Survey GDPI10 Interpretation Project, Southern Flank, Gippsland Basin

VicGCS

Victorian Geological Carbon Storage Initiative

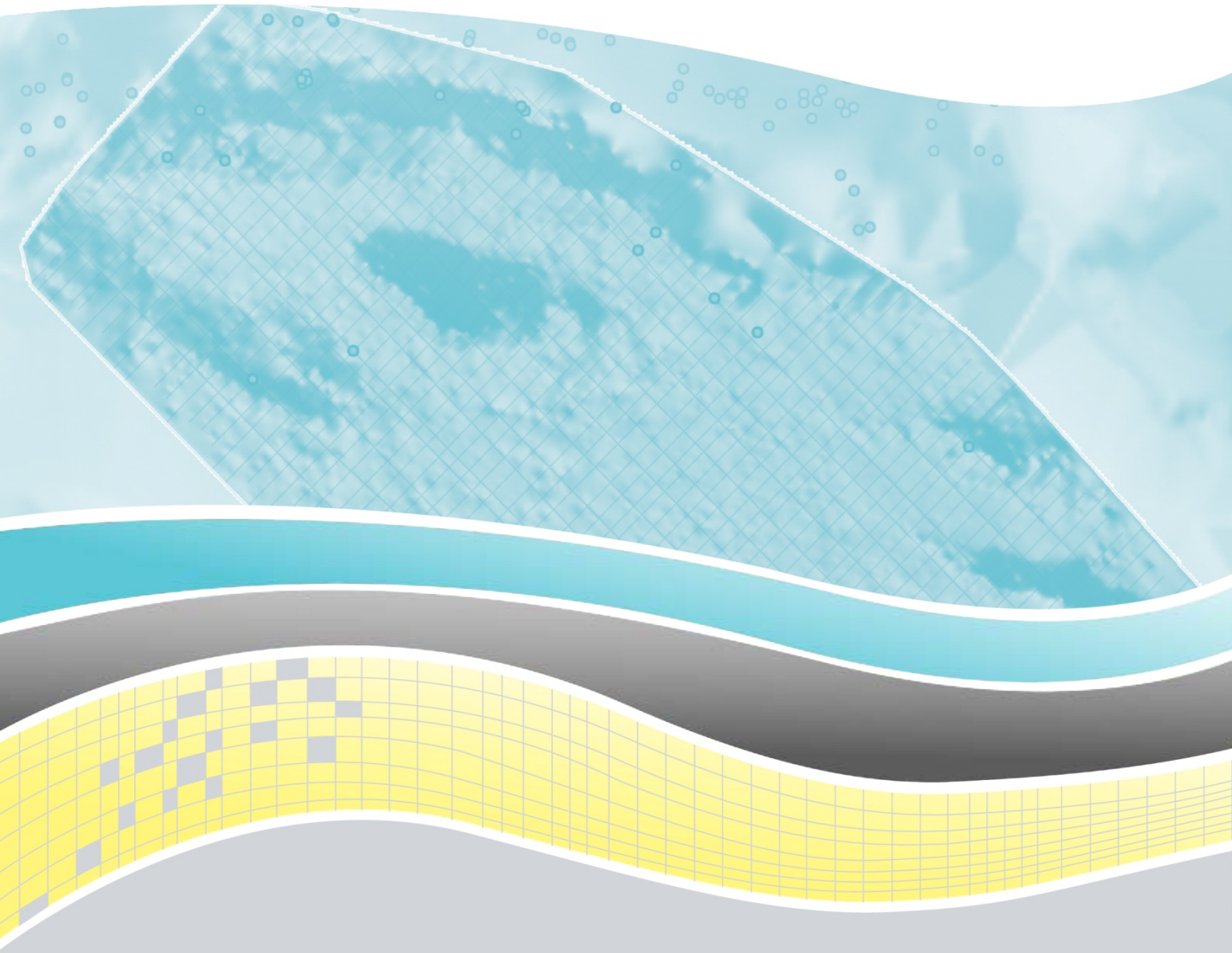

State Government Victoria

DEPARTMENT OF PRIMARY INDUSTRIES

VicGCS

Victorian Geological Carbon Storage Initiative

Survey GDPI10 Interpretation Project, Southern Flank, Gippsland Basin

J. BLEVIN, D. CATHRO, G. NELSON, J. VIZY & J.D. LEE

VicGCS Report 8
May 2013

Department of Primary Industries

If you would like to receive this information/publication in an accessible format (such as large print or audio) please call the Customer Service Centre on: 136 186, TTY: 1800 122 969, or email customer.service@dpi.vic.gov.au

Published by the Department of Primary Industries, Energy & Earth Resources Group, 1 Spring Street, Melbourne, Victoria 3000 Australia

May 2013

Authorised by the Victorian Government, 1 Spring Street, Melbourne, Victoria 3000 Australia

Bibliographic reference:
BLEVIN, J., CATHRO, D., NELSON, G., VIZY, J. & LEE, J.D., 2013. **Survey GDPI10 Interpretation Project, Southern Flank, Gippsland Basin.** VicGCS Report 8, Department of Primary Industries.

ISSN 1323 4536

ISBN 978-1-74326-433-1 (DVD)

ISBN 978-1-74326-434-8 (pdf)

Disclaimer:
This publication and all supporting components (seismic project, interpretation, depth conversion, wells etc) may be of assistance to you but the authors, FROGTECH Pty Ltd and the State of Victoria and its employees do not guarantee that the publication is without flaw of any kind or is wholly appropriate for your particular purposes and therefore disclaim all liability for any error, loss or other consequence which may arise from you relying on any information in this publication.

For more information about DPI visit the website at www.dpi.vic.gov.au or call the Customer Call Centre on 136 186.

Copies of this report may be obtained from:
Business Centre
Department of Primary Industries
16th Floor, 1 Spring Street
Melbourne, Victoria 3000

For further technical information and data packages contact:
Dr Louise Goldie Divko
Geological Survey of Victoria
Earth Resources Development Division
Department of Primary Industries
GPO Box 4440
Melbourne, Victoria, 3001
louise.goldie-divko@dpi.vic.gov.au

Acknowledgements:
FROGTECH Pty Ltd completed this regional stratigraphic interpretation of the GDPI10 Southern Flanks seismic survey in 2012 and was managed by Donna Cathro and Jane Blevin. Karen Romine of FROGTECH is thanked for her review of the work, as is Greg Blackburn of Terratek who provided technical advice throughout the project. FROGTECH's geophysicist Yvette Poudjom Djomani and data manager Christopher Pietrucha are thanked for their input, and Meredith Guy-Villon and Barbara Vanhoecke are acknowledged for their assistance with production of the report. Staff from the Geological Survey of Victoria and Geoscience Australia are acknowledged for their input and feedback and the Department of Resources, Energy and Tourism is acknowledged for their support through funds granted under the National Low Emissions Coal Council (NLEC).

Cover Image:
Top Basement depth structure map for the Gippsland Basin Southern Flank study area with well locations.

Contents

List of Figures

List of Tables

Executive Summary

The Gippsland Basin is a world-class hydrocarbon province and is widely viewed as highly prospective for large-scale geological greenhouse gas storage. Initial studies of the Gippsland Basin Central Deep identified large capacity storage opportunities, although the shallower southern and northern margins of the basin were viewed as less prospective due to seal capacity. More recently, the possibility for a good seal potential on the Southern Flank has led to further investigations of the area including the acquisition of the 2010 Southern Flank 2D Seismic Survey (GDPI10); an 8000+ line km grid of high quality, regional 2D seismic data across the Gippsland Basin's Southern Margin.

In February 2012, the Department of Primary Industries, Victoria (DPI) awarded FROGTECH the competitive Tender 314639 to undertake the regional stratigraphic interpretation of the GDPI10 seismic survey. The work was undertaken using IHS Kingdom™ (v. 8.7) as DPI's preferred software package. The GDPI10 data was loaded into an existing Kingdom project supplied by DPI. New synthetic seismograms, well composites, formation tops and biostratigraphic databases were created by FROGTECH in the Kingdom project.

FROGTECH has completed the seismic interpretation of 13 horizons on the 8000 km survey with ties to 20 key wells distributed across the Southern Flank (Figure 1). A velocity model was developed for the region, and calibrated to velocity information within the wells. Collectively, the resultant project is an integrated and depth-converted, seismic stratigraphic interpretation and geological model for the Southern Flank of the Gippsland Basin. The interpreted model will underpin further studies that assess geological factors relating to storage suitability and capacity.

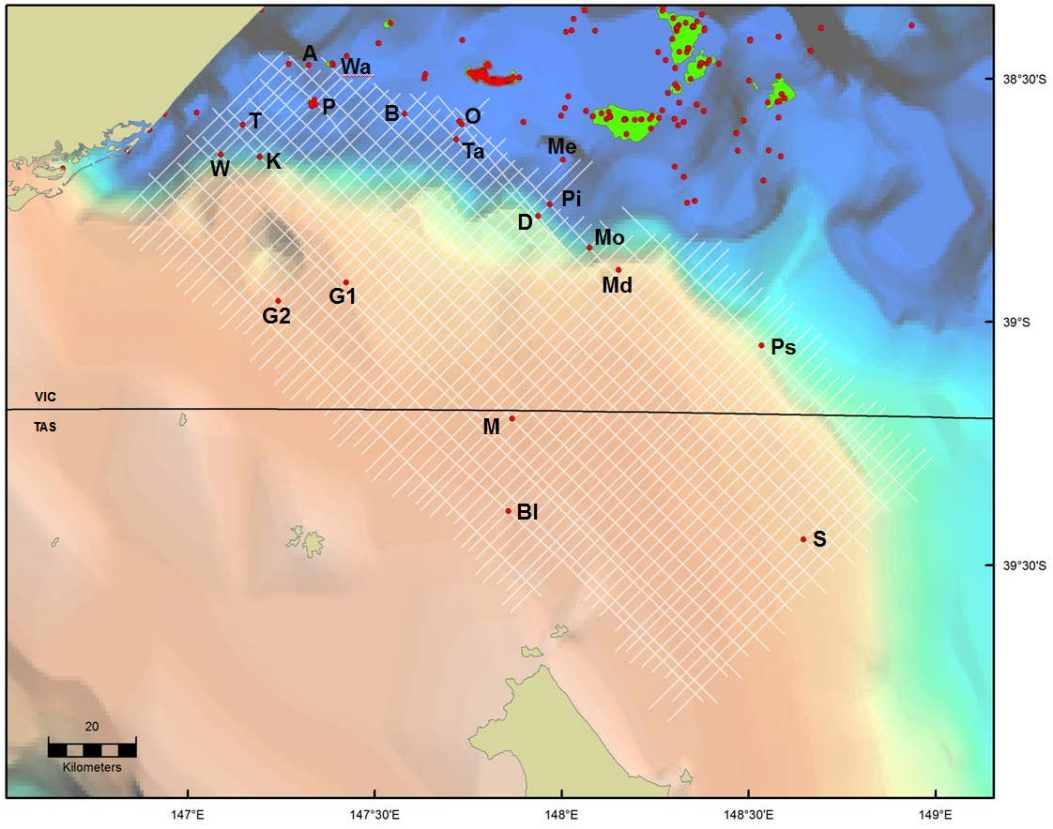

Figure 1 Location map of the key wells in the GDPI10 seismic interpretation. Well abbreviations: A = Amberjack-1, B = Bullseye-1, Bl = Bluebone-1, D = Devilfish-1, G1 = Groper-1, G2 = Groper-2, K = Kyarra-1A, M = Mullet-1, Me = Melville-1, Md = Mudskipper-1, Mo = Moray-1, O = Omeo-2A, P = Perch-1, Pi = Pike-1, Ps = Pisces-1, S = Sailfish-1, T = Tommyruff-1, Ta = Tarra-1, Wa = Wasabi-1 and W = Wyrallah-1.

The 13 interpreted horizons and 10 isopach intervals (listed below) are slightly different to those requested in the DPI Tender. Changes to the deliverables were made in consultation with DPI and were driven by the geological differences between significant stratigraphic intervals on the Southern Flank (study area) relative to the Central Deep:

REQUESTED HORIZONS	INTERPRETED HORIZONS
Seafloor	FrOG Tech 01 Seafloor
	FrOG Tech 02 Near Top Bassian Rise Unit 2
Mid-Miocene Marker	FrOG Tech 03 Top Bassian Rise Unit 3
	FrOG Tech 04 Top Bassian Rise Unit 4
Top Lakes Entrance Formation	FrOG Tech 05 Top Bassian Rise Unit 5
	FrOG Tech 06 Top Early Oligocene Wedge
Top of the Latrobe Group	FrOG Tech 07 Top Latrobe Group
	FrOG Tech 08 Top Halibut Subgroup
Top Cretaceous (near K-T boundary)	
Top of Golden Beach Sub-group	FrOG Tech 09 Top Golden Beach Subgroup
	FrOG Tech 10 Top Emperor Subgroup
Top of the Strzelecki Group	FrOG Tech 11 Top Strzelecki Group
	FrOG Tech 12 Top Pre-Strzelecki Group
Basement	FrOG Tech 13 Top Basement

Listing of originally requested and final interpreted horizons from the GDPI10 2D seismic survey on the southern flank of the Gippsland Basin. Additional horizons were interpreted (bold), with only the Top Cretaceous removed from the originally requested horizons.

ISOPACH/ISOCHRON UNIT	INTERPRETED HORIZONS
Total sediment thickness	FrOG Tech 01 to FrOG Tech 13
Mid Miocene and Younger	FrOG Tech 01 to FrOG Tech 03
Mid Miocene to top EOW	FrOG Tech 03 to FrOG Tech 06
EOW	FrOG Tech 06 to FrOG Tech 07
Latrobe Group	FrOG Tech 07 to FrOG Tech 11
Cobia Subgroup	FrOG Tech 07 to FrOG Tech 08
Halibut and Golden Beach subgroups	FrOG Tech 08 to FrOG Tech 10
Emperor Subgroup	FrOG Tech 10 to FrOG Tech 11
Strzelecki Group	FrOG Tech 11 to FrOG Tech 13
?Pre-Strzelecki Group	FrOG Tech 12 to FrOG Tech 13

Listing of isopachs/isochrons generated in the project and relationship to the interpreted horizons.

DPI identified the following key topics of interest for the Southern Flank Interpretation Project:

- A rigorous, regional sequence stratigraphic interpretation of the southern flank of the Gippsland Basin;
- Update the structural framework of the southern flank, including redefinition of the Pisces Sub-basin;
- A regional understanding of the distribution of potential reservoir/seal at the Top Latrobe level;
- Identification and mapping of seal failure indicators such as gas chimneys, shallow amplitude anomalies, hydrocarbon-related diagenetic zones (HRDZs) and seafloor anomalies; and,
- Capture of velocity variations within the stratigraphic succession on the southern flank and development of a 3D velocity volume.

Key Results

- **Structural Framework:** The Top Basement depth structure map and basement fault interpretation has defined the underlying structural framework of the study area (Figure 2). The main controlling features are the rigid, cratonised basement block which underlies the Southern Platform, and the Foster Fault System (FFS) which separates the Southern Platform and Southern Terrace. The Southern Platform displays a rugose topography with a central zone of basement highs that have acted as a sediment source during deposition of the Latrobe Group and the Early Oligocene Wedge. The Southern Platform experienced minimal subsidence and was a prominent sediment source until the Campanian. The FFS is a fundamental structural boundary that was reactivated in the early-middle Miocene, triggering instability and collapse of the overlying carbonate shelf. This lead to the development of a slump complex with subsequent canyon incision along the northern margin of the Southern Platform (Figure 3).

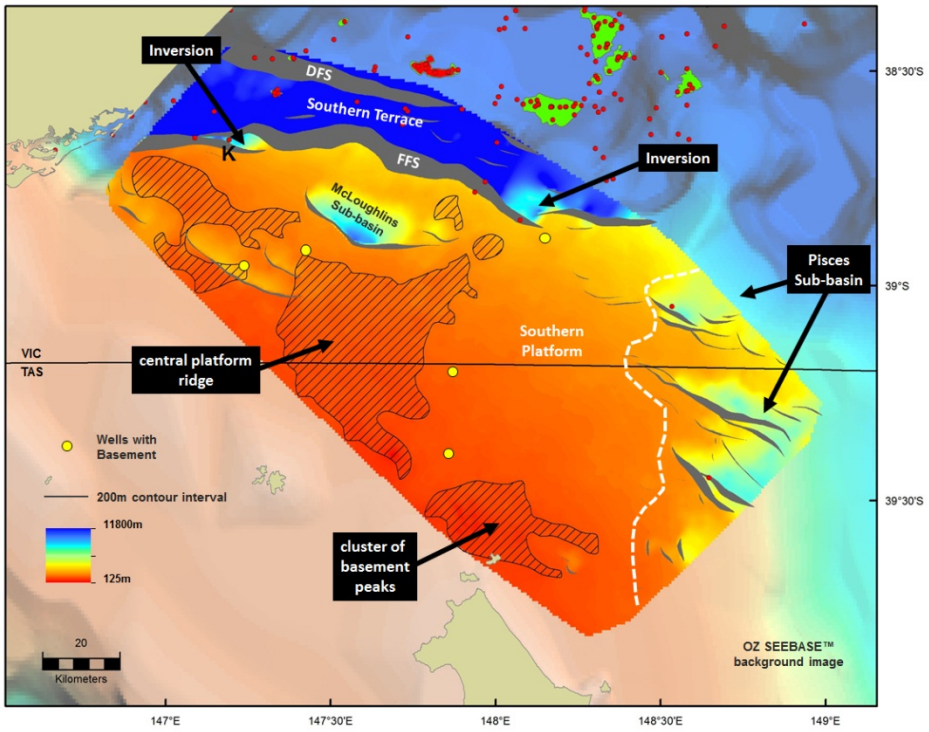

Figure 2 Top Basement depth structure map for the study area showing significant structural features. FFS = Foster Fault System. DFS = Darriman Fault System. Kyarra-1 (K) is drilled on the Kyarra anticline structure.

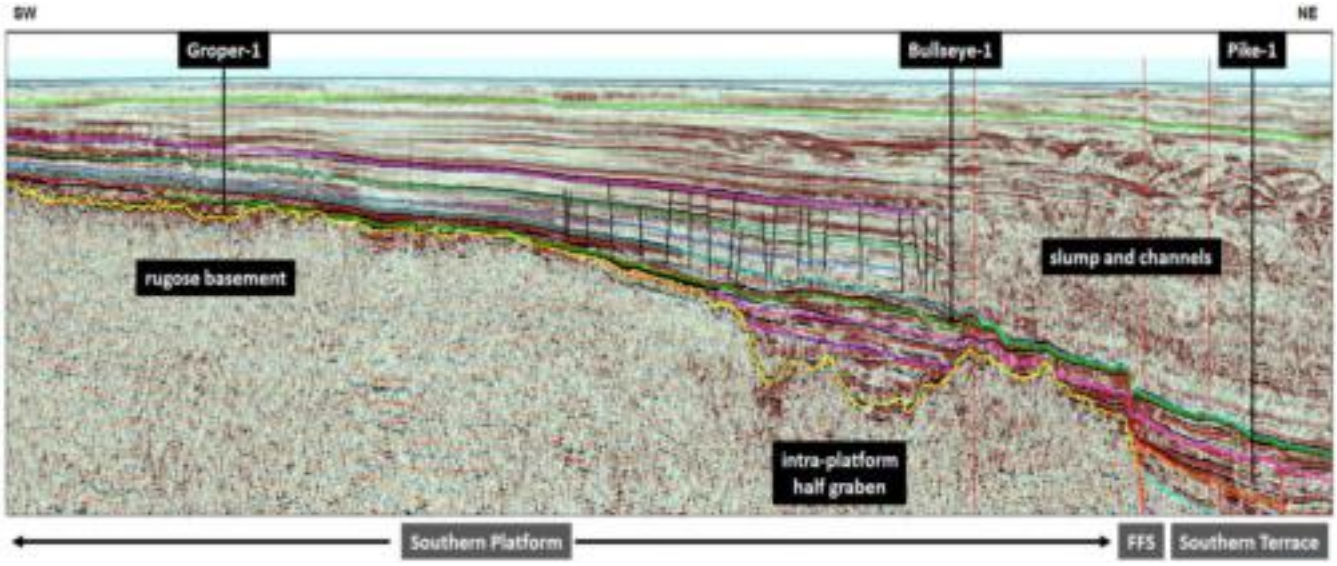

Figure 3 Representative seismic section across the Southern Platform and Southern Terrace. Other structural features of note are the intra-platform half graben, Foster Fault System (FFS) and the shelf margin slump and channel complex. Wells are not located on this line but are positioned to indicate the typical plays tested in the study area.

The FFS has also acted as a deep conduit for volcanic intrusions during periods of extension. Step-overs and relays along the extent of the FFS have been the focus of inversion such as observed near Moray-1, and also acted as conduits to funnel sands from the Southern Platform onto the Southern Terrace. Rigid basement has also acted as a buttress as observed in the formation of the Kyarra Anticline. The McLoughlins Sub-basin has been identified and mapped for the first time on the Southern Platform with up to 5.8 km interpreted Strzelecki-age equivalent sediments. The Pisces Sub-basin has been re-interpreted as a series of NE-trending en-echelon half graben that cut across the easternmost margin of the Southern Platform. The extensional faults were reactivated prior to breakup in the Tasman Sea off the Gippsland Basin. Here, sediments are locally disrupted by seismic anomalies suggesting vertical migration of fluids related to volcanism and igneous intrusions.

- **Latrobe Group Reservoirs:** New structure and isopach maps of the Cobia and Halibut subgroups (Latrobe Group) have been developed (Figures 4 and 5). Sands within these successions comprise the main reservoir intervals in the study area. New mapping clearly shows for the first time that the Halibut Subgroup extends from the Southern Terrace (where it has been intersected by drilling), across the Foster Fault System and well onto the Southern Platform. Seismic data also shows the development of extensive sand sheets which extend from the central platform basement ridge towards the Foster Fault System during Halibut deposition. These sands have been funneled from the Southern Platform onto the Southern Terrace at relay points along the FFS. The Cobia Subgroup has also been mapped and is more extensive across the Southern Platform than previously interpreted. The Cobia Subgroup thins on the updip and eastern parts of the Southern Platform where it infills the rugose basement topography and onlaps the basement highs. The broader extent of both Halibut and Cobia reservoirs will have implications for greenhouse gas injection models. New maps have also been produced for the older Latrobe Group intervals (Emperor and Golden Beach subgroups) where deposition has been strongly controlled by the Foster Fault System and related structures.

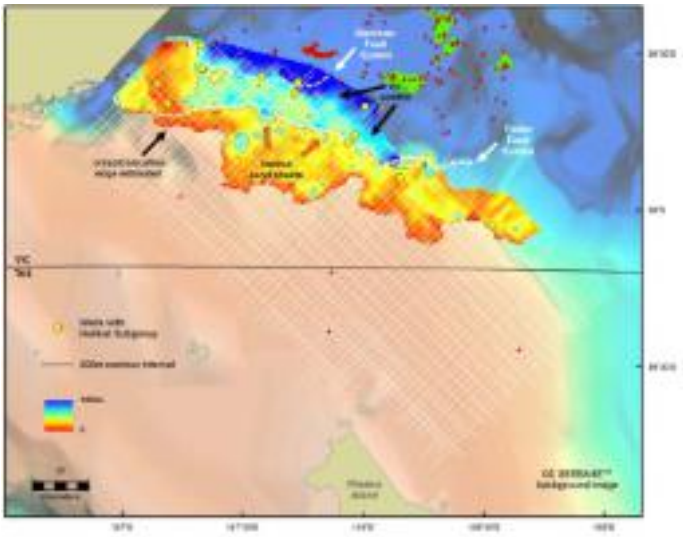

Figure 4 Halibut and Golden Beach subgroups (combined) isopach map for the study area.

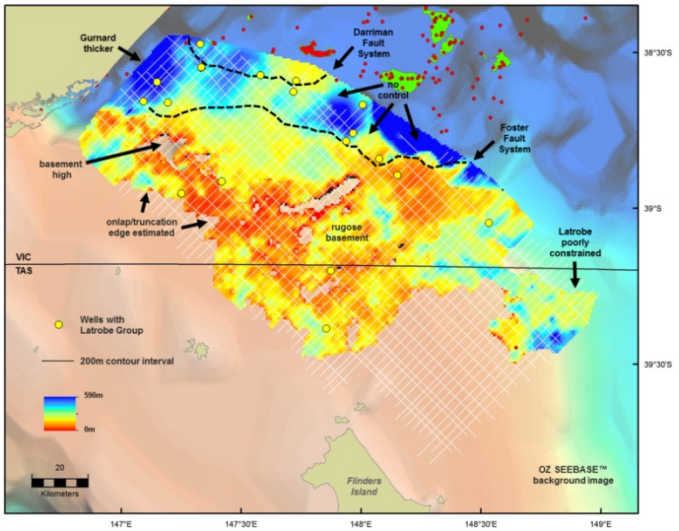

Figure 5 Cobia Subgroup isopach map for the study area.

- **Potential Sealing Facies:** The nature and distribution of sealing facies are relatively more complex in the study area than the central basin. Contrary to previous interpretations, the Lakes Entrance Formation is not the regional sealing facies for Top Latrobe reservoirs across the Southern Platform. Instead, an older, thick progradational, regionally extensive succession known as the Early Oligocene Wedge (EOW) overlies Latrobe Group sediments (Figure 6). The EOW forms the lowermost of a series of progradational carbonate

wedges that were deposited through to the late Miocene. The EOW displays mostly topset and low-angle progradational internal stratal geometries. The sealing characteristics of the basal EOW facies are here considered variable in age, thickness and lithology. The EOW is absent over the easternmost Southern Platform and thins to downlap across the Southern Terrace. In its condensed downlap location, sediments of the EOW could be confused with a thinned succession of the Gurnard Formation.

- **Risks:** It is interpreted that there are two potential scenarios where the EOW could have good sealing potential (Figure 6): 1) where the wedge is thickest; and, 2) where the wedge downlaps and the distal toes could represent fine-grained condensed sedimentation (Figure 7). The EOW is interpreted as a poor sealing facies where it thins over the central platform ridge. Areas proximal to the ridge are also downgraded for seal potential due to likely the input of sandy sediments. Identified risks associated with the EOW sealing potential include: 1) proximity to the central platform ridge; 2) post-depositional reactivation along the Foster Fault System; 3) the slump complex which may locally consume the upper part of the EOW; 4) local faulting of the EOW that occurs updip of the slump feature; and 5) inversion/uplift in the western basin. These risk polygons are shown in Figure 8. An optimal area has been predicted where the relative EOW seal potential is high and the risks are low (Figure 9).
- **Other Potential Seal Facies:** The seal assessment of the Southern Flank focused on the Cobia and Halibut subgroup reservoirs, and sealing facies of the EOW. The Gurnard Formation is here considered a more complex facies that requires further work beyond the scope of this study to determine its true age, lithology and sequence stratigraphic framework. The Gurnard Formation is predicted to be an important sealing facies in the western part of the study area. Elsewhere, the unit is too thin and underlies a condensed section of the distal EOW. The EOW does not directly overlie the Halibut Subgroup within the study area, thus seals for these reservoirs rely on intraformational shales or basal shales within the overlying Cobia Subgroup. The detailed mapping of individual intraformational seals within the Cobia and Halibut subgroups is beyond the scope of the current study but is recommended for future work.
- **Slump Complex**: Much of the EOW to mid-Miocene succession is consumed by a large slump zone that spans the length of the outer Southern Platform and extends across parts of the Southern Terrace. The slump is interpreted to have formed by shelf instability caused by late stage faulting along the western part of the Foster Fault System. The formation of release faults upslope from the slump complex have also affected the integrity of Oligocene and younger sediments that overlie the Latrobe Group. The slump feature breaches and reduces the effectiveness of possible sealing units. Greenhouse gases injected into underlying reservoirs may migrate into the slump zone, where containment and migration pathways may be complex and unconstrained.
- **Seal Failure Indicators**: An assessment of the GDPI10 2D seismic survey for evidence of seal failure, such as HRDZs and gas chimneys, has identified several clusters of seismic anomalies. Overall, these anomalies are interpreted to relate to the release of fluids associated with volcanic intrusions and with some component of associated fault breach. The clustering of the anomalies is more likely to relate to localised volcanic centres, rather than indicative of regional seal breach points. No pervasive hydrocarbon-related anomalies were identified.
- Other Points:
    - The stratigraphic surfaces mapped are referenced to the latest stratigraphic chart for the Gippsland Basin (Partridge et al., 2012). The timescale, in millions of years, differs from the stratigraphic chart of Bernecker and Partridge, 2001 and derivatives, typically used in GeoScience Victoria publications.
    - Seismic stratigraphic mapping suggest currently defined formation tops in some wells may be problematic at several levels and these are highlighted in Section 5. In particular, the "Devilfish Sand" has been reinterpreted and mapped as part of the Cobia Subgroup.
    - The most problematic picks are where a thinned section of the Gurnard Formation is overlain by the condensed distal toes of the progradational EOW. Here, there is likely to be bioturbation and the Gurnard picks often do not correlate well with the mapped Top Latrobe seismic horizon.
    - The "Top Lakes Entrance" pick at wells that lie within the slump (Bullseye-1, Mudskipper-1 and Tarra-1) are considered unreliable and were disregarded during the current study.

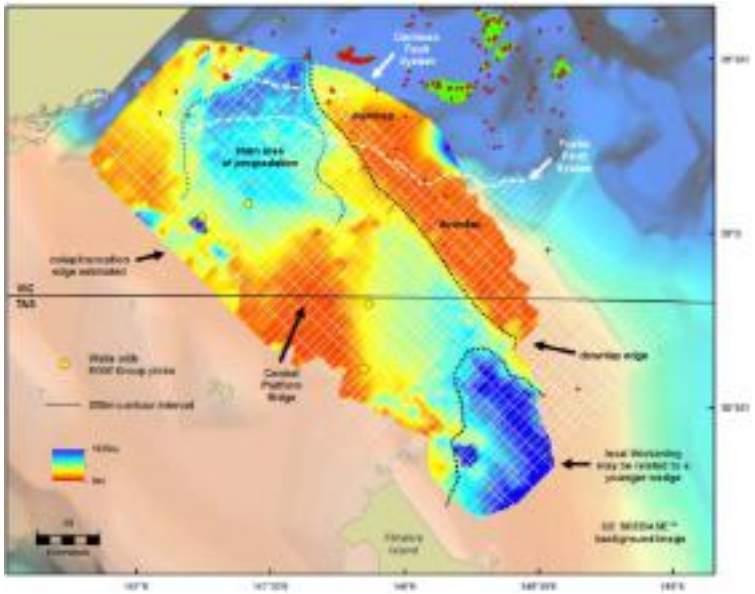

Figure 6 Early Oligocene Wedge (Seaspray Group) isopach map for the study area.

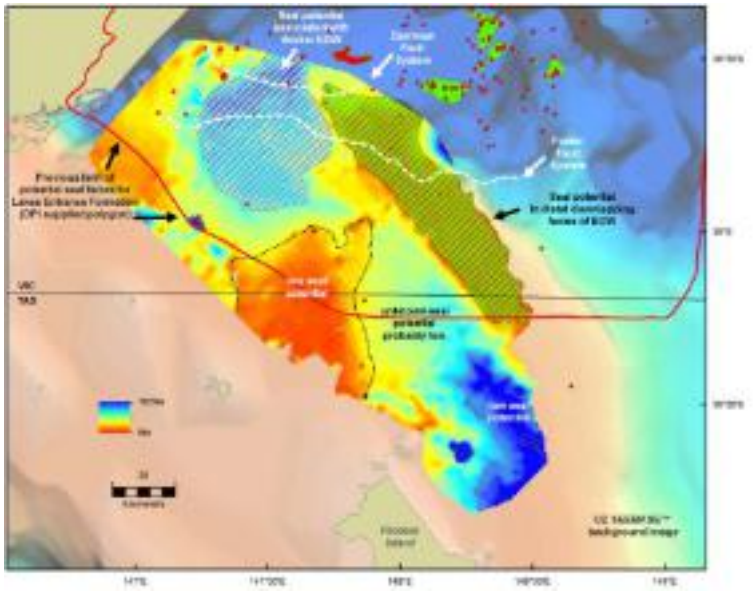

Figure 7 Map showing the potential for sealing facies associated with the EOW. The "Limit Top Seal Lakes Entrance Formation" polygon supplied by GeoScience Victoria is shown in red.

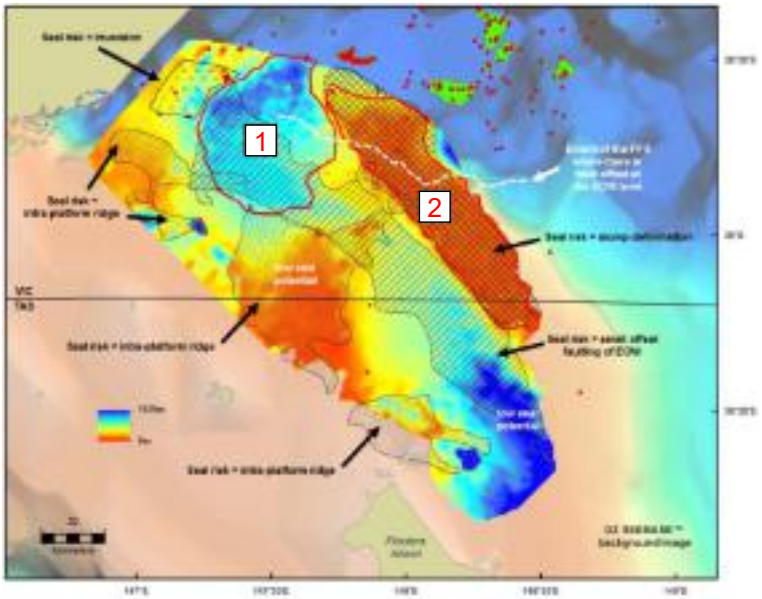

Figure 8 Map showing the risk polygons for the EOW sealing potential including: 1) proximity to the central platform ridge; 2) post-depositional reactivation along the Foster Fault System; 3) the slump complex which may locally consume the upper part of the EOW; 4) local faulting of the EOW that occurs updip of the slump feature; and, 5) inversion/uplift in the western basin. Note that only that part of the Foster Fault System (FFS) where there is offset of the EOW is shown in the figure. The red polygons indicate the potential seal facies distribution 1) thicker EOW and 2) Distal downlapping facies of EOW.

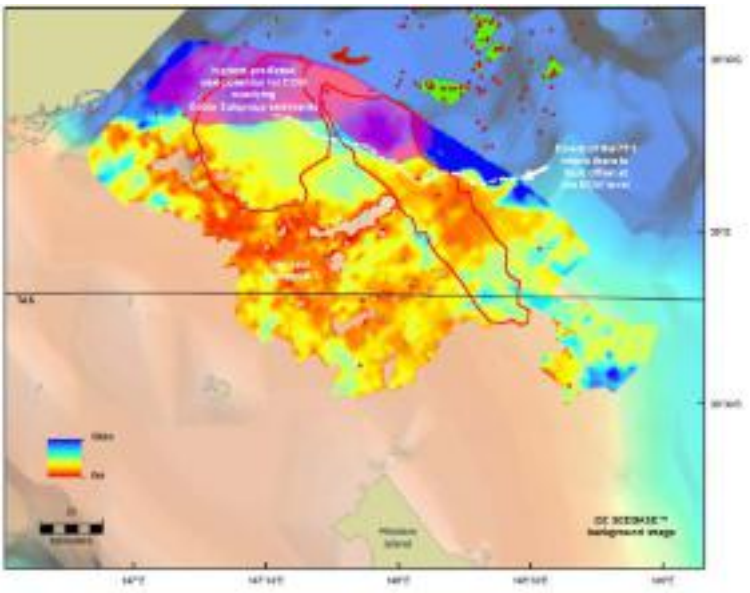

Figure 9 Summary map of the predicted high EOW seal potential overlying Cobia Subgroup sediments based on a first-pass analysis of regional geology and associated risk factors. The base map is the Cobia Subgroup isopach.

- The seismic interpretation is supported by synthetic seismograms generated for 20 key wells across the basin and tied to the GDPI10 seismic survey.
- Up to date geological information is summarised in well composites and includes the correlation between formation tops, biostratigraphy and seismic surfaces interpreted during this study.
- A 3D velocity model was developed using Kingdom VELPAK to generate a 3D average velocity volume which can be utilised in other software packages. This volume was used to depth convert the interpreted grids and other features. SEG-Y profiles of average velocities have also been created for the 2D seismic lines. These can be imported into Kingdom to depth convert interpretations in profile.

Recommendations for Future Work

- Undertake a full reinterpretation of the Gurnard Formation and the EOW to clearly distinguish the age, lithology and seal potential of these different facies. Integrate the new interpretation with wells that lie close to the Southern Platform (which are outside the current study area).
- Extend regional ties of the deeper horizons (Strzelecki, Emperor and Golden Beach) across the Darriman Fault and into the Central Deep to establish a continuous structural model for the Southern Flank. The GDPI10 2D seismic survey only crossed the Darriman Fault in the western part of the study area, and this has compromised ties along the northern boundary of the study area.
- Seismic interpretation and the resultant gridding performed on the regional GDPI10 survey could be used to highgrade areas for further investigation. As a first step, regridding any smaller area at a higher resolution to provide additional control on the gridding algorithm and allow for a smaller grid cell size would be beneficial. Including additional interpretations from the many vintage datasets where appropriate may also enhance the current interpretation in some locations. It is considered that additional modern seismic acquisition and interpretation would be required prior to siting greenhouse gas injection wells.
- Review the geographic location of wells on the southern flank, as the absolute confidence of the location of older wells is relatively low.
- Reprocessing of select GDPI10 lines may enhance the imaging of structural features on the Southern Platform or the deeper stratigraphy in the Southern Terrace.
- Formation tops need to be reviewed at a number of levels, including additional biostratigraphic analysis to investigate possible alternative interpretations.

- Melville-1 is a key tie well for the survey but contains limited biostratigraphic or formation top information. Additional work on this well may provide important linkage information between the Southern Flank and the Central Deep.
- The new stratigraphic and structural interpretation provides a framework to understand existing seal capacity results (MICP) and can be used to plan future program activities to test concepts and highlight areas of interest.
- The velocity model was developed on a regional scale, using broad stratigraphic intervals to capture velocity variations and assumed increasing velocity with depth. If a more accurate depth conversion is required in localised areas then the model should be reviewed taking into account the velocity inversions noticed in the pseudo-sonic logs. This could be achieved by 'mapping' the inversion in the pseudo-logs.
- The construction surfaces used to create the velocity model could be refined by using the final interpreted surfaces of this study. This should enhance the velocity model and give an improved depth result as the boundaries where the velocity changes would be more accurately defined.
- Ensure the GDPI10 2D seismic survey is released only after the SEG-Y have been regenerated referenced to shotpoint rather than CDP.

1 Introduction, Aims and Regional Setting

1.1 Introduction

The Gippsland Basin (Figure 1.1) is a world-class hydrocarbon province and is widely viewed as highly prospective for large-scale geological greenhouse gas storage. Initial studies of the Gippsland Basin Central Deep identified large capacity storage opportunities (Gibson-Poole et al., 2008), although the shallower southern and northern margins of the basin were viewed as less prospective due to seal capacity (O'Brien, et al., 2008). More recent work has identified good seal potential on the Southern Platform (Goldie Divko et al., 2010). This result has led to further investigations of the area including the acquisition of a new high quality 2D regional seismic survey (Figure 1.2).

In February 2012, the Department of Primary Industries, Victoria (DPI) selected FROGTECH Pty Ltd as the successful tenderer to undertake a regional seismic interpretation of the GDPI10 2D seismic survey. The 2D seismic survey of approximately 8,000 km was acquired on the southern flank of the Gippsland Basin in early 2010. Acquisition was jointly funded by DPI and the Federal Department of Resources, Energy and Tourism (RET). DPI's Earth Resources and Development Division (ERDD) and Geoscience Australia (GA; on behalf of RET) together administered the project.

1.2 Project Aims and Deliverables

The aim of the 2D seismic interpretation project was to undertake a geological interpretation of the regional seismic dataset to provide a framework for the future assessment of:

- top seal potential;
- fault seal integrity;
- reservoir quality, distribution and connectedness; and,
- petroleum systems and fluid migration.

The interpretation will be used by DPI and GA for continuing research on the greenhouse gas storage potential of the Gippsland Basin. Geological information will be used to construct regional injection and containment models, an attributed geological model, and regional petroleum systems and prospectivity assessments. The interpretation will form part of the pre-competitive data (along with the processed seismic grid) that will be open-file and available to Australian and State Governments, industry, research organisations and the geological community. As the interpretation will be open-file, the outputs are required in a range of formats compatible with commonly used geological software.

As stated in the request for Victorian Tender Document 314639 (September 2011), the scope of the interpretation includes the following outputs:

1) Regional stratigraphic surfaces, horizons and sequences in both two-way-time (TWT) and depth converted forms.
    a. Seafloor
    b. Mid-Miocene Marker
    c. Top Lakes Entrance Formation
    d. Top of the Latrobe Group
    e. Top Cretaceous (near K-T boundary)
    f. Top of Golden Beach Subgroup
    g. Top of the Strzelecki Group
    h. Basement
    i. Other mappable horizons identified

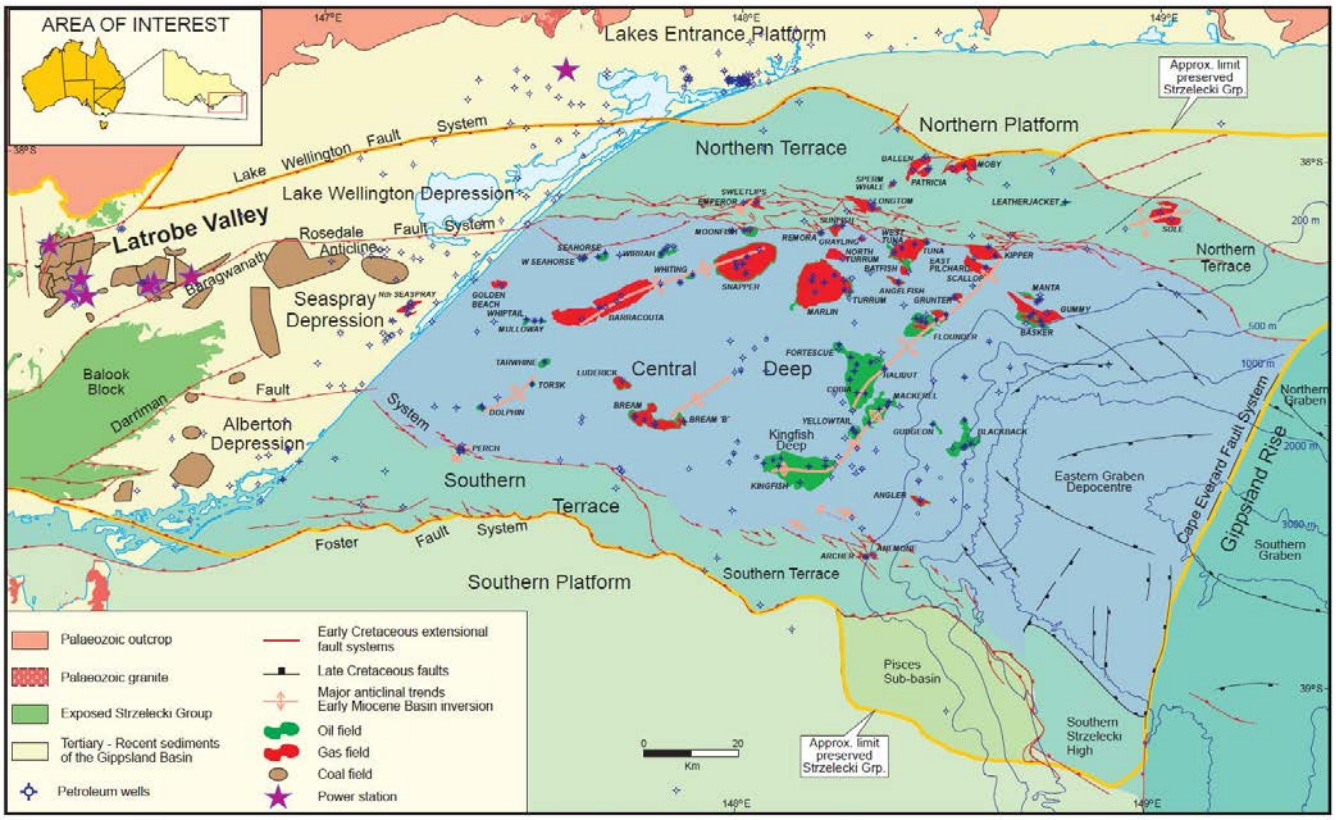

Figure 1.1 Tectonic elements of the Gippsland Basin, major oil/gas fields and hydrocarbon exploration wells (Goldie Divko et al., 2010).

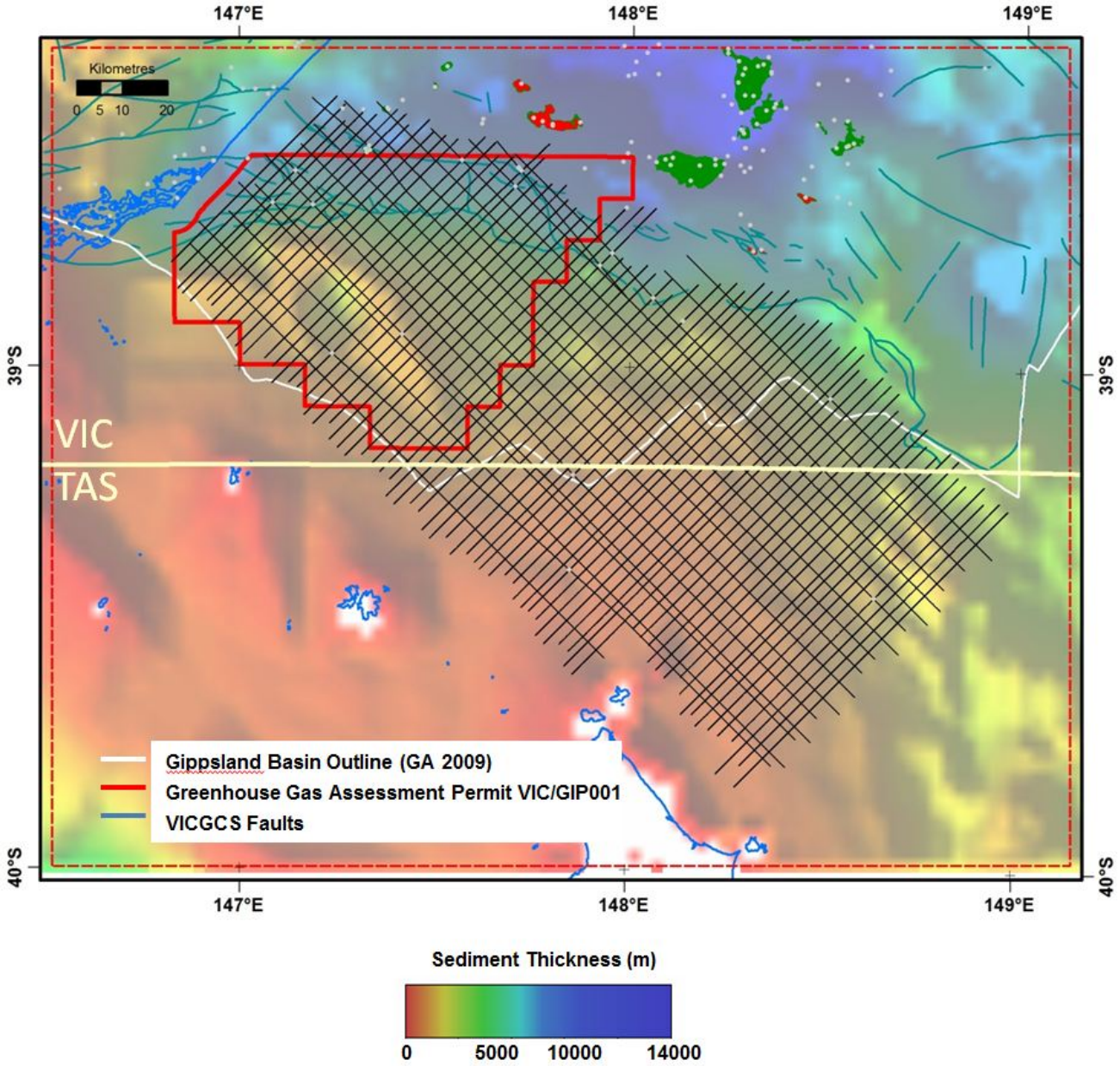

Figure 1.2 The GDPI10 2D seismic survey (black lines) acquired on the southern flank of the Gippsland Basin and the project area (red dashed line) for the current study are shown. Gas (red) and oil (green) fields, along with exploration wells (grey dots), and PSLA offshore boundaries for Victoria and Tasmania (yellow line) are also shown. Background is the total sediment thickness as calculated from the difference between DEM and OZ SEEBASE™ grids.

2) A structural interpretation in TWT and depth converted forms, showing fault linkages vertically and laterally; wherever possible correlating faults.
    a. Darriman Fault System
    b. Foster Fault System
    c. Intrabasinal Faults
    d. Basement Highs
    e. Definition of the Pisces and other sub-basins
    f. Channels and Canyons
3) A sequence-based seismic stratigraphic interpretation of the region including reflection terminations and associated unconformities.
4) Isochron and isopach maps of units, seal and reservoir extent; mapping of empirical indicators of seal failure, including gas chimneys, shallow amplitude anomalies, hydrocarbon-related diagenetic zones (HRDZs) and seafloor anomalies.
5) Velocity maps and the derived velocity model with interval velocities of key sequences and estimates of uncertainty. Interval velocities derived primarily from stacking velocity information and tied to time-depth relationships at a subset of the wells on the southern flank of the Gippsland Basin.
6) A report documenting the procedures and tools used in generating the geological interpretation, as well as the key findings and interpretative information outlining the stratigraphic and structural evolution of the Southern Flanks of the Gippsland Basin.
7) Up to three verbal presentations of the deliverables and key findings in Melbourne and/or Canberra.
8) Support for up to one year after delivery and acceptance of the 2D interpretation.

The project deliverables are provided to DPI Earth Resources Development Division as a Kingdom project (time and depth). Additional outputs are required to be compatible with loading into GOCAD, Permedia, Petrel, DUG, Petrosys, Landmark, GeoFrame and PetroMod.

The specific deliverables and mapped horizons were amended during the interpretation phase in consultation with DPI and GA, to better reflect the geology of the Southern Platform and Southern Terrace of the Gippsland Basin (Table 1.1). The significance of these changes to the regional interpretation is presented throughout this report.

1.3 Victorian Geological Carbon Storage Initiative and Southern Flanks Project

In July 2008, GeoScience Victoria (GSV) commenced the Victorian Geological Carbon Storage (VicGCS) Initiative sponsored by the Victorian State Government. The Gippsland Basin was identified as a key region for investigation and the work program focused on the offshore Gippsland Basin with three primary technical aims: containment, capacity/injectivity, and impacts. The program aimed to:

- identify areas with GCS potential; provide geological support for the State and Commonwealth GSC acreage release programs; and to provide open-file geoscientific data and information.
- in addition to the VicGCS program and to provide industry quality data across the southern margin of the Gippsland Basin, the federal Department of Resources, Energy and Tourism (RET) and the Victorian government funded the acquisition of the Southern Flanks 2D seismic survey in an area overlying the 2009 Greenhouse Gas Storage Assessment blocks. To facilitate the acquisition, processing and interpretation of the data, a National Geoscience Project Agreement was established between Geoscience Australia and GeoScience Victoria. Through GeoScience Victoria the GDPI10 2D seismic survey was acquired in 2010 and processed in 2011. The current study completes this work package and will provide a basis for future storage prospectivity work in the area.

HORIZONS (tender)	INTERPRETED HORIZONS
Seafloor	FrOG Tech 01 Seafloor
	FrOG Tech 02 Near Top Bassian Rise Unit 2
Mid-Miocene Marker	FrOG Tech 03 Top Bassian Rise Unit 3
	FrOG Tech 04 Top Bassian Rise Unit 4
Top Lakes Entrance Formation	FrOG Tech 05 Top Bassian Rise Unit 5
	FrOG Tech 06 Top Early Oligocene Wedge
Top of the Latrobe Group	FrOG Tech 07 Top Latrobe Group
	FrOG Tech 08 Top Halibut Subgroup
Top Cretaceous (near K-T boundary)	
Top of Golden Beach Sub-group	FrOG Tech 09 Top Golden Beach Subgroup
	FrOG Tech 10 Top Emperor Subgroup
Top of the Strzelecki Group	FrOG Tech 11 Top Strzelecki Group
	FrOG Tech 12 Top Pre-Strzelecki Group
Basement	FrOG Tech 13 Top Basement

Table 1.1 **Listing of originally requested and final interpreted horizons on the GDPI10 2D seismic survey on the southern flank of the Gippsland Basin. Changes from the horizons requested in the original Victorian Tender Document 314639 (September 2011) were made in consultation with DPI and GA staff. In general, additional horizons were interpreted (bold), with only the Top Cretaceous removed from the original requested horizons.**

1.4 A Geological Overview of the Gippsland Basin

The Gippsland Basin is one of Australia's most prolific hydrocarbon provinces with several giant oil and gas fields (Figure 1.1). The basin has onshore and offshore elements, with the vast majority of the hydrocarbon discoveries located offshore and reservoired in the Late Cretaceous to Paleogene Latrobe Group (Figure 1.3). The basin formed as part of the broader Southern Margin Rift System and the eastern margin Tasman rift system in response to the on-going fragmentation of eastern Gondwana. Rifting began in the Late Jurassic and continued episodically until breakup in the Tasman Sea off the Gippsland region in the Campanian (Norvick and Smith, 2001).

The basin succession can be broadly divided into syn-rift, post-rift and late post-rift/reactivation tectonostratigraphic megasequences. These megasequences roughly correlate to the Albian and older Strzelecki Group, the Late Cretaceous to early Oligocene Latrobe Group and the Oligocene and younger Seaspray Group (Bernecker and Partridge, 2001). The Latrobe Group has four subgroups (Emperor, Golden Beach, Halibut and Cobia) with several formations within each subgroup.

The horizons requested for interpretation and mapping by the DPI Tender relate to regionally significant geological surfaces that subdivide the stratigraphic groups (megasequences) and subgroups. The stratigraphic interval of particular interest for greenhouse gas storage is the Top Latrobe, as it represents the "top reservoir/base regional top seal" configuration across much of the basin. The DPI requested horizons were mostly based on the stratigraphic model of the broader Central Deep. During the current study, the presence and significance of the requested Central Deep horizons in the study area became clearer. While many of the key horizons defined in the Central Deep are also fundamental to the understanding of the development in the Southern Flank, others do not capture the distinct structural and depositional history of the area. Therefore, due to geological reasons, the list of requested horizons was changed to better reflect the unique geology of the area (Table 1.1). Further discussions on basin evolution, stratigraphy and mapped horizons in the Gippsland Basin are presented later in this report.

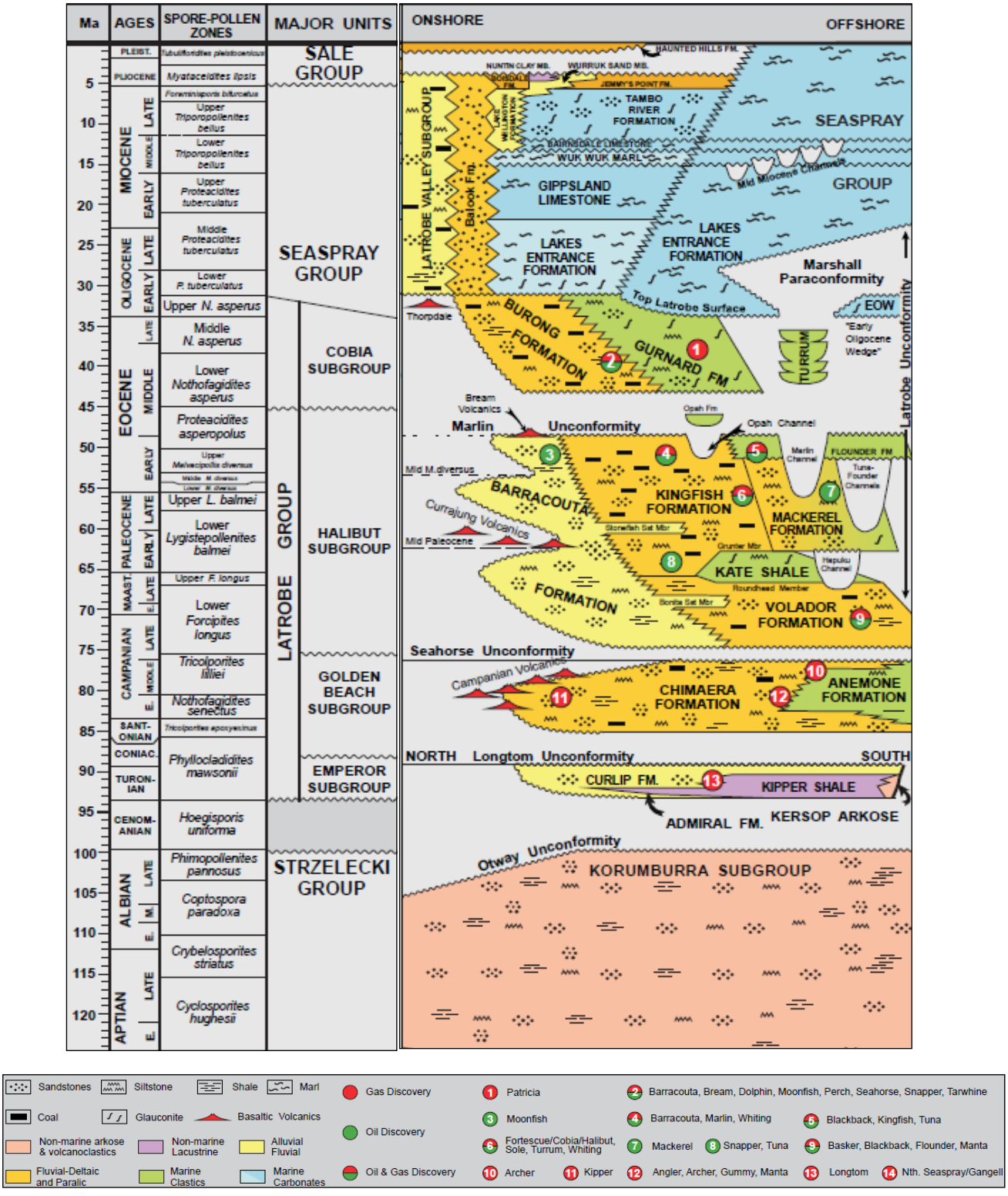

Figure 1.3 Gippsland Basin Stratigraphy (Bernecker and Partridge, 2001).

2 Data Compilation and Quality Assessment

2.1 Introduction

The primary dataset for this study is the GDPI10 2D seismic survey consisting of approximately 8,000 line km of 2D seismic data acquired on the southern flank of the Gippsland Basin (Figure 2.1). These data were provided to FROGTECH as SEG-Y data. Additional seismic and well data covering the entire Gippsland Basin were also provided as part of a Kingdom project supplied by DPI (Figure 2.2). Much of the seismic interpretation provided came from the regional interpretation project undertaken on multi-vintage 2D and 3D seismic surveys for DPI by 3D-GEO in 2010. As the Southern Flank is the focus for this study, the data were supplemented by a variety of reports on 20+ wells contained within the area of the GDPI10 survey (Figure 2.1). DPI also provided open file publications and reports covering the Gippsland and Otway basins. Each of these datasets will be discussed more fully in the following section.

2.2 GDPI10 Seismic Data

A detailed discussion of the seismic data quality is contained in an internal report to DPI by Terratek (2012), and is summarised below. The 8053.50 line kilometres of seismic data were acquired on 87 lines oriented approximately NE-SW and NW-SE with an approximate line spacing of 2.5 km and 5 km respectively (Figure 2.1). The data were acquired in 2010 with the general parameters as shown in Table 2.1.

Data processing of the GDPI10 2D seismic survey was awarded to Fugro Seismic Imaging Pty Ltd (Fugro) and completed in late 2011. For a full description of the processing steps please refer to "Seismic Data Processing Report for Victorian DPI" (Fugro, 2011). The main processing steps are summarised in Table 2.2.

FROGTECH received four stacks of each line from DPI: a final full stack and three partial angle stacks (near, 5-20^{o}; mid 15-30^{o} and far 25-40^{o}). No parameter documentation is provided with the Fugro processing report for the angle stacks. The angle windows were located within the SEG-Y headers (Figure 2.3).

All the SEG-Y stack data were loaded by FROGTECH into a pre-existing Kingdom project generated by 3D-GEO for DPI. FROGTECH loaded the data using the defined project coordinate system of GDA94 Zone 55S, which differs from the seismic projection of WGS84 UTM 55S as read from the SEG-Y headers. The difference between the two projections is often less than one metre.

During the QC of the data three issues were identified with the SEG-Y data:

- Common depth point vs. shotpoint referenced navigation;
- Incorrect fathometer data; and
- Shallow seafloor muting.

2.2.1 Common Depth Point vs. Shotpoint Referenced Navigation:

Once loaded into Kingdom, slight differences were noted between the base map provided in the data processing report by Fugro and the seismic base map generated from the Kingdom project (Terratek, 2012). Parallel seismic lines in the Kingdom project had terminations consistently along a straight line, while Fugro's base map (Fugro, 2011) had a more ragged edge appearance (Figure 2.4). The source of the discrepancy between the two displays is that the Fugro map in the processing report displays only the full-fold coverage, rather than the total coverage including seismic tails which is shown in the Kingdom project. While analysing this visual mismatch it was identified that the seismic data had been loaded into the Kingdom project assuming the SEG-Y navigation was relative to shotpoint (SP). Further examination of the SEG-Y header revealed that the navigation was actually related to common depth point (CDP) locations (Figure 2.5). The CDP location information was contained at the position where SP information is usually stored in SEG-Y data. As the SEG-Y data only contained CDP navigation, FROGTECH requested the supply of SP navigation to correct the problem. Once supplied, the data were corrected for the SP navigation in the Kingdom project. To prevent future confusion, FROGTECH also recommended that Fugro resupply the SEG-Y with the SP navigation embedded into the headers prior to the data being widely distributed.

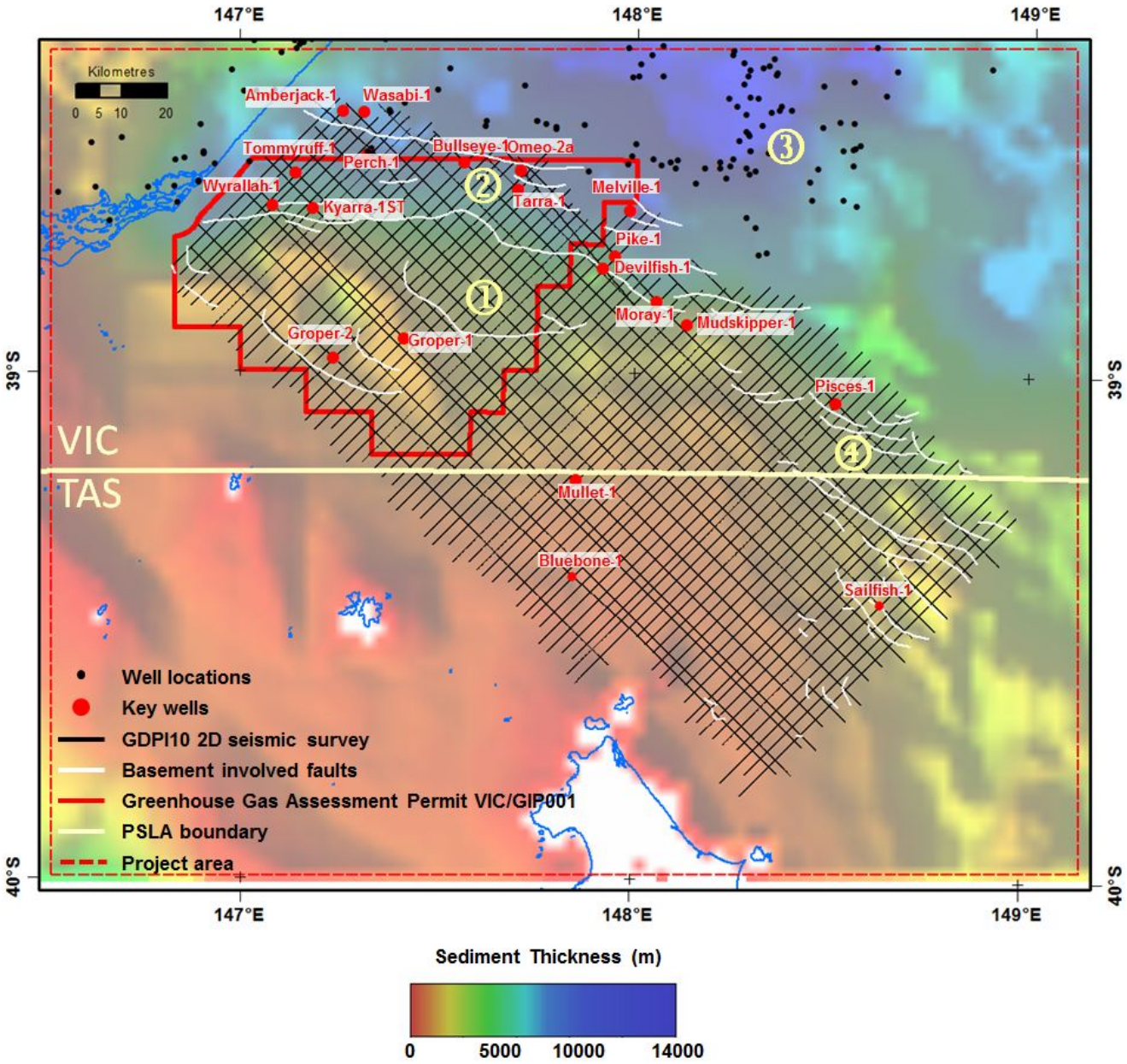

Figure 2.1 Seismic data and key wells (red dots) overlain on the total sediment thickness as calculated from the difference between DEM and OZ SEEBASE™ grids. Other wells in the Gippsland Basin are shown by black dots. The Southern Platform (1) and Southern Terrace (2) lie south of the Central Deep (3). Further east lies the Pisces Sub-basin (4). Fault traces (white lines) highlight the major basement-involved faults interpreted in this study.

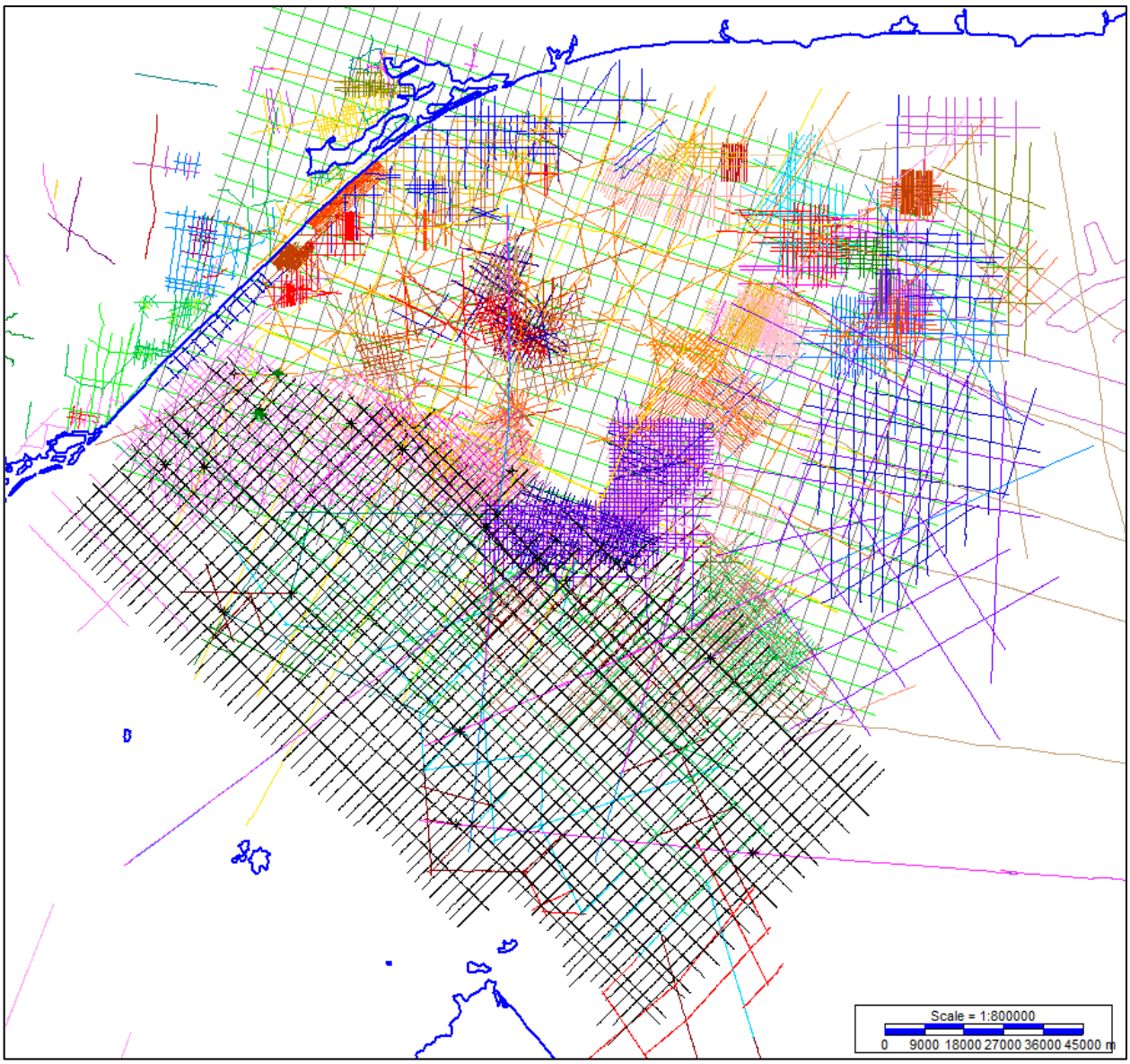

Figure 2.2 The suite of seismic data in the Kingdom project. The GDPI10 2D seismic survey that was interpreted during this study is shown in black. Multi-vintage 2D seismic data are in a variety of colours and the area of 3D megavolume generated by 3D-GEO is shown by the bright-green/grey crosshatch. The actual region covered by 3D data covers a smaller area than shown.

Vessel	: Seabird Exploration, M/V Aquila Explorer
Shot Interval	: 18.75 m
Group Interval	: 12.5 m
Cable Length	: 5087.5 m
Groups per Cable	: 408
Minimum Offset	: 113.68 m
Maximum Offset	: 5201.18 m
Sample Rate	: 2 ms
CDP Fold	: 136
Gun Depth	: 5-6 m
Cable Depth	: 7-8 m
Vertical datum	: Mean sea level
Record Length	: 5632 ms
Geodetic datum	: WGS 84
Projection	: UTM ZONE 55 S

Table 2.1 GDPI10 acquisition parameters.

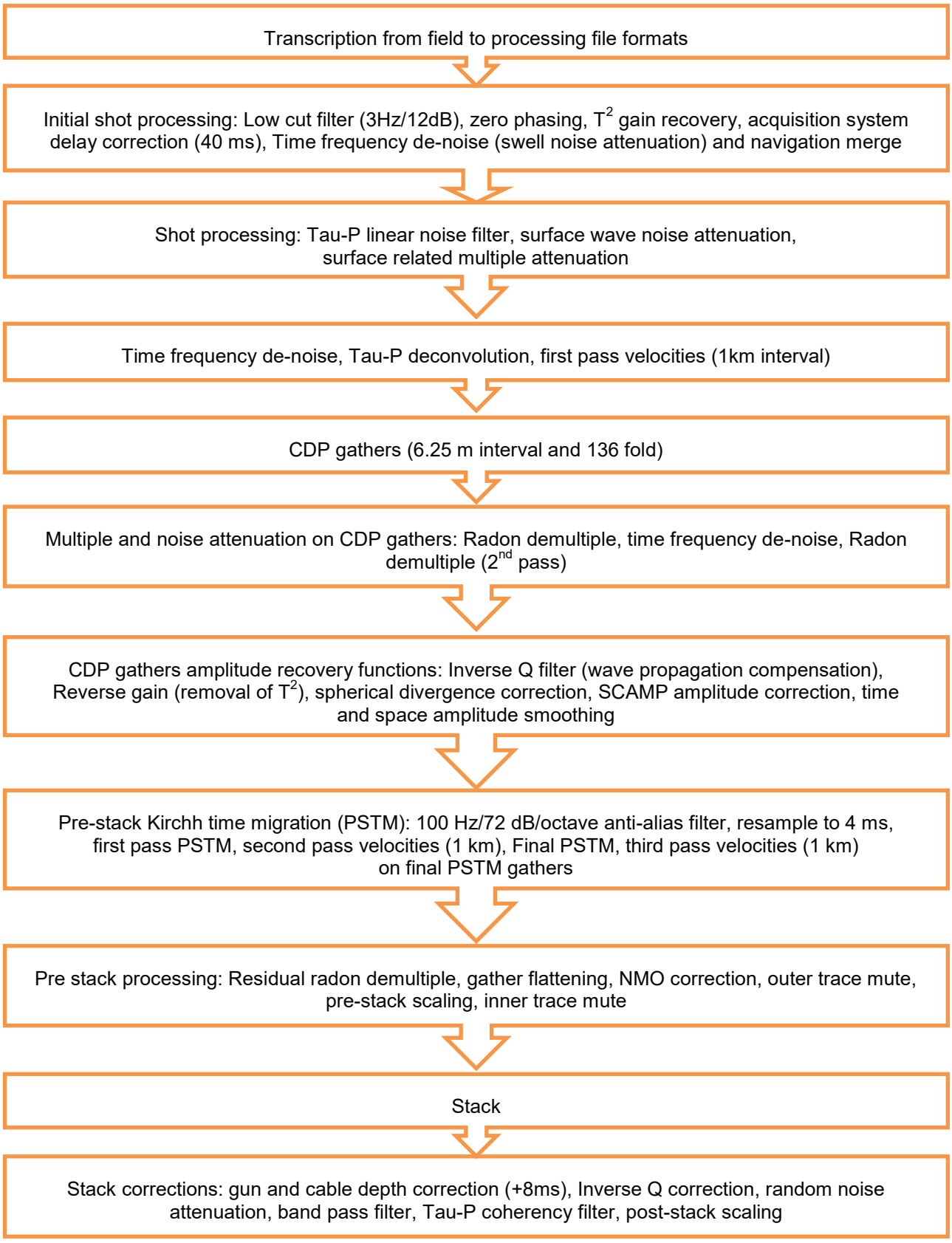

Table 2.2 Data processing steps performed on GDPI10 2D seismic data by Fugro.

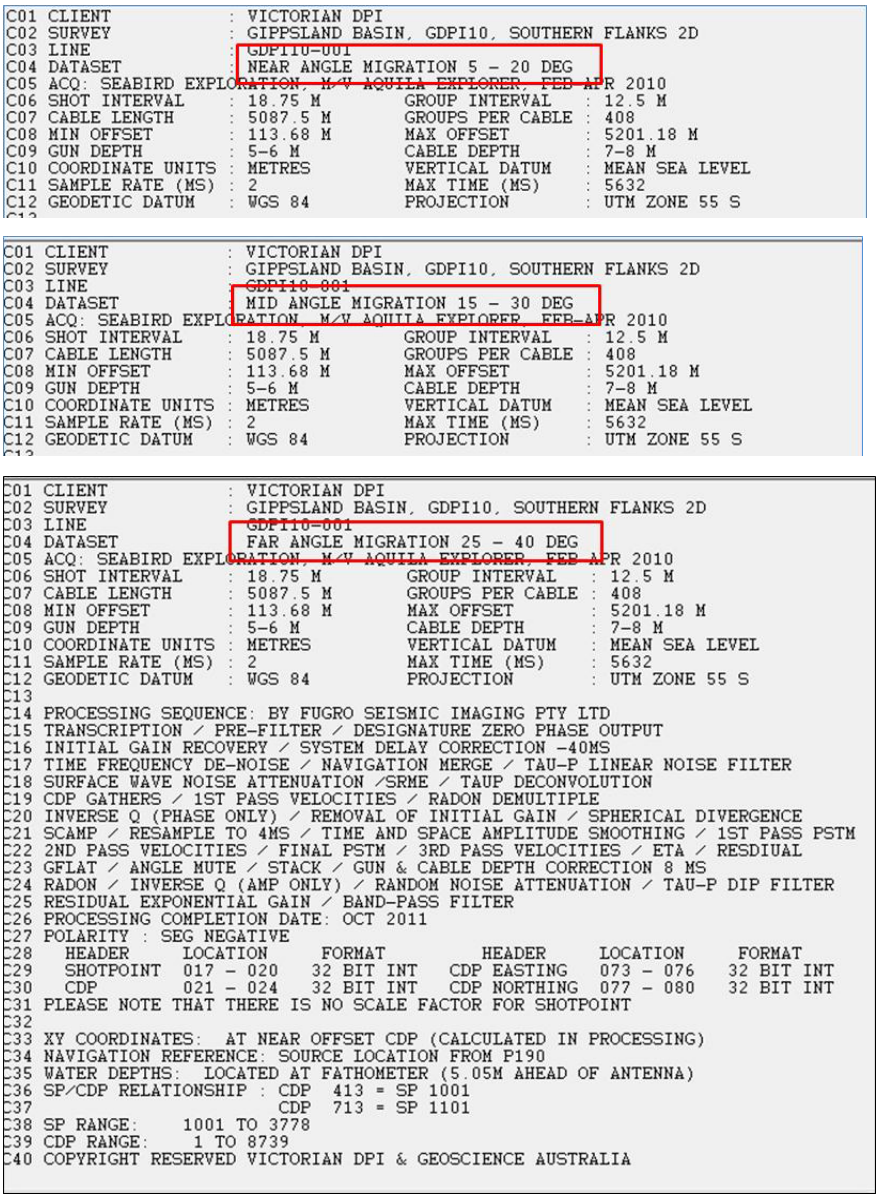

Figure 2.3 SEG-Y headers for near, mid and far angle stacks showing processing sequence, CDP XY coordinates, and shotpoint/CDP relationship.

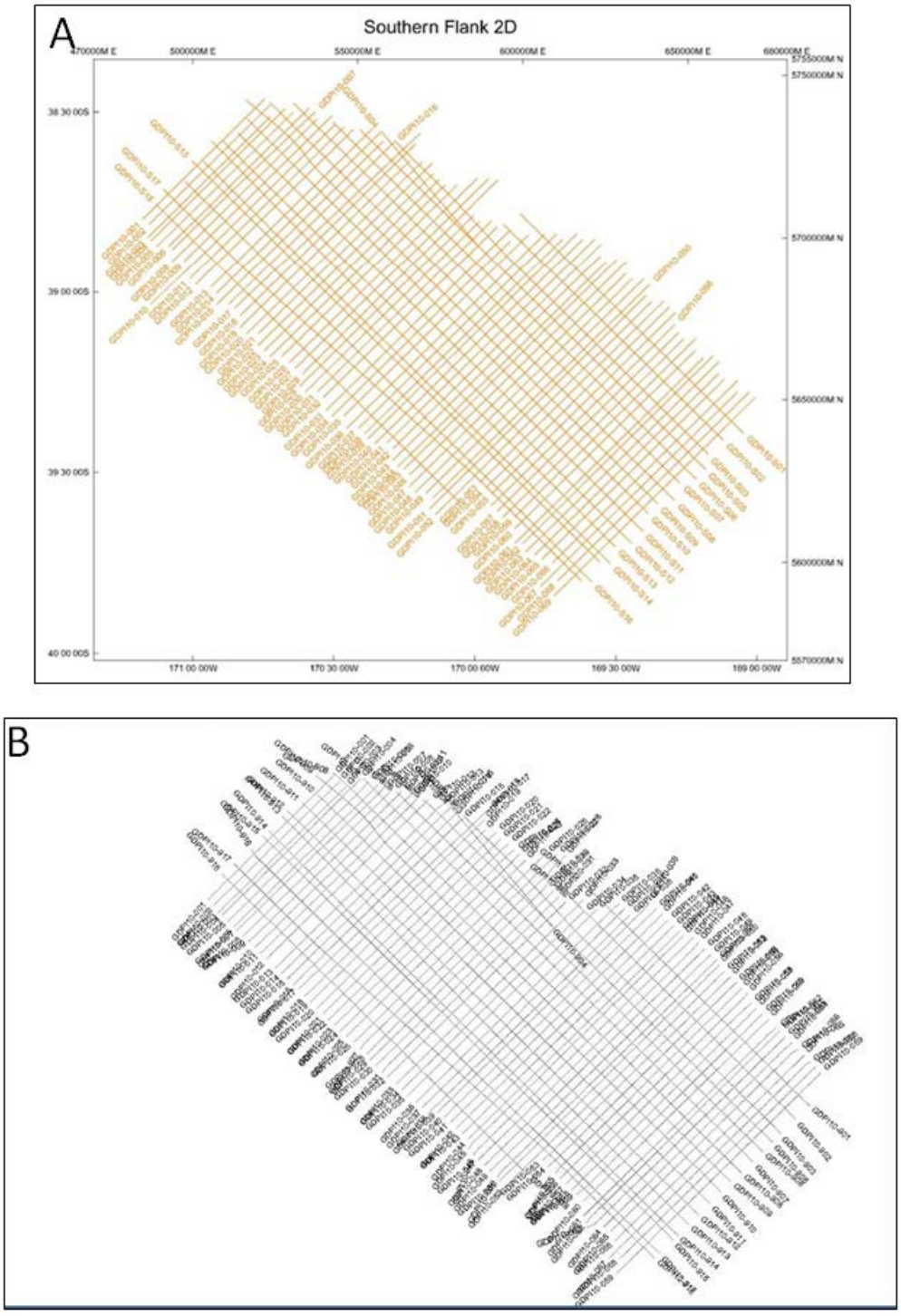

Figure 2.4 **Images of seismic location map showing discrepancies between the Fugro processing report (A) and from initial seismic data load (B). Both maps are shown on the same scale and are similarly located.**

GDPI10-001_agc_fmig SEG Y Text Header (EBCDIC)

```
C01 CLIENT          : VICTORIAN DPI
C02 SURVEY          : GIPPSLAND BASIN, GDPI10, SOUTHERN FLANKS 2D
C03 LINE            : GDPI10-001
C04 DATASET         : FINAL MIGRATION (SCALED)
C05 ACQ: SEABIRD EXPLORATION, M/V AQUILA EXPLORER, FEB-APR 2010
C06 SHOT INTERVAL   : 18.75 M       GROUP INTERVAL   : 12.5 M
C07 CABLE LENGTH    : 5087.5 M      GROUPS PER CABLE : 408
C08 MIN OFFSET      : 113.68 M      MAX OFFSET       : 5201.18 M
C09 GUN DEPTH       : 5-6 M         CABLE DEPTH      : 7-8 M
C10 COORDINATE UNITS : METRES       VERTICAL DATUM   : MEAN SEA LEVEL
C11 SAMPLE RATE (MS) : 2            MAX TIME (MS)    : 5632
C12 GEODETIC DATUM   : WGS 84       PROJECTION       : UTM ZONE 55 S
C13
C14 PROCESSING SEQUENCE: BY FUGRO SEISMIC IMAGING PTY LTD
C15 TRANSCRIPTION / PRE-FILTER / DESIGNATURE ZERO PHASE OUTPUT
C16 INITIAL GAIN RECOVERY / SYSTEM DELAY CORRECTION -40MS
C17 TIME FREQUENCY DE-NOISE / NAVIGATION MERGE / TAU-P LINEAR NOISE FILTER
C18 SURFACE WAVE NOISE ATTENUATION /SRME / TAUP DECONVOLUTION
C19 CDP GATHERS / 1ST PASS VELOCITIES / RADON DEMULTIPLE
C20 INVERSE Q (PHASE ONLY) / REMOVAL OF INITIAL GAIN / SPHERICAL DIVERGENCE
C21 SCAMP / RESAMPLE TO 4MS / TIME AND SPACE AMPLITUDE SMOOTHING / 1ST PASS PSTM
C22 2ND PASS VELOCITIES / FINAL PSTM / 3RD PASS VELOCITIES / ETA / RESDIUAL
C23 RADON / GFLAT / ANGLE MUTE / STACK / GUN & CABLE DEPTH CORRECTION 8 MS
C24 INVERSE Q (AMP ONLY) / RANDOM NOISE ATTENUATION / TAU-P DIP FILTER
C25 RESIDUAL EXPONENTIAL GAIN / POST-STACK SCALING / BAND-PASS FILTER
C26 PROCESSING COMPLETION DATE: OCT 2011
C27 POLARITY : SEG NEGATIVE
C28  HEADER   LOCATION   FORMAT      HEADER   LOCATION   FORMAT
C29  SHOTPOINT  017 - 020  32 BIT INT  CDP EASTING  073 - 076  32 BIT INT
C30  CDP      021 - 024  32 BIT INT  CDP NORTHING  077 - 080  32 BIT INT
C31 PLEASE NOTE THAT THERE IS NO SCALE FACTOR FOR SHOTPOINT
C32
C33 XY COORDINATES:  AT NEAR OFFSET CDP (CALCULATED IN PROCESSING)
C34 NAVIGATION REFERENCE: SOURCE LOCATION FROM P190
C35 WATER DEPTHS:  LOCATED AT FATHOMETER (5.05M AHEAD OF ANTENNA)
C36 SP/CDP RELATIONSHIP : CDP  413 = SP 1001
C37                       CDP  713 = SP 1101
C38 SP RANGE:   1001 TO 3778
C39 CDP RANGE:   1 TO 8739
C40 COPYRIGHT RESERVED VICTORIAN DPI & GEOSCIENCE AUSTRALIA
```

5 SEGY Header Information

Type	Start byte	Description	Type	Start byte	Description
I32	1	Trace number within line.	I16	99	Source static correction.
I32	5	Trace number within reel.	I16	101	Receiver static correction.
I32	9	Sequential record number.	I16	103	Total static applied.
I32	9	Original field record number.	I16	109	Delay recording time (ms).
I32	13	Trace number.	I16	111	Mute time start.
I32	17	Shot point number.	I16	113	Mute time end.
I32	21	CDP number.	I16	115	No. of samples.
I32	25	Trace no. within the CDP.	I16	117	Sample interval in microseconds.
I16	29	Trace identification code.	I16	157	Year of recording.
I16	31	No. of summed traces.	I16	159	Julian day number (1-366).
I16	33	Total number of traces in CDP.	I16	161	Hour of day (24 hour clock).
I16	35	Data use 1=production, 2=test.	I16	163	Minute of hour.
I32	37	Trace offset (integer).	I16	165	Second of minute.
I32	41	Elevation at receiver.	I16	167	Time base code 1.local,2.gmt
I32	45	Elevation at source.	I32	181	3D Line number.
I32	61	Water depth at source.	I32	185	CDP no. within 3D line.
I32	65	Water depth at receiver.	I32	189	2D shotpoint number (Maersk).
I16	69	Scaler to be applied to elevations.	I32	193	CDP easting.
I16	71	Scaler to be applied to coordinates.	i32	197	CDP northing.
I32	73	CDP easting.	I16	201	Scaler to be applied to SPNO.
I32	77	CDP northing.			
I32	81	Receiver easting.			
I32	85	Receiver northing.			
I16	89	Coordinate units (m/arc).			

Figure 2.5 Portion of seismic SEG-Y header showing CDP navigation rather than SP navigation.

2.2.2 Incorrect Fathometer Data

Fathometer readings were included in the original SEG-Y data referenced to 5.05 m ahead of the antenna. FROGTECH time-converted the data assuming 1521 m/s for water velocity (as used for stacking velocity by Fugro) and overlaid the data on the seismic data. Two problems exist in the fathometer data. Firstly there is a regular horizontal offset of approximately 340 m on the dip and strike lines. This problem is best observed in areas with rapid bathymetric variations such as at canyons or the shelf break (Figure 2.6). The second problem is restricted to deep water areas where large anomalies are observed where the fathometer appears to lose tracking of the seafloor (Figure 2.7). These errors made the fathometer data unusable for the project.

2.2.3 Shallow Water Seafloor Muting

During processing, the desired wavelet was SEG reverse, zero phase where an increase in acoustic impedance resulted in a negative number on tape and corresponded to a trough on the display (Figure 2.8). The zero phase wavelet can be easily recognised in the deep water allowing the seafloor to be accurately mapped on the seismic data (Figure 2.9). In very shallow water depths the seafloor event has been removed due to a combination of muting and the large shot to first receiver offset (113 m; Figure 2.10). Although there has been some truncation of the seafloor event, FROGTECH decided to use the interpretation from the seismic data for the following reasons:

1) The fathometer data supplied with the seismic data are corrupted with a regular offset and spurious datapoints in deep water (Figures 2.6 and 2.7). This data could not be used to replace the seafloor interpretation in the shallow water areas.

2) The seafloor event is removed when it shallows to 0.05s or less (approximately 38 m or less). Using the recently released 100 m Geoscience Australia bathymetry data, the area of the seismic grid where the waterdepth is less than 38 m is limited to the far western and southern edges of the data (Figure 2.11).

3) A comparison between the Geoscience Australia 30 m bathymetry grid and the depth converted interpreted seafloor horizon shows less than 15 m difference across most of the shelf (Figure 2.12). Larger variations (> 100 m) are present at the shelf break where there are rapid changes in water depth combined with canyon development. The differences seen here are likely to be related to gridding and input data differences. As gridding of the interpreted horizons is based solely on interpretation of the GDPI10 grid, the seafloor was treated in the same manner.

4) In the comparison grid some anomalies (up to 20 m) are evident on the shelf with a distinct acquisition footprint. The area immediately surrounding these lines shows little difference between the bathymetry grid and interpreted seafloor horizon (Figure 2.12). FROGTECH interprets that the anomalies point to some possibly spurious datapoints in the Geoscience Australia grid.

The vertical resolution of seismic data is generally calculated as a quarter of the dominant wavelength and generally decreases with depth (Yilmaz, 1987). The wavelength of a seismic wavelet is calculated by:

$$\lambda = {}^{v}/_{f}$$

where v is the velocity and f the dominant frequency. The frequency content of the GDPI10 survey has been calculated where wavelets have been extracted at 20 wells across the dataset (Figure 2.13). As the wavelets have been extracted over approximately a one second interval, the frequency content has a broad range (20 to 60 Hz). This can be reduced to 30 to 45 Hz if outliers are removed. The average velocity to the Top Latrobe Group varies across the shelf from 1900 to 2800 m/s (Figure 2.14). Using the formula above, the wavelength of the data ranges from 45 to 90 m. The vertical resolution (¼ wavelength) therefore ranges from around 11 to 23 m. Frequency content at the Top Latrobe Group level is likely to be at the lower end of the scale, so the vertical resolution will be around 20 to 23 m.

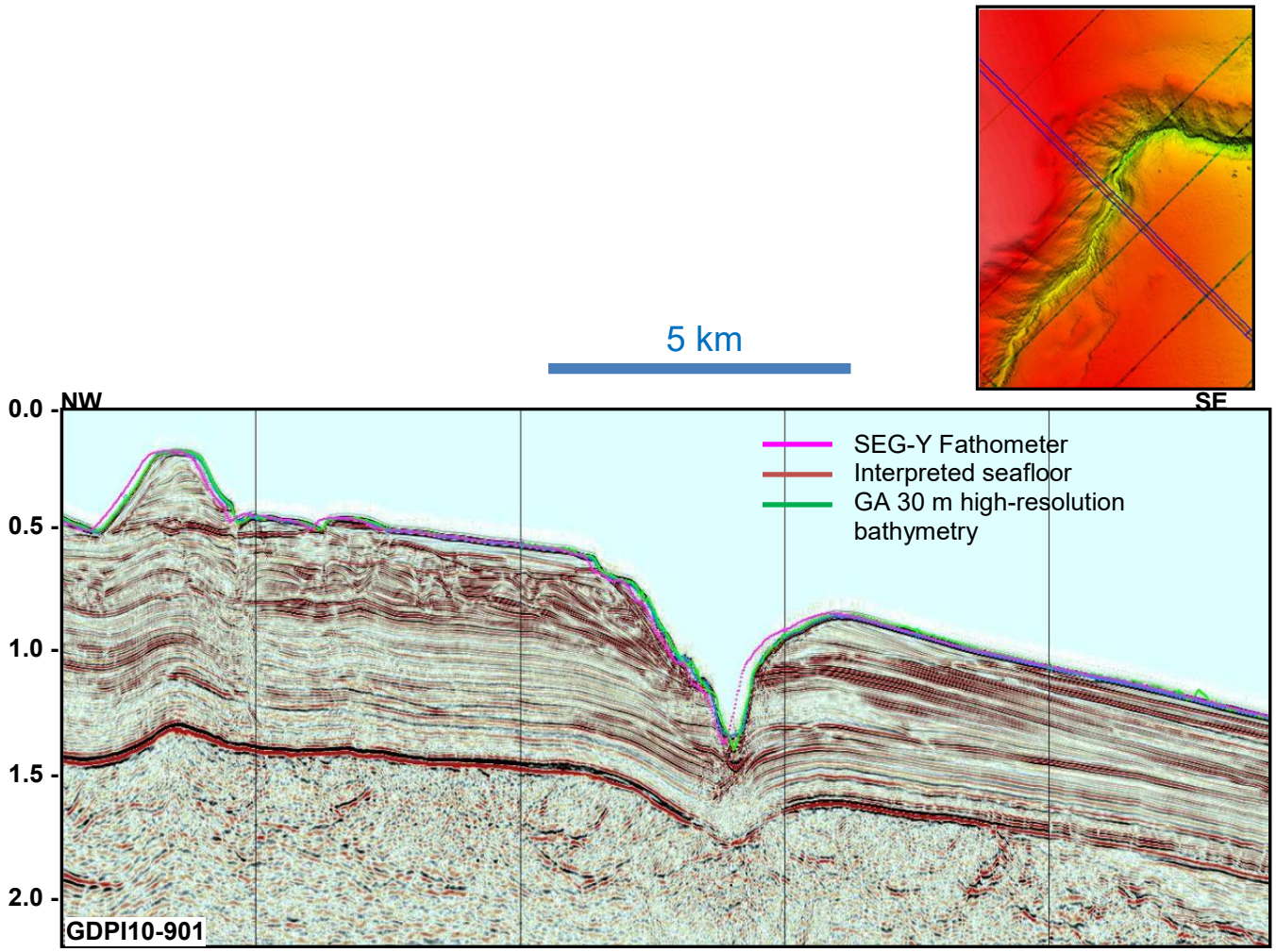

Figure 2.6 **Comparison of seafloor from several sources across a canyon. The fathometer embedded in the SEG-Y is offset relative to the seismic data, interpreted seafloor and the time-converted high resolution (30 m) bathymetry from Geoscience Australia.**

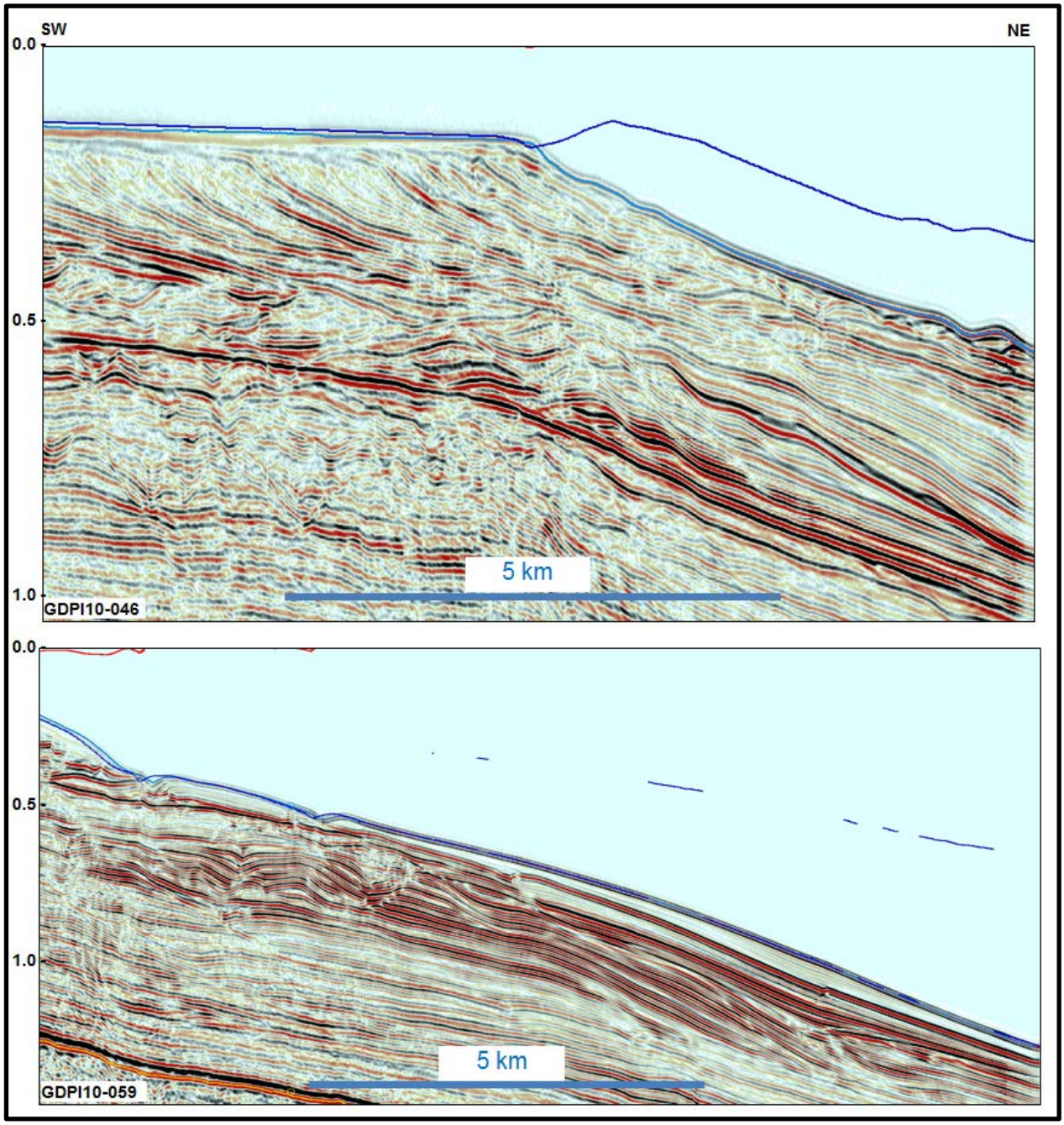

Figure 2.7 Two examples of errors in the fathometer readings due to a loss of tracking in deep water.

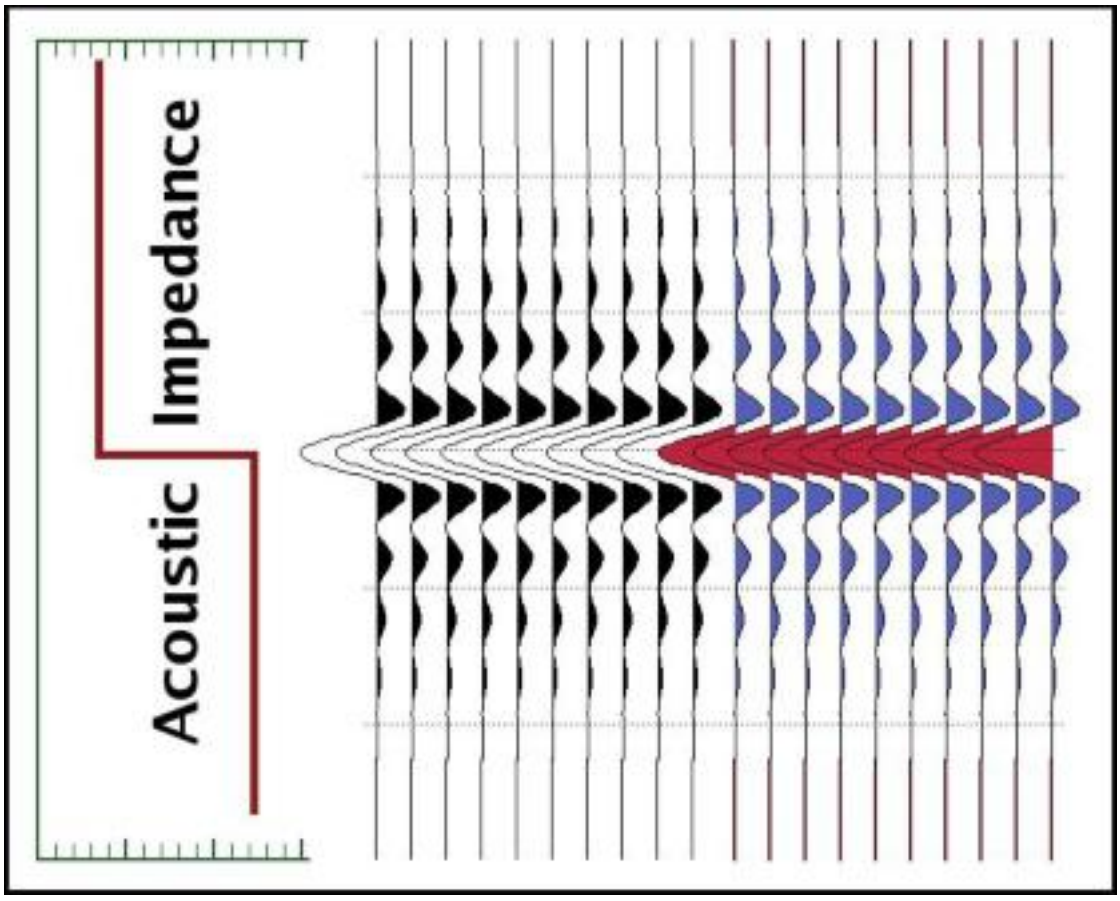

Figure 2.8 **The seismic data were processed to a SEG reverse zero phase wavelet resulting in a trough at an increase in acoustic impedance (Fugro, 2011).**

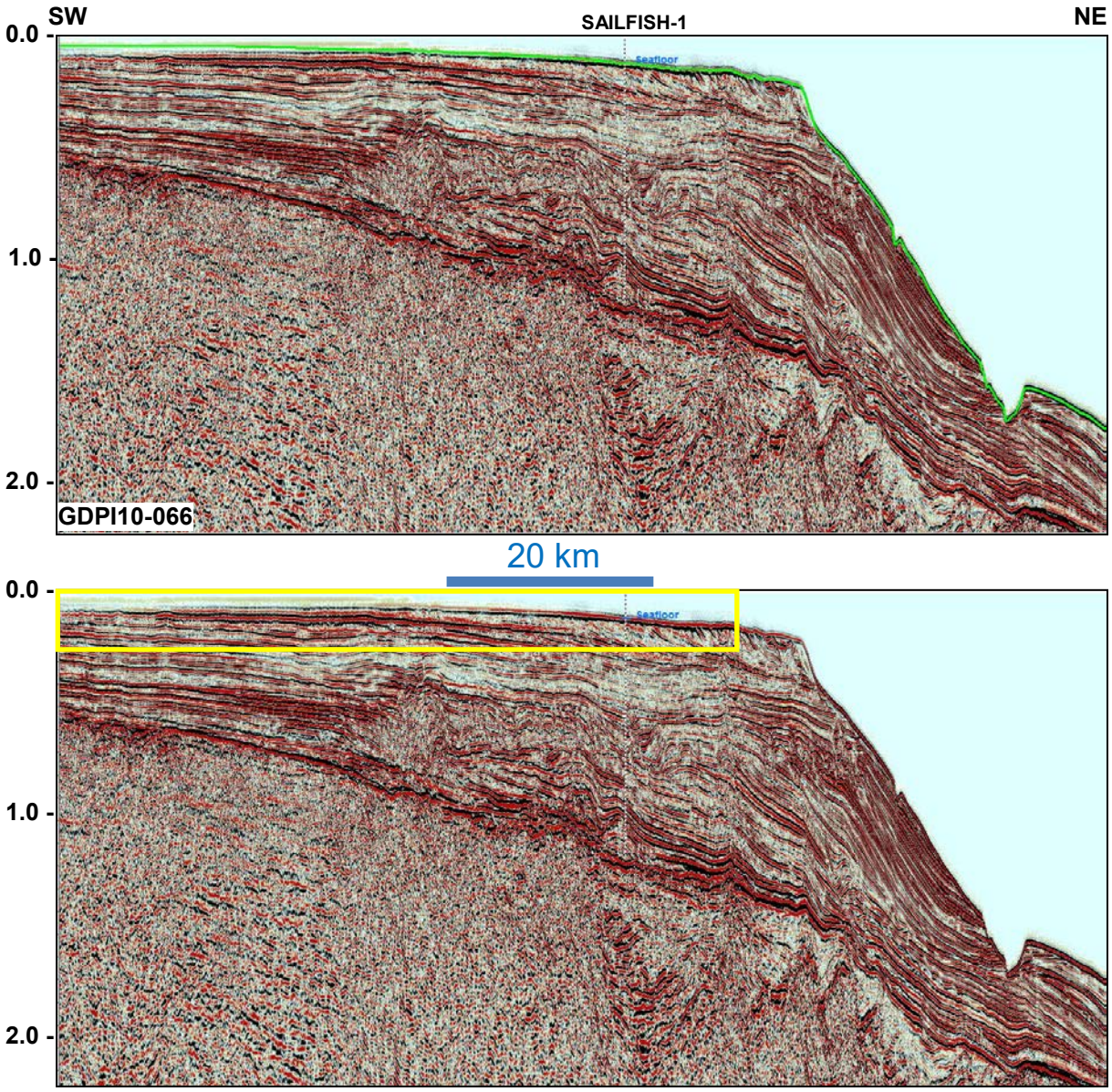

Figure 2.9 Example of seismic line GDPI10-066 showing interpretation at seafloor. The first coherent reflection in the deep water and just inboard of the Sailfish-1 well is a trough. In the very shallow area the initial reflection has been removed and it is not possible to confidently interpret seafloor morphology inboard of this location across a small number of dip lines in the survey. The yellow box is the zoomed in area shown in the next image.

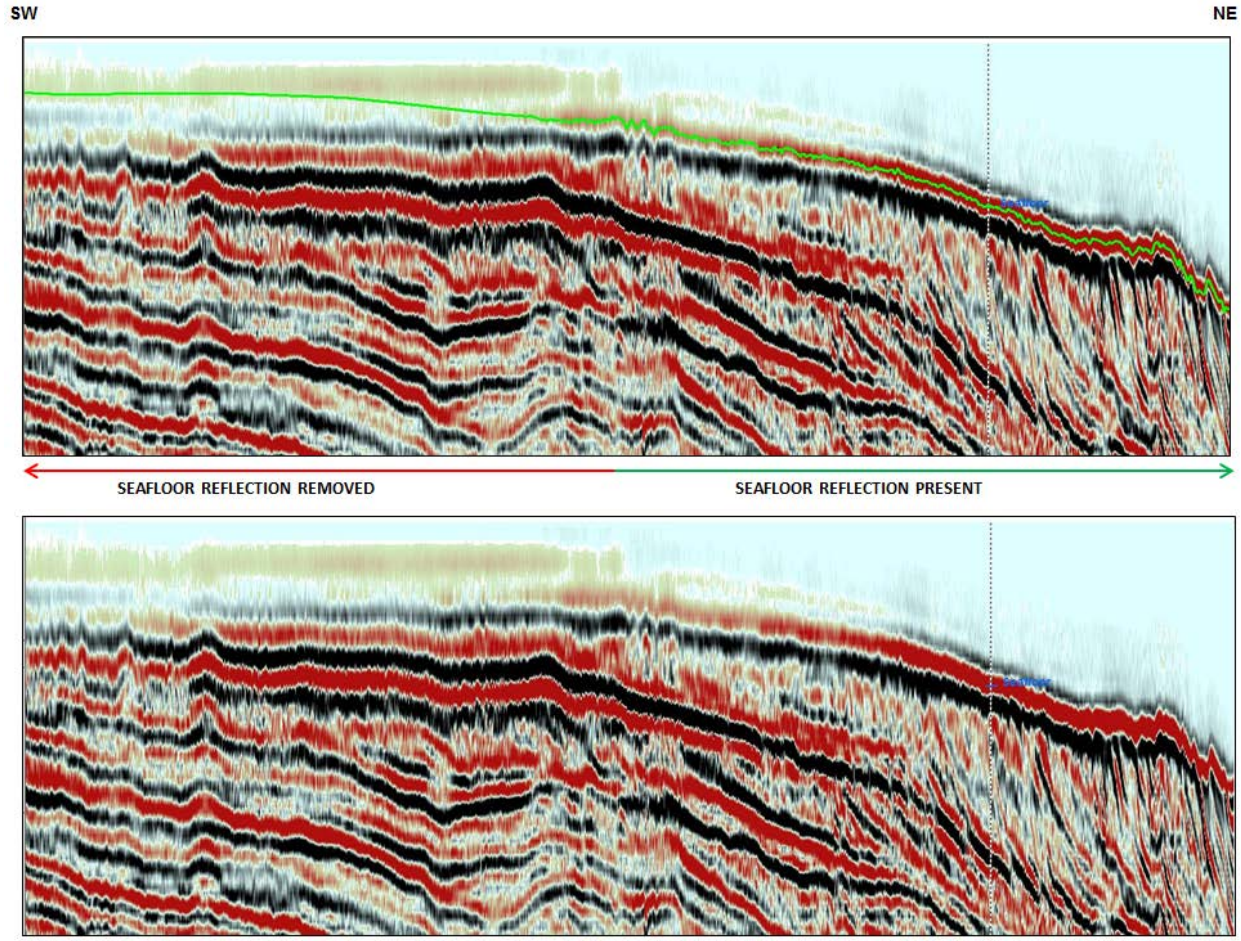

Figure 2.10 **Zoomed in to shallow section of GDPI10-066. Seafloor is a well-defined trough (red) reflection and is confirmed by the placement of the seafloor pick at the Sailfish-1 well. To the south the seafloor reflection shallows and loses character. The interpretation of seafloor in this region is an approximation only.**

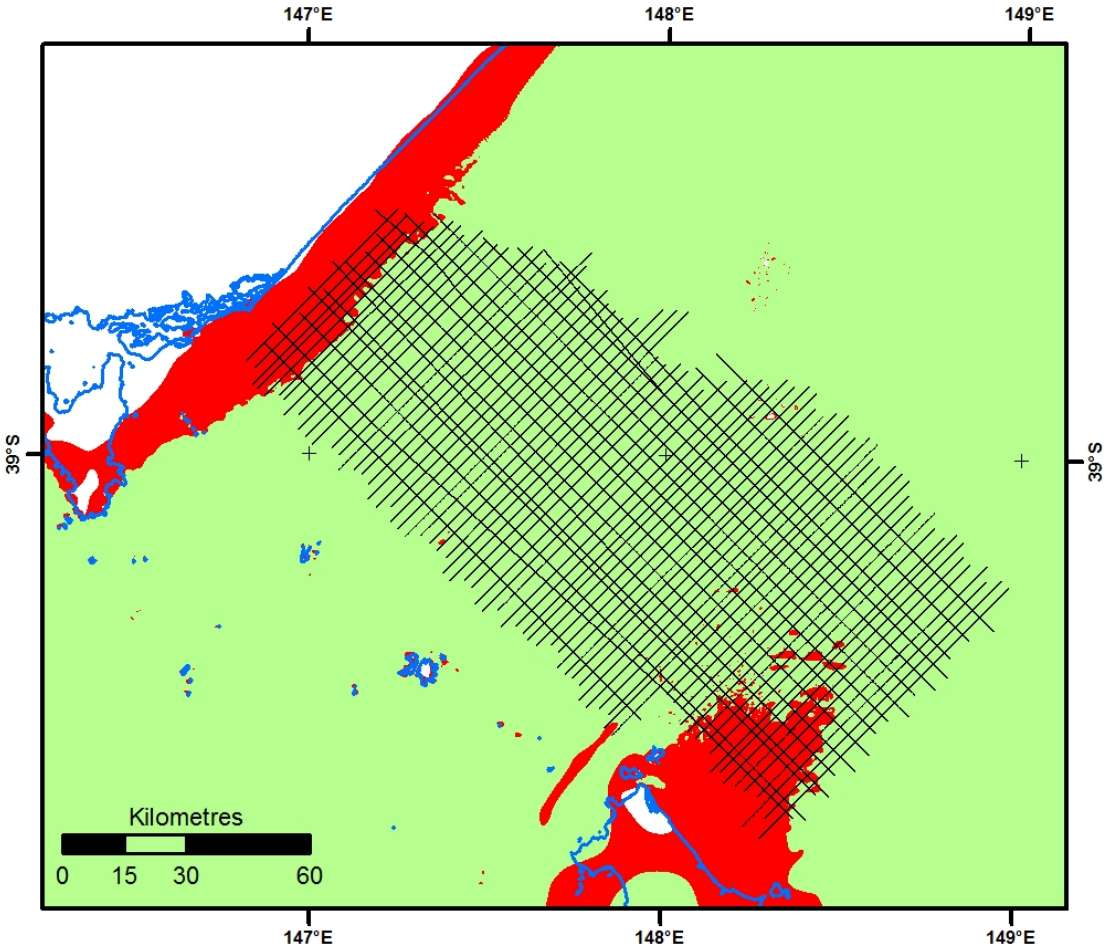

Figure 2.11 100 m Geoscience bathymetry data coloured up to show approximate extent seismic data that will show truncation of the seafloor reflection. The red areas are where bathymetry is 0-38 m and green is > 38 m. The data were obtained from the Geoscience Australia website in May 2012.

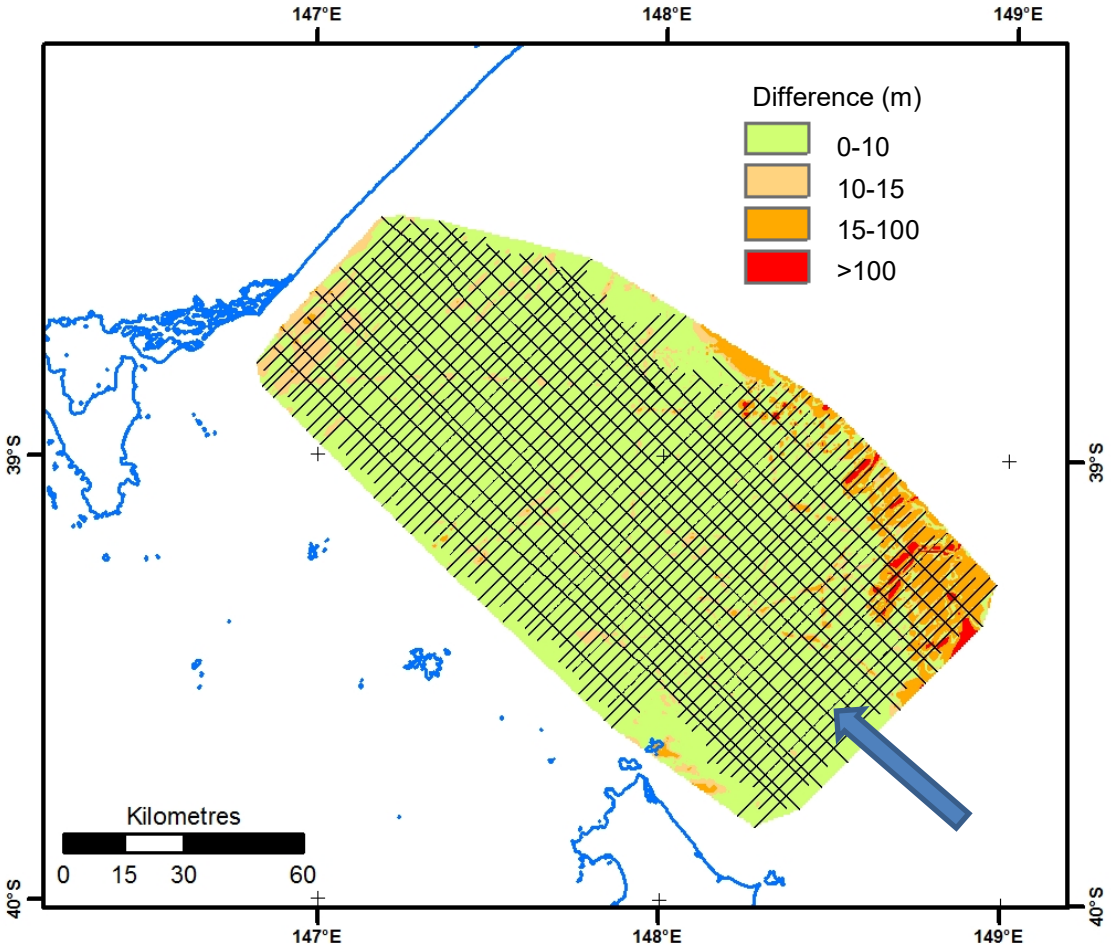

Figure 2.12 **Difference grid between the 30 m Geoscience bathymetry data and the depth converted grid of the seafloor interpretation from the GDPI10 2D seismic data. The grids are quite similar across most of the shelf with variations of less than 15 m. Differences of up to 20 m are seen on minor areas of the shelf and have the appearance of shiptrack traces (e.g. arrow). Large differences (> 100 m) are observed at the shelf break particularly where canyons are present.**

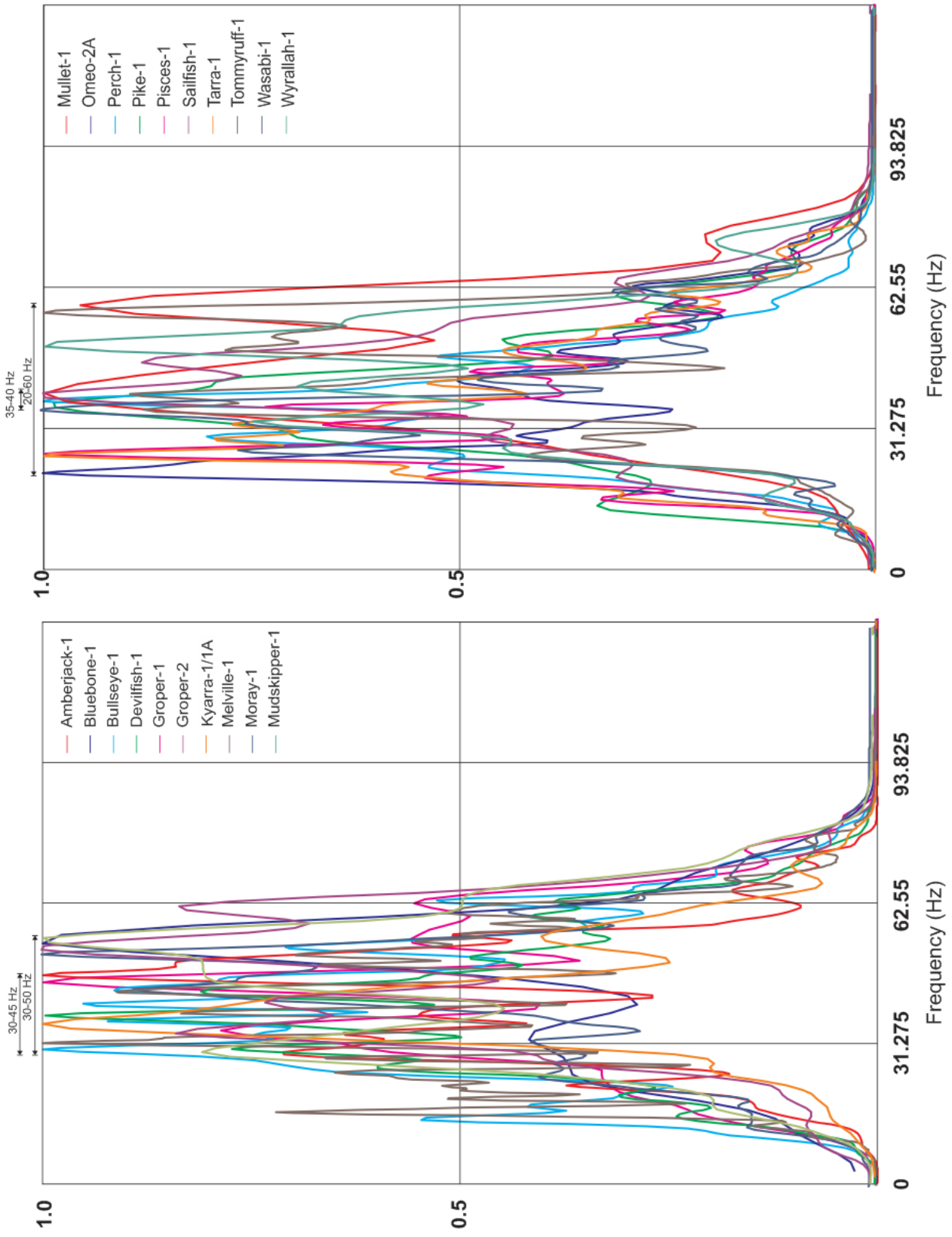

Figure 2.13 Frequency spectrum of wavelets extracted from seismic data at the 20 key wells.

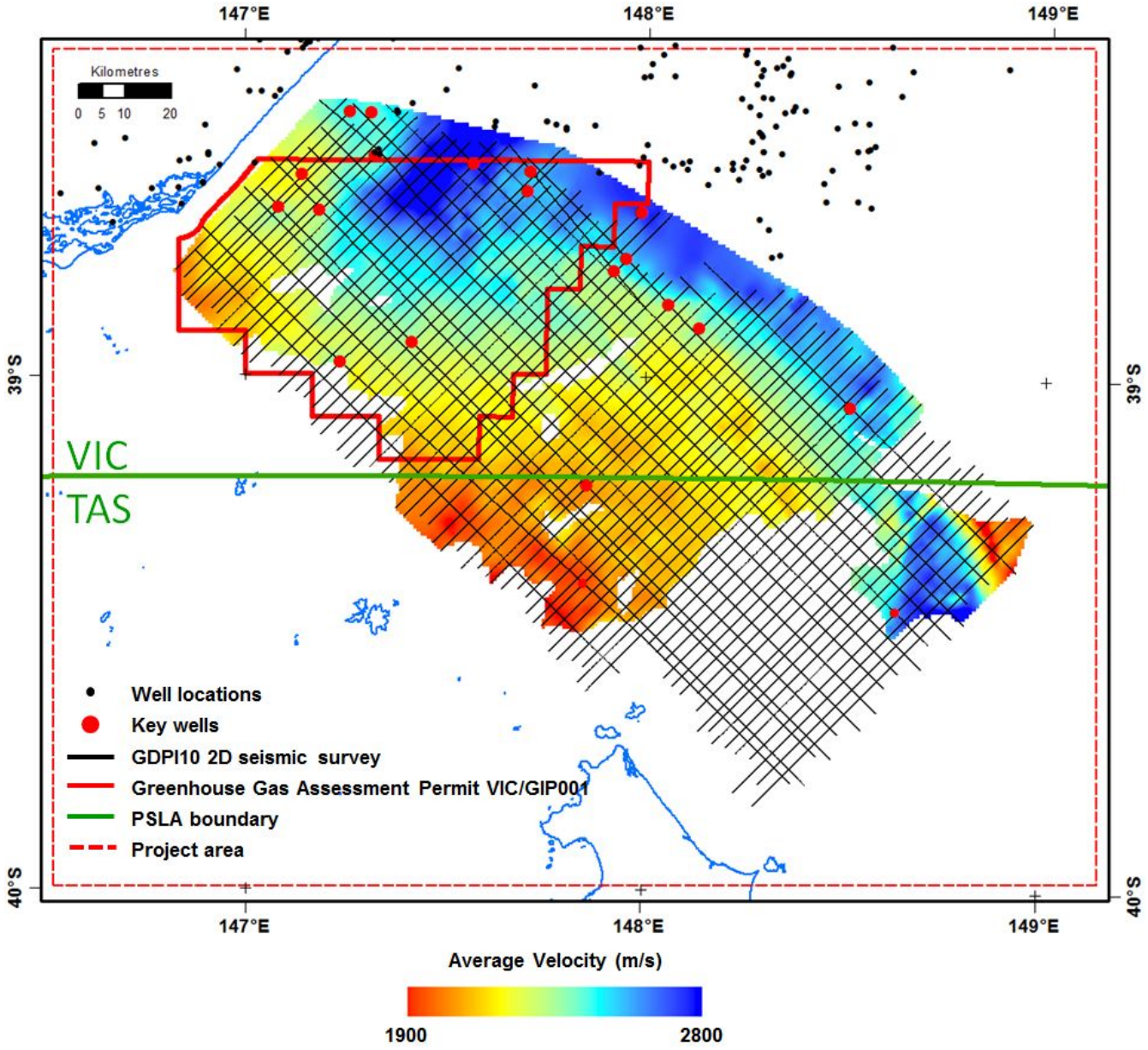

Figure 2.14 Average velocity to the Top Latrobe Group surface as determined from the velocity model developed for this study.

2.3 Seismic Data Provided in the Kingdom Project

The Kingdom project provided by DPI is a comprehensive database of 2D/3D seismic and well data available in the Gippsland Basin. On the Southern Platform, the 3D megavolume of 18 separate surveys (3D-GEO, 2010) and 35 2D seismic surveys intersect with the GDPI10 2D seismic survey (Table 2.3). Analysis of the 3D merged seismic dataset suggest that the data are quadrature phase, similar to the vintage 2D data in the Gippsland Basin (Figure 2.15; Terratek, 2012). This difference in phase makes direct comparison of interpretation between the GDPI10 and vintage datasets problematic. In general the GDPI10 2D seismic survey data quality is as good as, or better than the earlier surveys, particularly when imaging the deep reflections beyond the Foster Fault System and in the half graben depocentres identified on the Southern Platform (Figure 2.16 to 2.29; Terratek, 2012). Included in the Kingdom project is the interpretation from the 3D-GEO project for comparison with the current study.

2.4 Well Data

Thirty wells are located in the area covered by the GDPI10 2D seismic survey on the Southern Flank of the Gippsland Basin. Twenty wells were selected as key to the study (Table 2.4 and Figure 2.1). The wells cover all structural provinces of the Southern Flank of the Gippsland Basin: Southern Platform (Bluebone-1, Mullet-1, Groper-1, Groper-2 and Mudskipper-1); Pisces Sub-basin (Pisces-1; Sailfish-1); Southern Terrace (Bullseye-1, Pike-1, Omeo-2A, Moray-1, Tarra-1, Kyarra-1A, Wyrallah-1, Perch-1, Devilfish-1 and Tommyruff-1) and Central Deep (Amberjack-1, Wasabi-1, Melville-1). Basic and interpretation data for the wells was supplied in a variety of formats: as part of the Kingdom project, within DPI VIMP reports, spreadsheets, LAS files and an array of scanned pdf well reports and images. In addition, FROGTECH sourced data from the Geoscience Australia petroleum wells and the Mineral Resources of Tasmania publications.

Synthetic seismograms were generated for the key wells to allow a tie with the 2D GDPI10 seismic data (Appendix 1). Information from multiple sources was collated for the key wells and summarised in composite logs (Appendix 2). Methodologies for the preparation of the synthetics and composite logs are presented in Section 3 of this report.

2.4.1 Well Data Provided in the Kingdom Project

The Kingdom project provided by DPI is a comprehensive database of 2D/3D seismic and well data available in the Gippsland Basin. The well database in the Kingdom project includes onshore and offshore wells with a total of 1562 locations loaded. Basic data (location, KB, water depth) were loaded for all wells except for the more recently drilled Wasabi-1.

Time-depth relationships were provided in the database, referenced to GA, DPI_qc or unknown. As no synthetics were supplied, and the process histories of the time-depth relationships were unknown, they were used for comparison only with the synthetics generated as part of this project.

Two separate versions of formation tops were contained in the Kingdom project labelled as 3D-GEO and DPI-WCR and were used for comparison purposes only. A formation tops spreadsheet (fmtops_gipps_louise_monica.xls) supplied separately by DPI was indicated as the preferred dataset for stratigraphic picks. Biostratigraphic information labelled as GA_Bug was also contained within the Kingdom project and was included in the creation of the composites.

Basic wireline logs (i.e. CAL, GR, DT, RHOB) were included in the Kingdom project for all key wells except Bluebone-1, Melville-1, Pike-1, Sailfish-1 and Wasabi-1. Logs loaded from LAS files partially filled the gaps in the basic suite of logs, although some logs are still missing from Melville-1 and Sailfish-1. The well logs were generally spliced together, except Wasabi-1, which was separated into acquisition runs. Review of the sonic logs indicated they were scaled to μs/m rather than μs/ft and despiking at casing shoes was required before creating synthetics.

3D Megavolume (3D-GEO)
EO67 (G67B)
East Gippsland Basin (GMG68B)
EH-68
G69A and B
G80A
GBS-80
GC80
GBS-81
G81A
GA81A and EXTEND
GP-81A
GP81A-2D
GA82-B
GA-82B
G82D
GUT-83A
GA-84A
BMR1987-13
GF-88C
GS-88A
GC-89A
BLACKBACK
FORTESQUE
FLAGTAIL
FLAGTAIL and SW TORSK
NW FLOUNDER, S BARRAMUNDI, GOANAFISH
GF91A
REGIONAL BASINWIDE 2D
2D-SOUTH MARLIN CHANNEL
G92C

Table 2.3 Seismic surveys that intersect with the GDPI10 2D seismic survey.

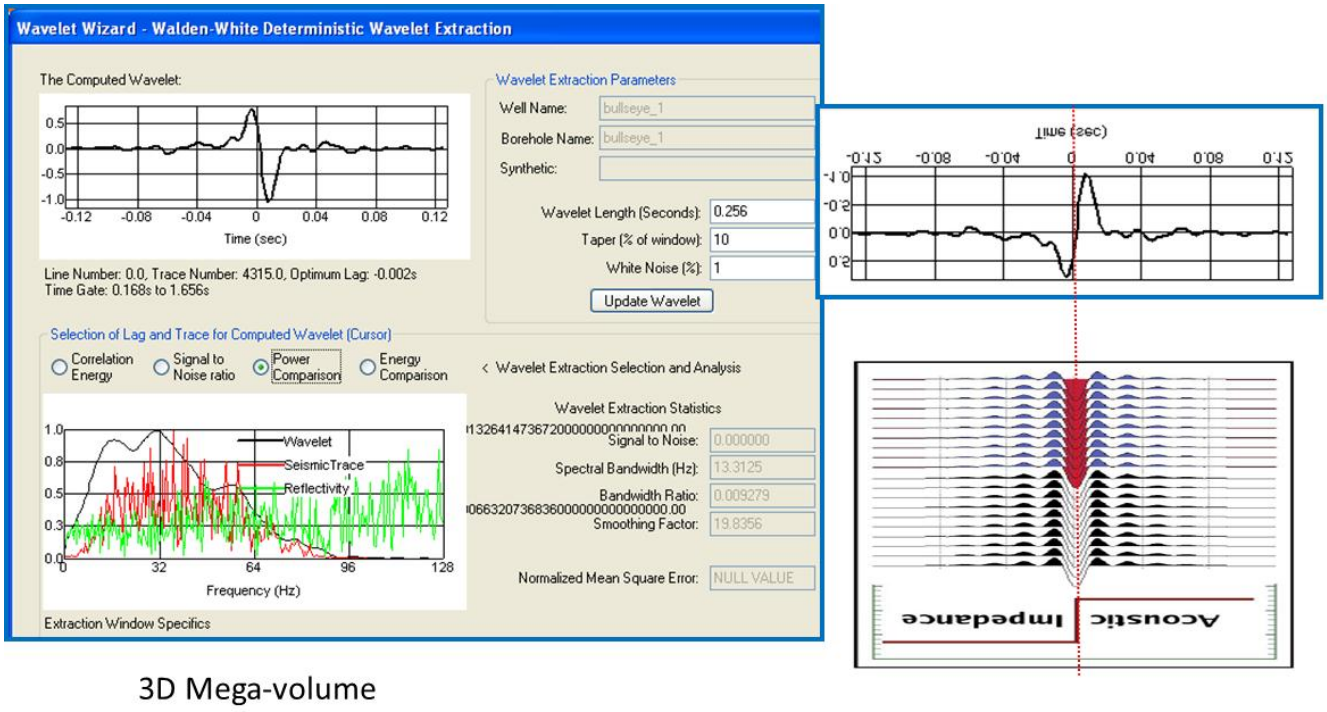

Figure 2.15 **A wavelet extracted from the 3D megavolume using the Walden White deterministic method at Bullseye-1 implies that an increase in impedance will be represented by a zero crossing in the 3D megavolume data compared with a trough in the GDPI10 data. The 3D megavolume data have been interpreted to be quadrature phase (Terratek, 2012).**

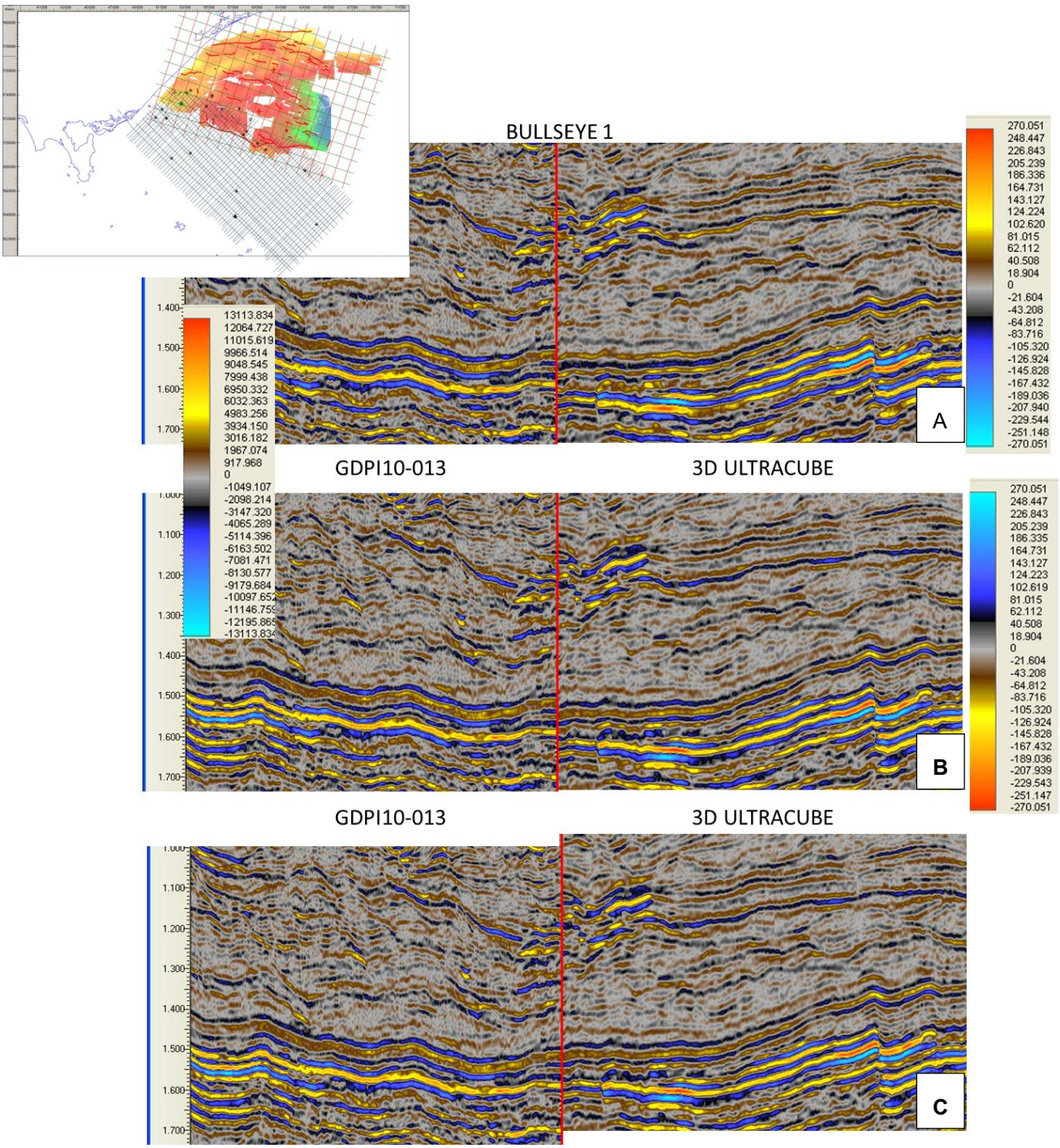

Figure 2.16 **Comparison of the GDPI10 seismic data along line 13 with equivalent data in the 3D megamerge data supplied in the Kingdom project. The data show a distinct mismatch (a) that can only be removed if the 3D data are first polarity flipped then (b) then bulk shifted (c). The area where the 3D megamerge that overlaps with GDPI10 seismic data as shown by the extent of the Latrobe interpretation in the inset.**

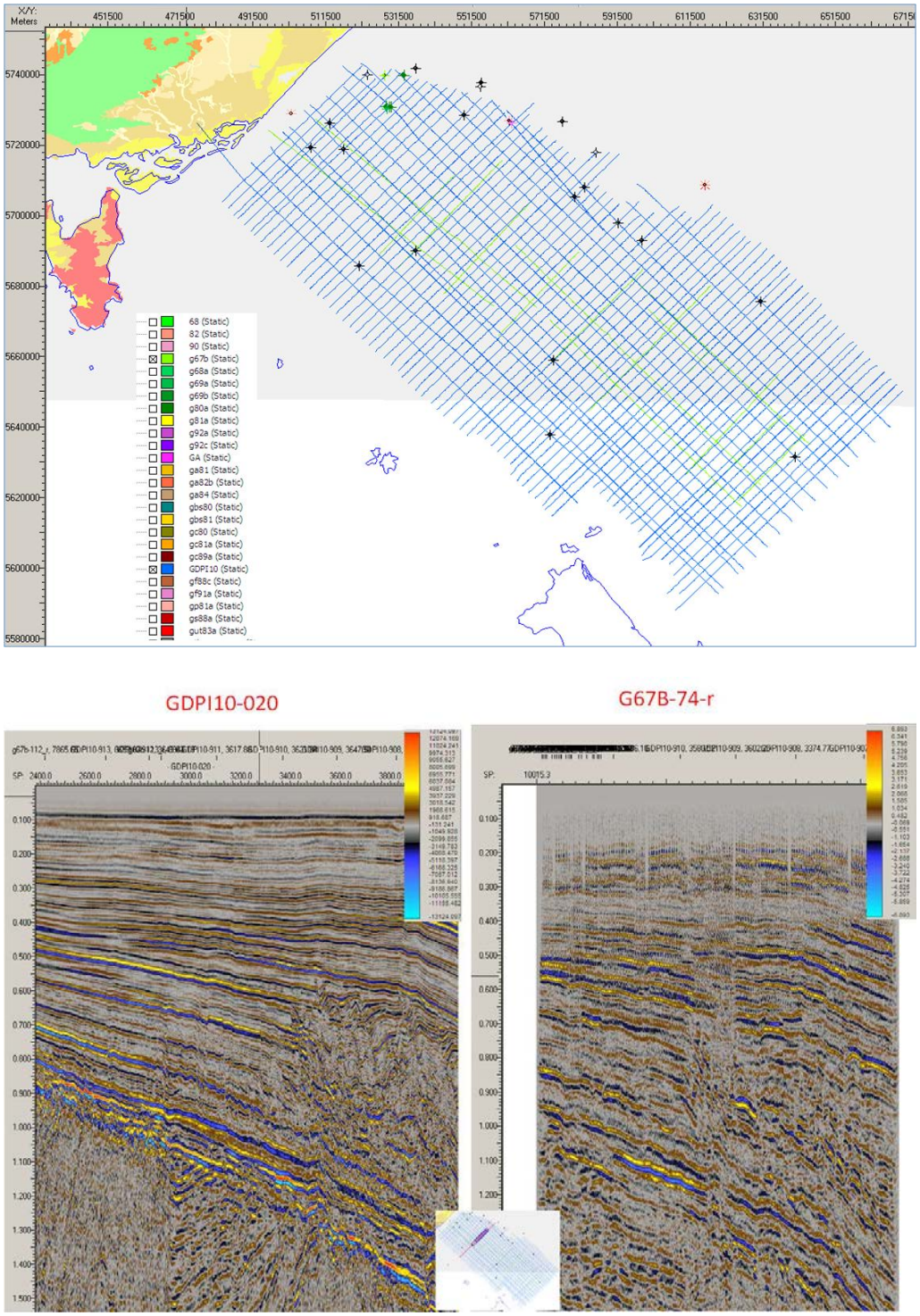

Figure 2.17 Extent of survey G67B (green) relative to survey GDPI10 (blue). Comparison of the two surveys at GDPI10-020 shows a dramatic increase in data quality at all levels but particularly in the very shallow and deeper sections of the data. Note the presence of a small half graben in GDPI10-20 that is not visible in the G67B line. (images supplied by G. Blackburn)

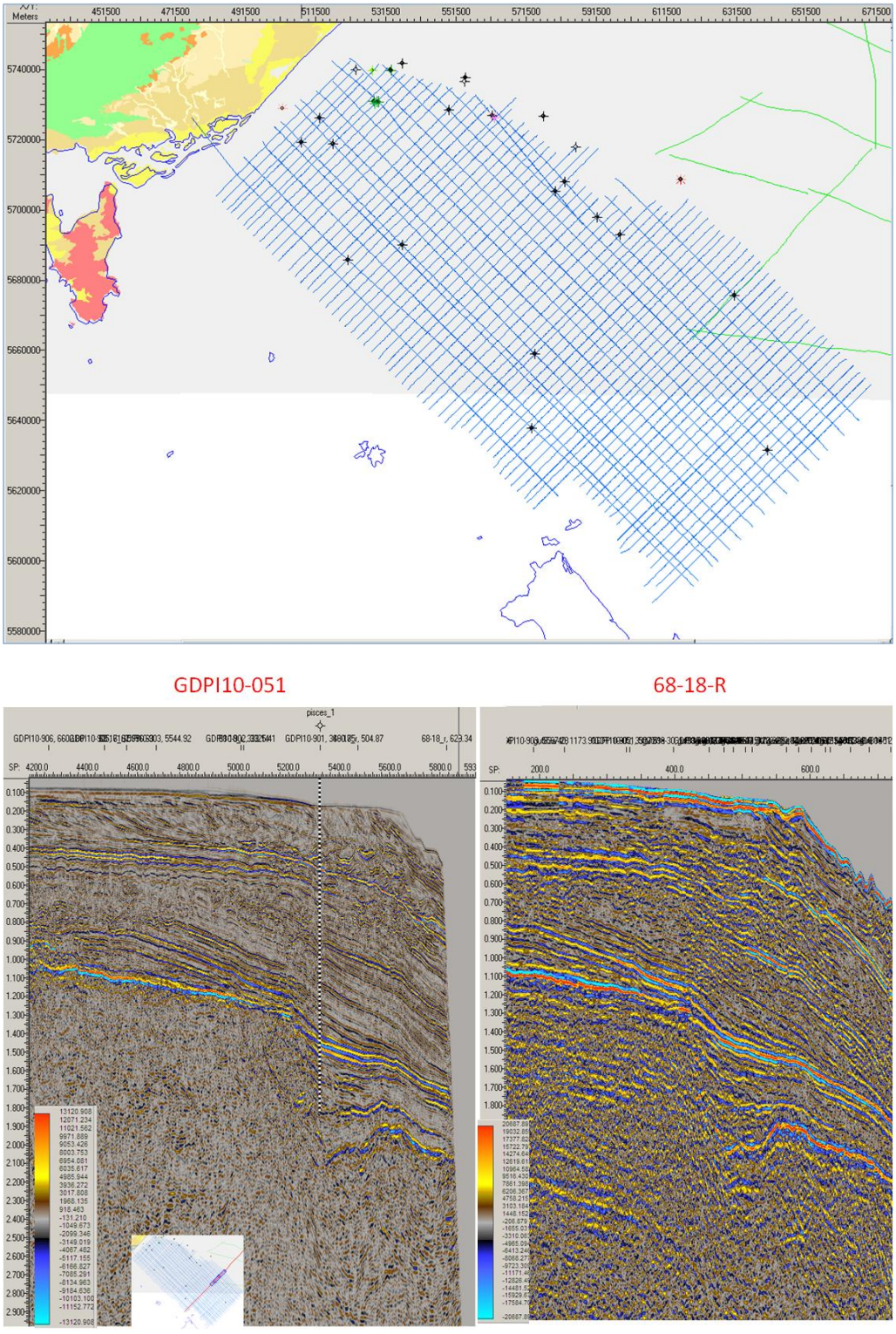

Figure 2.18 Extent of survey GMG68B (green) relative to survey GDPI10 (blue). Comparison of the two surveys at GDPI10-051 shows increased multiple energy in the survey 68 data. (images supplied by G. Blackburn)

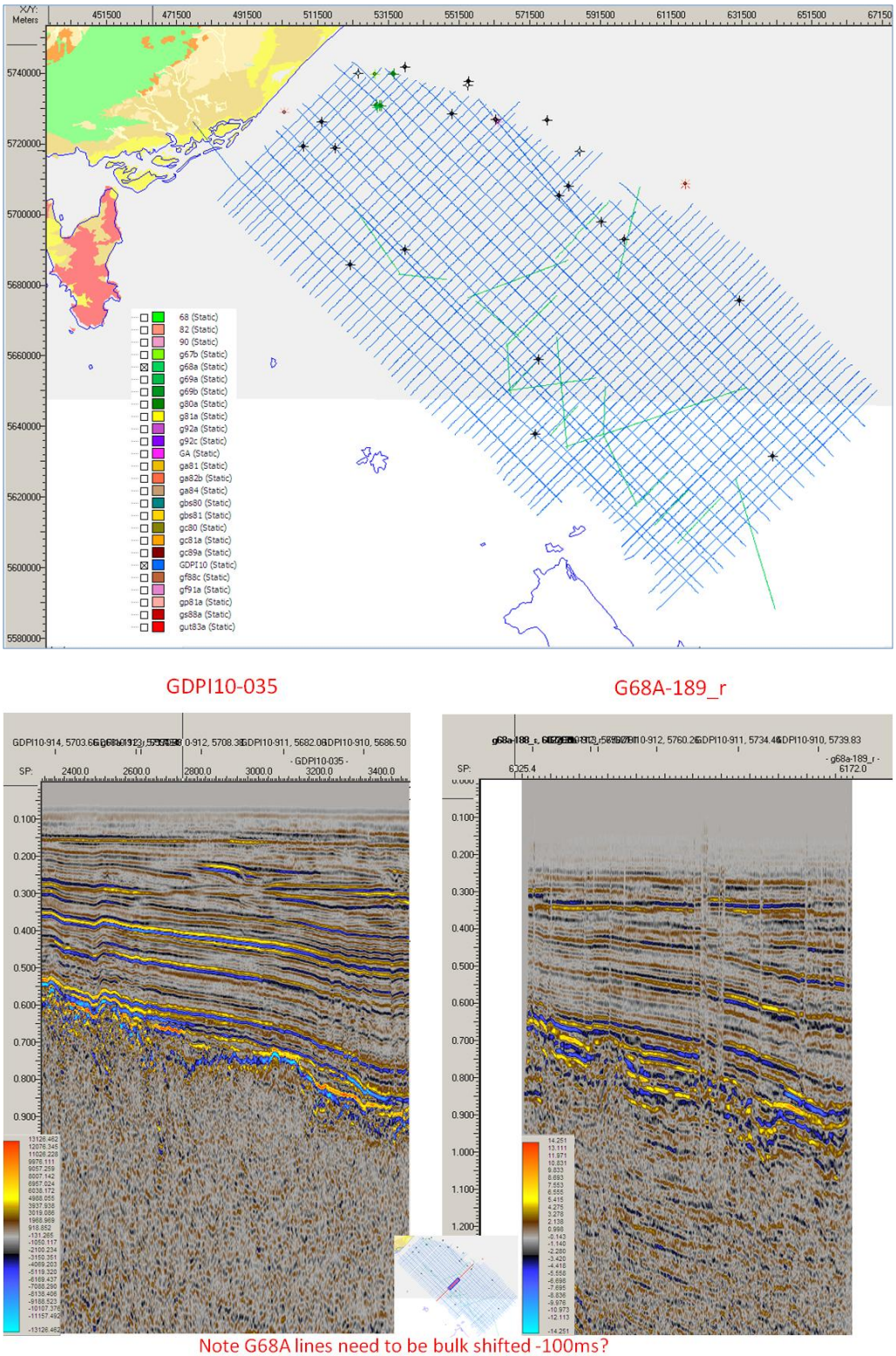

Figure 2.19 Extent of survey G68A (green) relative to survey GDPI10 (blue). Comparison of the two surveys at GDPI10-035 shows a dramatic increase in data quality. (images supplied by G. Blackburn)

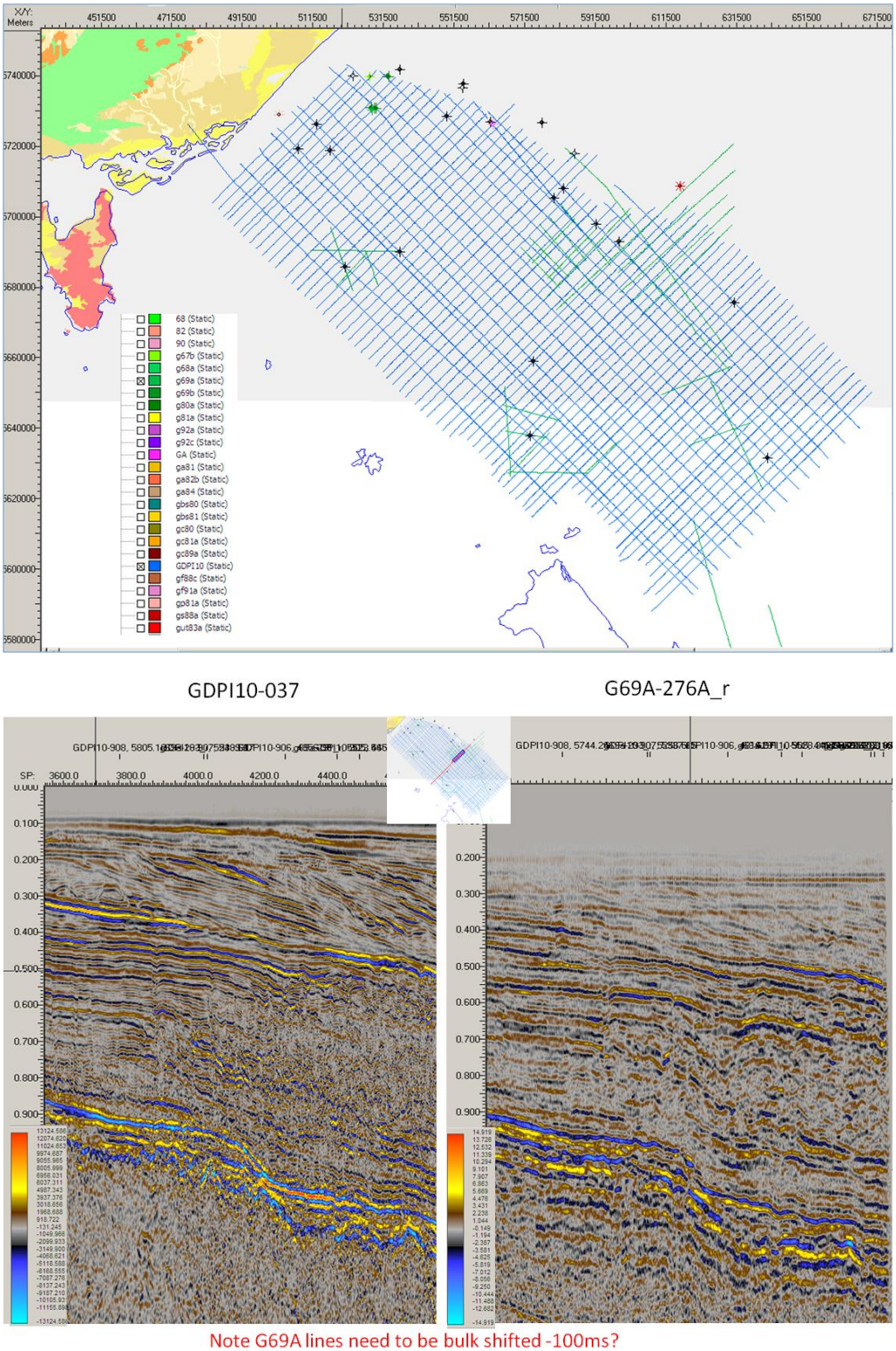

Figure 2.20 Extent of survey G69A (green) relative to survey GDPI10 (blue). Comparison of the two surveys at GDPI10-037 shows a dramatic increase in data quality. (images supplied by G. Blackburn)

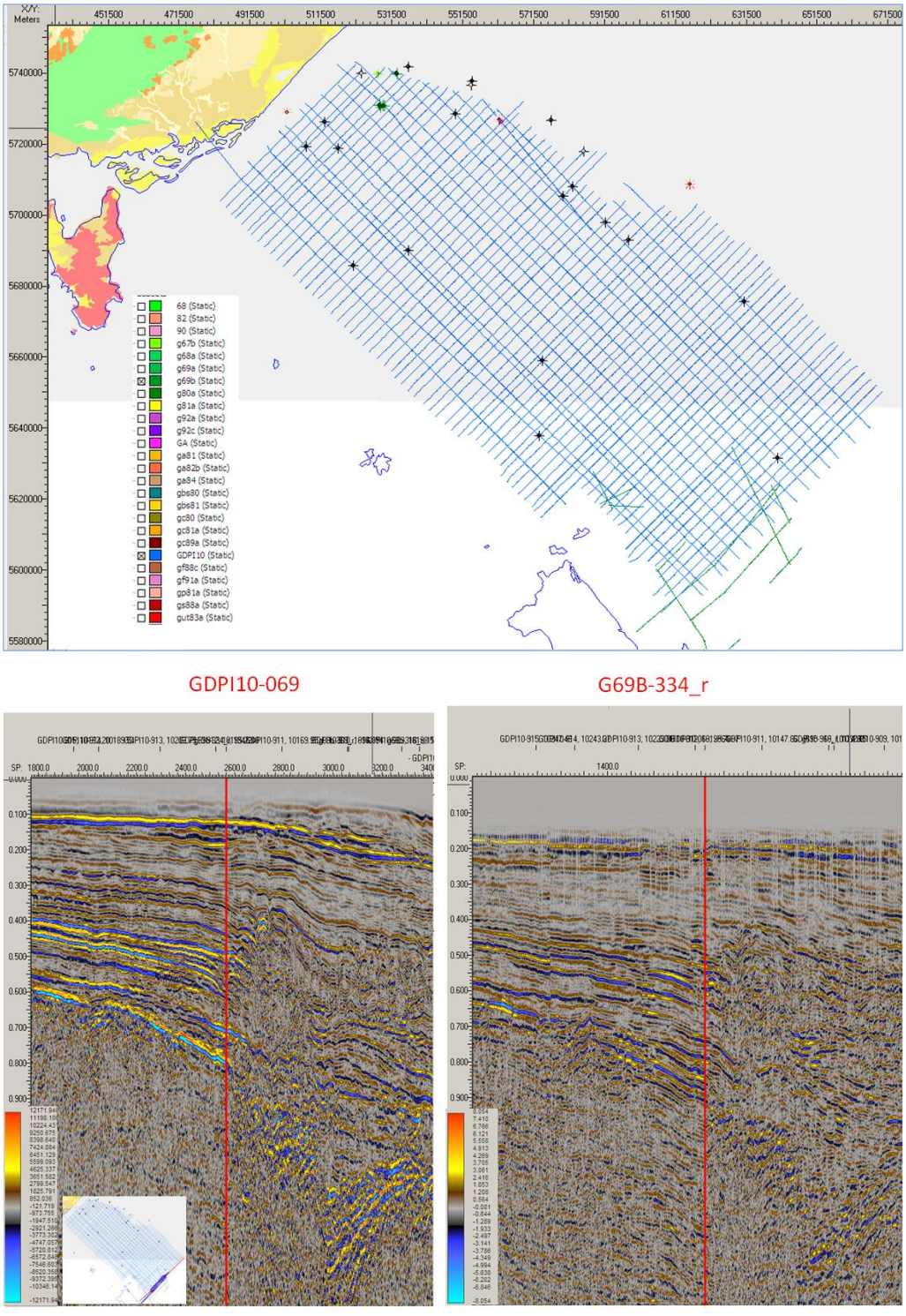

Figure 2.21 Extent of survey G69B (green) relative to survey GDPI10 (blue). Comparison of the two surveys at GDPI10-069 shows a dramatic increase in data quality at all levels but particularly in the very shallow and deeper sections of the data. Note the presence of a half graben in GDPI10-69 that is poorly resolved in the G69B line. (images supplied by G. Blackburn)

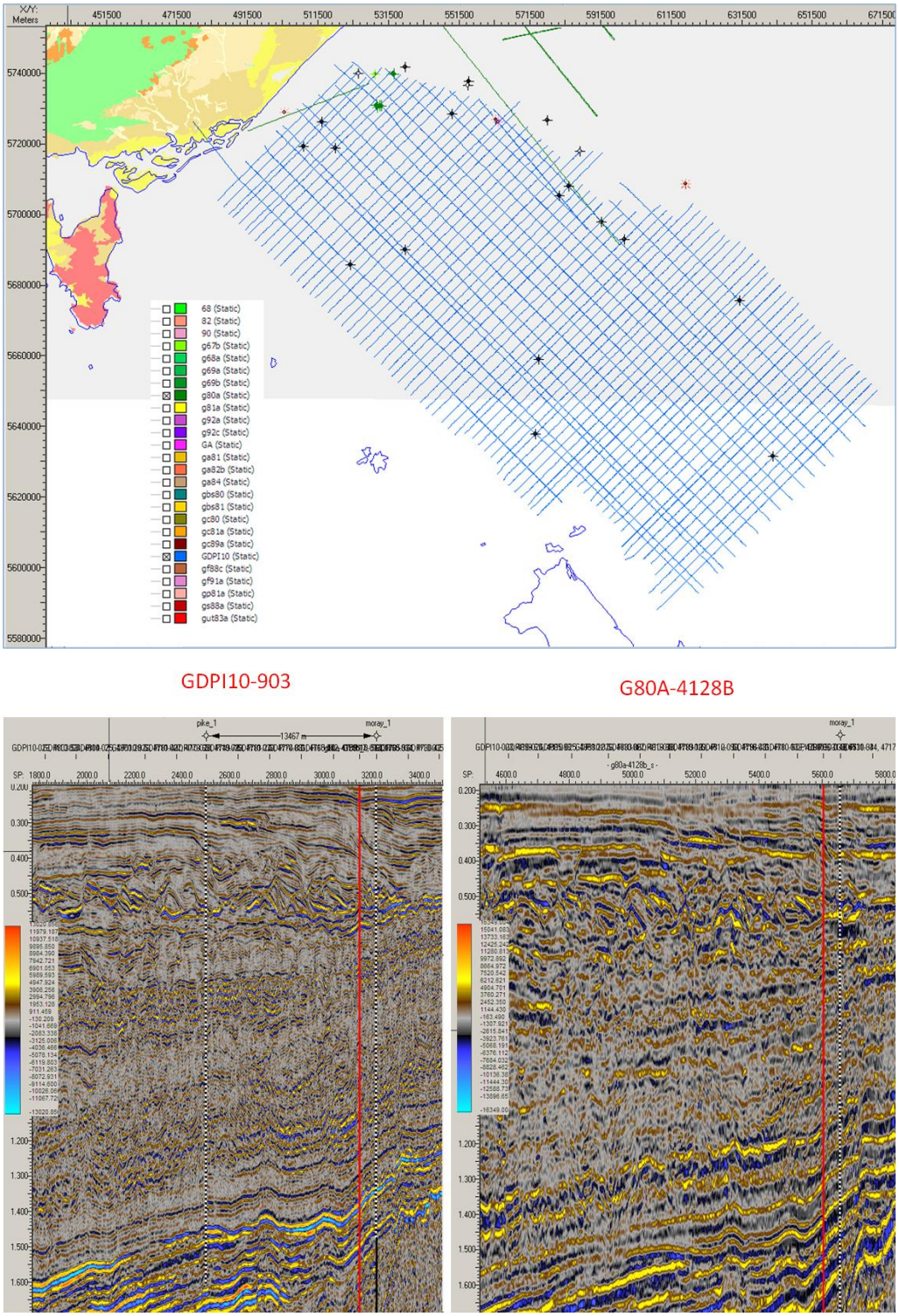

Figure 2.22 Extent of survey G80A (green) relative to survey GDPI10 (blue). Comparison of the two surveys at GDPI10-903 shows a dramatic increase in data quality. (images supplied by G. Blackburn)

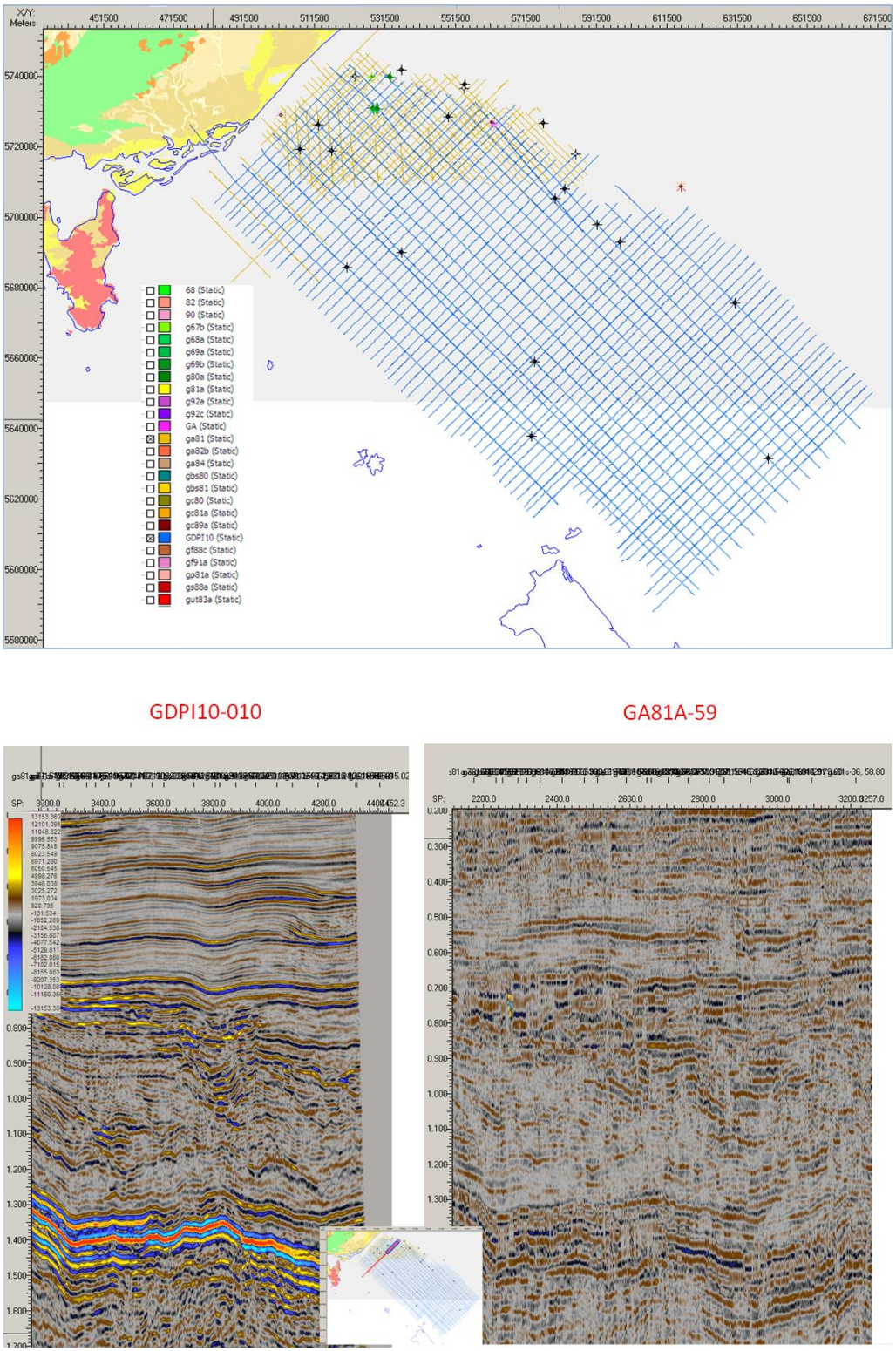

Figure 2.23 Extent of survey GA81A (yellow) relative to survey GDPI10 (blue). Comparison of the two surveys at GDPI10-010 shows a dramatic increase in data quality at all levels. (images supplied by G. Blackburn)

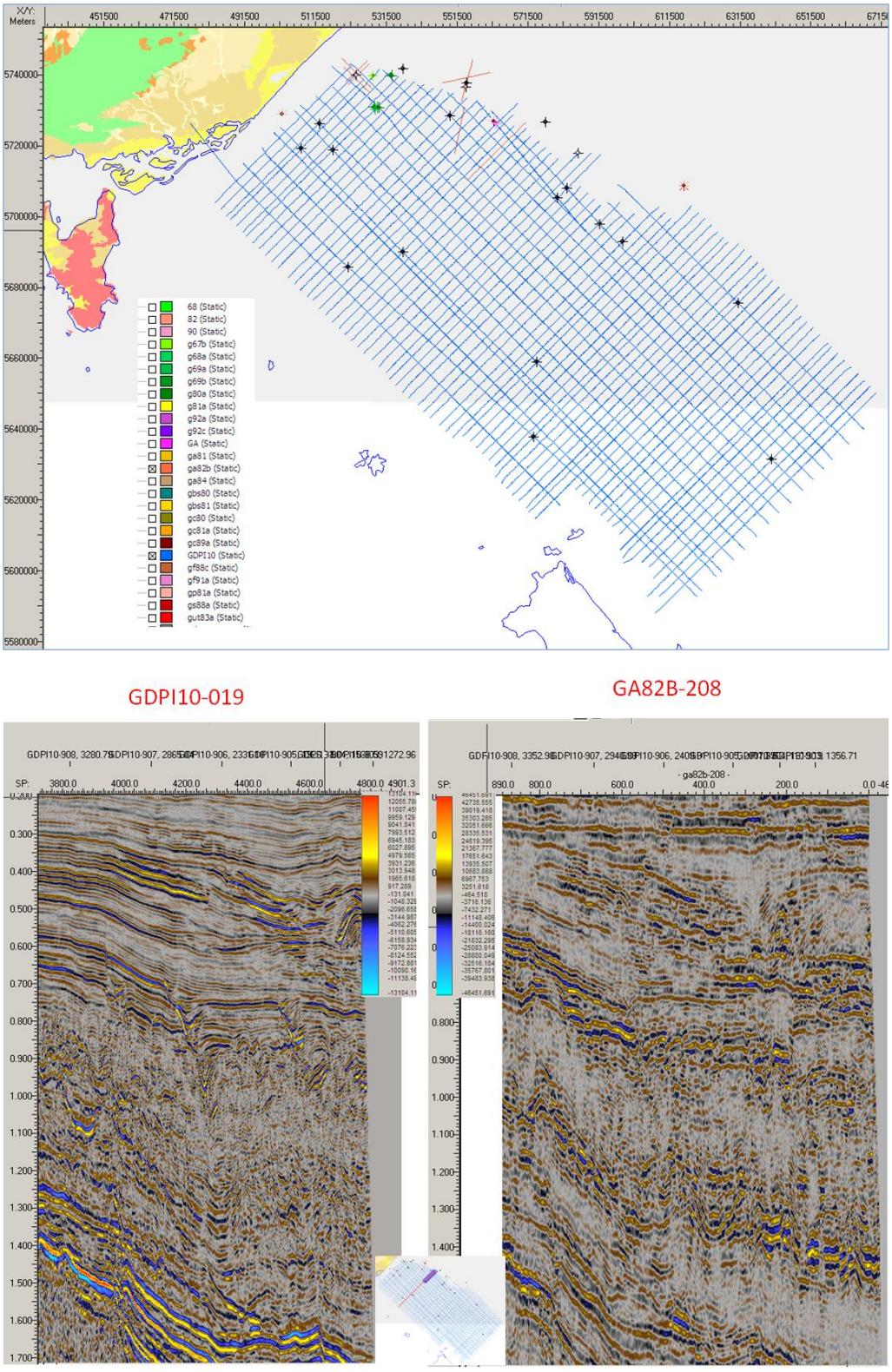

Figure 2.24 Extent of survey GA82B (red) relative to survey GDPI10 (blue). Comparison of the two surveys at GDPI10-19 shows a dramatic increase in data quality. (images supplied by G. Blackburn)

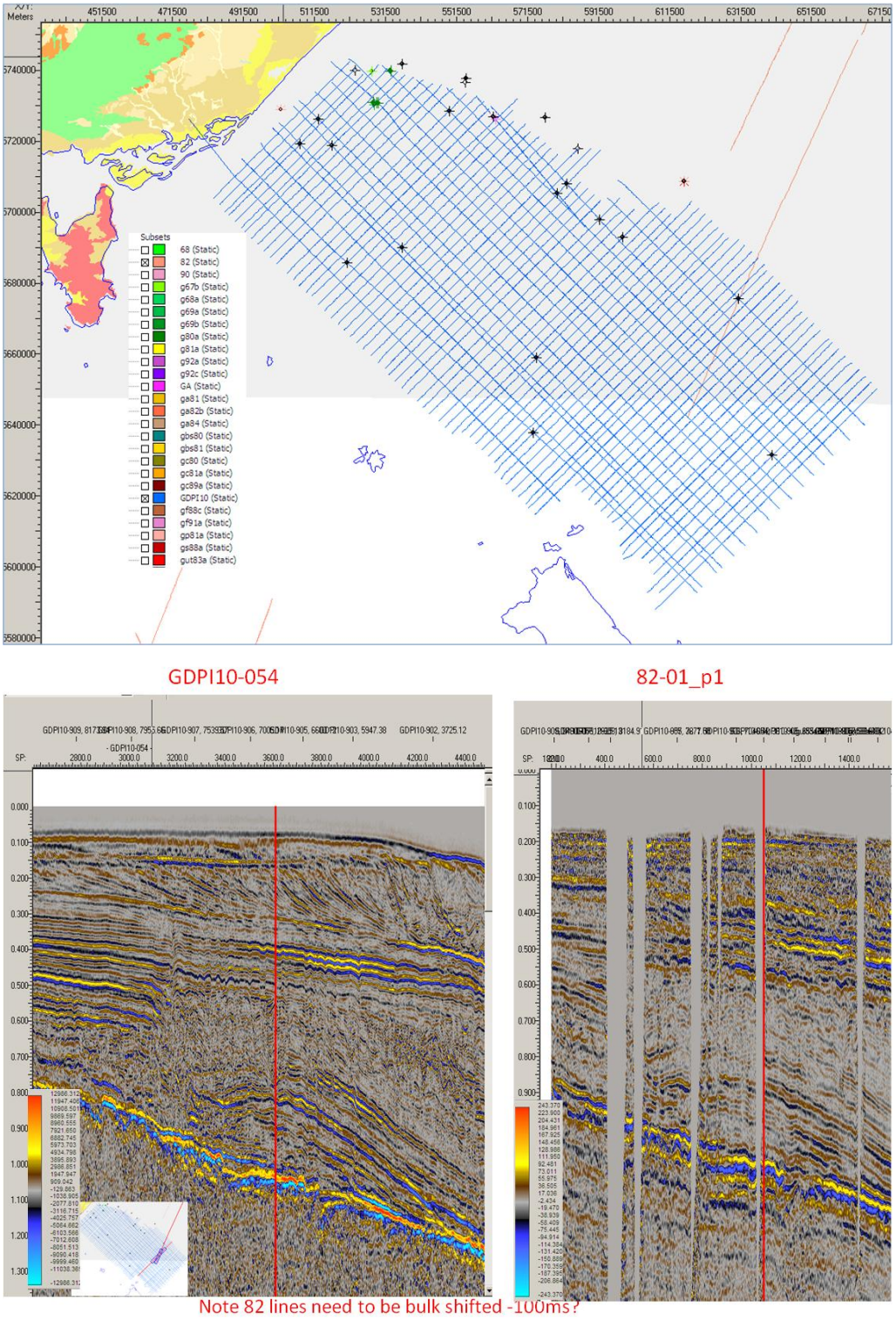

Figure 2.25 **Extent of survey G82D (red) relative to survey GDPI10 (blue). Comparison of the two surveys at GDPI10-054 shows a dramatic increase in data quality and consistent fold across the data. (images supplied by G. Blackburn)**

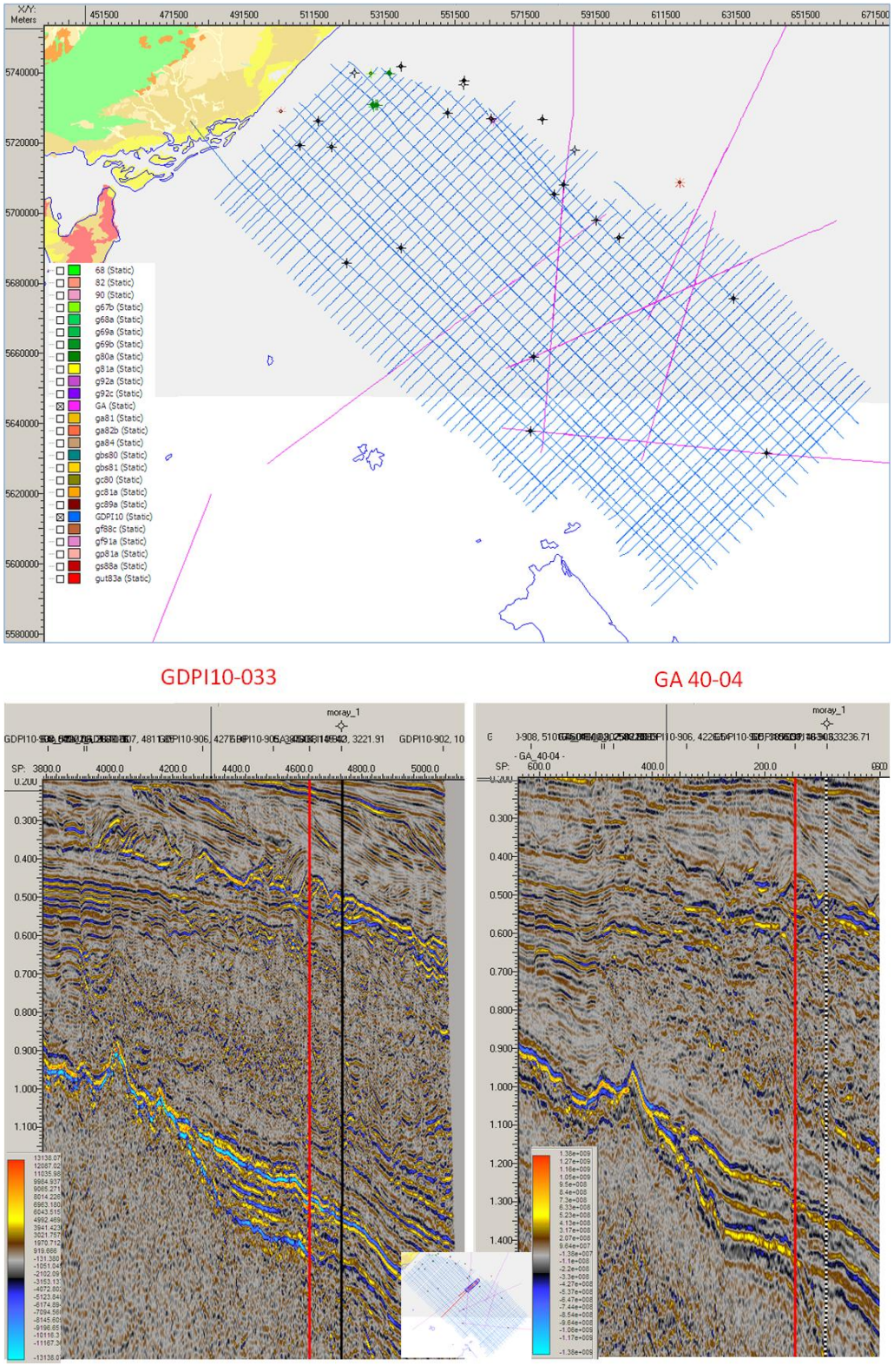

Figure 2.26 Extent of survey GA40 (purple) relative to survey GDPI10 (blue). Comparison of the two surveys at GDPI10-033 shows an increase in data quality. (images supplied by G. Blackburn)

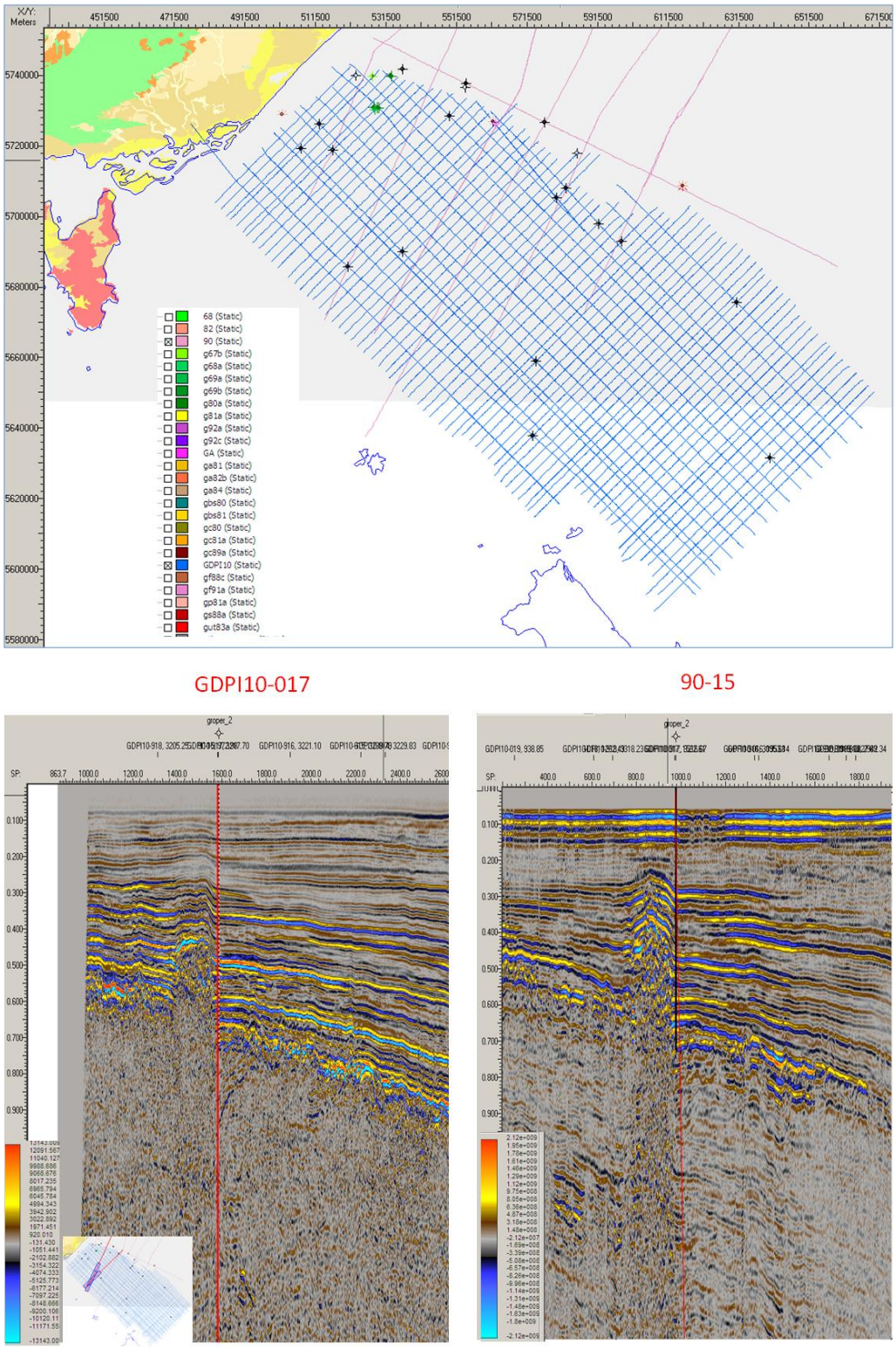

Figure 2.27 Extent of survey 90 (purple) relative to survey GDPI10 (blue). Comparison of the two surveys at GDPI10-017 shows similar data quality. (images supplied by G. Blackburn)

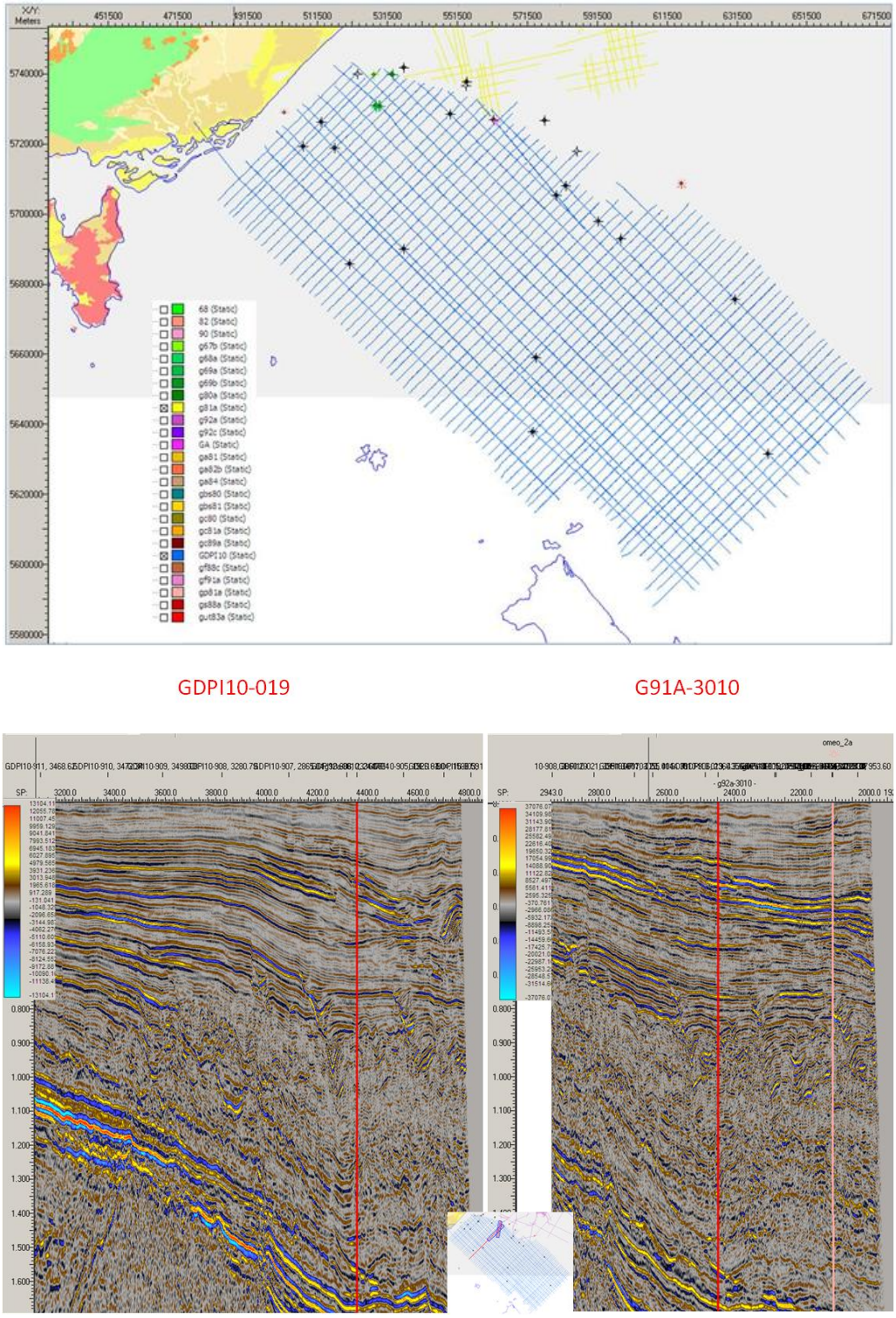

Figure 2.28 **Extent of survey G91A (yellow) relative to survey GDPI10 (blue). Comparison of the two surveys at GDPI10-019 shows similar data quality. (images supplied by G. Blackburn)**

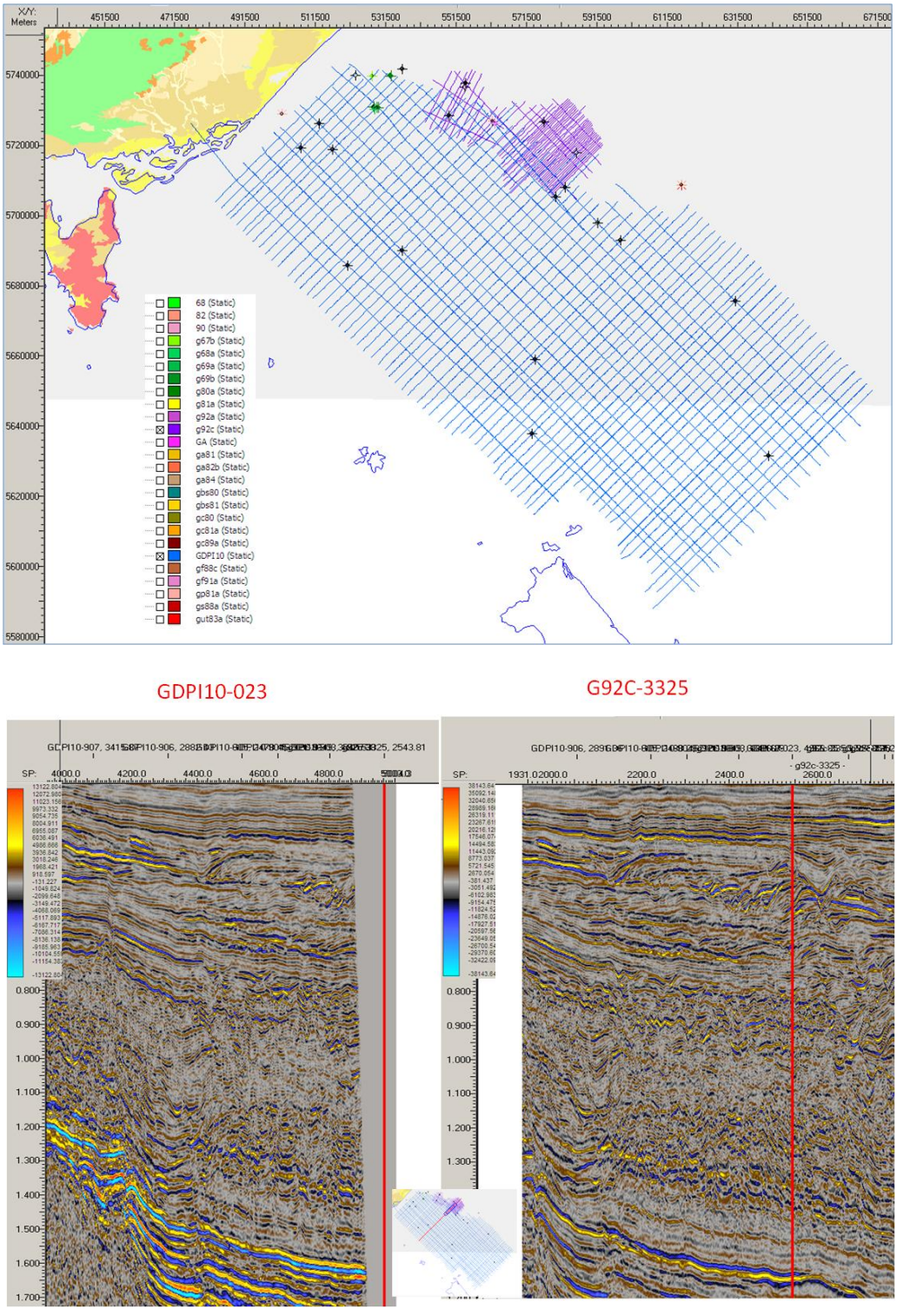

Figure 2.29 Extent of survey G92C (purple) relative to survey GDPI10 (blue). Comparison of the two surveys at GDPI10-023 shows an increase in data quality. (images supplied by G. Blackburn)

WELL	SPUD	GDPI10 TIE	DISTANCE FROM NEAREST GDPI10 LINE		TD	MAX AGE	TD FORMATION	KEY WELL	RATIONALE
amberjack-1	1990	NO	190 m NW	GDPI10-04	1750	Paleocene (Up. L. Balmei)	Barracouta	Yes	Location
bluebone-1	1969	YES		GDPI10-917	605	Eocene (Low N. asperus) above Basement	BASEMENT	Yes	BASEMENT Well
bullseye-1	1973	YES	<10 m away	GDPI10-906 and GDPI10-013	2386	Paleocene (A. hypercanthum)	Kingfish	Yes	Location
devilfish-1	1990	YES	<10 m away	GDPI10-028	2058	Maastrichtian (Up F. longus)	Volador	Yes	Location/stratigraphy
dolphin-1	1967	NO	610 m NE	GDPI10-907	2883.7	Campanian (N. senectus)	Chimaera	No	No checkshots
dolphin-2	1989	NO	720 m NE	GDPI10-907	1322	Unknown		No	Insufficient information and no seismic tie
dolphin-a3	1997	NO	720 m NE	GDPI10-907	1373	Unknown	BASEMENT	No	Insufficient information and no seismic tie
groper-1	1969	YES		GDPI10-914 and GDPI10-020	1035.4	Eocene (Low N. asperus) above Basement	BASEMENT	Yes	BASEMENT Well
groper-2	1969	YES		GDPI10-917 and GDPI10-017	875	Eocene (Low N. asperus) above Basement	BASEMENT	Yes	BASEMENT Well
kyarra-1	1983	YES	<10 m away	GDPI10-913	210	see Kyarra-1a		No	see Kyarra 1A
kyarra-1a	1983	YES	<10 m away	GDPI10-913 and GDPI10-007	1280	Aptian/Albian (C. striatus)	Korumburra	Yes	Location/stratigraphy
melville-1	2001	NO	210 m NW	GDPI10-026	3345	Turonian (P. mawsonii)	Emperor SG	Yes	Location/stratigraphy
moray-1	1972	YES	<10 m away	GDPI10-033	2669.7	Turonian (P. mawsonii)	Kersop Arkose	Yes	Line tie/Stratigraphy
mudskipper-1	1990	YES		GDPI10-036	1631	Paleocene (E. crassitabulata) above Baseme	BASEMENT	Yes	BASEMENT Well
mullet-1	1969	NO	25 m NW	GDPI10-039	751	Eocene (N. asperus) above Basement	BASEMENT	Yes	BASEMENT Well
omeo-1/ST1	1983	YES	<10 m away	GDPI10-904 and GDPI10-017	3379	Turonian (P. mawsonii)	Emperor SG	No	close to Omeo_2A
omeo-2	1985	YES	<10 m away	GDPI10-904	293	see Omeo-2a		No	see Omeo 2A
omeo-2a	1985	YES	<10 m away	GDPI10-904	3400	Maastrichtian (Up F. longus)	Chimaera	Yes	Line tie/Stratigraphy
palmer-1	1981	NO	270 m NE	GDPI10-909	1723	Turonian (P. mawsonii)		No	close to Perch 1/no tie
perch-1	1968	NO	16 m NW	GDPI10-007	2866.9	Aptian (C. hughesii)	Korumburra	Yes	near Line tie/Stratigraphy
perch-2	1985	NO	250 m SE	GDPI10-007	1321	Barremian (F. wonthaggiensis)		No	close to Perch 1/no tie
perch-3	1989	NO	615 m NW	GDPI10-007	1332	Eocene (Low N. asperus)		No	close to Perch 1/no tie
perch-4	1995	NO	650 m NW	GDPI10-007	2052	Unknown		No	close to Perch 1/no tie
pike-1	1973	YES	<10 m away	GDPI10-028	2134	Paleocene (L. Balmei)	Kingfish	Yes	Line tie
pisces-1	1982	NO	50 mNE	GDPI10-901	2580	Santonian (T.apoxyexinus)	Anenome	Yes	Location/stratigraphy
sailfish-1	1971	YES	<10 m away	GDPI10-907 and GDPI10-066	1422	Miocene	Unnamed volcanics	Yes	Location
tarra-1	1983	NO	35 m NE	GDPI10-905 and GDPI10-018	2905	Alb/Apt (C. striatus)	Korumburra	Yes	Stratigraphy
tommyruff-1	1990	NO	170 m SW	GDPI10-912	1550	Turonian (P. mawsonii)	Kipper Sh	Yes	Location/stratigraphy
wasabi-1	2008	NO	345 m SE	GDPI10-002	2125	NO INFORMATION		Yes	New well
wyrallah-1	1984	YES	<10 m away	GDPI10-914 and GDPI10-004	1160	Paleocene (Up L. Balmei)	Barracouta	Yes	Location

Table 2.4 **Basic information for wells intersecting the area covered by the GDPI10 2D seismic survey, highlighting the 20 key wells in green.**

Many of the wells were deviated and appropriate surveys were supplied within the Kingdom database and used in the creation of the synthetics. Three wells, Bluebone-1, Mullet-1, and Wasabi-1 were assumed to be vertical as directional surveys were not available in the WCR or from DPI. Deviation surveys supplied in the Kingdom project for Bluebone-1 and Mullet-1 were treated as suspicious and removed - it is unknown whether these wells are truly vertical. A summary of the basic well data supplied in the Kingdom project is shown in Table 2.5.

2.4.2 Biostratigraphy and Formation Tops

Two separate formation tops spreadsheets were supplied and FROGTECH was directed to the DPI preferred model to use as stratigraphic picks (fmtops_gipps_louise_monica.xls). The data contained in the spreadsheet were cross-checked with well reports and the Geoscience Australia petroleum wells database. Corrections were made to the formation tops as entered into the Kingdom project. A third and informal set of formation tops (Bassian Rise: BR1-BR5 and Early Oligocene Wedge: EOW) was derived from Partridge (2006), in the Oligocene to Recent for Mullet-1, Groper-1 and Bluebone-1 wells. Although, the tops are supported by biostratigraphic data, in these three wells interpretation of the EOW has been extended to nine other wells (Bullseye-1, Groper-2, Kyarra-1A, Melville-1, Moray-1, Mudskipper-1, Omeo-2A, Tarra-1, Wyrallah-1) based on log character alone.

The biostratigraphic data pre-loaded in the Kingdom project was augmented and cross-checked against additional data from a variety of sources, including Geoscience Australia's petroleum wells database, well completion reports with biostratigraphic analyses, VIMP reports and publications from Mineral Resources of Tasmania (e.g. Partridge, 2006).

Biostratigraphic and formation top information is available for all key wells except Wasabi-1. A listing of formation tops contained in the Kingdom project is provided in Appendix 3.

2.4.3 Porosity, Permeability and Seal Capacity Analyses

Porosity and permeability data were supplied in two excel spreadsheets (Offshore-PorosityPermDataMap-DPI-dbMap-Core-Log-data_copy 08032012.xls and Offshore-PorosityPermDataMap-ESSO-GA-data_copy 08032012.xls). The spreadsheets contain information for over 400 wells including data from the Otway Basin. When the data were distilled to the key wells from the Southern Flank of the Gippsland Basin, 13 contained porosity and/or permeability core analysis measurements or log analysis calculations (Amberjack-1*, Bluebone-1, Devilfish-1, Groper-1*, Groper-2*, Kyarra-1A*, Melville-1, Moray-1, Mudskipper-1, Mullet-1*, Perch-1, Pike-1, Tarra-1*). The datapoints were primarily restricted to the Latrobe Group. Only the six wells highlighted with an asterisk above had enough values (i.e. > 5) to warrant the generation of a separate datasheet. These datasheets are included with the well composites in Appendix 2.

Mercury Injection Capillary Pressure Analysis (MICP) data were provided for core (Groper-1), sidewall core (Groper-2) and cuttings (Kyarra-1A, Melville-1, Mudskipper-1, Omeo-1, Omeo-2A, Pike-1, Pisces-1, Tommyruff-1). Analyses from the Groper wells were taken from Goldie Divko et al. (2010), while the remaining analyses are unpublished. The wells with MICP analyses cover all the structural elements of the Southern Flank of the Gippsland Basin (Figure 2.1). All MICP data will need to be reviewed in the context of the seismic stratigraphic framework developed during the current study.

2.4.4 Additional Well Data

The Southern Flank of the Gippsland Basin has been involved in several acreage release rounds, and well data has been summarised in the supporting VIMP reports (Table 2.6). Time-depth information was supplied in a summary spreadsheet, containing data derived from WCR (checkshots, VSPs and read from time-depth curves). Each time-depth relationship was checked against information in the well reports and corrected if necessary, before loading into the Kingdom project.

The well data information described above was gathered from more than 200 separate pdf and image files that were supplied for the key wells.

WELL	KEY WELL	T/D-relationship	Synthetic	Formation tops 3D-GEO	Formation tops DPI-WCR	Deviation Survey	Biostrat GA_Bug	Cali	DT	GR	RHOB	DRHO	SP	NPHI	ILD	MSFL	SFL	LLD	LLS	others
amberjack -1	Yes	GA	NO	Yes	Yes (1 only)	Yes	NO													
bluebone-1	Yes	unknown	NO	Yes	NO	Yes-vert	Yes	las												
bullseye-1	Yes	GA	NO	Yes	Yes	Yes	Yes													
devilfish-1	Yes	DPI_qc	NO	Yes	Yes	Yes	Yes													
dolphin-1	No	NO	NO	Yes	Yes	Yes	Yes													
dolphin-2	No	NO	NO	Yes	Yes	Yes-vert	NO													
dolphin-a3	No	NO	NO	Yes	Yes	Yes	NO													
groper-1	Yes	GA	NO	Yes	Yes	Yes	Yes													
groper-2	Yes	DPI_qc	NO	Yes	Yes	Yes	Yes													
kyarra-1	No	DPI_qc	NO	NO	NO	Yes	NO													
kyarra-1a	Yes	GA	NO	Yes	Yes	Yes	Yes													
melville-1	Yes	unknown	NO	Yes	Yes	NO	NO	N/A	las	las	N/A									
moray-1	Yes	DPI_qc	NO	Yes	Yes	Yes	Yes													
mudskipper-1	Yes	GA	NO	Yes	Yes	Yes	Yes													
mullet-1	Yes	unknown	NO	Yes	Yes	Yes-vert	NO													
omeo-1/ST1	No	Yes	GA	Yes	Yes	Yes	Yes													
omeo-2	No	NO	NO	Yes	NO	NO	NO													
omeo-2a	Yes	GA	NO	Yes	Yes	Yes	Yes													
palmer-1	No	GA	NO	Yes	Yes	Yes	Yes													
perch-1	Yes	DPI_qc	NO	Yes	Yes	Yes	Yes													
perch-2	No	GA	NO	Yes	Yes	Yes	Yes													
perch-3	No	NO	NO	Yes	Yes	Yes	NO													
perch-4	No	NO	NO	NO	Yes	NO	NO			2 separate										
pike-1	Yes	GA	NO	Yes	Yes	Yes	Yes	las	las	las	las									
pisces-1	Yes	GA	NO	Yes	Yes	Yes	Yes													
sailfish-1	Yes	NO	NO	Yes	NO	Yes-vert	NO				N/A									
tarra-1	Yes	DPI_qc	NO	Yes	Yes	Yes	Yes													
tommyruff-1	Yes	GA	NO	Yes	Yes	Yes	Yes													
wasabi-1	Yes	NO	NO	NO	NO	NO	NO	las	las	las	las									
wyrallah-1	Yes	GA	NO	Yes	Yes	Yes	Yes													

Table 2.5 **Well information contained within the Kingdom project. Missing log information for Wasabi-1, Melville-1, Bluebone-1, Pike-1 and Sailfish-1 were supplied in LAS format and loaded into the project. Note that sonic logs are contained in the project as µs/m.**

WELL	KEY WELL	VIMP Reports	Checkshots spreadsheet	WCR
amberjack -1	Yes	VIMP79 (2003)	Yes	Yes
bluebone-1	Yes		supplied separately	Yes
bullseye-1	Yes	VIMP88 (2006)	Yes	Yes
devilfish-1	Yes	VIMP88 (2006)	Yes	Yes
dolphin-1	No	VIMP79 (2003)	No - none acquired	
dolphin-2	No	VIMP79 (2003)	No - none acquired	
dolphin-a3	No		No - none acquired	
groper-1	Yes	VIMP88 (2006)	Yes	summary
groper-2	Yes	VIMP88 (2006)	Yes	Yes
kyarra-1	No		Yes	
kyarra-1a	Yes	VIMP79 (2003), VIMP88 (2006)	Yes	Yes
melville-1	Yes		supplied separately	Yes
moray-1	Yes	VIMP79 (2003), VIMP88 (2006)	Yes	Yes
mudskipper-1	Yes	VIMP79 (2003), VIMP88 (2006)	Yes	Yes
mullet-1	Yes	VIMP88 (2006)	supplied separately	Yes
omeo-1/ST1	No	VIMP88 (2006)	No	Yes
omeo-2	No		No	
omeo-2a	Yes	VIMP88 (2006)	Yes	Yes
palmer-1	No	VIMP79 (2003)	Yes	Yes
perch-1	Yes	VIMP79 (2003)	Yes	summary
perch-2	No	VIMP79 (2003)	Yes	Yes
perch-3	No	VIMP79 (2003)	No	Yes
perch-4	No		No	Yes
pike-1	Yes	VIMP88 (2006)	Yes	Yes
pisces-1	Yes	VIMP79 (2003), VIMP88 (2006)	Yes	Yes
sailfish-1	Yes	VIMP88 (2006)	No - none acquired	Yes
tarra-1	Yes	VIMP88 (2006)	Yes	Yes
tommyruff-1	Yes	VIMP79 (2003)	Yes	Yes
wasabi-1	Yes		Supplied separately	Basic
wyrallah-1	Yes	VIMP88 (2006)	Yes	Yes

Table 2.6 Summary of the additional well information supplied for the study.

2.4.5 Wells with Limited or Erroneous Data

Several key wells had limited or erroneous data that reduced their utility. The wells were chosen as key due to their position and the problems encountered decrease the confidence in the well ties.

Pisces-1: The well was originally located greater than 50 m off the intersection with GDPI10-51 and GDPI10-901 to the north. The synthetic tie was problematic, with the seafloor pick too shallow, suggesting the well should be inboard of the original position. Further investigation (Terratek, 2012) identified that:

1) the position in the WCR was provided without a reference spheroid;
2) the position provided in the WCR summary differed from the position in the body of the report; and,
3) the intended position of the well was at SP1157 on line GC80-11A, and that the actual position was 14 m to the N30°W of the intended position.

Using this information, the well was moved approximately 200 m SW of the original position as provided in the Kingdom project. All the key wells, except Melville-1 and Wasabi-1, on the southern flank of the Gippsland Basin were drilled between 1969 and 1990. In general, in older wells, positioning was less accurate and location data records less complete relative to modern wells, which will affect all the key wells.

Melville-1: A relatively modern well (2001), sitting at the edge of the GDPI10 data grid in the Central Deep (Figure 2.1). The digital well logs were limited to deeper than 2600 m, with the caliper and density logs unavailable, reducing the ability to create an accurate synthetic tie. In addition, there were no biostratigraphic analyses above the Latrobe Group.

Wasabi-1: The most recent well within the GDPI10 survey area. As the well was drilled in 2008, only the basic data reports were available. There were no formation tops or biostratigraphic analyses to tie to the seismic data. Well logs were provided in LAS format but were split into acquisition runs.

Sailfish-1: Isolated to the far east of the GDPI10 seismic grid, the usefulness of this well was limited by the lack of checkshots or other time-depth data. When the synthetic was created an average sub-seafloor velocity of 2000 m/s was assumed to calibrate the sonic log. Combined with the complete lack of biostratigraphy and limited formation top information, this well provided no real constraints for this part of the project area.

3 Methodology and Data Delivery

3.1 Introduction

The interpretive phase of the GDPI10 2D seismic survey began after the compilation and review of well logs, biostratigraphy and the picks for formation tops were completed. The interpretation integrates the seismic and well information, via the synthetic ties at the 20 key wells. The process was an iterative one, and the seismic interpretation was correlated with the well ties and both were used to enhance the synthetic tie. The final output is a consistent, and tied seismic stratigraphic interpretation. The results are documented in this comprehensive report and appendices, and support the seismic horizons, synthetics and well composites contained within the Kingdom project. An ArcGIS project was developed as an additional means to illustrate the outcomes of the study.

3.2 Synthetics for Key Wells

Synthetic seismograms were used to relate depth-referenced well data to time-referenced seismic data at well-sites (Telford, 1985) and were created for the 20 key wells (Appendix 1).

Ideally, synthetic seismograms are generated using both sonic and density logs. However, density logs are often ignored in the calculation for two reasons:

- Density variations are small relative to changes in velocity (e.g. Table 2.5 in Telford, 1985); and
- Density logs are more susceptible to adverse effects of borehole rugosity, due to their smaller radius of penetration (< 13 cm) compared to sonic logs (< 25 cm; Rider, 1996). As logging runs are not continuous to the surface, the sonic log is calibrated to the seismic datum (mean sea level) using either a check shot survey or the results of a vertical seismic profile.

The density log was set to a constant in this study for the reasons above and because the density log often covered a much smaller interval than the sonic log.

The procedure used to create synthetic seismograms for the Southern Gippsland Basin using the Kingdom Software is presented in Figure 3.1 and outlined here:

i. Log Editing:

   The match between the synthetic seismogram and seismic data is dependent on the quality of the initial sonic log. Spurious peaks create false reflections in synthetic seismograms, lowering the quality of ties. Sonic logs were inspected with reference to caliper, bit-size, gamma logs and drilling reports (i.e. casing shoe locations and drilling problems) where available. Spikes in the sonic log were removed if coincident with washouts, which commonly occur near casing shoes.

ii. Checkshots and sonic calibration:

   Sonic logs were calibrated to checkshot surveys so that the average velocities between checkshots corresponded to the average velocities on the sonic log. A single checkshot placed at the top of the sonic log was the minimum required to make the depth conversion absolute from the surface. However, greater accuracy is achieved from multiple measurements down the borehole (Goetz et al., 1979). A reference checkshot was always placed at the seafloor, with an assumed average velocity of 1521 m/s, consistent with the velocity picking in the GDPI10 2D seismic survey. Sailfish-1 had no checkshot survey or VSP so an average velocity of 2000 m/s was assumed from seafloor to the top of the sonic log.

iii. Generate RC series:

$$RC(layer1/layer2) = \frac{Z_2 - Z_1}{Z_2 + Z_1}$$

   Where Z is the acoustic impedance of layers 1 and 2, which is the product of density (ϱ) and velocity (v). As density was assumed constant the RC was calculated by variations in velocity as determined from the calibrated sonic log.

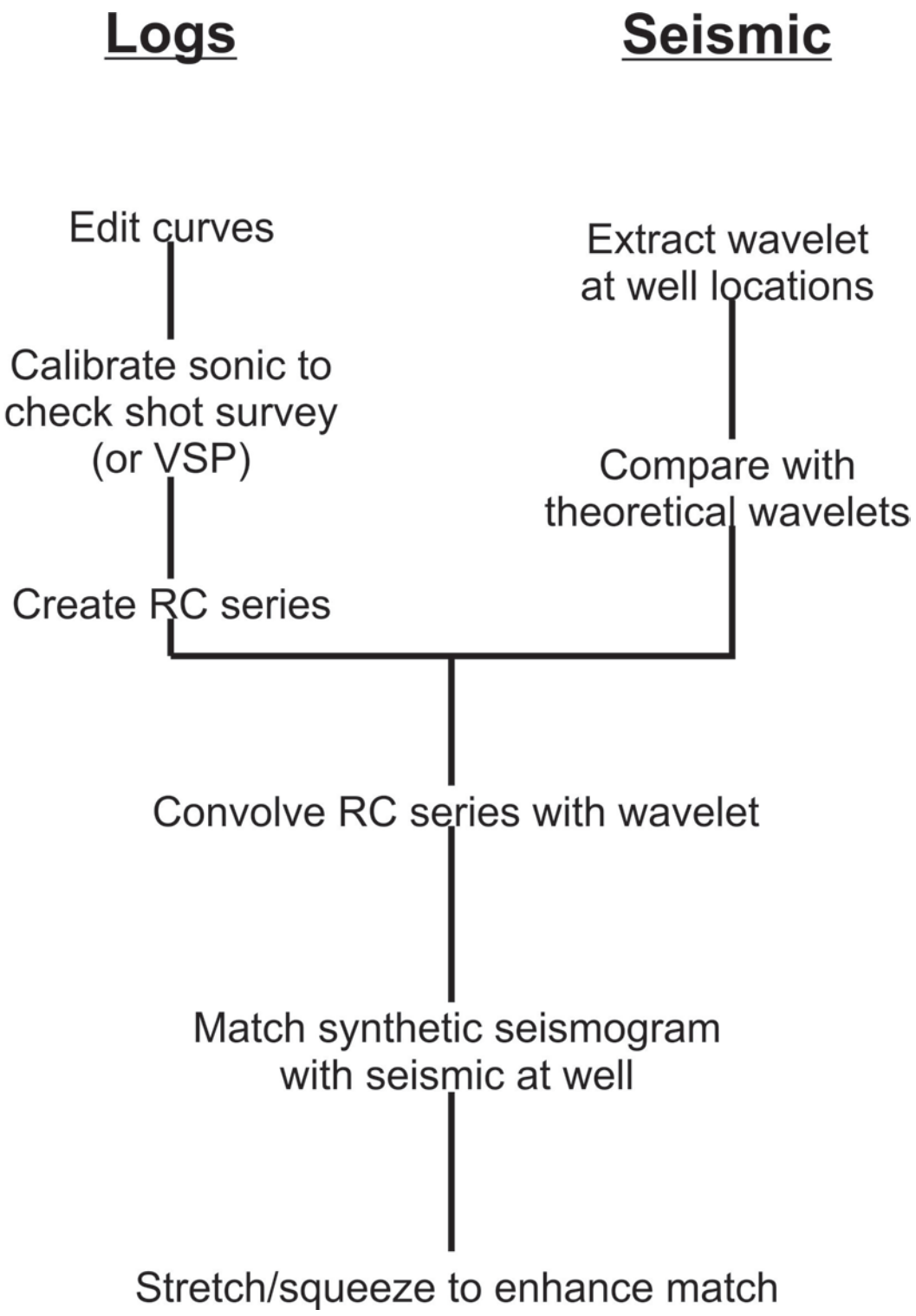

Figure 3.1 **Flow chart of generalised procedure to create synthetic seismograms for well ties with seismic data.**

iv. Create and match synthetic seismogram:

To create the synthetic seismogram, a suitable wavelet was convolved with the RC series. The processing report for the GDPI10 2D seismic survey (Fugro, 2011) indicated that these data were processed to zero phase and this was confirmed at seafloor in deeper water. Wavelets were extracted, assuming a zero phase, from seismic data adjacent to each well and compared with theoretical Ormsby and Ricker wavelets. Wavelets extracted from the GDPI10 survey ranged in dominant frequency (Figure 3.2) from less than 30 Hz (e.g. Omeo-2A) to greater than 50 Hz (e.g. Mudskipper-1) and commonly had a broad range of frequencies represented. Due to the variation between the extracted wavelets (Figure 3.2), it was decided not to approximate the wavelets with a single theoretical wavelet but to proceed with the wavelets as extracted at the wells.

Once these wavelets were extracted, they were convolved with the RC series, a linear filter that alters the shape of the source wavelet. The generated synthetic seismogram was then compared with the seismic data at the well location. When required, the synthetic was stretched and squeezed by inspection, anchored between selected tie points, to improve the match. Any stretching or squeezing will have affected the time-depth relationship and velocity profile at the well.

There are correlation resolution limits. Synthetic seismograms created from sonic logs are a composite response of closer spaced reflectors that can be detected using seismic frequencies (Yilmaz, 1987). This will result in inconsistencies in the detailed correlation between seismic data and the synthetic. Overall, sonic velocities tend to be greater than seismic velocities, although the dependency on frequency is not fully understood (Goetz et al., 1979). Spread lengths, fold, S/N ratio and deviation from the assumed hyperbolic path all impact seismic velocity picks. In contrast, the sonic log is affected by borehole conditions, instrumentation and calibration errors. Checkshot velocity surveys use frequencies comparable to seismic data, but are influenced by noise, picking methodology, formation variability and acquisition logistics.

The synthetics generated in the Kingdom project are presented in Appendix 1.

3.3 Composites for Key Wells

The composite logs were generated in Kingdom using data compiled from well and drill hole databases, digital logs, well completion reports (WCR), other reports and spreadsheets supplied by DPI and GA.

The different input datasets include:

- Spreadsheets - fmtops_gipps_louise_monica (the DPI preferred formation tops dataset), Alan_Tait_tops, DPI and ESSO Offshore-PorosityPermDataMaps;
- DPI supplied well information - WCRs, well composite templates, digital logs;
- Literature - VIMP and MRT reports; and,
- Geoscience Australia - Petroleum Wells Database.

The various multi-vintage datasets vary drastically in database structure and the quality and quantity of information available. Therefore, it was necessary to locate and extract the relevant information and restructure into a standardised spreadsheet with a focus on well header information and litho- and bio-stratigraphy (formation tops, palynology and their associated depths).

The client-supplied well composite templates were restricted to certain depth intervals and particular information. Nonetheless, they formed a good starting point for the generation of the well composite logs, consisting of:

Well header information from GA Well Reports and WCRs;

- Formation tops primarily sourced from the louise_monica spreadsheet and cross-referenced with WCRs, GA Well Reports and MRT reports;

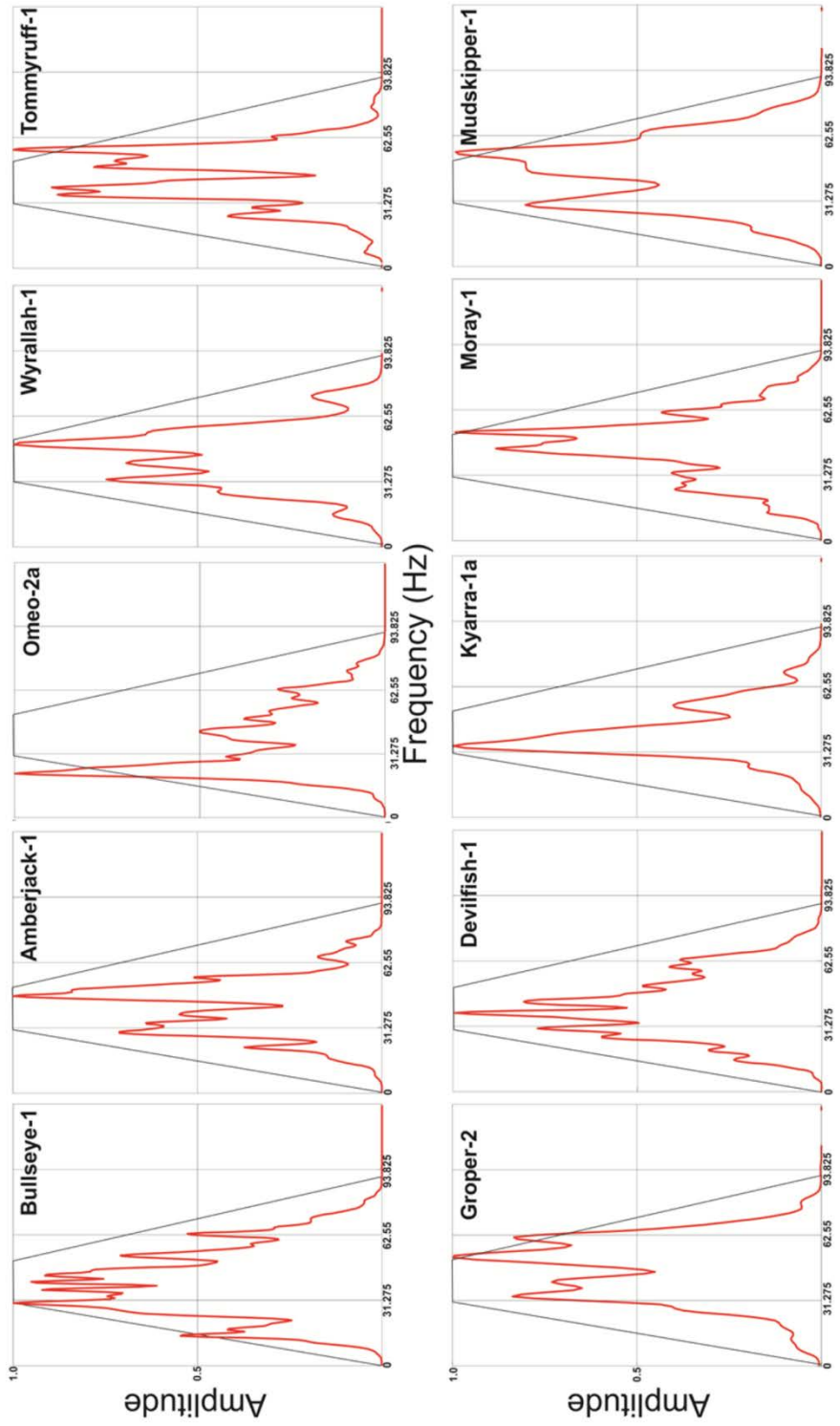

Figure 3.2 **Amplitude spectra for wavelets extracted from the GDPI10 2D seismic data at the well locations. The extracted data are overlain on the spectrum of a theoretical Ormsby wavelet with corner frequencies 0, 30, 50, 90 Hz.**

- Biostratigraphy data from GA Well Reports; cross-referenced with VIMP and louise_monica spreadsheet, and Biostrata reports from various WCR. All biostratigraphy was referenced to the latest Gippsland Basin stratigraphic chart (Partridge et al., 2012);
- A lithology log generated from cuttings descriptions from WCRs;
- Hydrocarbon shows;
- Client-supplied digital logs (GR, CALI, SP, DT, RHOB) where available;
- Seismic clips of each well and respective synthetic seismograms; and,
- FROGTECH-interpreted seismic horizons.

The information contained in the FROGTECH-interpreted seismic horizon track allows for the display and comparison of seismic horizons interpreted in the GDPI10 2D seismic survey relative to formation tops and biostratigraphy extracted from the various reports and databases. It is important to note that the seismic clips and associated TWT tracks are not at the same scale as the depth tracks of the composite logs.

Every effort has been made to collate and integrate all relevant information for entry into the composite logs in the Kingdom project. However, there are still some outstanding issues:

- Inconsistencies remain between the Gippsland Limestone and sea floor pick in some wells between different data sources;
- Some logs remain unavailable;
- Some logs are confidential and as such will only be available in the report, and not in the Kingdom project;
- Sonic logs in the Kingdom project and exported composite logs are scaled to μs/m and have been edited to remove spikes at the casing shoe;
- Information is limited for Wasabi-1 as only the basic data well completion report and raw log suites are currently available; and,
- Limitations with the Kingdom EarthPAK functionality for the display and update and transfer of data within and between projects.

Editing in Kingdom EarthPAK highlights the drawbacks in functionality where changes made to one composite (e.g. font, track widths, orientation) are reflected in all other composites. Therefore, once formatted consistently, the well composite logs are presented as PAKnotes within the Kingdom project, thereby allowing individual composites to be edited and saved without affecting the other composites.

In addition to the well composites, a supplementary set of porosity-permeability well composites were also generated, where poro-perm data for wells were available.

Images of the composites generated and stored in the Kingdom and the porosity/permeability summaries project are presented in Appendix 2.

3.4 Seismic Horizons and Interpretation Methodology

In the original tender documents, DPI specified the horizons of interest to be mapped in the study area. Some revision of the original list has been made in consultation with DPI to better reflect the significant stratigraphic and mappable units that are specific to the study area (Table 1.1). A number of supplementary horizons were also mapped for control purposes. The interpretation of the GDPI10 2D seismic survey was carried out using the Kingdom 2d/3dPak (version 8.7) software package. All faults and horizons were interpreted on the final time migration GDPI10 2D seismic survey provided by DPI Victoria. These horizons and their regional stratigraphic significance are discussed in subsequent sections.

Well logs were also provided by DPI in the Kingdom project. Synthetic seismograms were produced for key wells (Appendix 1). Grids produced for DPI by 3D-GEO (2010) were provided by DPI for comparative purposes in the current study. Biostratigraphic and formation top picks were provided in an Excel spreadsheet by DPI. These picks were entered into the Kingdom project Formation Tops database. Some suggested revisions to these picks are covered in Section 5.

3.4.1 Faults

Fault mapping was a three-step iterative process closely paired with peer review quality assurance. In the first step, fault sticks were interpreted along seismic lines trending close to the fault dip direction where vertical offset was evident in basement and overlying stratigraphy. In the second step, intersections of the fault sticks were correlated along perpendicular seismic lines, those closely trending the fault strike direction. Fully-tied interpretation along approximate fault strike and dip lines resulted in 48 fault and fault system surfaces. In the third step, a fault polygon map was constructed to show the horizontal offset of basement for all mapped faults and fault systems (Figure 3.3). No automated fault picking was used in this interpretation.

Quality assurance of the structural interpretation was carried out with an internal peer review process confirming that the faults and fault systems conform to conventional and reasonable models of fault development and geometry. This included qualitative fault offset analysis to assure a balanced unimodal distribution of offset along strike of individual faults (Figure 3.4), as well as assessment of the resultant structural model against the known regional tectonic evolution, and the presumed basement rheology.

3.4.2 Horizons

Each horizon was mapped along a particular seismic phase and along intersecting fault planes. Both manual and automated tools were used for horizon interpretation. Manual interpretation creates straight line horizon sections between successive mouse clicks and does not automatically conform to any seismic phase. Automated interpretation included fill and 2D hunt functions. The fill function automatically interprets the horizon along a defined seismic phase between successive mouse clicks. The 2D hunt function automatically interprets the horizon along a defined seismic phase in both directions from a single mouse click and continues to the end of the event within user defined parameters (e.g. search window size and largest or closest seismic phase matching). The horizons were extrapolated from and matched with well-derived formation boundary picks for 20 wells across the project area.

Early in the interpretation a series of construction horizons were generated as a control on the development of the seismic velocity model. Construction surfaces were mapped principally using manual picking tools with automated picking tools used when they could be efficiently applied. The Seafloor, Downlap, Mid-Miocene and Basement construction horizons were mapped on all lines and others were mapped along a subset of survey lines allowing for reasonable gridding across the rest of the survey. These horizons went through an expedited quality checking process which included qualitative matching of horizon cross-ties on part of the interpreter, with further correction applied during the gridding to create closed grids.

Construction horizons served as a first draft for the interpretation horizons. The interpretation horizons extend on each survey line to the seismically evident preservation limit. These horizons were quality checked to resolve and correct all mis-ties > 20 ms and to smooth or confirm rugosity evident in gridded horizons. The quality-check grids were generated with the flex gridding spline technique (Section 2) with a cell size of 50 m by 50 m. Unresolved correlation errors greater than 20 ms exist for the Seafloor in five locations in the eastern portion of the survey where steep canyon sides inhibited consistent seismic imaging of seafloor between perpendicularly acquired seismic lines (Figure 3.5).

All horizons were first interpreted with manual picking, and then automated-fill picking was used to better match the seismic phases, with further modification of manual editing to smooth out rough areas, improve interpretation ties, and extend interpretation between automatic picks and to the edges of the seismic survey data. The horizons were predominantly matched to particular phases and are therefore suitable for qualitative generation of horizon amplitude maps.

3.4.3 Gridding

Grid testing was performed on the Top Basement horizon which has the greatest variability and fault displacement. Prior to gridding it was noted that the seismic line spacing averages 2.5 km NW-SE and 5 km NE-SW. Previous gridding experience suggests the minimum grid cell size should be at least approximately ¼ of the distance between seismic lines (i.e. > 625 m). To illustrate the effects of over- and under-sampling the interpretation, grids with cell sizes ranging from 50 m to 1000 m were produced for some of the test runs. Details for the grid testing are discussed below for: single- and two-step flex gridding; and kriging with circular and elliptical search radii. All gridding was done within the Kingdom software.

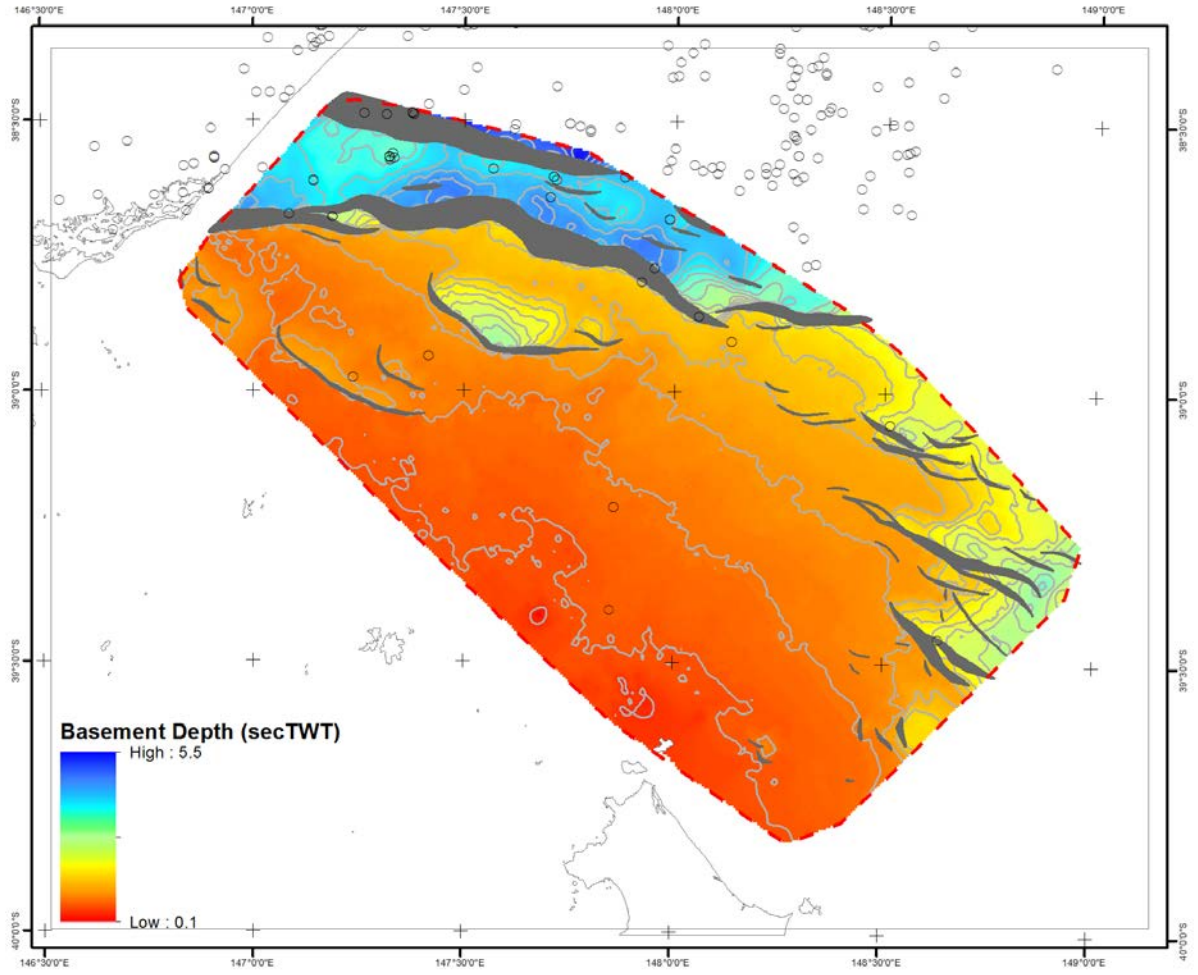

Figure 3.3 Gridded basement surface in seconds (TWT) with contours (grey lines) covering the GDPI10 seismic survey area (dashed red line). Also shown are basement faults (dark grey filled polygons) and wells (black circles).

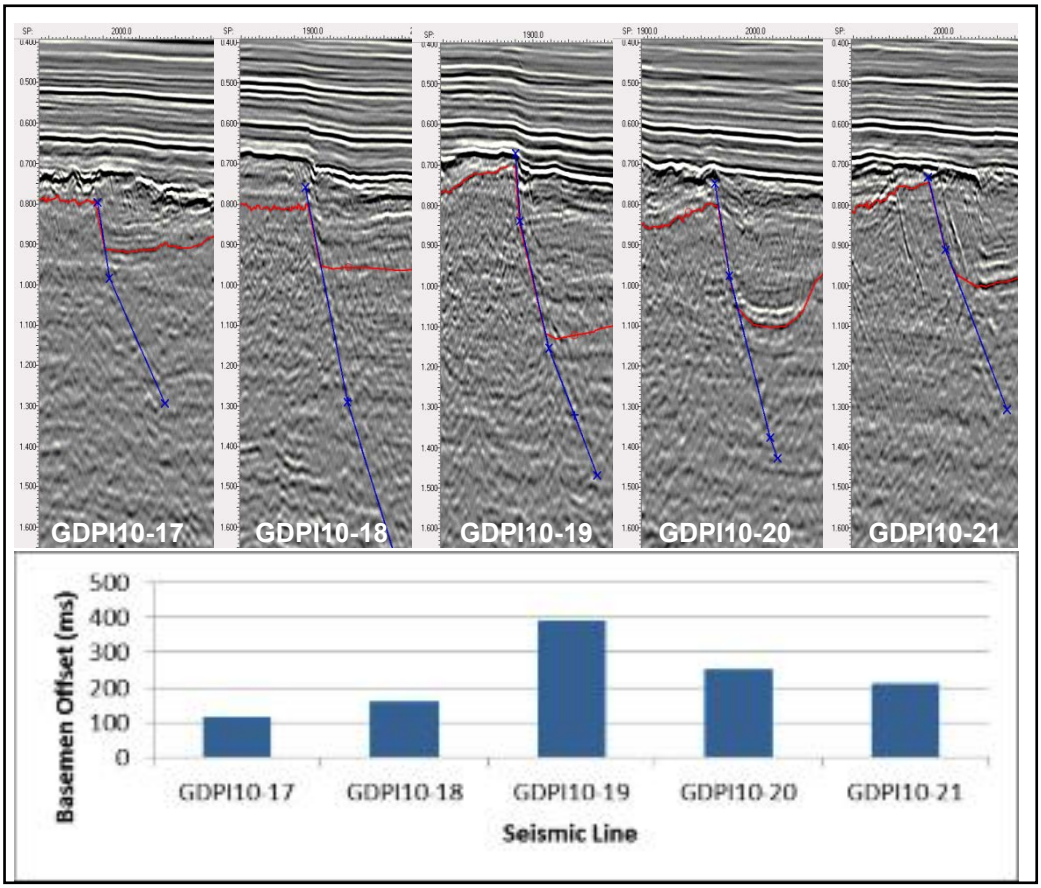

Figure 3.4 **Fault on the Southern Terrace showing vertical horizon offset along strike. This fault is steep and does not significantly change apparent dip angle, therefore vertical offset is a reasonable proxy for total apparent displacement. The unimodal distribution of vertical offset shown is also true of total apparent displacement along strike.**

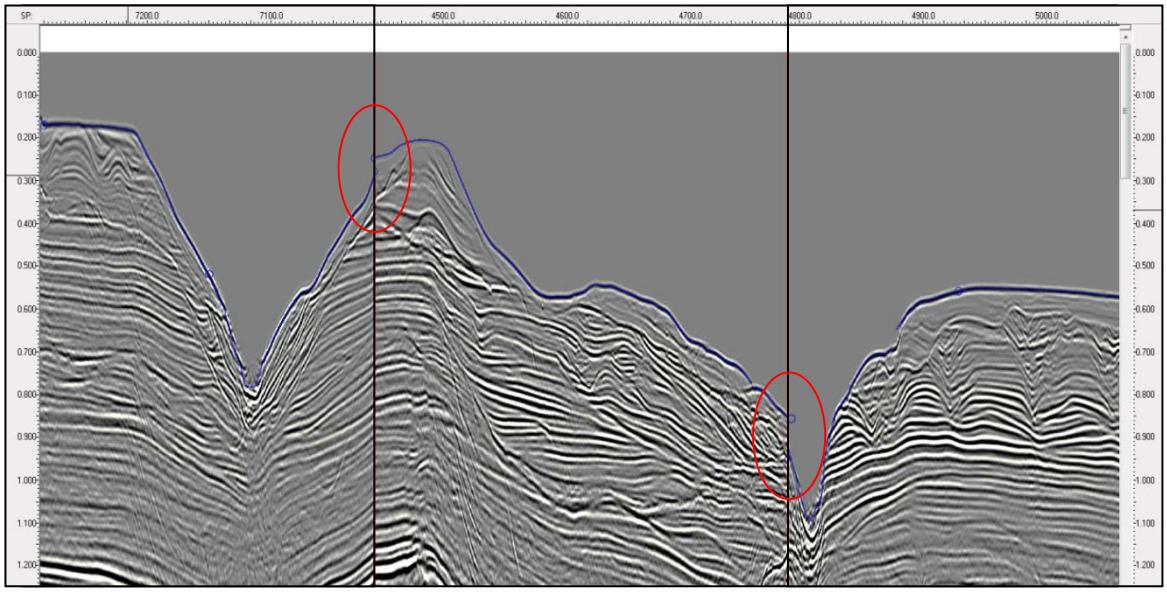

Figure 3.5 Merged seismic lines that meet at the vertical black lines (left to right, GDPI10-903, -62 and -902) show mis-ties (red ovals) of seismically imaged seafloor (blue horizon) between lines acquired perpendicular to and in proximity to canyons. The mis-ties shown are 30 ms and 91 ms respectively.

- *Single-Step Flex Gridding* – This is a spline gridding technique that combines minimum curvature and minimum tension algorithms. The aim of this combination is to reduce the tendency of minimum curvature grids to overshoot or undershoot in areas where the gradient changes within small distances. The strength of this algorithm is producing grids from data with an uneven distribution.

  Gridding using this algorithm was performed for grid cell sizes of: 50 m, 200 m, 500 m, 750 m and 1000 m, with tension and smoothing parameters set to average values. The finer grids of 50 m and 200 m produced rugose surfaces, that closely mimic the interpretation along the seismic line (Figures 3.6 and 3.7) but have surface variability between lines that is unsupported by interpretation and appears geologically unreasonable (Figure 3.8A). The coarse grid of 1000 m produces a smooth surface with too much averaging of the interpretation along the seismic line (Figures 3.8B and 3.9). The grids of 500 m and 750 m are very similar with a combination of moderate smoothing of the interpretation along the seismic lines and reasonable interpolation between seismic lines (Figures 3.10 and 3.11). Overshooting and undershooting observed in the early phases of gridding were significantly reduced when the horizon was mapped along the fault plane. Both grids display a scalloping along the fault trace between seismic lines, where the grid on the up-thrown side of the fault dips down between seismic line interpretations and on the downthrown side of the fault the grid curves up between seismic line interpretations. The 750 m grid is less affected by the scalloping and is therefore the preferred grid cell size for the single-step flex algorithm. Two-step flex gridding and oriented kriging grid algorithms were tested to remove the scallop effect.

- *Two-Step Flex Gridding* – Flex gridding using an initial fine cell size (20 m) without gridding of the offset fault planes and then smoothed by a second coarse gridding (500 m or 750 m) including the offset fault planes results in surfaces that closely correspond to the interpretation along seismic lines, including faulted areas with large offsets. The final grid extrapolates smoothly between seismic lines, and closely honours the interpretation. The advantage of the two-step process is that the initial gridding generates numerous points on the up-thrown and down-thrown side of the fault away from the seismic line, which minimise scalloping when the coarser grid is generated.

  The initial flex grid (20 m) was generated with minimum tension, maximum smoothing, and null values within fault polygons resulting in a high-resolution grid that smoothly interpolates between seismic lines, without connection on either side of the faults (Figure 3.12A). The 20 m grid was used as input into a second round of flex gridding with a cell size of 750 m, average tension and smoothness parameters, with gridding allowed within the fault polygons (Figure 3.12B). This second step retains a smooth accurate trend of the interpretation data while reducing high-frequency undulations related to automated seismic amplitude picking (Figure 3.11), and greatly reducing the scalloping along the fault trace (Figures 3.13, 3.14, 3.15). The final grid generates a small file size, convenient for further manipulation within the Kingdom software or other packages. This two-step technique is the method used to generate the interpreted grids.

- *Simple Kriging with a Circular Search Radius* – Geostatistical gridding technique that allows a map to be created from sparse data. Simple Kriging was tested in preference to Ordinary Kriging and Universal Kriging, gridding algorithms also available within Kingdom. While the Ordinary Kriging is meant to be more accurate than Simple Kriging, Simple Kriging was tested for the following reasons:

  - In simple tests there was no observed variation in kriging results (Figure 3.16);
  - The other kriging methods provided no additional parameters for modification;
  - Universal Kriging is better for data with a directional bias in data collection; and,
  - Simple Kriging is meant to produce smoother grids.

  Gridding using this algorithm was performed for grid cell sizes of: 200 m and 500 m, with tension and smoothing parameters set to average values. The kriging grids were very similar to the flex grids on the platform, smoothing the high-frequency, low-amplitude undulations. However, the kriging performed poorly where the basement interpretation had high-frequency topographic variability and at fault traces (Figures 3.17 and 3.18).

  .

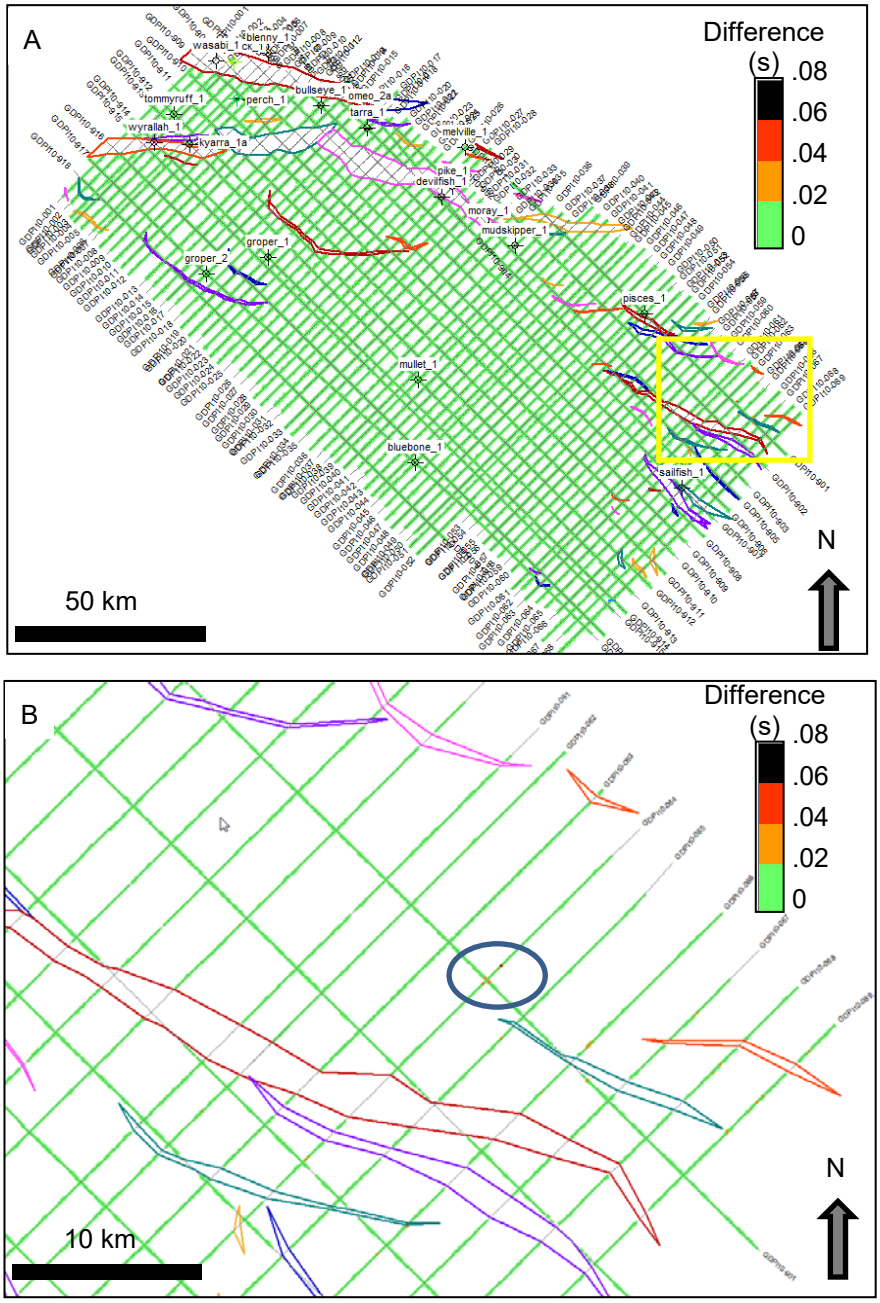

Figure 3.6 **Difference between the flex grid (200 m grid cell size) and picked horizon across the entire survey (A) and zoomed in to a smaller part of the survey (B). The yellow box in (A) shows the zoomed area, (B). The difference is generally < 0.02 s, but can be up to 0.08 s in very isolated areas (circled).**

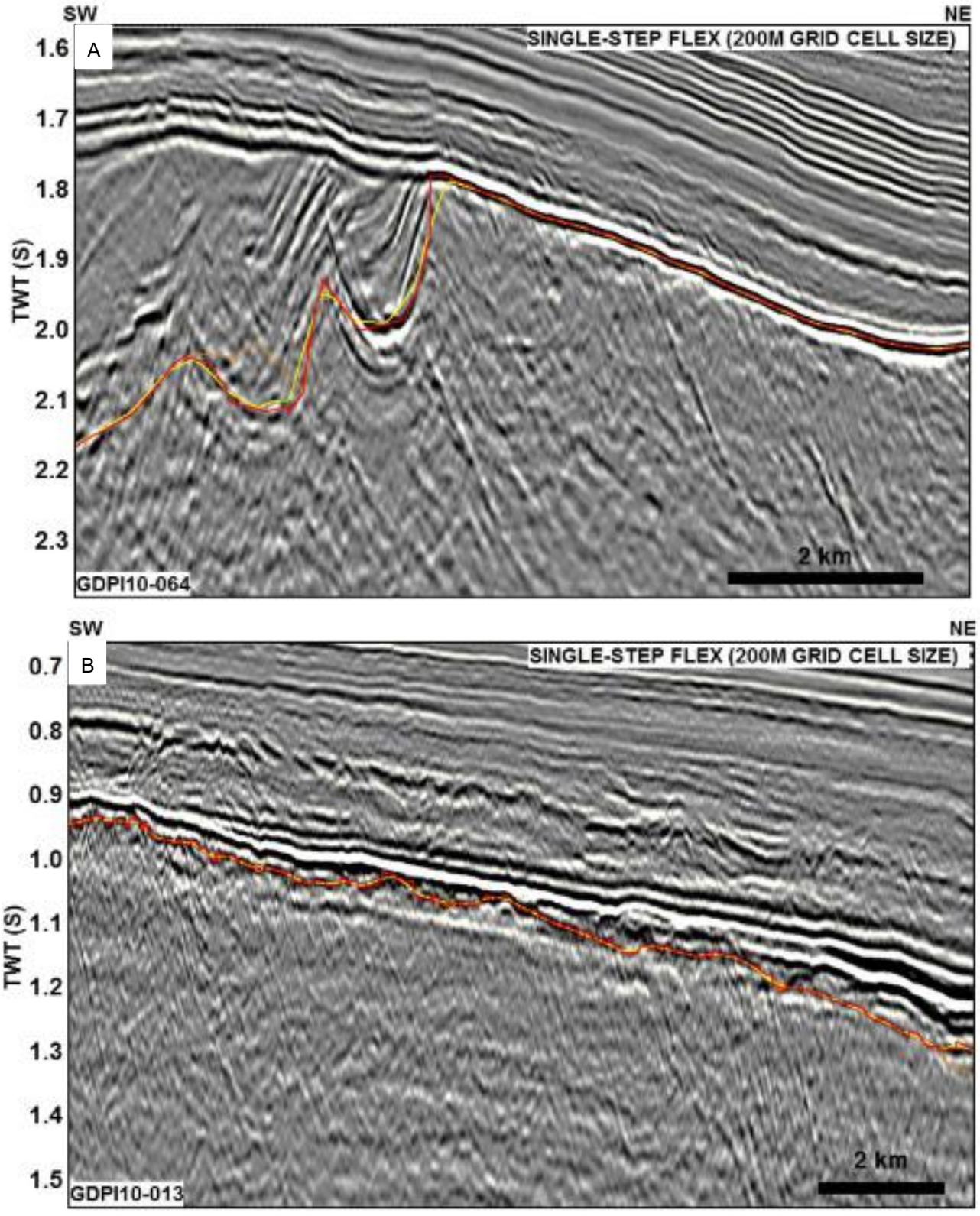

Figure 3.7 Examples from seismic lines GDPI10-64 (A) and GDPI10-13 (B) showing the close correlation between the interpreted basement horizon (red) and the surface derived from the single-step flex gridding algorithm with a 200 m grid cell size (yellow).

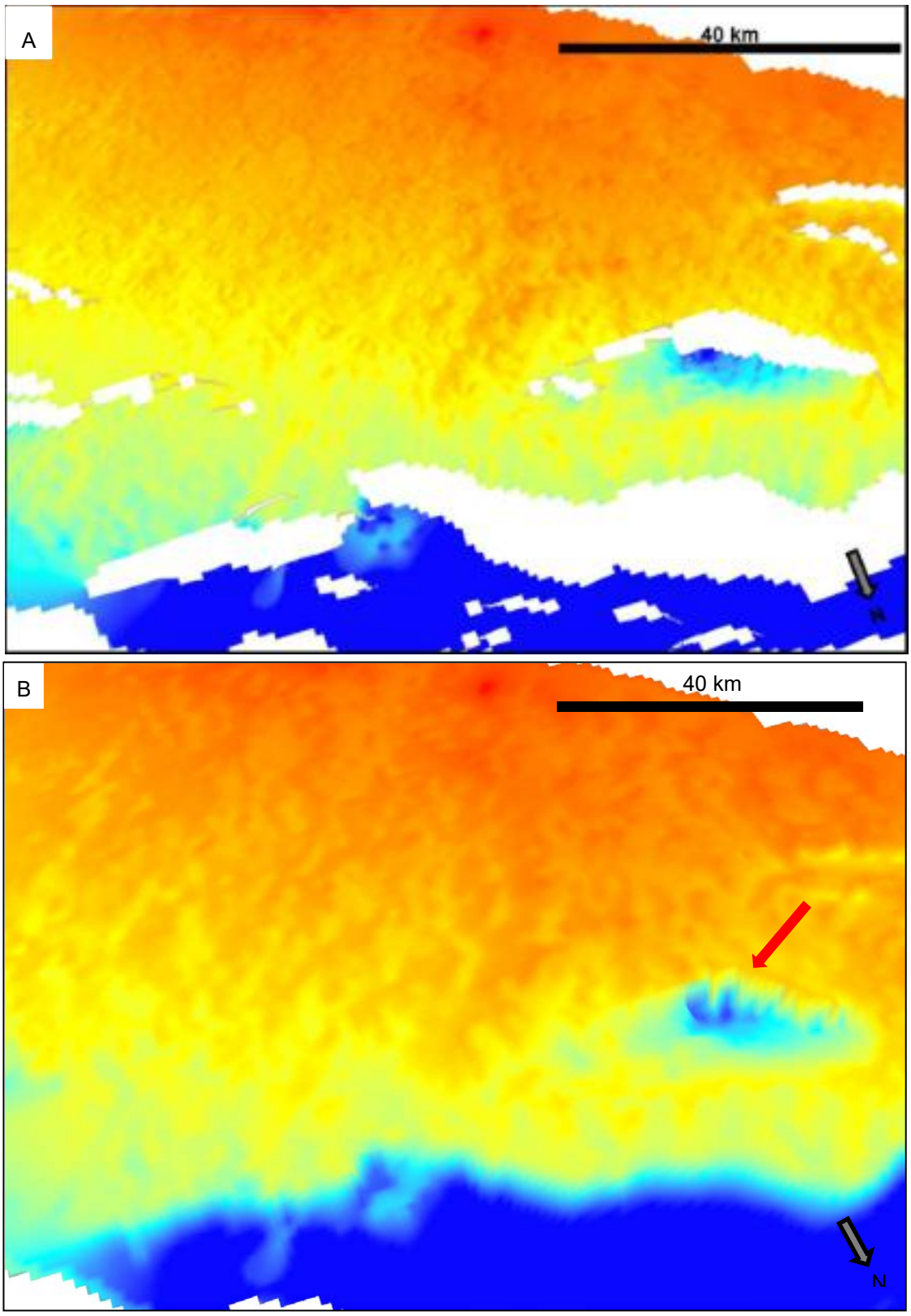

Figure 3.8 Three-dimensional ArcScene perspective view of a portion of the Top Basement surface generated using the single-step flex algorithm with a 200 m (A) and 1000 m (B) grid cell size. High-frequency gridding artifacts are present on the platform in the 200 m grid. Platform features on the 1000 m grid are smooth, while scalloping occurs along the fault plane in the intra-platform half graben (arrow).

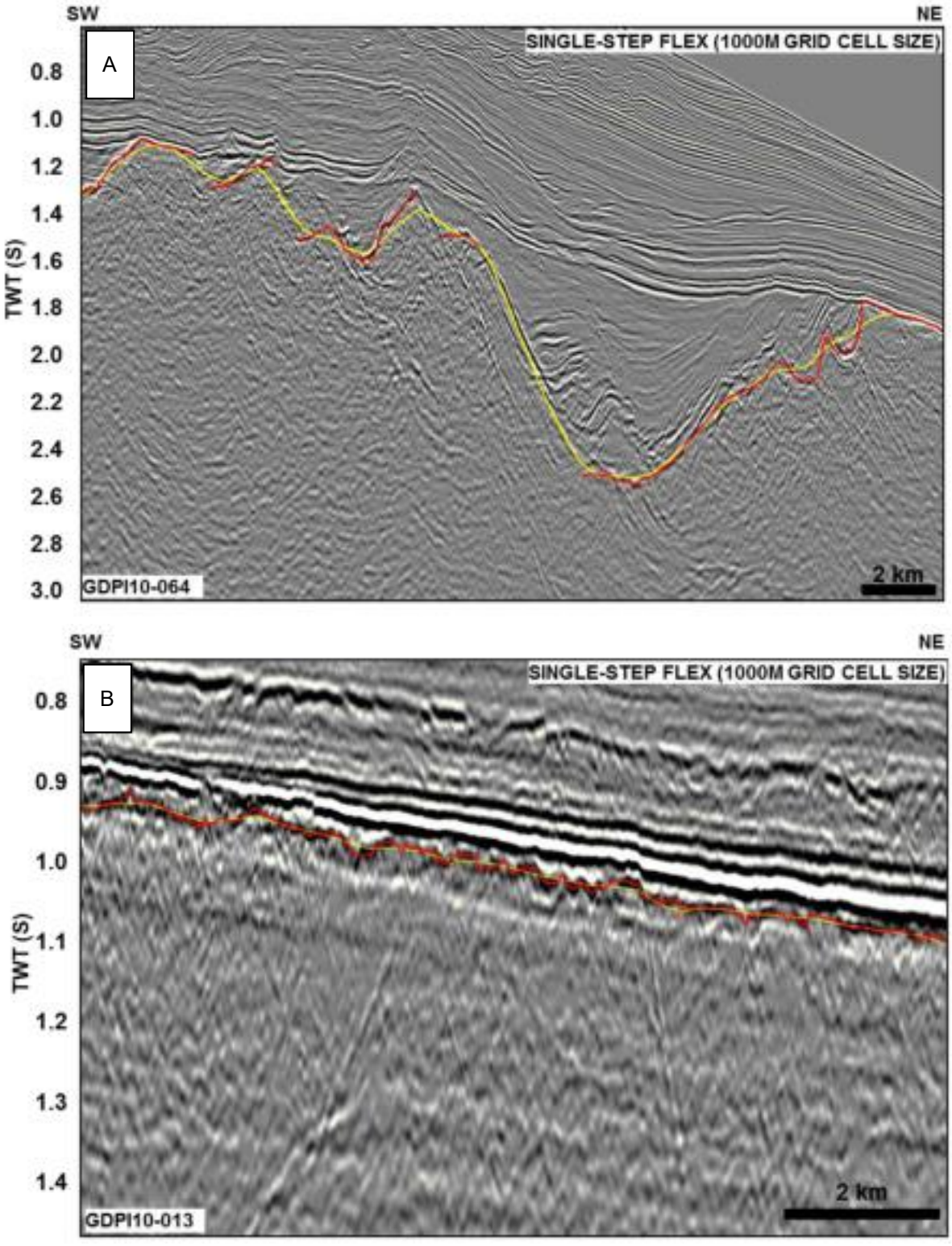

Figure 3.9 Examples from seismic lines GDPI10-64 (A) and GDPI10-13 (B) showing the correlation between the interpreted basement horizon (red) and the surface derived from the single-step flex gridding algorithm with a 1000 m grid cell size (yellow). The gridding is unable to track rapid changes in basement morphology, but does track up some fault planes.

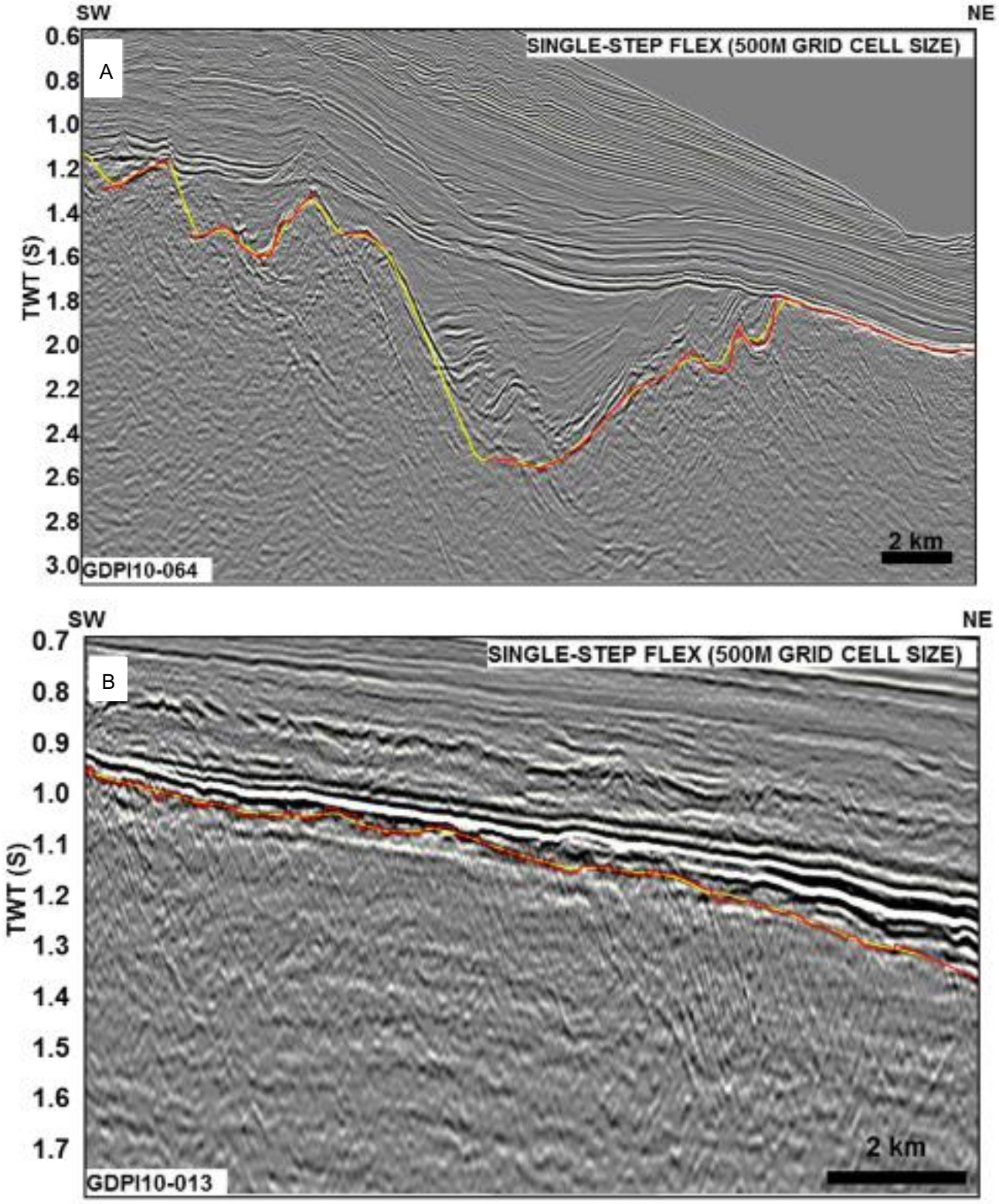

Figure 3.10 Examples from seismic lines GDPI10-64 (A) and GDPI10-13 (B) showing the correlation between the interpreted basement horizon (red) and the surface derived from the single-step flex gridding algorithm with a 500 m grid cell size.

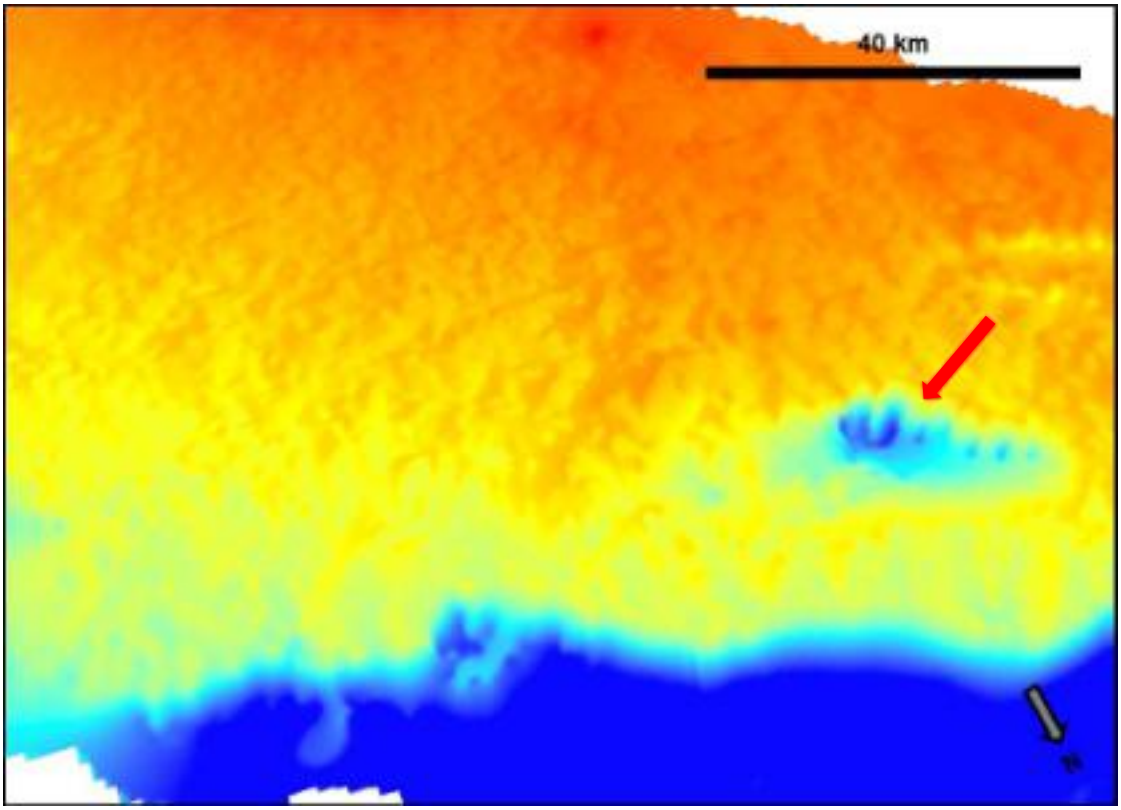

Figure 3.11 Three-dimensional perspective ArcScene view of a portion of the Top Basement surface generated using the single-step flex algorithm with a 500 m grid cell size. The resultant surface shows detail on the platform with scalloping along the fault plane in the intra-platform half graben (arrow).

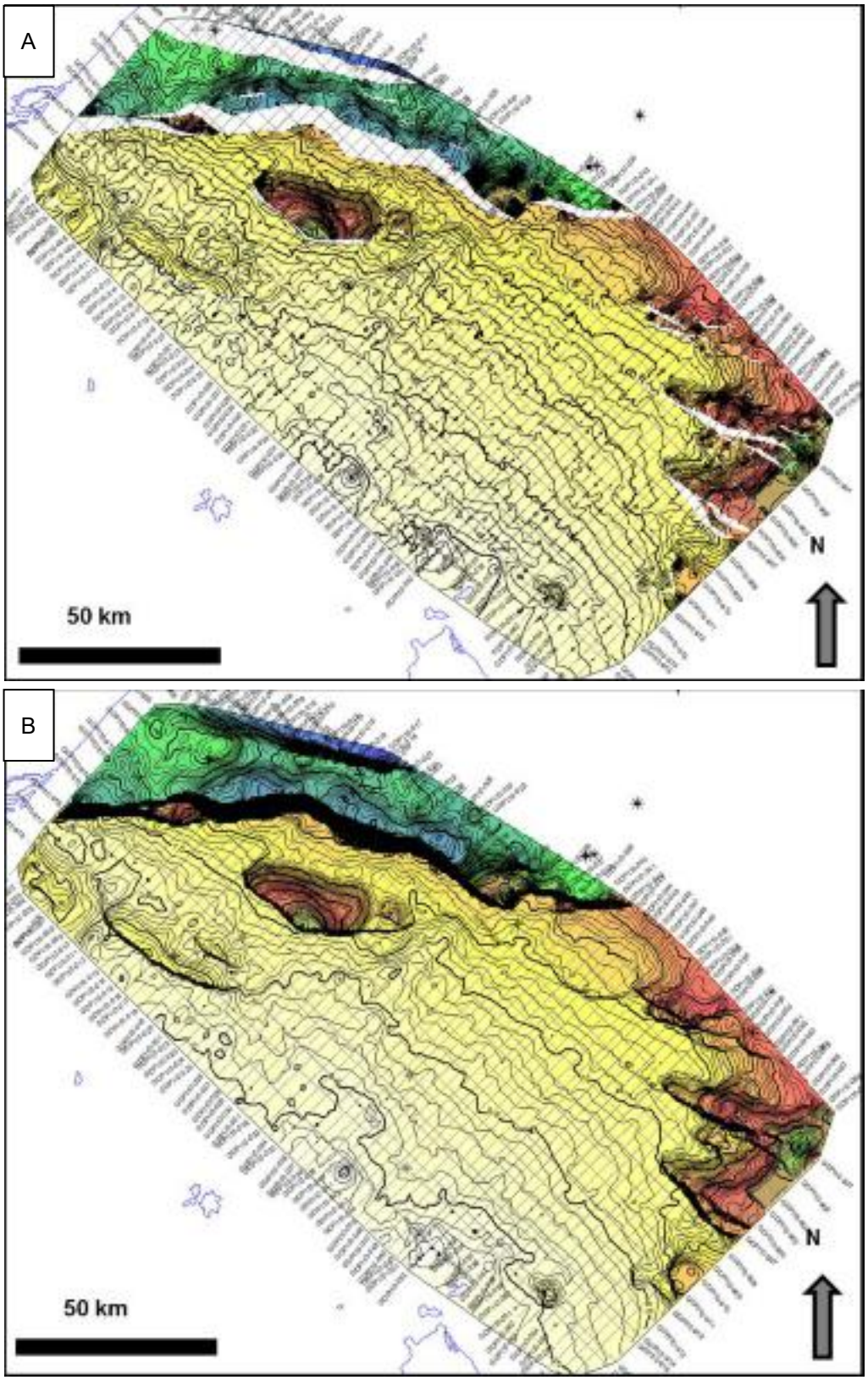

Figure 3.12 Structure contour map of the Top Basement surface generated during the two-step flex gridding workflow. (A) After the first step, with a 20 m grid cell size and no gridding within the fault polygons. (B) After the second step with a 750 m grid cell size. Contour interval is 50 ms.

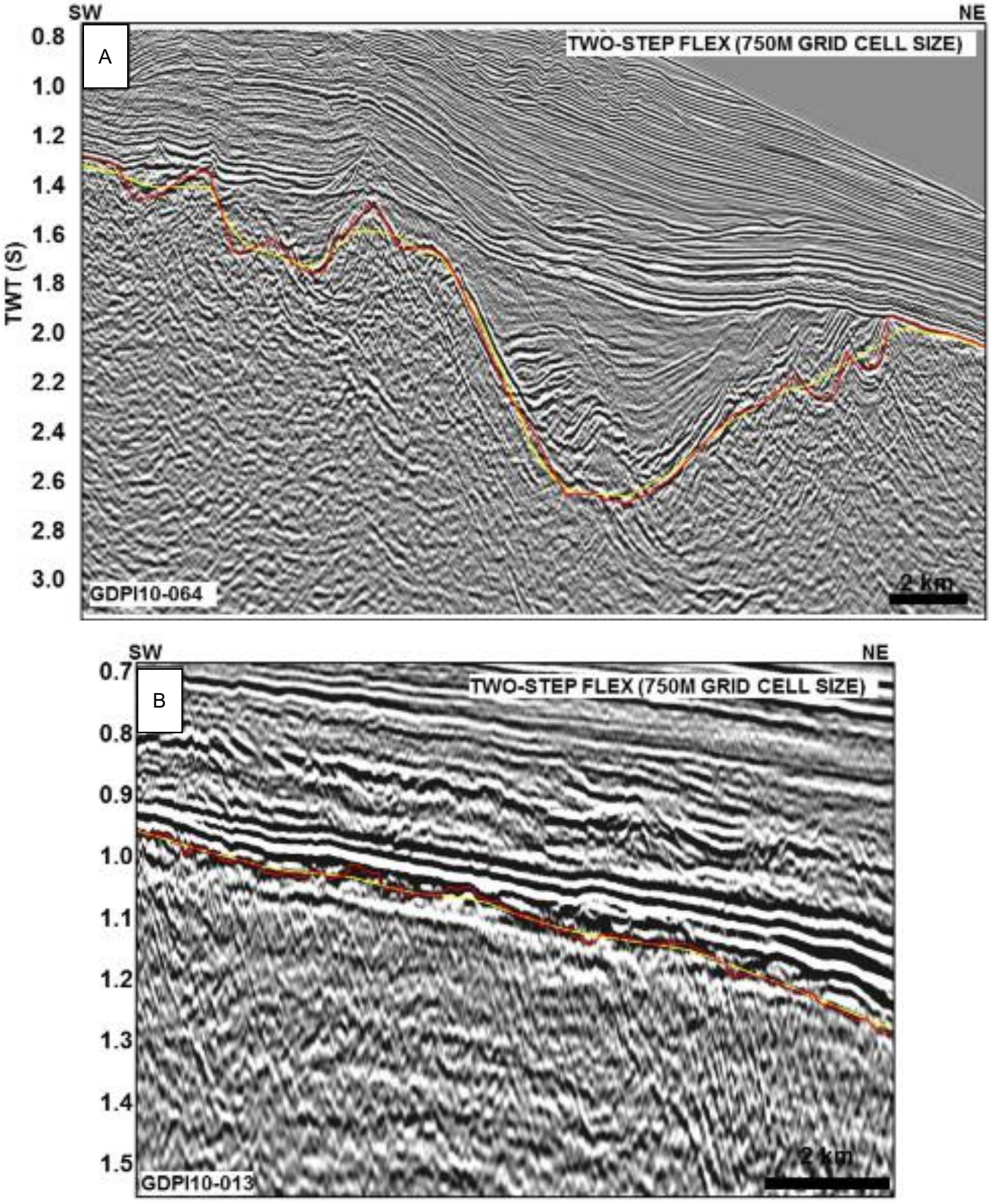

Figure 3.13 Examples from seismic lines GDPI10-64 (A) and GDPI10-13 (B) showing the correlation between the interpreted basement horizon (red) and the surface derived from the two-step flex gridding algorithm with an initial 20 m and second 750 m grid cell size.

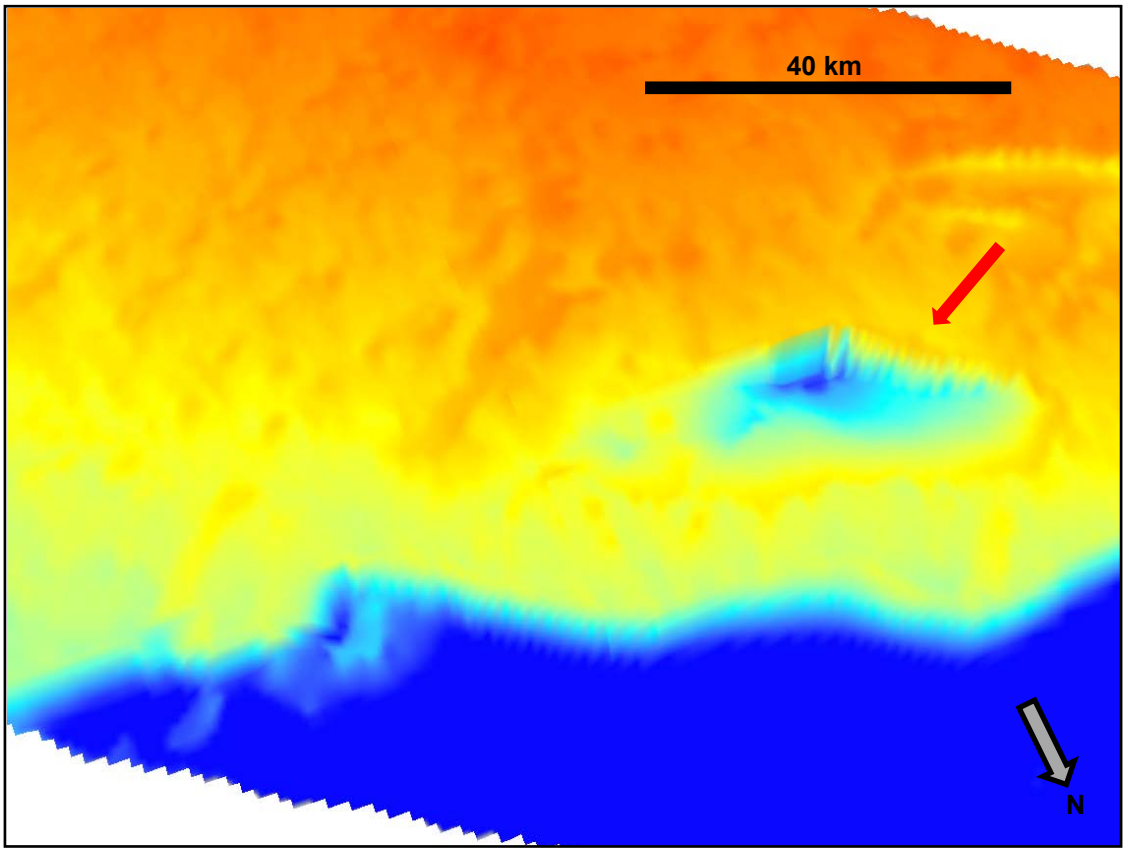

Figure 3.14 Three-dimensional perspective ArcScene view of a portion of the Top Basement surface generated using the two-step flex algorithm with an initial 20 m and second 750 m grid cell size. The resultant surface shows some smoothing on the platform while the amplitude of the scalloping along fault traces is reduced, particularly along the fault plane in the intra-platform half graben (arrow).

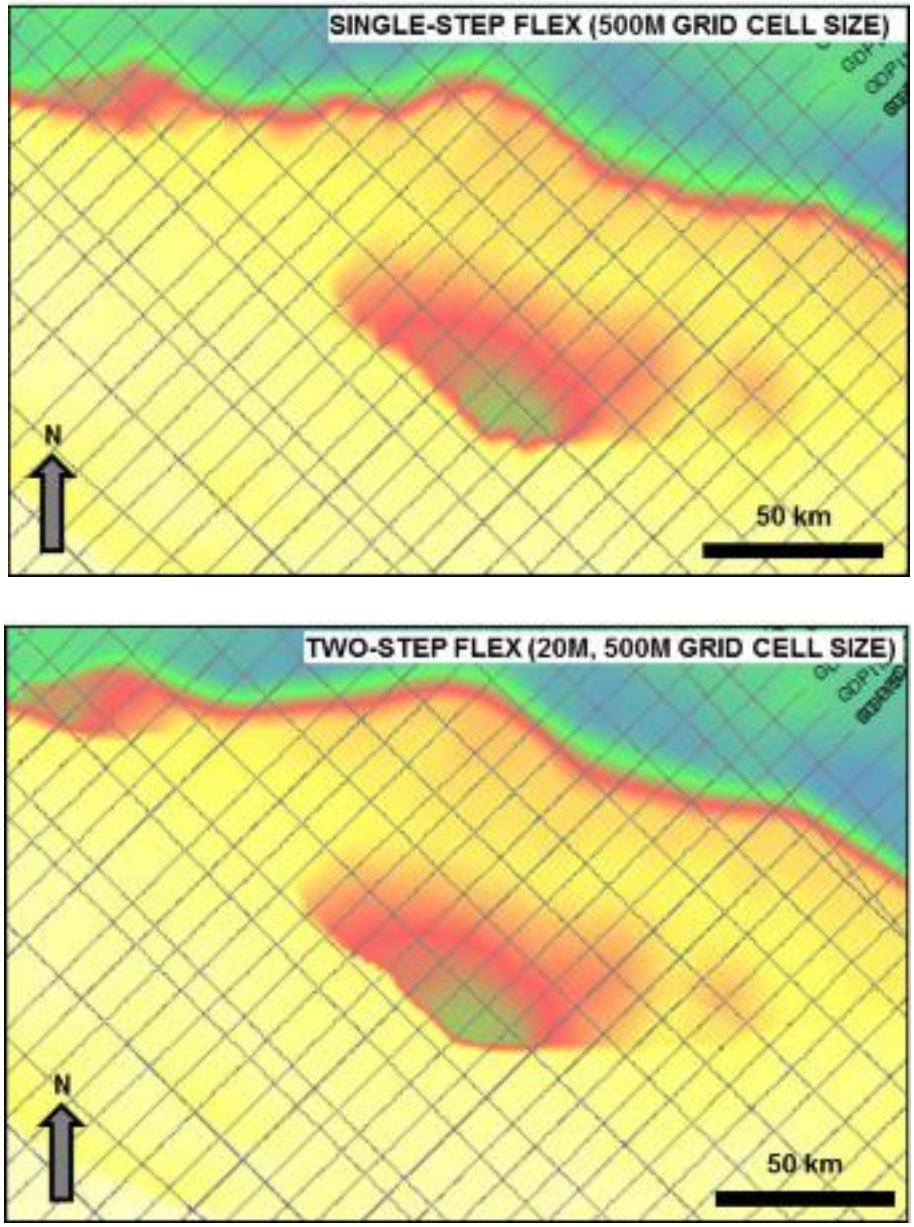

Figure 3.15 Comparison between the single- and two-step flex gridding methods with a final grid cell size of 500 m. Scalloping along the fault trace is reduced by the two-step process.

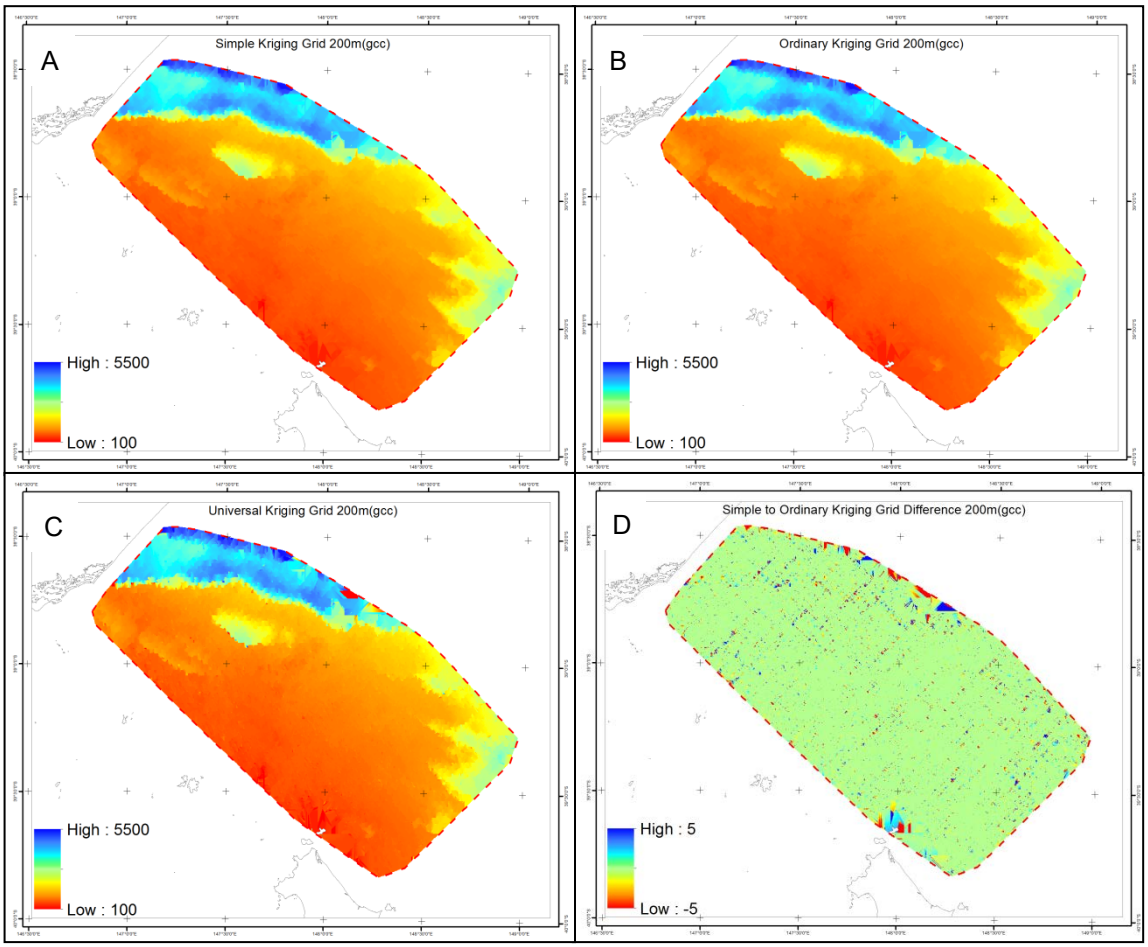

Figure 3.16 Kriging maps of the Top Basement horizon in milliseconds (TWT) with grid cell size of 200 m. Simple Kriging (A), Ordinary Kriging (B) and Universal Kriging (C) produced a similar coarse grid. The difference between the Simple and Ordinary Kriging grids (D) is minor.

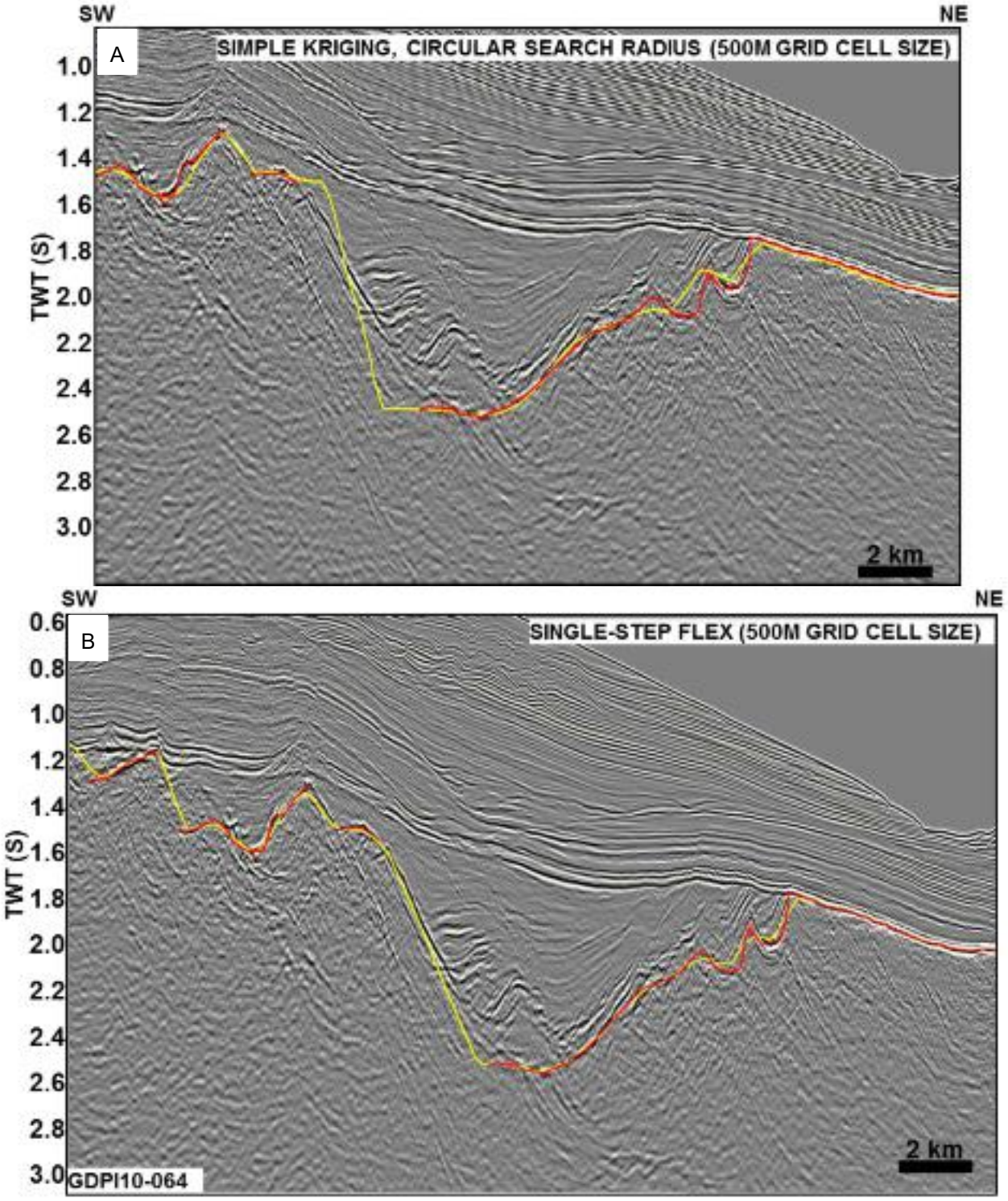

Figure 3.17 Examples from seismic line GDPI10-64 showing the correlation between the interpreted Top Basement horizon (red) and the surface derived from Simple Kriging (A) and single-step flex (B) gridding algorithms with a 500 m grid cell size. The kriging grid performs poorly along the fault trace and where the Basement amplitude variations are increased.

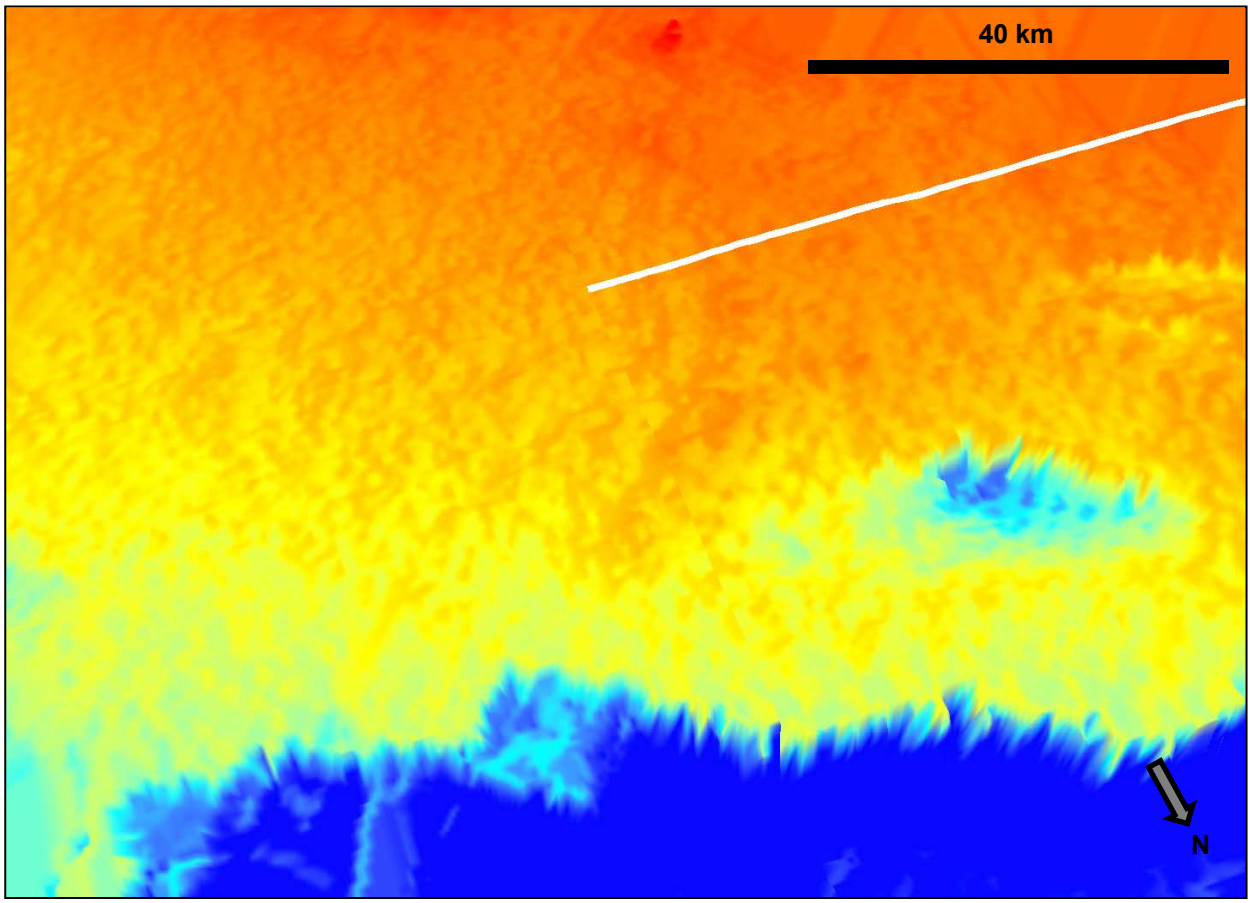

Figure 3.18 Three-dimensional perspective ArcScene view of a portion of the Top Basement surface generated using Simple Kriging with a circular search radius and a 500 m grid cell size. The resultant surface shows detail on the platform, similar to the single-step flex grid. Scalloping along the fault traces is severe, particularly along the Foster Fault System (arrow). The white line is an imaging artifact.

- *Simple Kriging with a Directional Search Ellipse (Anisotropic)* – This algorithm was tested as a method for the reduction of scalloping along the fault traces. The grid is generated using an elliptical data search, with the long axis parallel to the average trend of the faults. A series of grids were generated with the ellipse oriented E-W, N60°W or NW-SE to represent the range of fault trends observed along the Foster Fault System and along the intra-platform faults. In addition to the orientation of the search ellipse, the width was also varied to allow for strong continuity (thin) or less continuity (thick) along the major axis. In general, the grid along the faults is degraded except where the fault orientation is parallel with the long axis of the ellipse (Figures 3.19 and 3.20).

The interpreted horizons were gridded using the two-step flex gridding process with an initial 20 m grid and a second 750 m grid. After generation and depth conversion of the grids (see Section 7), they were exported from the Kingdom 2d/3dPak (version 8.7) software in a zmap format and imported into ArcGIS (version 10.0.0). Within ArcGIS the grids were clipped to the seismic limits and the polygon outlining digitised extent of the interpreted horizons. Internal grid clipping also occurred where the surface was interpreted to be absent. This includes where the surface was absent due to erosive removal or non-deposition of the unit, as interpreted from seismic (Figure 3.21). After clipping, the surface was exported in zmap format from ArcGIS (version 10.0.0) and imported into Kingdom 2d/3dPak (version 8.7).

A correction surface was generated from the difference between the depth-converted grids and the formation pick in the well. The correction was applied to the depth converted grids and the resultant grid files are identified by the suffix *_tied*. The correction grid at any surface is generated at well locations only, and is less constrained away from control points.

3.4.4 Isochron/Isopach Generation

Isochron and isopach grids were generated using the Kingdom 2d/3dPak (version 8.7) grid calculator on the gridded time and depth surfaces. The grid calculator produced a grid of the upper surface grid subtracted from the lower surface grid, and is suitable where the two grids are consistently present. The grid cell size of 750 m was conserved throughout this process and null values were produced where there was only one grid value present. Within the name of the isochron/isopach the upper surface is identified by the first two numbers and the lower surface is defined by the second two numbers such that:

- 01 corresponds to FrOG Tech 01 Seafloor grid;
- 02 corresponds to FrOG Tech 02 Near Top Bassian Rise Unit 2 grid;
- 03 corresponds to FrOG Tech 03 Top Bassian Rise Unit 3 grid;
- 04 corresponds to FrOG Tech 04 Top Bassian Rise Unit 4 grid;
- 05 corresponds to FrOG Tech 05 Top Bassian Rise Unit 5 grid;
- 06 corresponds to FrOG Tech 06 Top Early Oligocene Wedge grid;
- 07 corresponds to FrOG Tech 07 Top Latrobe Group grid;
- 08 corresponds to FrOG Tech 08 Top Halibut Subgroup grid;
- 09 corresponds to FrOG Tech 09 Top Golden Beach Subgroup grid;
- 10 corresponds to FrOG Tech 10 Top Emperor Subgroup grid;
- 11 corresponds to FrOG Tech 11 Top Strzelecki Group grid;
- 12 corresponds to FrOG Tech 12 Top Pre-Strzelecki Group grid; and,
- 13 corresponds to FrOG Tech 13 Top Basement grid.

In order to generate more complete isochrons/isopachs of the upper bounding horizon to the base of the respective stratigraphic interval, merged horizons were created. This allowed for the isochron/isopach to be calculated over the full extent of the upper bounding horizon, including areas where the base horizon terminates through onlap or downlap (Figure 3.21). Merged surfaces were generated by substitution using the grid calculator. The grid calculator produced merged surfaces using the shallowest depth/time value from a defined set of surfaces at any given location, where none of the set of surfaces was present, the value is null. For example, in Figure 3.21, to calculate the BR3 isopach, a merged surface was first calculated for the base of the isopach. Where Top Latrobe Group (green) exists, it was retained in the merged grid. If Top Latrobe Group was absent (in this case due to onlap), then the depth or time value for the next available surface in stratigraphic order was substituted (in this case the Basement surface; yellow).

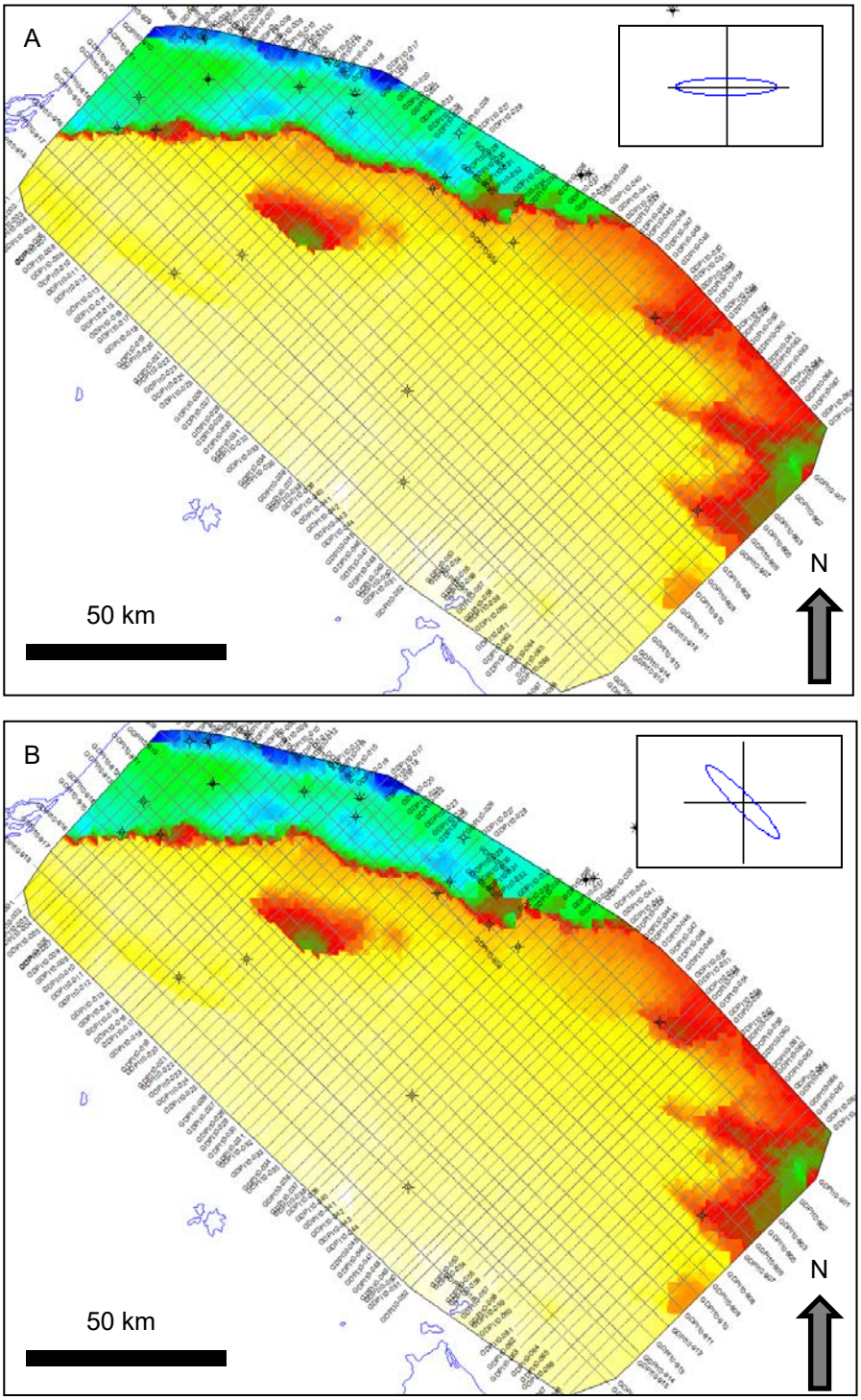

Figure 3.19 **Structure map of the Top Basement surface generated during gridding by Simple Kriging with a directional search ellipse set at E-W (A) and NW-SE (B). The resultant surface performs poorly along the fault trace in both examples. Ellipse axes are 30,000 X 5,000 and the grid cell size is 500 m.**

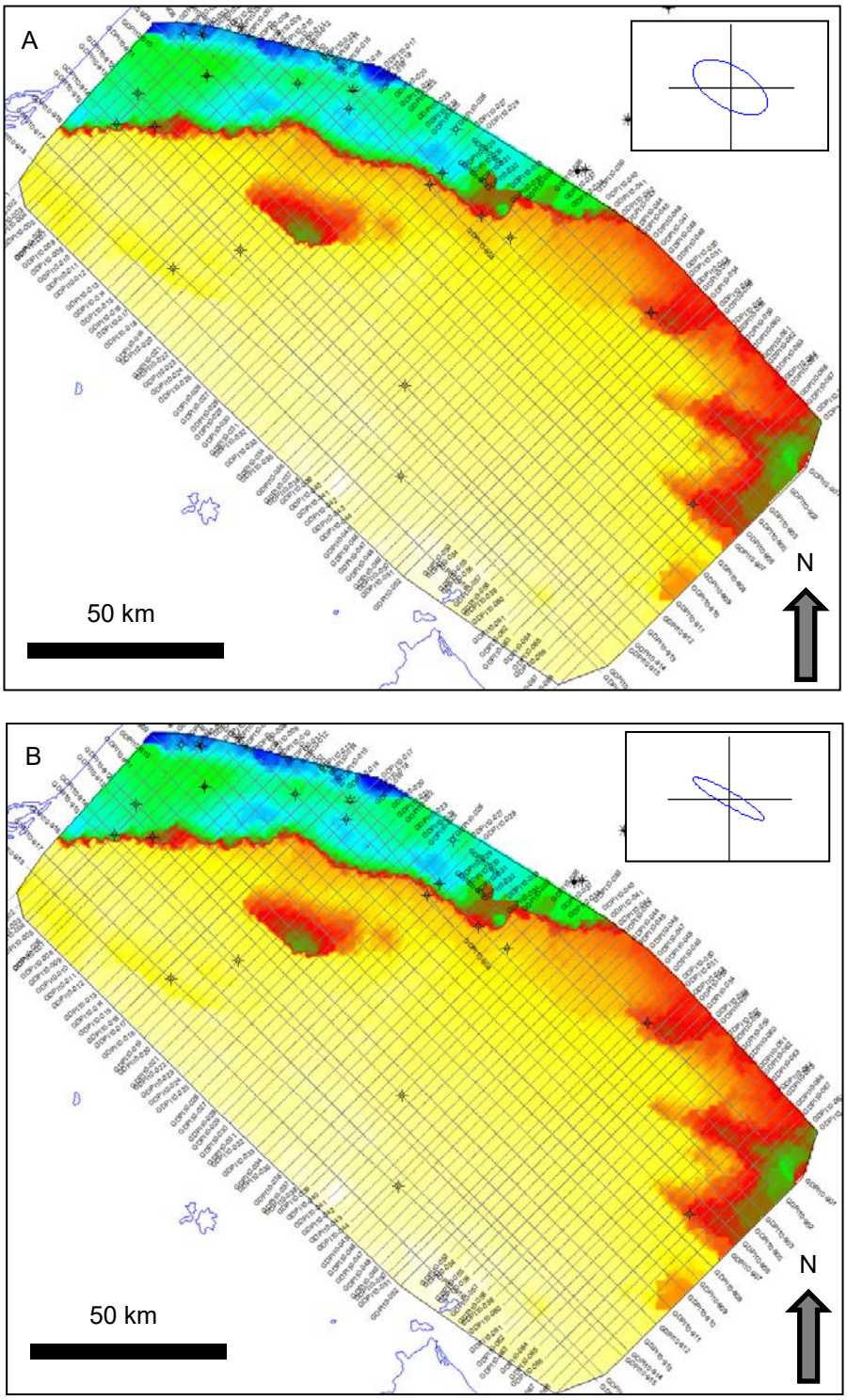

Figure 3.20 **Structure map of the Top Basement surface generated during gridding by Simple Kriging with a directional search ellipse oriented N60°W. The search ellipse axes are 40,000 X 20,000 (A) and 40,000 X 5,000 (B). The grid cell size for both examples is 500 m.**

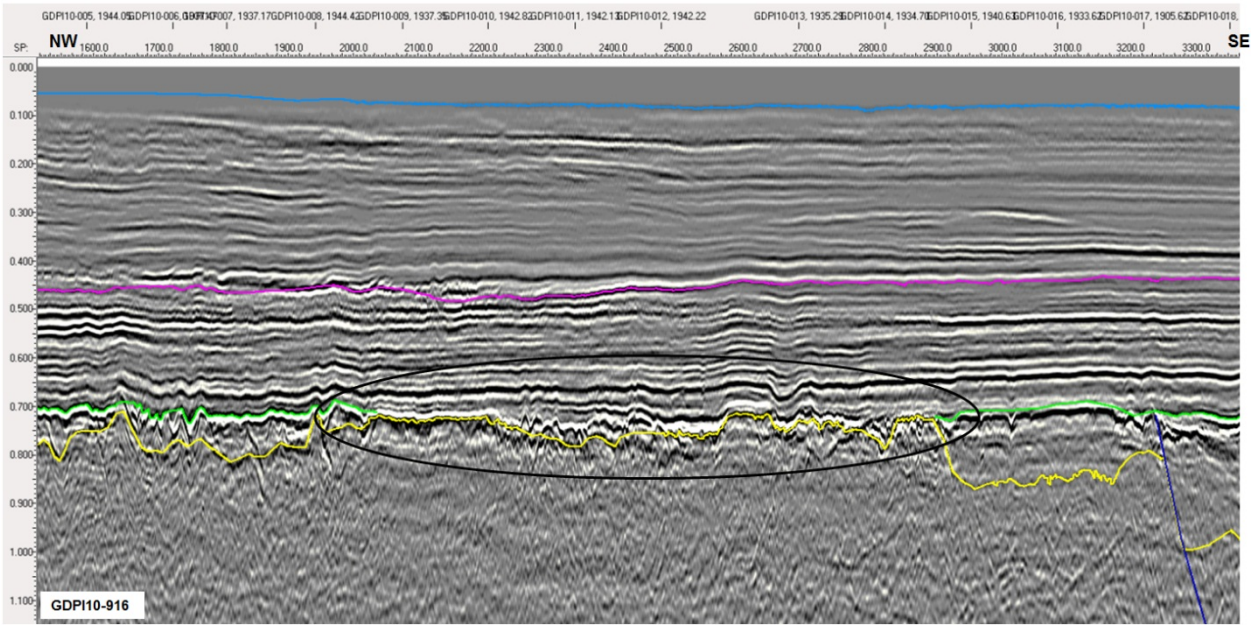

Figure 3.21 Local areas of non-deposition (black oval) of the Top Latrobe Group occur within the greater area of Latrobe Group deposition. Areas like these were clipped out during the generation of grids. Horizons shown include Seafloor (dodger blue), Top Bassian Rise Unit 3 (BR3; magenta), Top Latrobe Group (green), Basement (yellow). To calculate the BR3 isopach across these areas, the Top Latrobe Group is merged with the Top Basement surface. Vertical scale is in seconds (TWT).

The grid cell size of 750 m was conserved through the merging process. Merging by substitution occurred on six surfaces used in isochron/isopach calculations (Appendix 6). Isopach grids were produced with grids either corrected or uncorrected to well ties (Section 3.4.3, 7, and Appendix 6). Corrected grids were used if the generated isopach values appeared realistic and did not display a trend matching the applied correction. A bias could be manifest as a regional thinning trend reflected not in the change in unit thickness, but instead indicative of a stronger regional correction applied to one of the grids used in the isopach calculation. These corrected isopachs have the suffix _tied in the isopach name. Merged grids used to create corrected isopachs were merged from corrected grids only.

Following the creation of the isochron/isopachs, the grids were exported in zmap format, and imported into ArcGIS. Within ArcGIS the isochron/isopach grids were clipped:

- Within the project area boundary; and
- Within the "digitized extent" polygon for the horizon(s) defining the top of the isochron/isopach, so as
- To remove areas of non-positive values, zero edges; and
- To remove areas within the extent and project area polygons where the upper surface was absent.

After clipping, the surface was exported in zmap format from ArcGIS (version 10.0.0) and re-imported into Kingdom 2d/3dPak (version 8.7).

3.5 Data Delivery

The primary mode of data delivery is via the Kingdom seismic project. FROGTECH has loaded the GDPI10 2D seismic, and entered well data pertinent to this study to the Kingdom project supplied by DPI, which covers the entire Gippsland Basin. Quality control of the pre-existing data has only been undertaken within the study area. Well data available in the Kingdom project is also summarised in tables in this report (Tables 2.4, 2.5, 2.6, Appendix 3) and as Excel spreadsheets (Appendix 4). Raw stack and migration data provided by DPI are loaded and can be accessed as an option in the vertical display.

Interpretative data included in the Kingdom project include the final interpreted stratigraphic horizons in two-way time (TWT), gridded stratigraphic surfaces, isopachs and faults in TWT and depth and the associated interval and average velocity grids. Polygon and line datasets stored as culture in the Kingdom project show the interpreted morphology and distribution of basement faults, basin outlines, risk elements and stratigraphic pinchouts. 2D average velocity profiles derived from the 3D velocity model (Section 7) are loaded into the project and can be viewed as an attribute of each seismic line.

A separate Kingdom project has been built to deliver the velocity model (Section 7). This project contains all the input velocity, horizon and well information required to generate the velocity volume. Data contained in the VELPAK module are the horizon construction surfaces, velocity information from the key wells, PSTM stacking velocities and the VELPAK model. Grids of the depth, interval and average velocity for the construction surfaces only are contained in the 2D/3D module, as is the final average velocity volume.

To complement the Kingdom seismic project an ArcGIS project was created to deliver interpretative data, such as the gridded surfaces and isopachs in TWT and depth and their associated average and interval velocity grids. Interpreted line and polygon features of fault traces, basin outlines, risk elements and stratigraphic pinchouts are also provided in this format. Basic data in the ArcGIS project includes the GDPI10 seismic navigation, well locations, open file DEM, gravity and magnetic data, the current GCS permit boundary and general cultural data (e.g. coastline).

4 Tectonic Evolution of the Gippsland Basin

4.1 Regional Setting

The Gippsland Basin is one of Australia's most explored hydrocarbon provinces with the first commercial discovery dating back to 1965 (the Barracouta Field). The approximately east-west oriented basin has both onshore and offshore elements, with the Central Deep flanked to the north and south by fault-controlled terraces and platforms (Figure 1.1). The GDPI10 2D seismic survey covers most of the Southern Platform and Southern Terrace (collectively known as the "Southern Flank") on the southern margin of the basin.

Sediments in the basin range in age from Late Jurassic/Early Cretaceous to Recent, and reach a maximum thickness in the Central Deep of approximately 14 km (Figure 1.1). Early Cretaceous sedimentation was dominated by the non-marine volcaniclastics of the Strzelecki Group, followed by the largely non-marine siliciclastic succession of the Late Cretaceous to Eocene Latrobe Group, and the marine carbonate dominated Seaspray Group from the Oligocene to Recent (Figure 1.3).

Late Cretaceous to Eocene reservoirs (Gross, 1993) beneath the Top Latrobe Unconformity and, to a lesser extent, the intra-Latrobe reservoirs are estimated to contain approximately 85% of known hydrocarbons in the basin (e.g. Bishop, 2000). Coally intervals within the Latrobe succession are considered the main source rock as proposed by Brooks and Smith (1969) and supported by later studies (e.g. Burns et al., 1987; Moore et al., 1992; and Philp, 1994). Hydrocarbons below the Top Latrobe Unconformity are sealed by the regionally extensive marine calcareous mudstones and shales at the base of the Oligocene Lakes Entrance Formation (Bishop, 2000). The Lakes Entrance Formation generally thickens offshore to a maximum of greater than 400 m in wells of the Central Deep, thinning to less than 200 m in wells on the flanks and onshore to the west (O'Brien et al., 2008). The basin is considered mature for hydrocarbon exploration, with over 170 wells drilled offshore (mainly in < 200 m of water) and approximately 90,000 line km of 2D and more than 40 3D seismic surveys acquired across the basin (Department of Resources, Energy and Toursim, 2011). Exploration is not uniform across the basin, as the Southern Flank is relatively under-explored with only 24 wells drilled on the Southern Terrace and Platform (Figure 1.1).

4.2 Southern Margin and Tasman Rift Systems

The Gippsland Basin formed as one of a series of Mesozoic to Cenozoic depocentres along the southern margin of Australia (Figure 4.1). The basin was influenced by rifting associated with both the Southern Rift System (SRS; Fraser and Tilbury, 1979; Willcox and Stagg, 1990; Stagg et al., 1990; Norvick and Smith, 2001; Power, 2003) and the Tasman Rift to the east (Hayes and Ringis, 1973; Weissel and Hayes, 1977; Shaw, 1979; Royer and Rollet, 1997; Norvick and Smith, 2001). The SRS as described by Stagg et al. (1990) developed as a result of fragmentation of Gondwana, resulting in the extensional basins of the Southern Margin. Break-up of Australia and Antarctica was diachronous, commencing in the west during Late Jurassic, and propagating eastward during Early Cretaceous. Two distinct phases of extension with different orientations were proposed by Willcox and Stagg (1990). Phase one occurred in the Late Jurassic along a northwest-southeast azimuth, forming the Eyre, Ceduna and Duntroon sub-basins, and reactivating the Polda Trough. The second phase began in the Early Cretaceous (Figure 4.2), with a major change in the stress direction. The subsequent extension was oriented NNE-SSW and resulted in the development of the Otway, Sorell and Gippsland basins.

Alternatively, breakup of the southern Australian margin can be separated into three phases: Callovian-Tithonian, Cenomanian-Campanian and Eocene (Norvick and Smith, 2001). In phase one, rifting in the western Bight Basin (Callovian: 159 - 165 Ma) was followed by rift onset further east in the Duntroon, Otway and Gippsland basins during the Tithonian (142 - 146 Ma). The second phase commenced with uplift in eastern Australia, stress reorganisation and divergence of basin development in the Cenomanian (92 - 97.5 Ma). During this second phase, the Otway, Sorell and Great South basins (NZ) formed in a transtensional regime, while slow extension caused thinning of continental crust in the Bight and Otway basins. At this time, the Gippsland Basin represents the failed arm of the SRS as rifting preferentially continued west of Tasmania. Subsequently, rifting in the Gippsland Basin resulted from Tasman rifting to the south and east. Oceanic spreading began in the southern Tasman Sea (c. 85 Ma), followed by breakup south of the Bight Basin in the Early Campanian (c. 83 Ma; Sayers et al., 2001). The Tasman Sea rift tip propagated northward, passing the Gippsland Basin during the Early Campanian and on to the Coral Sea by the Paleocene (Norvick and Smith, 2001).

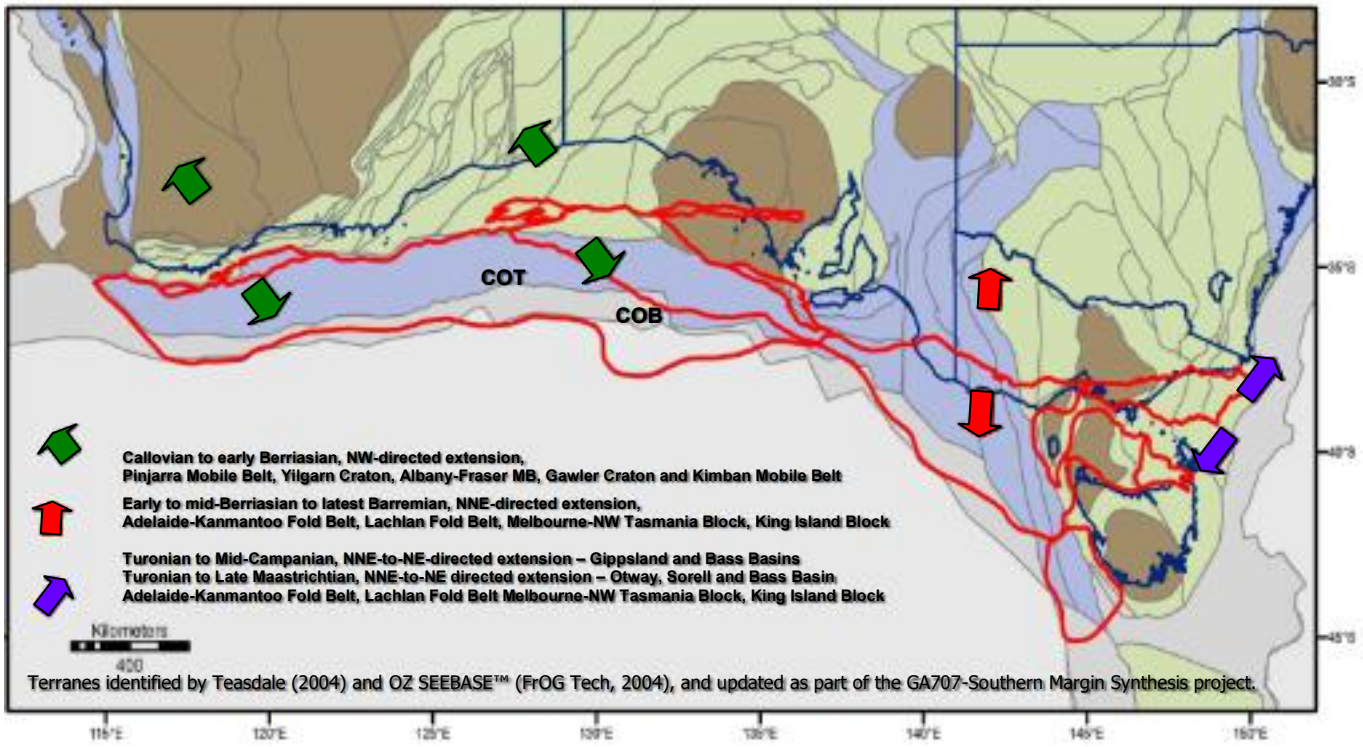

Figure 4.1 Basins of the Southern Rift System (red) including the Gippsland Basin (Blevin and Cathro, 2008).

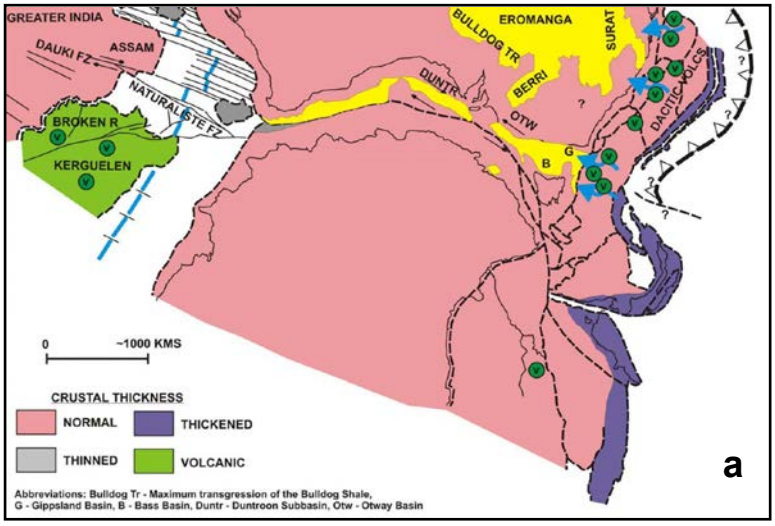

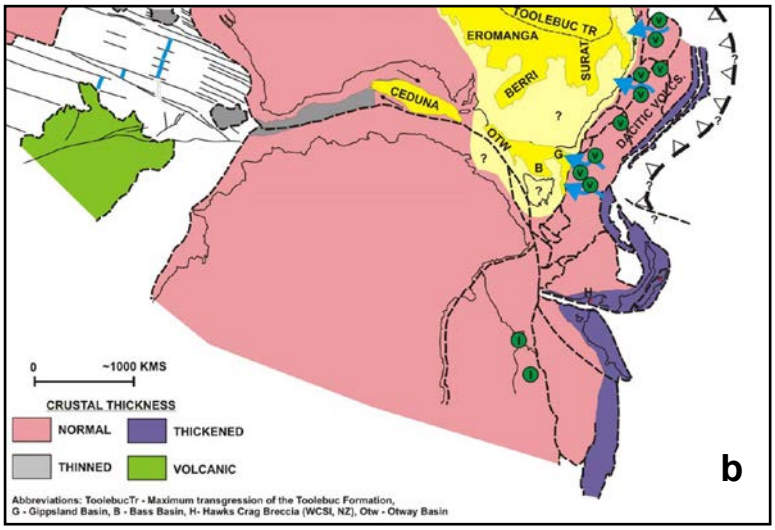

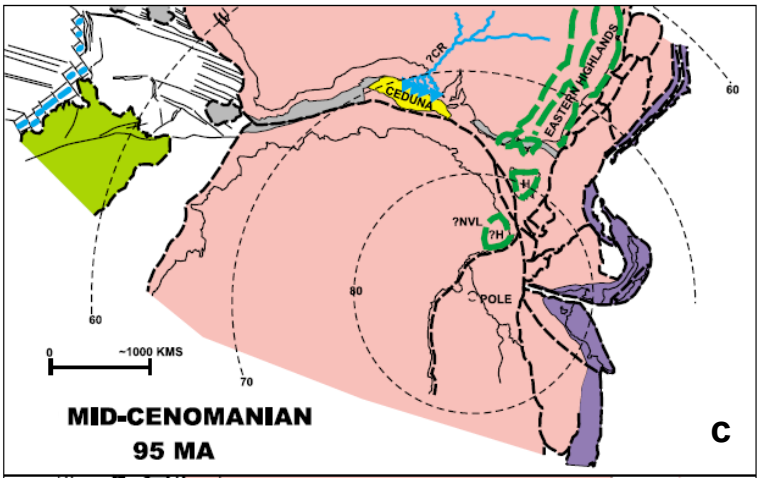

Figure 4.2 Plate tectonic reconstructions for the: (a) Late Aptian (110 Ma); (b) Late Albian (100 Ma) both from Norvick (2005); and (c) Mid Cenomanian (95 Ma) from Norvick and Smith (2001) illustrating the uplift that affected eastern Australia, Tasmania and Antarctica. GV - George V Coast, B - Bass, G - Gippsland, H - Hawks Crag Breccia, CR - Ceduna River.

Rifting in the Tasman Sea ceased in the early Eocene (Figure 4.3; c. 52 - 54 Ma) while slow spreading continued between Australia and Antarctica. Following this period of very slow spreading, the third and final tectonic phase was characterised by the change to fast spreading in the Southern Ocean during the middle Eocene (Cande and Mutter, 1982; c. 44 Ma) as Australia and Antarctica finally separated.

Building on these studies the Southern Margin Synthesis undertaken for Geoscience Australia (Blevin and Cathro, 2008) identified three major rift phases with a locus at different locations on the margin (see Figure 4.1):

- Callovian to Early Berriasian, NW-directed extension;
- Early to middle Berriasian to latest Barremian, NNE-directed extension; and,
- Turonian to Middle Campanian (Gippsland and Bass basins) and to Late Maastrichtian (Otway and Sorell basins) NNE- to NE-directed extension.

One transitional rift phase (Aptian - Albian) was also identified (Blevin and Cathro, 2008). While the entire SRS was the locus of crustal instability, rift basin formation is interpreted to propagate from west to east. It is suggested that evidence for the Mid-Callovian onset of extension in the Southern Margin is ambiguous (i.e. pervasive evidence of active faults) in the Otway, Bass and possibly the Gippsland basins. The oldest sediments in the Otway and Gippsland basin rifted successions, are represented by lacustrine and volcaniclastic deposits roughly coeval to the cessation of upper crustal extension in the Bight Basin. The second phase comprised the onset of extension in the Otway and Gippsland basins in response to a north-northeast-directed extensional stress – a shift from the earlier northwest-directed extension which affected the Bight Basin. The nature of the subsequent rift transition phase (Aptian - Albian) is also unclear, with differential movement on selected fault/fault sets across the southeastern basins. The final rift phase in the Late Cretaceous affected the south-eastern basins (i.e. Gippsland, Bass, Otway and Sorell basins) and was interpreted to be related to both the final fragmentation/clearance between Australia and Antarctica, and rifting in the Tasman Sea.

4.3 Basin Structure and Stratigraphy

The Gippsland Basin is an onshore and offshore, east-west trending rift basin on the south east coast of Victoria (Figure 1.1). The basin has an offshore area of approximately 35,000 km^2, and is separated from the Bass Basin to the west by the Bassian Rise. To the north and onshore, the Gippsland Basin is adjacent to the Eastern Highlands. A summary of the Gippsland Basin was presented in the Australian Margin Synthesis Report prepared for Geoscience Australia (Blevin and Cathro, 2008). Much of the information provided in Sections 4.3 and 4.4 has been sourced from the earlier synthesis report and references therein.

The Gippsland Basin was strongly affected by rifting in eastern Gondwana and breakup in the adjacent Tasman Sea. However, evidence of Late Jurassic extension onshore, suggests that initial development of the rift basin was linked to tectonic events involved in Southern Margin rifting. Power et al. (2001) interpreted and depth-converted more than 4000 km of 2D seismic and generated 15 regional horizon maps from Palaeozoic to late Tertiary to develop a 3D model for evolution of the Gippsland Basin. This work undertook a more detailed mapping approach than the previous work of Willcox et al. (1992) and used reprocessed Geoscience Australia deep seismic data.

Mapping of the latest Jurassic - Early Cretaceous rift phase (Strzelecki Megasequence) indicates that the main depocentres were the Central Deep (CD), Eastern Graben (EG), Northern Graben (NG), Southern Graben (SG) and SE Strzelecki Graben System (SGS; Figure 1 of Power et al., 2001). Faulting within the rift was oriented NE-SW, while faulting on the outer northern and southern rift flanks exhibits a more E-W trend (Figure 4.4). More than 10 km of Strzelecki Group sediments were deposited during this initial rift phase, representing the most significant amount of extension in the basin. Cenomanian uplift preceded the second phase of rifting with kilometre-scale uplift interpreted along eastern Australia, Tasmania and possibly Antarctica (Duddy and Green, 1992; Hill et al., 1998; O'Sullivan et al., 2000).

In the Gippsland Basin, NE-trending depocentres along the northern and southern flanks of the Gippsland Basin were preferentially inverted. The middle Cretaceous rift phase obliquely reactivated the underlying Early Cretaceous and basement structures with deposition largely confined within the Foster (FFS) and Rosedale (RFS) fault systems.

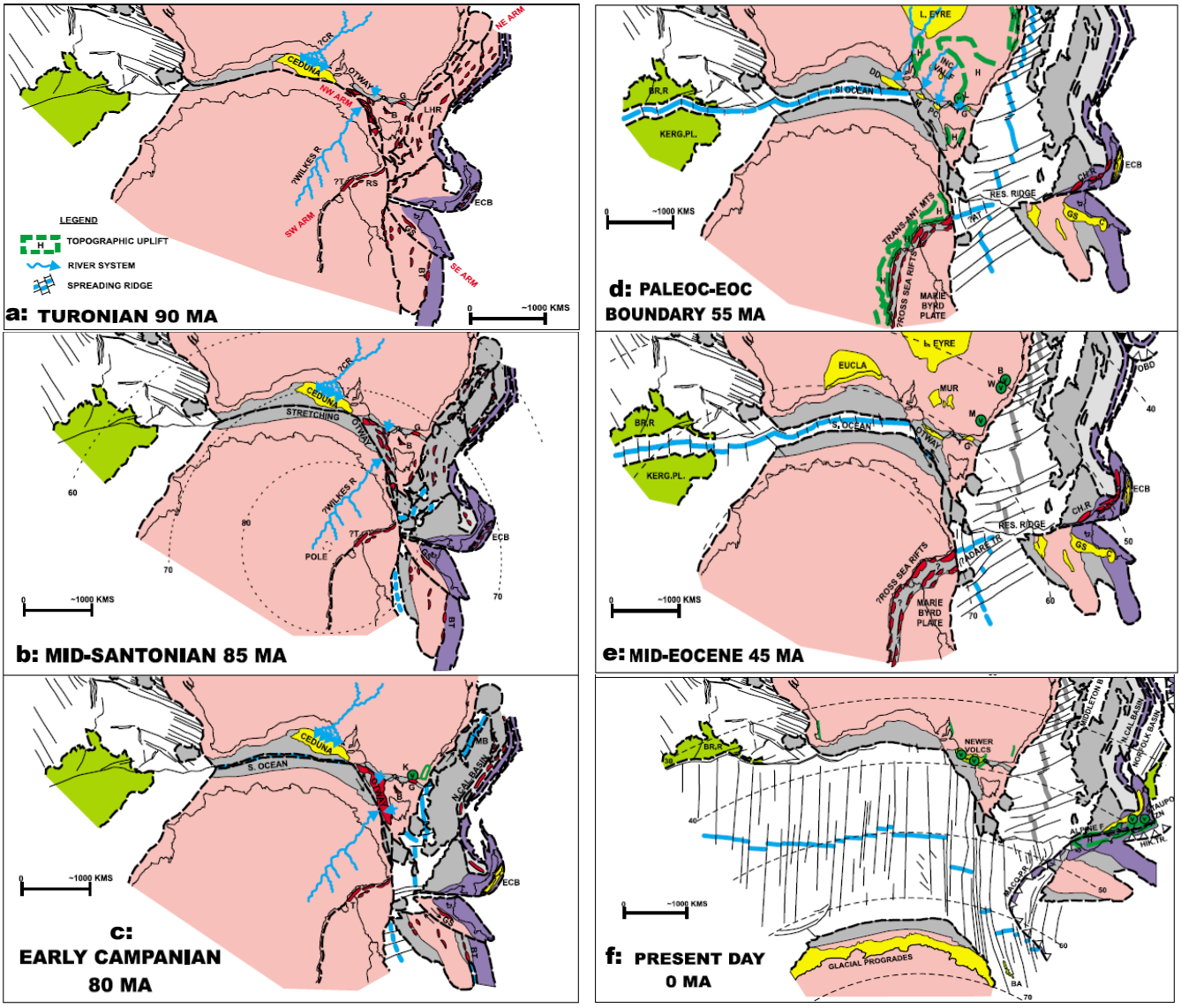

Figure 4.3 Plate tectonic reconstructions for the: a) Turonian (90 Ma), b) Mid-Santonian (85 Ma), c) Early Campanian (80 Ma), d) Paleocene-Eocene Boundary (55 Ma), e) Mid-Eocene (45 Ma), and f) Present Day from Norvick and Smith (2001). B - Bass, G - Gippsland, CR - Ceduna River, LHR - Lord Howe Rise, BT - Bounty Trough, NVL - North Victoria Land, T - Terror Rift, GS - Great Southern Basin, ECB - East Coast Basin, RS - Ross Sea, K - Kipper Volcanics, MB - Middleton Basin, N Cal - New Caledonia, inc.val.f – incised valley fills, Ch.r - Challenger rifts, C - Canterbury Basin, L - Latrobe Basalts, Mur - Murray Basin, obd - obduction, B - Barrington basalts, W - Walcha basalts, M - Monaro basalts.

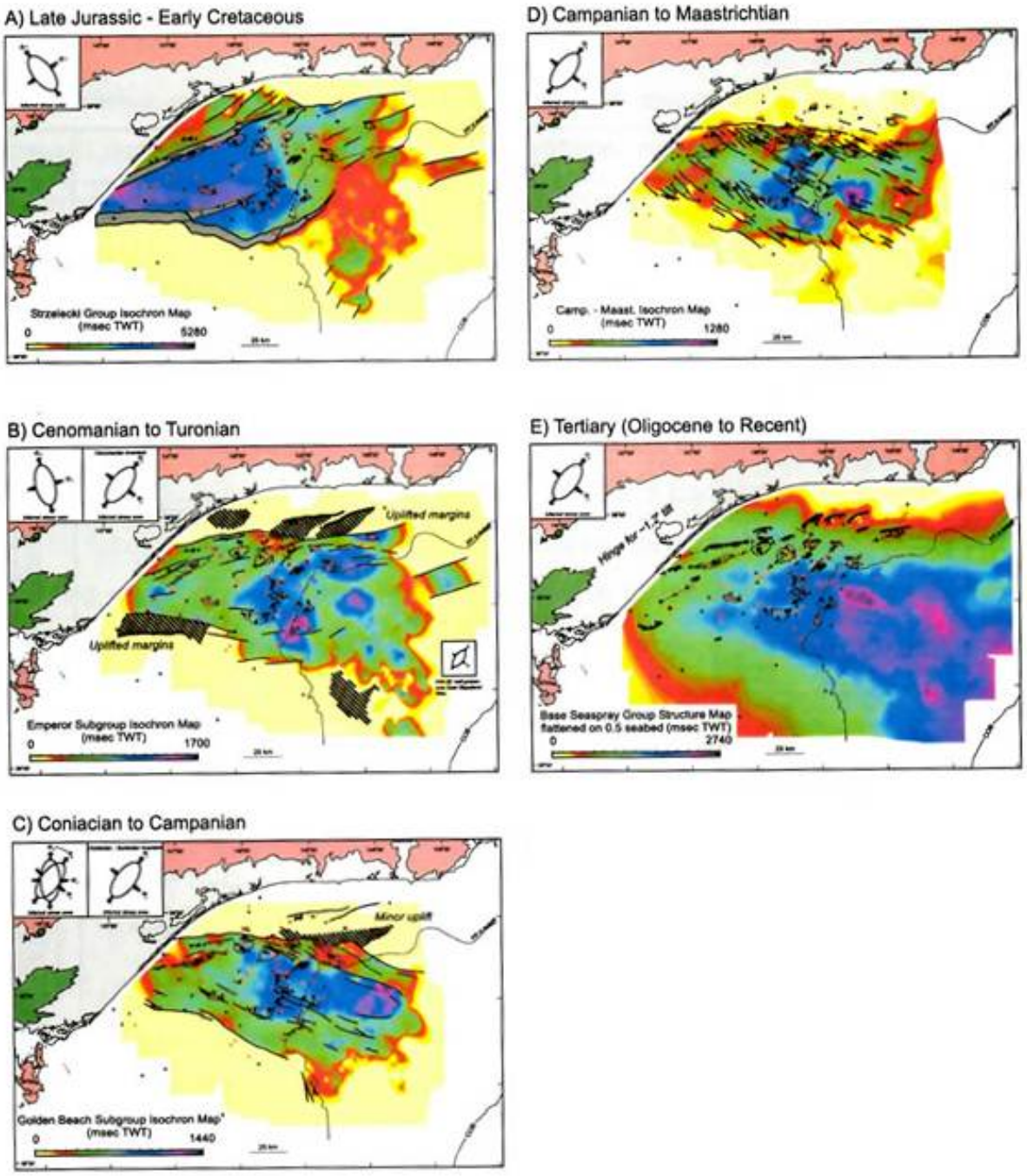

Figure 4.4 **Structural architecture as interpreted by Power (2003). (A) Latest Jurassic to Early Cretaceous, (B) Cenomanian to Turonian, (C) Coniacian to Campanian, (D) Campanian to Maastrichtian, (E) Oligocene to Recent. Images (A) to (D) are shaded isopachs, with (E) a TWT structure map of the base Seaspray Group.**

The Rosedale Fault System was a major feature during the Turonian, while the greatest amount of extension probably occurred through the Eastern to Southern graben and Central Deep. The influence of the Rosedale Fault System is interpreted to diminish significantly during the Coniacian and Santonian as the Central Deep narrows with the gradual clockwise rotation of propagating fault tips. The Darriman Fault System became more prominent along with the initiation of other NW-SE oriented faults throughout the basin. Volcanic centres developed along the traces of the south Rosedale and Darriman fault systems during the Santonian to Campanian (Power et al., 2003; Bernecker et al., 2006) in response to the northward propagation of the Tasman rift system past the Gippsland Basin. Mafic flows derived from these centres covered the Golden Beach deltaics and the Central Deep continued to narrow as it was bypassed by the propagating rift system.

The change from rift to spreading in the Tasman Sea during the Santonian-Campanian was accompanied by a rotation of the stress field by 45^{o} to arrive at the present-day orientation. The Campanian to Paleocene is described by Power et al. (2003) as a time of fault-controlled subsidence to differentiate it from the preceding active rift and the following flexural sag geometries. The period is characterised by development of NW-SE-trending normal faults and the widening of the Central Deep and Eastern Graben. EW-oriented segments of the Rosedale Fault System were preferentially reactivated, resulting in a highly oblique relationship between intra-basinal and border faults (Figure 4.4). Fault-controlled subsidence was replaced by flexural sag in the Eocene, coeval with the cessation of Tasman seafloor spreading and the start of rapid spreading between Australia and Antarctica.

The entire offshore basin was in deep water by the Eocene and as thermal subsidence continued, carbonates of the Seaspray Group were deposited. Thermal subsidence was interrupted by inversion events in the early Eocene, Oligocene - early Miocene, mid-late Miocene and Pliocene - Recent resulting in broad NE-SW-oriented anticlines and the development of extensive submarine channels in the Central Deep and eastern Gippsland Basin (e.g. Bass Canyon). Although important for trap creation, the inversion pulses were not significant enough to negate the effects of thermal subsidence. The cause of the inversion events is unknown, but the effects of distal plate interactions along the southern and northern Australian margins are interpreted as likely contributors to the compression.

Based on the seismic cross-section published by Power et al. (2001; Figure 4.5), it would appear that extensional geometries within the Early Cretaceous rift succession are best developed in Strz1 (Berriasian to Hauterivian) and Strz2b (Aptian to Early Albian). The intervening section (Strz2a; Barremian to earliest Aptian) appears to be more continuous in thickness across the basin thinning only onto the basin margins, thus it may be more sag or 'waning rift' related. Power et al. (2001) do not mention Late Jurassic involvement in the offshore rift development, as most evidence of these older sediments is known from onshore well intersections. However, this does not preclude the occurrence of Late Jurassic sediments within the basal section of Strz1. The middle Cretaceous rift phase (Emperor and Golden Beach subgroups; Turonian to Mid-Campanian) is chronostratigraphically equivalent to the Durroon Rift Phase in the Bass Basin, and was related to extension in eastern Gondwana prior to breakup in the Tasman Sea.

Rift phase Strz1 correlates closely with the timing of extension in the onshore Otway Basin and parts of the offshore basin. Sediments of this age have not been penetrated in the Bass Basin, but Cummings et al. (2004) have inferred their presence from seismic data in the western part of the basin. Rift Phase 2 (Emperor and Golden Beach subgroups) is confined to the Central Deep and modelled extension is relatively minor at 5%. The interpreted interval appears to grow into faults to the SSW in the Central Deep and towards the flanks. Volcanics associated with breakup are not evident from the cross-section, but are interpreted to exist from the latest Santonian to Campanian within the Golden Beach Subgroup (Bernecker et al., 2006) suggesting that at least part of this interval is post-rift.

Evidence for the separation of the post-rift interval (LS1-SS4; Figure 4.5) into fault-controlled and flexural phases as suggested by Power et al. (2003) is limited in the published example. However, minor fault activity can be interpreted in the LS1-LS2 sequences (Campanian-Paleocene Latrobe Siliciclastics), with no fault activity identified in the Paleocene-Recent Latrobe and Seaspray sequences (LS3, SS1-4). Overall the locus of deposition for the post-rift interval overlies the rifted depocentres resulting in a steers-head geometry from south to north across the Central Deep.

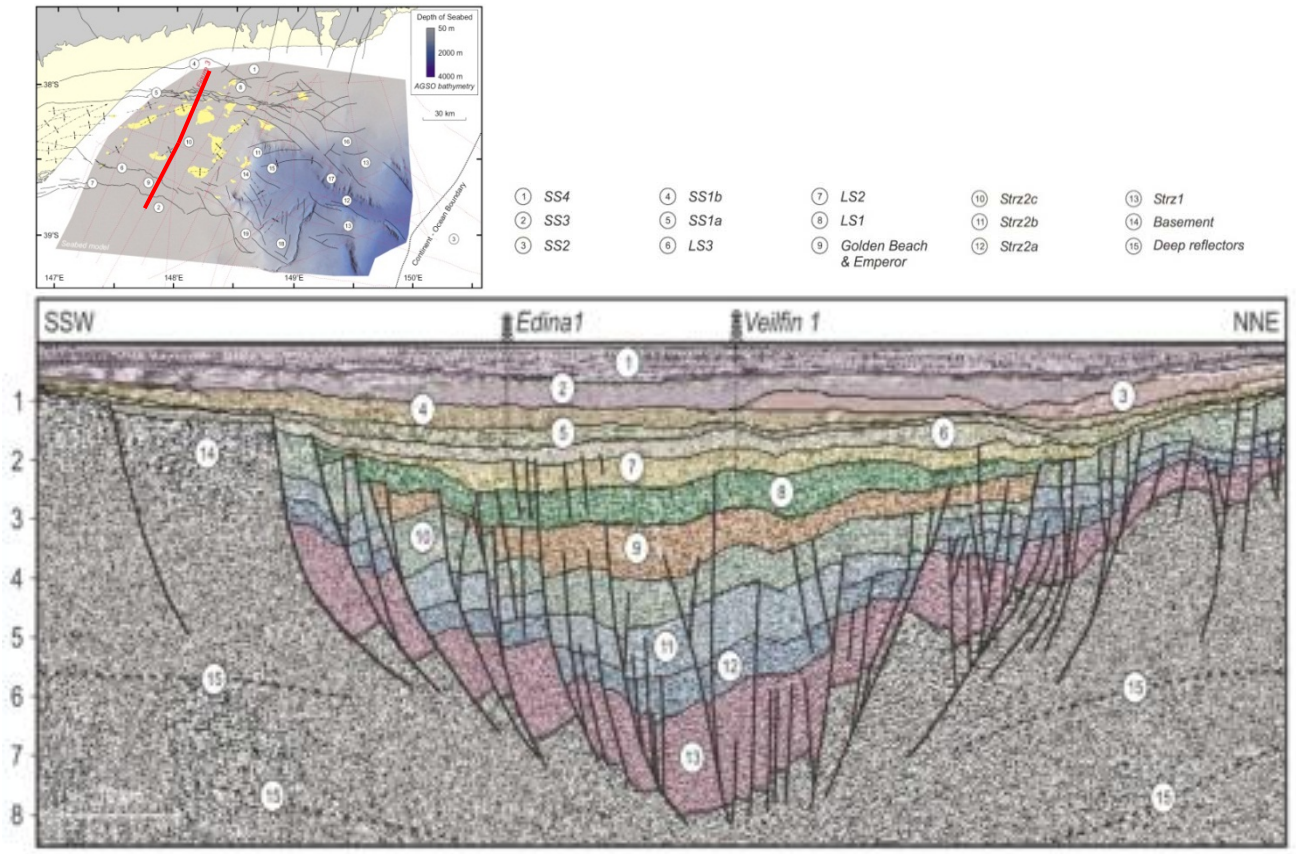

Figure 4.5 **Interpreted seismic line (red line on location map) across the Gippsland Basin showing the major megasequences mapped by Power et al. (2001). According to the stratigraphic chart within Power et al. (2001) Strz1 = Neocomian Lower Strzelecki Group, Strz2a = Barremian Upper Strzelecki Group, Strz2b = Aptian Upper Strzelecki Group, Strz2c = Albian Upper Strzelecki Group, LS1 = Campanian-Maastrichtian Latrobe Siliciclastics, LS2 = Maastrichtian-Paleocene Latrobe Siliciclastics, LS3 = Paleocene-Eocene Latrobe Siliciclastics, including the Gurnard Formation, SS1a = Oligocene Seaspray Group, SS1b = Oligocene-Miocene Seaspray Group, SS2 & SS3 = Miocene Seaspray Group. After Power et al. (2001).**

4.4 Southern Flank of the Gippsland Basin

The southern flank of the Gippsland Basin has several tectonic elements that trend approximately WNW-ESE to E-W (Figure 4.6). From south to north, these elements are the shallow basement area of the Southern Platform and the Southern Terrace separated by the Foster Fault System. The Southern Terrace was formerly known as the Southern Strzelecki Terrace. Further basinward, the Darriman Fault System forms the northern limit of the Southern Terrace, beyond which lies the Central Deep.

The exact nature of this system is difficult to define using the GDPI10 2D seismic data alone as the complex fault system lies at the edge of the seismic grid.

The Pisces Sub-basin lies along the eastern edge of the Southern Platform and is represented very generally on many maps. The limits of this depocentre have been revised during the current study, and additional half graben of interpreted similar age have been identified on the Southern Platform. The Bassian Rise demarcates the southern limits of the flank and is a long-lived Paleozoic basement high.

Sediments on the Southern Flank are thin relative to the Central Deep. The siliciclastics of the Cretaceous Strzelecki Group and Emperor, Golden Beach and Halibut subgroups are confined to the Southern Terrace, with the Cobia and younger subgroups present on the Southern Platform (Figure 4.7). The oldest confirmed sediments in the Pisces Sub-basin are from the Santonian (*T. apoxyexinus*) Anenome Formation of the Golden Beach Subgroup, although there is a deep, syn-rift section that is not penetrated in the well (see Section 5). Although the stratigraphy in the Pisces Sub-basin is referenced to the Mudskipper-1 well, Pisces-1 is the only well drilled in the sub-basin. The Halibut and Cobia subgroups are also intersected at Pisces-1. The Oligocene to Recent limestones of the Seaspray Group are identified across the southern flank with the oldest interval (Oligocene to early Miocene) missing over the Pisces Sub-basin.

Relative to the broader Gippsland Basin, the Southern Flank has received limited exploration activity with only 24 wells drilled on the platform and terrace. The main target for exploration in this area has been the stratigraphic pinch-out play of the upper Latrobe Group on basement overlain by the regional seal of the Lakes Entrance Formation carbonates (e.g. Groper-1, Groper-2, Mullet-1 and Bluebone-1). Other plays include intra-Latrobe sands (e.g. Moray-1, Mudskipper-1), structural closures (e.g. Devilfish-1, Tarra-1, Kyarra-1A, Wyrallah-1, Tommyruff-1). Sailfish-1 was drilled to test interpreted biohermal reefs which turned out to be volcanic mounds. There are no significant hydrocarbon discoveries on the southern flank. The absence of accumulations has been attributed to a number of risk factors such as long-distance migration from the Central Deep, a lack of reservoir pinch-out against basement or lack of sufficient seal at the base Lakes Entrance and intra-Latrobe levels (Thomas et al., 2003; Bernecker et al., 2003, 2006).

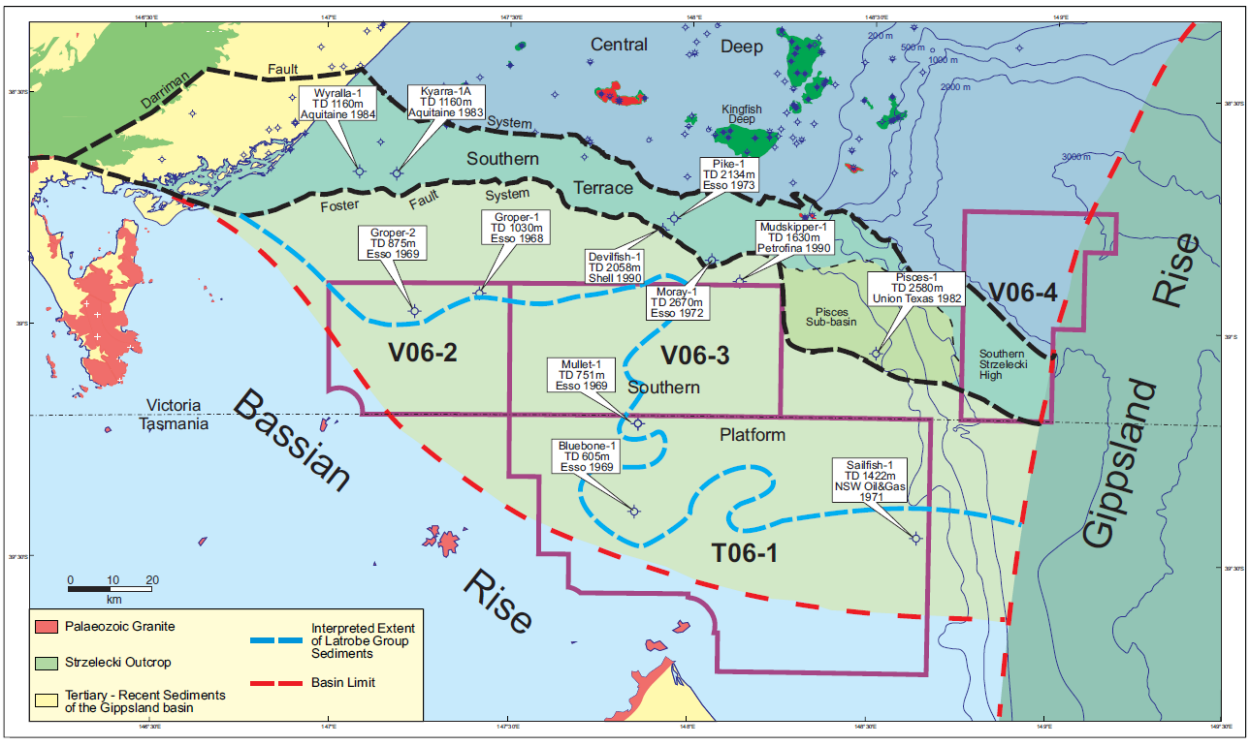

Figure 4.6 **Tectonic elements of the Southern Flank of the Gippsland Basin showing basin limits and interpreted extent of Latrobe Group sediments across the region (after Bernecker et al., 2006).**

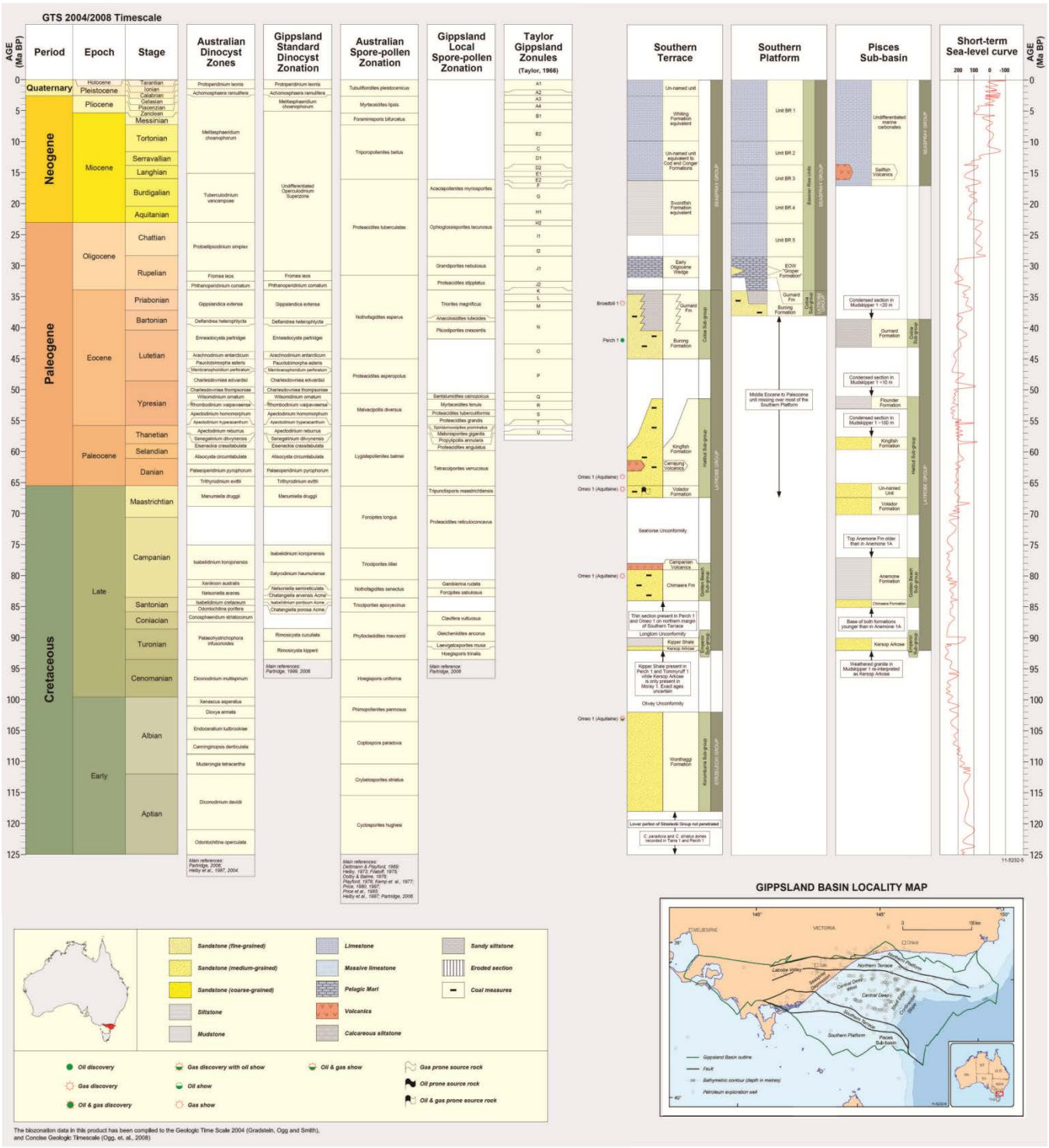

Figure 4.7 Tectonostratigraphic chart of the Southern Flank of the Gippsland Basin separated into the Southern Platform, Southern Terrace and Pisces Sub-basin (Modified after Partridge et al., 2012).

5 Stratigraphy, Well Ties and Horizon Interpretations

5.1 Horizon Interpretation

The horizon interpretation was undertaken using IHS Kingdom Core software. The preferred stratigraphic picks of formation tops at the 20 key wells were supplied by DPI Victoria in an Excel spreadsheet (Figure 5.1). These picks were entered into the Formation Tops table in Kingdom. While most picks have been validated through the seismic ties and regional correlations, there were some errors in the Excel spreadsheet which have been highlighted in this section. In addition, some alternate picks have been suggested based on correlations between wells, seismic geometries and other criteria.

Figure 5.2 shows a typical seismic section across the study area. Here, the broad tectonic and structural elements of the Southern Platform, Southern Terrace, Foster Fault System, intra-platform half graben and the shelf margin slump/channel complex are evident. A total sediment thickness map (Figure 5.3) shows these tectonic elements in a regional setting. It is clear that the attenuated basin stratigraphy in the study area differs significantly from the Central Deep due to lower rates of subsidence and the shallow basement setting of the Southern Platform. The following sections detail the horizon ties at key wells and their regional correlation across the GDPI10 2D seismic grid. The mapped extent of each horizon is shown in Appendix 5. Maps and grids of the interpreted horizons are presented in Section 6.

5.2 Stratigraphic Charts and Timescales

The stratigraphy of the Gippsland Basin can be subdivided into three broad, tectonically defined megasequences which correlate to the following basin phases: 1) Late Jurassic to Early Cretaceous syn-rift associated with formation of the Southern Margin Rift System and southeast margin breakup; 2) Late Cretaceous to early Eocene post-rift sag (or drift and seafloor spreading of Bernecker and Partridge, 2001); and, 3) late Eocene to Recent late stage subsidence and compressive reactivation. These basin phases correlate to the syn-rift Strzelecki Group, post-rift Latrobe Group, and the Seaspray Group which was deposited during late-stage subsidence and reactivation.

The stratigraphic framework used in the Gippsland Basin has evolved from a confusing formation-based system into nomenclature based on formal ranking of groups, subgroups and formations (Partridge, 1999; Bernecker and Partridge, 2001; Bernecker and Partridge, 2005). The stratigraphic chart published by Bernecker and Partridge (2001; and subsequent variations to the chart) has been used by DPI in recent publications and remains as the standard nomenclature (Figures 5.4a and 5.4b). In a review of the Eocene to Recent stratigraphy of the Bassian Rise (Southern Platform), Partridge (2006) formally defined the terminology of the Early Oligocene Wedge (EOW) and five Bassian Rise Units (Figure 5.5).

In 2011, Geoscience Australia revised and updated the Gippsland Basin Biozonation and Stratigraphy Chart 40 (Partridge et al., 2011). A subsequent revision to this chart in 2012 was supplied by Geoscience Australia for the current study (Figure 5.6). Importantly, the revised chart incorporates the stratigraphy of Bernecker and Partridge (2001) and Partridge (2006), and provides a correlation of the different nomenclature used across the basin in specific tectonically-defined regions (e.g. Onshore Basin, Central Deep). For the purposes of the current study, elements of Southern Terrace, South Platform and Pisces Sub-basin were extracted from the Geoscience Australia chart (Partridge et al., 2012). It should be noted that the timescale (millions of years) differs between the DPI chart and Geoscience Australia chart. The Geoscience Australia chart uses the 2004 Geological Time Scale (Gradstein et al., 2004) and the Concise Geological Time Scale (Ogg et al., 2008). There is no reference to the timescale used in the DPI Victoria stratigraphic chart. In addition, there is further detailed breakdown of the spore/pollen zonations (i.e., early, middle, late) in the DPI chart in comparison with Partridge et al. (2012).

5.3 Basement

The study area covers two principal tectonic elements in the southern Gippsland Basin: the Southern Platform and the Southern Terrace (Figures 5.2 and 5.3). The Southern Terrace was previously known as the Strzelecki Terrace. These tectonic elements are bounded by the Foster Fault System (between the Southern Platform and Southern Terrace) and the Darriman Fault System (which extends from onshore and separates the Southern Terrace from the Central Deep). Basement rocks underlying the study area are Paleozoic metasediments and volcanic rocks of terranes that were accreted to eastern Australia and extensively intruded by Devonian granites. The Bassian Rise is the bathymetric name

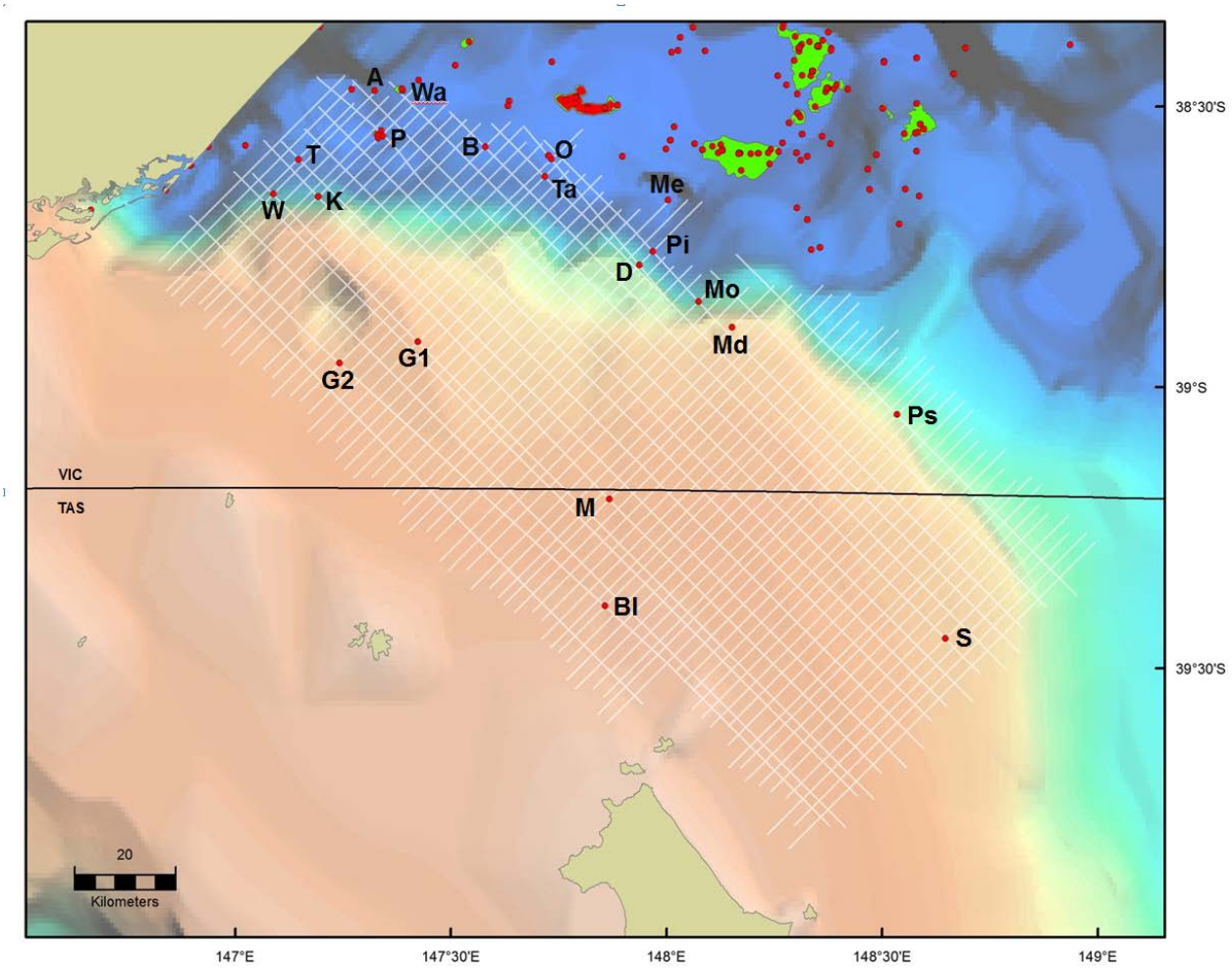

Figure 5.1 Location map of the key wells in the GDPI10 seismic interpretation. Well abbreviations: A = Amberjack-1, B = Bullseye-1, Bl = Bluebone-1, D = Devilfish-1, G1 = Groper-1, G2 = Groper-2, K = Kyarra-1A, M = Mullet-1, Me = Melville-1, Md = Mudskipper-1, Mo = Moray-1, O = Omeo-2A, P = Perch-1, Pi = Pike-1, Ps = Pisces-1, S = Sailfish-1, T = Tommyruff-1, Ta = Tarra-1, Wa = Wasabi-1 and W = Wyrallah-1.

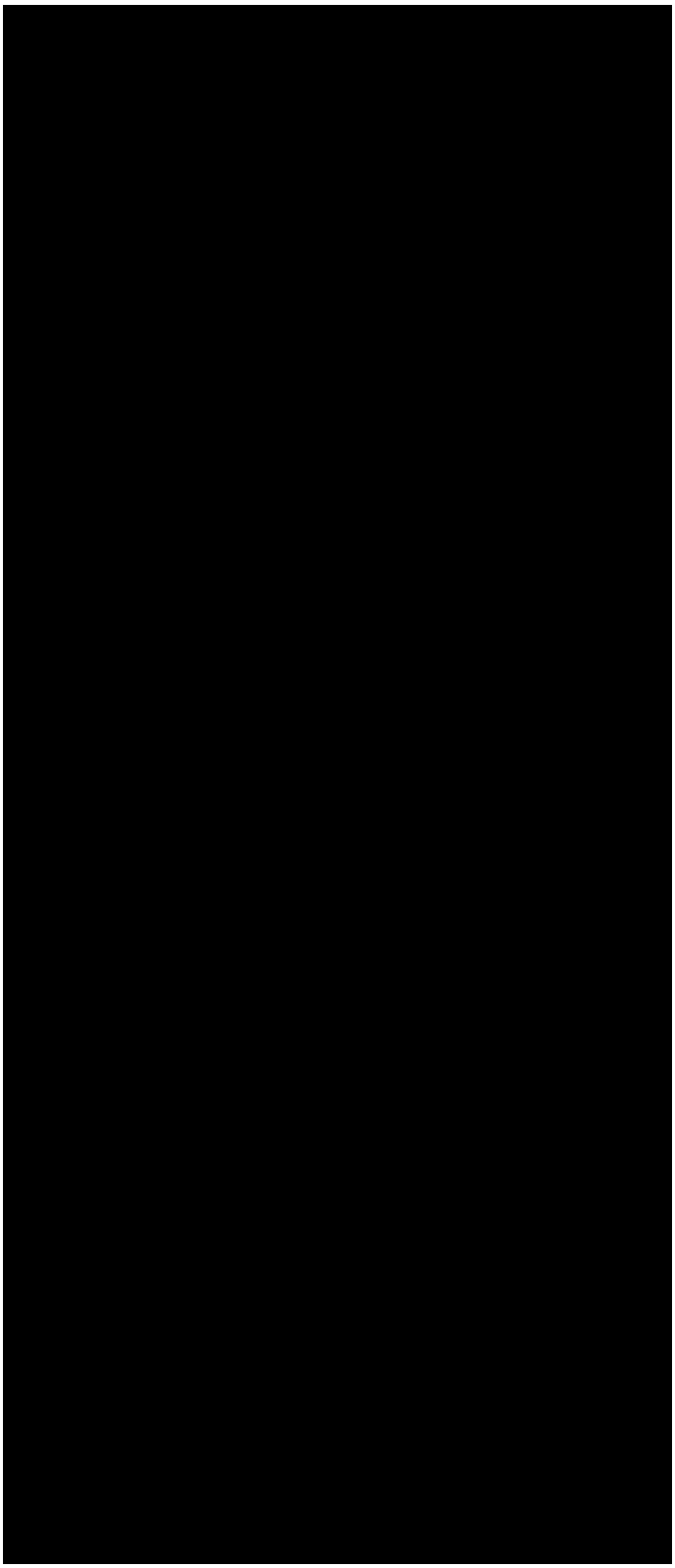

Figure 5.2 **Representative seismic section across the Southern Platform and Southern Terrace. Other structural features of note are the intra-platform half graben, Foster Fault System (FFS) and the shelf margin slump and channel complex. Well locations are not on this line but positioned to indicate the typical plays tested in the study area.**

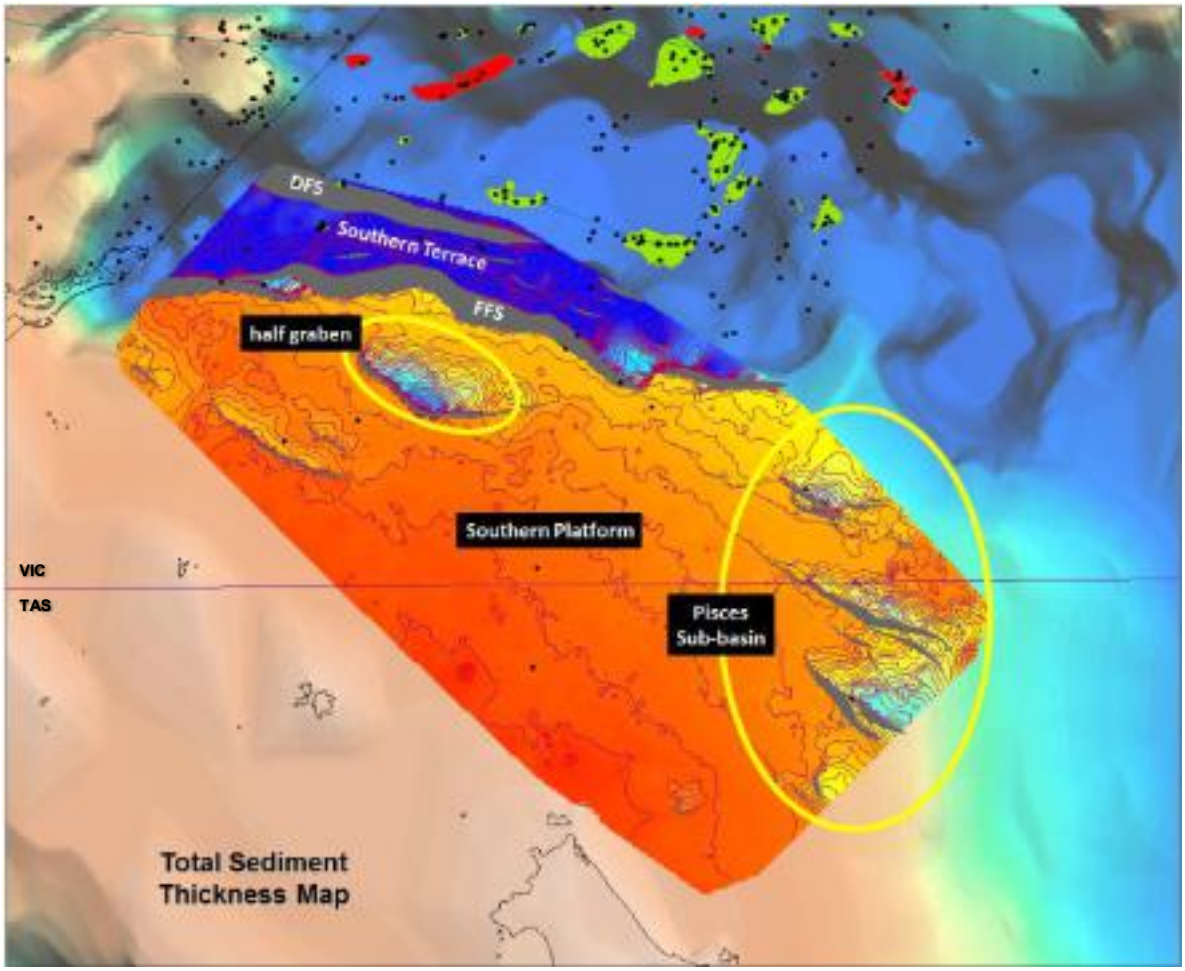

Figure 5.3 Total sediment thickness map with yellow circles indicating locations of the intra-platform half graben and the Pisces Sub-basin. Other structural elements shown are the Southern Platform, Southern Terrace, Foster Fault System (FFS) and the Darriman Fault System (DFS).

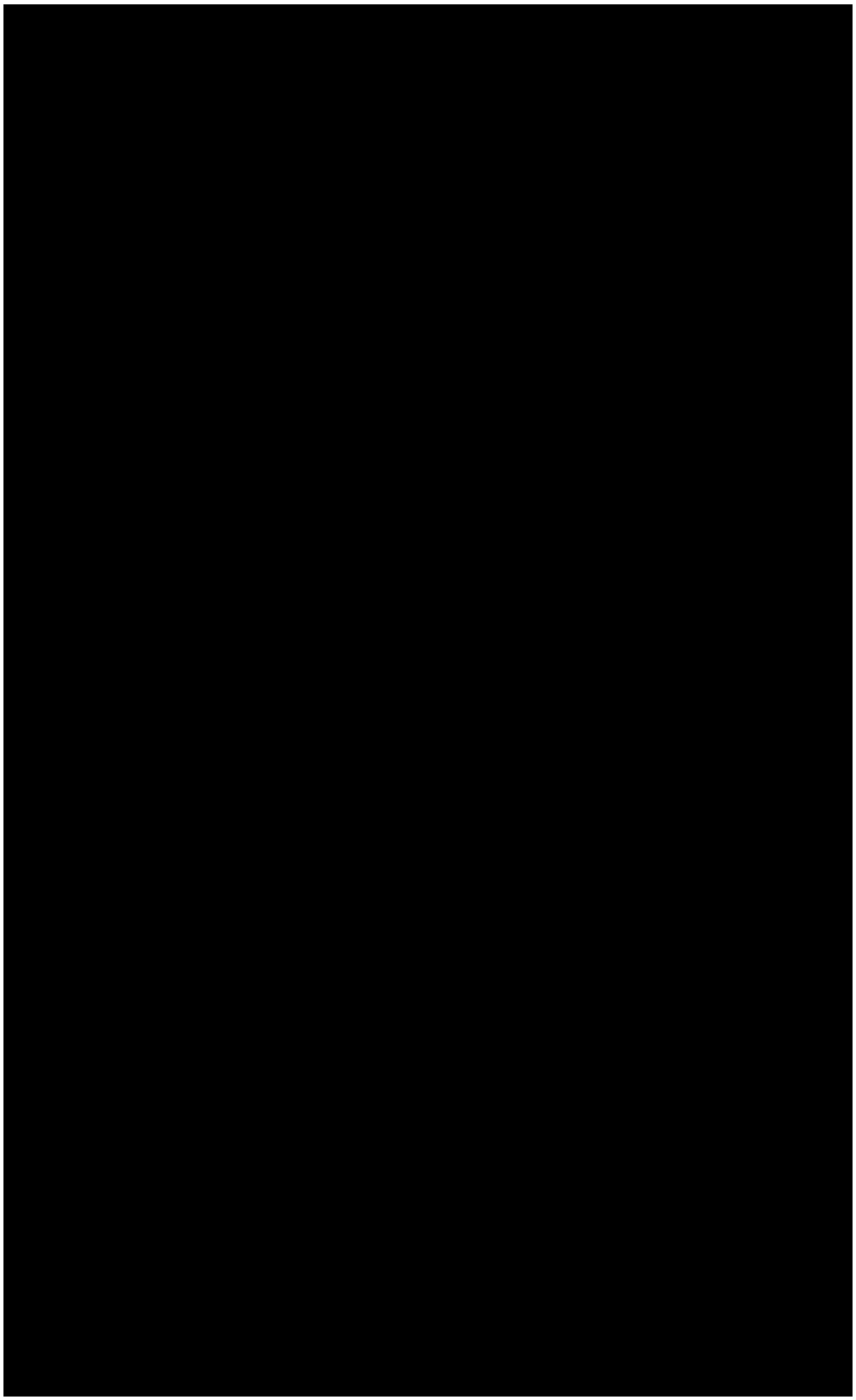

Figure 5.4a Summary of seismic horizons plotted against DPI Victoria stratigraphy and timescale (image modified from Goldie Divko et al., 2010).

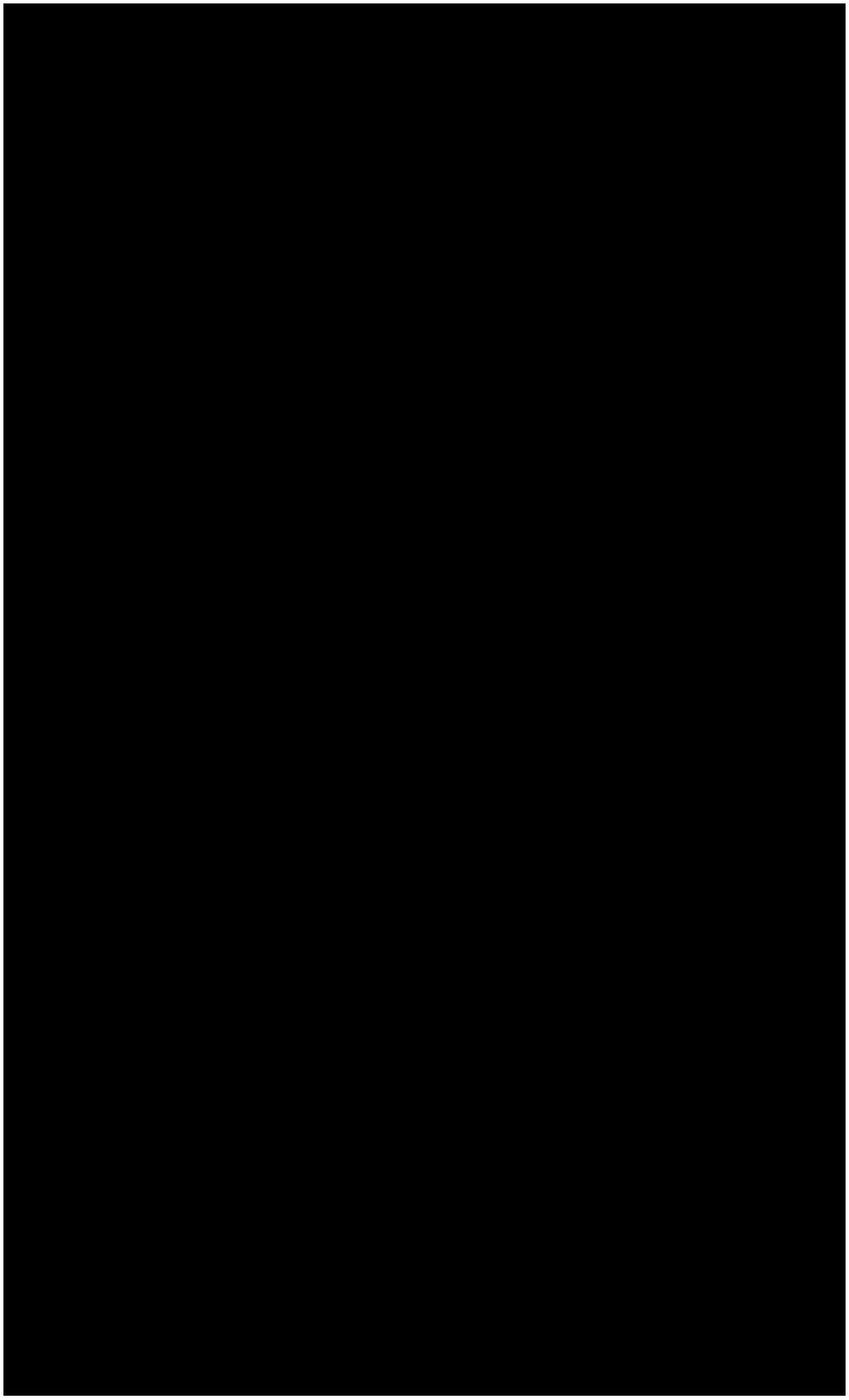

Figure 5.4b Summary of seismic horizons plotted against DPI Victoria stratigraphy and timescale with mapping comments (image modified from Goldie Divko et al., 2010).

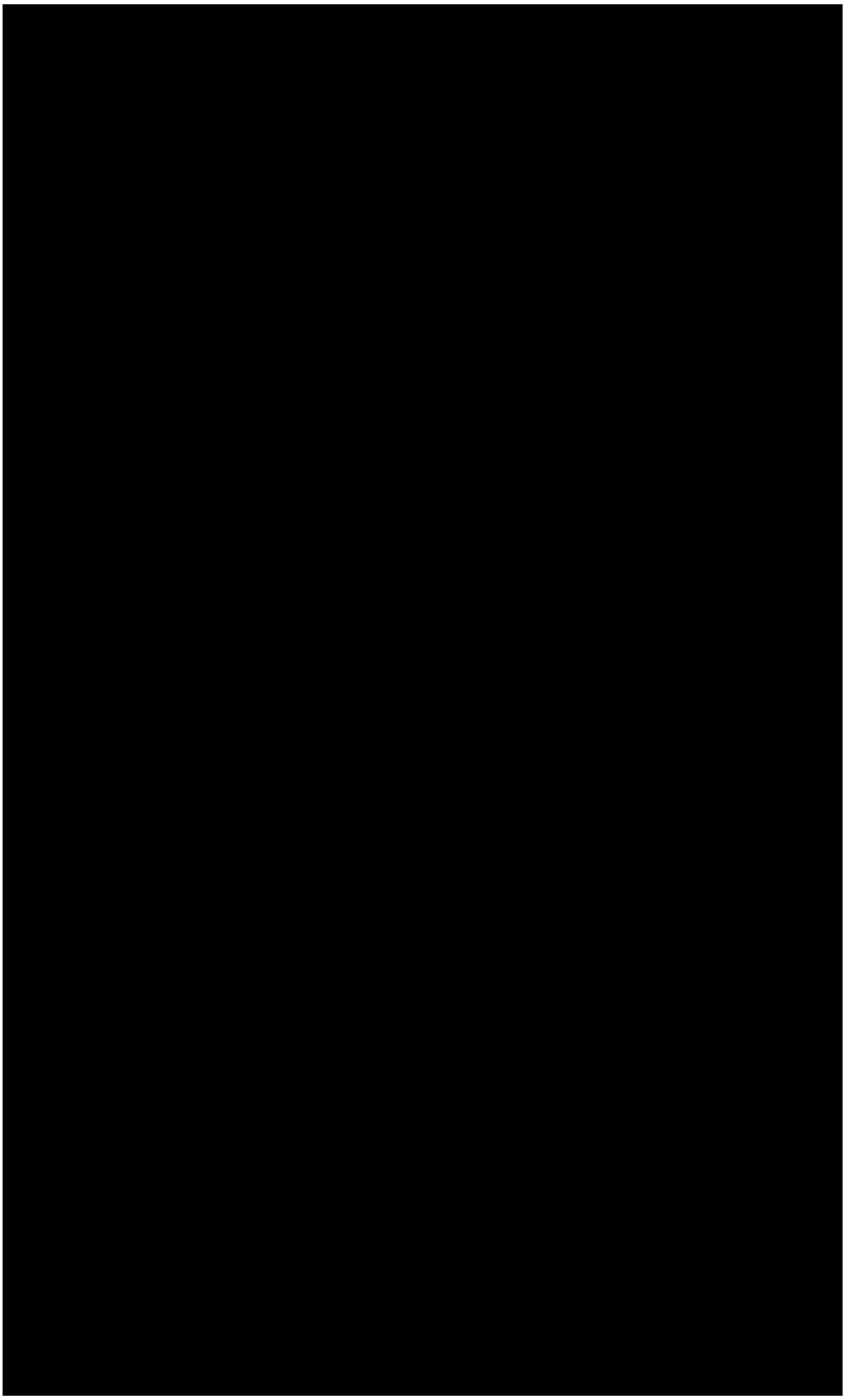

Figure 5.5 Summary stratigraphy of the Bassian Rise and comparison to broader Gippsland Basin (image from Partridge, 2006).

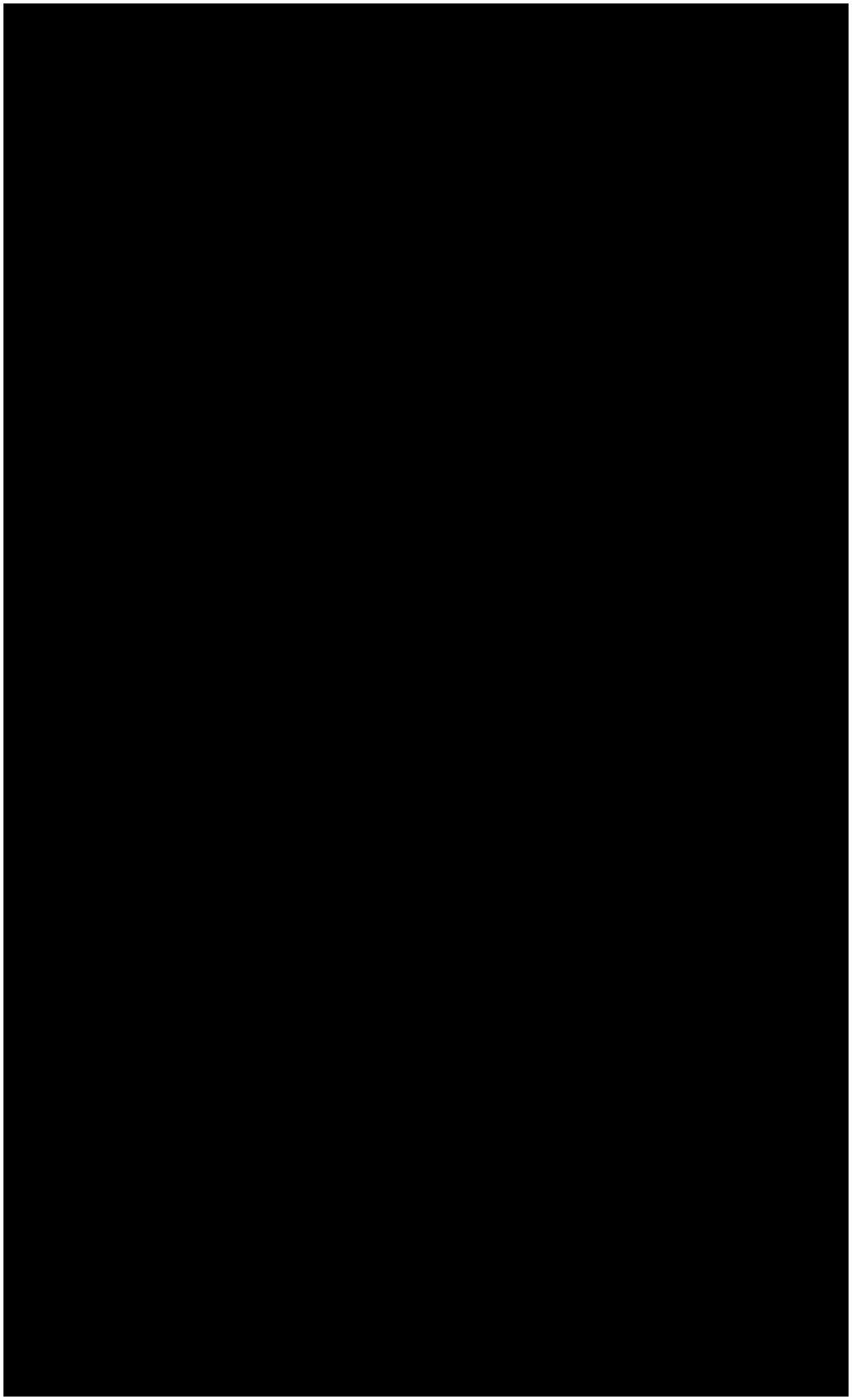

Figure 5.6 Summary of mapped seismic horizons plotted against the updated Geoscience Australia stratigraphy and timescale (image modified from Partridge et al., 2011; digital copy supplied by Geoscience Australia).

given to the large basement high that runs between Wilson's Promontory and Flinders Island. Geologically, this basement high separates the Gippsland and Bass basins.

The basement topography of the Southern Platform was mapped as the Top Basement horizon, and largely reflects the Bassian Rise with basement rising to the south. Within the study area, basement reaches a minimum depth of approximately 200 m along the southwestern margin of the seismic survey grid near Bluebone-1. Although slightly outside of the seismic coverage, the granitic basement is exposed in the Kent Group of islands on the Bassian Rise. The typical depth to basement across the Southern Platform is approximately 1000 m. Finer features along the Southern Platform include half graben, a NS-trending topographic ridge, volcanogenic highs and older isolated peaks along the Bassian Rise – all features that are important to local sediment supply.

Five wells within the study area reach total depth (TD) in basement. Four of these wells (Bluebone-1, Groper-1, Mudskipper-1 and Mullet-1) intersect weathered granite to granodiorite (Figure 5.7). The basement intersected in Groper-2 is reported as a dense red and brown shale and siltstone shale unit with lithology similar to the Upper Devonian Avon River Group. This interval in Groper-2 is most evident from the angular unconformity recorded in the dipmeter (Curnow, 1969).

It is interpreted here that Groper-2 does not penetrate basement, but alternatively an unconformity bound half-graben succession consisting of pre-Strzelecki or early Strzelecki age sediments. This unconformity capped half-graben succession is evident on seismic (Figure 5.8) and similar features occur across the Southern Platform (Figure 5.3). Evidence to support this interpretation includes the orientation of the half graben which is consistent with the extensional direction during early development of the Gippsland Basin. While the Groper-2 succession does not show obvious growth into the footwall, there is no conclusive evidence to discount the package as a pre- to early extensional sequence.

Similar features on the Southern Platform include the shallow half graben southwest of Groper-1 and -2, and a single isolated half graben in the far western corner of the seismic grid (Figure 5.3). These half graben are defined by down to the NE normal faults with approximately 400 to 900 m offset in the basement. The half graben are approximately 4 km wide and 15 to 30 km long. A significantly larger half graben, herein informally referred to as McLoughlins Sub-basin, is located about 10 km NE of Groper-1. The McLoughlins Sub-basin is 15 km wide, 40 km long with more than 4 km offset of basement. It also has a similar orientation to the other half graben in the area. The pre-Strzelecki or early Strzelecki stratigraphic fill in the half graben is capped by a major angular unconformity with the overlying Latrobe or Seaspray groups.

There is a prominent, NNE-trending basement ridge with approximately 150 m relief located about 10 km north of Mullet-1. The ridge terminates near the Foster Fault System (Figure 5.9). Seismically, this elongate ridge appears to be a series of conical peaks across the generally elevated surface. There is degradation of seismic quality beneath these conical peaks, with the exception of high-amplitude reflections at depth within the basement. Sediments overlying the peaks display near vertical faulting and uplift that effects strata to the top of the Bassian Rise Unit 2. Just overlying the Top Bassian Rise Unit 2 are high-amplitude and discontinuous reflections. This ridge is likely the topographic expression of an igneous intrusion into the basement and the overlying strata. The intrusion is evident from deep reflections within the basement, forced uplift and folding, and the near-extrusive to extrusive volcanism that occurred in the late Miocene as determined by the age of the Bassian Rise Unit 2.

On the southern edge of the seismic grid in proximity to Bluebone-1 is a cluster of small isolated topographic highs with 50 m to over 400 m of relief (Figure 5.9). Some of the highs are peaks that extend to near seafloor, while others with low relief have a flat peneplaned surface. Sediments onlap these highs, skirting around the bases as alluvial fans. These features, along with the NNE-trending basement ridge, would have acted as a control on depositional paths and flow direction through most of the deposition of the Latrobe Group to Recent sediments. These basement highs also provided a local source of sediment during the Latrobe Group deposition.

The basement surface mapped in seismic over most of the Southern Platform coincides principally with the last major trough beneath the high-amplitude continuous reflections of the Gippsland Basin succession and overlying the disrupted lower amplitude reflections of older basement lithologies. The basement reflection is highly rugose (Figure 5.10) across the Southern Platform. Most of the basement rugosity is not reflected in the overlying stratigraphy which drapes and fills in the rough topography within approximately 150 m. The continuity and amplitude of the basement reflection is less prominent in the Southern Platform half graben and Southern Terrace. In these locations the basement horizon is mapped along reflections best defining an unconformable contact with comprehensive cross-line ties.

The basement surface is shallow in the southern extent of the grid along the Bassian Rise and gently deepens to the north, before it is offset by the Foster and Darriman fault systems. The Foster Fault System is an EW-striking system of large basement offset consisting of anastomosing and amalgamating faults, with steeply deepening relay ramps in the area of

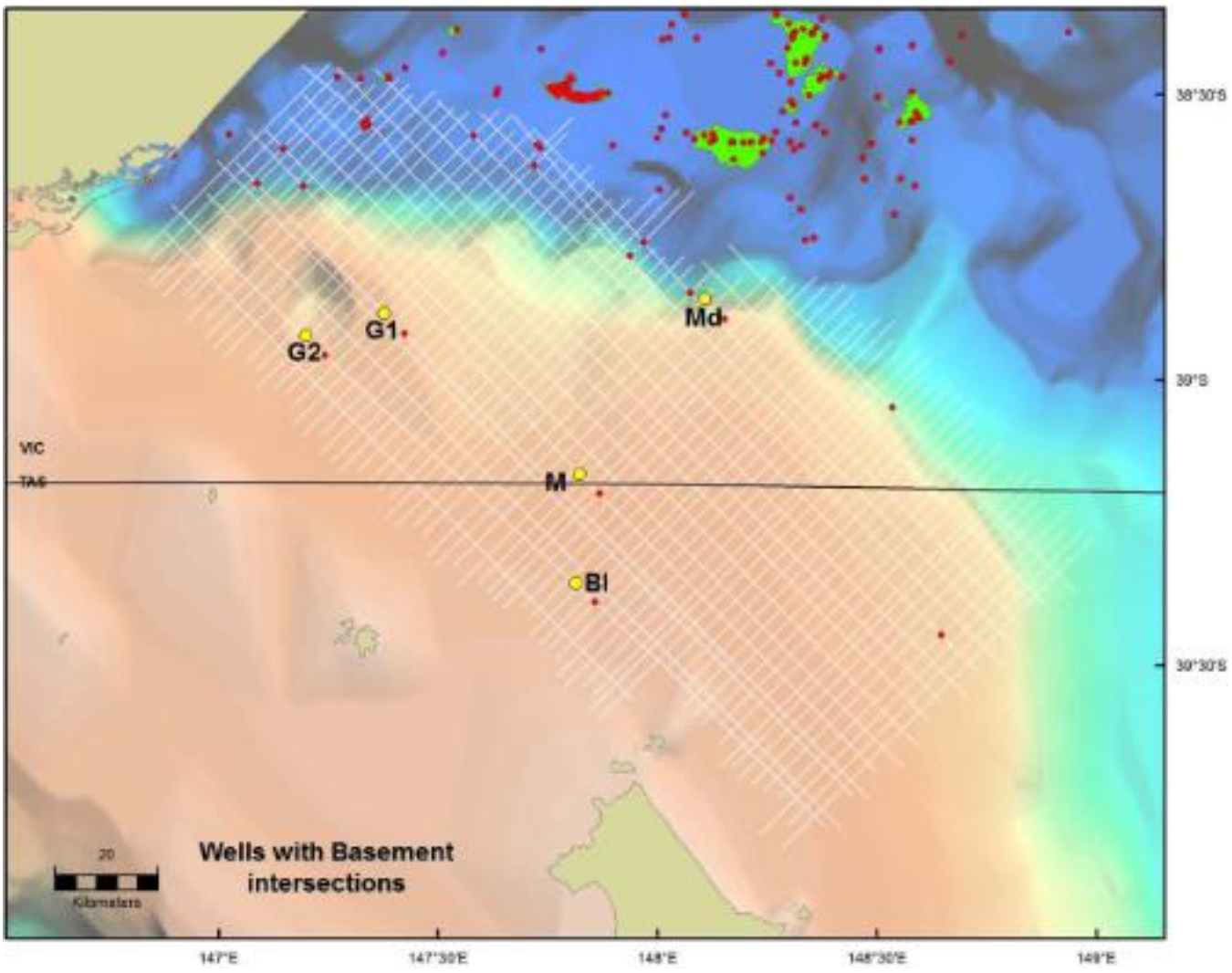

Figure 5.7 Map showing wells that intersected basement. Well abbreviations: Bl = Bluebone-1, G1 = Groper-1, G2 = Groper-2, M = Mullet-1 and Md = Mudskipper-1. Note that Groper-2 has been interpreted to intersect Paleozoic basin sediments rather than igneous basement.

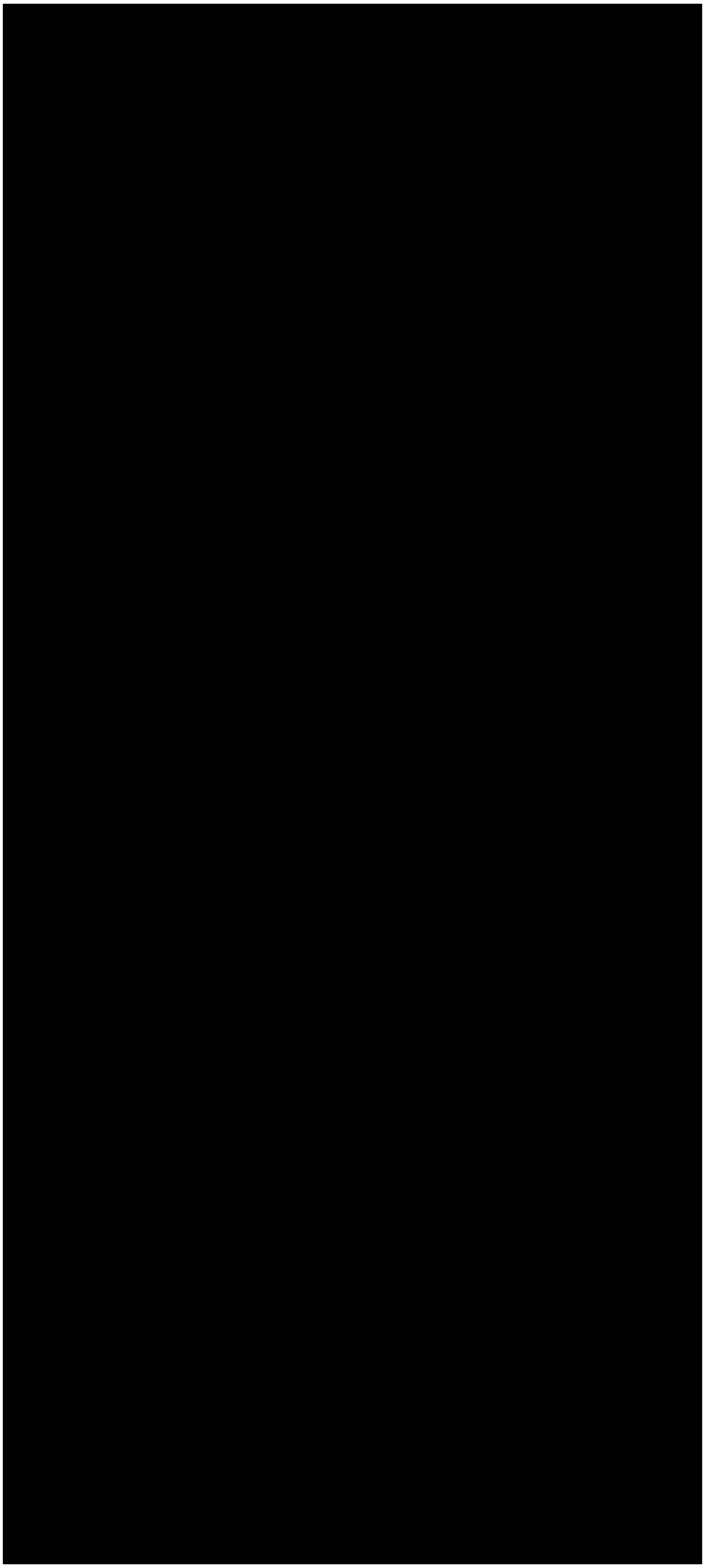

Figure 5.8 Seismic strike line GDPI10-917 showing an interpreted Paleozoic half graben near Groper-2 on the Southern Platform.

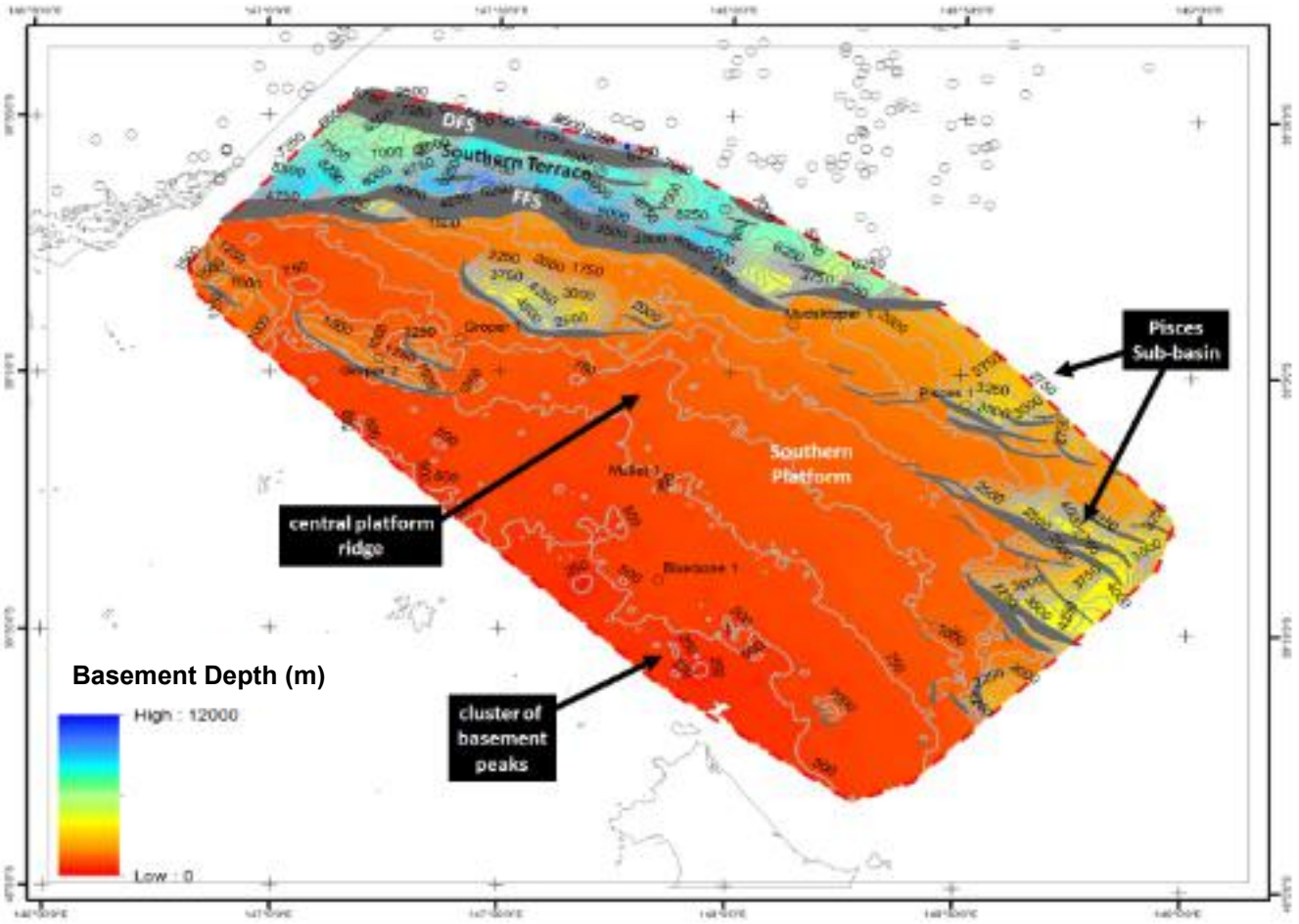

Figure 5.9 Depth grid of Top Basement surface with depth contours, fault polygons (grey polygons) and well locations shown. The prominent basement ridge on the central part of the Southern Platform, the clusters of basement peaks near Bluebone-1 and the Pisces Sub-basin are also labelled.

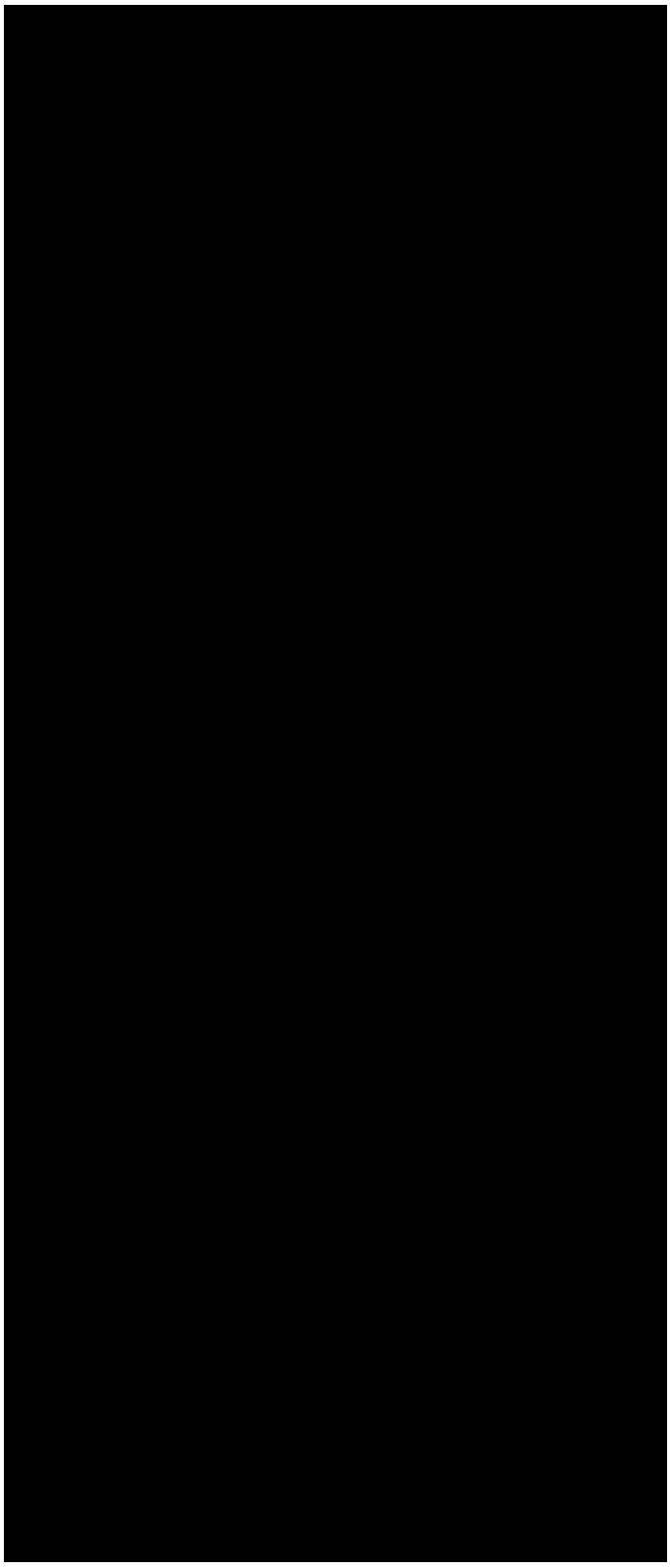

Figure 5.10 Seismic Line GDPI10-59 showing the rugose basement surface and topographic highs along southern edge of the seismic grid.

Kyarra-1A and Moray-1. The Foster Fault System displaces the basement surface close to six kilometres. Outboard of the Foster Fault System is the Darriman Fault System. The Darriman Fault System consists of normal faults sub-parallel to the Foster Fault System. Here, apparent offset of the basement horizon is greater than 4 km, as shown on seismic line GDPI10-17. Other seismic lines crossing the Darriman Fault System are interpreted not to extend far enough to the north to show the basement horizon in the hanging wall. Interestingly, the general E-W trend of the basin-bounding fault systems is interpreted as perpendicular to the underlying boundaries of the accreted terranes which run north-south. This change may reflect deeper crustal features, or more likely the presence of rigid, cratonised basement (granite) and the focusing of faults along weaker boundaries around the granites.

In the eastern part of the grid, a series of smaller down-to-the-north half graben define the structural extent of the Pisces Sub-basin as covered by the GDPI10 2D seismic grid. The half graben are bounded by a series of normal faults with a basement offset of 1.4 to 2.0 km. Between the faults, the basement ramps down from 1.25 km on the platform to greater than 3.5 km depths where the thickest sedimentary succession of the Pisces Sub-basin is observed. Faulting in the region has a similar trend to the Foster and Darriman fault systems, but the character of the faulting is that of discrete faults rather than a larger amalgamated fault system. The Pisces Sub-basin faults clearly display half graben and relay ramp geometries (Figure 5.9). This style of faulting resulted from extension affecting a more brittle basement rather than a main extensional fault zone cross-cutting basement. The distinctive Pisces Sub-basin faults could be due to rheological differences in the basement or the manifestations of a different extension event during the extensional phase prior to breakup and seafloor spreading. The GDPI10 2D seismic grid also provides the opportunity to re-map a portion of the Pisces Sub-basin. The geographic extent of the Pisces Sub-basin in the Gippsland Basin was defined by Bernecker et al. (2001) based on the depositional extent of the Strzelecki Group.

Figures 5.11 and 5.12 display the nature of faulting along the eastern margin of the Southern Platform and the formation of isolated half graben across the platform. High-angle normal faulting formed along the margins of the rigid granitic basement block that underlies the Southern Platform (Figure 5.11). The inversion anticline that formed at Kyarra-1A is the result of later compression of weaker sediments against the basement buttress of the Southern Platform. The different styles and possibly age of half graben that formed across the Southern Platform are indicative of localised faulting within an otherwise rigid basement block (Figure 5.12). The Foster Fault System formed at the margin of the rigid basement block that underlies the Southern Platform.

5.4 Strzelecki Group

The Late Jurassic to Late Albian Strzelecki Group was deposited as a syn-rift succession during Southern Margin rifting. The Strzelecki Group consists of interbedded lithic and volcaniclastic sandstones, mudstones and minor coals that overlie igneous and folded sedimentary rocks of Paleozoic age. Strzelecki sandstones were deposited in meandering to braided fluvial systems with volcaniclastic sediments derived from active volcanoes to the east (Norvick and Smith, 2001). In general, Strzelecki Group sediments have poor reservoir quality due to unstable lithic and volcaniclastic components which have altered to clays and occlude porosity. For these reasons, the Strzelecki Group is unlikely to be a target for greenhouse gas storage. Potential reservoirs are also likely to be strongly faulted and fractured.

The thickness of the Strzelecki Group is poorly constrained in parts of the Gippsland Basin, in part due to lack of well penetrations and poor imaging on seismic data in the Central Deep. The Strzelecki Group is exposed in the Strzelecki Ranges and along parts of the Victorian coast, with a maximum thickness of 2,503 m penetrated in the onshore Wellington Park-1 well (Bernecker and Partridge, 2005).

In the current study area, Strzelecki Group sediments are penetrated in only four wells: Kyarra-1A, Perch-1, Tarra-1 and Omeo-1 (Figure 5.13). With the exception of Omeo-1, the other three wells penetrating the Strzelecki Group were drilled on the Southern Terrace over rotated extensional fault blocks (Tarra-1) or basement inversion structures (Kyarra-1A and Perch-1).

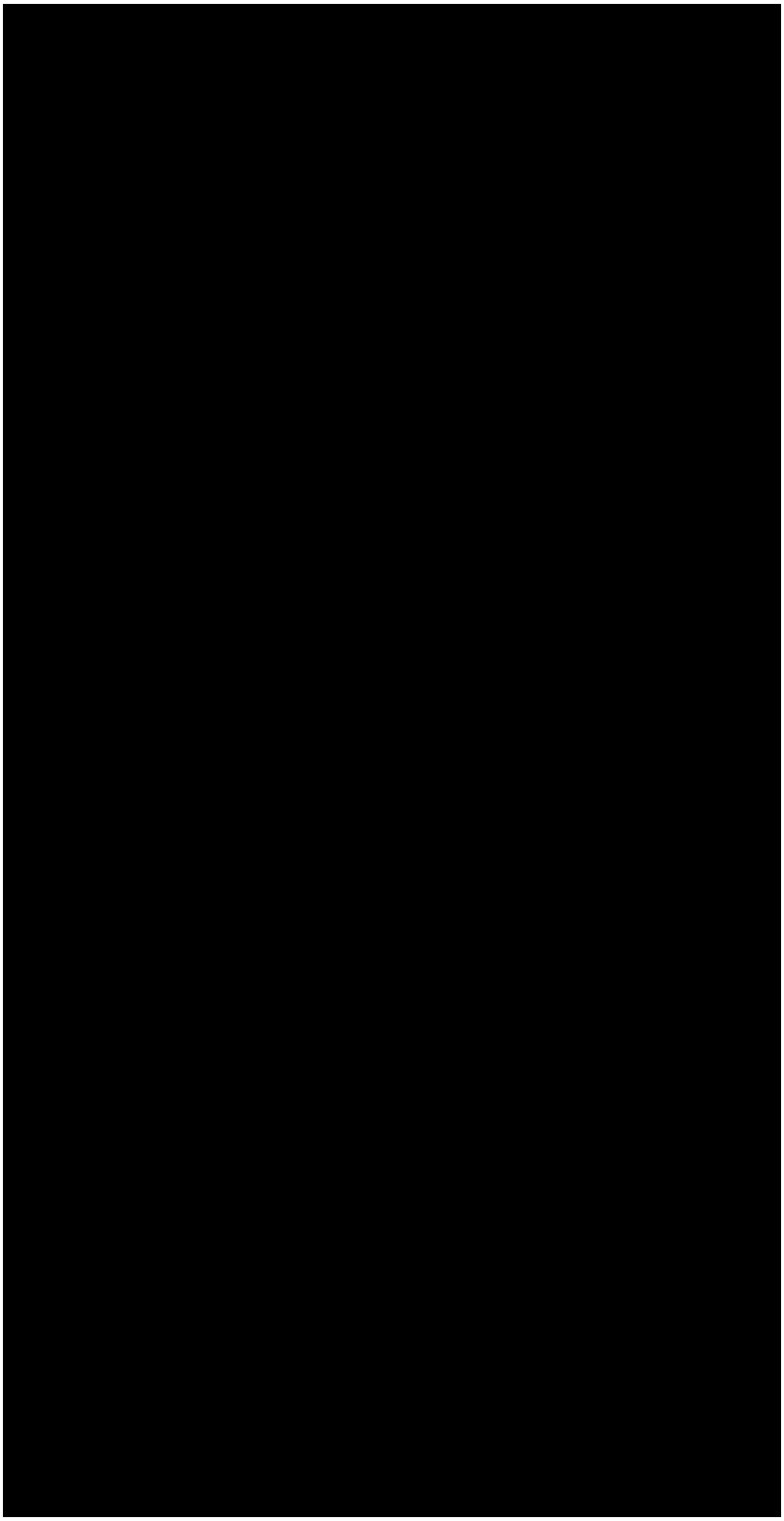

Figure 5.11 Seismic strike line GDPI10-913 showing the nature of faulting around the margins of the Southern Platform. High-angle normal faults occur along the margins of the rigid granitic basement block that underlie the Southern Platform. The inversion anticlines that formed at Kyarra-1A are the result of later compression of weaker sediments against the basement buttress of the Southern Platform.

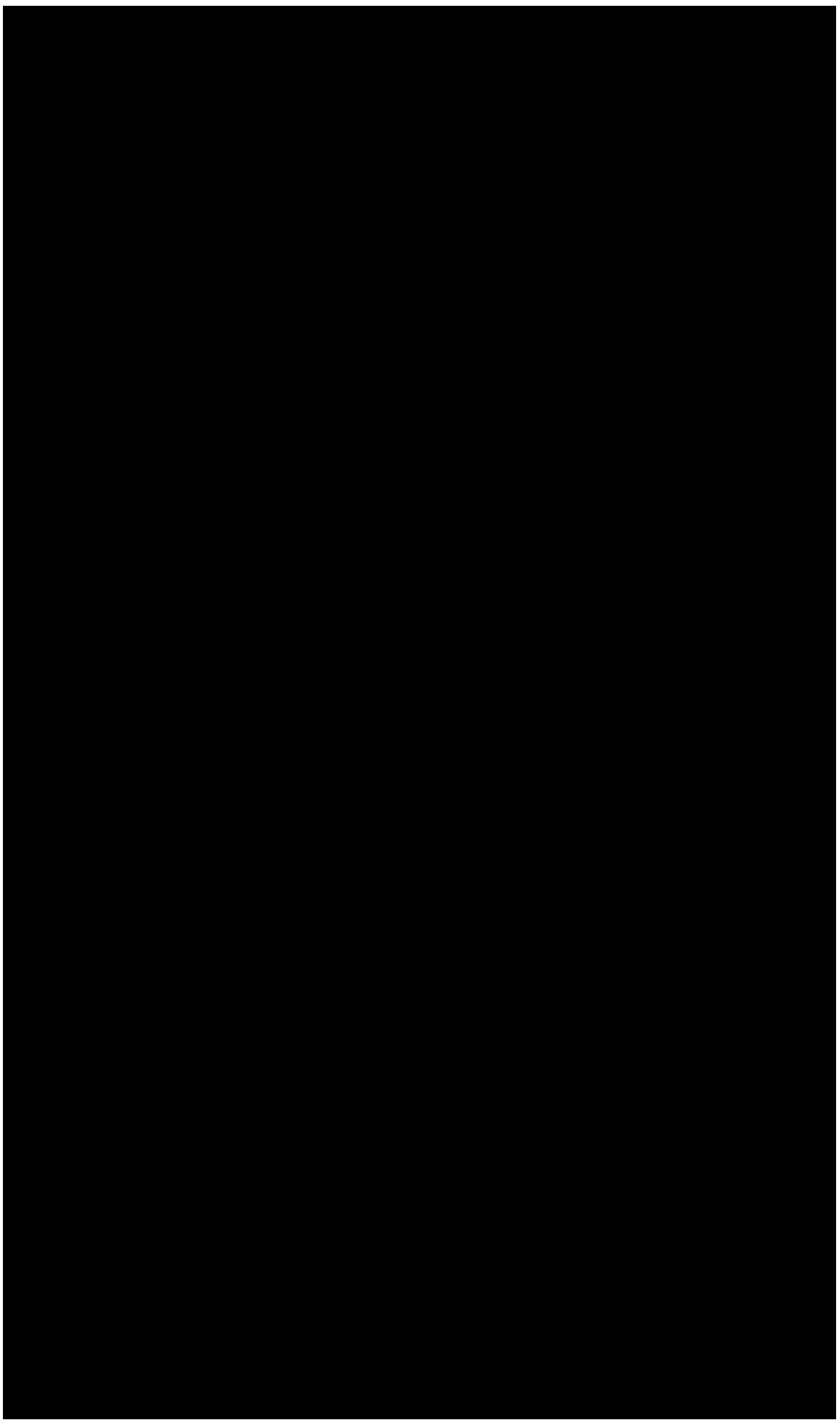

Figure 5.12 The composite seismic line shows the different styles and possibly age of half graben that formed across the Southern Platform. The isolated nature of these structures is indicative of localised faulting within an otherwise rigid basement block. The Foster Fault System (FFS) formed at the margin of the rigid basement block that underlies the Southern Platform.

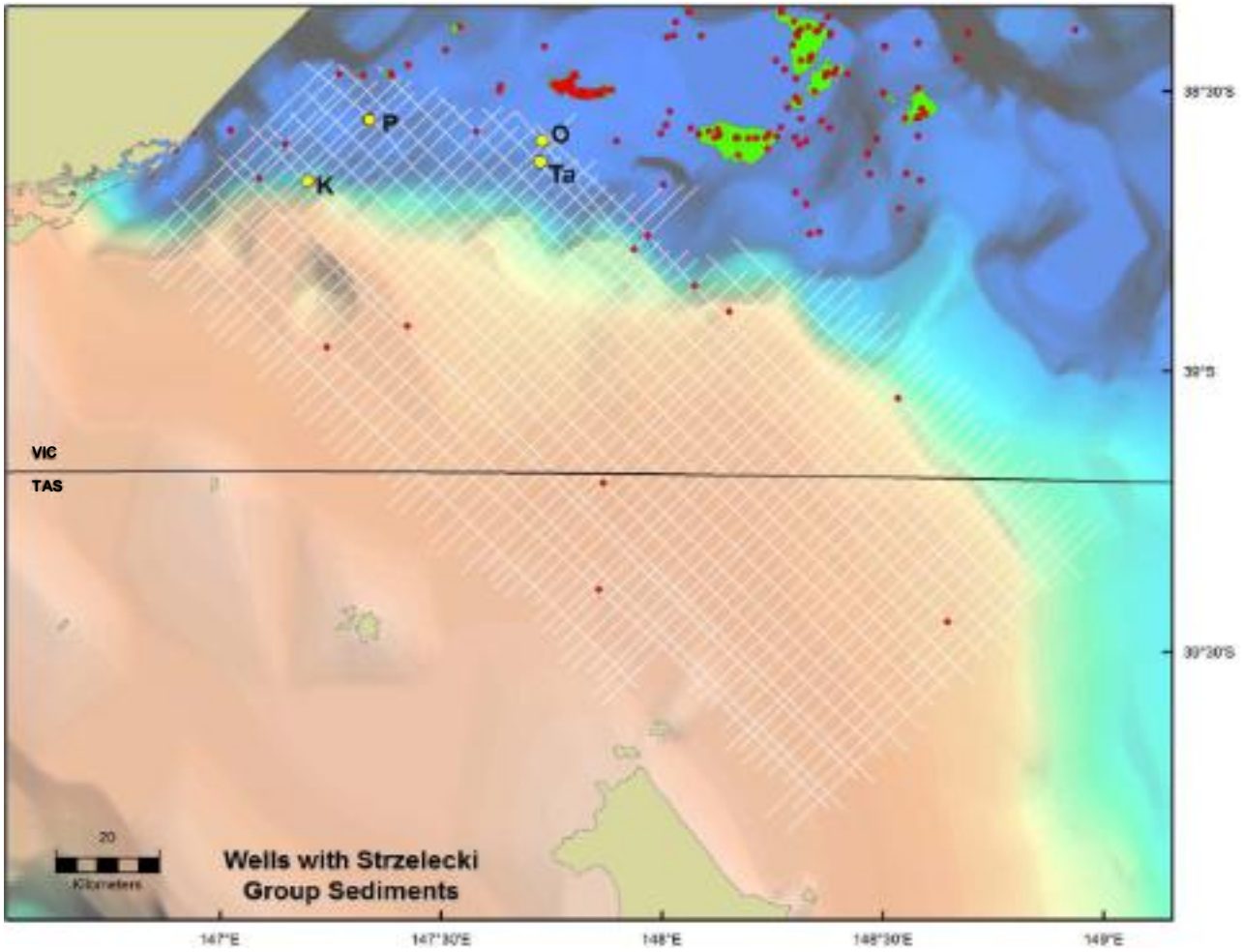

Figure 5.13 Location map of the wells that intersected Strzelecki Group sediments. Well abbreviations: K= Kyarra-1A, O = Omeo-1, P = Perch-1, Ta = Tarra-1.

Strzelecki Group sediments at Kyarra-1A consist of interbedded grey to green-grey siltstones that are micaceous, carbonaceous, lithic and slightly weathered. The Kyarra structure is a basement fault block that has been strongly inverted against a basement buttress (Figure 5.14). Golden Beach Subgroup age equivalent volcanics are interpreted to overlie the Strzelecki Group. Clasts of Strzelecki Group sediments in the overlying Gurnard Formation (1020 m) indicate that nearby inverted structures remained high for an extended time. Flattening on the Top Halibut Subgroup horizon shows that the Kyarra Anticline underwent inversion in the early to mid-Eocene. The structure was reactivated again in the early Miocene and as recently as Pliocene.

At Perch-1, Strzelecki Group sediments are described as lithic sandstones interbedded with shale and coal, overlying interbedded sandstone, siltstone and coals. The fault offset between Perch-1 and Kyarra-1A suggests that the latter well could intersect older Strzelecki Group sediments (Early Albian/Late Aptian), although the spore/pollen analysis contradicts this interpretation (Figure 5.14).

Omeo-1 was drilled on the downdip side of the Darriman Fault System within the Central Deep. The well drilled through the fault plane near TD and into Strzelecki Group sediments in the footwall block (Figure 5.15). The fault is evident on the dipmeter and log evidence from 3310 to 3319 m. Omeo-1 was one of a few deep wells in the current study that were drilled on the basinward side of the Darriman Fault System. However, as the logs provided for the study did not extend to TD, a tie to the Strzelecki Group was made through extrapolation. The Strzelecki Group "formation" top provided for the current study (3195 m) appears to be high on the seismic tie, and a depth below the fault plane at 3310-3319 m is the preferred interpretation (consistent with the original interpretation in the well completion report). The Geoscience Australia well summary indicates that sediments of Turonian age (*P. mawsonii*) occur at 3164 m (high reading) and 3212 m (low reading), and this is consistent with a deeper pick for Top Strzelecki Group. Omeo-2A (TD = 3369 mKb) was drilled further away from the fault plane and did not intersect Strzelecki Group sediments in the footwall.

Nearby at Tarra-1, Strzelecki Group sediments were intersected in the footwall of a rotated fault block located between the Foster and Darriman fault systems (Figure 5.16). Sediments were described as fine-grained lithic to sub-arkosic sandstones with poor to moderate sorting and well cemented by diagenesis (clays and quartz overgrowths). It has been inferred that the sediments were deposited in a distal alluvial fan and braided stream complex (Chan, 1983).

The four well ties to the Strzelecki Group within the GDPI10 2D Seismic Survey grid provide only poor to moderate control on the mapped Top Strzelecki Group horizon. In particular, working the ties on the uplifted/rotated fault block away from well control is problematic near Kyarra-1A and Perch-1 due to complex faulting, inversion and poor imaging/resolution of the deeper section (Figure 5.14). Here, the interpretation of Top Strzelecki Group is largely based on the geometry of the rotated fault blocks on key lines, and extrapolation to parallel lines and cross-ties. It should be noted that most of the seismic grid near Kyarra-1A and Perch-1 is oriented obliquely to the structural trend, and many line intersections occur in faulted zones, which adds to the complexity of mapping the fault blocks.

The fault blocks along the Southern Terrace near Bullseye/Omeo/Tarra show a more consistent geometry of rotation and multiple periods of syn-rift growth against the Foster Fault System (Figures 5.14 and 5.15). The Darriman Fault System at the outer edge of the Southern Terrace is more complex and composed of multiple narrow fault blocks which increase in throw to the north. The large offset at Top Strzelecki along the outer boundary of the Darriman Fault System is relatively easy to pick on longer seismic lines because of the change in seismic character between the down-stepping Strzelecki fault blocks and the juxtaposed sediments of Golden Beach and Emperor subgroups. However, several of the seismic lines have poor resolution on their most northerly extents and the massive fault throw that displaces the Top Strzelecki Group cannot be confidently picked. It is recommended that future work include the extension of these lines to well/horizon ties into the Central Deep, so that the Top Strzelecki offset can be more confidently mapped. An attempt was made to use the gridded data (in Kingdom) supplied by DPI from the 3D-GEO regional study of the Gippsland Basin, however this data was not at a sufficient resolution to be useful.

Previous workers have interpreted the Strzelecki Group as syn-rift and this is not disputed. Bernecker and Partridge (2001) also attribute deposition of the overlying Emperor Subgroup as syn-rift ("basin formation"), and describe the subgroup to be "preserved in rotated fault blocks on the northern side of the Rosedale Fault System" (Figure 5.17). This same scenario has been utilised during the current study interpretation; that is, the rotated fault blocks that occur on the Southern Platform consist of both Strzelecki Group and Emperor Subgroup age sediments.

The key well for this interpretation is Perch-1 which intersected 48 m of Emperor Subgroup sediments unconformably overlying the Strzelecki Group (Figure 5.14). The geometry of these sediments suggests a second phase of limited

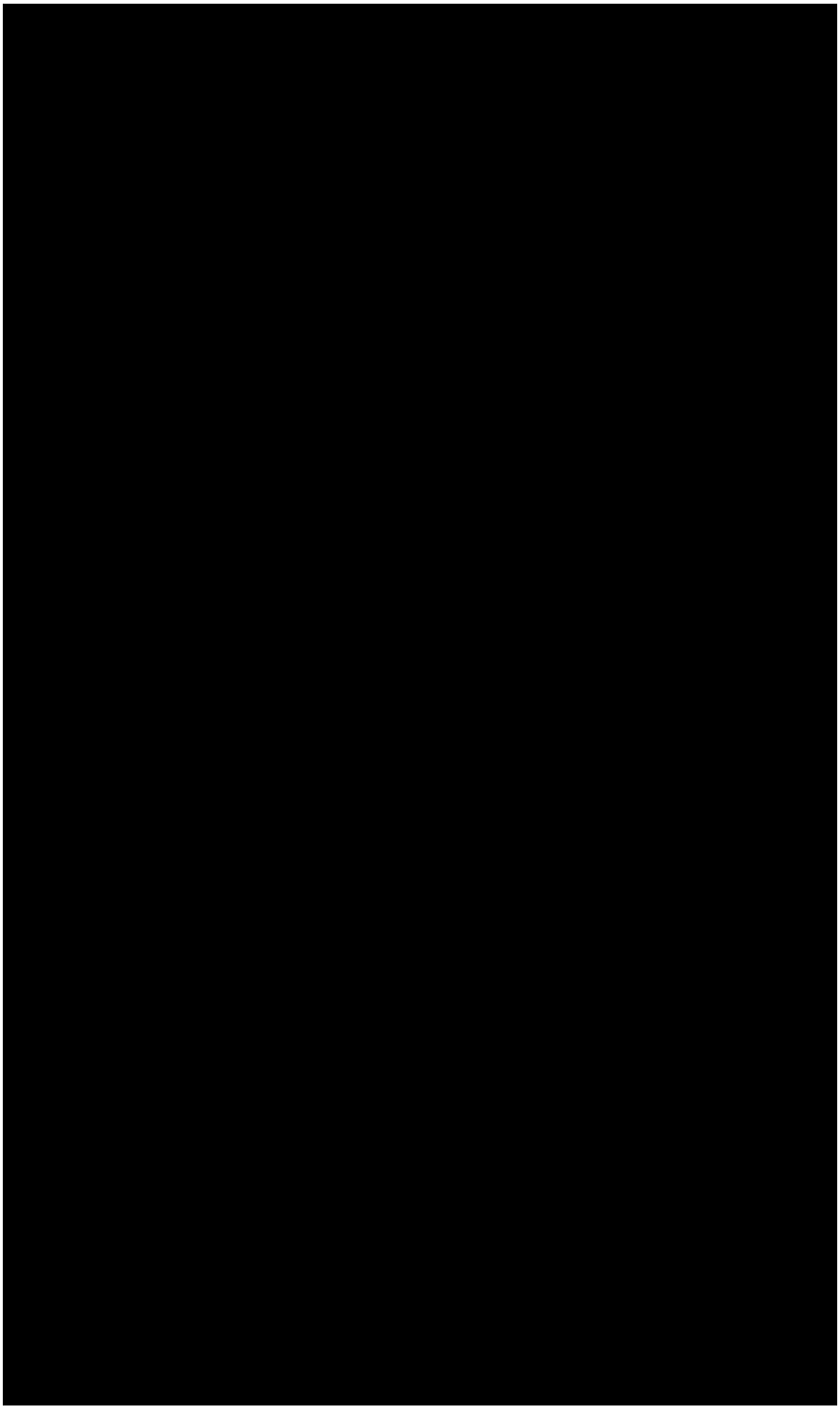

Figure 5.14 Seismic line GDPI10-07 showing the intersections of Strzelecki Group sediments at the Kyarra-1A and Perch-1 wells. Note that Emperor Subgroup sediments were intersected at Perch-1, while volcanic flows of Golden Beach Subgroup equivalent-age were intersected at Perch-1 and Kyarra-1A.

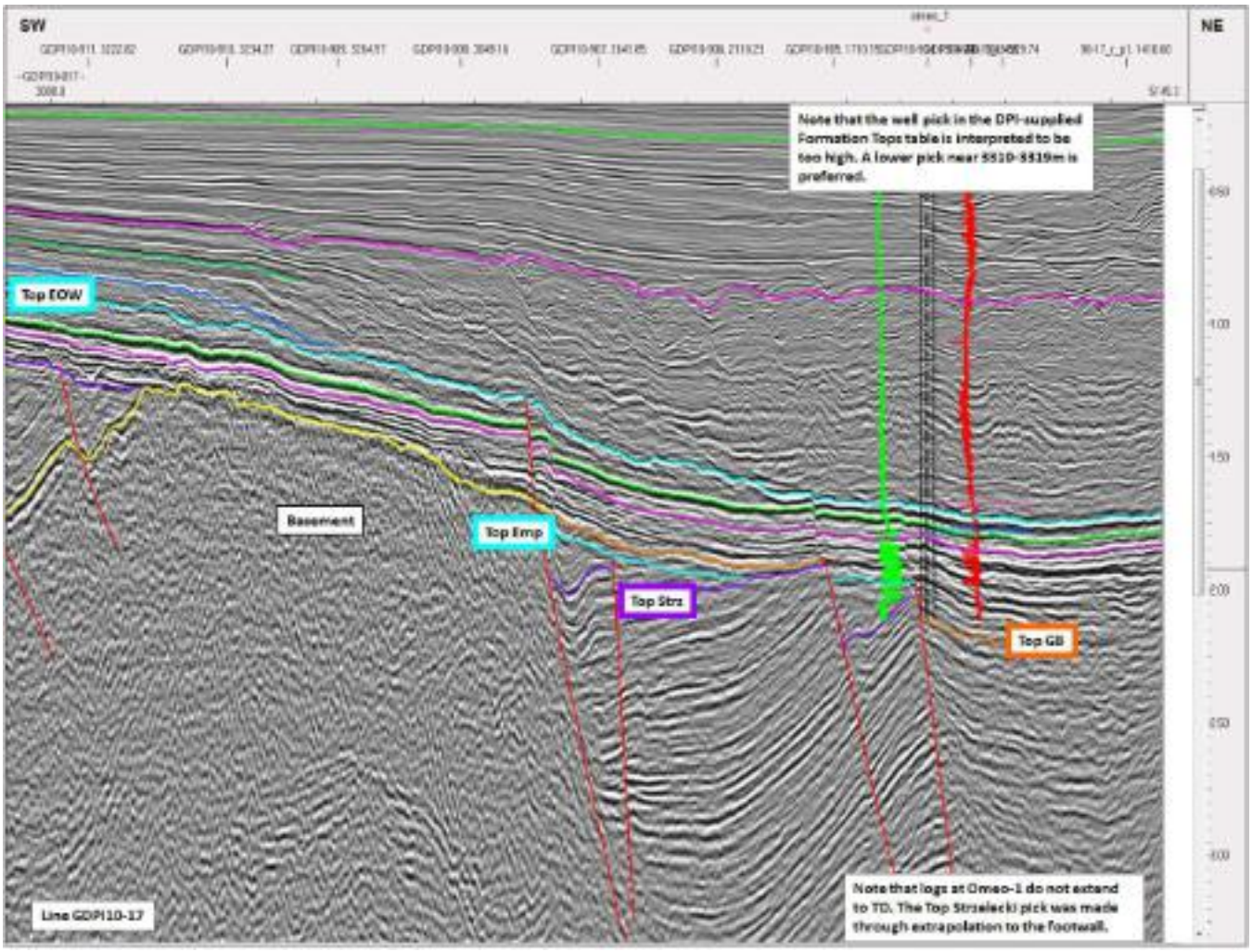

Figure 5.15 Seismic line GDPI10-17 showing the intersection of Strzelecki Group sediments at the Omeo-1 well. Note that Omeo-1 was not designated as a key well and a synthetic was not available.

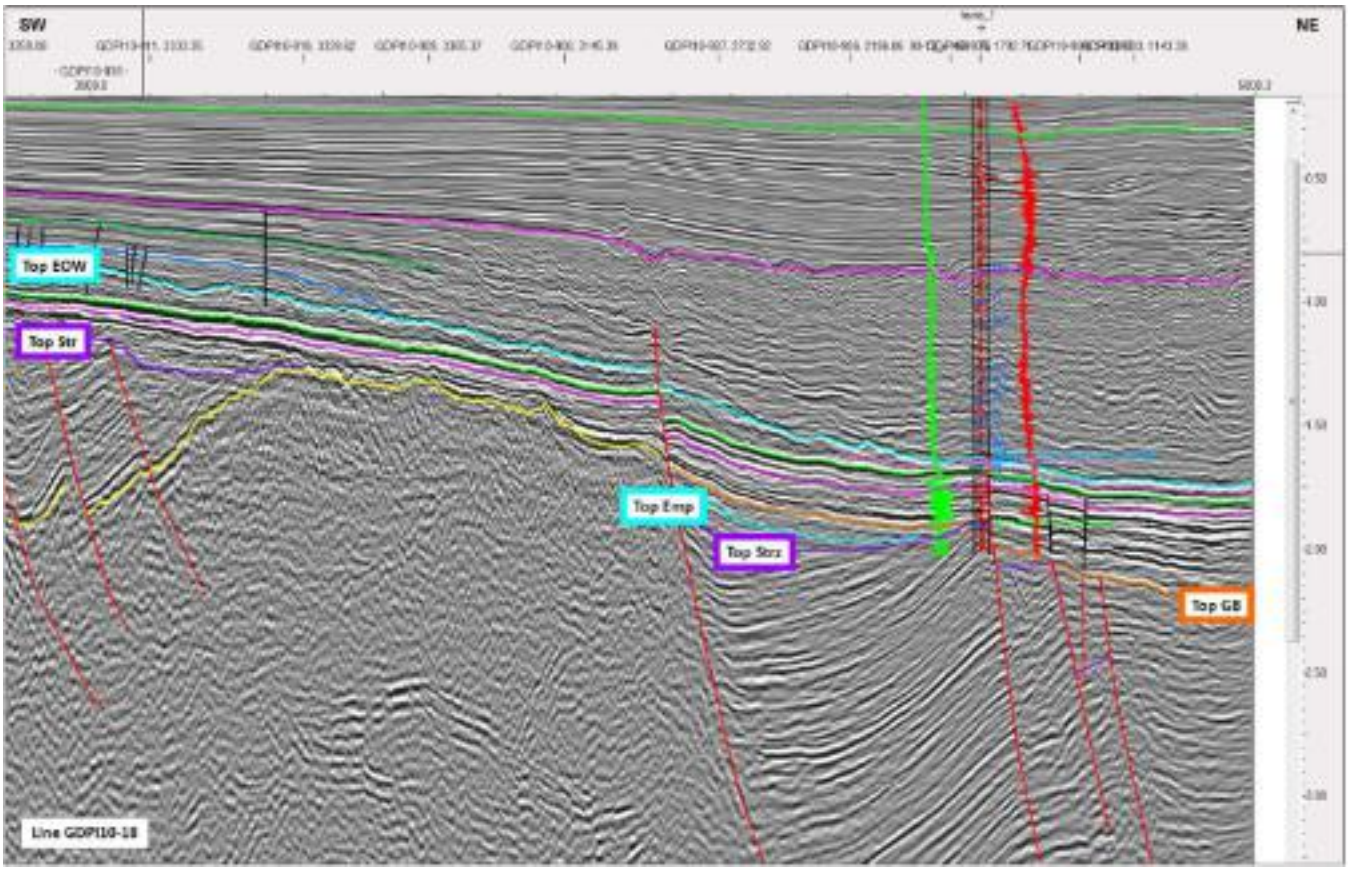

Figure 5.16 Seismic line GDPI10-18 showing the intersection of Strzelecki Group sediments at the Tarra-1 well.

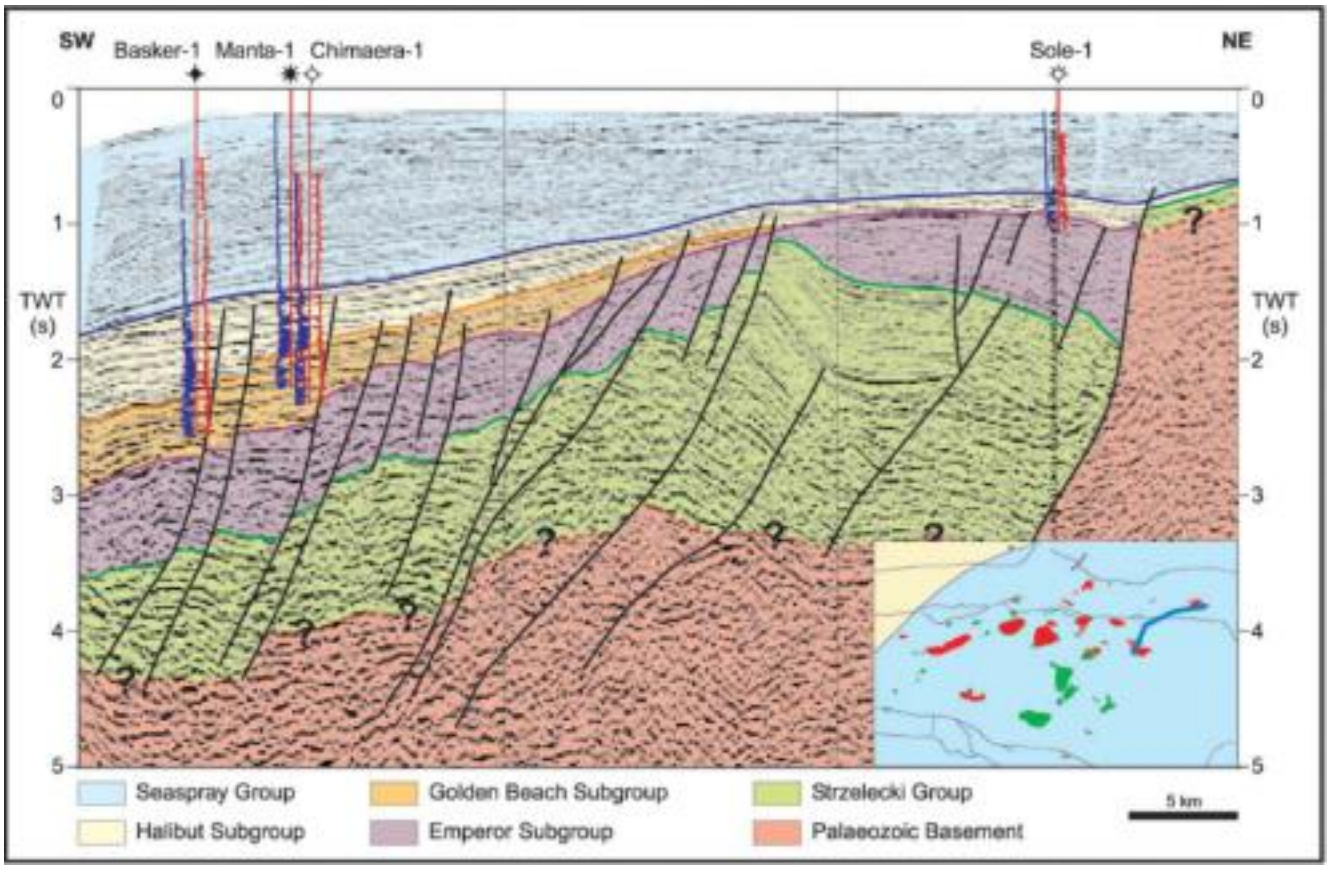

Figure 5.17 Seismic sections along the Northern Flank from Bernecker and Partridge (2001) showing the interpretation of syn-rift geometries within the Strzelecki Group and Emperor Subgroup sediments.

extension in the Turonian prior to breakup in the Tasman Sea at 83Ma (chron 33). In addition, the "transitional beds" described at Omeo-1 could be interpreted as possible Emperor Group. Figures 5.15 and 5.16 near Tarra-1 and Omeo-1, show that Strzelecki was the main syn-rift phase. Emperor is interpreted as a late syn-rift section that thickens variably against the same basin-bounding fault that controlled deposition of the Strzelecki Group. In this instance, the strong rotation of the footwall means that the subcrop across the top of the fault block could be of variable age (Figure 5.18). The Kersop Arkose penetrated at Moray-1 is interpreted to have intersected a similar pocket of isolated syn-rift sediment near the Foster Fault System.

The GDPI10 2D seismic grid has also helped define a previously poorly known depocentre situated in the middle of the Central Platform (Figures 5.19 and 5.20). The depocentre was previously transected by Geoscience Australia line 90-13 (Figure 5.21), however multiples riddled the underlying section and obscured the feature. The basin has a distinct half graben geometry, is up to 6 km deep and bears a strong structural resemblance to the half graben to the north of the Foster Fault System (Figure 5.22). Sediments infilling the basin have been interpreted as Strzelecki Group age equivalent, as seismic character suggests it is distinctly different to infill of smaller half graben on the upper flanks of the Southern Platform. The Groper-1 well was drilled over an older half graben and reached TD in Paleozoic rocks (Figure 5.22). The newly defined half graben on the platform is interpreted to be a younger feature associated with Southern Margin extension.

In tectonostratigraphic terms, it would be appropriate to consolidate sediments of syn-rift deposition (Strzelecki Group and Emperor Subgroup) to distinguish them from overlying post-rift section (Golden Beach Subgroup and younger). This would apply only to the Southern and Northern terraces where Golden Beach Subgroup sediments are patchy in distribution and mostly sag related. In addition, the current interpretation has included Emperor Subgroup as part of the fault block. Evidence of the "uplift/compression with reverse faulting" event (Otway Unconformity; Bernecker et al., 2001) which separates the Strzelecki Group and Emperor Subgroup successions is not observed in the current study area. However, the Strzelecki Group and Emperor Subgroup are well entrenched in the nomenclature and sediments are distinctively different in lithology and composition, so this proposition to consolidate them into one tectonic phase may cause confusion.

5.5 Latrobe Group

The Turonian to basal Oligocene age Latrobe Group has been subdivided into the Emperor, Golden Beach, Halibut and Cobia subgroups (Bernecker and Partridge, 2001). Previously, the Latrobe Group was informally referred to as the undifferentiated "Latrobe Siliciclastics". The revised nomenclature of Bernecker and Partridge (2001) recognised significant lithostratigraphic and chronostratigraphic breaks within a mostly non-marine siliciclastic succession. The Latrobe Group hosts most of the discovered commercial oil and gas accumulations in the Gippsland Basin, and is viewed as the most prospective interval for potential greenhouse gas storage.

The Latrobe Group was deposited under changing tectonic conditions with an initial rift phase (Emperor Subgroup), followed by margin sag and rapid subsidence in the Central Deep associated with Santonian to early Eocene Tasman Sea spreading (Golden Beach and Halibut subgroups; Bernecker and Partridge, 2005). While it is beyond the scope of the current study to review regional tectonic settings and events, it seems unlikely that seafloor spreading in the Tasman (which is east/west) would result in N/S-to-NE/SW directed extension. Events further afield such as the final stages of separation along the active transform margin along western Tasmania and the South Tasman Rise, may have given rise to continued and selective reactivation of major faults in appropriate orientations. In the Bass Basin, minor reactivation of extensional faults continued into the early Eocene (Ypresian/50Ma; Blevin et al., 2003). This age is approximately time equivalent to the interpreted end of extension in the broader Gippsland Basin (Bernecker and Partridge, 2001). Given that much of the extension was largely focused on the major east/west-tending, basin-bounding faults, far-field stresses may have provided the driver.

The final phase of slower margin sag (Cobia Subgroup) was characterised by declining sediment supply and widespread transgression of the basin margins (Bernecker and Partridge, 2005). The reservoir, source and seal rocks within the Latrobe Group are often difficult to correlate because of similar and recurring lithologies, and broad biostratigraphic zonations.

Formations within the subgroups are used to distinguish different facies and depositional settings contained in each unconformity-bounded unit (subgroup). In general, more marine and nearshore environments are recorded in sediments of the deeper offshore Gippsland Basin (particularly the eastern part of the Central Deep), with facies grading to paralic and non-marine in the present-day onshore region, and across the shallow basement platforms and terraces that bound the Central Deep. Deposition was principally controlled by the interplay of subsidence, sediment supply and relative sea level changes in response to the opening of the Tasman Sea (Bernecker and Partridge, 2001).

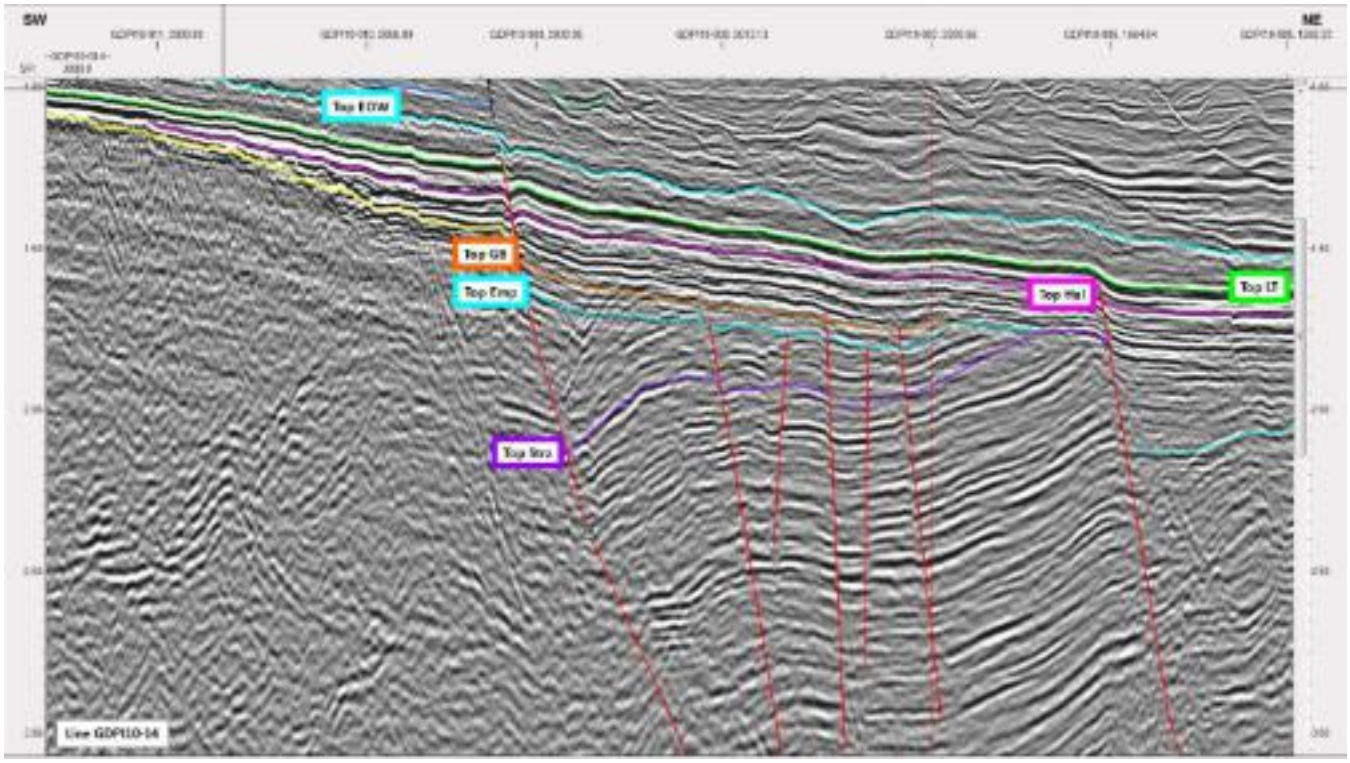

Figure 5.18 Seismic line GPDI10-14 showing the complex truncation of the Emperor Subgroup on the footwall of fault blocks on the Southern Terrace.

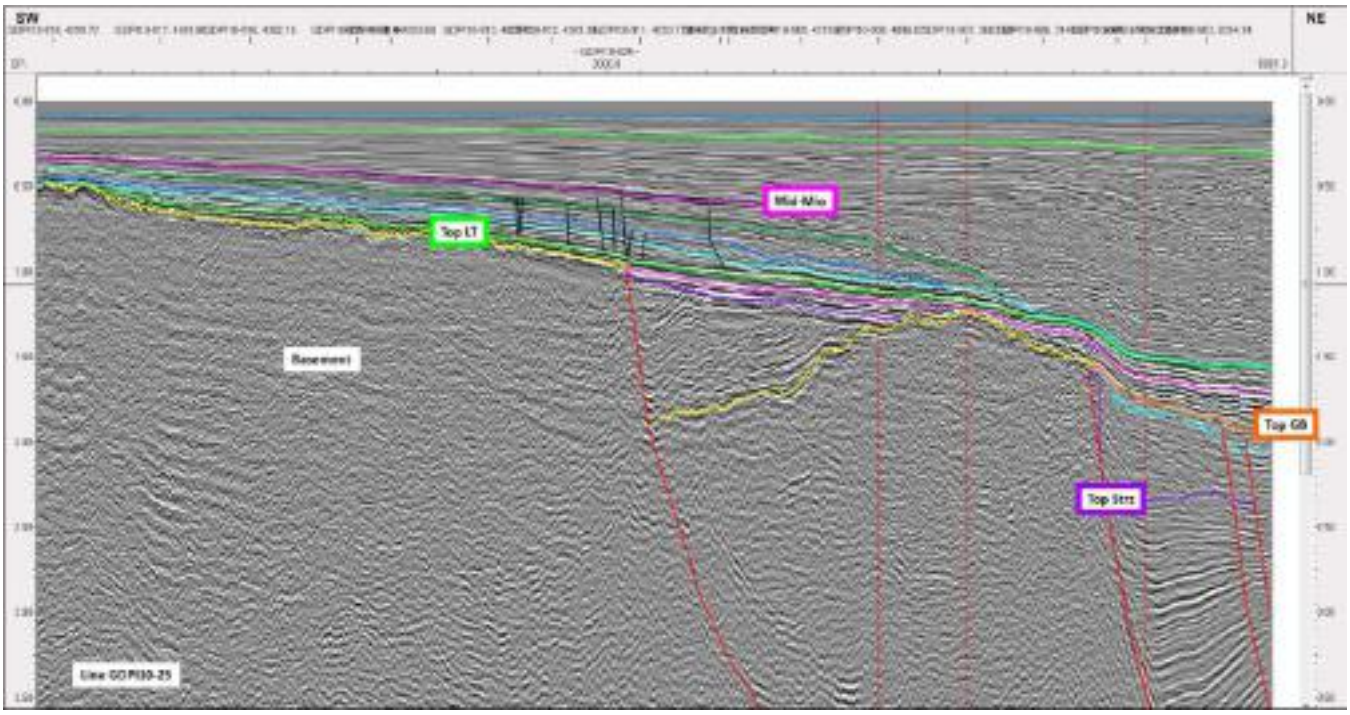

Figure 5.19 Seismic line GPDI10-25 showing the newly mapped half graben on the Southern Platform.

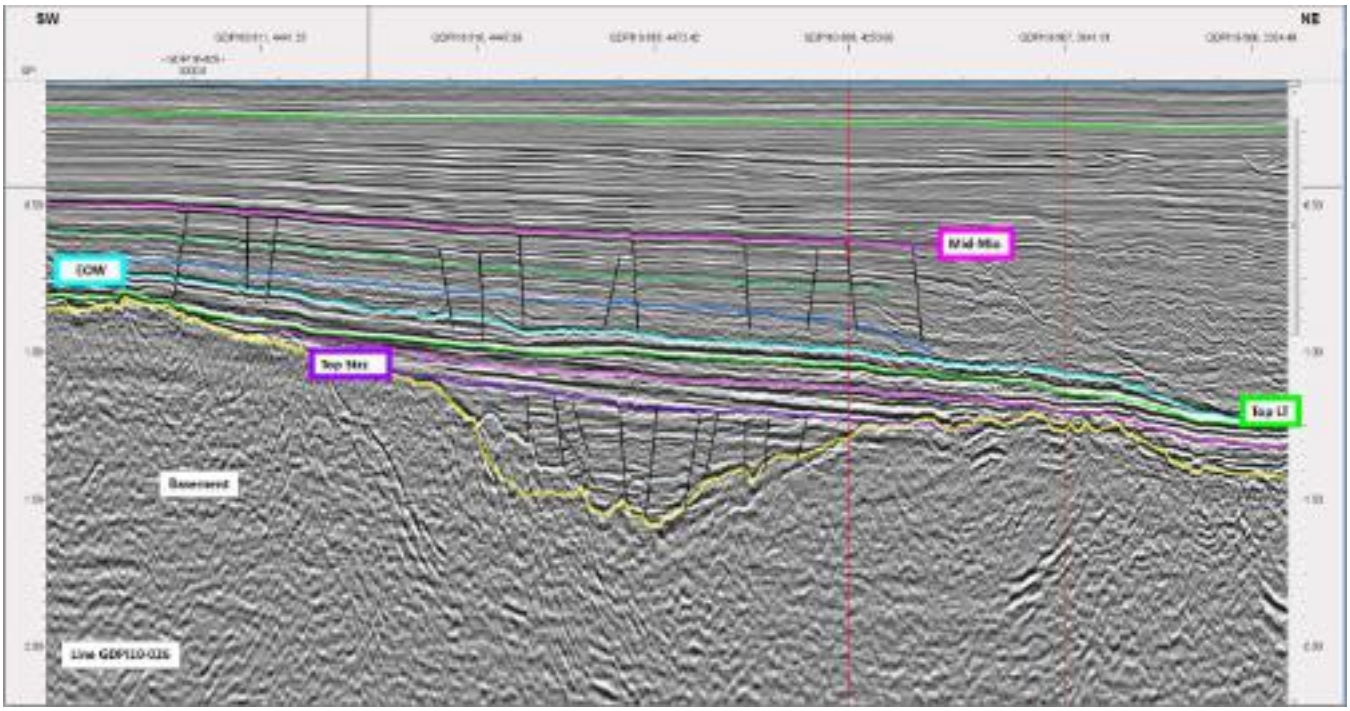

Figure 5.20 Seismic line GPDI10-26 showing the newly mapped half graben on the Southern Platform.

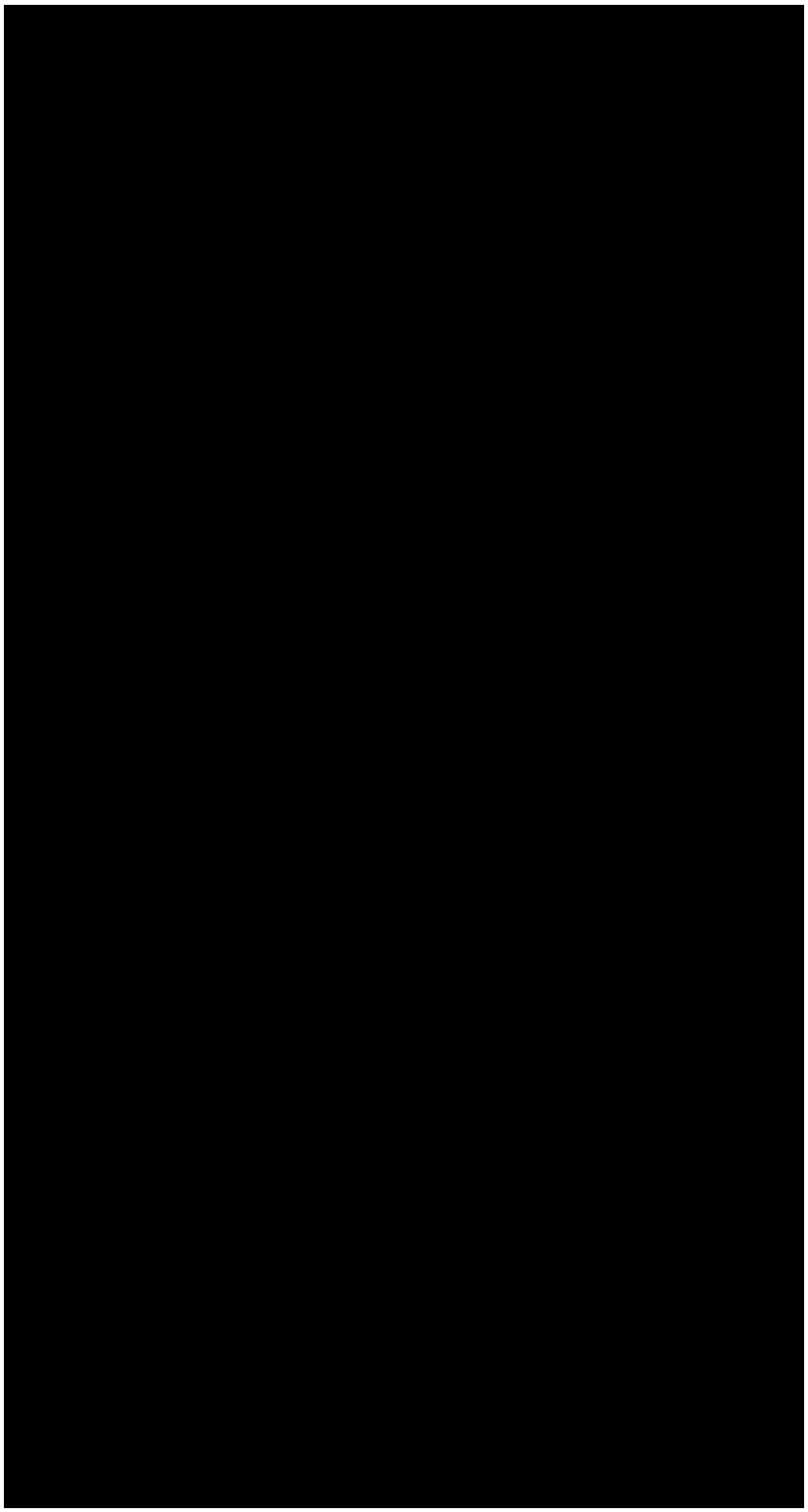

Figure 5.21 Geoscience Australia seismic line 90-13 across the intra-platform half graben (yellow box). Note that multiples obscure the imaging of this feature.

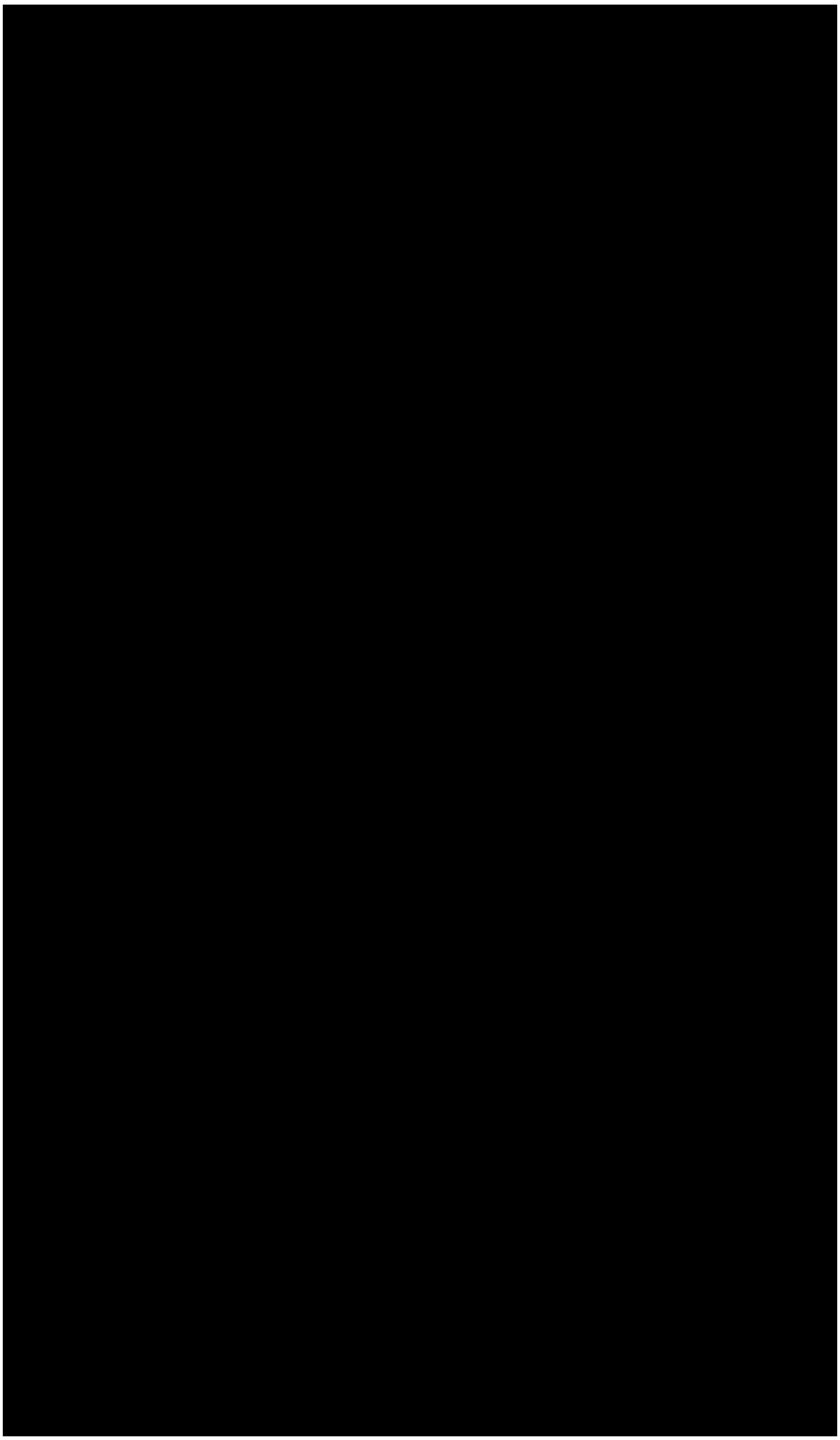

Figure 5.22 Seismic line GPDI10-20 comparing the seismic character of Paleozoic half graben near Groper-1 and the interpreted Strzelecki age half graben on the Southern Platform. A possible pre-rift section is also present within the Strzelecki half graben.

The Latrobe Group unconformably overlies the syn-rift Strzelecki Group, while the top of the group is marked by a condensed interval (depositional hiatus). Bernecker and Partridge (2001) have proposed regionally extensive unconformities between the subgroups of the Latrobe Group: 1) Longtom Unconformity between the Emperor and Golden Beach subgroups; 2) Seahorse Unconformity between the Golden Beach and Halibut subgroups; and, 3) Marlin Unconformity between the Halibut and Cobia subgroups. In a series of chronostratigraphic cross-sections, 3D-GEO (2010) suggest there is only one regional unconformity between the Strzelecki Group and the Emperor Subgroup as all other age zones are represented in at least one well. The biostratigraphic breaks observed by Bernecker and Partridge (2001) are most pronounced along the basin margins where accommodation is low, and over hydrocarbon fields which have been periodically uplifted with erosion or non-deposition (3D-GEO, 2010). The chronostratigraphy of Norvick et al. (2001); modified by 3D-GEO (Figure 5.23) also suggests that the intra-Latrobe unconformities may be more local in their development.

5.5.1 Emperor Subgroup

The Emperor Subgroup is "preserved in rotated fault blocks on the northern side of the Rosedale Fault System signifying compressional tectonism and tilting of the northern basin margin during the development of the Longtom Unconformity" (Bernecker and Partridge, 2001; Figure 5.17). The syn-rift nature of the Emperor Subgroup on the Southern Terrace and its relationship to the Strzelecki Group has been discussed in the previous section. The basal Emperor Subgroup is *P. mawsonii* age and unconformably overlies the Strzelecki Group on the Southern Platform and Southern Terrace. A thick, undrilled section of the Emperor Subgroup is interpreted to underlie the Central Deep at depths below 4 to 6 km.

The Emperor Subgroup contains the clastic Curlip Formation, Kipper Shale, Admiral Formation and the Kersop Arkose, although the age of the latter is poorly constrained. Sandstones within the Emperor Subgroup typically contain lithic fragments and arkosic sand that has been reworked from the underlying Strzelecki Group, particularly in areas affected by Cenomanian uplift. The Kipper Shale was deposited as part of a basin-wide lacustrine system that filled the rift valley of the Central Deep. Sediments are silty claystones with lacustrine shoreline sands and turbidites. The overlying Curlip Formation represents the termination of lake sedimentation and the return to a largely fluvial depositional regime (Bernecker and Partridge, 2001).

In the current study area, the Emperor Subgroup is penetrated in Tommyruff-1, Perch-1, Melville-1 and Moray-1 (Figure 5.24). Each well has a different lithology or facies. In Tommyruff-1, 243 m of Emperor Subgroup sediments (Curlip Formation and Kipper Shale) were intersected (Figure 5.25). The well section consists of a repetitive sequence of thinly bedded sandstone, siltstone and claystone units with some volcanic lithics towards the base of the interval. The sandstones (ditch cuttings) are loose, unconsolidated and medium- to coarse-grained. In Perch-1, 48 m of Emperor Subgroup sediments (Curlip Formation) consist of sandstones with minor siltstone and coals (Figure 5.14). The Emperor Subgroup is also interpreted to lie just below TD at Palmer-1 (Figure 5.26), just north of the Perch oil field.

The Emperor Subgroup (Curlip Formation) is 323 m thick at Melville-1 (Figure 5.27). Here, the section is predominantly siltstone interbedded with claystone and sandstone. Siltstones near the base contain more lithic grains, while the unit also contains thin coals with the biostratigraphic results suggesting sediments are younger than the lacustrine Kipper Shale (Partridge, 2002). The basal 15 m of the well section contained volcanic rocks and altered claystones; suggestive of a local intrusion. Sandstones at Melville-1 are relatively tight and have marginal reservoir potential.

At Moray-1, the Emperor Subgroup (Kersop Arkose) consists of a massive 765 m of continuous sandstones with an increasing arkosic component and conglomerates toward the base (Figure 5.28). However, given the location of the well in a fault sliver near the Foster Fault System, the coarse clastic component is considered typical of a fault-associated alluvial fan. The section from 1905 to 2670 m at Moray-1 is the type section for the Kersop Arkose (Bernecker and Partridge, 2001).

Similar to the underlying Strzelecki Group, the sparse intersections of Emperor Subgroup in the study area supports limited confident mapping of the Top Emperor Subgroup away from the wells. The thickness of the Emperor Subgroup is also poorly constrained due to limited confidence in the deep Strzelecki seismic picks. However, the mapping suggests that the active faults played a significant role in the distribution and facies of the Emperor Subgroup. Due to the diversity of lithologies and depositional settings of the tie wells, the Top Emperor Subgroup has a different seismic character between wells. For this reason, the Top Emperor Subgroup was primarily a manual pick and often correlates to a weak peak (zero phase) on the seismic data.

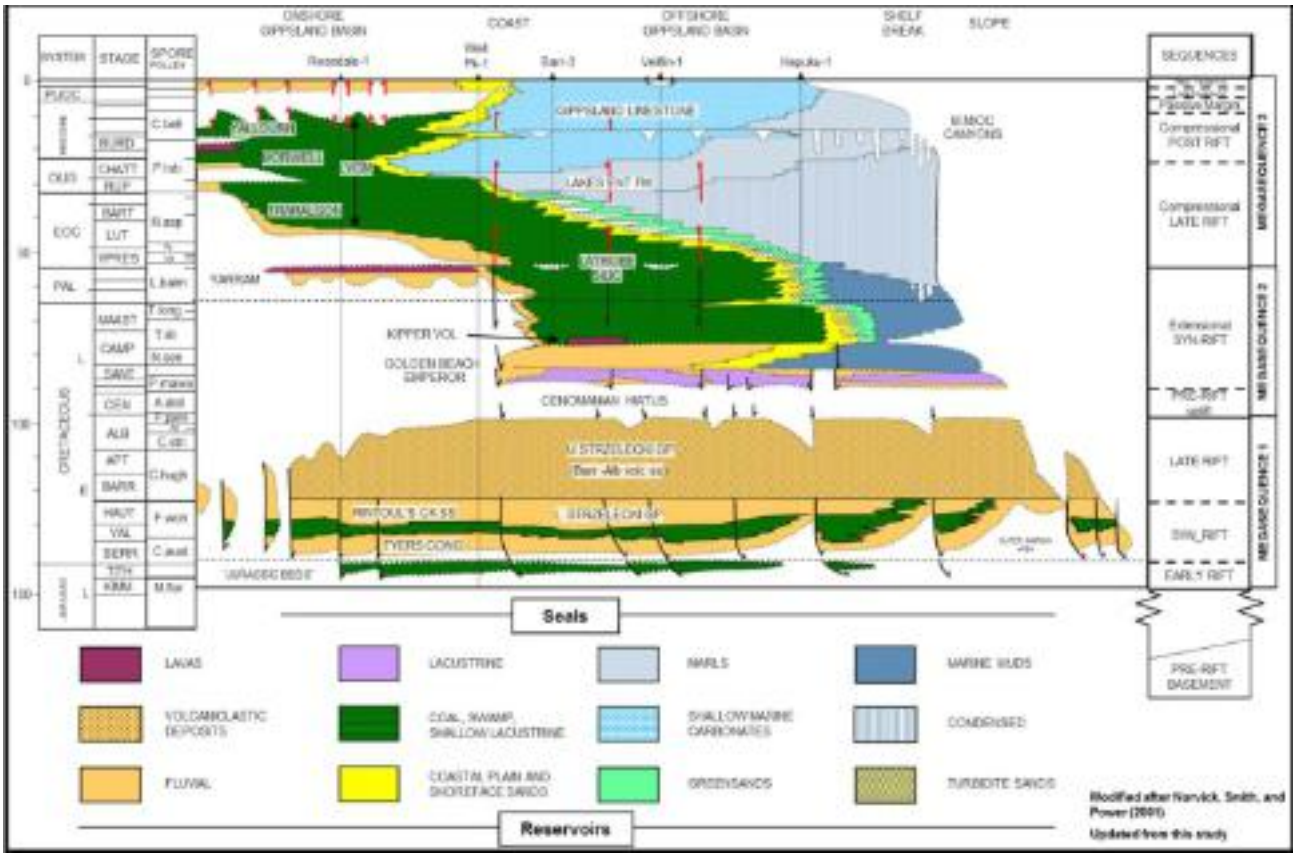

Figure 5.23 Chronostratigraphic chart of Norvick et al. (2001) modified by 3D-GEO (2010) showing that the Cenomanian hiatus is the main regional unconformity in the Gippsland Basin.

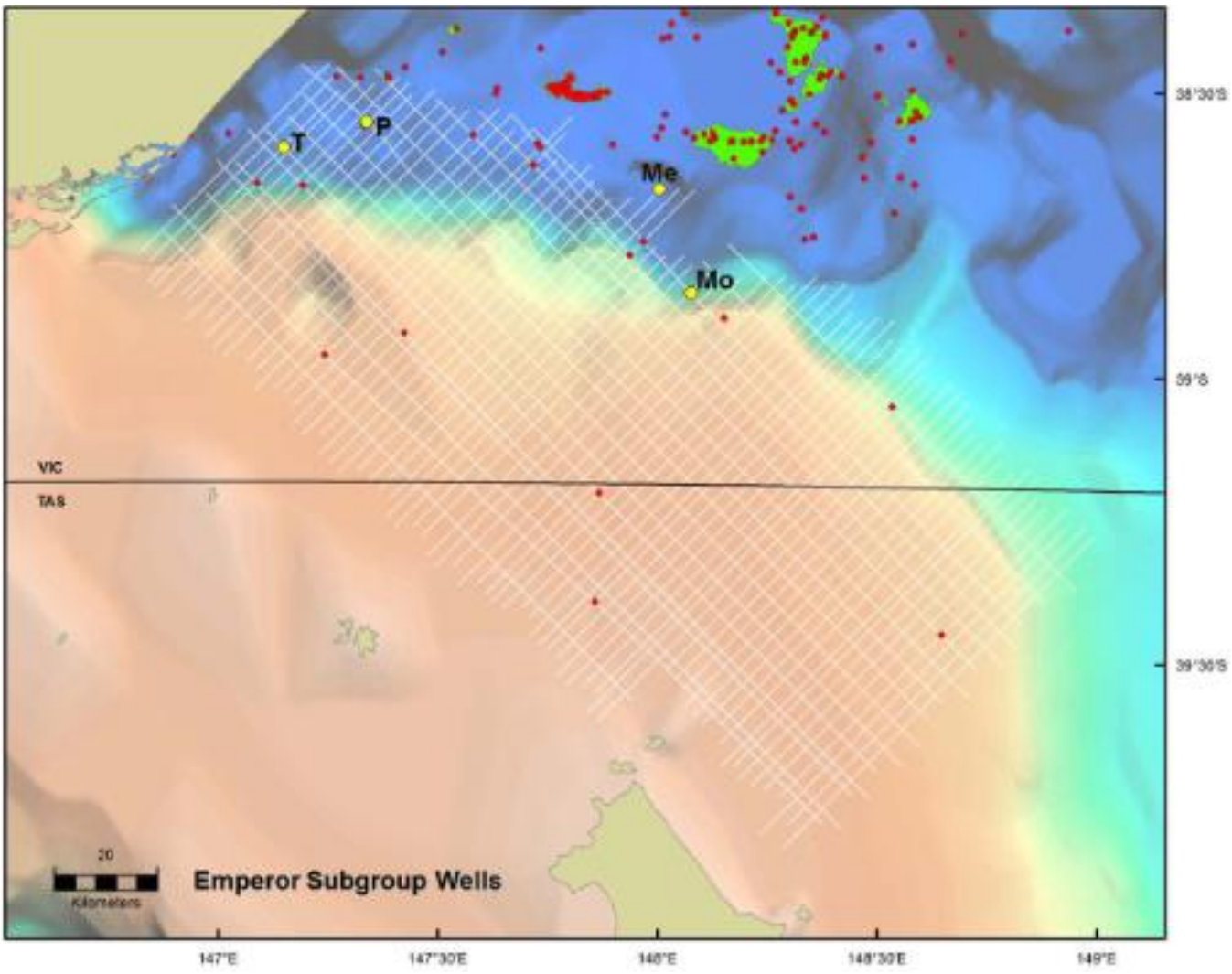

Figure 5.24 Location map of the wells that intersected Emperor Subgroup sediment. Well abbreviations: Me = Melville-1, Mo = Moray-1, P = Perch-1 and T = Tommyruff-1.

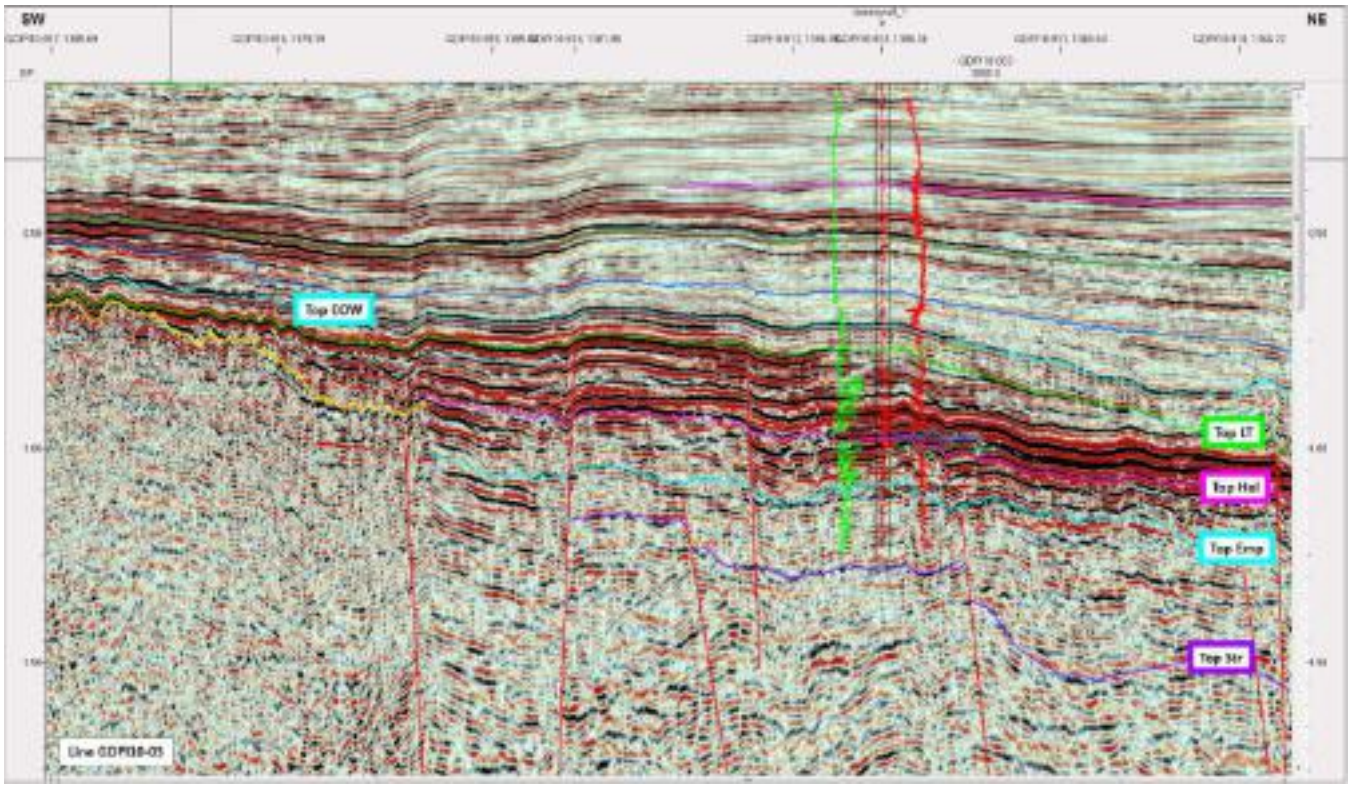

Figure 5.25 Seismic line GPDI10-03 showing the intersection of Emperor Subgroup (Kipper Shale) sediments at Tommyruff-1. Deposition of the Emperor Subgroup is interpreted to be within a restricted, fault-controlled setting during a late stage phase of extension.

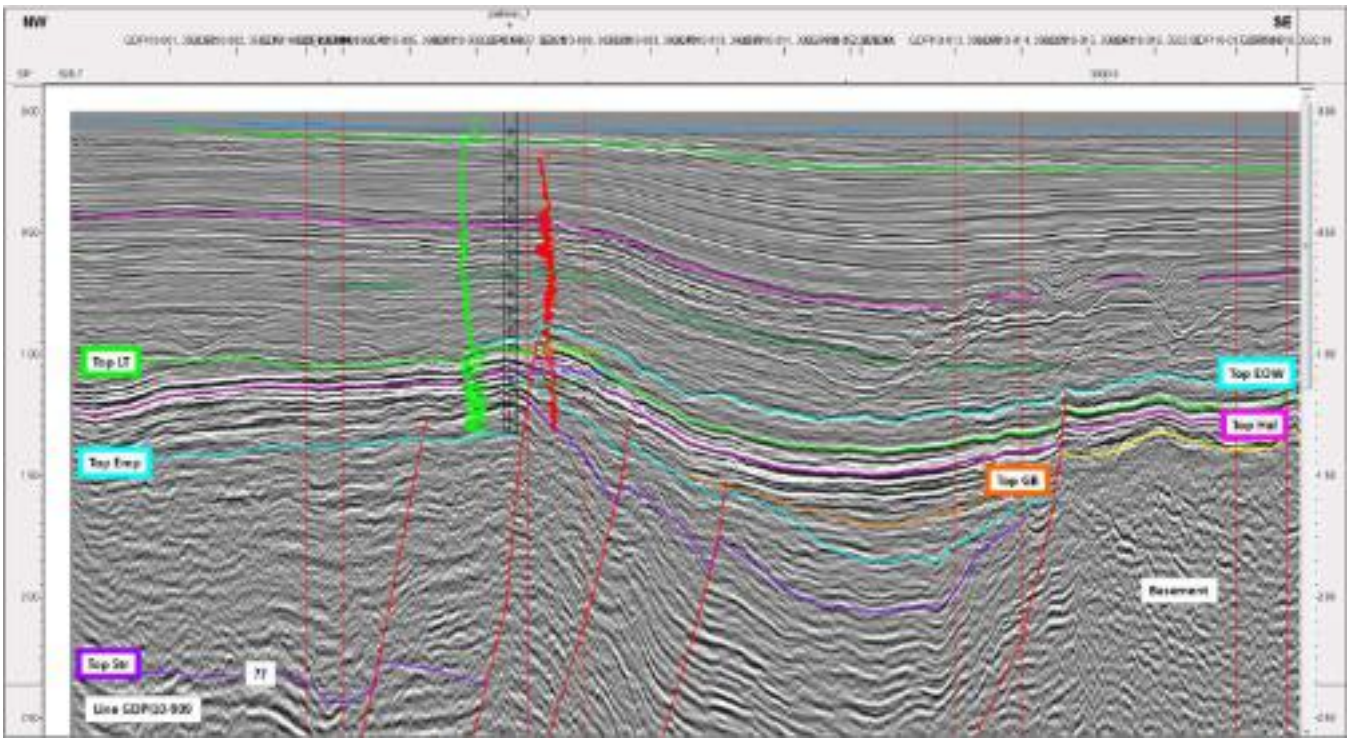

Figure 5.26 Seismic strike line GPDI10-909 showing the interpretation of Emperor Subgroup (Kipper Shale) sediments just below TD at Palmer-1.

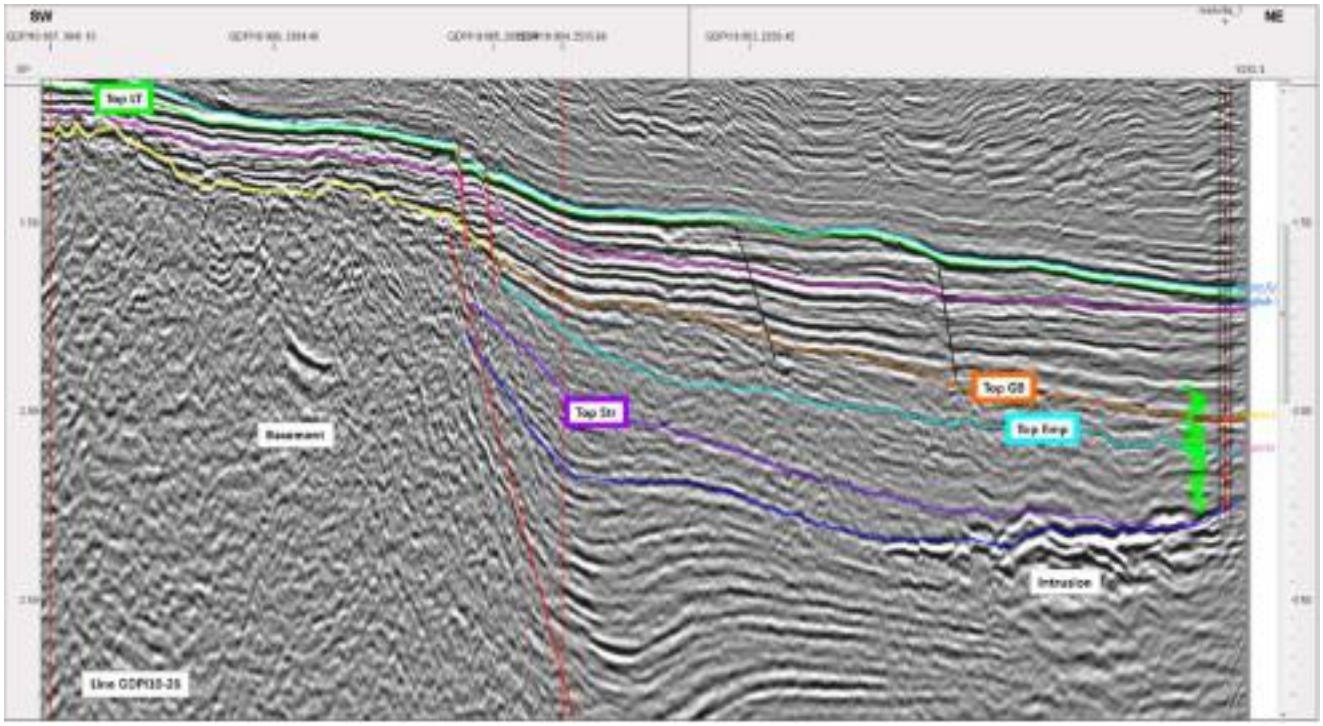

Figure 5.27 Seismic line GPDI10-26 showing the intersection of Emperor Subgroup (Curlip Formation) sediments at Melville-1. The pick at the Top Emperor Subgroup should be reviewed. Note the interpretation of volcanic intrusions near the base of the well.

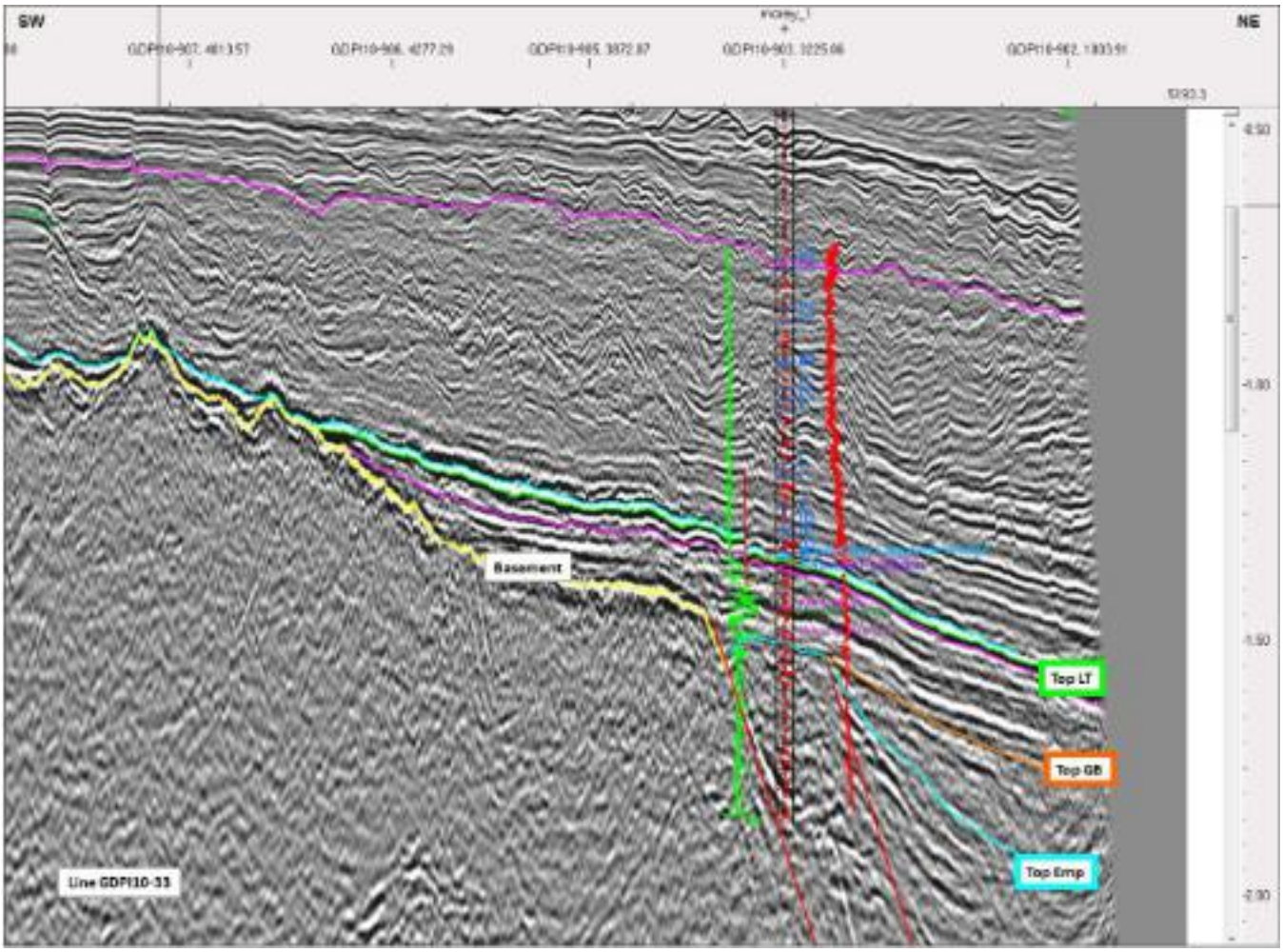

Figure 5.28 **Seismic line GPDI10-33 showing the intersection of Emperor Subgroup (Kersop Arkose) sediments at Moray-1. The well was drilled on a fault sliver against the Foster Fault System. The arkose is interpreted as typical of a fault-related alluvial succession.**

The geometry of the Emperor Subgroup between the Tommyruff-1 and Wyrallah-1 wells, supports the development of a local, fault-controlled depocentre (Figure 5.29). These structures provided for the development of semi-restricted lacustrine systems, and this scenario helps to explain the thick intersection of monotonous and repetitive sediments at Tommyruff-1. It is expected that facies closer to the bounding faults will be coarser-grained due to proximity to local sediment sources. A similar feature is interpreted from seismic to occur near Palmer-1, although the well reached TD in the overlying Halibut Subgroup (Figure 5.26). To the east of Palmer-1, the Golden Beach Subgroup has been interpreted to be sparsely present within the deeper parts of the fault-controlled depocentres.

Despite tying at the end of the line (GDPI10-026) and limited geophysical logs, Melville-1 provides an excellent stratigraphic tie in a key area of the outer Southern Terrace (Figure 5.27). The well confirms the presence of a 323 m thick section of Emperor Subgroup sediments, although the Top Emperor Subgroup (and Top Golden Beach Subgroup) pick can only be confidently mapped along the most northerly strike line in this part of the grid (GDPI10-903), so it has limited use across the broader seismic grid. Similarly, the fault-related alluvial fan intersected at Moray-1 is expected to extend along most of the Foster Fault System. However, due to the deformation of the alluvial fan section at its location in a fault corner, the Top Emperor Subgroup pick has limited confidence away from the well.

5.5.2 Golden Beach Subgroup

The Santonian to earliest Maastrichtian Golden Beach Subgroup is mostly restricted to the Central Deep (Bernecker and Partridge, 2001), but extends onto the Southern Terrace and to the southeastern part of the Southern Platform (Pisces Sub-basin). The Golden Beach Subgroup consists of the non-marine clastic Chimaera Formation and the shaley marine Anemone Formation. The subgroup covers the *T. apoxyexinus*, *N. senectus* and *T. lilliei* spore/pollen zones. Lithologically, the subgroup comprises mainly lithic or arkosic sandstones, with claystones and coals deposited in fluvial and floodplain environments. The Golden Beach Subgroup often contains volcanic intrusions and flows that occur mostly within the middle to upper part of the Chimaera Formation ("Campanian Volcanics" of Bernecker and Partridge, 2001). These volcanics include stacked flows of subaerial basalts that are commonly found along the northern and southern faulted margins of the basin, and in other areas of active faulting.

In the current study area, the Golden Beach Subgroup is penetrated in Kyarra-1A, Perch-1, Melville-1, Omeo-1, Omeo-2A and Pisces-1 (Figure 5.30). At Kyarra-1A, the Golden Beach Subgroup pick corresponds to the top of an approximately 35 m thick undated volcanic unit (1215 – 1251 mKb) comprising interbedded pyroclastics and basalt flows that overlie sediments of the Strzelecki Group (Figure 5.14). At Perch-1, the Golden Beach Subgroup consists of a thinner basalt (12.2 m/1481.3-1493.5 mKb) which appears to unconformably overlie the Emperor Subgroup (48 m thick section of Curlip Formation). Both of these volcanic intervals have been correlated to the "Campanian Volcanics" which are interbedded and overlie the Chimaera Formation. As well ties at Kyarra-1A and Perch-1 correlate to non-sedimentary rocks, they are of limited use in regionally mapping the Top Golden Beach Subgroup stratigraphic section due to the thin and sporadic nature of their geological occurrence in the region.

The tie at Melville-1 occurs just at the end of seismic line GDPI10-026, although it provides a good tie to the Golden Beach Subgroup (Figure 5.27). There were no client-supplied preferred stratigraphic picks for the Melville-1 well. In addition, no DPI-generated composite log was supplied for this study, thus stratigraphic picks were taken from Partridge (2002). These formation top picks are different from those cited by the well operator (Bass Strait Oil Company, 2001). The main difference is the recognition by Partridge (2002) of the Emperor Subgroup in the well, whereas the well operator had included this section within the Golden Beach Subgroup. Melville-1 penetrated 175 m of Golden Beach Subgroup, which includes 16.5 m of volcanics, 108.5 m of Chimaera Formation and 50 m of "transitional beds" (Partridge, 2002).The age of the "transitional beds" is unclear and Partridge (2002) would equally favour assignment to the underlying Curlip Formation (Emperor Subgroup). At Omeo-1, the Golden Beach Subgroup is 176 m thick, and consists of sandstone, siltstone and shale interbeds with some conglomerate and coal (Figure 5.31). The well intersected the section just before drilling through the fault plane. At Omeo-2A, drilled further away from the fault plane, the well intersected a 439 m section of Golden Beach Subgroup (Chimaera Formation) before reaching TD. The section consisted

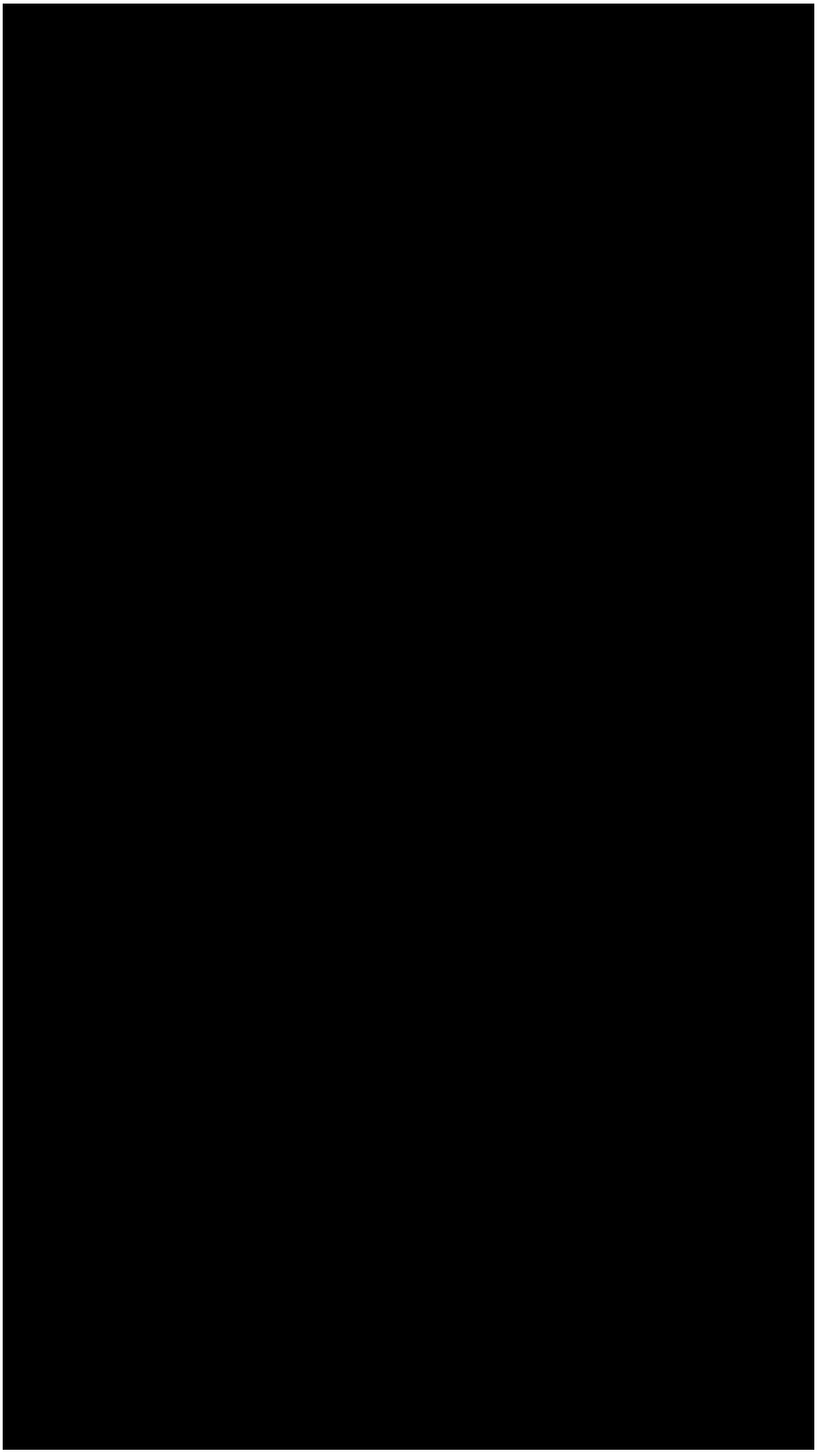

Figure 5.29 Arbitrary seismic line from the GDPI10 survey flattened on Top Latrobe showing the intersection of Emperor Subgroup (Kipper Shale) sediments at Tommyruff-1. Note that the well logs are not flattened. Also note the distinctive seismic character of the Halibut and Cobia subgroups. At the Wyrallah-1 and Tommyruff-1 well, these sediments are stacked fluvial sandstones with interbedded shales.

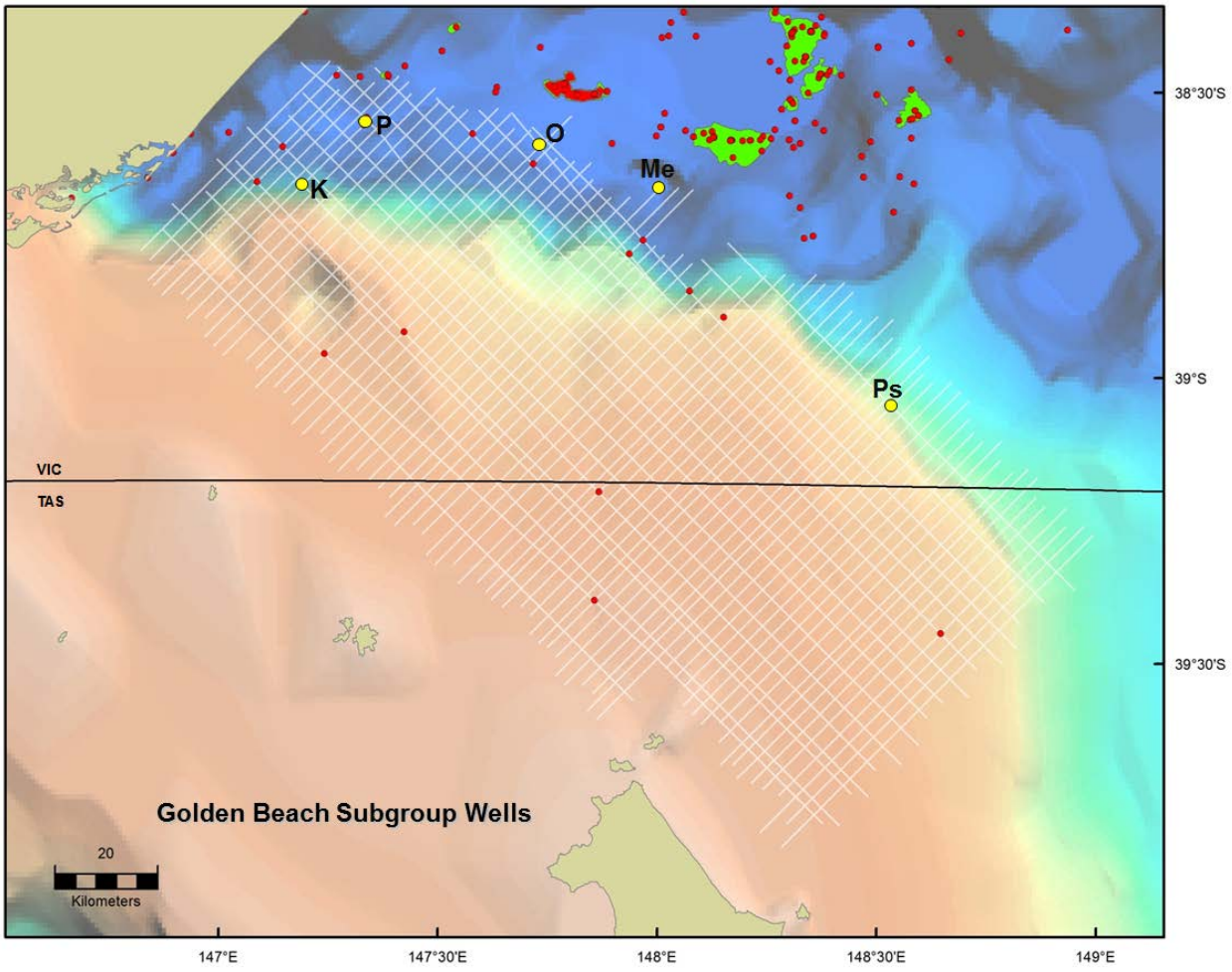

Figure 5.30 Location map showing wells that intersected Golden Beach Subgroup sediments. Well abbreviations: K = Kyarra-1A, Me = Melville-1, O = Omeo-1, -2A, Ps = Pisces-1 and P = Perch-1.

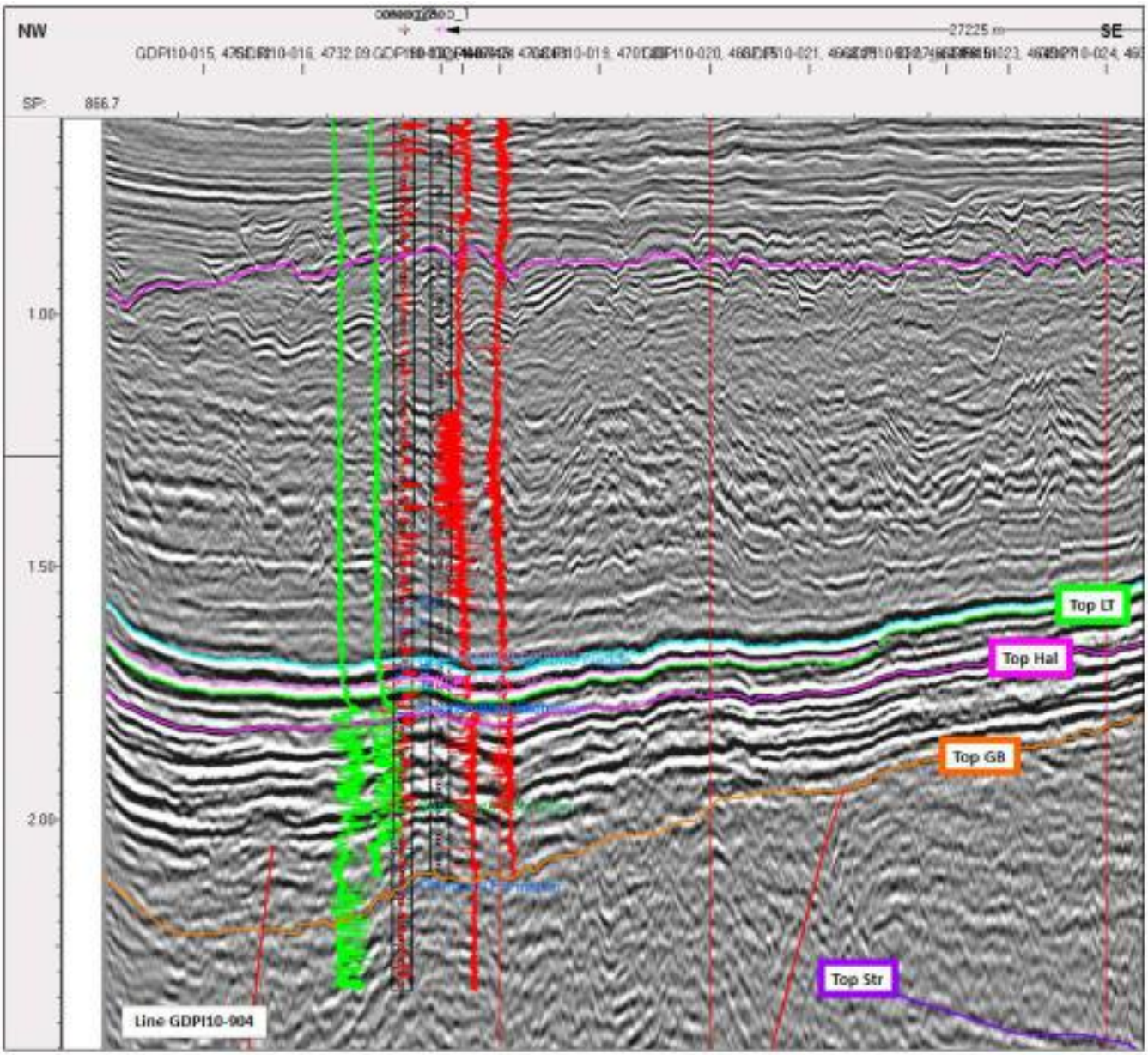

Figure 5.31 Seismic strike line GPDI10-904 showing the intersection of Golden Beach Subgroup sediments near TD at Omeo-1 and -2A.

of medium- to fine-grained sandstone and shale interbeds with some coal present as minor stringers. Pisces-1 intersected 655 m of Golden Beach Subgroup (Anemone Formation) sediments comprising interbedded siltstone, claystone and sandstone in a poorly known half graben on the outer margin of the Southern Platform. Seismic data show that the Golden Beach Subgroup in the half graben has a distinct wedge geometry indicative of syn-rift deposition (Figure 5.32).

As noted, the seismic ties at Kyarra-1A and Perch-1 are of limited use in the regional mapping as they penetrate volcanic rocks and not sediments. Nonetheless, the Golden Beach Subgroup has been interpreted to have been deposited in fault or subsidence-controlled settings in this area (Figure 5.33). The Golden Beach Subgroup ties at Melville-1, Omeo-1 and -2A provide some constraint along the outer part of the Southern Terrace. Here, the interpreted distribution of the Golden Beach Subgroup is limited to a relatively thin unit next to the Foster Fault System, which thickens to the north across a series of down-stepping faults into the Central Deep via the Darriman Fault System. The tie at Pisces-1 has allowed the Top Golden Beach Subgroup horizon to be mapped along-strike within the Pisces Sub-basin. However, extending that tie beyond the spatial limits of the half graben where the well was drilled is problematic due to increased volcanic intrusions and flows, canyons and complex faulting of the outer platform margin. The Top Golden Beach Subgroup ties to the seismic as a peak (zero phase) and can be locally picked near the well using the auto-pick tool. Elsewhere, the horizon has been manually interpreted on the seismic data.

5.5.3 Halibut Subgroup

The Maastrichtian to early Eocene Halibut Subgroup contains the reservoir sandstones of the giant oil fields in the Gippsland Basin (Bernecker and Partridge, 2001). Deposition of the subgroup spans the *F. longus* to *P. asperopolus* spore/pollen zones, and occurred under conditions of waning subsidence. The bulk of sediments in the Halibut Subgroup occur in two coal-bearing successions, the Maastrichtian Volador Formation and the Paleocene to early Eocene Kingfish Formation, both of which were deposited in lower coastal plain environments (Bernecker and Partridge, 2005). The Barracouta Formation is the landward and more coarse-grained lateral equivalent of the Volador and Kingfish formations (Bernecker and Partridge, 2005). Overall, the Halibut Subgroup consists of fine- to coarse-grained quartzose sandstones with claystones and coals. Major channels (canyons) also formed within the Gippsland Basin during the early Eocene (Marlin and Tuna channels).

The two lithologically similar Volador and Kingfish formations are separated in the eastern part of the basin by the thick marine Kate Shale (up to 120 m thick) which straddles the Cretaceous/Tertiary boundary. The Top Cretaceous horizon (or Top Kate Shale) was requested to be mapped in the original DPI tender documents. However, the Kate Shale is thin (< 20 m) in the current study area, and thus is seismically unmappable. It is also clear that the Kate Shale has a limited distribution on the Southern Terrace and is absent from the Southern Platform. As an alternative, FROGTECH have recommended mapping of the Top Halibut Subgroup as a substitute horizon, as the Halibut Subgroup has demonstrated reservoir capacity.

In the current study area, Halibut Subgroup sediments are penetrated at Amberjack-1, Bullseye-1, Devilfish-1, Kyarra-1A, Moray-1, Melville-1, Mudskipper-1, Omeo-1, Omeo-2A, Palmer-1, Perch-1, Pike-1, Pisces-1, Tarra-1, Tommyruff-1 and Wyrallah-1 (Figure 5.34). However, upon further investigation, it is recognised that the DPI-supplied spreadsheet of formation tops has mistakenly listed the Mullet-1 pick at 698 m and the Groper-1 pick at 952 m as Kingfish Formation, while Partridge (2006) has called this unit Burong Formation in both wells. The Burong Formation is the preferred interpretation, as the current mapping shows that while the Halibut Subgroup (Kingfish Formation) extends onto the Southern Platform, it is unlikely to be present at the Mullet-1 and Groper-1 wells. In addition, the Kyarra-1A, Perch-1 and Wyrallah-1 wells were picked to contain the Barracouta Formation, but this is not supported by the Lower *N. asperus* palynology pick. This discrepancy is noted on the DPI formation tops spreadsheet.

The thickness and relative abundance of Halibut Subgroup intersections in wells on the Southern Terrace make correlation of the Top Halibut a relatively straightforward exercise. In addition, the Halibut Subgroup has a distinctive seismic character (high amplitude, low frequency) which is easily recognised on the seismic data. A seismic cross-section between Wyrallah-1 and Tommyruff-1 shows this distinctive character, although the Miocene deformation makes the correlation somewhat difficult (Figure 5.35). However, when the section is flattened on the Top Latrobe the continuous strata within the Kingfish Formation is clear (Figure 5.29). The Kingfish Formation at Wyrallah-1 (1099-1935 m) is described as white, soft claystones interbedded with minor sandstones. Good reservoirs described from the well all occur above the Top Halibut Subgroup horizon (within the Burong Formation). The flattening suggests this area was a depositional low during Halibut time, thus the absence of reservoir quality sands is consistent.

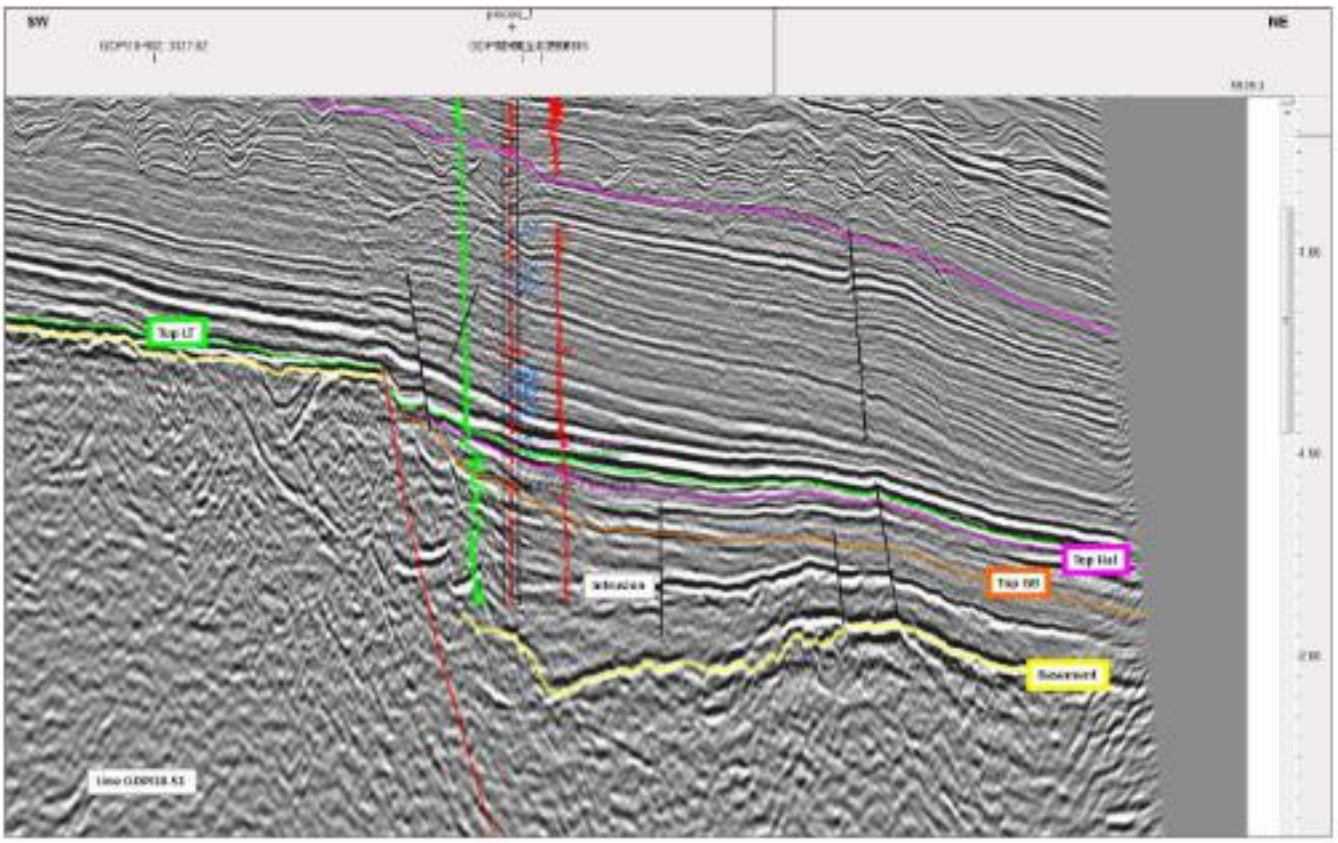

Figure 5.32 Seismic dip line GDPI10-51 showing the intersection of Golden Beach Subgroup sediments at Pisces-1. Here, the Golden Beach Subgroup is a syn-rift section and nearby intrusions (sills) are interpreted. Note the exact location of the well is problematic.

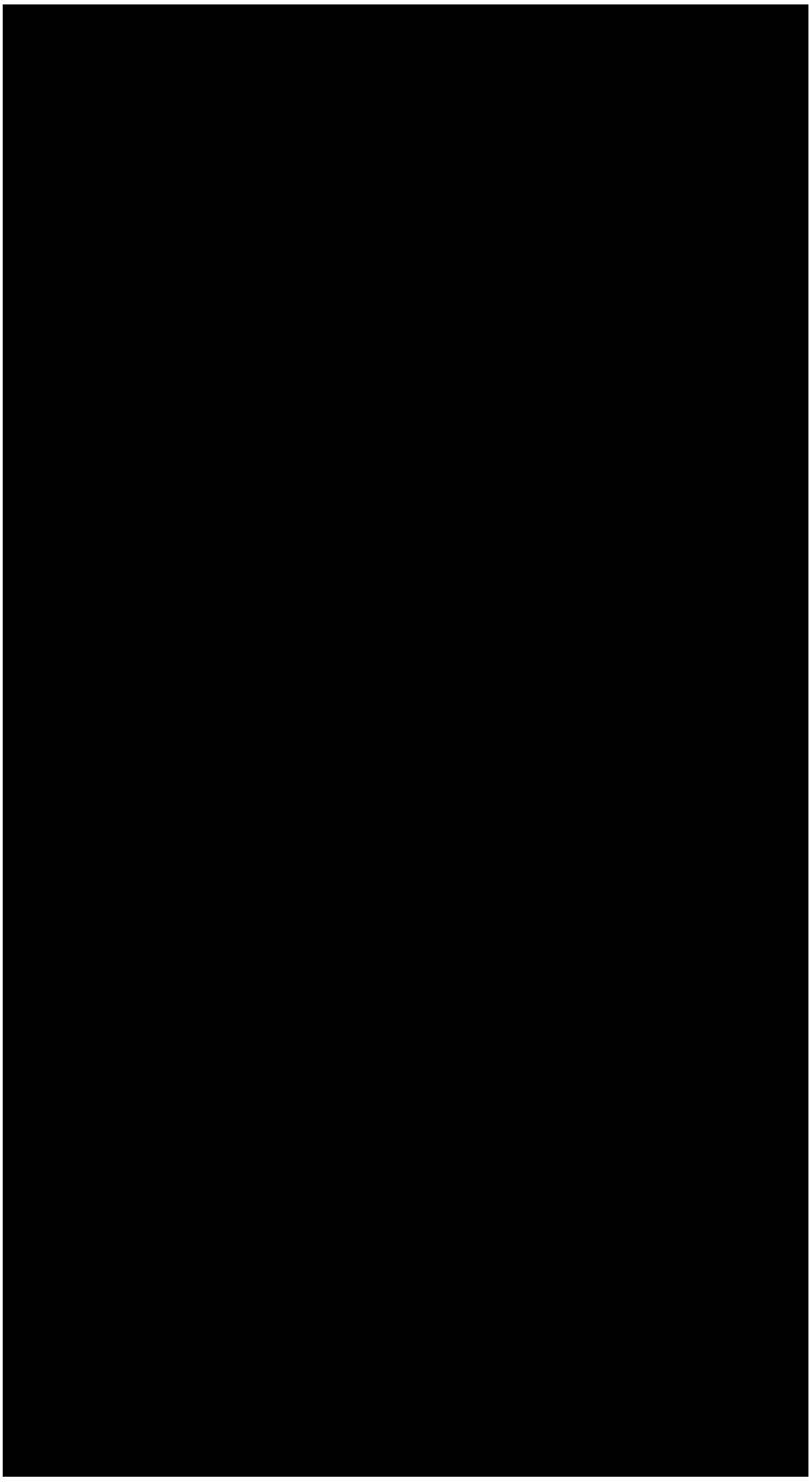

Figure 5.33 Seismic strike line GDPI10-909 showing the interpreted deposition of Golden Beach Subgroup sediments as a late stage syn-rift or early post-rift infill within restricted depocentres between fault blocks.

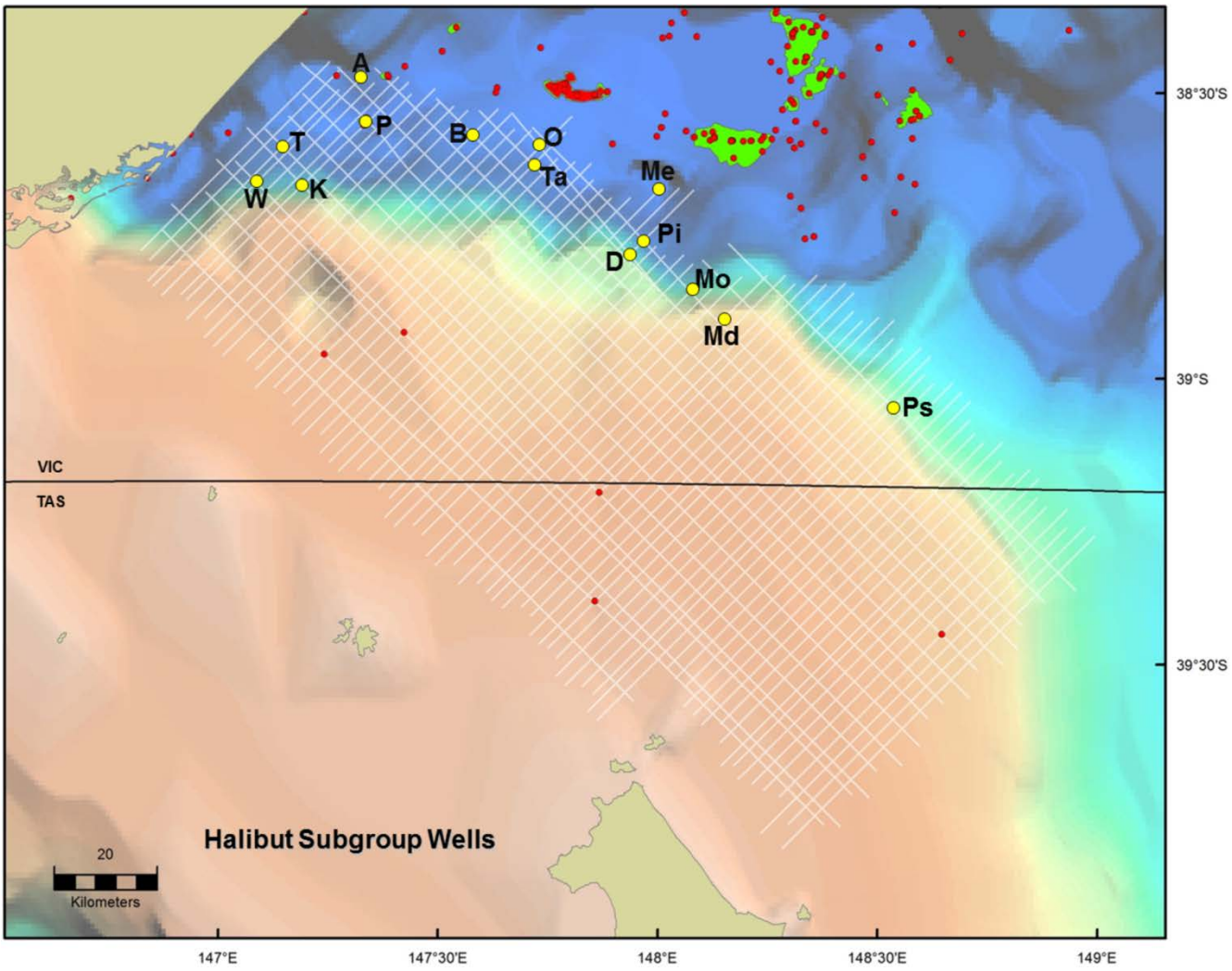

Figure 5.34 Location map of the wells intersecting Halibut Subgroup sediments. Well abbreviations: A = Amberjack-1, B = Bullseye-1, D = Devilfish-1, K = Kyarra-1A, Me = Melville-1, Mo = Moray-1, Md = Mudskipper-1, O = Omeo-2A, P = Perch-1, Pi = Pike-1, Ps = Pisces-1, T = Tommyruff-1, Ta = Tarra-1 and W = Wyrallah-1.

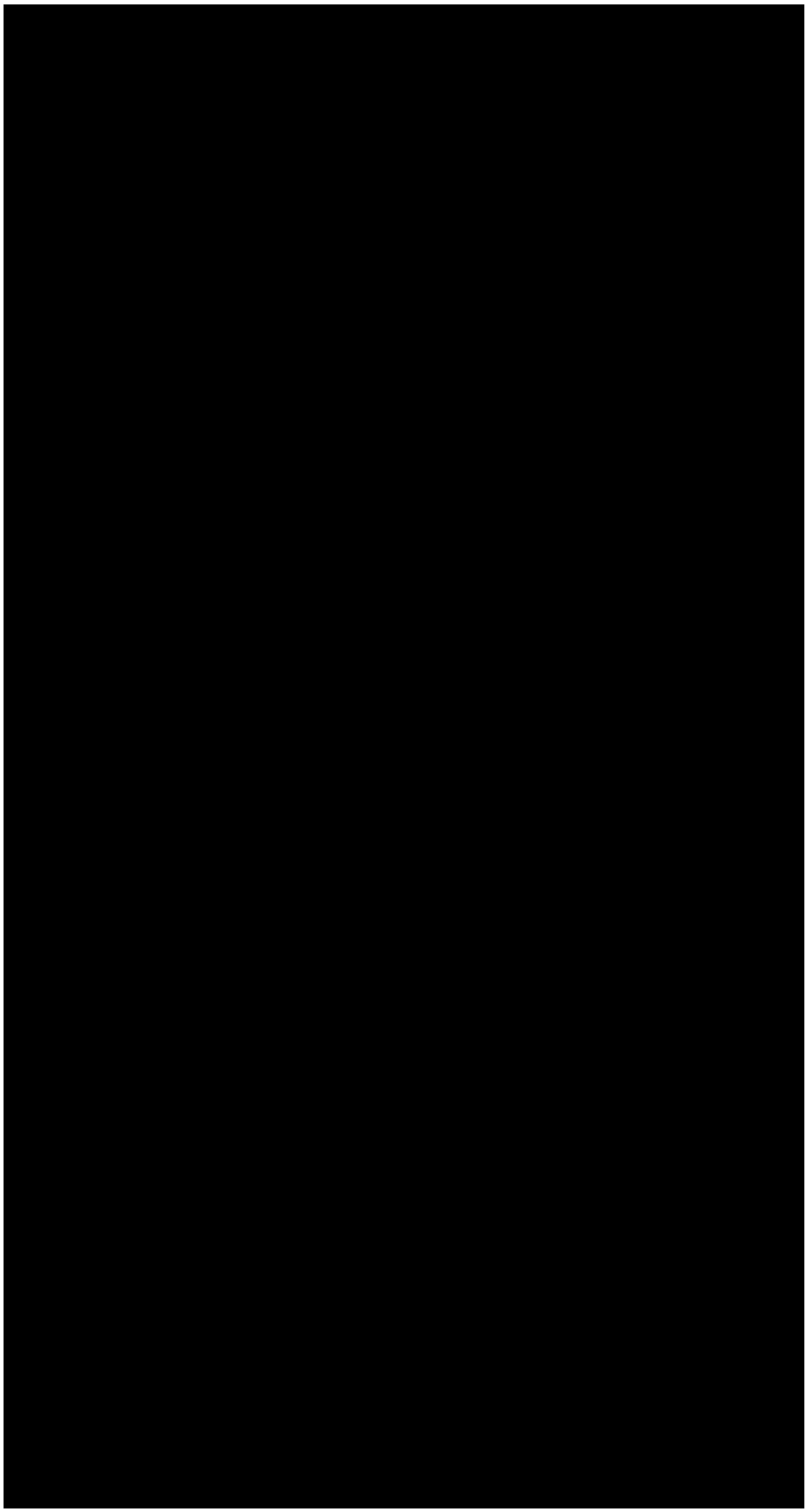

Figure 5.35 Arbitrary seismic line from the GPDI10 survey showing the distinctive character of the Halibut Subgroup sediments at Tommyruff-1 and Wyrallah-1.

The correlation of Kingfish Formation between Devilfish-1 (263 m) and Pike-1 demonstrates that the Top Halibut horizon extends well onto the Southern Platform (Figure 5.36). It is likely that the basement ridge that lies updip from this area (see Basement section) is the source of the sediment. Close examination and correlation to Devilfish-1 shows that the DPI-preferred pick at Pike-1 for Top Halibut Subgroup (1828 m) is incorrect (Figure 5.37). The Top Halibut Subgroup pick should be at around 2023 m (supported by the palynology), while the current pick should be reclassified as the Top Burong. The Top Halibut correlation between Moray-1 and Pike-1, using the revised pick at Pike-1, confirms that the revised pick is correct (Figure 5.38). The tie between these two wells also shows the thickening of the overlying Burong Formation at Pike-1 which correlates to the distinctive "Devilfish Sandstone" in the well section.

In Omeo-1 and -2A, the Halibut Subgroup is > 600 m thick and both units of the Kingfish and Barracouta formations are easily distinguished on the seismic data (Figure 5.39). Further ties were undertaken between Omeo-1, Omeo-2A, Bullseye-1, Tarra-1 and Moray-1. There appears to be a slight thickness and/or change of facies in this area, and the Top Halibut Subgroup horizon begins to wobble between lines. The problem may lie in trying to tie the younger Kyarra-1A, Perch-1 and Wyrallah-1 (Lower *N. asperus*) correlations of Top Halibut Subgroup picks to the west, with the slightly older Top Halibut Subgroup picks at Omeo-1, Tarra-1, Pike-1 and other wells along the central part of the Southern Platform. There may be a slight mis-tie of around one cycle between these two areas.

Mapping of the Top Halibut Subgroup from Devilfish-1 and Tarra-1 from the Southern Terrace onto the Southern Platform clearly shows significant sand sheets that formed around the basement highs (Figure 5.40). The seismic correlations indicate that approximately half of the thickness (TWT) of Latrobe Group that is present is Halibut Subgroup age. Given the distance to sediment source and the geometry of the unit, there is little doubt these sediments would have good reservoir quality. However, sealing facies may be a problem, as the Gurnard Formation at the nearby Groper-1 well contains glauconitic sandstones with little sealing capacity (Figure 5.40). The sand lobes appear to be in part continuous between the Southern Platform and the Southern Terrace around the Devilfish-1 region. This correlation also supports the local sourcing of the younger "Devilfish Sand" (Cobia Subgroup) from the Southern Platform. On seismic data, the Top Halibut generally correlates to a strong peak, although this varies considerably across the Southern Platform, particularly near the sand wedges.

5.5.4 Cobia Subgroup

The uppermost unit of the Latrobe Group is the middle Eocene to basal Oligocene Cobia Subgroup (*N. asperus* spore/pollen zone). This subgroup contains the non-marine (paralic) Burong Formation and the glauconitic-rich marine facies of the Gurnard Formation. All formations of the Cobia Subgroup are typically non-calcareous and thereby readily distinguished from the overlying Seaspray Group (Bernecker and Partridge, 2001). The Burong Formation consists of interbedded sandstones, siltstones, shales and coals. The Gurnard Formation is recognised as a marine condensed section that was deposited across the Gippsland Basin in a distal offshore and open-marine environment (Partridge, 2003). As all wells in the current study have Cobia Subgroup sediments present, the Top Latrobe horizon is picked at the top of the Burong or Gurnard formations.

A review of the literature on the Cobia Subgroup highlights the importance and economic significance of this interval, but also a range of different interpretations of the Gurnard Formation. In addition, interpretations of the "unconformities" that bound the unit also vary.

Lithology of the Gurnard Formation varies from greensands with some reservoir potential to potential sealing facies over accumulations, depending on its location within the basin (Gibson-Poole et al., 2006). The thickness and distribution of the formation is also highly variable across the basin (Goldie Divko et al., 2010). Overall, the Gurnard Formation is generally thin and can be hard to map as a separate unit on seismic data. The sequence stratigraphic analysis of the Kingfish field by Gibson-Poole et al. (2006) clearly shows the truncation at the top of the underlying Halibut Subgroup (Kingfish Formation; Marlin Unconformity), and the subsequence onlap and erosion of the Gurnard Formation which is present across part of the Kingfish structure (Figure 5.41). In this interpretation, the "Latrobe Unconformity" is indicated at the Top Gurnard Formation.

3D-GEO (2010) describes the "so-called Latrobe unconformity below the Gurnard" as a "composite ravinement surface produced by shallow marine erosion during transgressive phases of Latrobe Group deposition", and the Gurnard Formation as "the transgressive glauconitic sandstone veneer deposited across the top of the Latrobe siliciclastics". The glauconitic veneer is condensed, bioturbated, and has most or all of its calcareous microfossils removed by diagenetic processes (3D-GEO, 2010). 3D-GEO also made the following observations about the Gurnard Formation from their regional study of wells and seismic mapping:

- The Gurnard Formation can be a reservoir where it contains enough quartz sand and minimal clay introduced by bioturbation. Otherwise, the glauconitic pellets are soft and deform with compaction to reduce porosity.

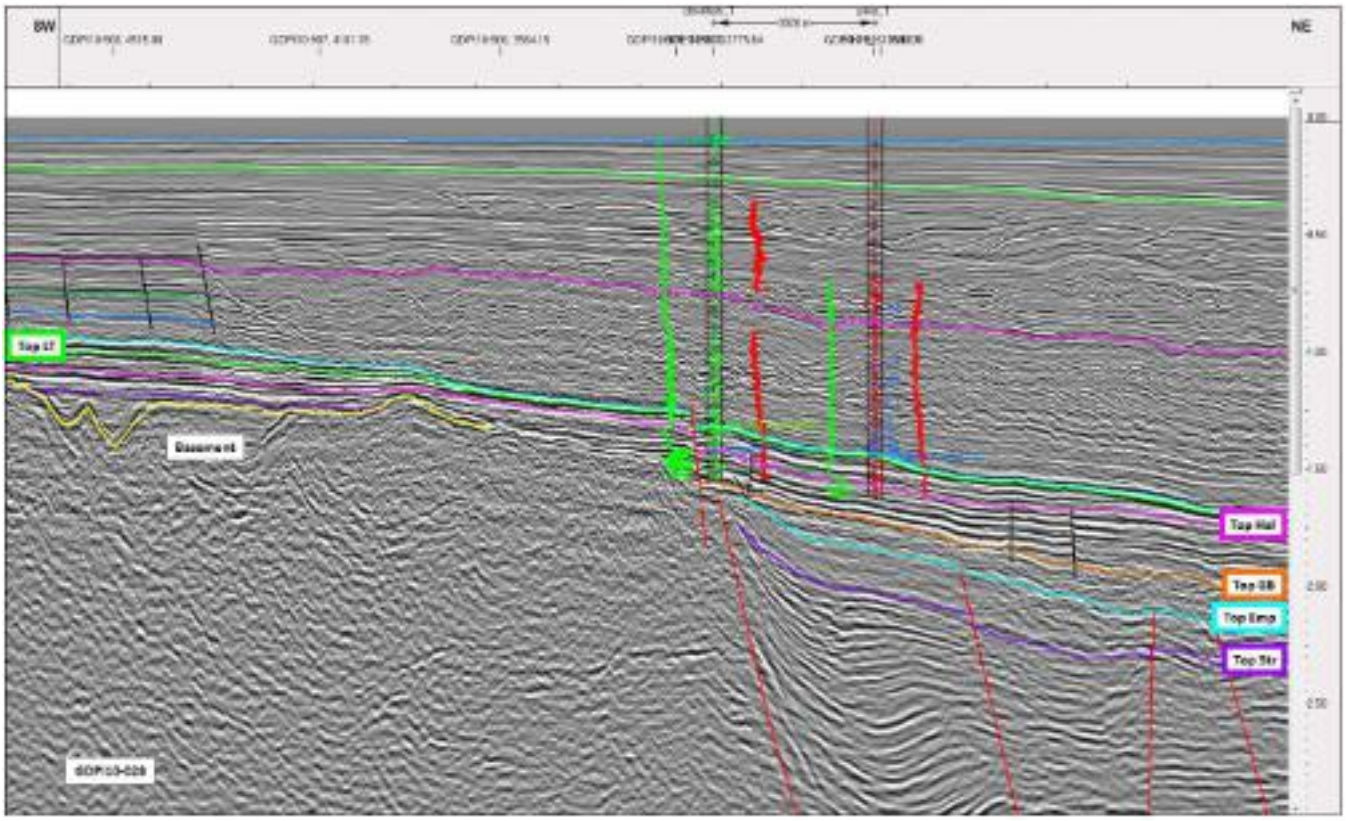

Figure 5.36 Seismic line GDPI10-28 survey showing the correlation of Halibut Subgroup sediments between Devilfish-1 and Pike-1. The Halibut Subgroup is interpreted to extend southward onto the Southern Platform.

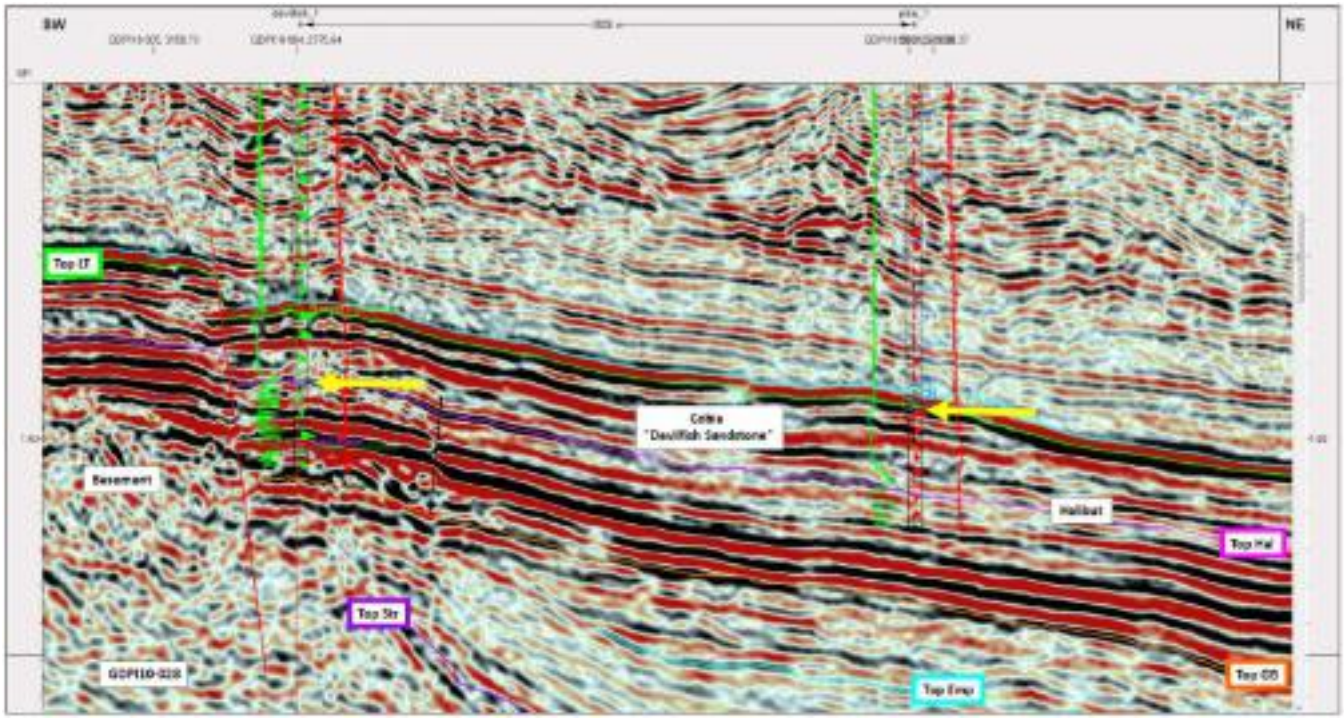

Figure 5.37 Seismic line GDPI10-28 showing that the correlation of the DPI-preferred Top Halibut pick at Devilfish-1 (yellow arrow) does not correlate downdip to the DPI-preferred Top Halibut pick at Pike-1 (yellow arrow). The DPI pick of Top Halibut (yellow arrow) at Pike-1 has been revised to be the Top Latrobe (Cobia Subgroup). The seismic correlation of the Top Halibut pick to the Pike-1 well is shown. The "Devilfish Sandstone" is interpreted as the thick Cobia Subgroup sand unit between the two wells.

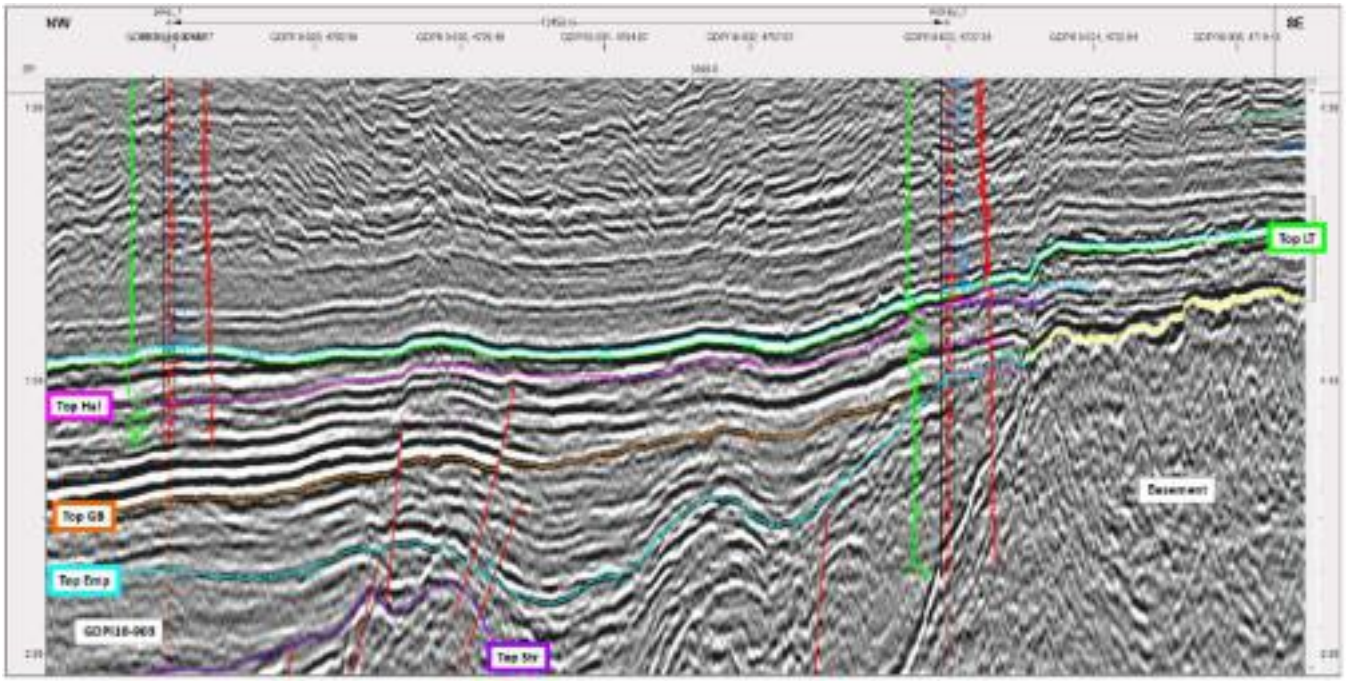

Figure 5.38 Seismic strike line GDPI10-903 showing that the revised pick of Top Halibut at Pike-1 correlates well along strike to the Top Halibut Subgroup pick at Moray-1.

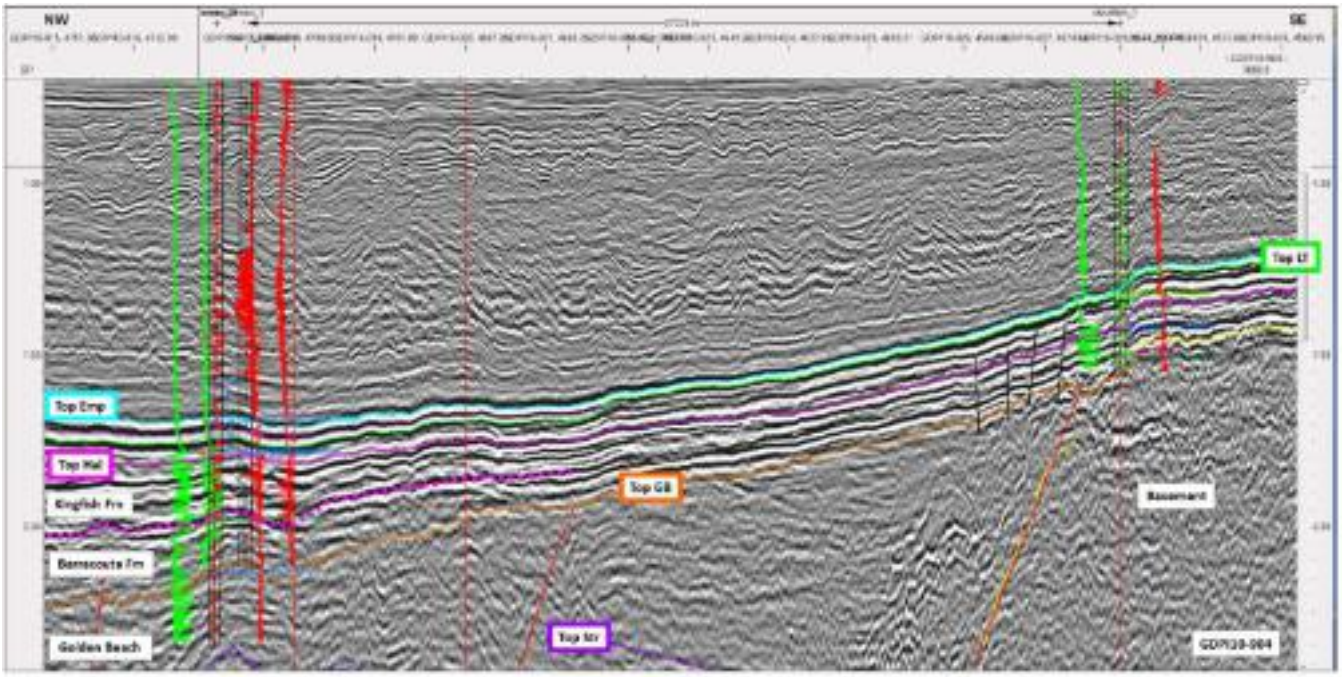

Figure 5.39 **Seismic strike line GDPI10-904 showing that the Top Halibut Subgroup at Devilfish-1 correlates well along strike to the Top Halibut picks at Omeo-1 and Omeo-2A. Note that both the Kingfish and Barracouta formations of the Halibut Subgroup can be distinguished and mapped on the new seismic data.**

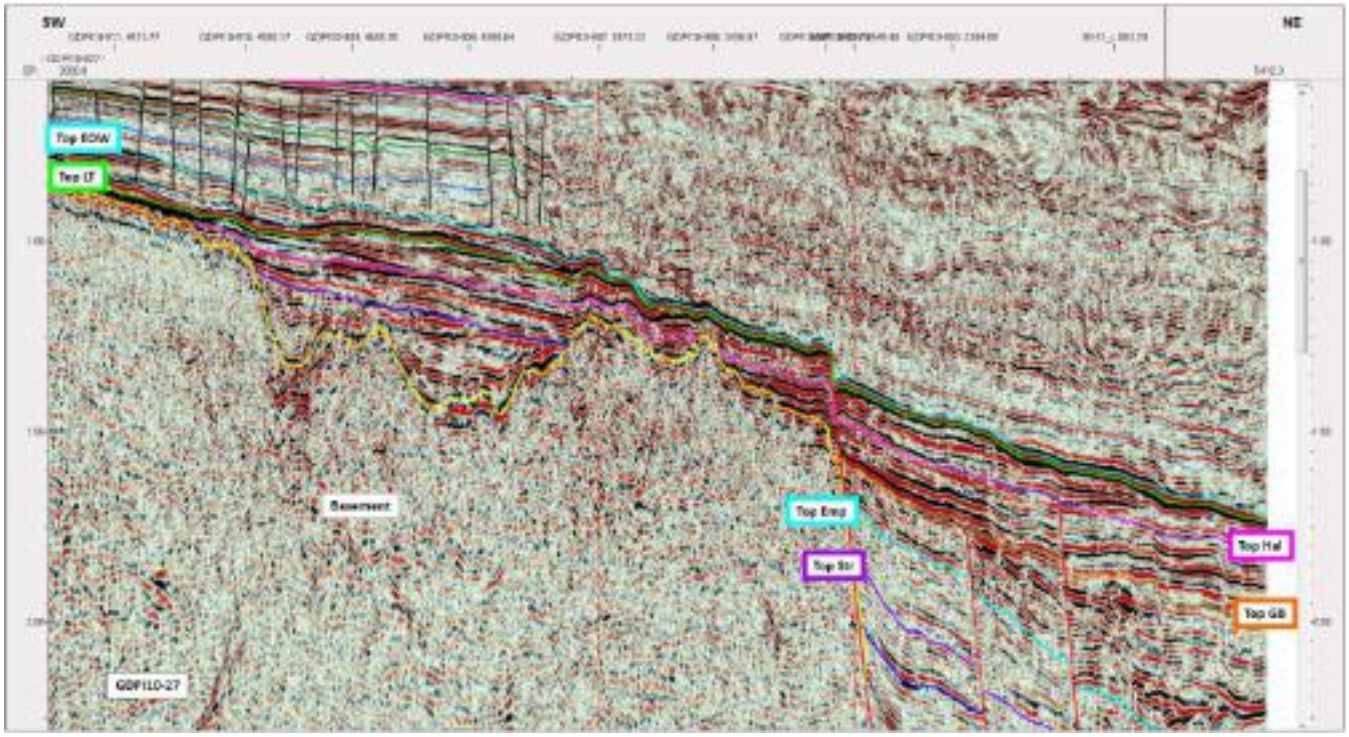

Figure 5.40 Seismic line GDPI10-27 showing the thickening of sand units of the Halibut and Cobia subgroups across the outer Southern Platform. These sands are interpreted to continue downdip towards Pike-1.

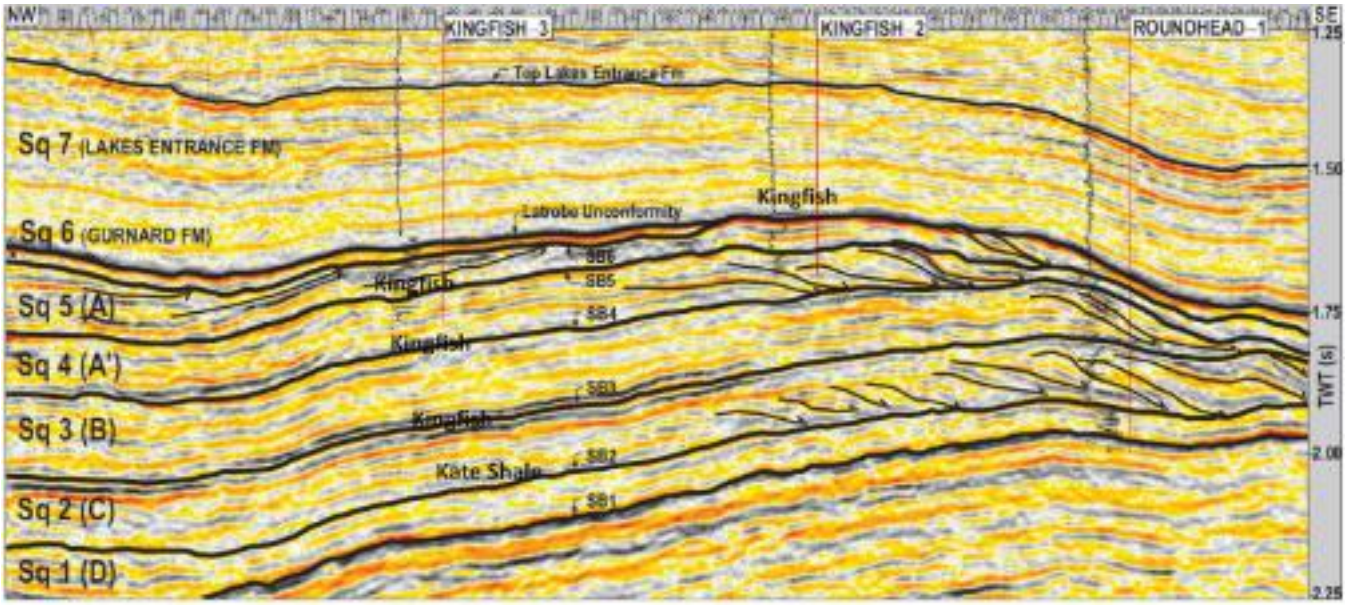

Figure 5.41 Seismic line across the Kingfish Field area (line G92A-3074A) showing the sequence interpretation and key stratal relationships such as truncation and downlap (image from Gibson-Poole et al., 2006). In particular, note the thin onlap of the Gurnard Formation across part of the field.

- Intervals within the Gurnard Formation show limonitic alteration of iron-bearing minerals and a lack of calcareous microfossils. The limonitic alteration is usually attributed to weathering, but 3D-GEO (2010) proposes that the oxidation occurred when acidic freshwater from the underlying Latrobe Group flowed through the greensand soon after deposition. The acidic waters also dissolved the calcareous microfossils.
- Often there are problems with dating the Gurnard Formation by palynology and micropalynology because of its depositional and diagenetic features.
- The Gurnard Formation is generally non-reservoir because of burial compaction, but contains producible gas on the Northern Terrace where it is much shallower. As the Gurnard is often non-reservoir, the top reservoir level is commonly picked at the Top Latrobe siliciclastics and this surface can be difficult to pick precisely on seismic data.

All of the wells in the current study intersect Cobia Subgroup sediments and the clastic Burong Formation is volumetrically the most significant (Figure 5.1). The thickest section of the Cobia Subgroup occurs in Tommyruff-1 where the Burong Formation is 265 m thick and overlain by a thin Gurnard Formation (4 m thick; Figures 5.29 and 5.35). Nearby wells Wyrallah-1 (197 m), Kyarra-1A (145 m), Palmer-1 (126 m), Perch-1 (148 m) and Amberjack-1 (209 m) also have thicker sections of the Burong Formation. Except for Kyarra-1A where the Gurnard Formation is absent, these wells also have thinner overlying sections of the Gurnard Formation. The flattened section between Wyrallah-1 and Tommyruff-1 shows the distinctive seismic character, thickening and lateral continuity of the Burong Formation section in this part of the Southern Terrace (Figure 5.29).

Elsewhere on the Southern Terrace, the Burong Formation is thin or absent (Omeo-1/absent, Omeo-2A/absent, Tarra-1/16 m, Moray-1/absent, Mudskipper-1/absent and Pisces-1/absent. The exception is Devilfish-1 (150 m) and Pike-1 (135 m; see revision of picked section from Halibut Subgroup to Burong Formation). The Burong Formation at Pike-1 is a thick section of unconsolidated, well-sorted quartzose sandstones with excellent porosity and permeability. A similar lithology is present at Devilfish-1, and the unit is informally known as the "Devilfish Sandstone" (Figure 5.37).

Bernecker et al. (2006) correlated this unit with the Oligocene Sand Member of the overlying Lakes Entrance Formation (Seaspray Group; Figure 5.42). Although the sediments are barren of diagnostic spore/pollen assemblages, the seismic mapping clearly shows that the "Devilfish Sandstone" belongs to the Latrobe Group (Cobia Subgroup), and not the overlying Seaspray Group as suggested by Bernecker et al. (2006; Figure 5.42). Similar to the underlying Halibut Subgroup which thickens in this same area, the seismic mapping shows that sediments are being sourced locally from the emergent granitic hills that occur in the central region of the Southern Platform. Sand distribution is expected to localise along the edge of the Foster Fault System, as the strike-line tie between Devilfish-1 and Omeo-1 and Omeo-2A show that this seismic package (Top Halibut Subgroup to Top Latrobe Group) correlates with a basal sand and thicker overlying greensand (Gurnard Formation) away from the fault system (Figure 5.39). A full sequence stratigraphic interpretation of these units would yield a different correlation to the present lithology-based system of formation tops.

On the Southern Platform, the total thickness of the Latrobe Group thins markedly southward towards the shallowing Bassian Rise (Figure 5.43). The ties to Groper-1, Groper-2, Mullet-1 and Bluebone-1 that have been reviewed by Partridge (2006) at Top Latrobe Group level are very good and allow a confident correlation between wells and across the broader Southern Platform (Figure 5.44). Notably, the Gurnard Formation is present only at Groper-1, Groper-2 and Mullet-1, and is thin in all instances (8.2 to 17.7 m). The best seismic tie is at Groper-1 where all the stratigraphic units are thickest (Figure 5.45). Here, the Top Latrobe Group (Top Gurnard Formation) ties at a (zero phase) negative to positive, and shows a strong regionally consistent seismic character that can be mapped across the platform. Other ties to Groper-2, Mullet-1 and Bluebone-1 are shown in Figures 5.46 to 5.48. North of Groper-2 the thickness of the Latrobe Group section reduces to a single cycle (reflection) on the seismic data. The truncation of Latrobe Group updip from Groper-1 is clear and shows that the overlying sediments belong to the Early Oligocene Wedge (Seaspray Group).

The new seismic coverage around Bluebone-1 allows the Top Latrobe Group to be mapped more broadly on the Southern Platform than before. In particular, there are many sediment wedges trapped within the network of rugose basement topography. These sediments are likely to be coarse-grained arkosic sands grading to alluvial granite-wash.

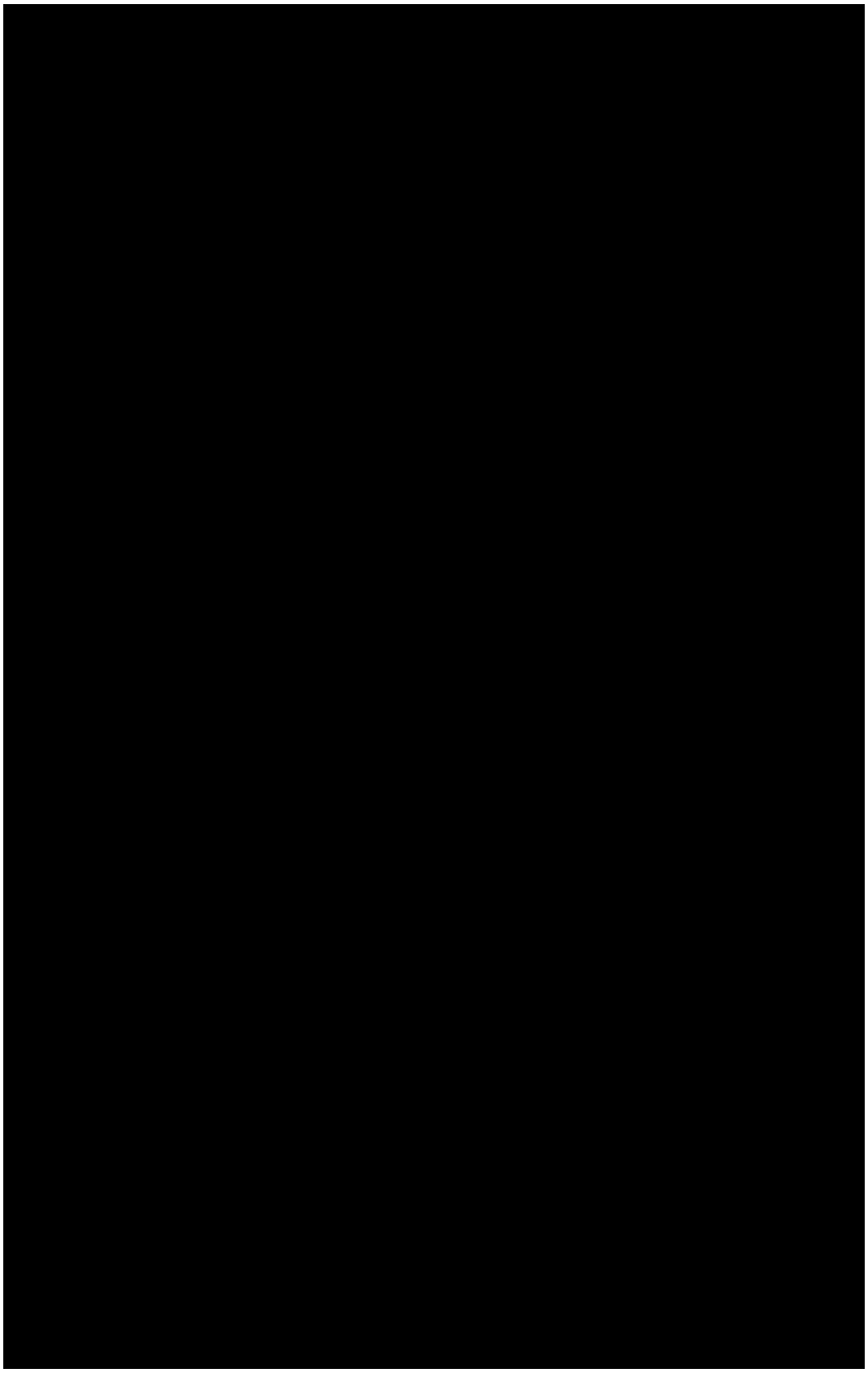

Figure 5.42 Horizon picks and correlations for the Top Latrobe Group from Bernecker et al. (2006). In this interpretation, the thick sand unit at Devilfish-1 was revised from Cobia Subgroup (Burong Formation) to the "Oligocene Sand Member". Correlations undertaken for the current study suggest that the original interpretation of the sand unit as Cobia Subgroup is correct.

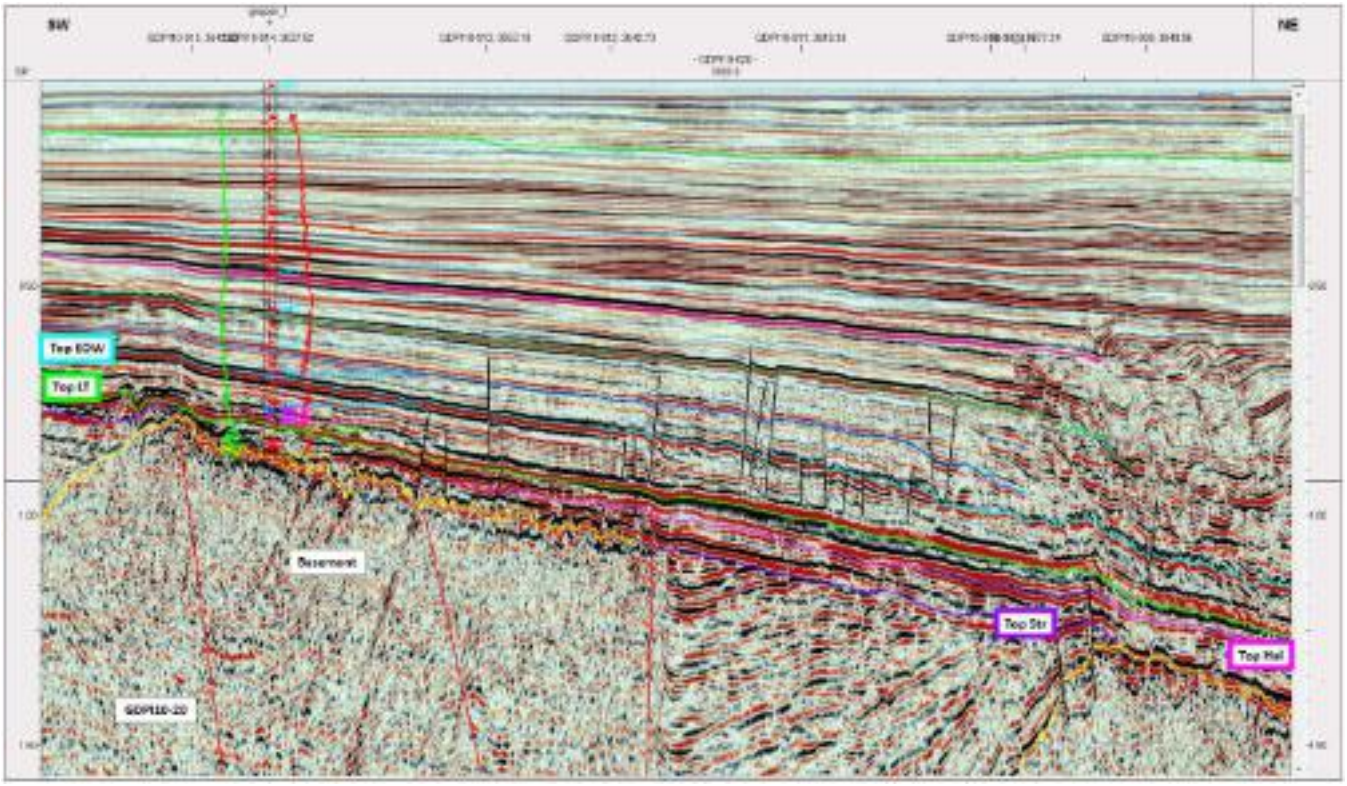

Figure 5.43 Seismic line GDPI10-20 showing the overall thinning of the Halibut and Cobia subgroups from the Southern Terrace across the Southern Platform. Note that the Halibut Subgroup sediments pinchout before reaching the Groper-1 well.

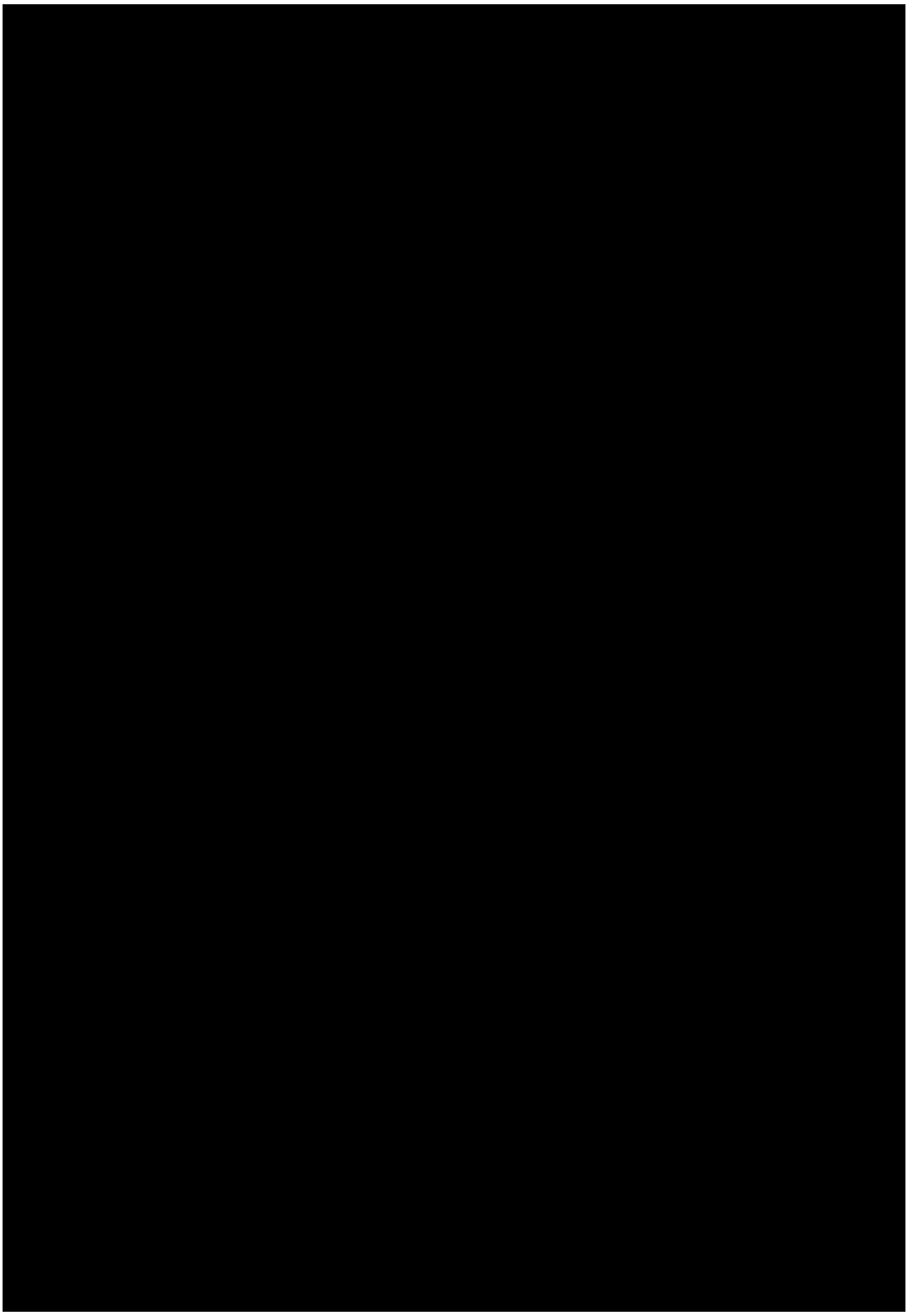

Figure 5.44 Well correlations of Partridge (2006) for the Latrobe Group, Early Oligocene Wedge and Bassian Rise Units across the Southern Platform.

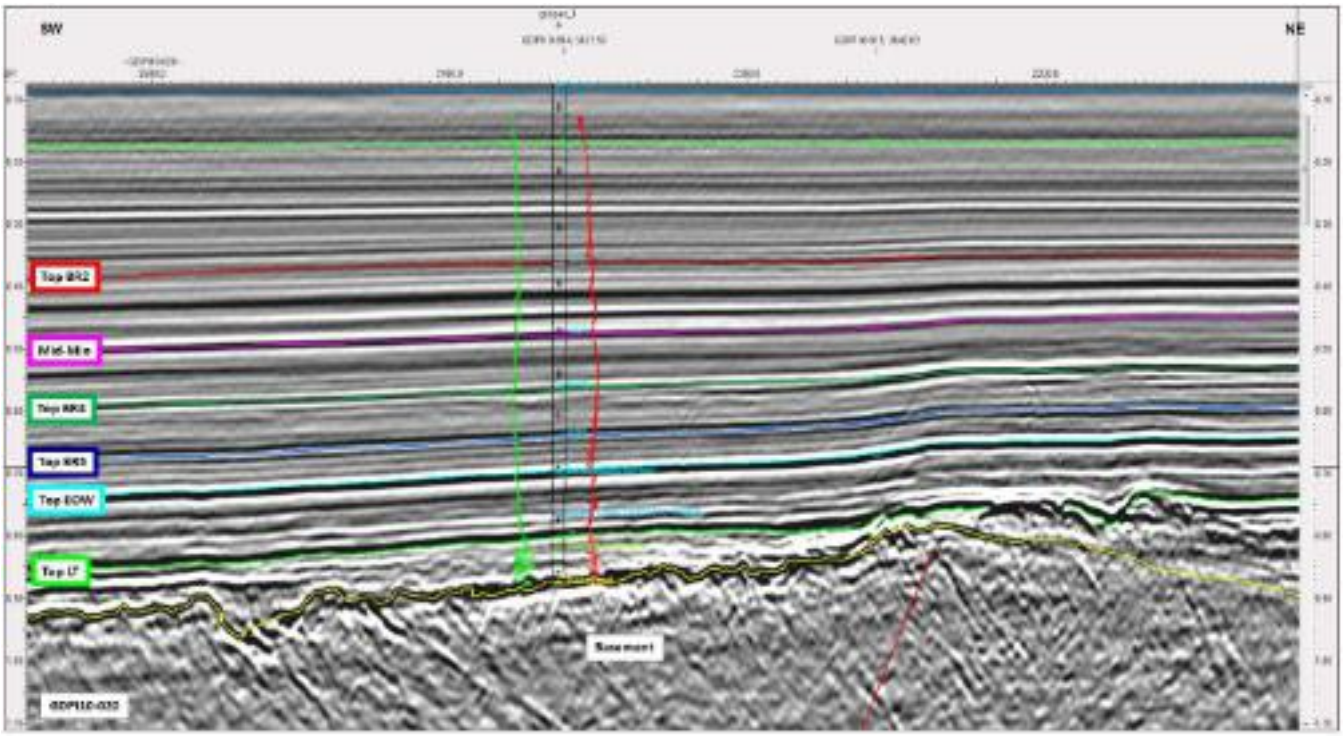

Figure 5.45 Seismic line GDPI10-20 showing the correlation of Partridge's (2006) picks for the Latrobe Group, Early Oligocene Wedge and Bassian Rise Units at Groper-1.

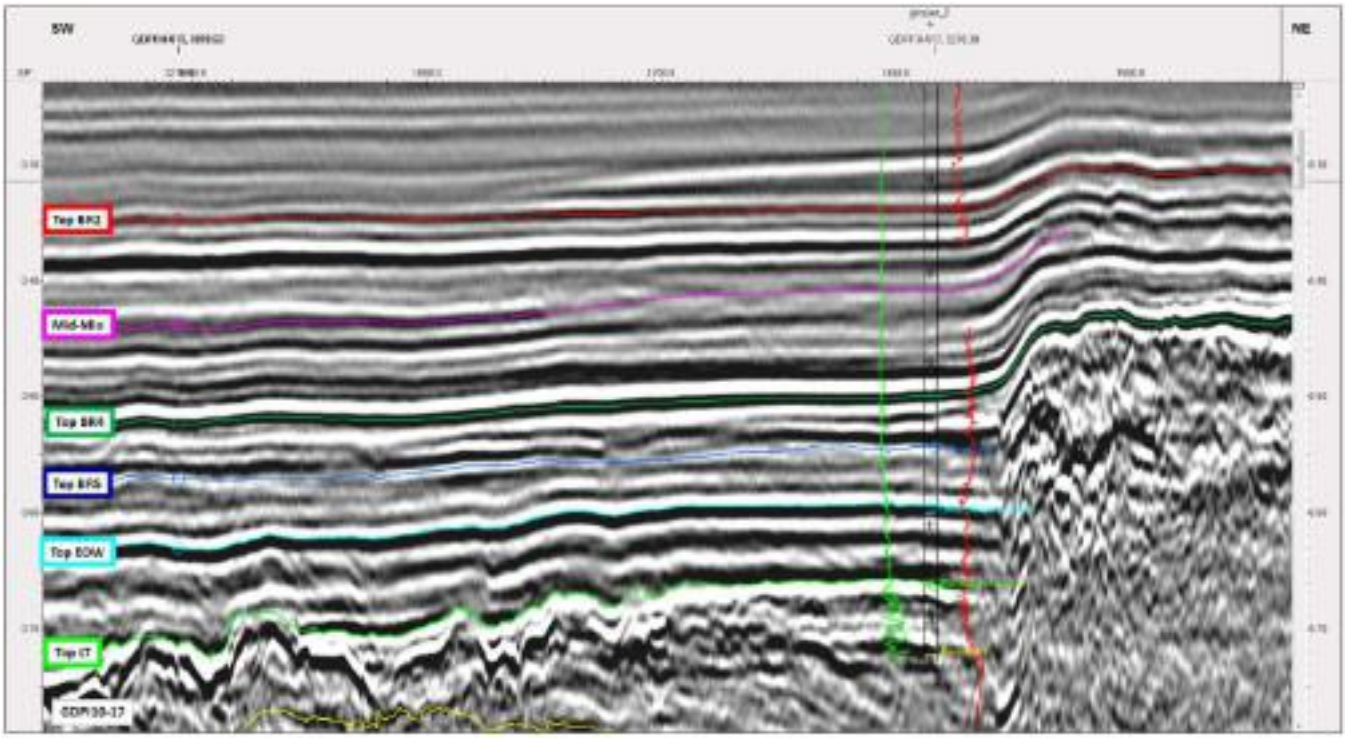

Figure 5.46 Seismic line GDPI10-17 showing the correlation of Partridge's (2006) picks for the Latrobe Group, Early Oligocene Wedge and Bassian Rise Units at Groper-2.

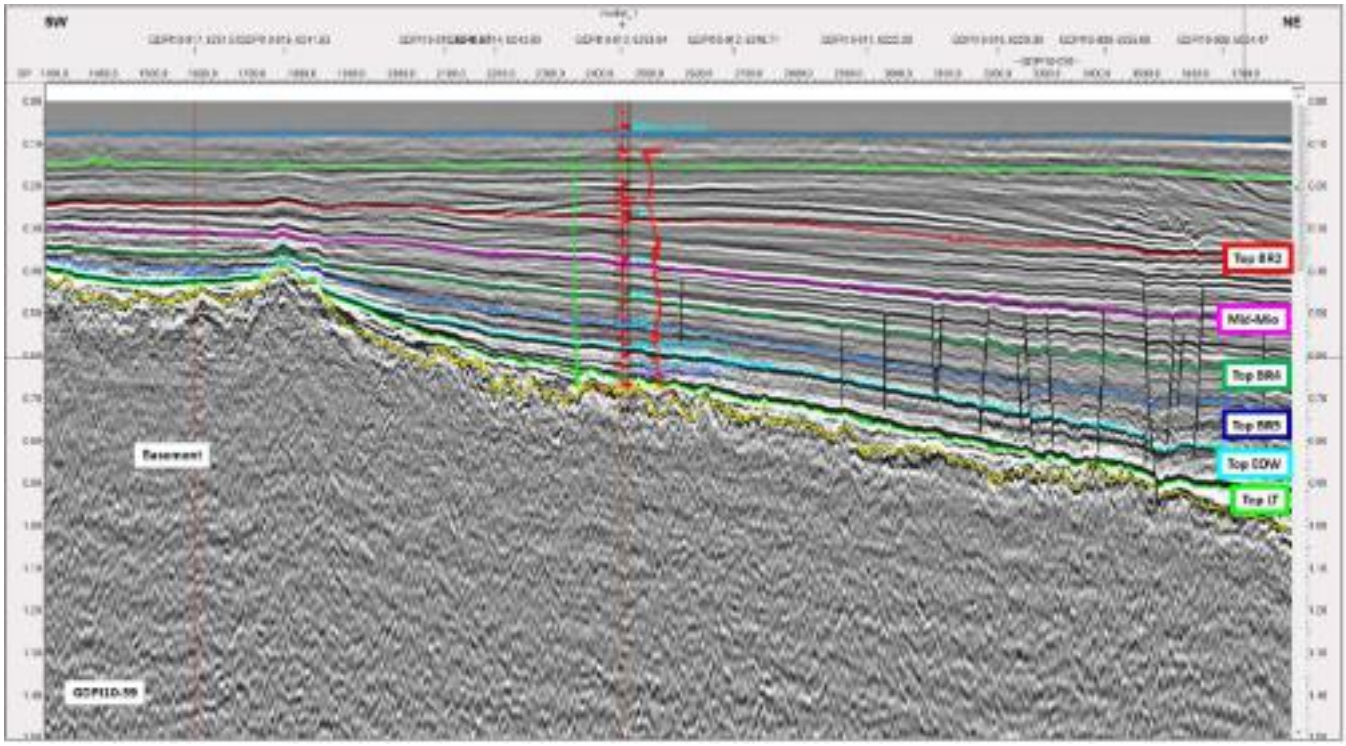

Figure 5.47 Seismic line GDPI10-39 showing the correlation of Partridge's (2006) picks for the Latrobe Group, Early Oligocene Wedge and Bassian Rise Units at Mullet-1.

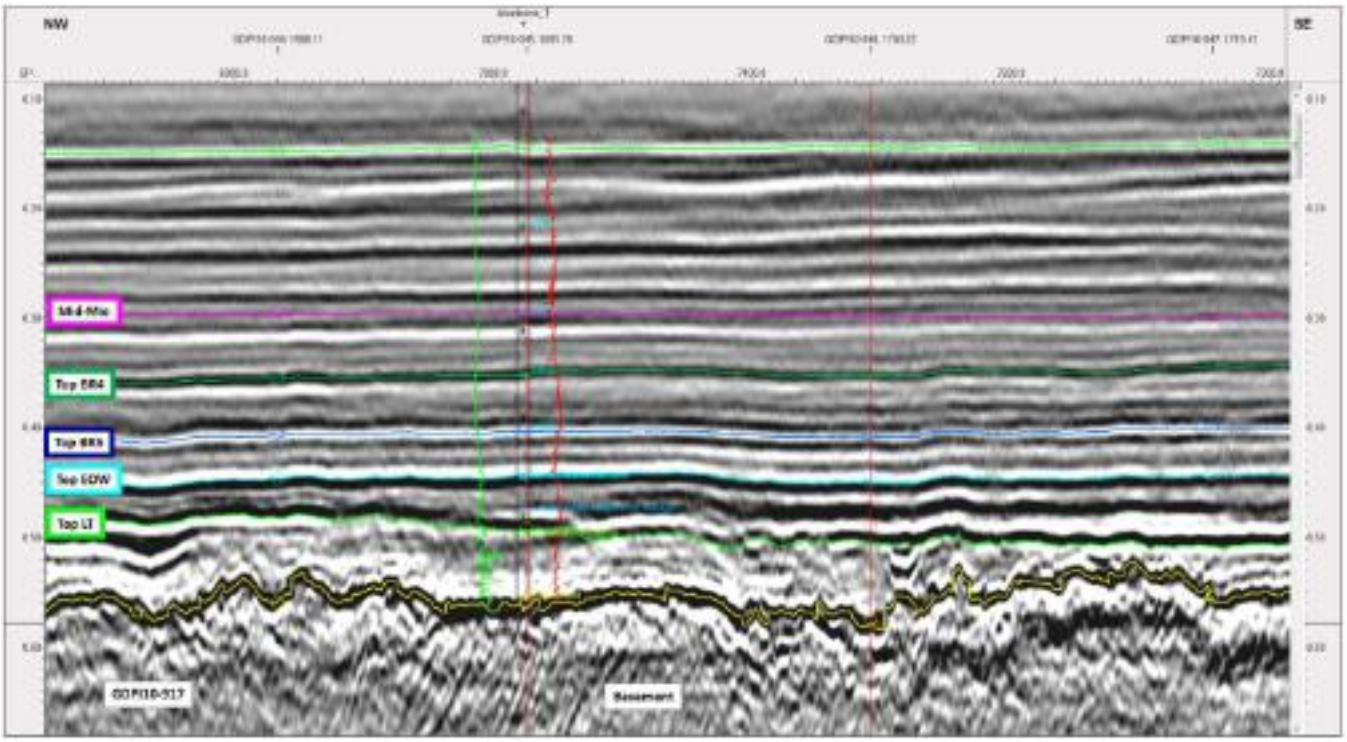

Figure 5.48 Seismic strike line GDPI10-917 showing the correlation of Partridge's (2006) picks for the Latrobe Group, Early Oligocene Wedge and Bassian Rise Units at Bluebone-1.

The sediments have a distinct bland seismic character that can be recognised as discontinuous pockets along strike lines (Figure 5.49). The age of some sediments maybe older, although ties to Bluebone-1 suggest they are Latrobe age. The updip termination of Latrobe Group sediments on the Southern Platform is mapped as a truncation/onlap against rugose basement highs and generally shallowing basement. The single-cycle nature of mapping thin units on seismic make this exercise highly interpretive. The western extent of the Latrobe Group on the Southern Platform is easier to map and suggests the western platform is barren of Latrobe Group sediments.

Shallow, stable basement underlying the Southern Platform has meant tectonic-related accommodation was low and most post-Latrobe Group deposition was driven by eustasy (mostly transgressive and highstand deposits). As described previously, the basement surface of the Southern Platform is marked by an overall rugose topography and a central region of large high-standing hills near the present-day Kent and Furneaux Groups of islands. These basement highs acted as local sediment sources on the Southern Platform and Southern Terrace during deposition of the siliciclastic Latrobe Group, and may have continued to act as a sediment source until the early Miocene when most of the relict basement topography was draped by marine sediments.

While mapping the Top Latrobe Group surface on the Southern Platform is relatively straightforward given the consistency of well ties and seismic character, the well ties between the platform and the Southern Terrace are more problematic. This is particularly the case when a thick section of the Gurnard Formation is present. There are five wells with thick Gurnard Formation present: Omeo-1 (159 m), Omeo-2A (101 m), Tarra-1 (116 m), Melville-1 (54 m) and Bullseye-1 (78 m). A review of these well ties has yielded mixed results.

The tie between Omeo-1 and Omeo-2A shows a mis-tie at the Top Gurnard Formation based on the DPI-supplied picks of formation tops (Figure 5.50). At Omeo-1, the Top Gurnard Formation pick is at 2188 m, while at Omeo-2A the pick is at 2246 m. Figure 5.50 shows there is a clear mis-tie using these picks, and the deeper pick at Omeo-2A is the preferred interpretation. The incorrect pick at Omeo-1 actually ties to the seismically-defined Top Oligocene Wedge, and this is confirmed by Partridge (2006). Furthermore, the Top Gurnard Formation pick at Omeo-2A is interpreted to be too high. The preferred interpretation would bring the Top Gurnard Formation pick down to a log break at 2263 m (a difference of 17 m). This is confirmed by Partridge (2006) who has placed the base of the Early Oligocene Wedge at 2260 m in Omeo-2A. The lower pick is consistent with the foramiferal zonules of J2 below and G above the revised pick. More importantly, the regional seismic character of Top Latrobe Group that is mapped across most of the area ties at the deeper level. This revised pick would make the thickness of the Gurnard Formation more consistent with other wells in the area.

At Tarra-1, the Top Gurnard Formation is picked within the J2 foraminiferal zonule which correlates to the basal part of the Early Oligocene Wedge according to the stratigraphic chart of Partridge (2006; Figure 5.5). It is suggested here, that the Top Gurnard Formation be moved down to somewhere between 2165 and 2175 m (Figure 5.51). At this level, the well report records a lithological break between an underlying late Eocene highly glauconitic sand that is dominantly rusty brown in colour, and an overlying Oligocene calcareous sandstone/calcarenite deposited in a shallow marine setting. Similar to the suggested changes to Omeo-2A, the lower pick at Tarra-1 for Top Gurnard Formation would tie the regionally mapped Top Latrobe Group surface. A lower pick would also be consistent with the foraminiferal zonules at the well. This is further supported by the base of the Early Oligocene Wedge placed at 2165 m at Tarra-1 by Partridge (2006). Similar to Omeo-1 and Omeo-2A, this suggested revision of the Top Gurnard Formation pick would make the thickness of the Gurnard Formation more consistent with other wells in the area. Although Melville-1 also has an interpreted thick section of Gurnard Formation, we are unable to evaluate the well tie properly due to an absence of logs across this interval, and the well tie at the end of the line.

At Bullseye-1, the Top Gurnard Formation pick also appears to be slightly high with reference to the mapped regional Top Latrobe Group seismic surface (Figure 5.52). Interestingly, Bullseye-1 has a thick interpreted Gurnard section that is described as Lower *N. asperus* age, and consists of claystone and siltstone with glauconite, coal and traces of pyrite. This unit is overlain by a thinner section of more glauconitic-rich sediments that have the typical Gurnard Formation sonic log kick. The relatively good correlation between the Top Gurnard Formation pick at Bullseye-1 and the regionally mapped seismic surface suggests that the Top Latrobe Group can be picked at the Top Gurnard Formation and mapped around with careful discrimination and integration of biostratigraphy and lithology at each location. However, the typical Gurnard Formation log-kick still lies slightly above the mapped seismic surface, and there may be alternate reasons for this situation.The regional correlation of the Top Latrobe Group seismic horizon from the Southern Platform (where it is solidly constrained/tied to four wells with consistant characteristics) onto the Southern Terrace is clearly problematic. This is in part because of the occurrence of the overlying Early Oligocene Wedge (see following text section). However, it is suggested here that picking a significant, regional boundary such as Top Gurnard Formation, based on where sediments become more calcareous seems to place some uncertainty in the evaluation. Clearly, the

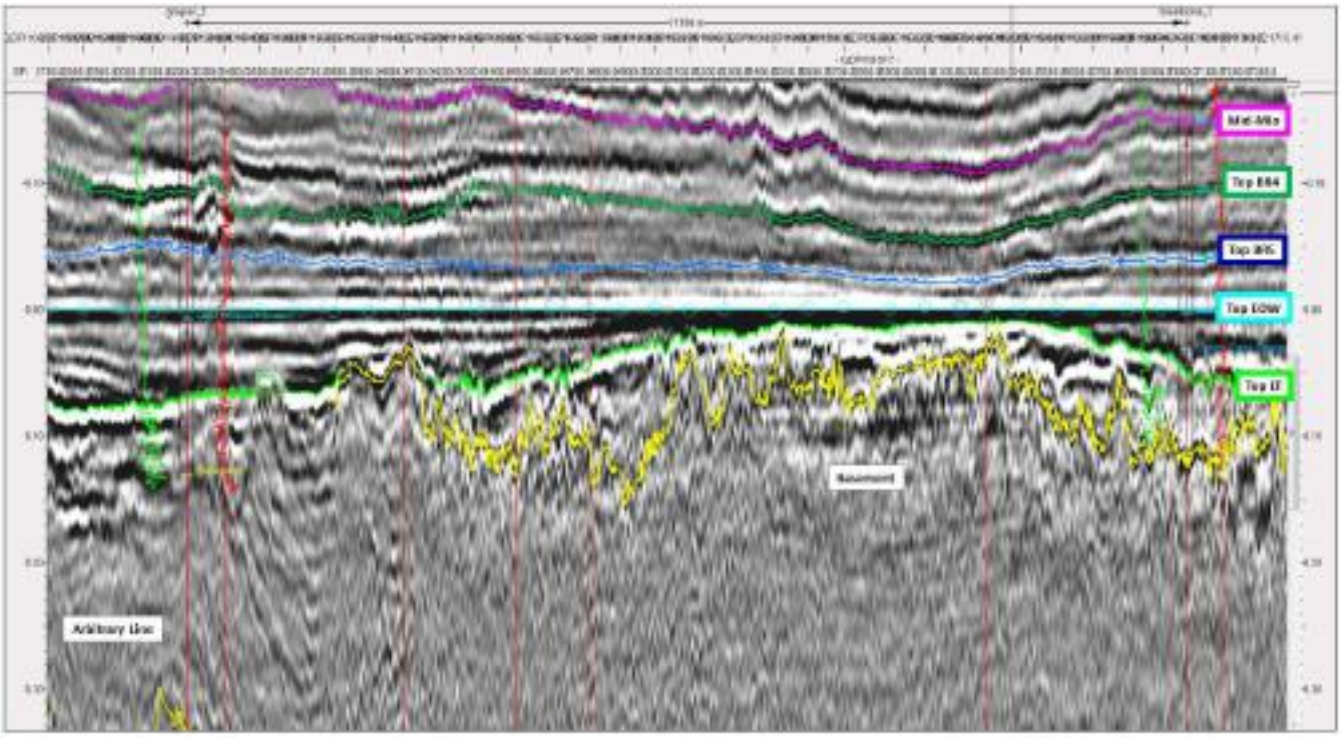

Figure 5.49 Highly-squeezed and flattened arbitrary line between Groper-2 and Bluebone-1 showing the variable thickness and nature of Latrobe Group sediments. The sediments are largely constrained to valleys formed by the rugose topography of the basement surface.

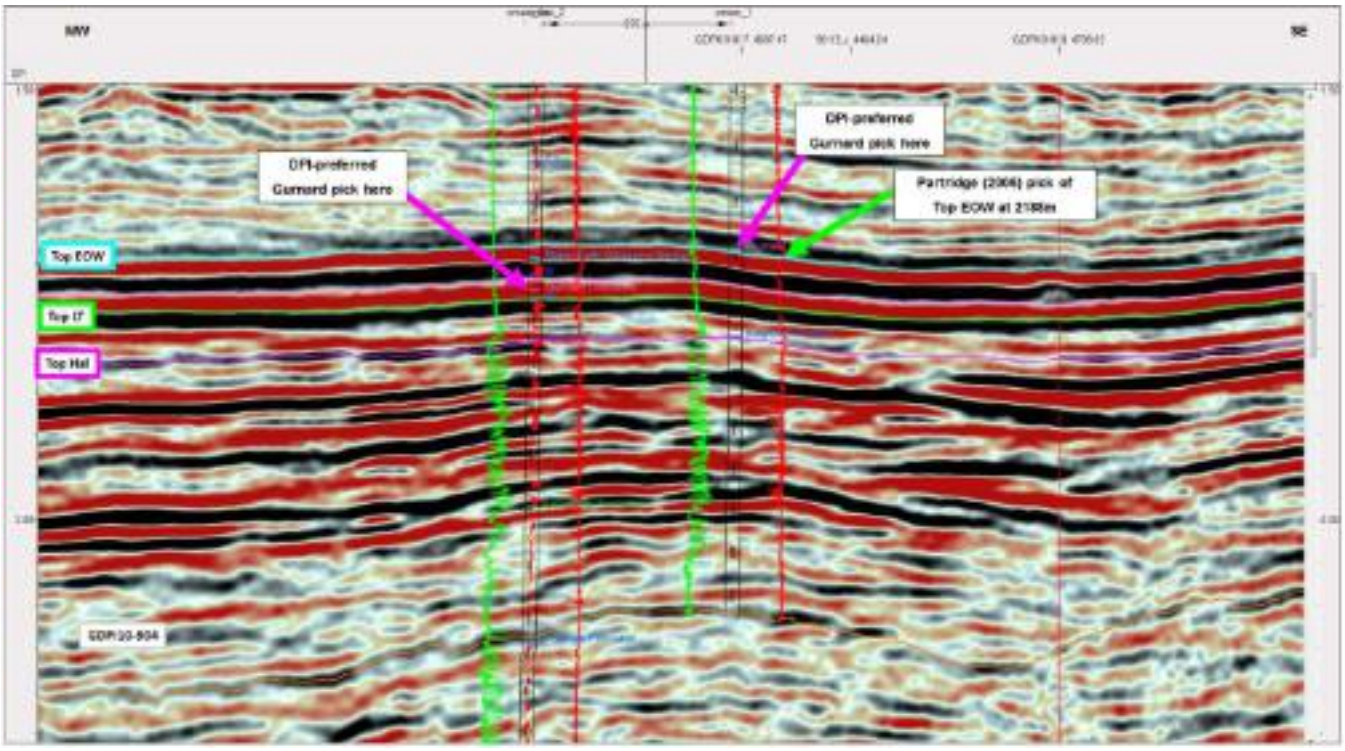

Figure 5.50 Seismic strike line GDPI10-904 showing the mis-correlation between the DPI-preferred picks of Top Gurnard Formation between Omeo-1 and Omeo-2A. The deeper pick at Omeo-2A is the preferred interpretation. Regional seismic correlations suggest that the (high) Gurnard Formation pick at Omeo-1 is the top of the Early Oligocene Wedge (also confirmed by Partridge, 2006).

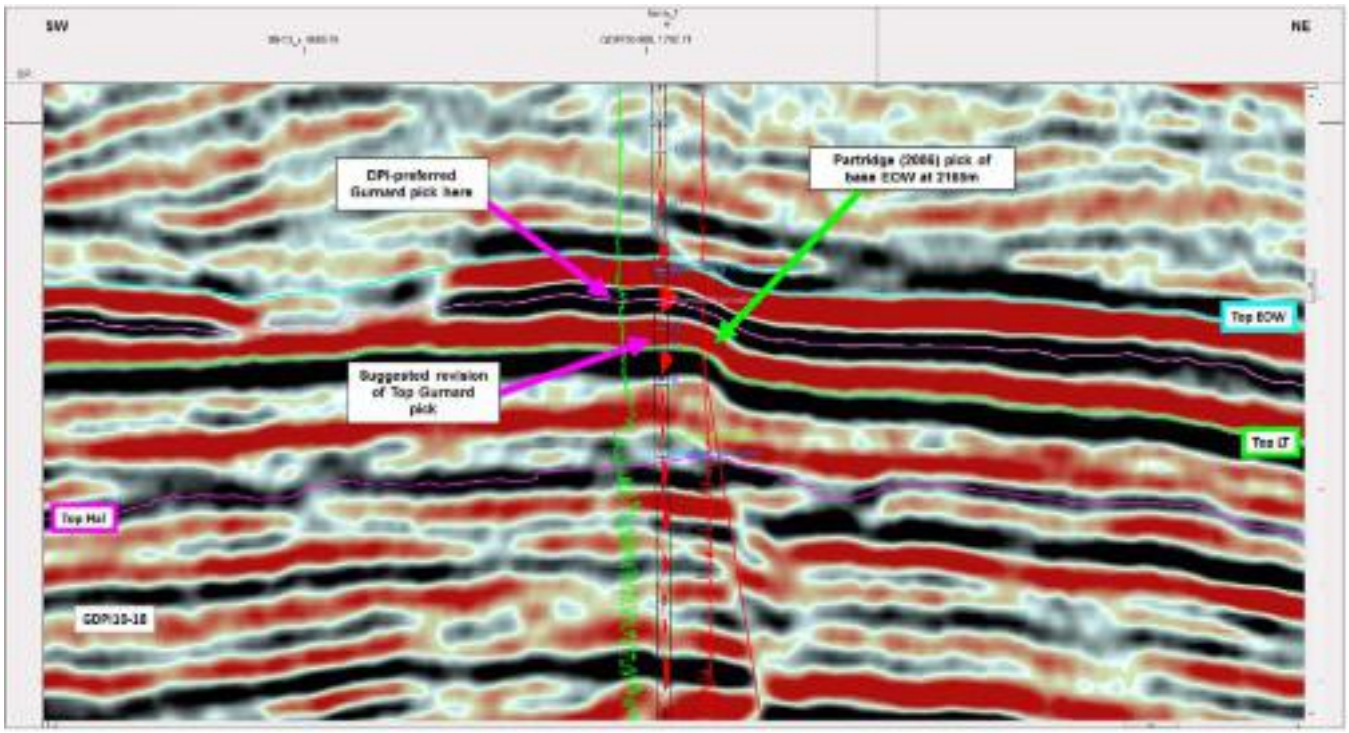

Figure 5.51 **Seismic line GDPI10-18 showing the DPI-preferred pick for Top Gurnard Formation at Tarra-1. In this position, the "Top Latrobe" horizon does not tie well with the regional seismic correlations. Note that the "Gurnard" interval at Tarra-1 has been picked by Partridge (2006) as the base of the Early Oligocene Wedge (2165m).**

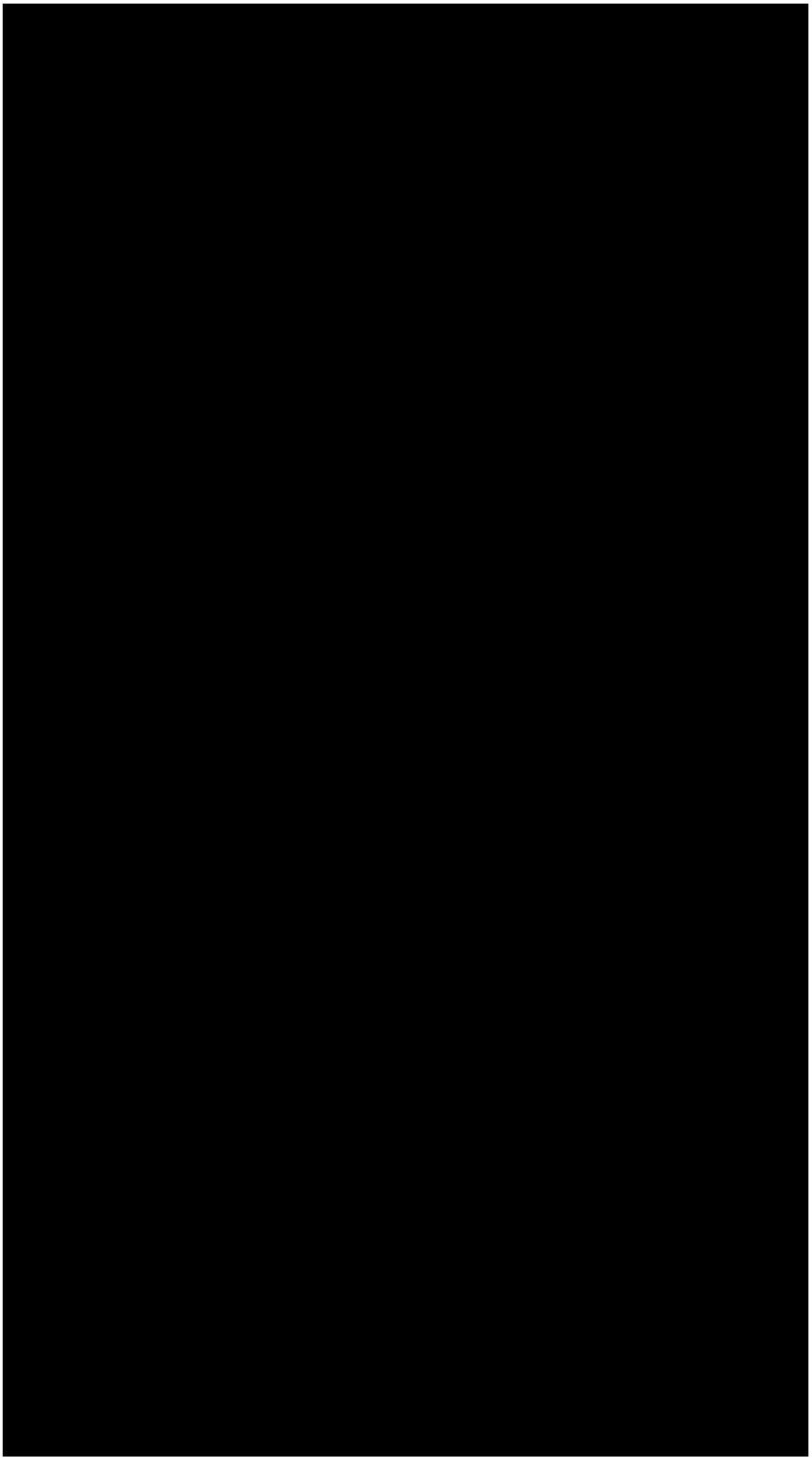

Figure 5.52 Seismic line GDPI10-13 showing the DPI-preferred pick for Top Gurnard Formation at Bullseye-1. In this position, the seismically mapped "Top Latrobe" horizon lies within a half cycle of the well tie. Note that Bullseye-1 has a thick Gurnard Formation that is characteristically claystone and siltstone, overlain by a thin glauconitic sandstone/siltstone.

timing/onset of a calcareous environment will differ across the basin, and will be highly dependent on the relict topography of the transgressive surface. An assessment of the literature (e.g. Gibson-Poole et al., 2006) would suggest that the Gurnard Formation is a complex and diverse stratigraphic unit with many different interpretations. It also represents a time of significant environmental change in the basin; an event which is time transgressive and not necessarily tied to a single lithology. Noting the physiographic difference between the Southern Flank and the Central Deep, the timing of the transgression is expected to be later on the Southern Terrace and Southern Platform. This may explain why the Gurnard Formation at Bullseye-1 has a stronger terrestrial signal when similar age sediments in the Central Deep are glauconitic. The thin overlying glauconitic interval at Bullseye-1 may not be typical Gurnard glauconitic sands, but rather a similar facies associated with the flooding of the Southern Flank and the onset of deposition of the Early Oligocene Wedge. Further work is required before these scenarios can be confirmed.

5.6 Seaspray Group (Bassian Rise Units)

Overlying the Eocene Latrobe Group are the Oligocene and younger cool-water carbonates of the Seaspray Group (Bernecker et al., 1997). A marine transgression which began in the latest Eocene (Gurnard Formation) continued into the early Oligocene, and resulted in the transition of the basin depositional system from largely non-marine clastics (Latrobe Group) to open marine fine-grained calcareous mudstones, marls and fossiliferous limestones. By the middle Eocene, seafloor spreading had ceased in the Tasman Sea and the start of compressional tectonism began to affect the Gippsland Basin, initiating a series of NE- to NNE-trending anticlines (Smith, 1988; Bernecker and Partridge, 2005). Compression and structural growth peaked in the middle Miocene, and many of the major hydrocarbon accumulations in the basin are hosted within the structures that formed during this time.

In the Central Deep to continental slope regions of the Gippsland Basin, the Seaspray Group is subdivided into the Angler, Albacore and Hapuku subgroups each with a number of formations (e.g. Holdgate et al., 2000; Bernecker and Partridge, 2001; Partridge et al., 2012). The basal unit of the Seaspray Group in these areas is the Early Oligocene Wedge (EOW; see Partridge, 2006; Partridge et al., 2012). However, some authors continue to use the more traditional "Lakes Entrance Formation" and "Undifferentiated Gippsland Limestone" nomenclature to describe the Seaspray Group. These works includes a recent study of the whole Gippsland Basin undertaken by 3D-GEO (2010) for DPI Victoria, whereby they describe that "regional containment is provided by the regional top seal, the Lakes Entrance Formation". This may be the case for the Central Deep, but it is clear from the current study that the Southern Platform is different.

On the Southern Platform, the Seaspray Group has been subdivided into the EOW and the overlying Bassian Rise Units (BR1/youngest to BR5/oldest; Partridge, 2006; Figure 5.5). Across the platform, the Seaspray Group is thinner (464 m/ Bluebone-1 to 866 m/Groper-1) although lithologically similar to the significantly thicker progradational carbonates of the Gippsland Basin Central Deep (2653 m at Volador-1). The Seaspray Group thickens over the adjacent Southern Terrace, but here much of the succession consists of a massive remobilised slump deposit that has been strongly affected by canyon incision (Figure 5.2). Characteristically, stratigraphic picks within the Seaspray Group slump deposit appear to be "random" (i.e. Top Lakes Entrance Formation picks at Bullseye-1, Mudskipper-1 and Tarra-1), and do not provide useful surfaces which can be regionally correlated or mapped on seismic data. The "Top Lake Entrance" pick at wells that lie within the slump are considered unreliable and were disregarded during the current study.

The mapping undertaken during this study has delineated a stacked succession of shallow marine, largely progradational carbonate wedges that were deposited from the early Oligocene until the late Miocene. These wedges were correlated to the Early Oligocene Wedge and Bassian Rise Units defined by Partridge (2006; Figures 5.44 to 5.48). Partridge (2006 and references therein) recognised the deepest wedge as the EOW at Bluebone-1, Mullet-1, Groper-1 and -2. The top of the EOW was previous described as the "Top Lakes Entrance Formation" in the original well completion reports from the late 1960s.

The EOW is best dated and constrained at Groper-1 (Partridge, 2006) where its Oligocene age lies within the I1 (top) and J1 (base) foraminiferal zonules of Taylor (1966). However, at Groper-2, the EOW corresponds to zonules H1 to G. Interestingly, the Bassian Rise stratigraphic chart of Partridge (2006) indicates that the EOW age correlation to Taylor's (1966) zonules is Base J2 (base of EOW) and mid-I2 (top of EOW), while the newer Geoscience Australia Chart 40 (Partridge et al., 2012) puts the EOW at Base J2 (base) and Top J1 (top). There are clearly some discrepancies between the spore/pollen and foraminferal results, and further work is needed. Partridge (2006) has delineated a Lower EOW and Upper EOW (Bluebone-1, Mullet-1 and Groper-1), and a Yellow Sandstone member within the Lower EOW at Bluebone-1.

Seismic ties of the Bassian Rise well picks at Groper-1 and Mullet-1 are excellent with the megasequence packages showing a strong correlation with the well picks (Figures 5.45 and 5.47). On seismic data, the EOW has an overall thick wedge geometry with mostly top-set internal geometries on the shallower parts of the southern platform (Figures 5.47

and 5.53). Along the outer margin of the platform, internal geometries become progressively more progradational in nature. The EOW and the BR5 and BR4 wedges clearly prograde to the outermost edge of the Southern Platform (Figure 5.53). The thickest part of the wedge only extends beyond the platform onto the Southern Terrace in a region roughly between Tarra-1 and Bullseye-1. Here, the thinned edge of the EOW has been cut by the Foster Fault System (Figures 5.16 and 5.22). The extent of the BR3 and BR4 wedges is unclear, as these units are mostly consumed within the slump complex. Wedges BR2 and BR1 are the mostly basinward extensive units (Figure 5.53).

The Top EOW horizon is correlated on the GDPI10 2D seismic grid at a well-defined (zero phase) positive-to-negative crossover. The well and seismic correlation between the Partridge (2003, 2006) picks at Bluebone-1, Mullet-1, Groper-1 and Groper-2 are generally very good (Figures 5.45 to 5.48). It is clear that the recognition of the EOW on the Southern Platform by Partridge (2006) can be supported by the seismic mapping where the wedge is thick. The correlation of Top EOW well picks beyond the outer part of the Southern Platform into more distal environments is also clear from the seismic data, as the top of the wedge is a strong and continuous reflector. In the more distal environments, a thin condensed section of the EOW is preserved and overlies the Top Gurnard Formation. Distinguishing between the EOW and the Gurnard Formation in the wells is more problematic.

On the western part of the Southern Terrace, Partridge (2006) suggests that the EOW is present at the Bullseye-1 (24 m; 2048-2072 m), Wyrallah-1 (73 m; 840-913 m) and Kyarra-1A (17 m; 995.5-1013 m) wells. However, when the EOW (as identified and tied at Groper-1) is correlated directly with these wells on seismic data, it would suggest the "wedge" feature is much thicker than proposed by Partridge (2003, 2006). The seismically-defined wedge is an estimated 166 m thick at Bullseye-1(1906-2072 m; Figure 5.52), 65 m thick at Wyrallah-1 (810-875 m), and 94 m thick at Kyarra-1A (919-1013m; Figure 5.14). It should also be noted that well data suggest that the seismically-defined wedge is no longer constrained within Taylor's (1966) foraminiferal zonules J2 (base) and mid-I2 (top). At Wyrallah-1 the wedge base is J1 zonule/early Oligocene [consistent with the Partridge (2012) definition]), and younger at the top [H1 zonule/early Miocene; younger than the Partridge et al. (2012) definition]. In this well, the lower wedge is described as a light-to-medium grey, soft, glauconitic calcareous claystone, while the upper part of the wedge is marl. The younger age at the top of the wedge is simply part of the progradational nature of the wedge, so this correlation is not surprising. There is also a disconformity (?hiatus) within the wedge at Wyrallah-1 between the late Oligocene and early Miocene. The top of the EOW is clearly an unconformity on the seismic data, and locally shows large-scale scouring and incision (Figures 5.14, 5.15 and 5.18).

An attempted correlation of the EOW between the Wyrallah-1 and Kyarra-1A wells by Partridge (2003) can be shown as invalid when correlated on the new seismic data. The error was the incorrect picking of the Gurnard Formation too deep in the Wyrallah-1 well. In Partridge's (2003) correlation, the thick sand unit near 900 m (which is actually Burong Formation age) is correlated to a condensed interval at Kyarra-1A. This interpretation is not supported by results of the current study.

Other picks of the EOW by Partridge (2006) in the Tarra-1, Omeo-1, Omeo-2A, Devilfish-1, Moray-1 and Mudskipper-1 wells are very close to those interpreted on the seismic grid. Only minor adjustments are suggested. Similarly, a pick of the EOW at Melville-1 by Partridge (2002) also agrees very closely with the seismically mapped Top EOW. Importantly, these wells are located at the seismically defined downlapping toes of the prograding wedge where the interval is thin and condensed. Collectively, the seismic interpretation supports the EOW with modifications (as noted above), and the EOW is validated as a regional continuous unit across the seismic grid. Partridge (2006) also notes that the "micaceous marl" portion of the traditional Lakes Entrance Formation is equivalent to the Bassian Rise Unit 5 (BR5). The Top BR5 horizon has also been mapped during this study as a proxy for the Top Lakes Entrance Formation horizon.

In the regionally constrained framework, where the well-defined picks of the EOW and younger wedges have been tied and mapped across the Southern Platform and Southern Terrace, the concept of a single early Oligocene age wedge as proposed by Partridge (2006) should be amended to one of a longer-lived, carbonate progradational system that formed within an overall ramp-like setting (Figure 5.53). Indeed, the overlying BR5 and BR4 units of Partridge (2006) can also be mapped as large progradational systems. The downlapping margins of the BR5 and BR4 progradational systems are best imaged in the western part of the GDPI10 2D seismic grid, as elsewhere this part of the Seaspray Group is often consumed within the slump system that occurs along the northern margin of the platform. BR3 also appears to be a progradational system but this succession is almost entirely consumed within the slump system at its most northern (?progradational) extent. BR2 does not appear to have a progradational geometry within the current study area, but may show this character in the deeper Gippsland Basin.

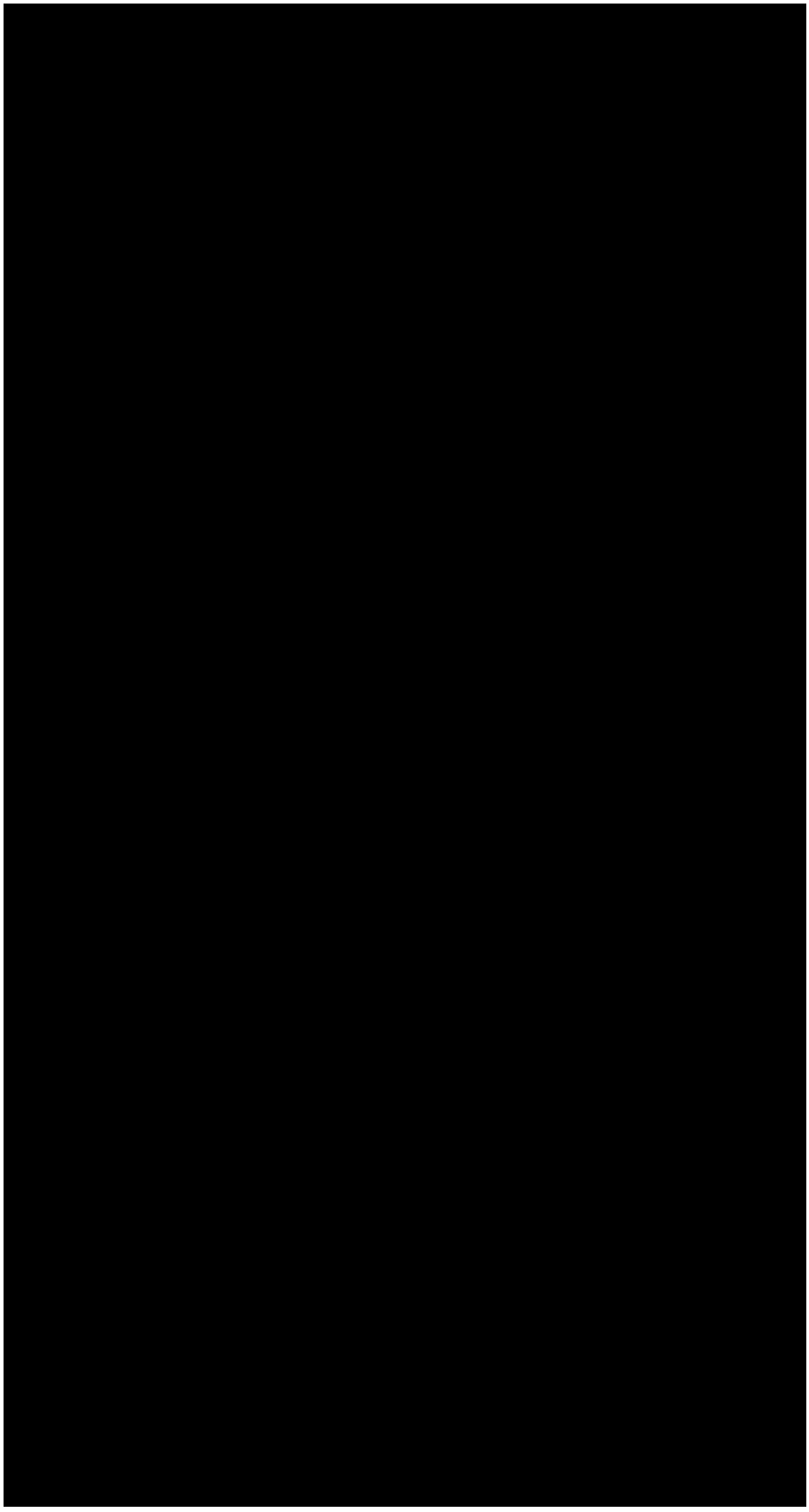

Figure 5.53 Seismic line GDPI10-45 showing the correlation of Partridge's (2006) picks for the Latrobe Group, Early Oligocene Wedge and Bassian Rise Units at Bluebone-1. Note the varying extent of each of the progradational wedges onto the outer Southern Platform and Southern Terrace.

There are several key implications of the EOW and Bassian Rise Units' seismic correlation:

1) The traditional Lakes Entrance Formation regional sealing facies does not directly overlie the Top Latrobe Group in the study area on the Southern Flank of the Gippsland Basin.

2) The distal toes of the EOW may be mistaken for a condensed section of the Gurnard Formation, particularly if the section is bioturbated and there are no microfossils preserved due to diagenesis as suggested by 3D-GEO (2010). This will alter the picks and correlation of the Top Latrobe Group regionally.

3) The BR5 (Lakes Entrance equivalent sealing facies) is thickest on the Southern Platform and does not appear to extend onto the Southern Terrace.

4) The top seal that directly overlies the Top Latrobe Group reservoirs is extremely variable in age, thickness and lithology. The MICP analyses which were undertaken on the Gurnard Formation at Groper-1 yielded poor storage capacity potential (Goldie Divko et al., 2010), while the single sample with good capacity came from the "Lakes Entrance Formation". The current mapping study has confirmed that the high capacity storage results came from a sample within the EOW – not the Lakes Entrance Formation.

5) There are high risks for the integrity of the EOW and BR5 units as seals due to late stage faulting along the Foster Fault Zone, deformation by the slump complex, and Miocene uplift and faulting near Kyarra-1A. Risks for sealing facies are discussed further in Section 6.

6 Mapping, Risks and Key Results

6.1 Introduction

A series of structure (TWT and depth) isochron and isopach grids were produced from the horizon interpretations and velocity model. Previous sections of this report have presented the datasets, interpretation and gridding methodology used in the study. Section 5 has assessed the stratigraphy, well picks and ties, as well as highlighting any issues or observations. The compilation and testing of the velocity model for depth conversion is covered in Section 7. The interval velocities for all generated isopachs are shown in Appendix 7, as well as the average velocity of each of the mapped surfaces.

Presented in this section are the depth grids of the structure surfaces and isopachs as a series of annotated maps that highlight the regional features of each mapped stratigraphic interval. Emphasis has been placed on understanding the reservoir and seal intervals in the upper Latrobe Group (Cobia and Halibut subgroups) and lower Bassian Rise units , respectively. A regional assessment of key risks and results was also undertaken.

The GDPI10 2D seismic grid provides a "new look" into an area that was previously covered by sparse and vintage datasets. The data has provided insights into the complexity of the stratigraphy and structure – both of which have implications for potential storage capacity and risks. Despite the high quality of the seismic data, some drawbacks are present. The grid was oriented with NE/SW-trending dip lines, and NW/SE-trending strike lines (Figure 6.1). This orientation provides the best result for imaging structures and stratigraphy across the central and eastern part of the study area. However, a change in structural trend in the western part of the study area has meant that lines GDPI10-01 to GDPI10-10 are oriented oblique to the structure which makes the mapping of the intra-basinal faults and the pre-Latrobe Group stratigraphy difficult. This is particularly evident on the western ends of the "strike lines". In addition, many of the line intersections in the same area cross-tie at major structures and faults, and this has introduced some apparent mis-ties in the grid. Lastly, the Darriman Fault System is only transected in the western part of the study area. In the central region, only three lines extend close to the fault system. Therefore, the Darriman Fault System was only interpreted where transected, and the interpretation of the deep horizons on the northernmost parts of the lines was not undertaken due to inadequate control on fault offsets. The 3D-GEO grids were available to help with extending ties from the deep basin into the study area, but these grids were of insufficient resolution to provide confident input.

6.2 Depth Structure and Isopach Maps

6.2.1 Top Basement

The Top Basement depth structure map shows the underlying structural framework of the study area (Figures 6.2 and 6.3). Across the seismic grid, basement depth ranges from 125 m to 12 km with the largest offset occurring along the Foster Fault System (FFS). The FFS has acted to control deposition in the rifted depocentres that abut the Southern Flank since the Early Cretaceous. This fundamental boundary has continued to be active periodically until the mid-Miocene when minor fault reactivation resulted in instability in the overlying Miocene progradational carbonate shelf. Fault movement resulted in shelf collapse, and the development of a slump complex with subsequent canyon incision along the northern margin of the Southern Platform (see section 6.4). The FFS has also acted as a deep conduit for volcanic intrusions during periods of extension. Step-overs and relays along the extent of the FFS have been the focus of inversion such as observed near Moray-1 (Figures 6.2 and 6.3). Rigid basement has also acted as a buttress as observed in the formation of the Kyarra Anticline.

The McLoughlins Sub-basin has been defined as an isolated, intra-platform rift basin up to 5.8 km deep. Strzelecki age equivalent sediments have been interpreted to infill the depocentre. Older Paleozoic half graben have also been mapped around the Groper-2 well and further to the west. Along the eastern boundary of the Southern Platform, parts of the Pisces Sub-basin have been systematically mapped for the first time. Although not fully covered by the grid, the basin-boundary faults appear to be defined as a series of en-echelon half graben that deepen to the east. Limited well control (Pisces-1) suggests that the deep syn-rift fill is Golden Beach age (Campanian).

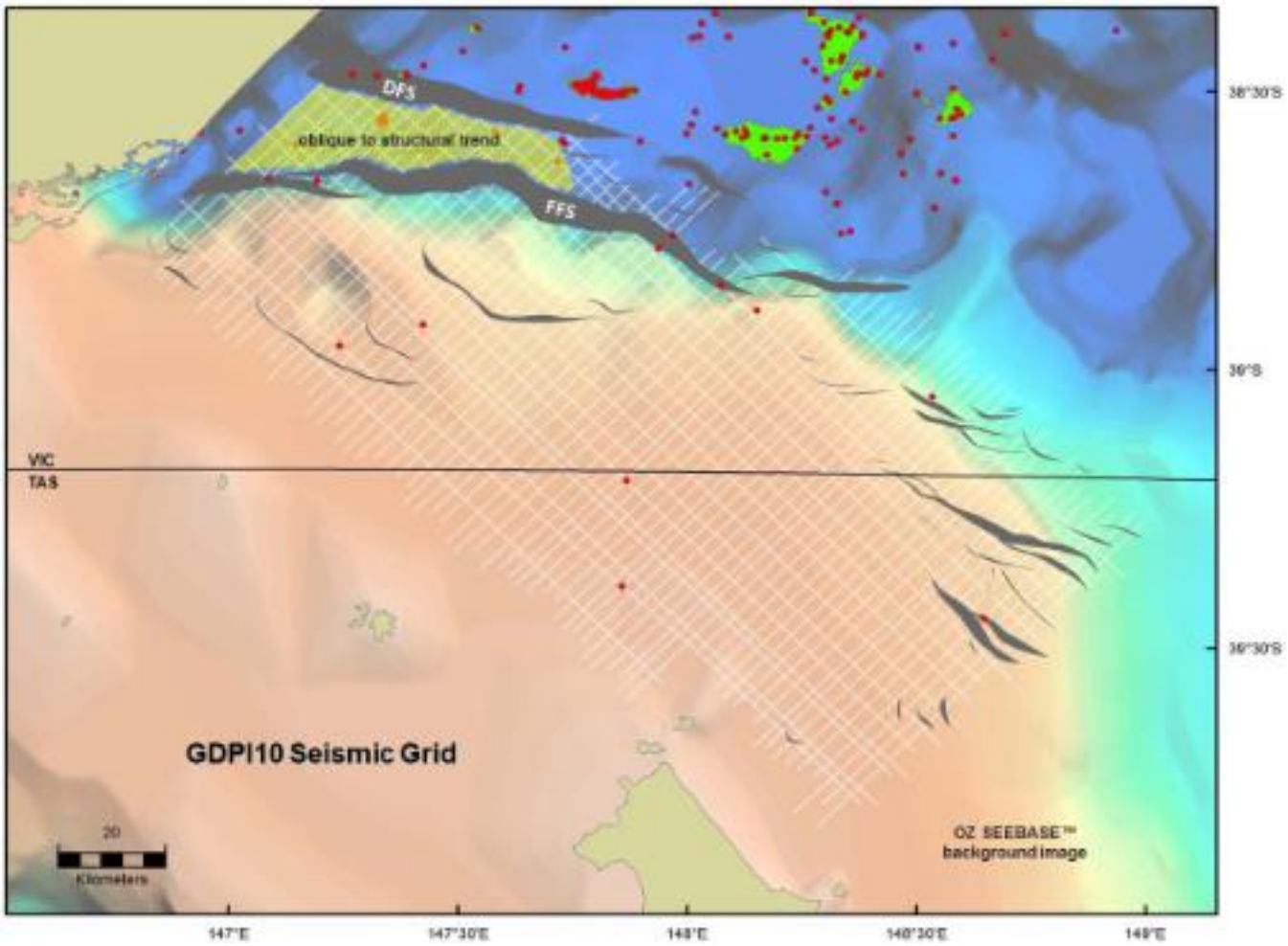

Figure 6.1 Map showing the GDPI10 2D seismic survey grid relative to underlying structural features. Note that parts of the western grid are oriented oblique to structural trend. The Darriman Fault System (DFS) is only transected in the western part of the grid. Only three lines in the central part of the grid cross the major structural boundary. FFS = Foster Fault System.

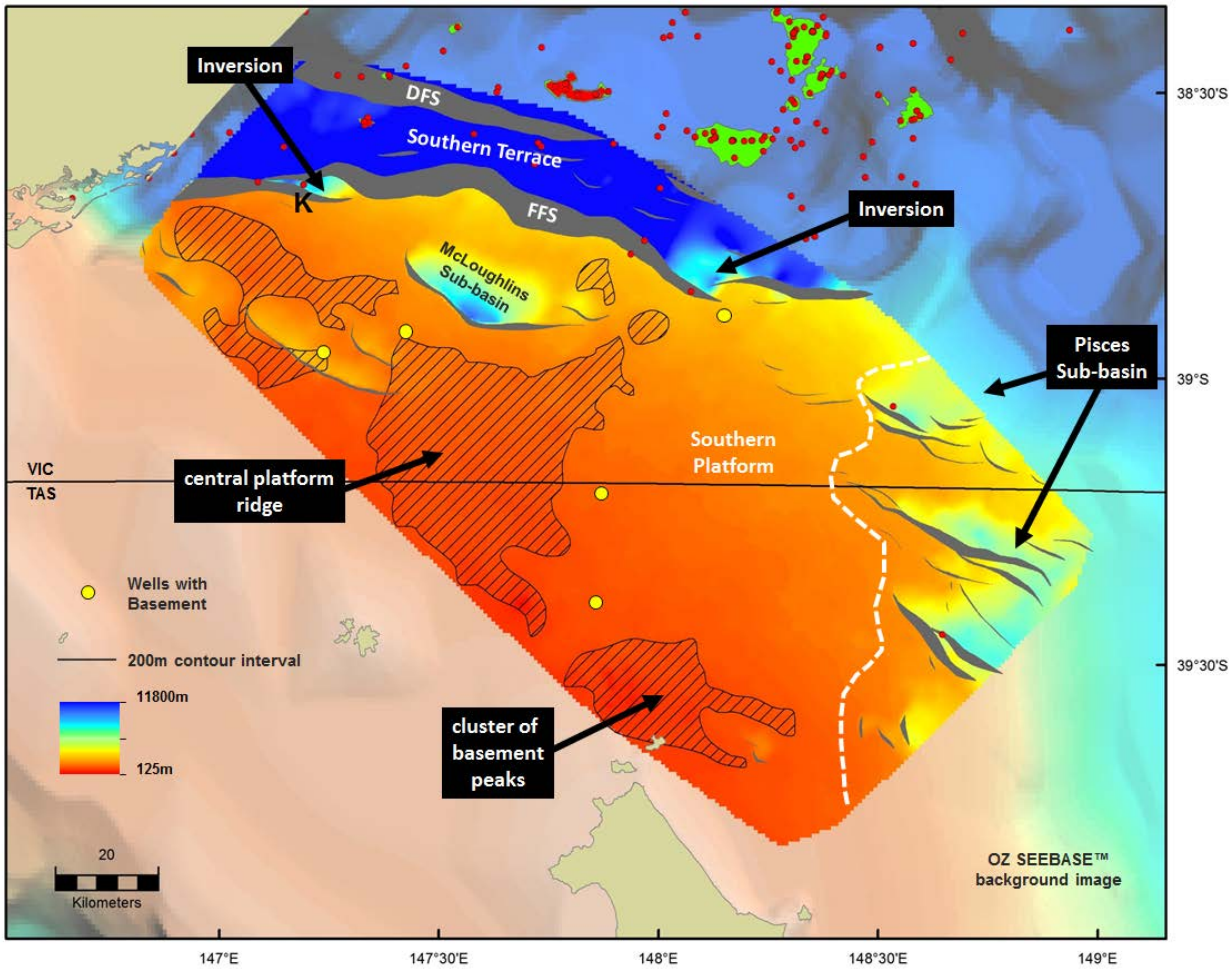

Figure 6.2 Top Basement depth structure map for the study area showing significant structural features. FFS = Foster Fault System. DFS = Darriman Fault System. Kyarra-1A (K) is drilled on the Kyarra structure.

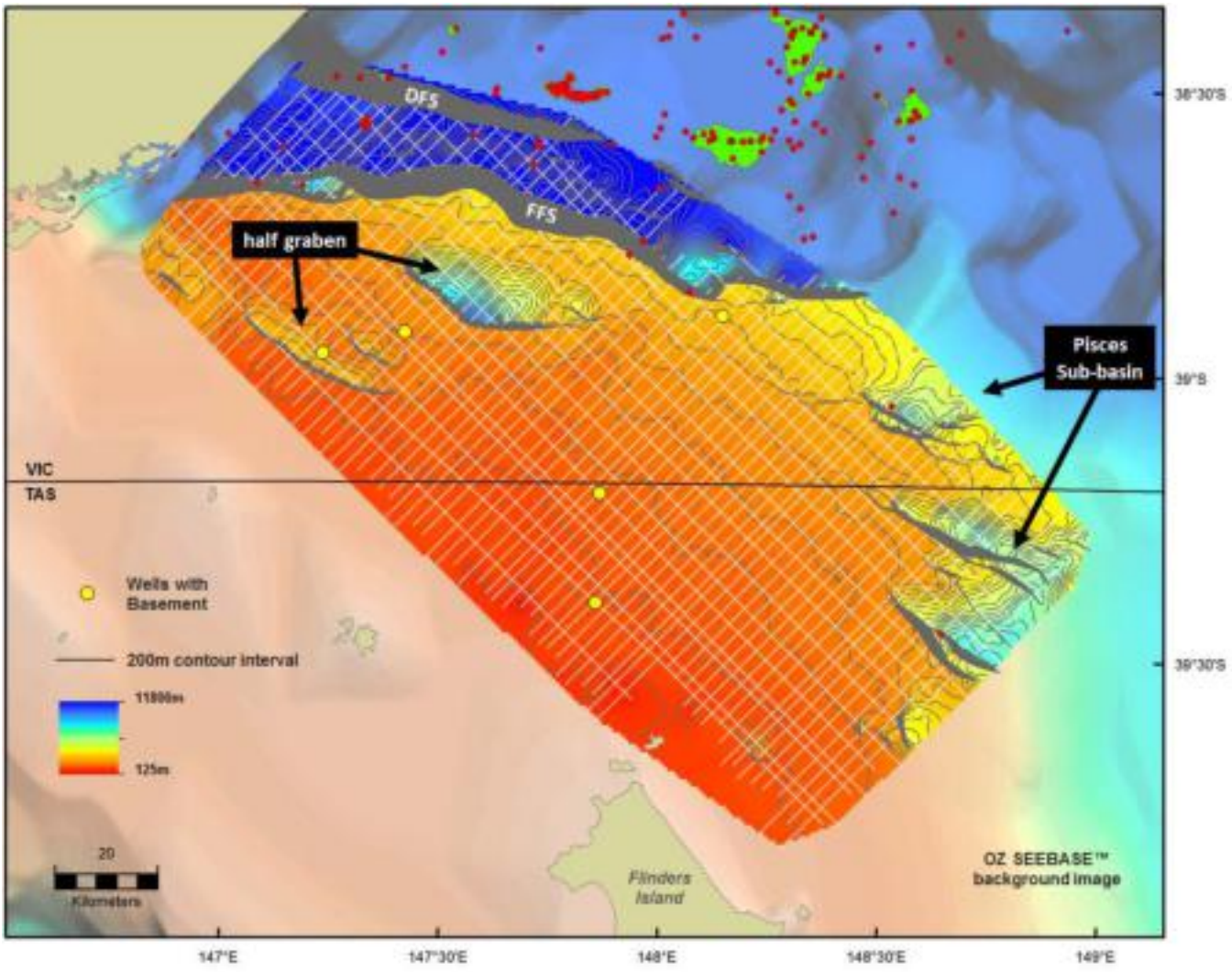

Figure 6.3 Top Basement depth structure map showing the underlying structural framework of the study area. FFS = Foster Fault System. DFS = Darriman Fault System.

These structures formed during extension prior to breakup in the Tasman Sea off the main Gippsland Basin. Massive volcanics were intruded and extruded around the margins of the Pisces Sub-basin during breakup. The volcanics commonly have associated fluid leakage features (see Section 6.5). If prospective source rocks are present, the depth of the Pisces Sub-basin is sufficient for maturation to have occurred.

Elsewhere, the Southern Platform is characterised by overall rugose basement topography with shallow hills and ridges. The overlying structure maps and isopachs suggest that sediment was shed from these features to the north and northwest. These structures were particularly important for sediment provenance during deposition of the Latrobe Group.

6.2.2 Total Sediment Thickness

The total sediment thickness depth map shows the thinning of sediments across the Southern Platform and thickening with local fault-controlled structures such as the McLoughlins and the Pisces sub-basins (Figure 6.4). Sediments thicken significantly across the Foster Fault System with local thinning in the vicinity of the Kyarra Anticline and Moray-1 where an inverted fault sliver lies near the main fault. Sediments range in thickness from 80 m near Flinders Island to 12 km across the outer Southern Terrace near the Darriman Fault System.

6.2.3 Strzelecki Group

Mapping of the Top Strzelecki Group is controlled by only four wells in the survey area: Kyarra-1A, Perch-1, Tarra-1 and Omeo-1. With the exception of Omeo-1, the other three wells penetrating the Strzelecki Group were drilled on the Southern Terrace over rotated extensional fault blocks (Tarra-1), or basement inversion structures (Kyarra-1A and Perch-1). These wells provide only poor-to-moderate control on the mapped horizon. In particular, working the ties on the uplifted/rotated fault blocks away from well control is problematic due to complex faulting, inversion and poor imaging/resolution of the deeper section. The oblique orientation of the seismic grid in the western part of the study area also significantly impeded imaging of the Strzelecki fault blocks and their correlation (see Section 6.1). Much of the Top Strzelecki Group mapping in that area is based on seismic character.

The Top Strzelecki depth structure map (Figure 6.5) shows prominent high features such as the Kyarra-1A inversion anticline and the Perch fault block in the western study area. The prominent McLoughlins Sub-basin on the Southern Platform has been interpreted as filled with Strzelecki age equivalent sediments. Overall, the Strzelecki Group is confined to the Southern Terrace with deposition controlled by the Foster Fault System. Some fault slivers off the Foster Fault System are evident near the Moray-1 well.

The Strzelecki Group is downfaulted along the Darriman Fault System into the Central Deep; however the fault has only been interpreted where it crosses the grid in the northwestern part of the study area. In the central and northern parts of the terrace, only three seismic lines extend across the width of the Southern Terrace (Lines GDPI10-026, -027 and -028). These lines terminate at or before the Darriman Fault System, and the Strzelecki Group picks at the ends of these lines are poorly constrained. East and west of these lines, there is no seismic control and the gridding process has extrapolated the interpretation into these areas (Figure 6.5). It is recommended that several transects be interpreted into the Central Deep to better constrain the interpretation of basement, the Strzelecki Group and younger sediments near the Darriman Fault. The 3D-GEO grid was of insufficient resolution to provide confident constraints.

The Strzelecki Group depth isopach map is probably not a true reflection of Strzelecki thickness because of the low confidence in picking deep basement north of the Foster and Darriman fault systems (Figure 6.6). In addition, the Top Strzelecki horizon is poorly constrained due to reduced quality of the deeper seismic data and sparse intersections. However, the isopach of the McLoughlins Sub-basin is well constrained and shows a slightly asymmetrical, fault-bounded depocentre with up to 8.2 km of sediment. Due to its poor reservoir quality the Strzelecki Group sediments are unlikely to have any significant greenhouse gas storage potential.

6.2.4 Emperor Subgroup

Similar to the Strzelecki Group, the Emperor Subgroup is poorly constrained by only four well intersections (Tommyruff-1, Perch-1, Melville-1 and Moray-1). Perch-1 and Tommyruff-1 intersected Emperor Subgroup sediments in fault-bounded depocentres in the western part of the study area. Moray-1 intersected arkosic sands and conglomerate proximal to the Foster fault scarp, while Melville-1 is located on a basinward thickening wedge. The Top Emperor Subgroup depth structure map shows its distribution is strongly controlled by the Foster Fault System (Figure 6.7).

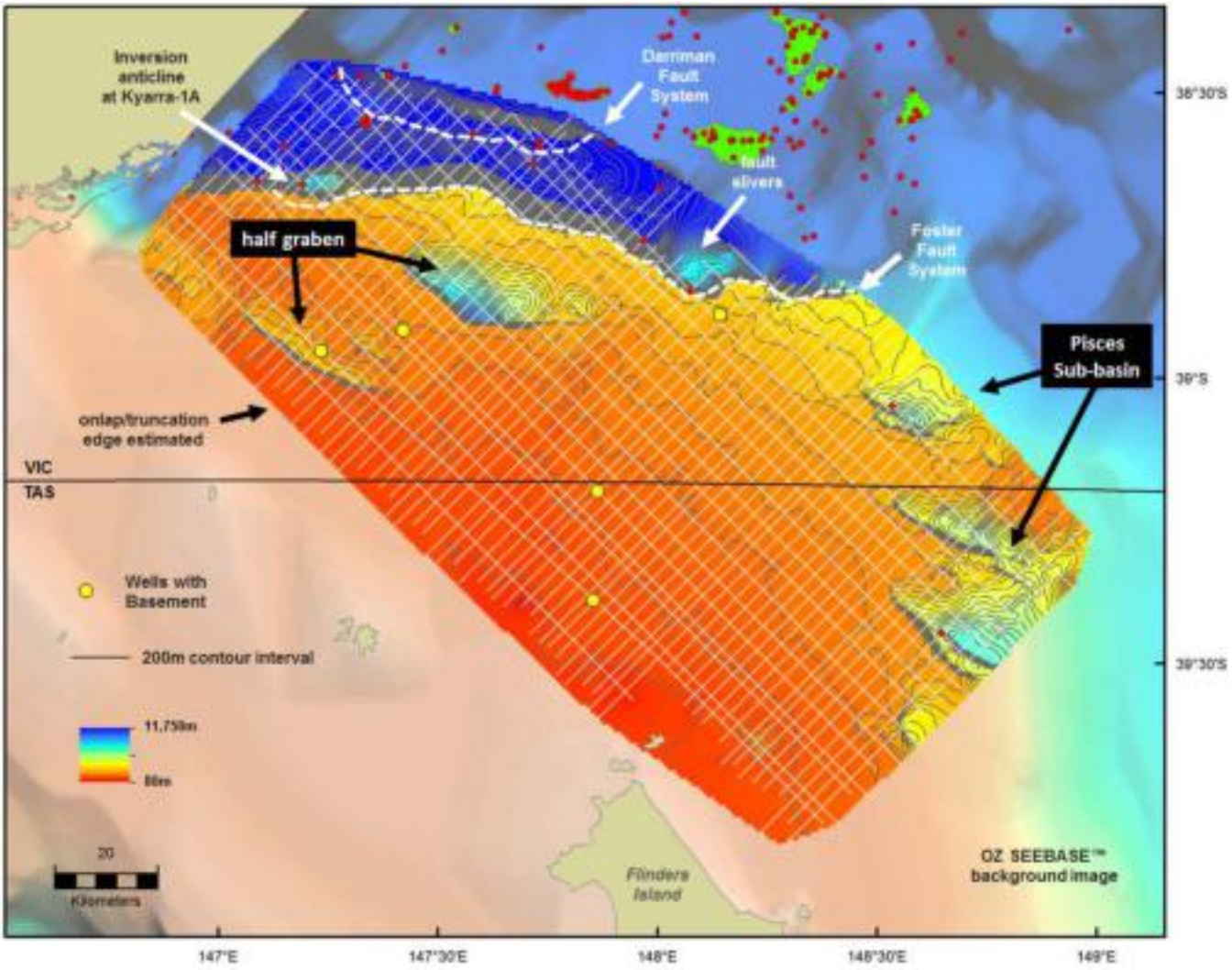

Figure 6.4 Total sediment thickness depth map for the study area.

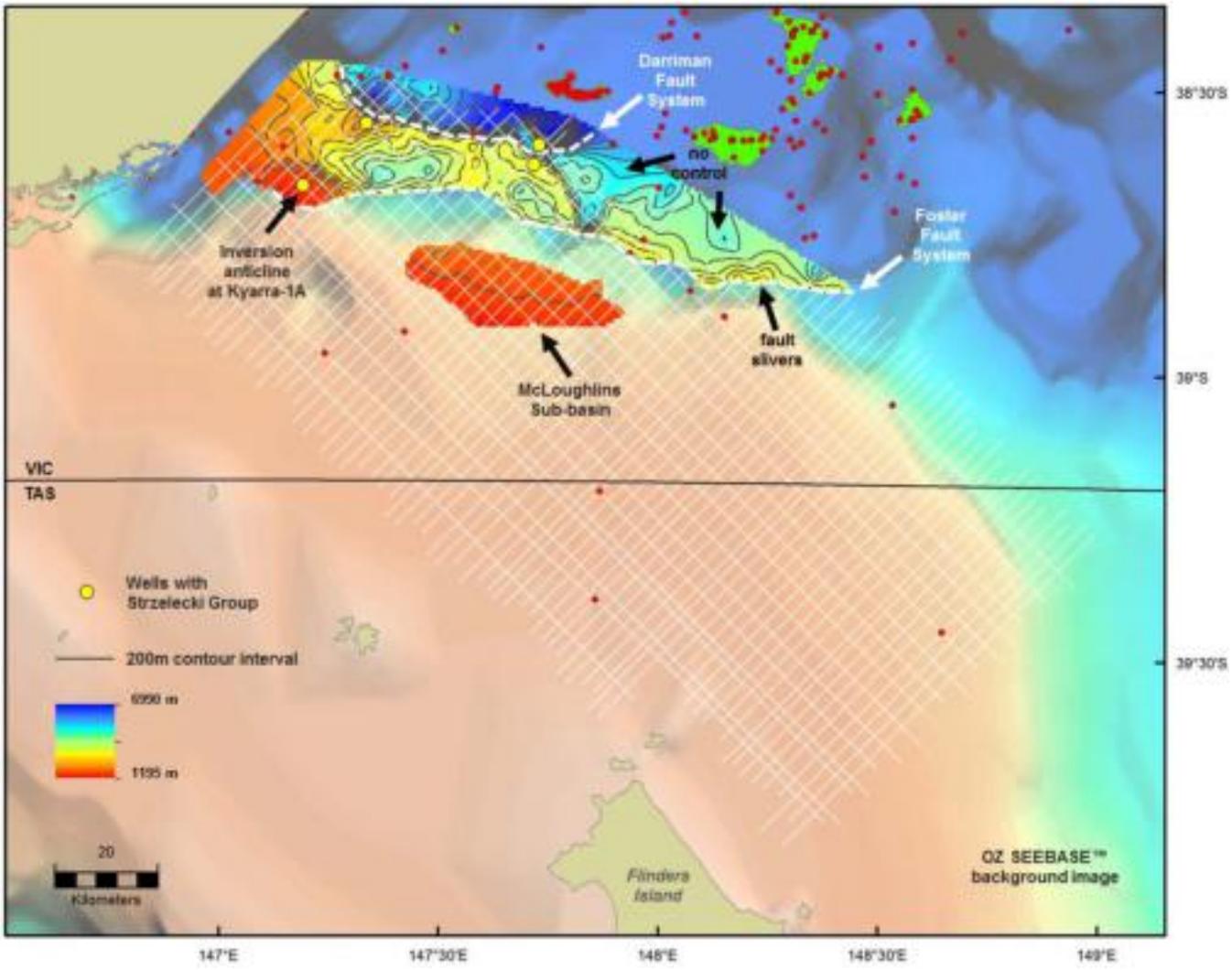

Figure 6.5 Top Strzelecki depth structure map for the study area.

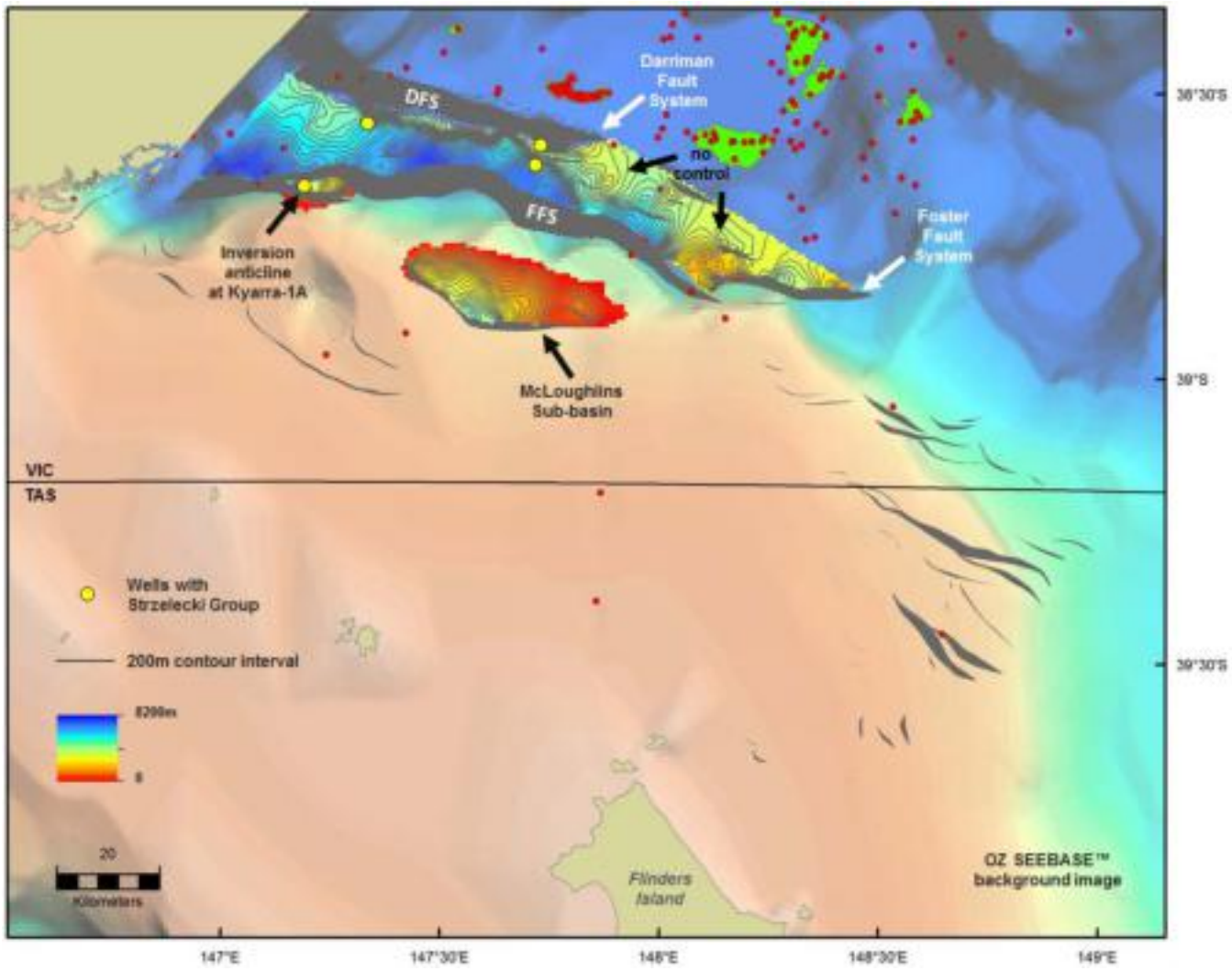

Figure 6.6 Strzelecki Group sediment isopach map for the study area. FFS = Foster Fault System. DFS = Darriman Fault System.

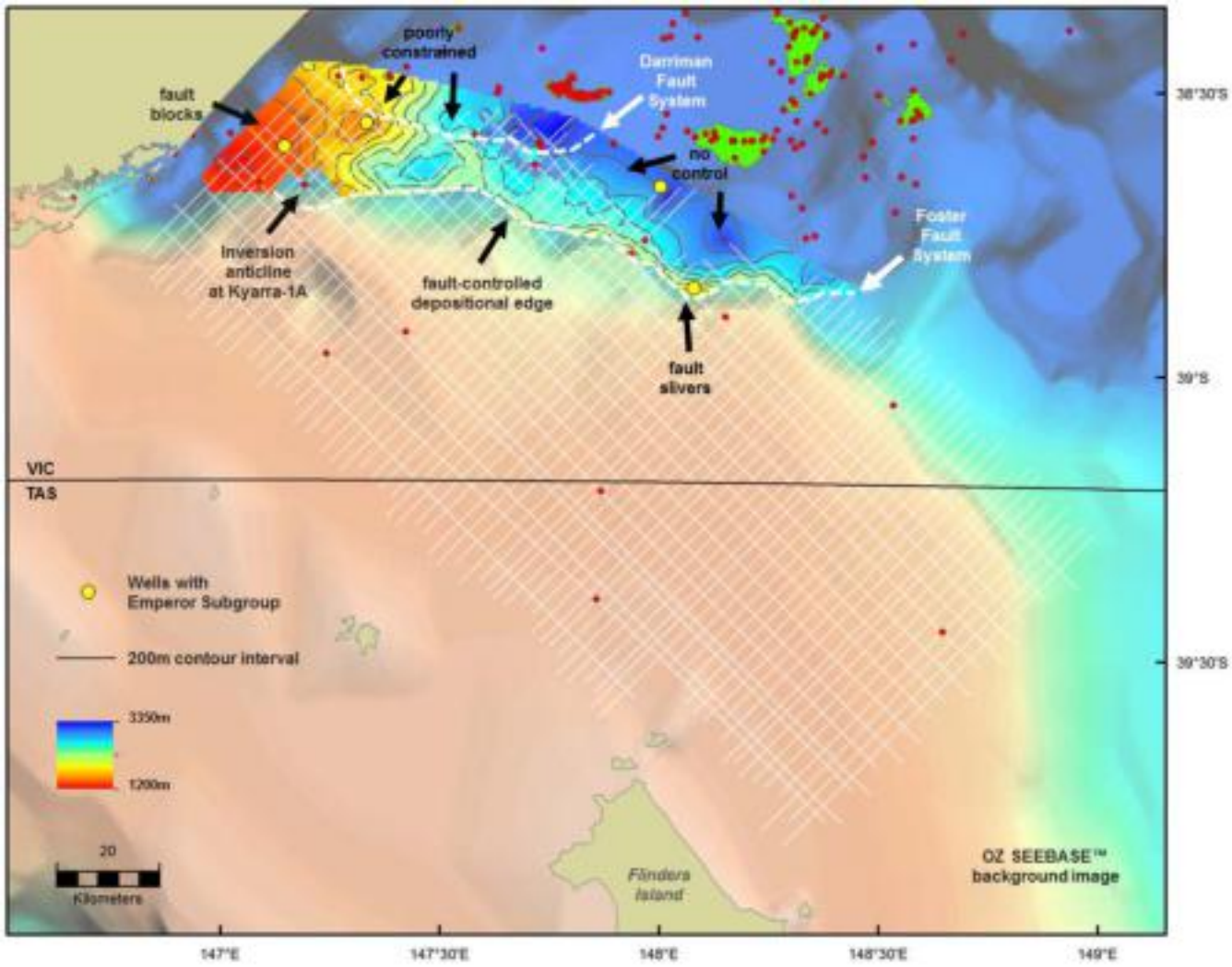

Figure 6.7 Top Emperor Subgroup depth structure maps for the study area.

A general basinward deepening trend is observed north of the Foster Fault System, although deepening across the Darriman Fault System is poorly constrained due to data distribution and quality. The shallowing of the surface in the western part of the study area is due to recent structural uplift, rather than original deposition environment. The Emperor Subgroup is absent over the Kyarra-1A inversion anticline and shallows locally against the Foster Fault System due to inversion against the fault.

The Emperor Subgroup depth isopach map shows significant thickening north of the Darriman Fault System (Figure 6.8), although this could be misleading because of difficulty in accurately picking the top of the underlying Strzelecki Group (i.e. the lower constraining surface). The Emperor Subgroup is absent over the Kyarra-1A anticline but present in an E/NE-trending, fault-controlled depocentre present just north of the anticline. Some local thickening is observed on the downthrown side of the Foster Fault System due to rotation of fault blocks. The Emperor Subgroup is also unlikely to be a target for storage, although there may be some potential for lacustrine source rock deposition in the western study area.

6.2.5 Golden Beach Subgroup

Strata of the Golden Beach Subgroup are penetrated in only four wells: Omeo-1 and Omeo-2A, Melville-1 and Pisces-1. The Top Golden Beach Subgroup depth structure map shows deposition is fault controlled and confined to outboard of the Foster Fault System and within the Pisces Sub-basin half graben (Figure 6.9). Mapping of the Golden Beach Subgroup in the Pisces Sub-basin shows there is a significant thickness present in the easternmost half graben which may be prospective for hydrocarbon generation (if source facies are present). In the western part of the study area, the presence of the Golden Beach Subgroup is mostly inferred from volcanics and thus is not well constrained. A general deepening trend is observed towards the Darriman Fault System where the Golden Beach Subgroup thickens significantly into the Central Deep. Due to low confidence in the regional mapping, limited well control and the thin nature of the succession, no isopach of the Golden Beach Subgroup was produced. The Golden Beach Subgroup is also unlikely to be a storage target.

6.2.6 Halibut Subgroup

The Halibut Subgroup has sufficient well control, stratigraphic thickness and distinctive seismic character to allow this interval to be confidently mapped across the study area. The Halibut Subgroup is present in Amberjack-1, Bullseye-1, Devilfish-1, Kyarra-1A, Moray-1, Melville-1, Mudskipper-1, Omeo-1, Omeo-2A, Palmer-1, Perch-1, Pike-1, Pisces-1, Tarra-1, Tommyruff-1 and Wyrallah-1. The subgroup is potentially a good reservoir for both petroleum accumulations and CO_2 storage, although the presence of intraformational and top seals are risk factors. The Halibut Subgroup lies at depths of 960 to 2500 m which is within the depth window for storage of supercritical CO_2.

The new seismic grid shows clearly for the first time that the Halibut Subgroup extends from the Southern Terrace, across the Foster Fault System and well onto the Southern Platform (Figure 6.10). It is also likely that a thinned succession of the Halibut Subgroup is present in the eastern part of the Pisces Sub-basin; however current well control does not allow a continuous tie from Pisces-1 into this area. This tie is also compromised by the development of the outer platform slump complex (see Section 6.4) and extensive volcanic intrusions which locally degrade data quality. Similar to previous maps, the extent of the Halibut Subgroup northward beyond the Darriman Fault System is poorly constrained.

Seismic data also shows the development of sand sheets which extend from the central platform basement ridge (see Figure 6.2) towards the Foster Fault System. In this scenario, fault relays in the Foster Fault System may have acted as conduits for sands to funnel from the Southern Platform locally onto the Southern Terrace (Figures 6.10 and 6.11). The shallowing of the Halibut Subgroup in the western study area is due to inversion rather than original depositional environment. A strong west-to-east deepening trough is observed east of this uplifted area (Figure 6.10), and this trend is present in subsequent structure maps. The trend is likely to reflect post-depositional movement on the Foster Fault System.

The Halibut Subgroup sediment thickness depth map shows the extent and interpreted thickness of the succession beyond the Southern Terrace and onto the Southern Platform (Figure 6.11). Locally thick occurrences of this interval are highlighted along the Foster Fault System. Sediments of the Halibut Subgroup are the first widespread succession to onlap the basement surface on the Southern Platform. Local thickening observed on the Southern Platform is highly speculative and mostly reflect areas with rugose basement topography. The Halibut Subgroup is thinner in the western study area, although the well ties indicate some differences in the Top Halibut Subgroup picks between the western wells and the Southern Terrace wells. The structural trend may reflect some influence from the picks. The Halibut Subgroup reaches a maximum of almost 1500 m.

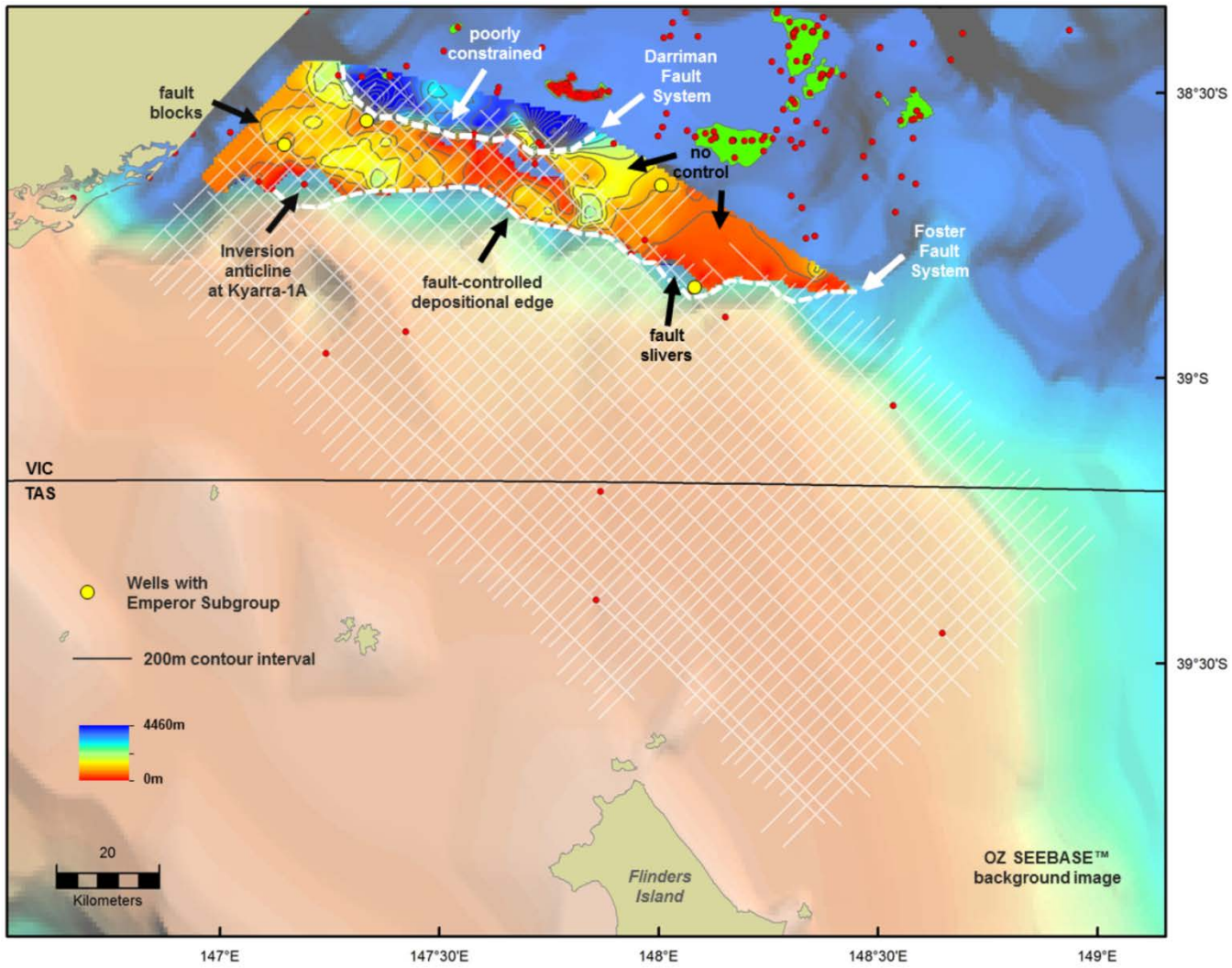

Figure 6.8 **Emperor Subgroup sediment isopach map for the study area.**

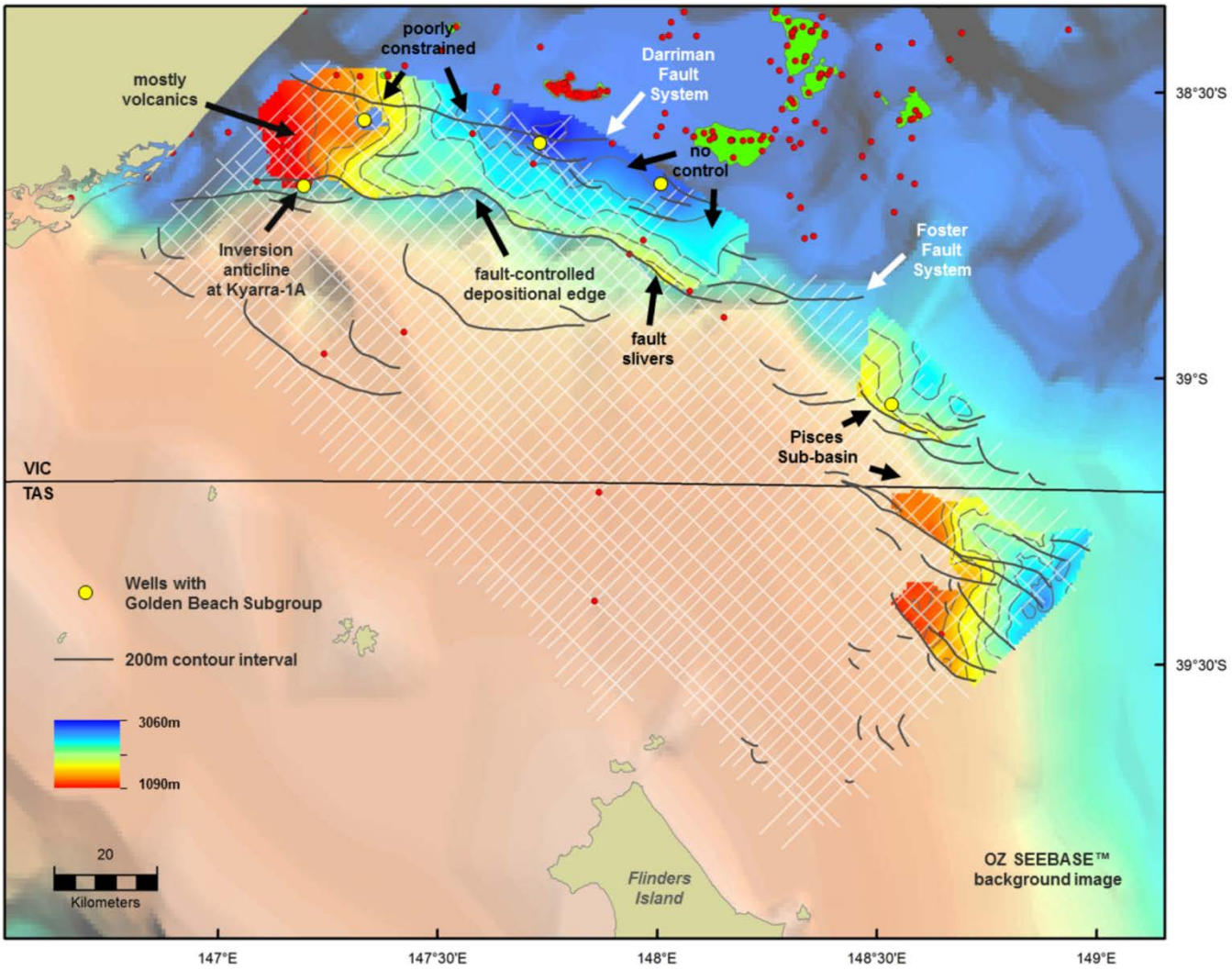

Figure 6.9 Top Golden Beach Subgroup depth structure map for the study area. Note that a clipped version of this grid is supplied with the ArcGIS project that accompanies this report. The clipped area excludes areas where data is poorly constrained.

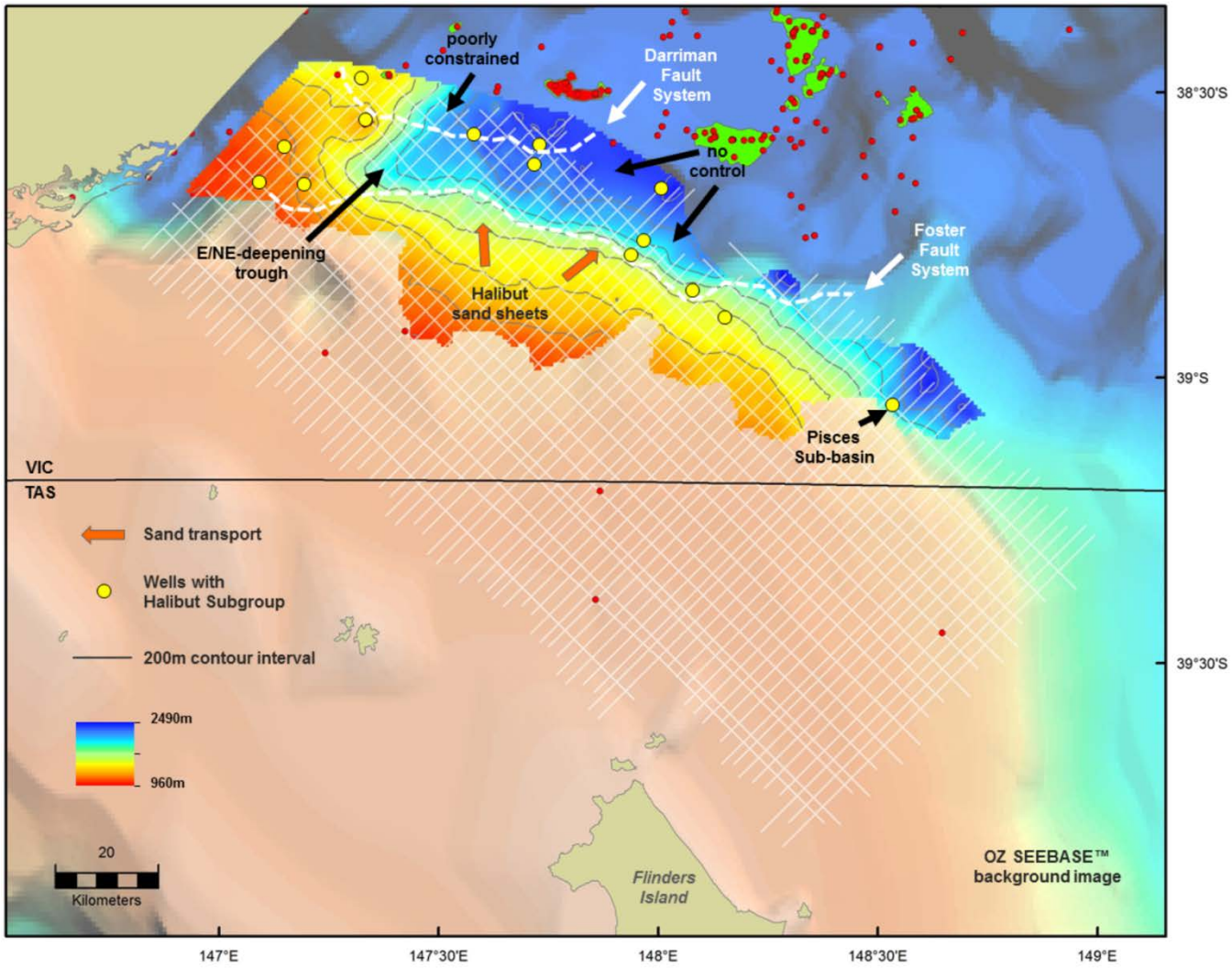

Figure 6.10 Top Halibut Subgroup depth structure map for the study area.

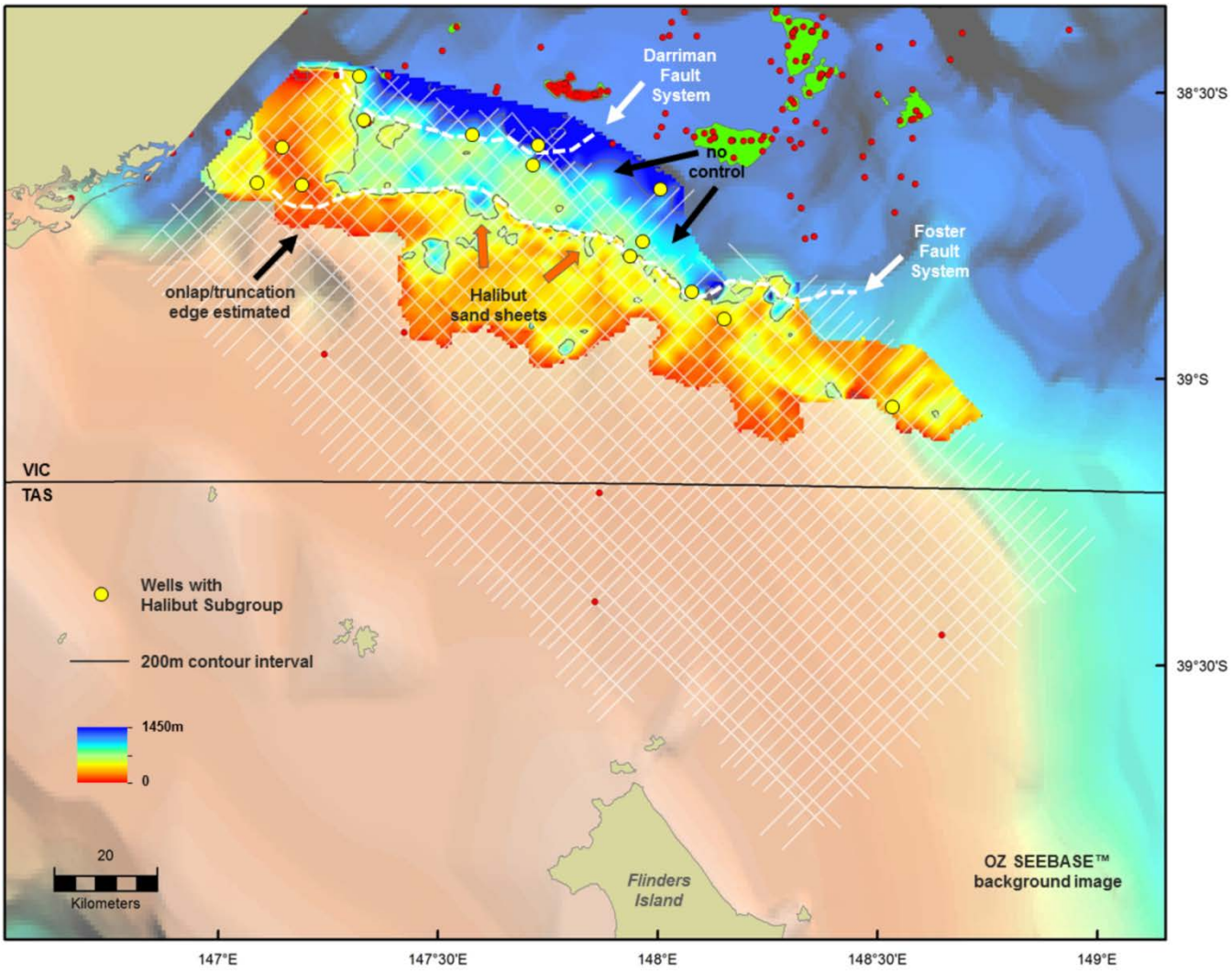

Figure 6.11 Halibut Subgroup sediment isopach map for the study area. Note that a combined Halibut and Golden Beach subgroups sediment isopach map is supplied with the ArcGIS project that accompanies this report.

6.2.7 Cobia Subgroup

The Top Latrobe Group (Cobia Subgroup) has sufficient well control, stratigraphic thickness and distinctive seismic character to allow this interval to be confidently mapped across the study area. All of the wells in the study area with the exception of Sailfish-1 intersect some thickness of Cobia Subgroup. The depth structure map shows that the Cobia Subgroup is the most widespread of the largely terrestrial Latrobe Group sediments (Figure 6.12). The Cobia Subgroup thins across the Southern Platform and in the western study area, and deepens northward beyond the Foster Fault System. Cobia sediments are absent over the intra-platform basement highs. The updip limit of the Cobia Subgroup is difficult to map as the succession thins to a single cycle (loop), thus exact onlap/truncation points are highly interpretative. The western limit of the Cobia Subgroup is similarly difficult to map because of its extremely thin nature. The presence of the Latrobe Group in the easternmost Pisces Sub-basin is highly speculative. The same east-to-west deepening structural trough that was noted in the previous Halibut Subgroup map is also clearly present in the Cobia Subgroup depth structure map. The trend is likely to reflect post-depositional movement on the Foster Fault System, although it also coincides with the area where Gurnard Formation sediments begin to thicken. The Cobia Subgroup lies at depths of between 960 and 2500 m.

The Cobia Subgroup thickness depth map shows a clear patchy distribution of sediments across the Southern Platform (Figure 6.13). The Cobia Subgroup is absent over intra-platform basement highs, and locally thins and thickens over the basement rugose topography. Here, the mapping of a single-cycle thickness is highly interpretative. Similarly, the thickness of the Cobia Subgroup in the Pisces Sub-basin is highly speculative due to lack of well control and direct seismic ties. In the western study area, the thickening of the Cobia Subgroup also coincides with the area where Gurnard Formation sediments also thicken. There is little well control and good seismic constraints on the mapping north of the Darriman Fault System. Some thinning across the Southern Terrace is controlled by progradation and shallow structures where the overall succession thins. The Cobia Subgroup is thickest near the Pike-1 and Devilfish-1 wells, and this is due to the re-interpretation of the "Devilfish Sand" as Cobia age (rather than the "Oligocene Sand Member" as suggested by Bernecker et al., 2006). The Cobia Subgroup reaches a maximum thickness of almost 600 m.

6.2.8 Early Oligocene Wedge (Seaspray Group)

The Early Oligocene Wedge (EOW) depth structure map shows the broad and uniform distribution of this progradational system across most of the study area (Figure 6.14). Where appropriate facies and thicknesses are present, the EOW has the potential to be the regional top seal over the Latrobe Group. The EOW thins and is absent in the most eastern part of the study area, and thins due to downlap across the Foster Fault System. The interpreted updip/truncation edge of the EOW is highly speculative due to thinning of the unit. The EOW has been formally picked in only four wells on the Southern Platform, but inferred from logs picks in other locations (Partridge, 2006). Similar to previous maps, a present-day E/NE deepening trough is evident on the structure map. The trend is likely to reflect post-depositional movement on the Foster Fault System. The EOW lies at present-day depths of between 275 and 2260 m.

The EOW sediment isopach map shows the strongly progradational nature of the succession in the eastern study area with a prominent thickening to the north (Figure 6.15). The Foster and Darriman fault systems appear to have had minimal control on the deposition of the EOW. The EOW thins across the central platform basement ridge (see Figure 6.2). The thinned downlapping margin of the EOW is clear across the eastern part of the Southern Platform, and extending west across the Southern Terrace. The prominent thickening observed in the southeast part of the study (near Flinders Island) may be coming from a younger wedge that has built out from the east. The EOW reaches a maximum thickness of approximately 1050 m.

6.2.9 Bassian Rise Unit 5 (Seaspray Group)

The Bassian Rise Unit 5 (BR5) coincides approximately with the Top of the Lakes Entrance Formation, and is picked in only four wells on the Southern Platform. Similar to the underlying EOW, the BR5 depth structure map shows the broad and uniform distribution of this progradational system across most of the study area (Figure 6.16). BR5 deepens to the north/northwest across the Foster and Darriman fault systems, although these systems do not appear to have controlled deposition. Along most of the outer Southern Platform and parts of the Southern Terrace, BR5 and younger units have been strongly deformed by their consumption within the slump complex. Here, BR5 cannot be mapped and its thickness/distribution is largely chaotic. For these reasons, no depth or time isopach maps were produced for the BR5 succession.

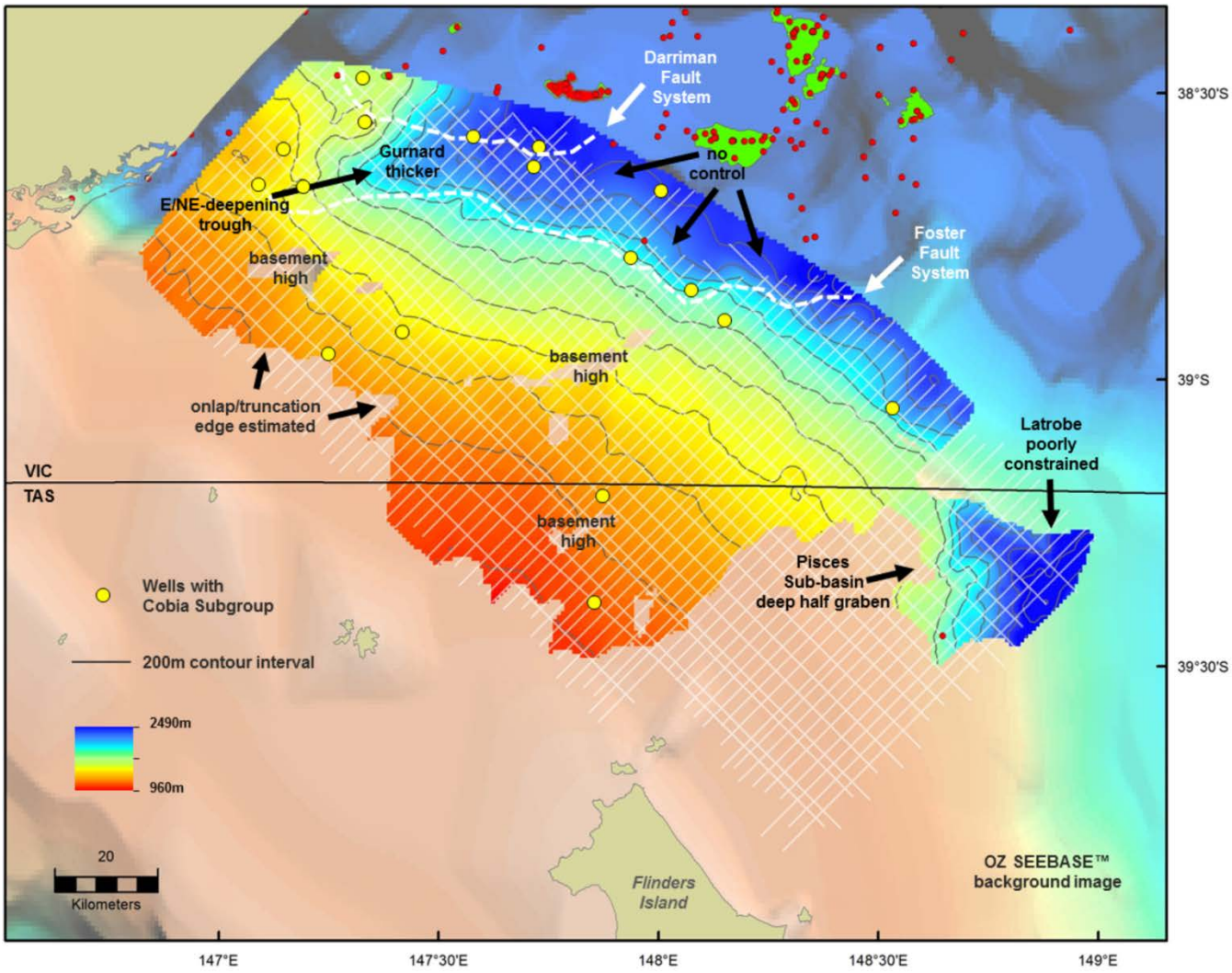

Figure 6.12 Top Latrobe Group (Cobia Subgroup) depth structure map for the study area.

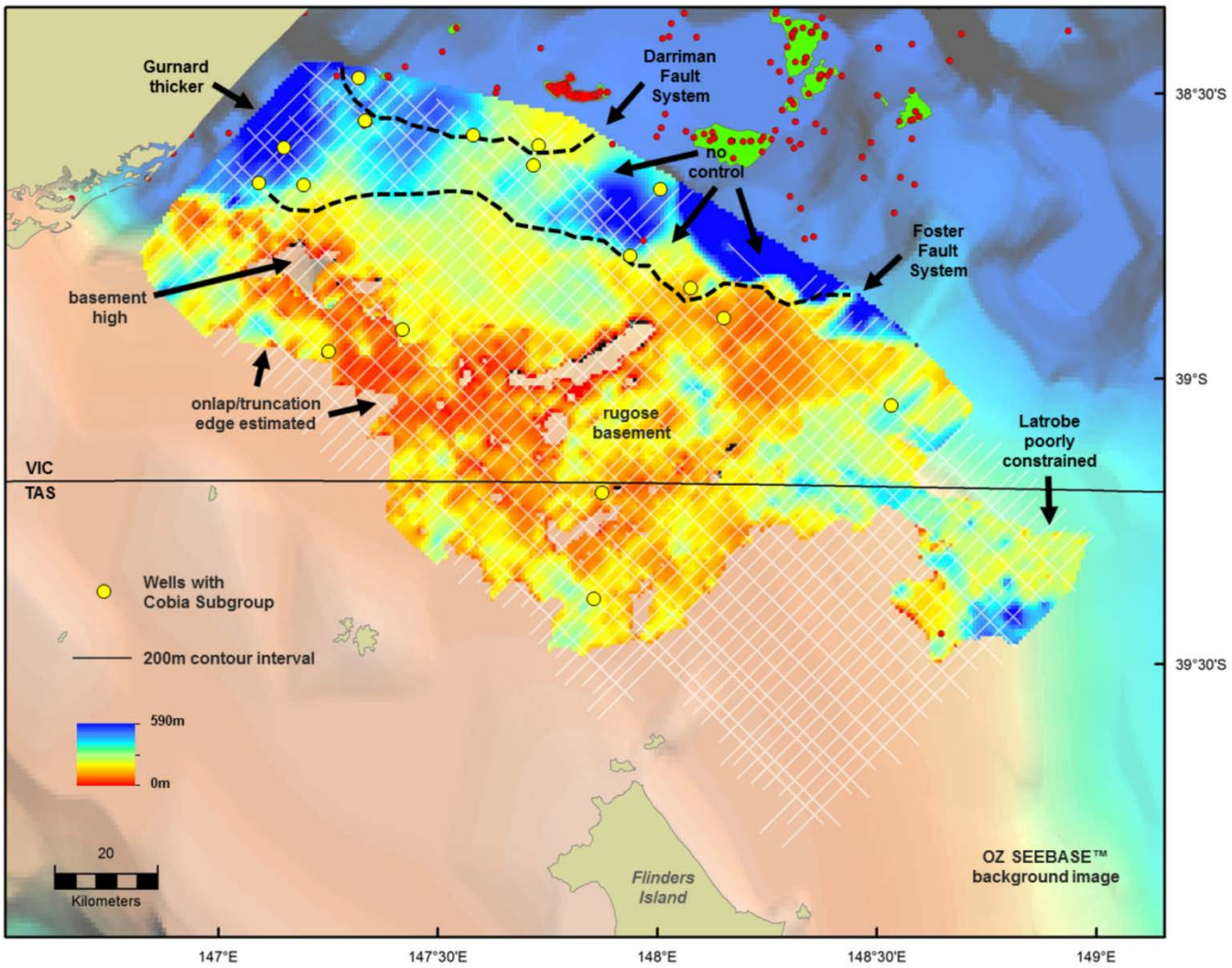

Figure 6.13 Cobia Subgroup sediment isopach map for the study area.

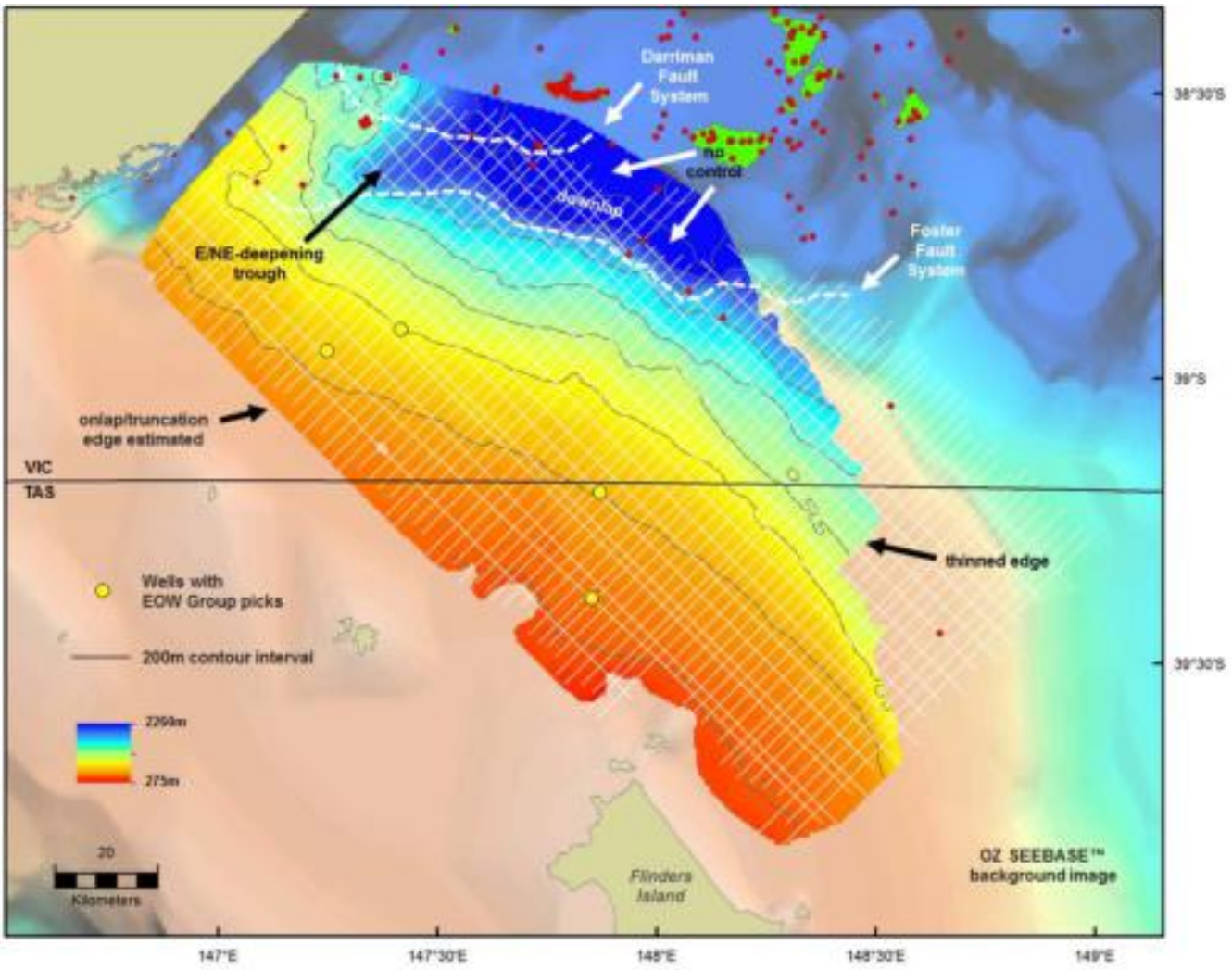

Figure 6.14 Top Early Oligocene Wedge (Seaspray Group) depth structure map for the study area.

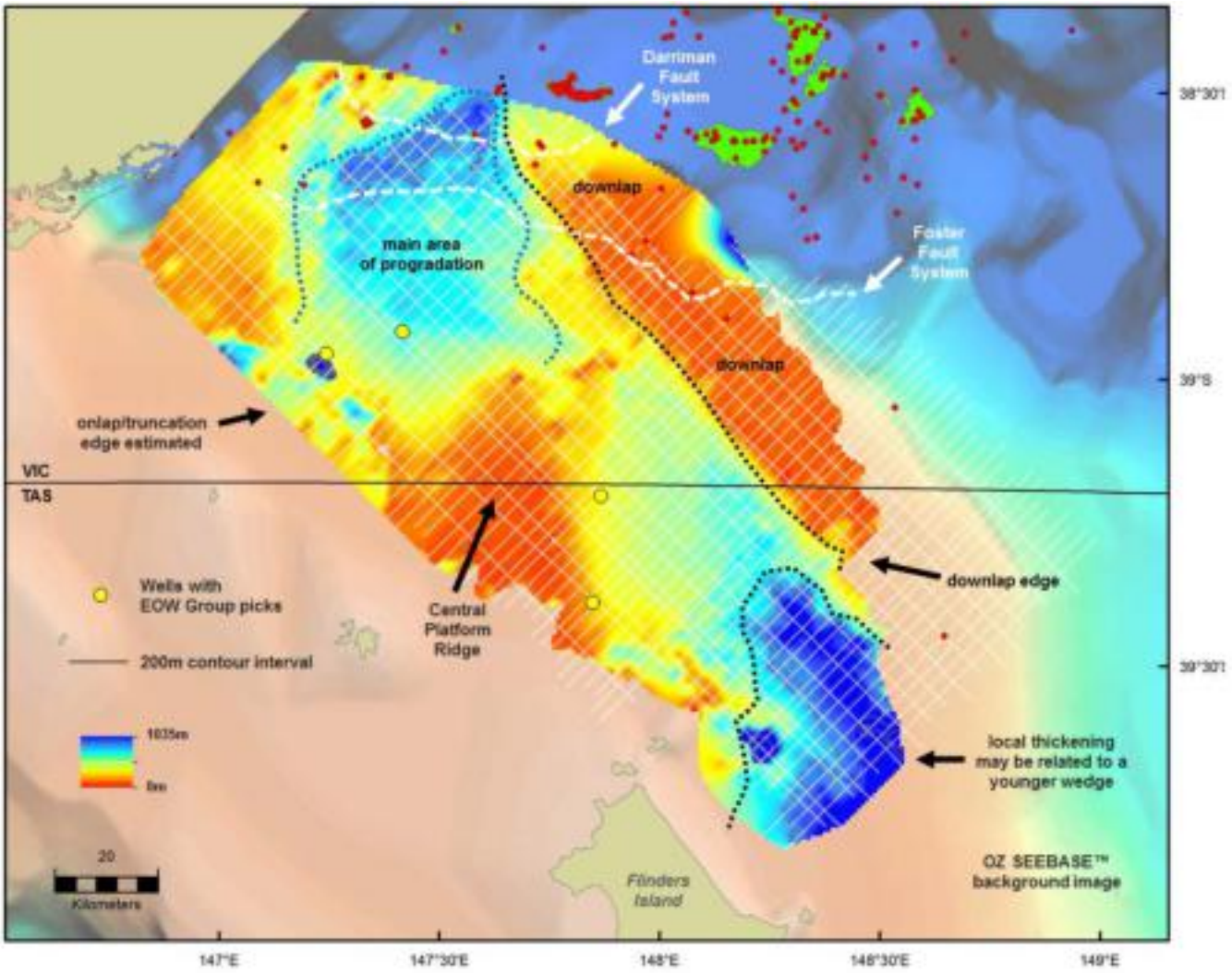

Figure 6.15 Early Oligocene Wedge (Seaspray Group) sediment isopach map for the study area.

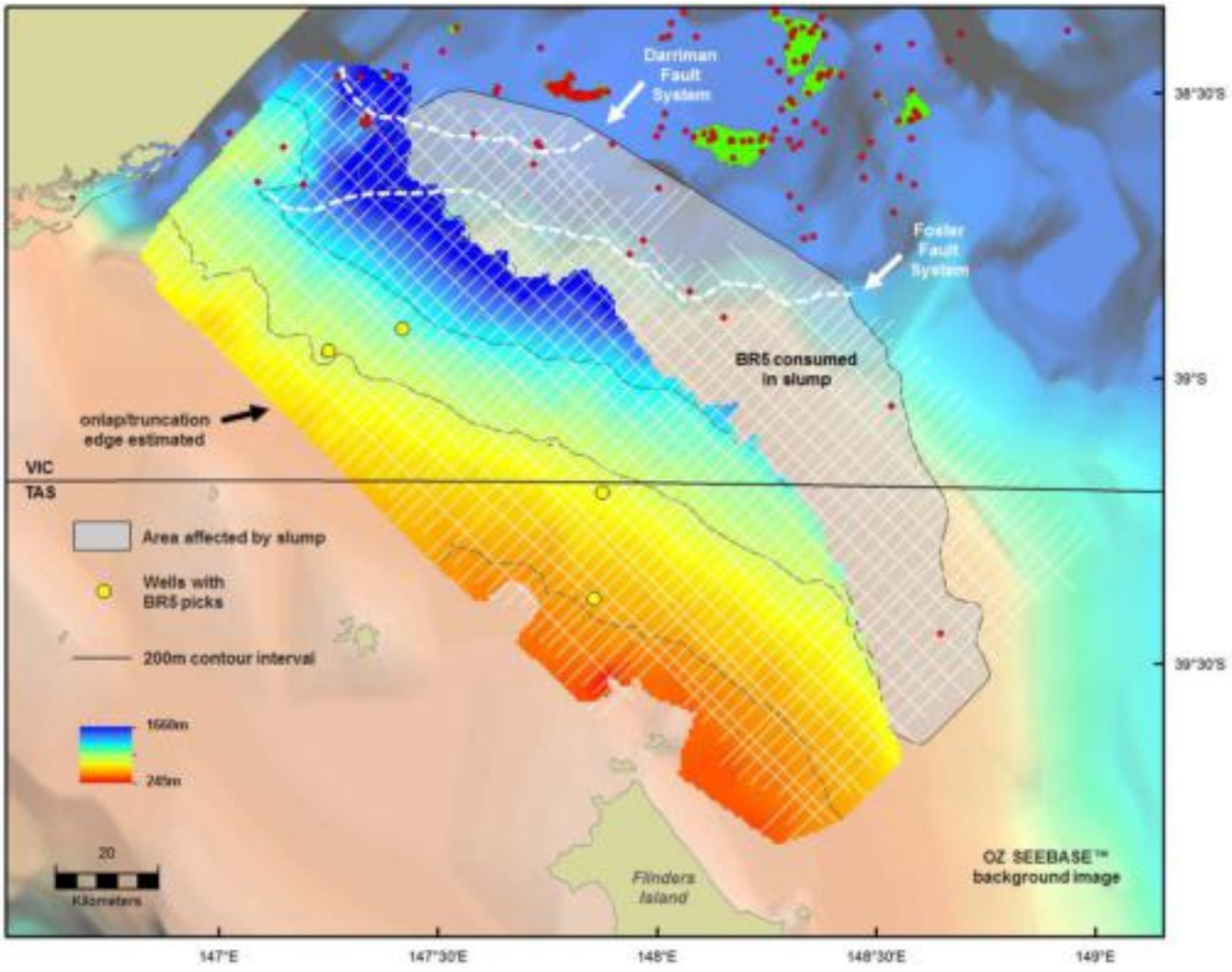

Figure 6.16 Top Bassian Rise Unit BR5 (Seaspray Group) depth structure map for the study area.

6.2.10 Bassian Rise Unit 3 (Seaspray Group)

The Top Bassian Rise Unit 3 (BR3) coincides with the Mid-Miocene marker. No DPI-preferred picks were supplied for the Mid-Miocene horizon, and its mapping was tied to the Bassian Rise picks of Partridge (2006) for the four wells on the Southern Platform. Structurally, BR3 maps across the top of the slump complex, although the horizon locally coincides with some areas of canyon incision. Similar to the underlying EOW and BR5 surfaces, the BR3 depth structure map shows the broad and uniform distribution of this progradational system across most of the study area (Figure 6.17). The Top BR3 surface deepens beyond the Foster and Darriman fault systems and also in the Pisces Sub-basin.

The isopach for this interval was constructed for a combined BR3-BR4-BR5 succession (equivalent to Top BR3 to Top EOW). As the BR4 and BR5 successions are affected by the slump complex, this deformed area has been clipped from the eastern part of the grid. The combined sediment isopach map shows a uniform thickness across most of the Southern Platform (Figure 6.18), and thickening across the Foster and Darriman fault systems. The BR3-BR4-BR5 succession ranges from 80 m to approximately 1100 m thick, and are likely to be more important as overburden units, rather than as potential reservoir and seal units.

6.2.11 Bassian Rise Units BR1 and BR2 (Seaspray Group)

The Top BR1 horizon coincides with the Top Seaspray Group and seafloor. The combined BR1 and BR2 sediment thickness depth map shows the broad and uniform distribution of this progradational system across most of the study area (Figure 6.19). The BR1-BR2 succession thickens mid-way across the Southern Platform, and thickens significantly beyond the Foster and Darriman fault systems and in the Pisces Sub-basin. The succession is locally thinned in the Pisces Sub-basin due to canyon incision. The succession ranges from 35 m to approximately 1250 m thick.

6.3 Seal Potential and Risk Maps

The GDPI10 2D Seismic Survey was acquired to improve geological knowledge of the Southern Platform and Southern Terrace. In particular, the interpreted dataset aimed to provide a regional framework to better understand the nature and distribution of reservoir and seal units which may have potential for greenhouse gas storage. The regional geological dataset will also provide a better assessment of potential risks. The Cobia and Halibut subgroups of the Latrobe Group are the main reservoir intervals (see Figures 6.10 to 6.13). The original tender for this study called only for mapping of the Top Latrobe (top reservoir) surface. However, it became apparent during the study that the 2D seismic dataset and well ties were sufficient to map the Cobia and Halibut subgroups as separate units. The distribution and thickness of these individual units has been discussed in the previous section.

The nature and distribution of sealing facies are more complex and therefore higher risk. Prior to the acquisition of the GDPI10 2D seismic grid, the assessment of seal potential on the Southern Platform and Southern Terrace was assessed as "very good" across most of the area, and "moderate-to-poor" on the shallow up-dip flanks of the Southern Platform (Figure 6.20**;** Goldie Divko et al., 2010). This assessment was largely based on a view that the Lakes Entrance Formation was the main sealing facies across most of the Gippsland Basin. It should be noted that only one analysis in a single well from that study area yielded analytical results indicative of good sealing capacity (Groper-1; Goldie Divko et al., 2010). Where tested, the Gurnard Formation did not yield good seal potential results in the current study area.

Overall, intraformational seals within the largely terrestrial Cobia and Halibut subgroups are thin and laterally variable in lithology and extent, particularly across the Southern Platform where overall accommodation is low. Sediment supply on the platform is also high and there are multiple local sources associated with the intra-platform basement ridge, clusters of hills and generally rugose basement topography. Thus, there is a higher likelihood of coarse-grained, non-sealing facies to locally dominate the sedimentary succession. It is beyond the scope of the current study to undertake detailed mapping of individual facies within a group/subgroup/formation, and this is what is required to fully understand the distribution and potential of intraformational seals within the Latrobe Group, in particular within the Halibut Subgroup as these are the prime sealing facies.

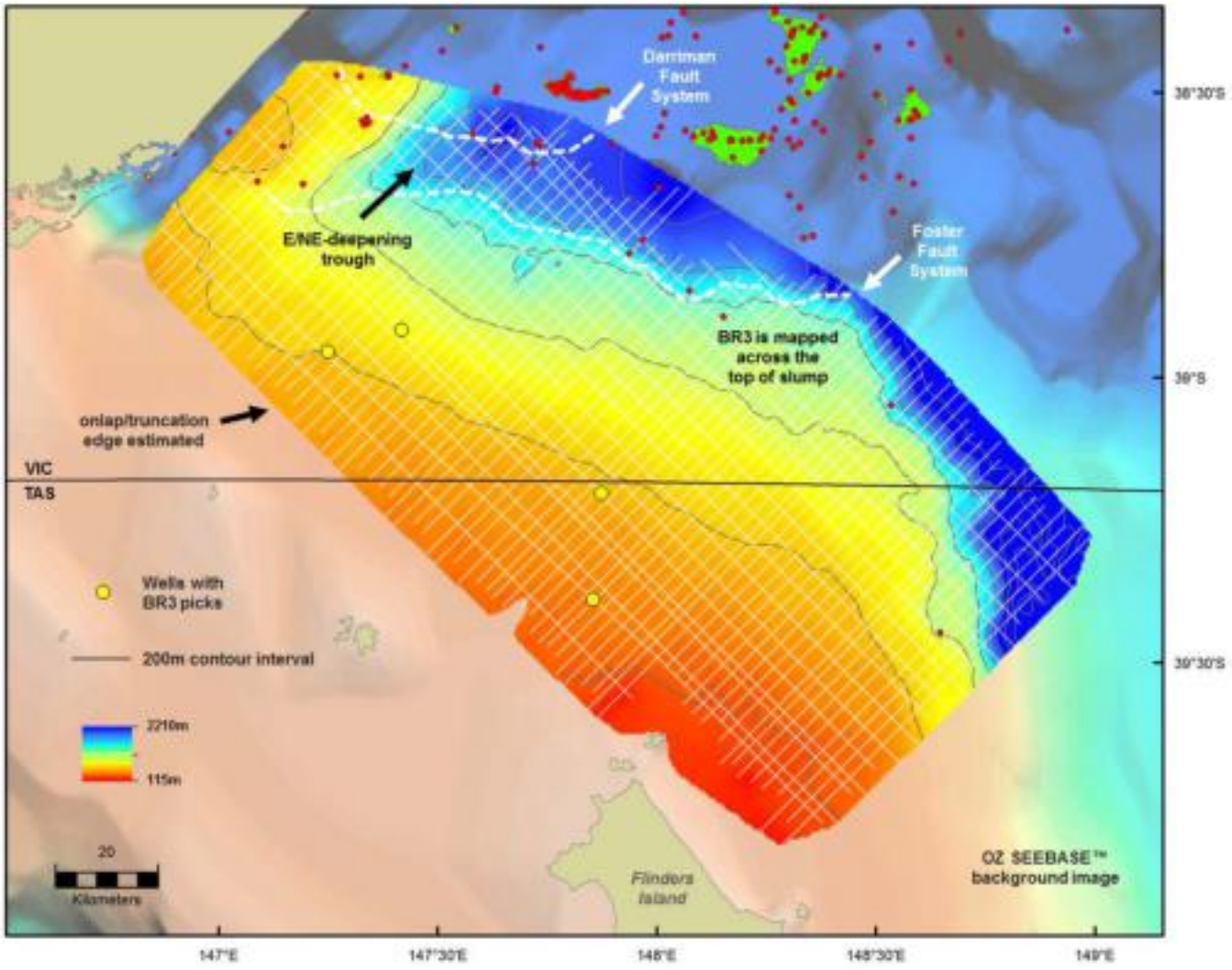

Figure 6.17 Top Bassian Rise Unit BR3 (Mid-Miocene Marker Equivalent; Seaspray Group) depth structure map for the study area.

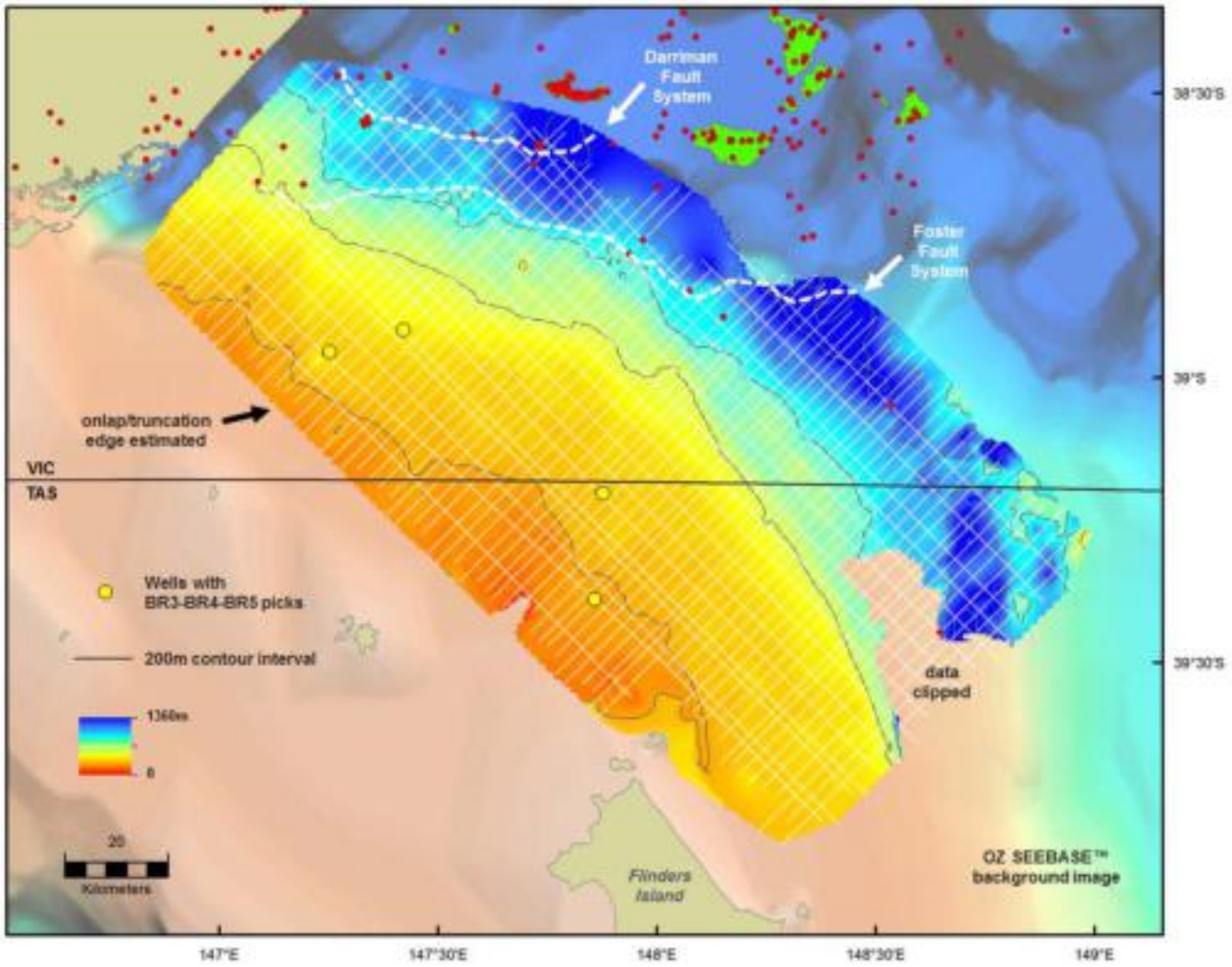

Figure 6.18 Combined BR3-BR4-BR5 (Seaspray Group) sediment isopach map for the study area.

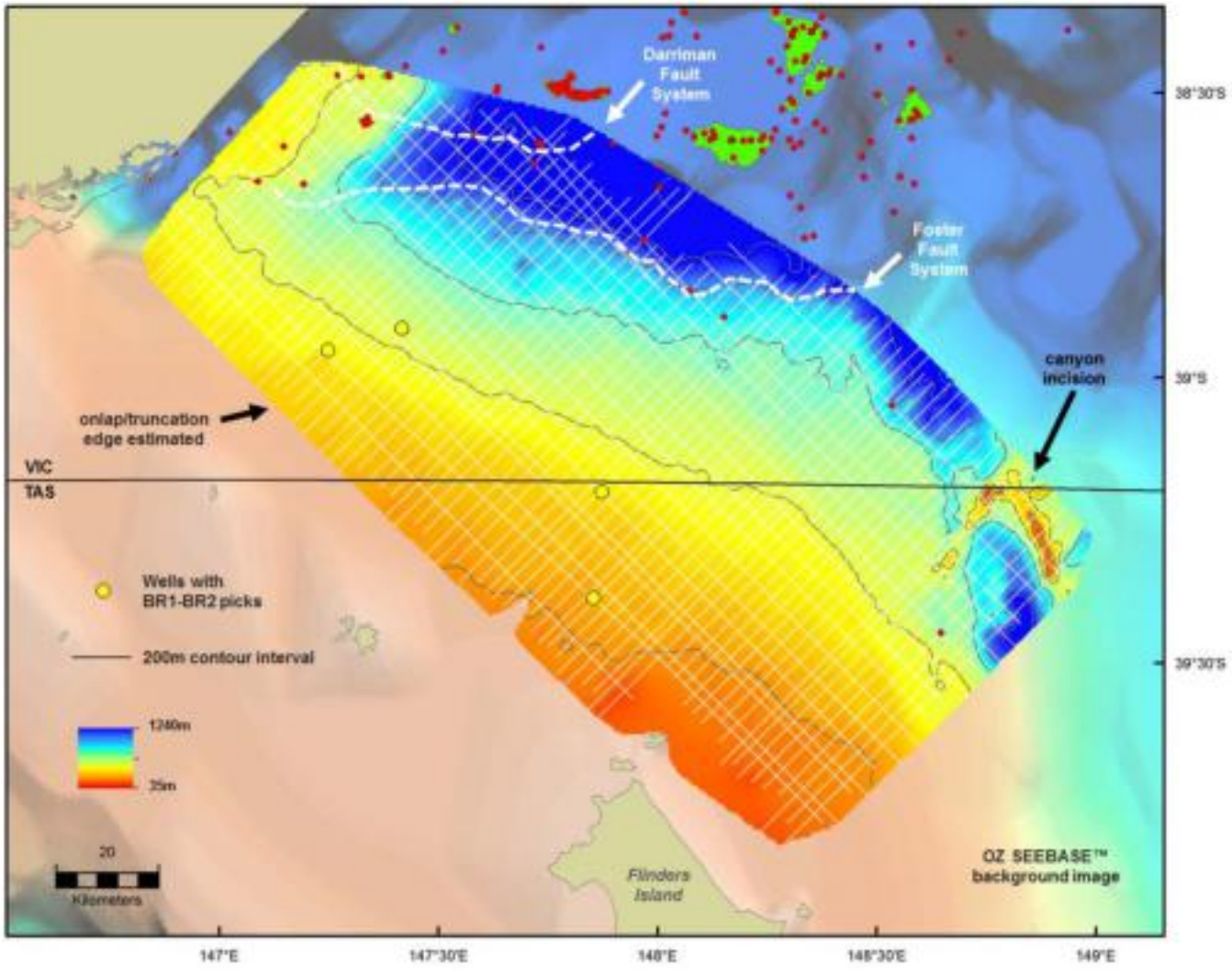

Figure 6.19 Combined BR1-BR2 (Seaspray Group) sediment isopach map for the study area.

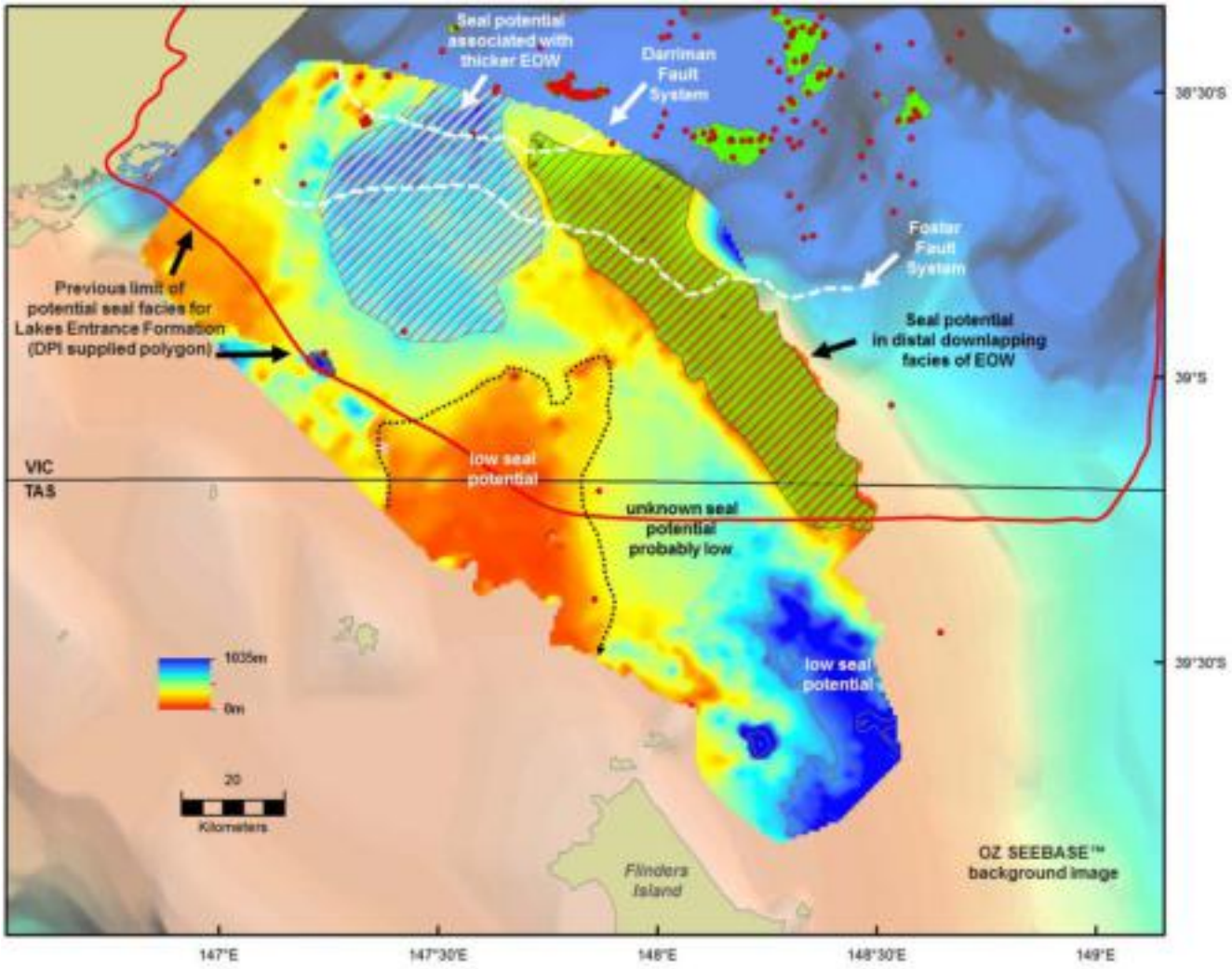

Figure 6.20 Maps showing the potential for sealing facies associated with the EOW. The "Limit Top Seal Lakes Entrance Formation" polygon supplied by GeoScience Victoria is shown by the red polygon.

The Kate Shale (Halibut Subgroup) is also a thick, intraformational sealing facies within the Central Deep, but it is largely absent in the study area except for a thin interval at Devilfish-1 and Moray-1 which is largely unmappable in a regional context. The Gurnard Formation (Cobia Subgroup) is cited by previous studies as both a potential reservoir and potential seal. Reservoir potential in the Gurnard Formation is highest where there is enough quartz sand and minimal clay introduced by bioturbation (3D-GEO, 2010). Otherwise, the glauconitic pellets within the Gurnard Formation are soft and deform with compaction to reduce porosity. Across most of the current study area, the Gurnard Formation is a thin glauconitic sandstone or siltstone with some claystone. In this context, the Gurnard Formation most likely acts as a potential reservoir, although further petrographic-based studies are required to confirm this assessment.

On the Southern Flank, the unit overlying the Latrobe reservoirs has been previously cited as the regional seal (the Lakes Entrance Formation) but has been shown by the current study to be a fundamentally different stratigraphic unit than observed in the Central Deep. Specifically, the sediments overlying the Latrobe Group are early Oligocene age, and therefore older than the "micaceous marl" facies of the traditional Lakes Entrance Formation which is distributed across the northern and western margins of the Gippsland Basin (Partridge, 2006). Instead, the Early Oligocene Wedge (EOW) directly overlies the Latrobe Group – not the Lakes Entrance Formation. The significance of the EOW has been discussed previously in Section 5. Wells ties and mapping of the EOW show that this unit is widespread across the study area. The marly facies of the traditional Lakes Entrance Formation occur above the EOW within Bassian Rise Unit 5. While these BR5 facies may have "better" sealing potential (although unproven in the area), the age-equivalent BR5 succession does not directly overlie the Top Latrobe Group reservoirs.

In summary, the regional risk assessment for the current study has focused on the reservoirs of the Cobia and Halibut subgroups, and sealing facies of the EOW. The Gurnard Formation is considered to be a more complex facies that requires further work beyond this study to determine its true age, lithology and sequence stratigraphic framework. Similarly, the mapping of individual intraformational seals within the Cobia and Halibut subgroups is beyond the scope of the current study, but is recommended for future work.

The EOW is present across most of the study area, although its thickness is variable (Figures 6.14 and 6.15). The EOW has the potential to be a sealing facies over the Cobia Subgroup only. Nowhere in the study areas does the EOW directly overlie the Halibut Subgroup. The base of the EOW is a transgressive surface that represents flooding of the Southern Platform prior to the highstand progradational phase when the bulk of sediments were likely to have been deposited. While the overall geometry of the total EOW succession (package) is clearly a wedge, the internal stratal geometries within the EOW are mostly featureless. Most of the strata appear to be topsets or very low angle progrades.

It is interpreted that there are two potential scenarios where the EOW could have good sealing potential (Figure 6.21): 1) where the wedge is thickest; and, 2) where the wedge downlaps and the distal toes could represent fine-grained condensed sedimentation. The EOW is interpreted to be a poor sealing facies where it thins over the central platform ridge. Areas proximal to the ridge are also downgraded for seal potential due to likely input of sandy sediments (Figure 6.21). Finally, the area to the east of Bluebone-1 and Mullet-1 could have seal potential but this is unclear with the current dataset. In a regional context, this area sits between the central platform ridge and a very thick wedge which has prograded onto the eastern part of the Southern Platform. The EOW is locally thick in the western basin and could have seal potential here.

Identified risks associated with the EOW sealing potential include: 1) proximity to the central platform ridge; 2) post-depositional reactivation along the Foster Fault System; 3) the slump complex which may locally consume the upper part of the EOW; 4) local faulting of the EOW that occurs updip of the slump feature; and 5) inversion/uplift in the western basin. These risk polygons are shown in Figure 6.21.

The nature and degree of small-scale faulting within the EOW is shown in Figure 6.22, and can be locally significant. Figure 6.23 shows the offset associated with the Foster Fault System at the EOW level – which can also be significant. The slump complex which formed over the EOW is also shown in Figure 6.23. Several examples of inversion in the western basin are shown in Section 5.

It is clear from the regional analysis that there are several key risks associated with the potential for the EOW to be a sealing facies for the Top Latrobe Group reservoirs. The clearest risks are the intra-platform ridge which can locally contribute sand in the Latrobe Group sediments, particularly in updip locations on the southern part of the platform. The degree of small-scale offset within the EOW is variable but widespread in occurrence. More work is required to

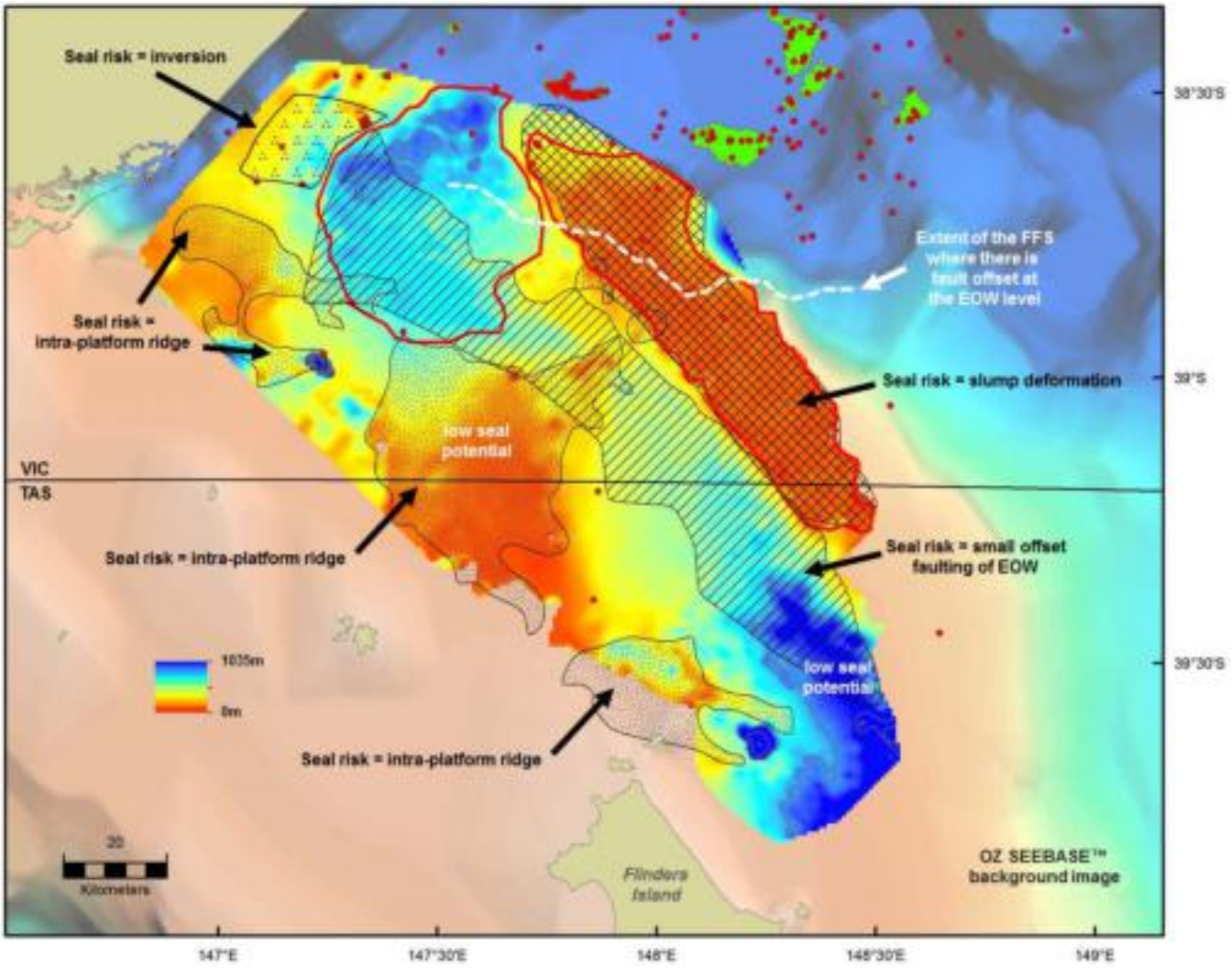

Figure 6.21 Map showing the risk polygons for the EOW sealing potential including: 1) proximity to the central platform ridge; 2) post-depositional reactivation along the Foster Fault System; 3) the slump complex which may locally consume the upper part of the EOW; 4) local faulting of the EOW that occurs updip of the slump feature; and, 5) inversion/uplift in the western basin. Note that only that part of the Foster Fault System (FFS) where there is offset at the EOW is shown in the figure. The red polygons indicate the potential seal facies distribution as shown in the previous figure.

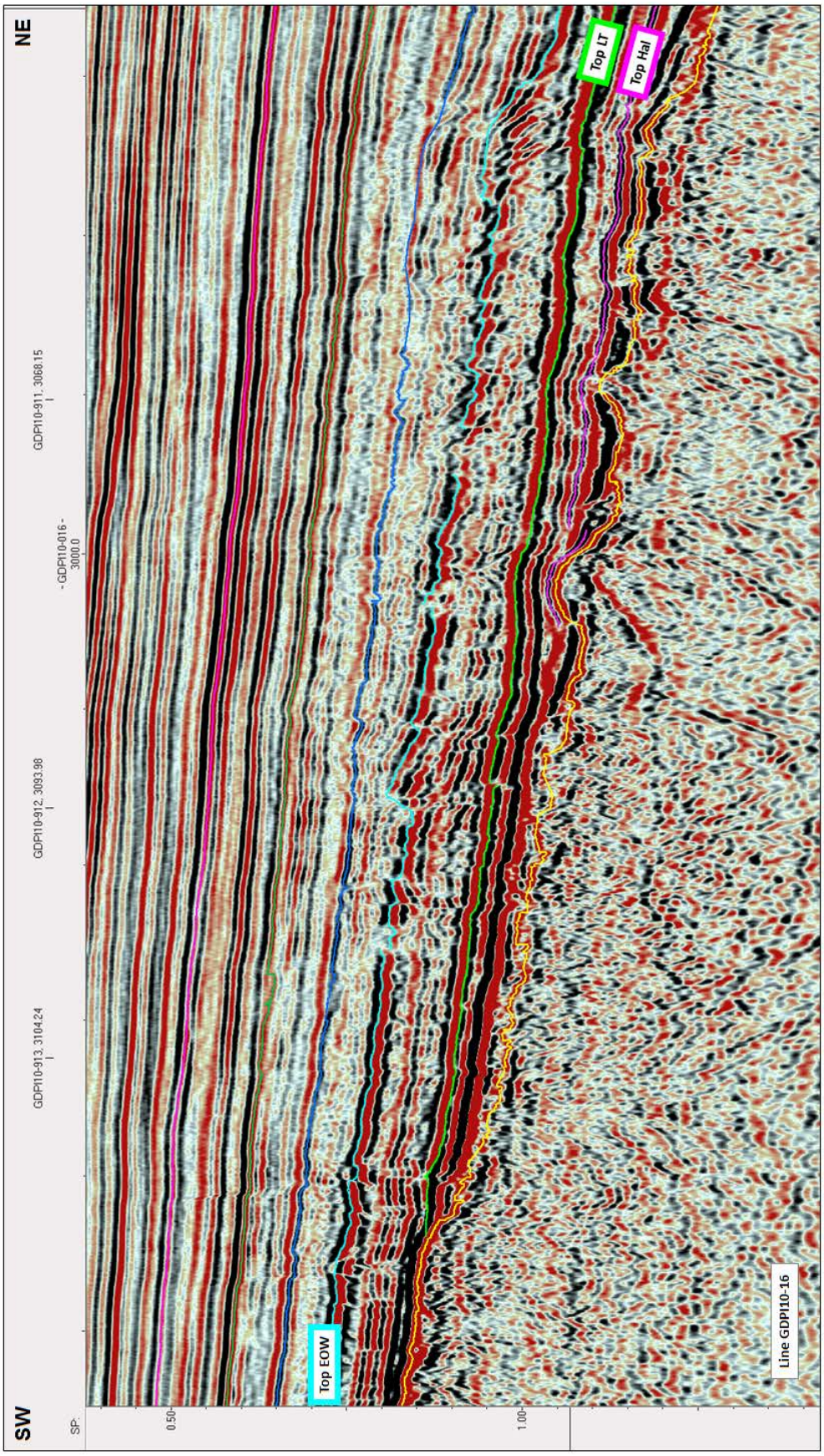

Figure 6.22 Seismic line GDPI10-16 showing the nature of small-scale fault offset affecting the EOW.

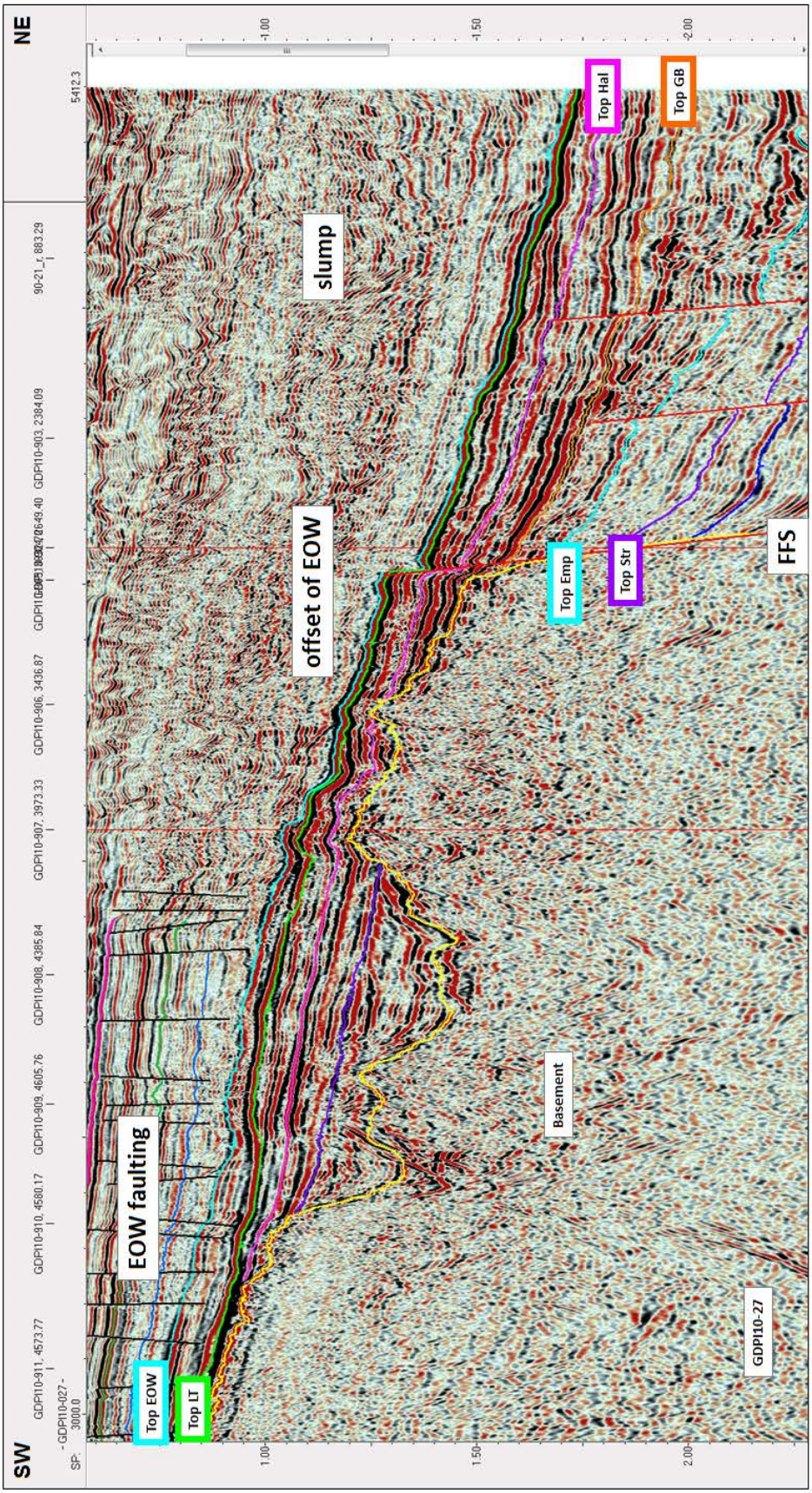

Figure 6.23 Seismic line GDPI10-27 showing the nature of offset along the Foster Fault System (FFS) that displaces the EOW potential sealing facies. Also note the EOW small-scale faulting that occurs updip.

further understand the relative degree of risk associated with this faulting. The risk from the slump deformation was not quantified during the current study, and further work is needed to assess the finer-scale effects of the slump on the sealing potential of the EOW. Offset of the EOW along the Foster Fault System (FFS: Figure 6.21) is much more apparent and straightforward to quantify. The FFS offsets the EOW along most of the length of the fault system east of Bullseye-1. West of Bullseye-1, reactivation of the FFS does not propagate into the EOW, and this is indicative of the relative timing of fault movement. Although the GDPI10 grid does not cover the full length of the Darriman Fault System, there is little apparent offset of the EOW along the fault that was mapped during the current study. Inversion does not appear to have significantly faulted the EOW in the western basin. In addition, the potential for Gurnard Formation seals is also higher in the region west of Bullseye-1. However, movement on some structures in the west has continued until as recently as Pliocene, thus the risk of neotectonic influences on possible injection scenarios should be further assessed.

Areas of predicted high seal potential and the associated EOW risk polygons are shown overlain on the Cobia Subgroup (reservoir) sediment thickness map in Figure 6.24. Collectively, the EOW risk polygons indicate the best area with the highest predicted sealing potential and the lowest associated risk (Figure 6.25). This first-pass assessment of seal risk has used the geological framework that was interpreted during the current study. Clearly, further work is required to understand the details of specific risks to more accurately predict and model injection sites.

6.4 Slump Deformation and the Outer Shelf Mound

Along the outer edge of the Southern Platform a large slump feature has been mapped as input into the velocity model generated as part of this study (see Section 7). The interval of disrupted stratigraphy was originally isolated as a unit suspected to have a different interval velocity relative to the surrounding undisturbed stratigraphy. Overall, the slump unit was shown to have a lower interval velocity than the adjacent stratigraphy with details illustrated in Section 7. The slump unit is defined at the base by a "slump container" horizon. The upper limit of the slump unit is generally marked by the "FrOG Tech 03 Top Bassian Rise Unit 3" (BR3) horizon, although there are areas where the faulting and slumping terminates lower in the stratigraphy. Both horizons are supplied in the Kingdom seismic project, with a reminder that the "slump container" horizon is at a level of interpretation and detail suitable for creation of the velocity model. Further work is required to fully define the nature of the slump zone.

The slumped unit forms a prominent feature along the outer edge of the Southern Platform. The slump zone is at least 160 km wide, interpreted to continue beyond the eastern and northern limits of the GDPI10 2D seismic survey. The slump zone has two segments; with the eastern side oriented generally NNW-SSE approximately centred over the western tips of the Pisces Sub-basin boundary faults. Further west, the slump appears to have a more NW-SE orientation, sub-parallel to, and overlapping the Foster Fault System. The two overlapping segments vary in width, internal structuring and relationship to adjacent stratigraphy. These variations are described briefly here but require further mapping to fully understand the implications and development of the slump across the platform edge.

The eastern segment (Figure 6.26) is relatively narrow, 20-25 km wide, and the disrupted interval relatively thin, generally less than 300 ms, with local thickening to 400 ms or more adjacent the slump boundary faults. A narrow zone of listric faulting, with rotation of coherent fault blocks containing traceable stratigraphy is common at the headwall location of the slump (Figure 6.27). The inboard edge of the fault system truncates the progradational "FrOG Tech 04 Top Bassian Rise Unit 4" (BR4) and "FrOG Tech 05 Top Bassian Rise Unit 5" (BR5) horizons, with the downlapping toes of the "FrOG Tech 06 Top EOW" horizon forming the lowermost decollement for the listric faulting. Internal detachments may also be present at shallower levels in the faulted succession. The listric faulting is observed to displace reflections up to BR3, with limited rotation observed at this level. BR3 is interpreted to be consistently present over the slumped zone and is not truncated. The central portion of the slump is dissected by numerous faults both synthetic and antithetic to the listric boundary faults. In general, the internal faults are contained by the lower "slump container" horizon but can, at times, be observed to continue in to the mid-Miocene stratigraphy above the BR3 horizon. The internal faults progress from predominantly synthetic to predominantly antithetic in < 15 km from the boundary fault. However, landward dipping thrust faults associated with asymmetric fault-related folds common in the contractional domain of large slumps (e.g. Orange Basin; de Vera et al., 2010) are absent. The disrupted zone thins to around < 100 ms to the NE, with canyon incision and fill dominating the internal morphology.

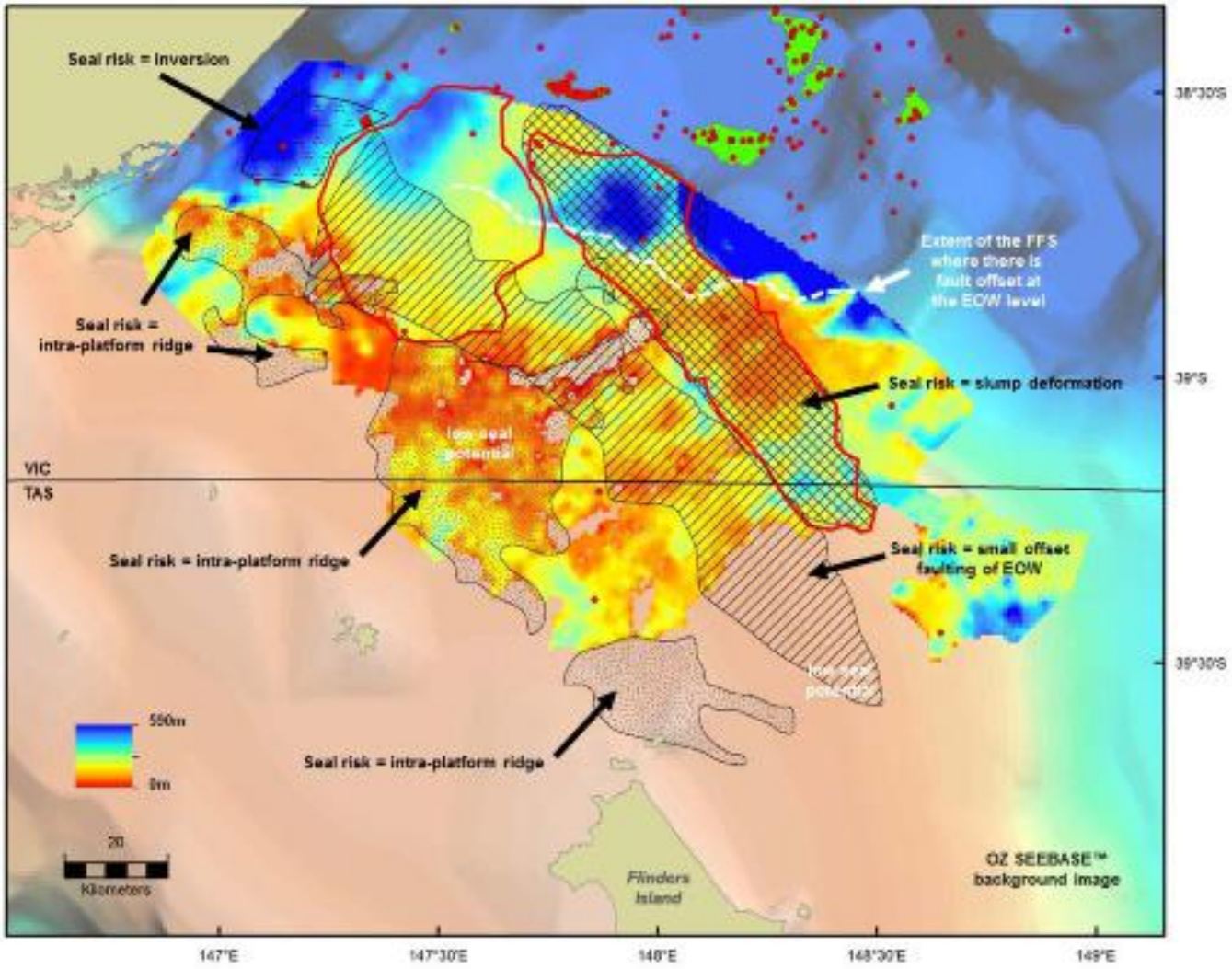

Figure 6.24 Risk polygons for the Early Oligocene Wedge overlain on the isopach of the Cobia Subgroup. See Figure 6.21 for further details of associated risk segments. The red polygons indicate areas where the EOW seal potential is predicted to be high.

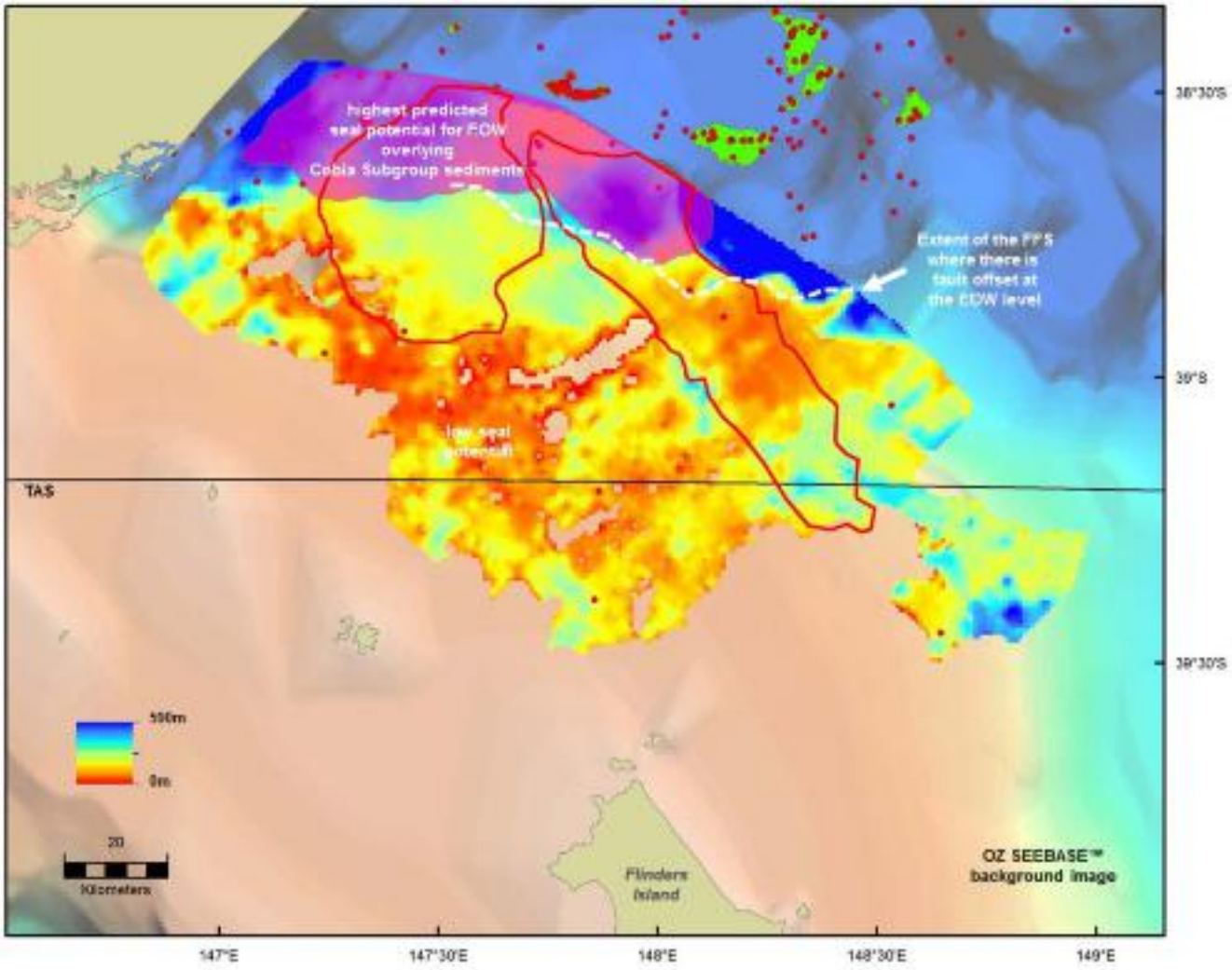

Figure 6.25 Summary map of the predicted high EOW seal potential overlying Cobia Subgroup sediments based on a first-pass analysis of regional geology and associated risk factors. The base map is the Cobia Subgroup isopach.

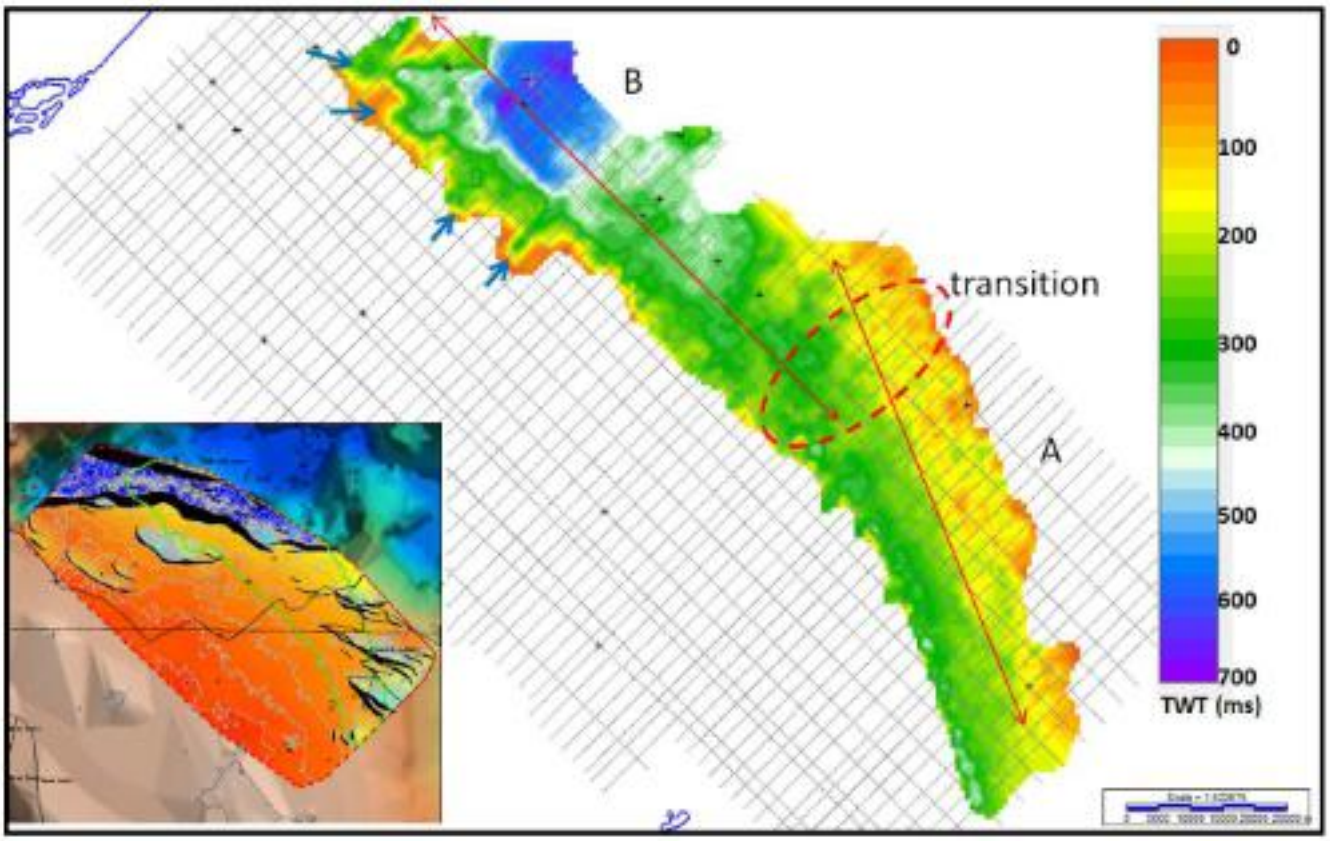

Figure 6.26 Approximate thickness of the slump feature showing A, the eastern segment, B the western segment, with the overlapping area of transition between the two segments. Note the difference in orientation between the two segments, the linearity of segment A to the east and the shelf re-entrants in segment B to the west– see inset for relationship between faults and slump.

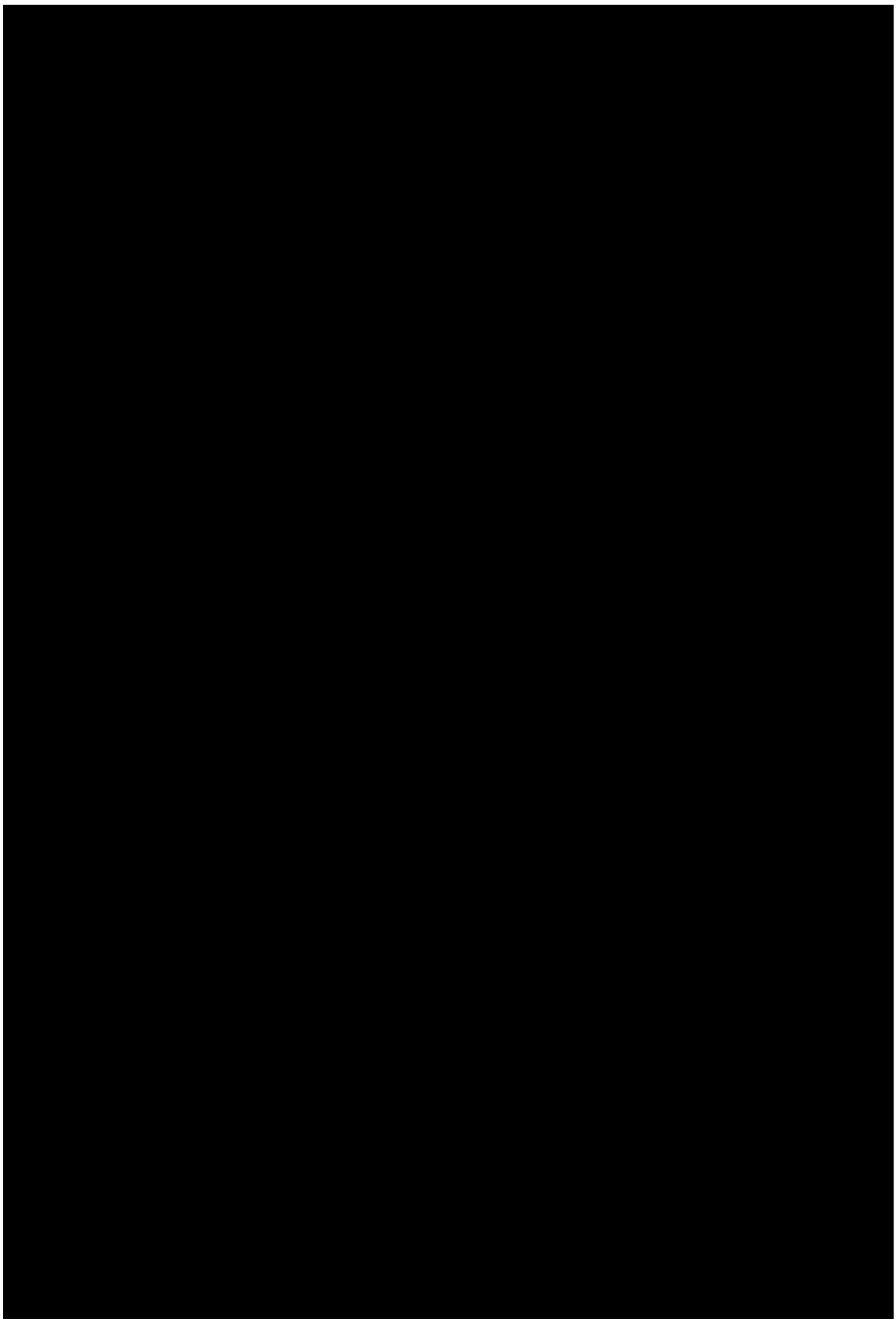

Figure 6.27 Interpreted and uninterpreted seismic line GDPI10-55 showing the eastern segment of the slump and relationship to the Oligocene-Miocene shelf stratigraphy in the SW and the underlying sedimentary mound. Surfaces M1, M2, M3 have been mapped at a broad scale to identify the external geometry of the mound.

A large, convex upward sedimentary package or mound exists below the disrupted zone in the eastern segment, and to a lesser extent in the western segment of the slump within the bounds of the GDPI10 2D seismic survey. Four horizons, M1, M2, M3, and M4 have been mapped within the mound to provide insight into the gross morphology and thickness variations. The horizons were interpreted on a subset of the GDPI10 2D seismic survey and further work is required to fully understand the mound geometry and evolution. The age of the mound is poorly constrained as the relationship to the prograding late Oligocene-Miocene shelf cannot be determined from the seismic grid other than in the broadest terms (i.e. equivalent to the BR3-BR5 interval). Three wells intersect the mound: Pisces-1 (M2 horizon and above), Pike-1 and Moray-1 (both intersecting the M1-M2 intervals). Pisces-1 is interpreted to contain foraminiferal zonules D1-E2 (Taylor, 1966; 12-16 Ma) in the mound. This time period is equivalent to the BR2-BR3 units (Partridge et al., 2012), which is inconsistent with the seismic interpretation. Further north, only the lower portion of the mound is preserved and intersected in Pike-1 and Moray-1. The interval is interpreted to contain foraminiferal zonule G (BR3-BR4) in Pike-1 and H1-H2 (BR4-BR5) in Moray-1.

Internally, the mound is characterised by sub-parallel, moderate to low amplitude, continuous reflections. Downlap in opposite directions is present in the lower parts of the mound, while the middle and upper sections are truncated by the slump (Figure 6.28). The mound can be mapped as a NW-NNW oriented lenticular body that appears to migrate to the east, with a northward shift of the depocentre during the M2 interval. Whether the depocentre persists to the north during the M3 interval is unknown as it is beyond the limits of the GDPI10 2D seismic survey. Above the M3 interval the seismic data are characterised by a thick succession of low amplitude semi-continuous reflections truncated and incised by the slump. Faults propagated upward from the basin boundary faults of the Pisces Sub-basin intersect the slump stratigraphy, and provide evidence of continued movement along these structures (Figure 6.29). The instability caused by this movement may have been sufficient to trigger slumping along an oversteepened progradational front to the south. The external and internal geometries of the elongate mound are consistent with a contourite developed by variations in bottom currents. Further subdivision of the mound is possible and more detailed mapping could identify sedimentary phases separated by periods of non-deposition/erosion allowing for a greater understanding of the significance of this feature (Stow et al., 1998; Koenitz et al., 2008).

The western segment is greater than 30 km wide, extending beyond the limits of the seismic data and the disrupted interval reaches up to 700 ms across a broad region (Figure 6.26). Slump boundary faults are at a lower angle and less distinct than in the eastern segment (compare Figures 6.27 and 6.30). However, the shelf stratigraphy truncated by the inboard edge of the fault system are the same late Oligocene-Miocene progradational units. The headwall escarpment is irregularly shaped, with re-entrants onto the platform, potentially located at less stable areas along the platform margin. The slump overlies the Foster Fault System, with the headwall located 12-15 km south of the major structural boundary. The internal morphology of the slump in the western segment is highly chaotic; internally coherent rotated fault blocks are generally absent and the central portion of the slump is characterised by closely spaced faults and discontinuous reflections. The slump toe is north of the limits of the GDPI10 2D seismic survey.

The two segments overlap in a transition zone 10-15 km wide (Figure 6.26), where the orientation of the slump zone changes and complex internal geometries are present. The seismic lines across this interval show a broad zone of listric headwall faulting terminating at the toe of the EOW and within the mounded succession. The faulted succession to the SW is overlain by the topsets of the BR3 ?progrades, which are disrupted by the listric faulting further NE, suggesting that within the transition zone, slumping progressed from south to north, or from the western segment to the eastern segment (Figure 6.31). The disrupted zone thins basinward over the mounded succession, consistent with the eastern segment of the slump.

Inboard of the slumped zone is a zone of high density (1.5-6 km spacing) of sub-vertical extensional faults with small throw (10 ms or less). This zone extends along the length of the slump area and is approximately 20 km wide (Figure 6.32). The faults typically extend up to the mid-Miocene level, and the bottoms of the faults terminate near the top of the Latrobe Group or Top Basement where the top of the Latrobe Group is thin or absent. The location, of these faults updip of a major slump zone suggests they may be the result of extensional release along the platform during slumping. The faulting will affect the integrity of Oligocene and younger sediments that overlie the Latrobe Group.

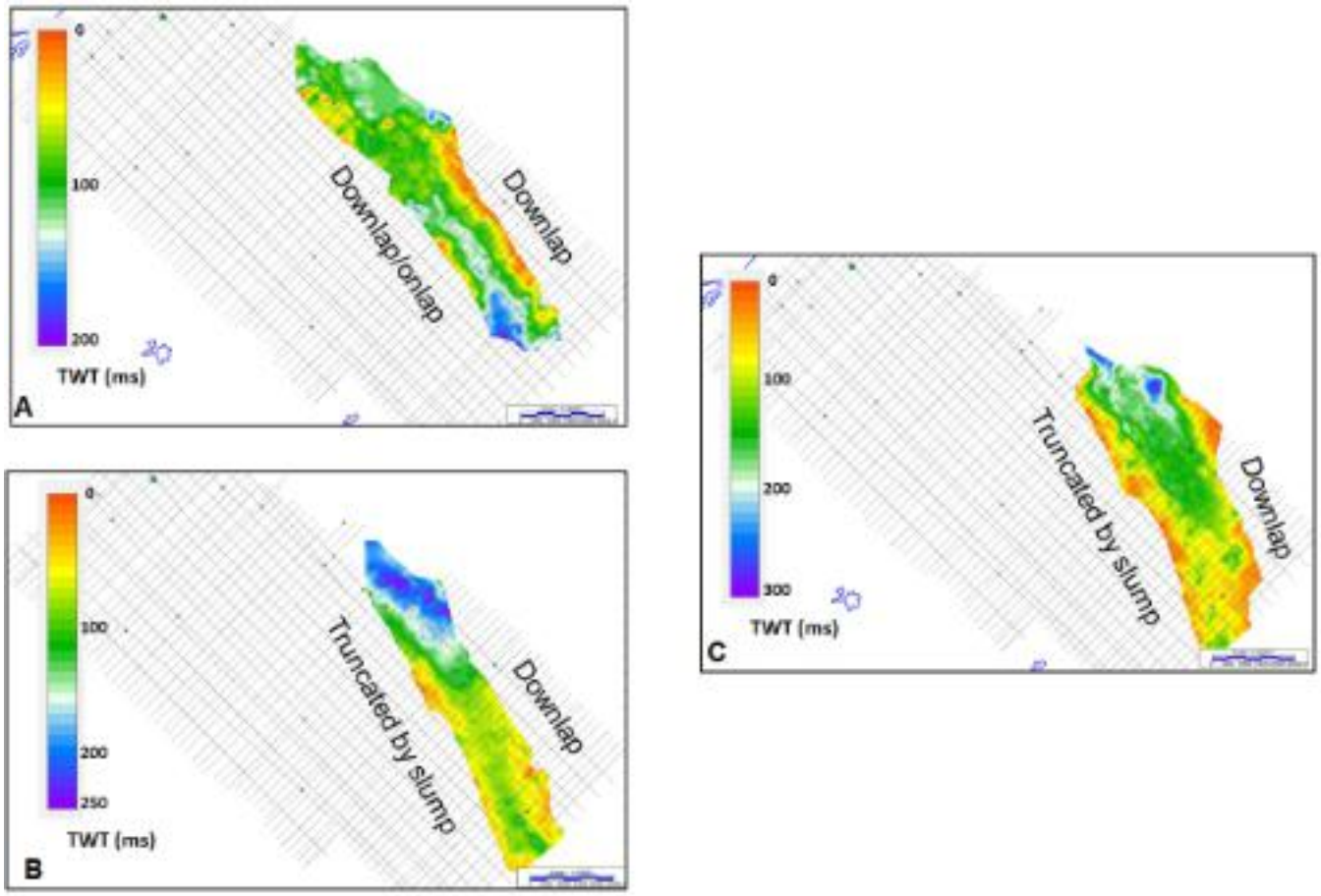

Figure 6.28 TWT thickness variations within the sedimentary mound beneath the slump. A) M1 to Top Latrobe Group, B) M2 to M1, C) M3 to M2. The three mapped intervals show a NW-NNW oriented lenticular body potentially migrating eastward overall and showing northward movement of the depocentre in the M2 interval. Truncation by the slump, particularly at the M3 level skews the location of the thickest part of the mound to the east. All intervals thin by downlap to the east.

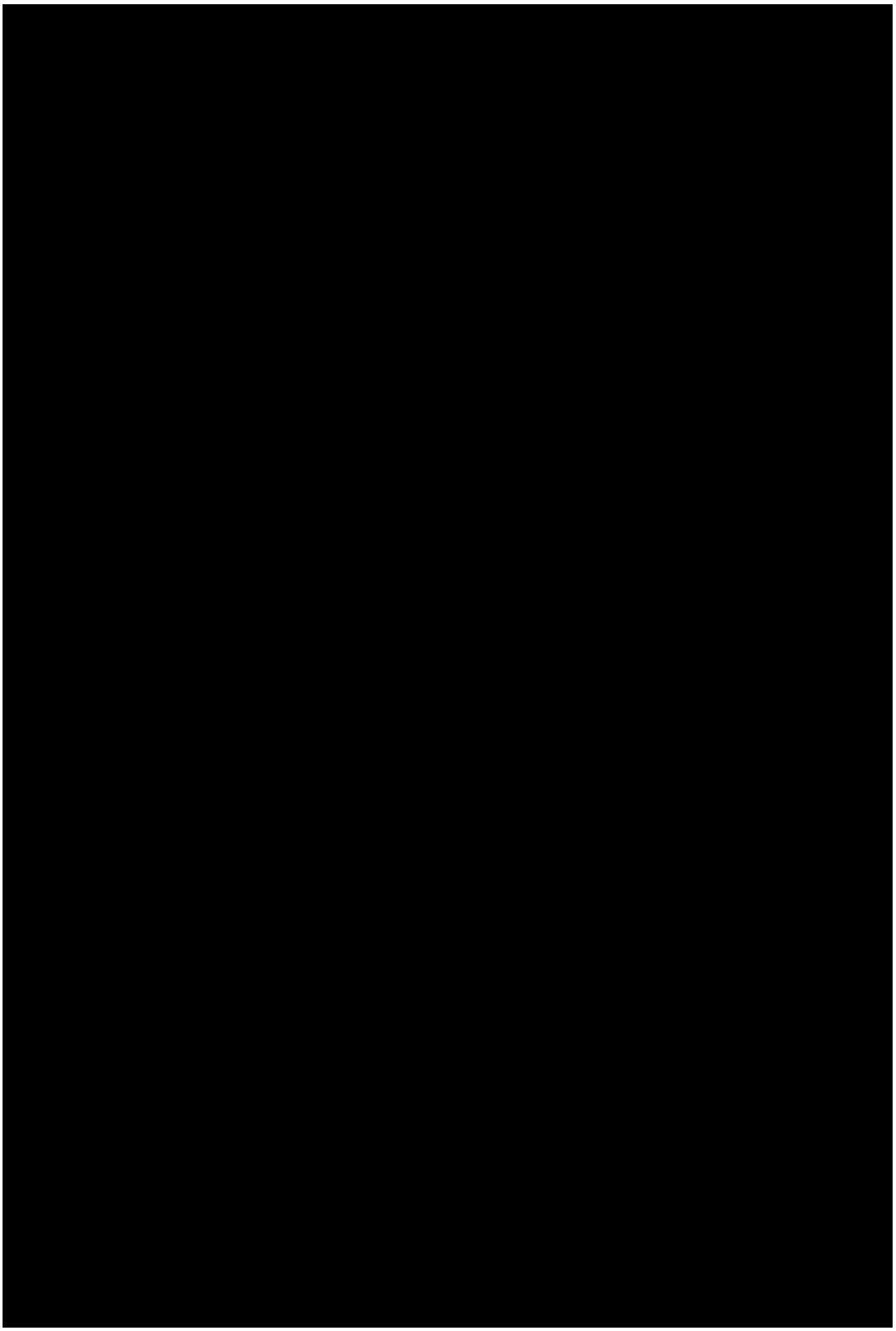

Figure 6.29 Interpreted and uninterpreted seismic line GDPI10-64 showing the eastern segment of the slump and relationship to the Oligocene-Miocene shelf stratigraphy in the SW and the underlying sedimentary mound. Surfaces M1, M2, M3, and M4 have been mapped at a broad scale to identify the external geometry of the mound. The slump partially overlies the basin boundary faults of the half graben that collectively form the Pisces Sub-basin. Movement on these faults continues into the mound stratigraphy and could provide a potential mechanism to trigger failure along the shelf margin, gravitationally unstable due to progradation in the late Oligocene-Miocene.

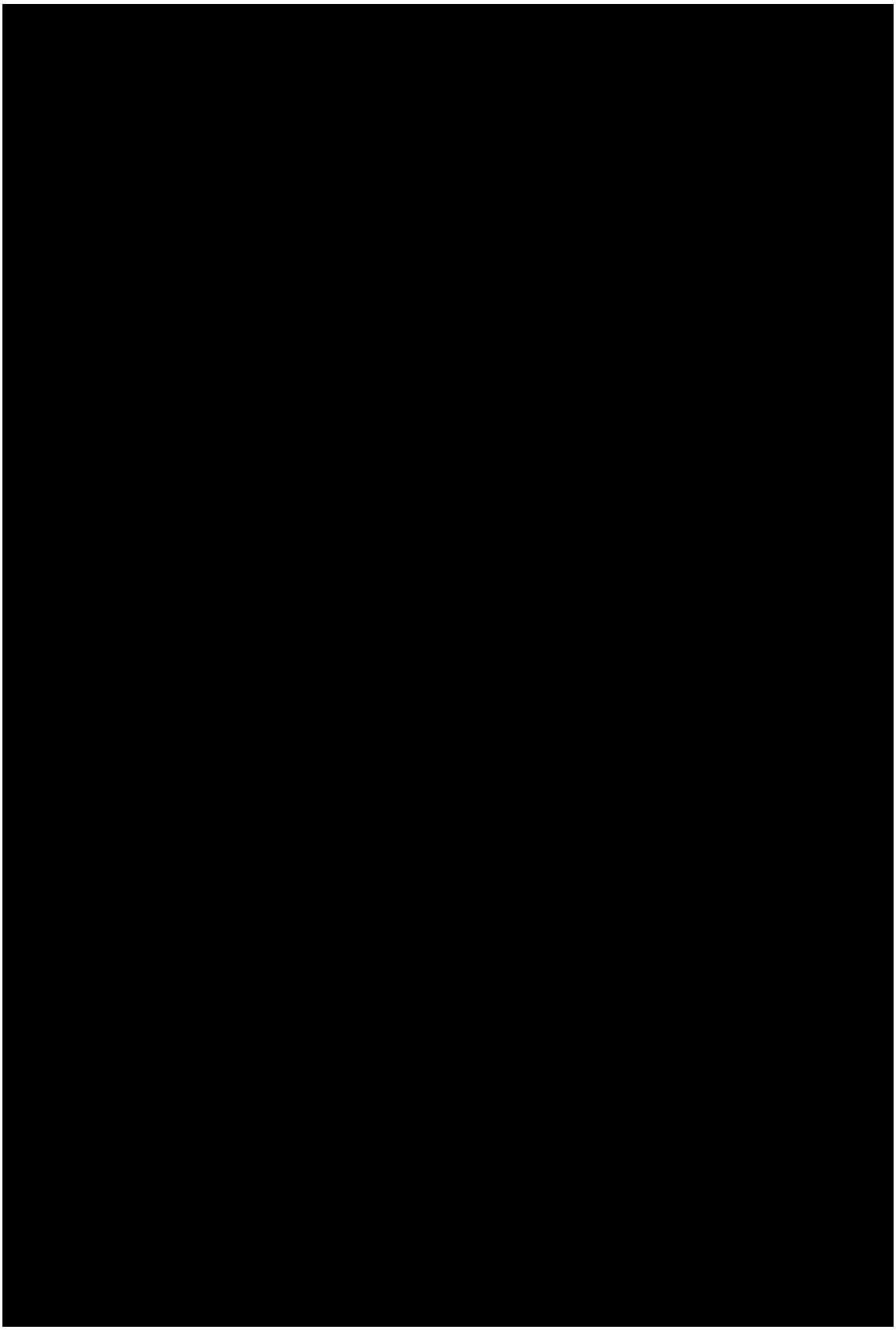

Figure 6.30 Interpreted and uninterpreted seismic line GDPI10-26 showing the western segment of the slump and relationship to the Oligocene-Miocene shelf stratigraphy in the SW. The sedimentary mound is less pronounced at this location, with only top M1 preserved. Headwall faulting is less defined and at a lower angle relative to the eastern segment of the slump (see Figure 6.27). The internal geometry is chaotic and is dissected by numerous closely spaced faults.

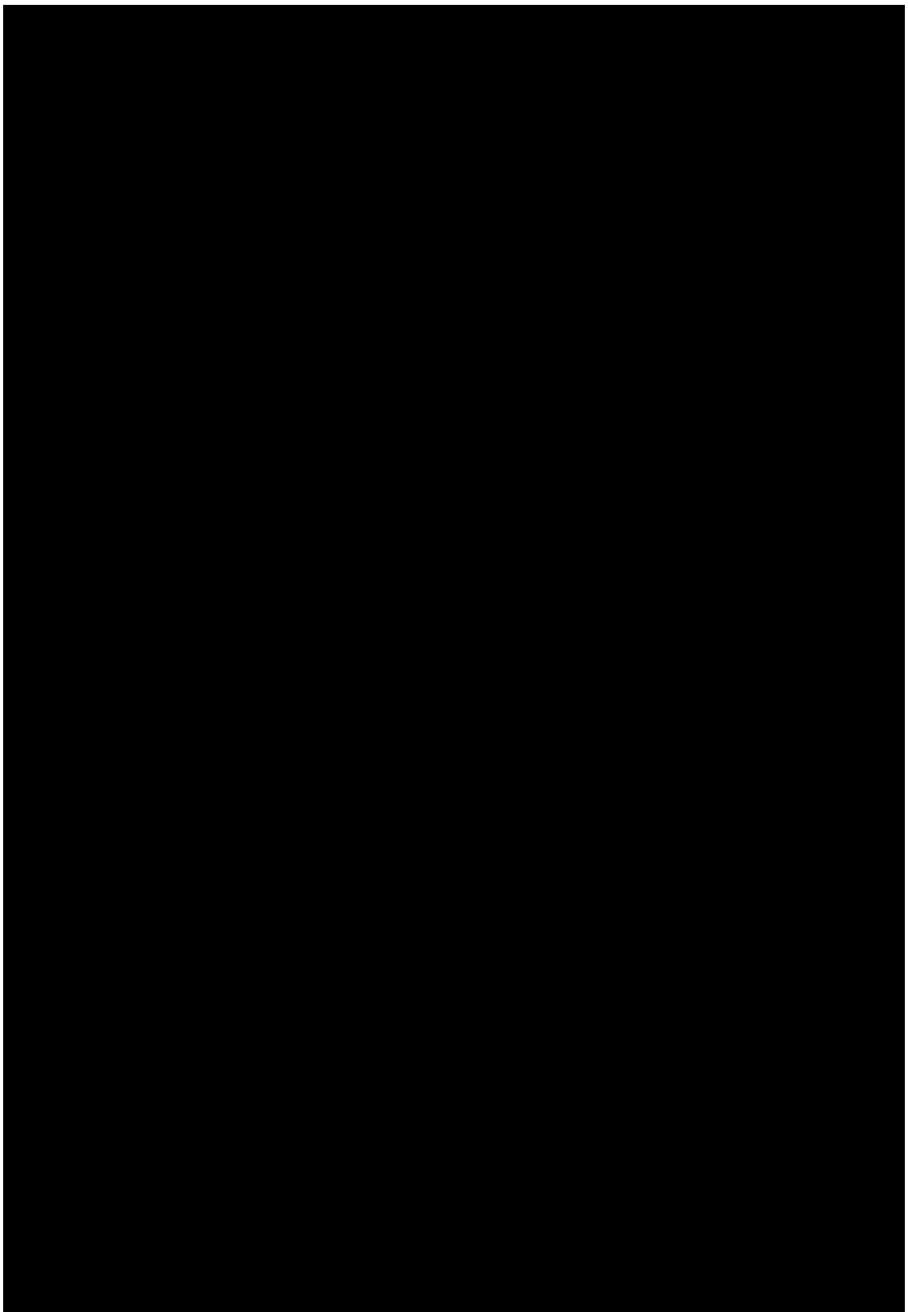

Figure 6.31 Interpreted and uninterpreted seismic line GDPI10-40 showing the transition zone between the western and eastern segments of the slump and relationship to the Oligocene-Miocene shelf stratigraphy in the SW. A wide zone of listric faulting is present, involving younger stratigraphy to the NE, suggesting a progression from the western segment to the eastern segment.

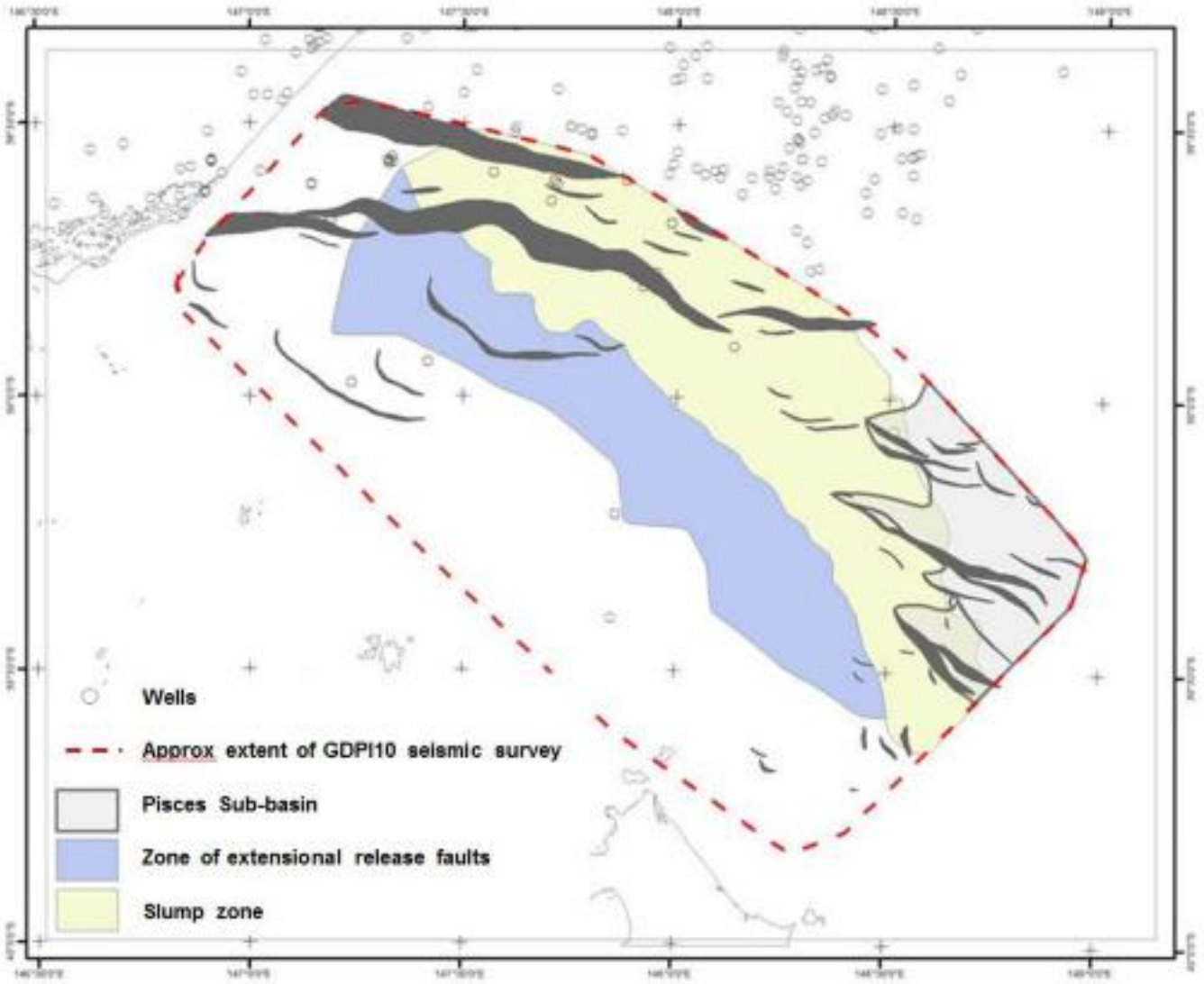

Figure 6.32 Geographical extent of slump zone and associated extensional release fault system. Also shown is the Pisces Sub-basin, and basement fault polygons (grey polygons).

6.5 Leakage Indicators

Leakage indicators such as Hydrocarbon Related Diagenetic Zones (HRDZ) and gas chimneys form when hydrocarbon containment fails due to seal pinchout, trap or seal breach due faulting, or when hydrocarbon charge exceeds seal capacity (O'Brien and Woods, 1995). Leakage features can be imaged on seismic data due to the acoustic, mechanical or diagenetic alterations that result from the flow of fluids or gas through a formation. Non-hydrocarbon related fluids such as those related to volcanic intrusions can also have similar degradational effects on seismic data. Both hydrocarbon and non-hydrocarbon related leakage indicators can be used as first-order proxy to assess seal or trap containment properties.

The GDPI10 2D seismic grid has been assessed for the presence of leakage indicators, and several seismic anomalies have been identified with most being present in the shallow seismic record (< 2 s TWT). Some of the anomalies are clearly associated with volcanic features (sills or dykes), although the origin of others are unclear. The highest numbers of anomalies are present in or around the Pisces Sub-basin. The anomalies occur as isolated features and within clusters.

The seismic anomalies were mapped as leakage indicators on the basis of a confidence ranking of strong, moderate or weak (Figure 6.33). The ranking does not imply a hydrocarbon or non-hydrocarbon origin, but provides a framework to understand the distribution and significance of the features. Strong indicators exhibit pervasive stack degradation and seismic pull-up, and have associated high-amplitude anomalies on seismic data. Moderate indicators have moderate stack degradation and seismic pull-up, with some associated high-amplitude anomalies. Weak indicators have broad areas of minor stack degradation and occasional minor seismic pull-up, and some associated moderately high-amplitudes anomalies.

6.5.1 Distribution

Strong leakage indicators were identified in eight locations. Seven of the indicators are relatively closely spaced, and this has been identified as a high density area, five within 15 km of Sailfish-1 and the others within 10 km of Pisces-1 (Figure 6.34). The other occurrence is at the NE end of line GDPI10-40.

Moderate possible fluid indicators occur predominantly within the high density area noted above. Within this area they are more than 30 observed indicators. The moderate indicators also cluster in one area approximately in the middle of the seismic grid (9 observed occurrences). Aside from these two locations there is one other observed occurrence 25 km NW of the cluster in the centre of the grid.

The weak indicators are distributed across the survey, although they are less common on the shallower parts of the Southern Platform. The weak indicators are the most ambiguous in terms of their definition and origin. The highest density of weak indicators (approximately 30 observed occurrences) is in the eastern portion of the survey and is coincidence with a high density of moderate and strong indicators (Figure 6.34). There is also a smaller cluster of weak possible fluid indicators (6 observed occurrences) located 20 km to the SW of the high density area.

6.5.2 Significance of Clusters

The possible fluid migration anomalies within the high density cluster include strong, moderate and weak indicators. They are spatially associated with the structurally defined Pisces Sub-basin. The strong and moderate anomalies typically extend from the basement to the seafloor. The anomalies occur in proximity to basin boundary faults, but do not typically lie directly above them. The features are closely associated with conical build-ups and high amplitude crosscutting reflections (Figure 6.35).

It is inferred that the fluid migration anomalies within the high density cluster are genetically related to igneous emplacement, volcanism and fluid generation. While the apparent conical volcanic features (Figure 6.35) overlie the Top Latrobe Group surface, the linkage of vertical fluid migration anomalies to these features as well as to other dikes and sills indicates that fluid migration of likely igneous fluids continued to Recent. It is possible that there are also depositional facies changes in this area delineating a terminal edge of effective seal, allowing for the vertical migration of fluid, but this is not considered necessary. Igneous emplacement and fluid generation is capable of creating vertical migration pathways through otherwise effective fluid seals. The high density cluster of anomalies is inferred to define a zone of igneous activity from post Latrobe Group time with ongoing fluid generation to Recent.

The moderate indicator cluster is located within the centre of the seismic survey area. Similar to the high density cluster, this area is inferred to be associated with igneous activity. This area is in proximity to a basement ridge that extends across the middle of the seismic survey area from the SW to NE. In this area there are high amplitude crosscutting

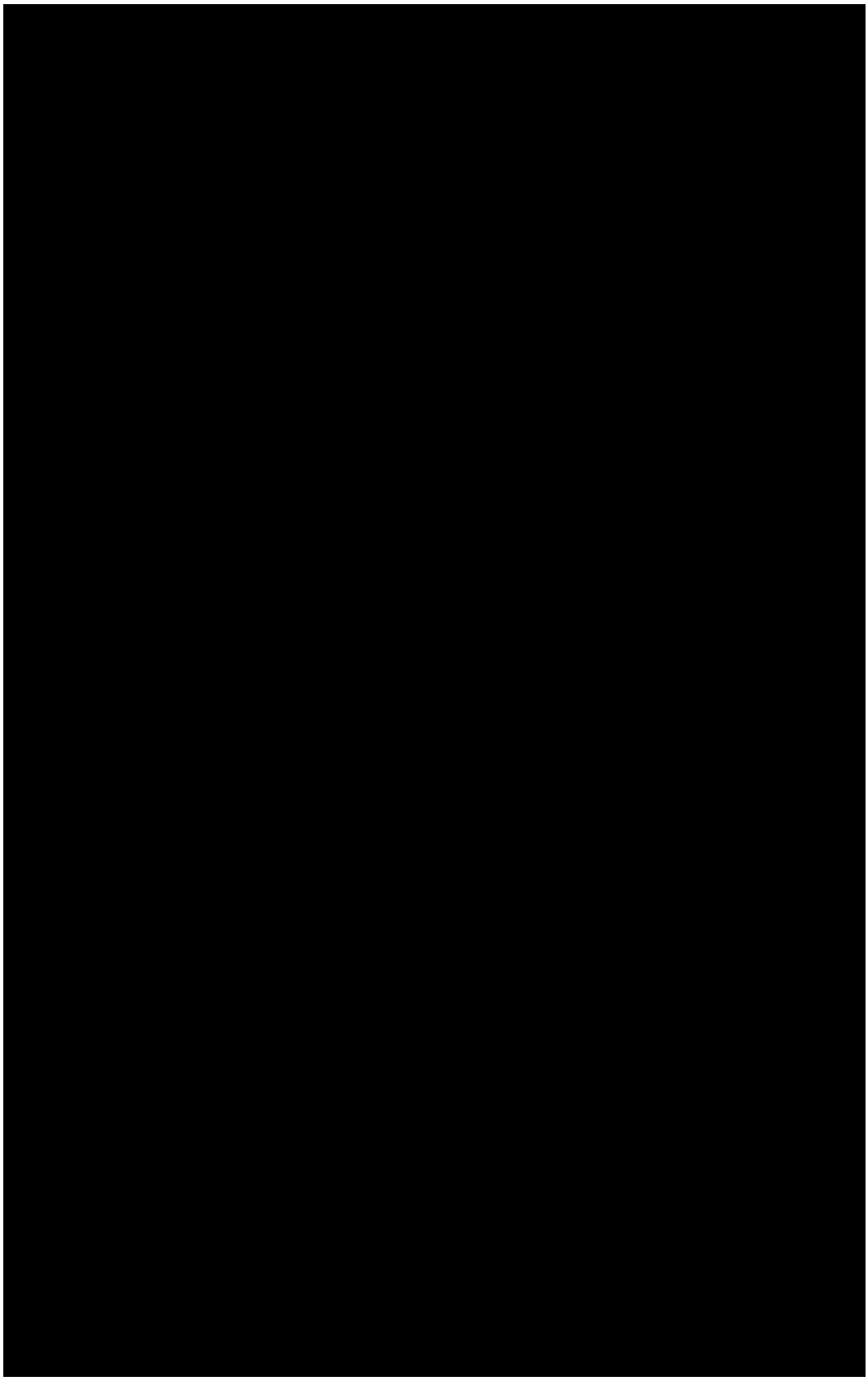

Figure 6.33 Possible leakage indicators of weak (A), moderate (B) and strong (C) confidence (grey ovals). Some indicators also occur with high amplitude anomalies, including high amplitude seafloor anomalies (C, black arrow). Vertical scale is TWT (s).

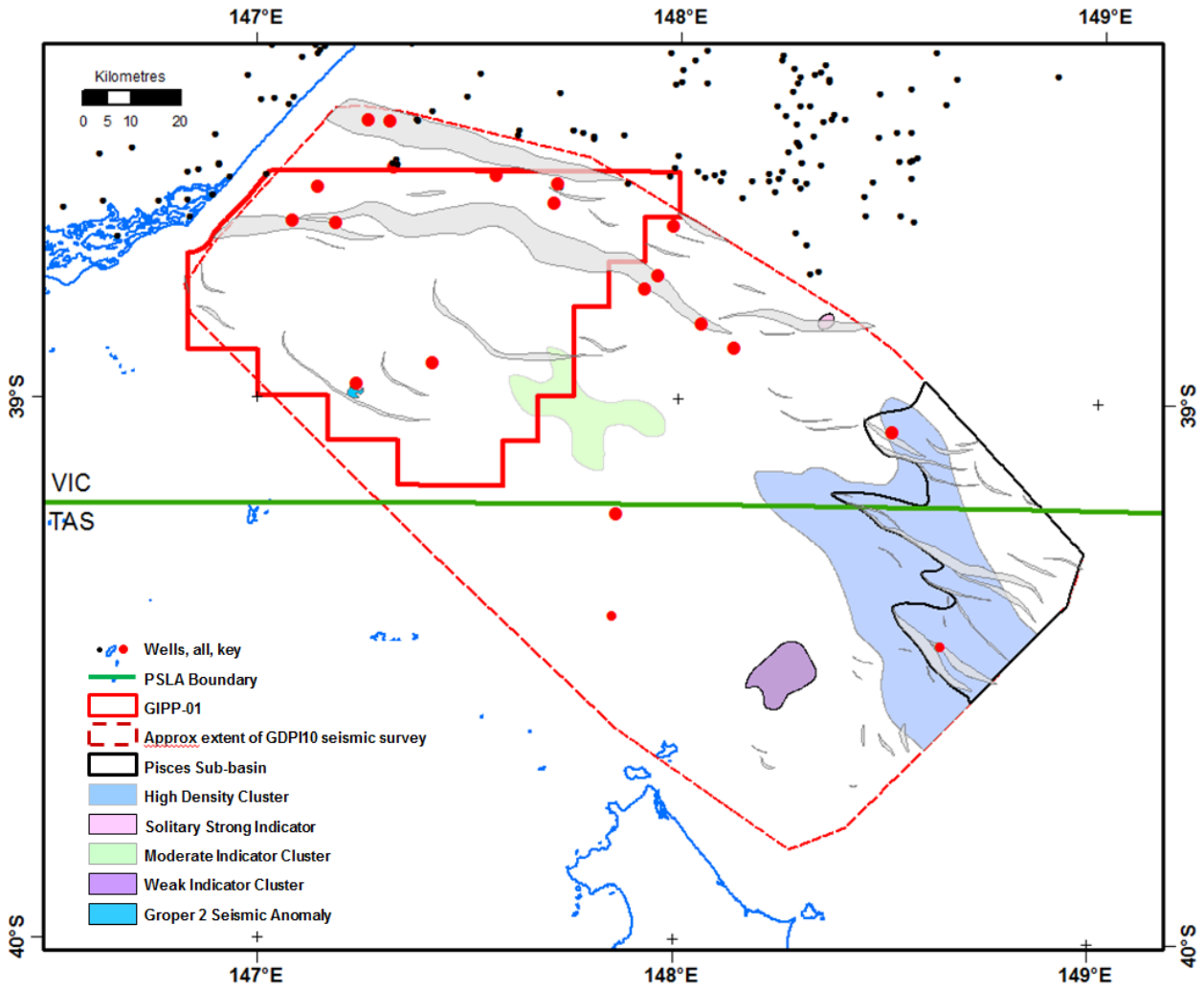

Figure 6.34 Distribution of possible fluid migration indicators (coloured polygons). Grey polygons are basement faults.

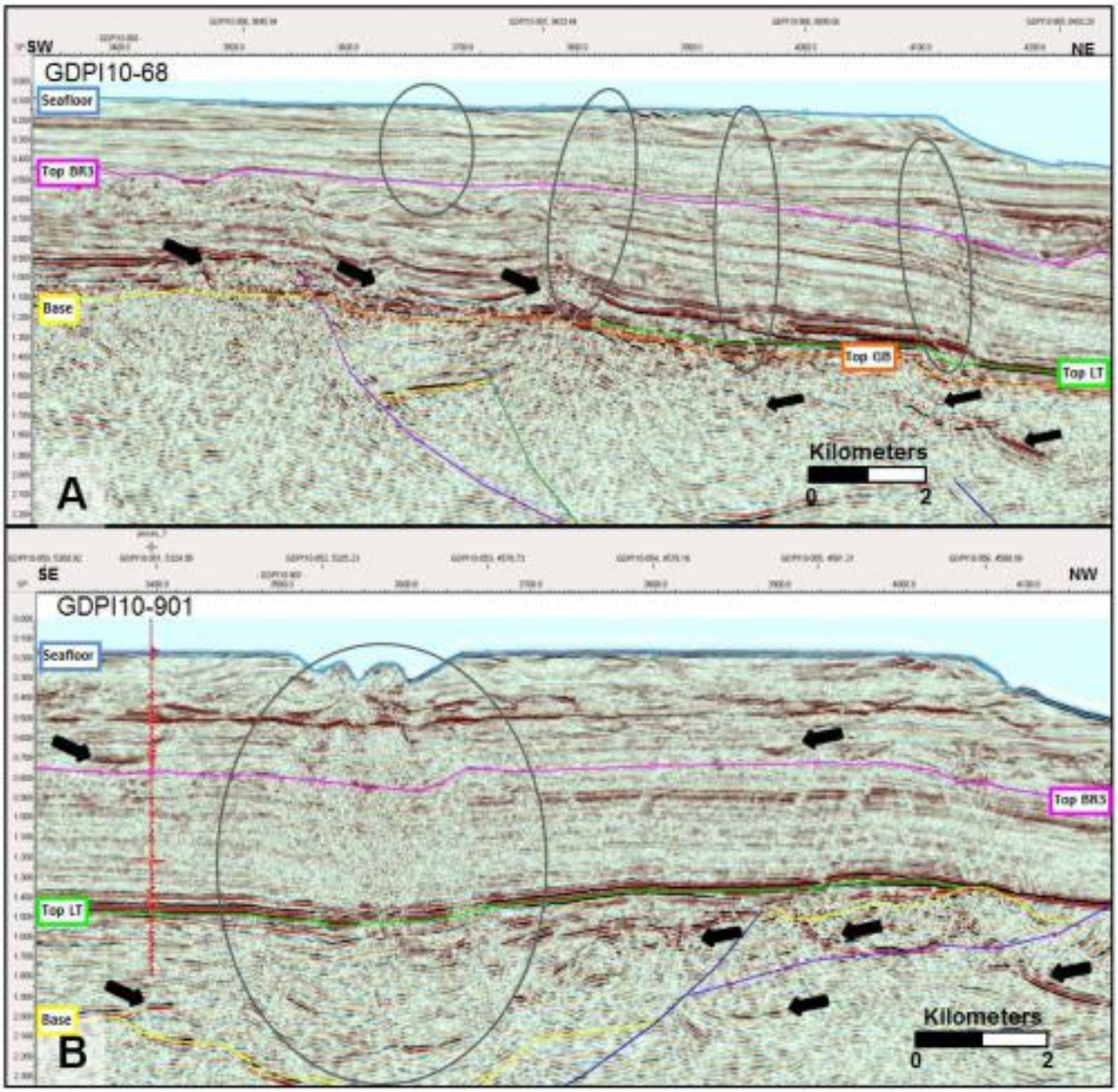

Figure 6.35 Possible fluid migration indicators within the high density cluster include moderate indicators (A) and strong indicators (A, black ovals). Likely volcanic conical features are evident in some locations above Latrobe Group Stratigraphy (A, right pointing black arrows). Many possible igneous features are present in the high density cluster (black arrows). Vertical scale is TWT (s).

reflections in the basement and possible small intrusive bodies in the overlying stratigraphy. Closely linked with these features are possible fluid migration anomalies. The anomalies do not appear to extend to the shallow subsea levels, where there are observed disruption zones and high amplitude reflections. In this area, there are also small scale reflection offsets (less than 0.02 ms). While the small faulting offset may form a conduit for vertical fluid migration this is not evident from seismic (Figure 6.36). It is likely that the faulting is related to differential compaction of sediment in proximity to the basement ridge, caused by variable sediment thickness or possible local facies variations.

The weak indicator cluster located to the SW of the high density cluster is also inferred to be related to igneous fluids. The features extend from moderate to high amplitude crosscutting basement reflections to mounds at or near the seafloor. In addition to this are features that appear to be small intrusive bodies causing some force folding within the Cenozoic stratigraphy (Figure 6.37).

The weak possible fluid migration anomalies in the western portion of the seismic survey area predominantly occur high in the stratigraphy near the seafloor. They are broad areas of disruption not necessarily connected to features at depth (Figure 6.38). These features are of equivocal origin and may be the result of seismic acquisition and processing, locally generated fluids or slow vertical fluid migration rates. Given the equivocal nature and origin of these weak indicators it is difficult to ascertain the significance without future detailed investigation.

6.5.3 Significance of Single Occurrences

A solitary, strong possible fluid migration indicator is located at the NE end of GDPI10-40. This occurrence is similar to the strong occurrences within the high density cluster, and may also be related to igneous activity. There are high amplitude crosscutting reflections evident near the seafloor above these features, which may be a direct indication of relatively late igneous activity along this margin, as inferred by the possibly igneous related seafloor anomalies elsewhere (Figure 6.39).

A large disruptive feature observed in seismic images south of Groper-2 is of interest. This feature is has an amorphous distribution of approximately 3.5 km across (Figure 6.34) and is best imaged in seismic lines GDPI10-017 and gbs80_04a (Figure 6.40). In seismic this feature appears to be an intrusive igneous body. The characteristics indicative of this origin are:

- Down-warping of underlying beds
- Up-warping of overlying beds
- Chaotic high amplitude reflections internally
- Short discontinuous reflections leading to the body
- Degradation of seismic imaging underlying the feature

This feature is not caused by fluids breaching a seal, but instead an igneous emplacement. Similar features are evident in Planke et al. (2005)

6.5.4 Fluid Migration or Volcanogenic Generation through Seaspray Group in Wells

The well completion reports of wells within the seismic survey area were examined for evidence of fluid migration and hydrocarbon alteration within the upper section of the wells. This included features such as hydrocarbon indicators, volcanics, altered volcanics, ash layers, alteration zones, degraded sand zones, and other anomalies. The well completion report for Wasabi-1 was not included as only the basic data was available. Only Amberjack-1 and Tommyruff-1 showed evidence of nonintersitial fluids. In Amberjack-1 this was very dull yellowish-white to greenish-white direct fluorescence in sandstone and calcarenite cuttings at 400-480 mKB. In Tommyruff-1 the fluorescence was trace to 3% dull pale yellow pinpoint hydrocarbon fluorescence in sandstone cuttings at 375-385 mKB. Both of these occurrences are close to the Top of the Bassian Rise Unit 3, mapped at 460 mKB in Amberjack-1 and 400 mKB in Tommyruff-1. The seismic imaging around these wells also shows weak possible fluid migration anomalies, but this also occurs near many other wells in the western portion of the survey area, without evidence for hydrocarbons in the well completion reports. Therefore the significance of the trace fluorescence in these wells is not substantive and equivocal but may be evidence of limited local fluid migration, not clearly imaged in the seismic data.

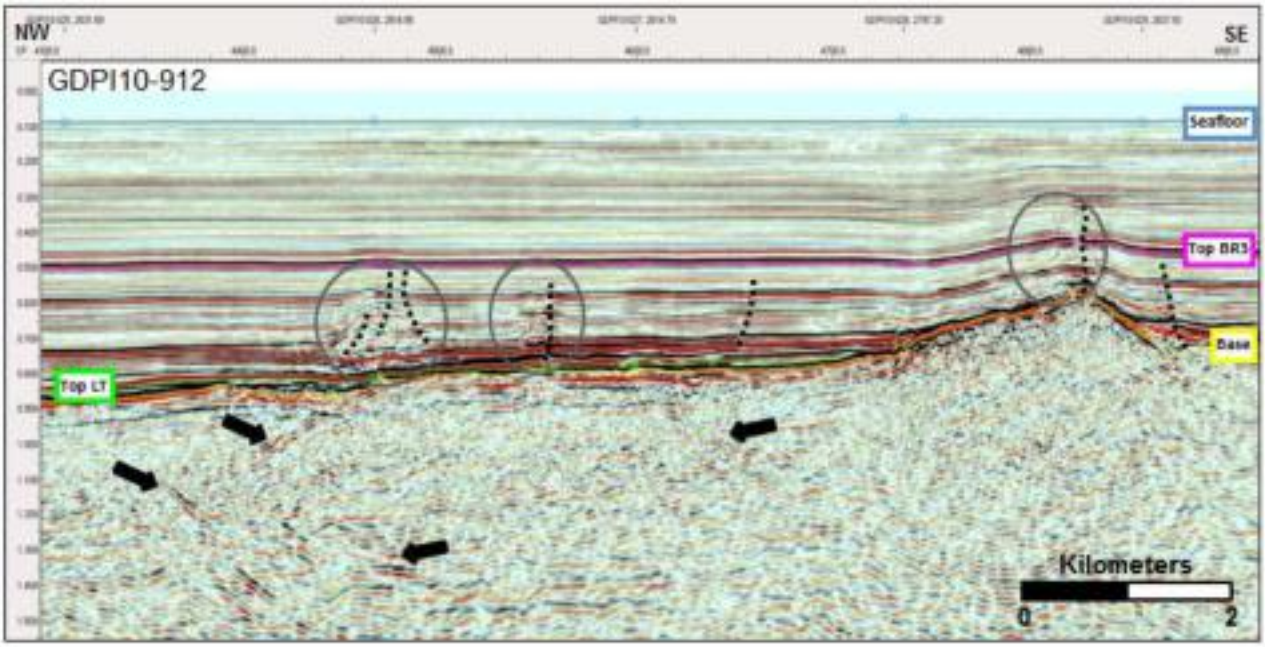

Figure 6.36 Possible fluid migration indicators within the moderate indicator cluster (black ovals). Also evident in this area are small stratigraphic offsets (dashed black lines) and possible igneous features (black arrows). Vertical scale is TWT (s).

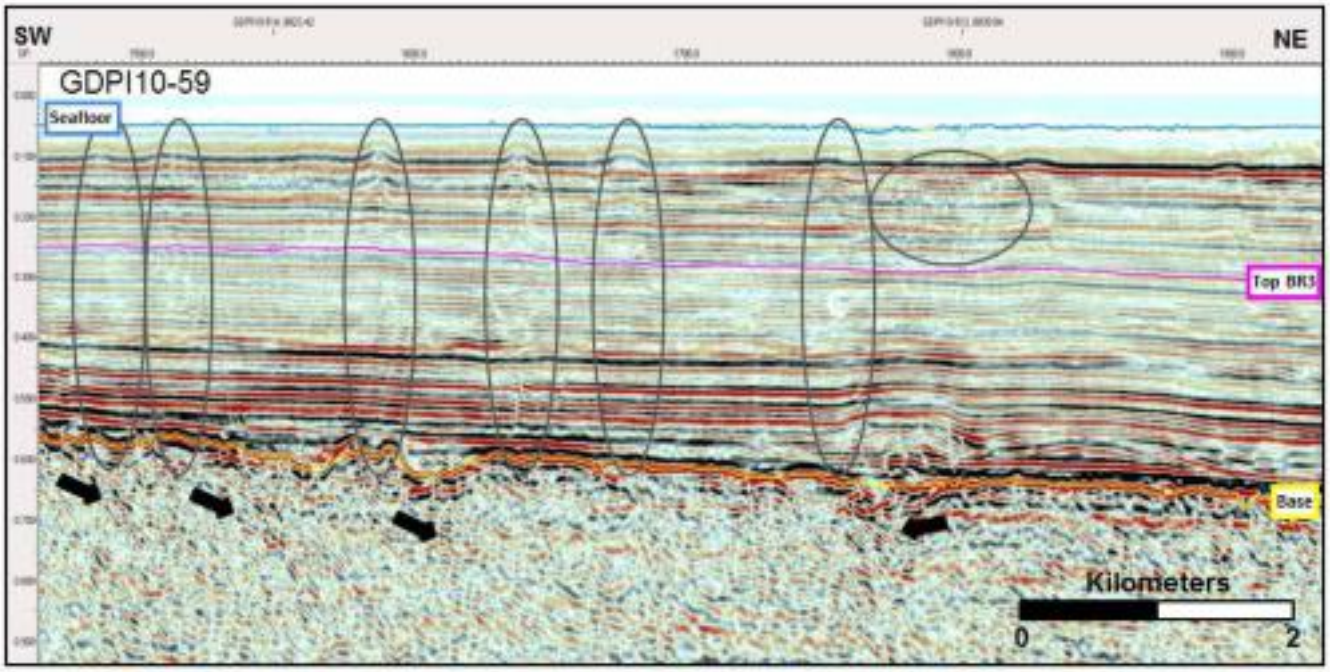

Figure 6.37 Possible fluid migration indicators within the weak indicator cluster (black ovals). Possible igneous features are indicated by black arrows. Vertical scale is TWT (s).

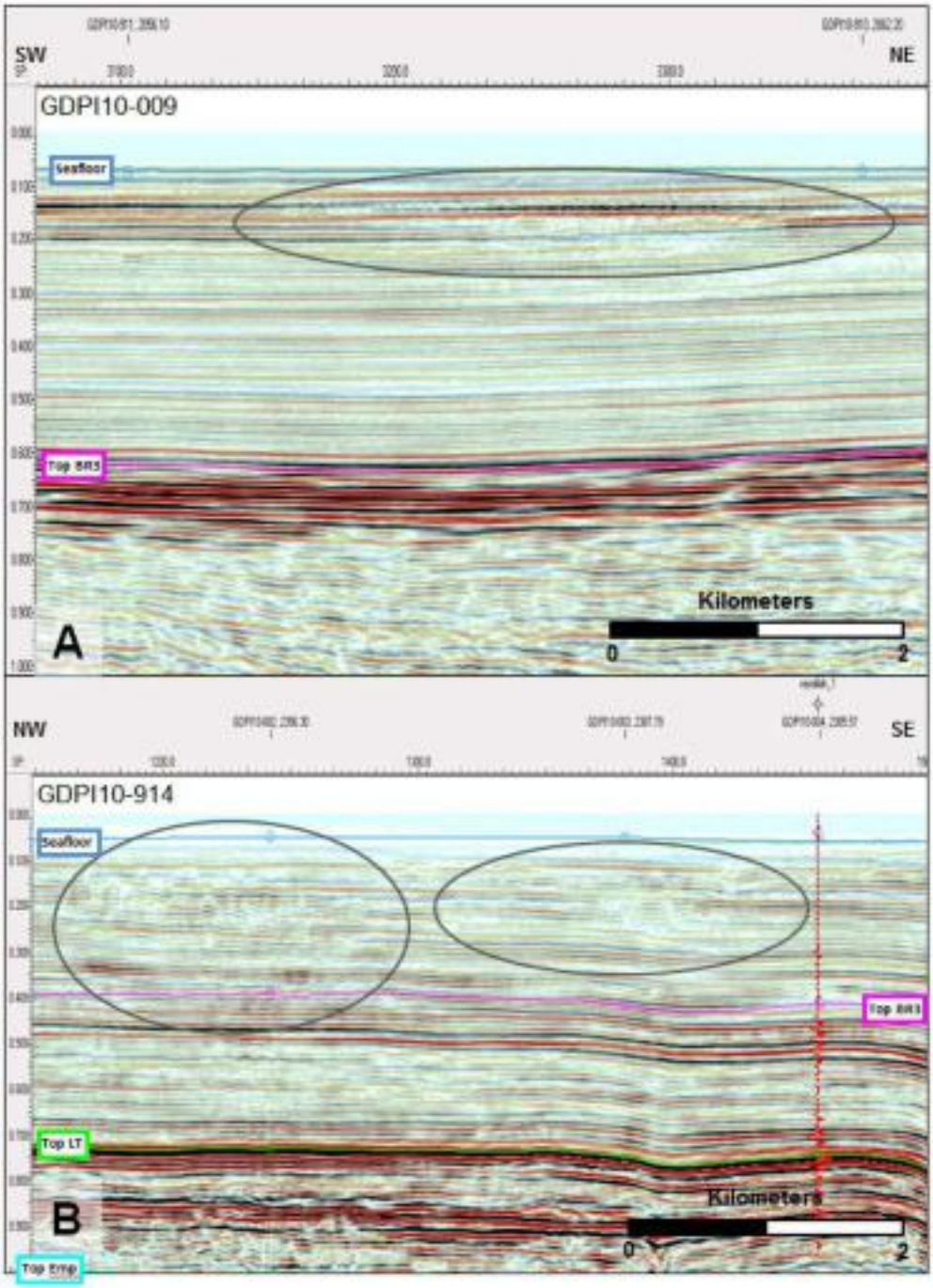

Figure 6.38 **A and B, Weak possible fluid migration indicators in the western portion of the seismic survey area (black ovals). Gamma ray log is shown along the project well path of Wyrallah-1 (B). Vertical scale is TWT (s).**

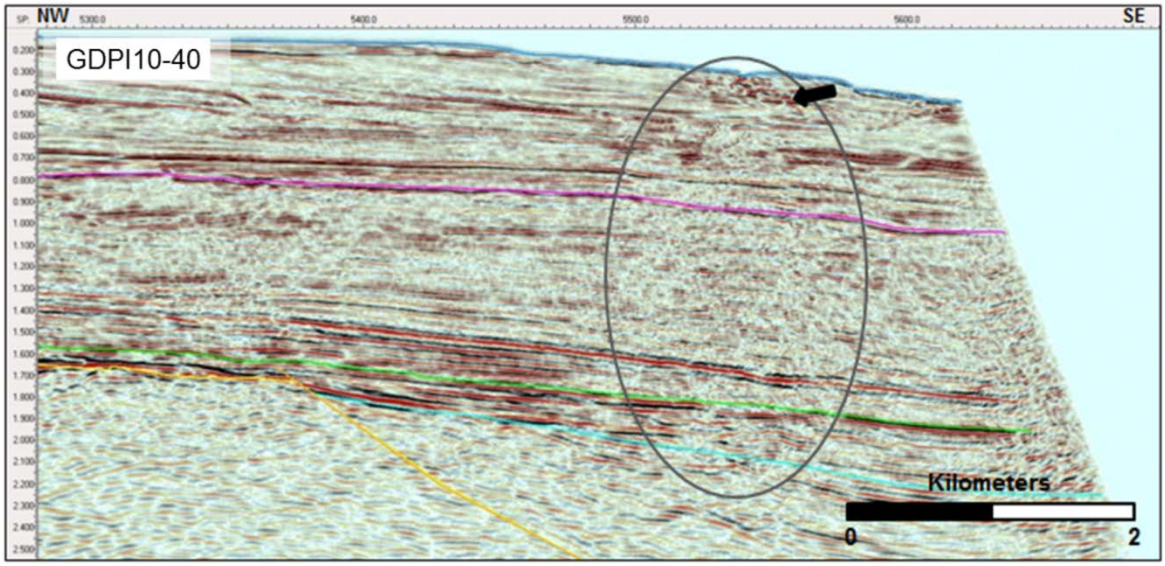

Figure 6.39 The solitary, strong possible fluid migration indicator (black oval). Near seafloor possible igneous features are evident here as well (black arrow). Vertical scale is TWT (s).

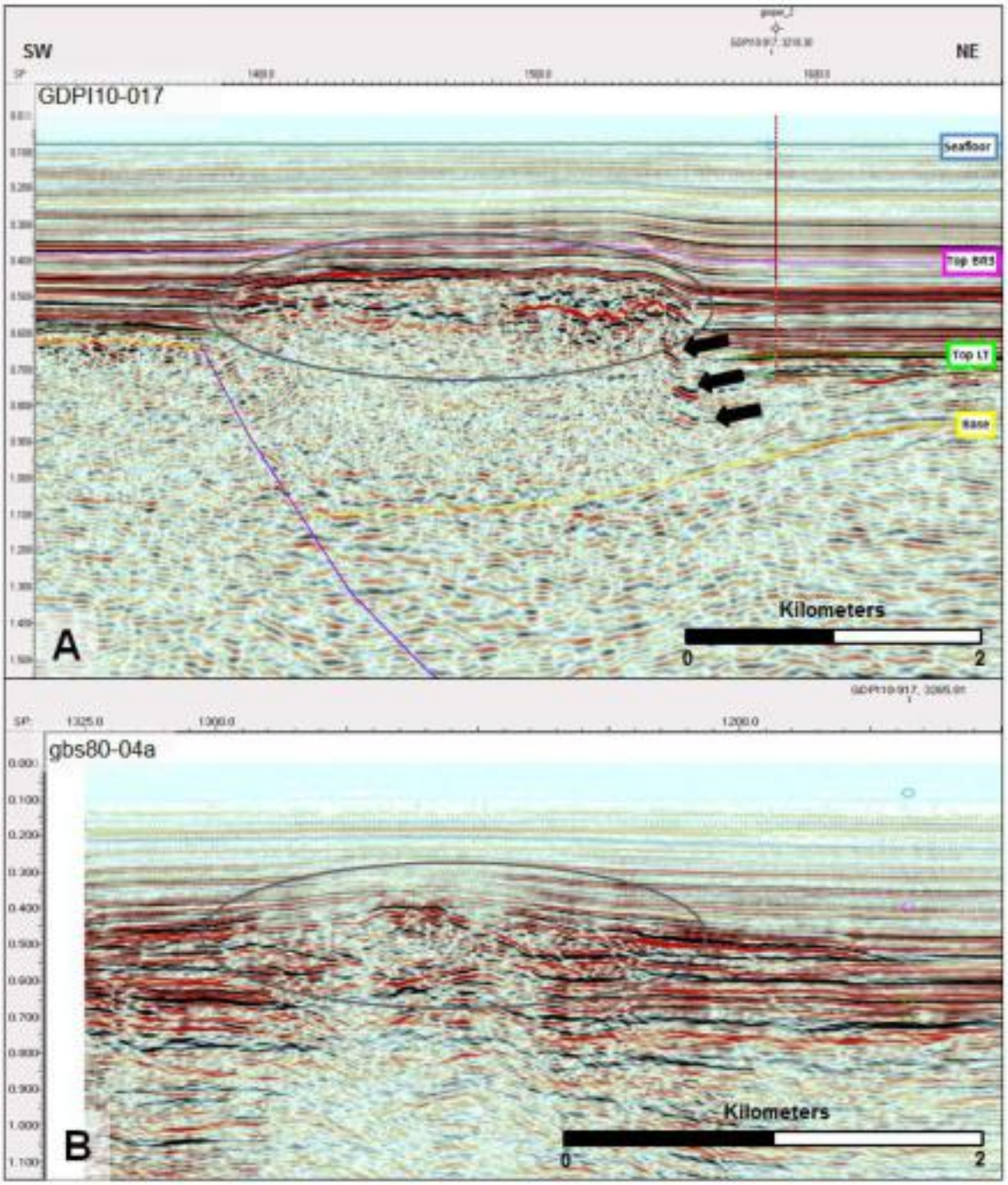

Figure 6.40 Groper-2 seismic anomaly (black oval) as seen in GDPI10-017 (A) and gds80-04a (B). Associated possible igneous features are evident in proximity to the feature (black arrows). Vertical scale is TWT (s).

7 Velocity Model

7.1 Introduction

The process to derive the velocity model and depth convert the horizons was undertaken primarily within the IHS Kingdom suite of software (VELPAK and Kingdom 2d/3dPak), with additional functionality provided by entering the average velocity model into the GOCAD software. An overview of the processes involved is summarised in Figure 7.1.

7.2 Generating the Velocity Volume using Kingdom VELPAK

7.2.1 Event Interpretation

Prior to entering VELPAK, seismic interpretation was undertaken to subdivide the stratigraphy into packages (or events) that may be significant for the definition of the velocity model due to lithologic, stratigraphic or structural variations. In this model, nine separate velocity events were chosen (Figures 7.2 and 7.3). The horizons used to separate these events were, in part, early tied versions of the final stratigraphic surfaces. Additional construction surfaces were interpreted to further subdivide intervals that could have significant velocity variations. The relationship between the construction surfaces and the final tied stratigraphic surfaces is given in Table 7.1.

A brief description of each of the events follows:

Event 1: C00 Sea Level to C01 Seafloor. This interval was given a constant interval velocity of 1521 m/s.

Event 2: Interval between C01 Seafloor and C02 Toplap surface with sub-parallel to progradational seismic reflections, likely composed of carbonate sediments. This interval also included the topsets of some (the most basinward) of the prograding packages of Event 3.

Event 3: Interval between C02 Toplap or C01 Seafloor surfaces and C03 Downlap surface, capturing a progradational package stepping basinward.

Event 4: Interval between C03 Downlap surface and C04 Mid Miocene, where seismic is dominated by parallel to sub-parallel reflections and the event has a relatively consistent thickness across the shelf. Basinward small incisions are present in this interval.

Event 5: This event from C04 Mid Miocene to C05 Slump Top was incorporated late in the process to fill the gap in those regions where the slump did not impact on the stratigraphy of the Mid Miocene construction surface. It was not defined as a region where there was no geological reason for a velocity variation. The interval is null over the majority of the area of interest and thin relative to the other intervals. As this interval is thin, there are fewer values available to make statistically robust velocity calculations. Slight variations in the thickness may be translated into large interval velocity variations.

Event 6: This event from the C05 Slump Top to C06 Slump Container is restricted to the basinward portion of the area of interest where there is much disruption to the seismic horizons due to slumping and incision. The seismic character in this zone is highly variable ranging from rotated fault blocks with well-defined stratigraphy to totally chaotic reflectivity.

Event 7: Interval between the C06 Slump Container or C04 Mid Miocene and the C07 Near Top Latrobe surface or older surfaces. This interval represents the deepest of the predominantly carbonate units and has a strong progradational character. Seismic reflections are typically well resolved on the platform, losing character adjacent to the slump zone. High angle to vertical faults with limited displacement are a common feature of this interval south of the slump zone.

Event 8: This event represents the interval between the C07 Near Top Latrobe and C08 Base Latrobe. The interval thins on the platform onto a basement with rugose topography in places. Interval velocity may be influenced by the thin interval as small thickness variations can lead to large interval velocity variations. This interval was identified as an interval of interest to sub-divide the Latrobe Group from the older Strzelecki Group

Event 9: Interval between C08 Base Latrobe and C09 Basement. Restricted to the half graben, contains the oldest sediments in the area of interest.

Figure 7.1 Overview of Depth Conversion Workflow.

Figure 7.2 Events used as input into the velocity model.

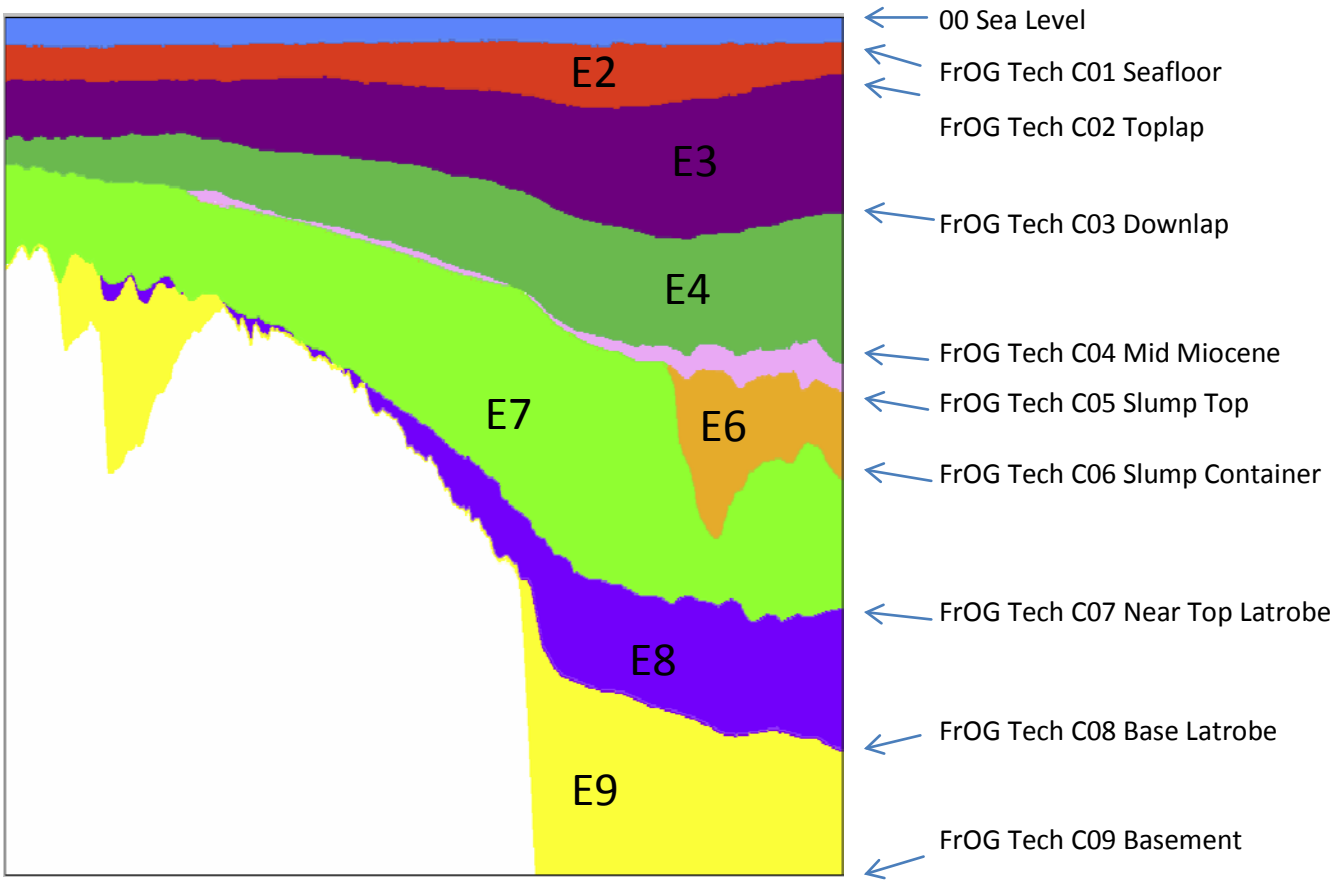

Figure 7.3 Events used as input into the velocity model.

CONSTRUCTION SURFACE	STRATIGRAPHIC SURFACE
FrOG Tech C01 Seafloor	FrOG Tech 01 Seafloor
FrOG Tech C02 Toplap	construction surface only
FrOG Tech C03 Downlap	FrOG Tech 02 Near Top Bassian Rise Unit 2
FrOG Tech C04 Mid Miocene	FrOG Tech 03 Top Bassian Rise Unit 3
FrOG Tech C05 Slump top	construction surface only
FrOG Tech C06 Slump Container	construction surface supplied in interpretive Kingdom project
FrOG Tech C07 Near top Latrobe	FrOG Tech 07 Top Latrobe Group
FrOG Tech C08 Near Base Latrobe	FrOG Tech 11 Top Strzelecki Group
FrOG Tech C09 Basement	FrOG Tech 13 Top Basement

Table 7.1 **Relationship between construction surfaces used to generate the depth conversion model and the final interpreted horizons. Please note that the construction surfaces only approximate the final horizons.**

7.2.2 Event Gridding

VELPAK requires all events to be gridded and to cover the entire depth conversion area of interest. This requires a series of horizon substitutions to generate "construction horizons" to cover the area of interest. The construction horizons were gridded (100 m grid cell size) to generate a series of "construction surfaces".

7.2.3 Importing Seismic Processing Velocities

Velocities used for the Pre-stack time migration (PSTM) were loaded into VELPAK and converted to average velocity using the Dix equation.

7.2.4 VELPAK Process 1 - Creating Pseudo-wells/Velocity Smoothing

The input seismic velocity profiles were smoothed for each model event during the creation of pseudo-wells. Pseudo-wells were reviewed and those with anomalous velocity variations were deleted.

Much of the description below has been summarised from the VELPAK user guide and online presentations provided by IHS.

- The "amalgamation" velocity smoothing process averages the time-depth curves from adjacent stacking velocity analysis points (1000 m spacing) generating a regional grid of combined time-depth curve (pseudo-wells) via the Dix process.
- For each model event, VELPAK generates a cylinder at the pseudo-well location, with a radius of the search distance set to include adjacent velocity analysis points. In this analysis the search radius was set to 2500 m, allowing for the inclusion of five stacking velocity analysis points within each pseudo-well. The pseudo-wells are spaced at 4000 m allowing an overlap of a single common velocity analysis point (Figure 7.4). The top and base of the cylinder are the time grids for the top and base of the layer.

Only data points from within this cylinder are considered in the analysis (Figures 7.4 and 7.5).

- VELPAK then combines the data points within the cylinder, and rearranges them to form a pseudo-sonic log. It does this by calculating an interval velocity between each sample down each stacking velocity analysis curve, and a midpoint depth for each of these sample pairs. It then sorts these midpoint depths into order, and re-integrates to get a time-depth curve.
- A matrix of pseudo-wells has been created using a spacing of 4000 m. During the "amalgamation" process if the pseudo-well doesn't find curve data for the layer then it is deleted (Figure 7.5).
- The time-depth curve for each pseudo-well is only defined for a single layer so the process is repeated for each layer of the model.

7.2.5 VELPAK Process 2 - Optimisation of the Instantaneous Velocity Function at each Pseudo-well

This process calculates the best parameters for instantaneous velocity function for each model event used for the depth conversion. Much of the description below has been summarised from the VELPAK user guide and online presentations provided by IHS.

- The "optimise" process uses polynomial curve fitting to derive the best instantaneous velocity function parameters using the pseudo-sonic logs derived from the "amalgamation" process at each event (Figure 7.6).
- The method used in this model is instantaneous velocity (Figure 7.7) as this is an industry standard and allows for capture of the lateral and vertical variability of velocity.
- The "optimise" process is run to derive the best set of parameters for the instantaneous velocity function for any particular layer (Figures 7.8 to 7.10). A tight cluster of velocity functions indicates a well constrained estimate.
- The Depth Conversion Intercept (V_0) is gridded and used to depth convert using $Vz=V_0+kZ$.

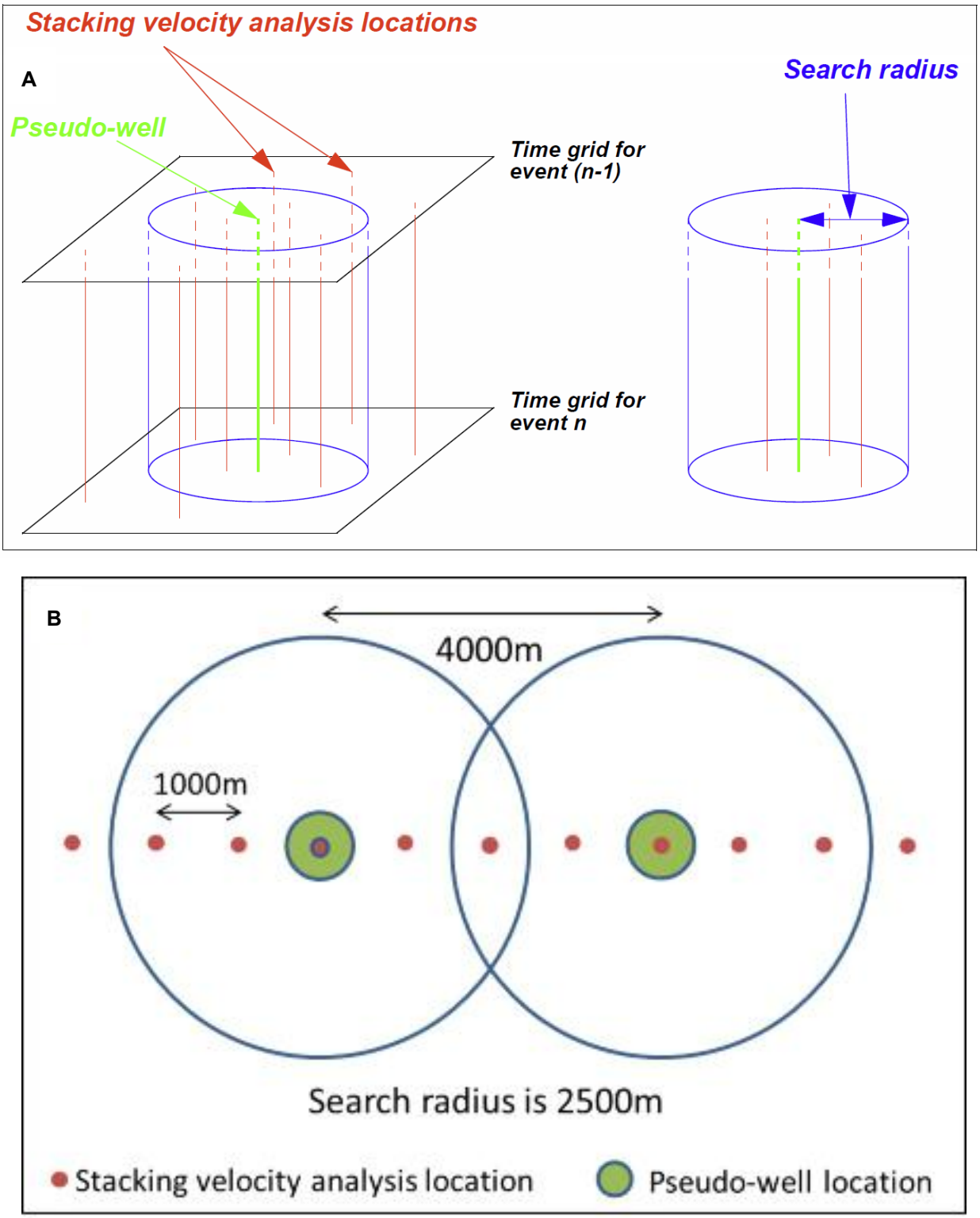

Figure 7.4 Pseudo-well search geometry used during the "amalgamation" process in VELPAK showing vertical (A) and horizontal (B) inclusion areas.

Before

A

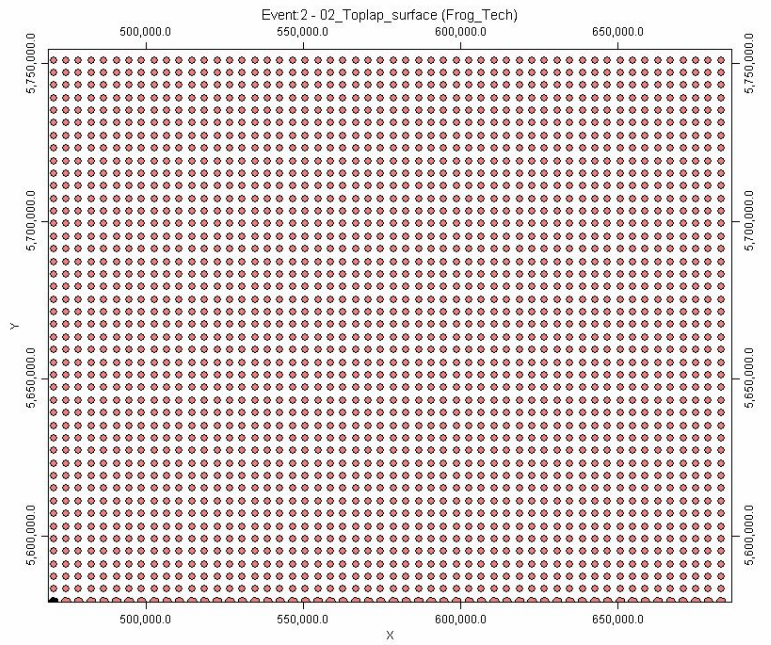

After

B

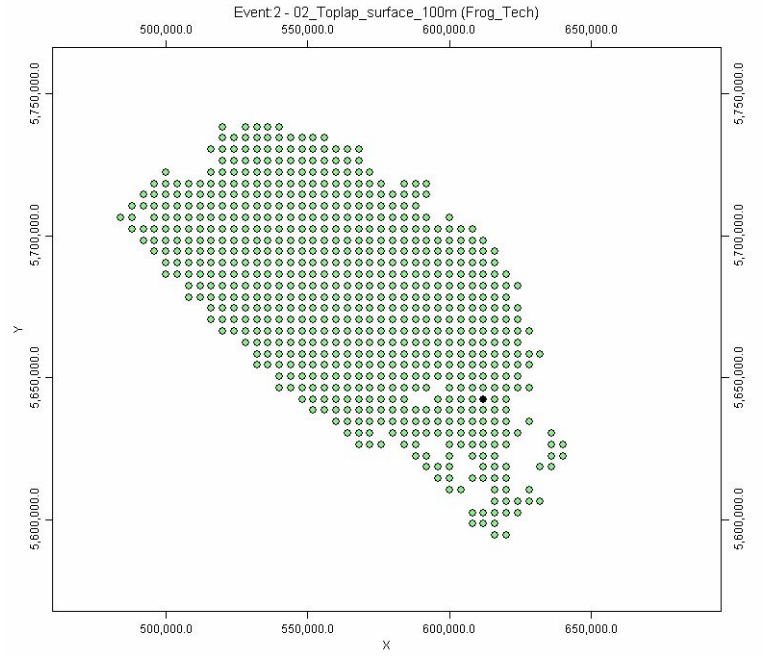

Figure 7.5 Creation of the pseudo-well matrix over the entire area of interest (A) and then with pseudo-wells that contain information in a particular interval (B).

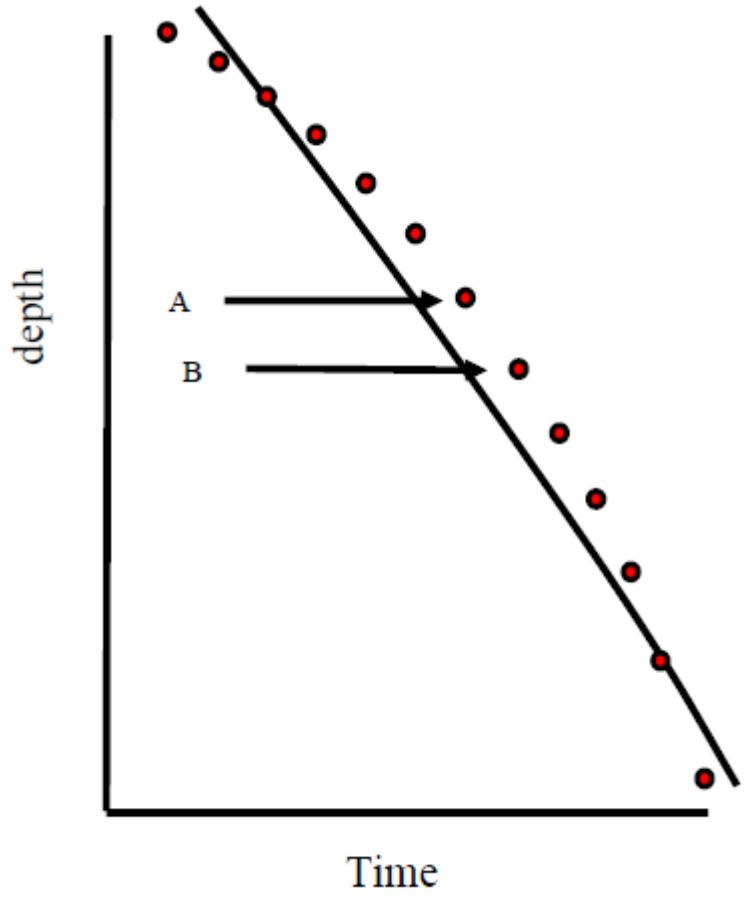

$$Z_b = \frac{1}{k}\left[\left(V_0 + kZ_t\right)e^{k\Delta t} - V_0\right]$$

Figure 7.6 Explanation of the optimisation process. For each pair of points on the time-depth curve we compare the known depth predicted by the function parameters. In the case of $Vz=V_0+kZ$ the depth conversion formula is shown in the yellow box. The best fit function is derived by minimising the RMS residual at each possible V_0, k pair.

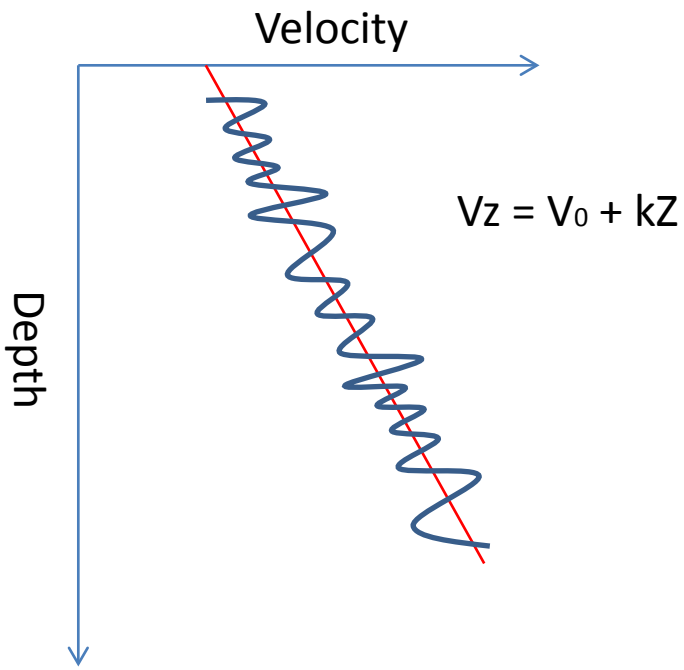

Vz = Instantaneous velocity at depth z
V_0 = Intercept of the line
k = Gradient of the line
Z = Depth

Figure 7.7 **Instantaneous velocity function used in this model. Blue is a velocity generated from a sonic log, red is the best fit straight line of the sonic log described by the function Vz.**

A

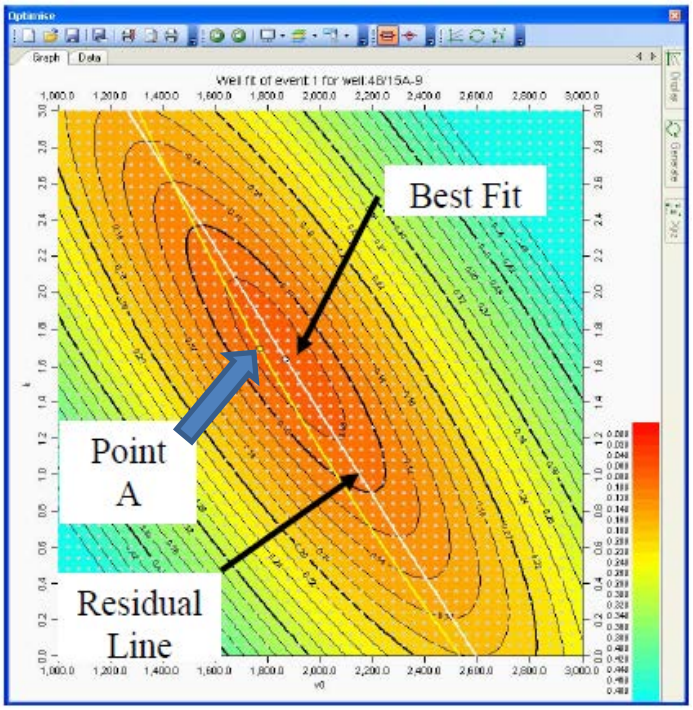

B

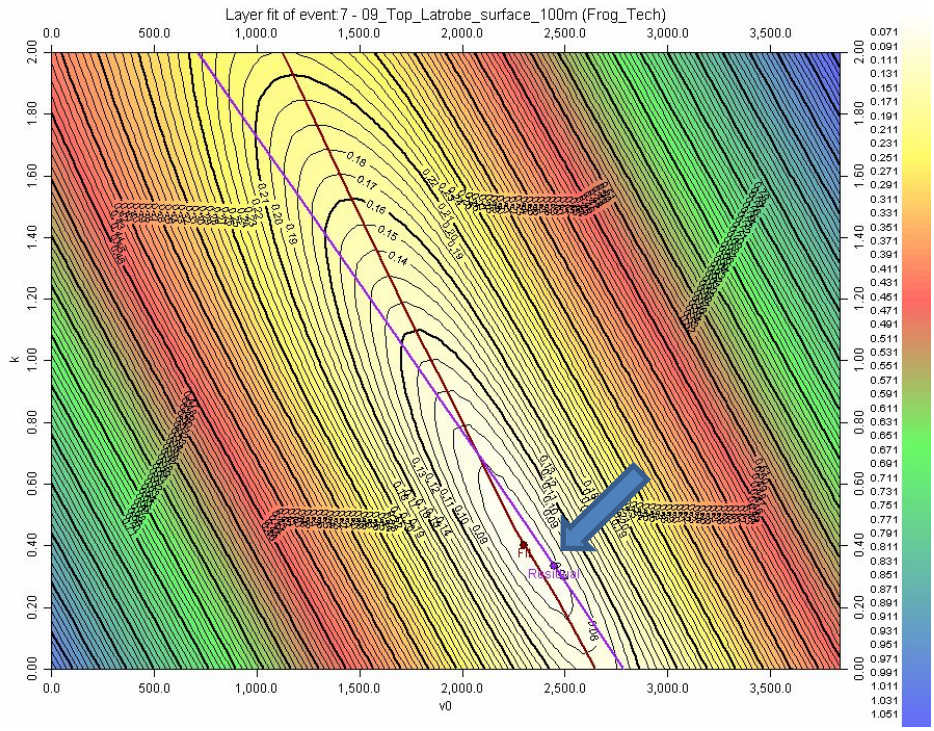

Figure 7.8 **Calculation of the residual and best fit instantaneous velocity using a single well for synthetic (A) and real data (B) from this study. For each node on the grid the fit for V_0, k pair with the log data at a single well is calculated. The residual line (yellow on A and purple in B) is also calculated such that any parameter pair down this line would result in a zero depth error. The optimal point on the residual is shown with the blue arrow on both plots and represents the calculated best combination of zero residual and best fit. This process is completed for each well.**

A

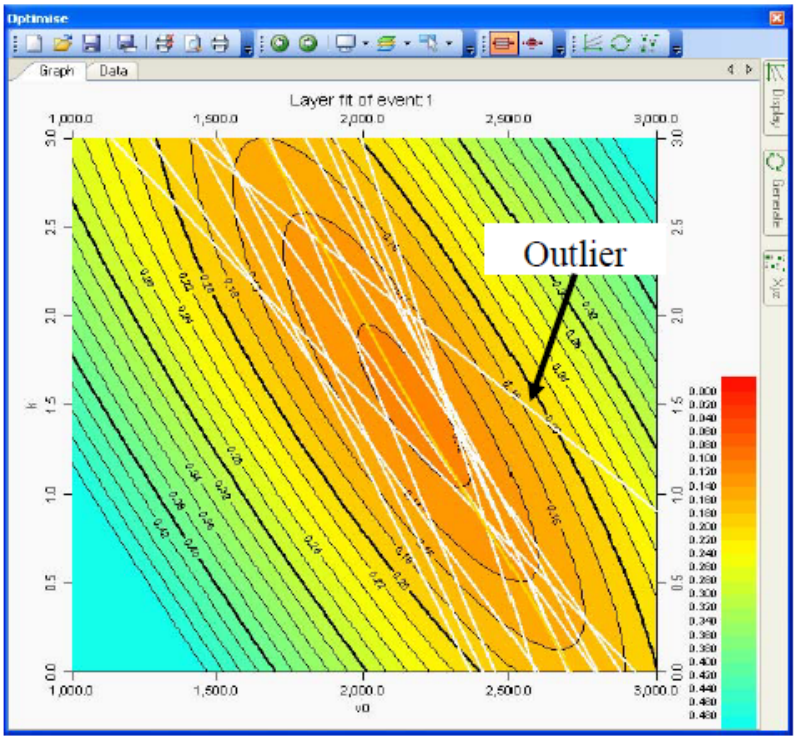

B

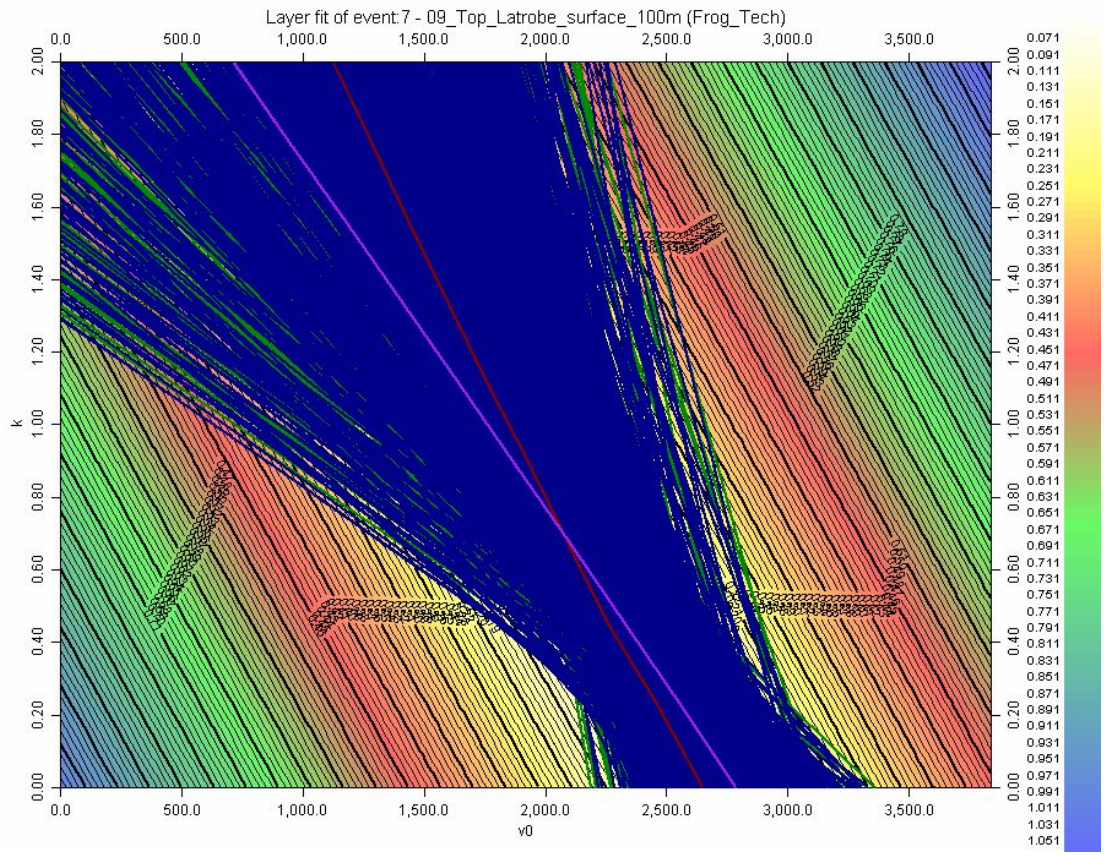

Figure 7.9 **Calculation of the mean best fit using all wells using synthetic (A) and real data (B) from this study. The tighter the cluster of lines the better the fit. Outliers can be identified and removed or re-assessed as required.**

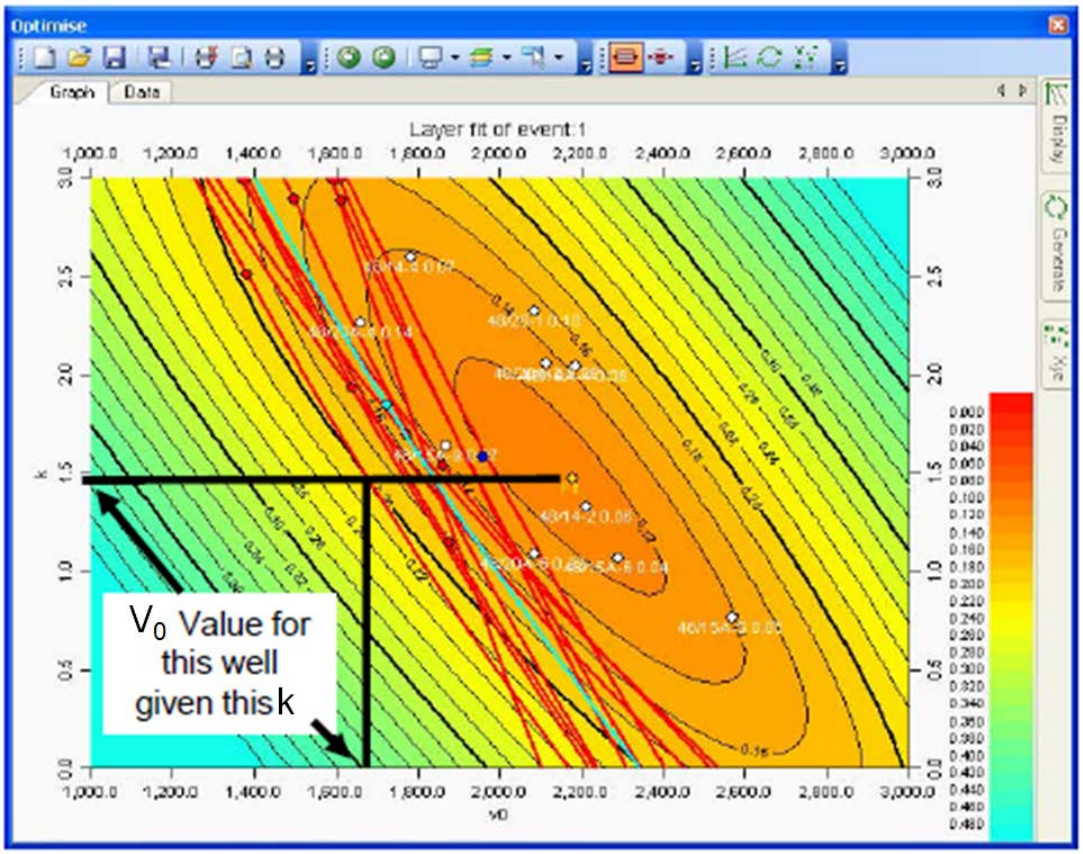

Figure 7.10 **Finally in the optimisation process one of the parameters can be fixed and the other contoured to provide a smooth variation between the wells and retain a reasonable velocity gradient. In the synthetic example above, the k value is set constant at the point of best fit and V_0 value determined at each well. The derived V_0 values are then gridded to produce the depth intercept grid (examples shown later – see Figure 7.21).**

7.2.6 Gridding and Depth Conversion

During the depth conversion process a series of grids are generated as standard output. The grids include average velocity, interval velocity (at midpoint of event), instantaneous velocity at construction surfaces, depth surfaces, isochrons and isopachs all of the construction surfaces. These outputs have been used as a broad QC of the distribution of velocities.

7.2.7 VELPAK Process 3 - Tie to Wells

Wells ties and corrections were applied where required. Twenty wells were available for this step, but not all wells contained every event (Table 7.2; Figures 7.11 to 7.14).

The main aim of this process was to understand how the distribution of velocities compared between the stacking velocities in the pseudo-wells and the sonic calibrated checkshot logs. This then allowed for a suitable correction to be applied to the instantaneous velocity function, where required for each event. The time-depth curves (Figures 7.11 to 7.14) show a general agreement between the calibrated checkshots and the time-depth pairs for the pseudo-logs in events 2 (C01 Seafloor – C02 Toplap), 3 (C02 Toplap – C03 Downlap), 5 (C04 Mid Miocene – C05 Slump Top), and 7 (C06 Slump Container – C07 Near Top Latrobe). At events 4 (C03 Downlap – C04 Mid Miocene), 6 (C05 Slump Top – C06 Slump Container) and 8 (C07 Near Top Latrobe – C08 Base Latrobe), the pseudo-well time-depth pairs show a higher velocity than reported from the real well data points. The instantaneous velocity function was decreased in each of these events to allow a good fit to the drilled wells. The amount of correction was 8% for event 4, and 15% for both events 6 (C05 Slump Top – C06 Slump Container) and 8 (C07 Near Top Latrobe – C08 Base Latrobe). Event 9 (C08 Base Latrobe – C09 Basement) shows a wide distribution of velocity both above and below the values from the wells. As velocities at depth are poorly constrained no correction was made to this level but the correlation to the wells is affected by the corrections made to the shallower surfaces. The match between the wells and the model surface before and after correction is given in Table 7.2.

The interval velocity plots (Figures 7.15 to 7.18) display a general increase in mean interval velocity except at events 5 (C04 Mid Miocene – C05 Slump Top) and 6 (C05 Slump Top – C06 Slump Container). The reduction in velocity seen at these levels relative to Event 4 (C03 Downlap – C04 Mid Miocene) is within statistical error given the complete range of velocity. However, more significant is the difference seen between events 6 (C05 Slump Top – C06 Slump Container) and 7 (C06 Slump Container – C07 Near Top Latrobe). These events are partially time equivalent and there is a significant decrease in average interval velocity in the disrupted area within the slump zone. Interval velocity in Event 8 (C07 Near Top Latrobe – C08 Base Latrobe) is highly variable, particularly on the southern half of the grid where the Latrobe Event is thinning onto the basement. Access to a reduced number of data points in this area may be contributing to the variability, along with the problem of calculating interval velocity in thin intervals. Although there is much variability, the overall thinness of the unit, particularly on the platform, means that this interval will have minimal impact on the velocity volume. As construction surfaces are slightly different to the interpreted stratigraphic surfaces, the ultimate impact of this variability needs to be assessed using the final interpretation. Figure 7.19 (A and B) shows the interval velocity within, and average velocity at the base of the Latrobe Group. Significant variability is observed in the interval velocity across the platform and at fault traces further to the north (Figure 7.19A). The variability is not observed in the average velocity (Figure 7.19B). Comparison between profiles in TWT and depth (Figure 7.20), across the region of high interval velocity variability show similar trends. There is no discernible footprint of the interval velocity variability.

7.2.8 VELPAK Process 4 - Generate Average Velocity Volume

An average velocity volume was generated using a 100 m grid, 4 ms vertical sample rate (Figures 7.21 to 7.24). The actual algorithm used to generate the velocity volume is not revealed in the VELPAK documentation. The inputs required to create the velocity volume are the interpreted construction surfaces (in time), intercept velocities (V_0) and the gradient value which is a measure of the variability of the intercept velocity (Figures 7.21 to 7.24). The intercept velocity (V_0) plots show a general increase in intercept velocity where data exist as indicated by the location of the pseudo-well points. Outside the area covered by the pseudo-well points there is no interval thickness and the velocity calculation is null for that interval. The sample interval used in the calculation of the average velocity model is 4 ms.

Mid Miocene Surface	Depth seismic datum (m)	Depth Conversion depth (m)	Difference (m)	% Difference	Depth conversion depth after correction (m)	Corrected difference (m)	Corrected % difference
Bluebone-1	272	286	14	4.90	276	4	-1.47
Groper-1	499	508	9	1.77	497	-2	0.40
Mullet-1	373	388	15	3.87	372	-1	0.27
Near Top Latrobe Surface							
Amberjack1	1238	1256	-18	1.43	1255	17	-1.37
Bullseye-1	2062	2100	38	1.81	2025	-37	1.79
Devilfish-1	1617	1682	65	3.86	1554	-63	3.90
Groper-1	922	929	7	0.75	929	7	-0.76
Kyarra-1A	982	1000	18	1.80	998	16	-1.63
Melville-1	2189	2271	82	3.61	2220	31	-1.42
Moray-1	1630	1659	29	1.75	1596	-34	2.09
Mudskipper-1	1448	1334	-114	-8.55	1438	-10	0.69
Mullet-1	680	684	4	0.58	684	4	-0.59
Omeo-2a	2224	2281	57	2.50	2170	-54	2.43
Perch-1	1097	1141	44	3.86	1145	48	-4.38
Pike-1	1808	1808	0	0.00	1800	-8	0.44
Pisces-1	1774	1919	145	7.56	1870	96	-5.41
Tarra-1	2109	2106	-3	-0.14	2106	-3	0.14
Tommyruff-1	876	871	-5	-0.57	871	-5	0.57
Wyrallah-1	853	854	-1	0.12	855	2	-0.23
Base Latrobe Surface							
Kyarra-1A	1220	1274	54	4.24	1224	4	-0.33
Perch-1	1528	1571	43	2.74	1517	-11	0.72
Tarra-1	2551	2571	20	0.78	2507	-44	1.72
Basement_surface							
Bluebone-1	582	610	28	4.59	587	5	-0.86
Groper-1	1009	1048	39	3.72	1047	38	-3.77
Mudskipper-1	1585	1589	4	0.25	1599	14	-0.88
Mullet-1	728	757	29	3.83	741	13	-1.79

Table 7.2 Comparison between depth-converted construction surfaces and formation tops in wells.

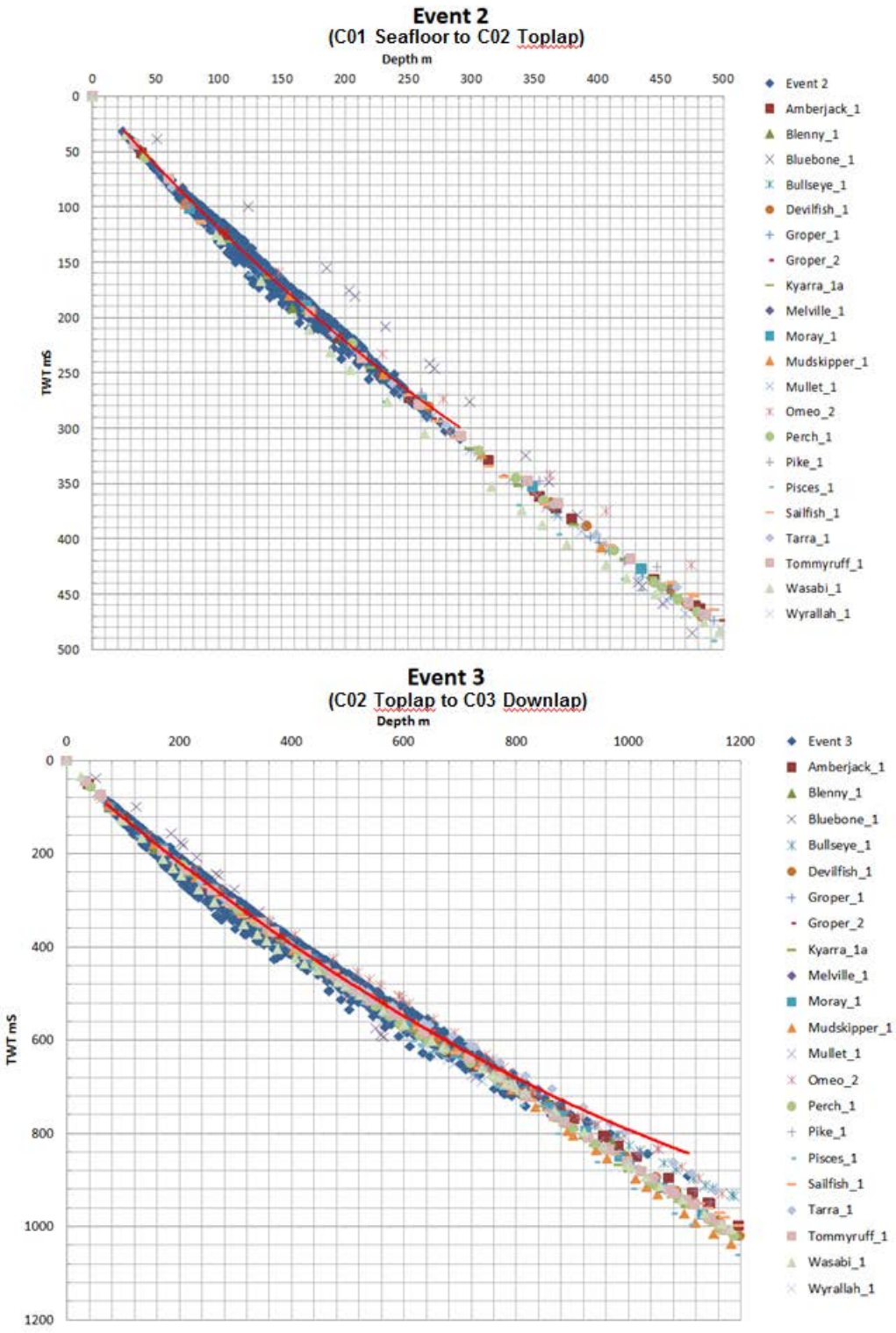

Figure 7.11 Time-depth pairs derived from pseudo-sonic logs (blue diamonds) compared with time-depth pairs from checkshot-calibrated sonic logs at wells for events 2 and 3.

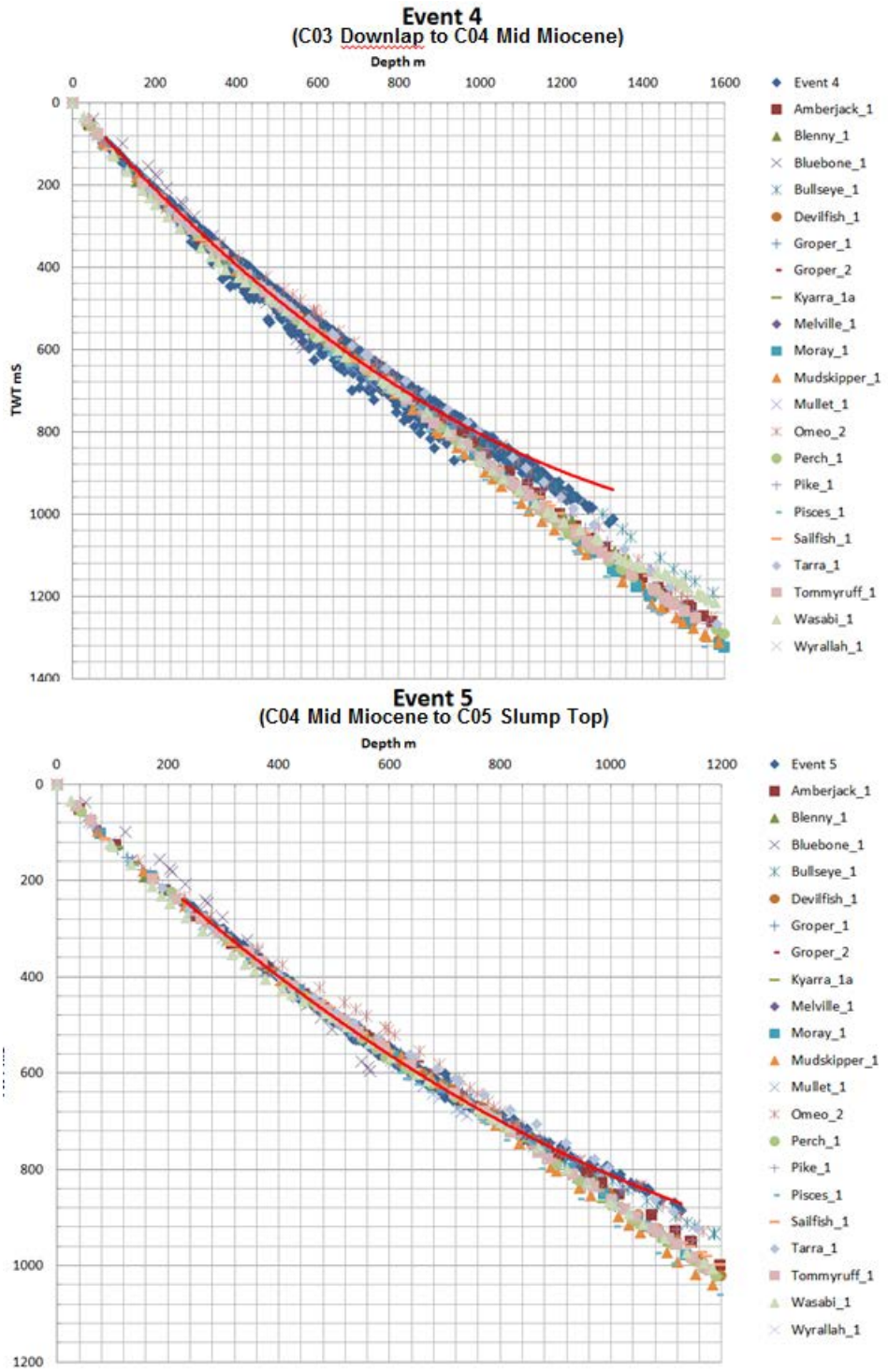

Figure 7.12 Time-depth pairs derived from pseudo-sonic logs (blue diamonds) compared with time-depth pairs from checkshot-calibrated sonic logs at wells for events 4 and 5.

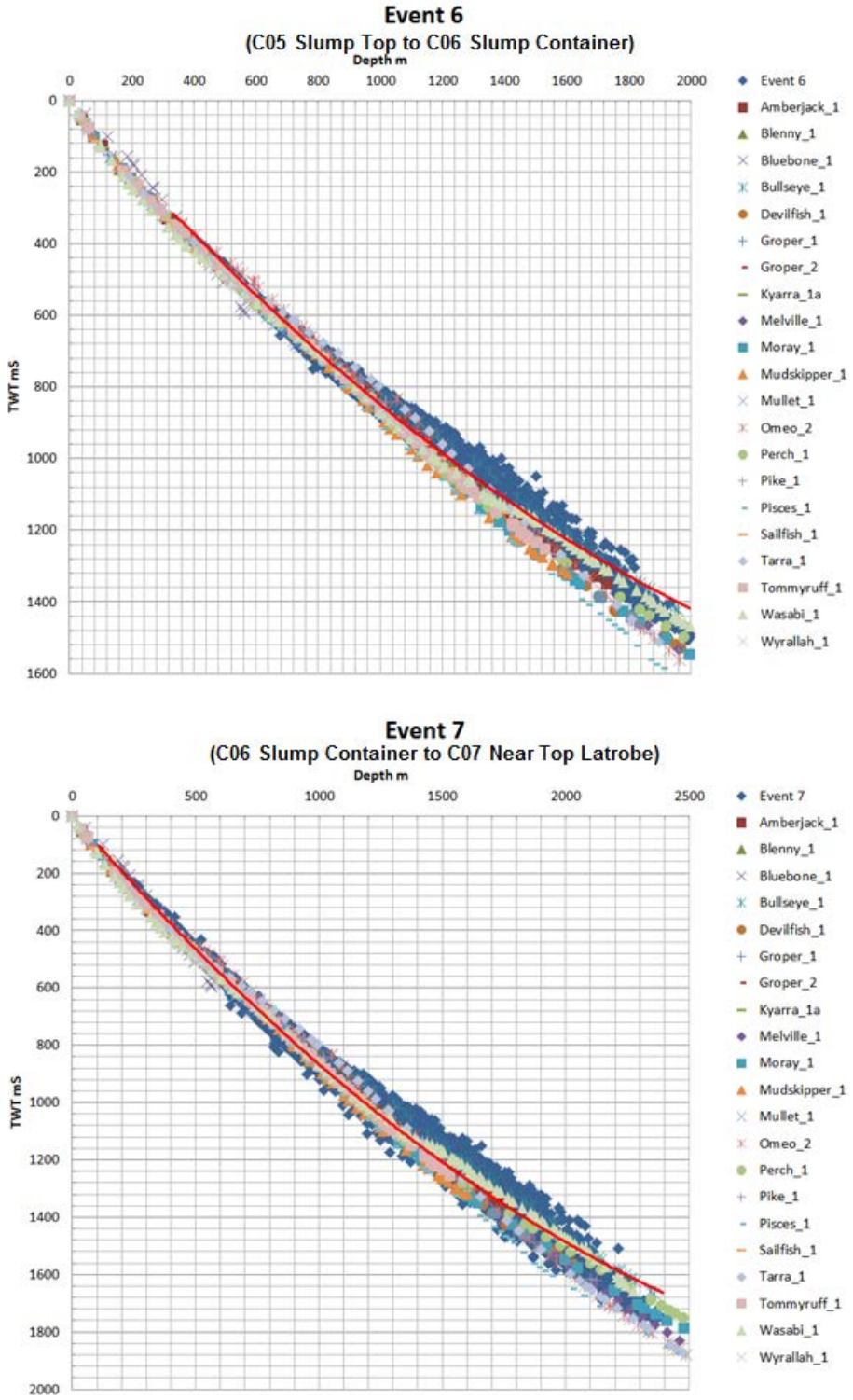

Figure 7.13 Time-depth pairs derived from pseudo-sonic logs (blue diamonds) compared with time-depth pairs from checkshot-calibrated sonic logs at wells for events 6 and 7.

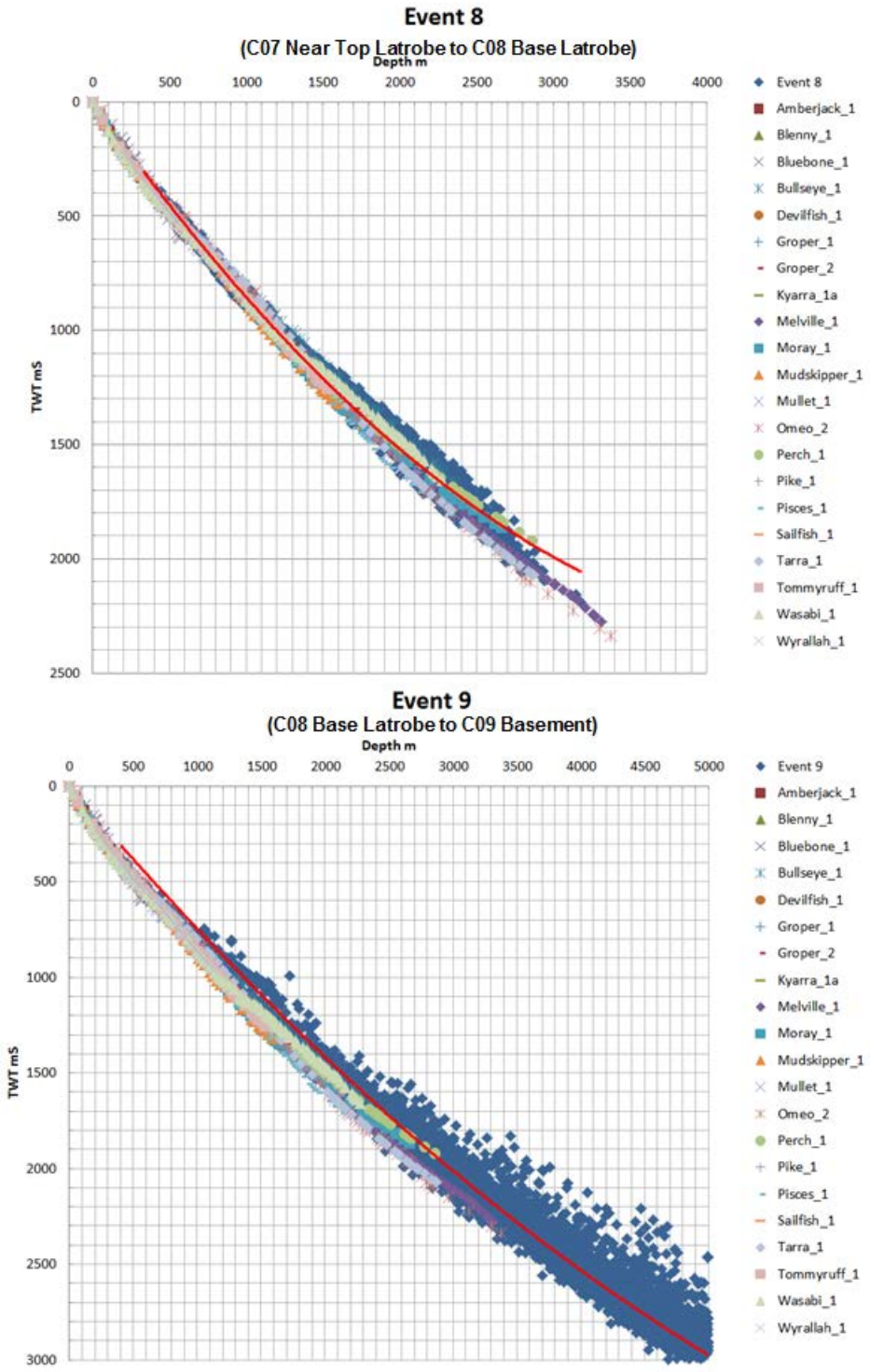

Figure 7.14 Time-depth pairs derived from pseudo-sonic logs (blue diamonds) compared with time-depth pairs from checkshot-calibrated sonic logs at wells for events 8 and 9.

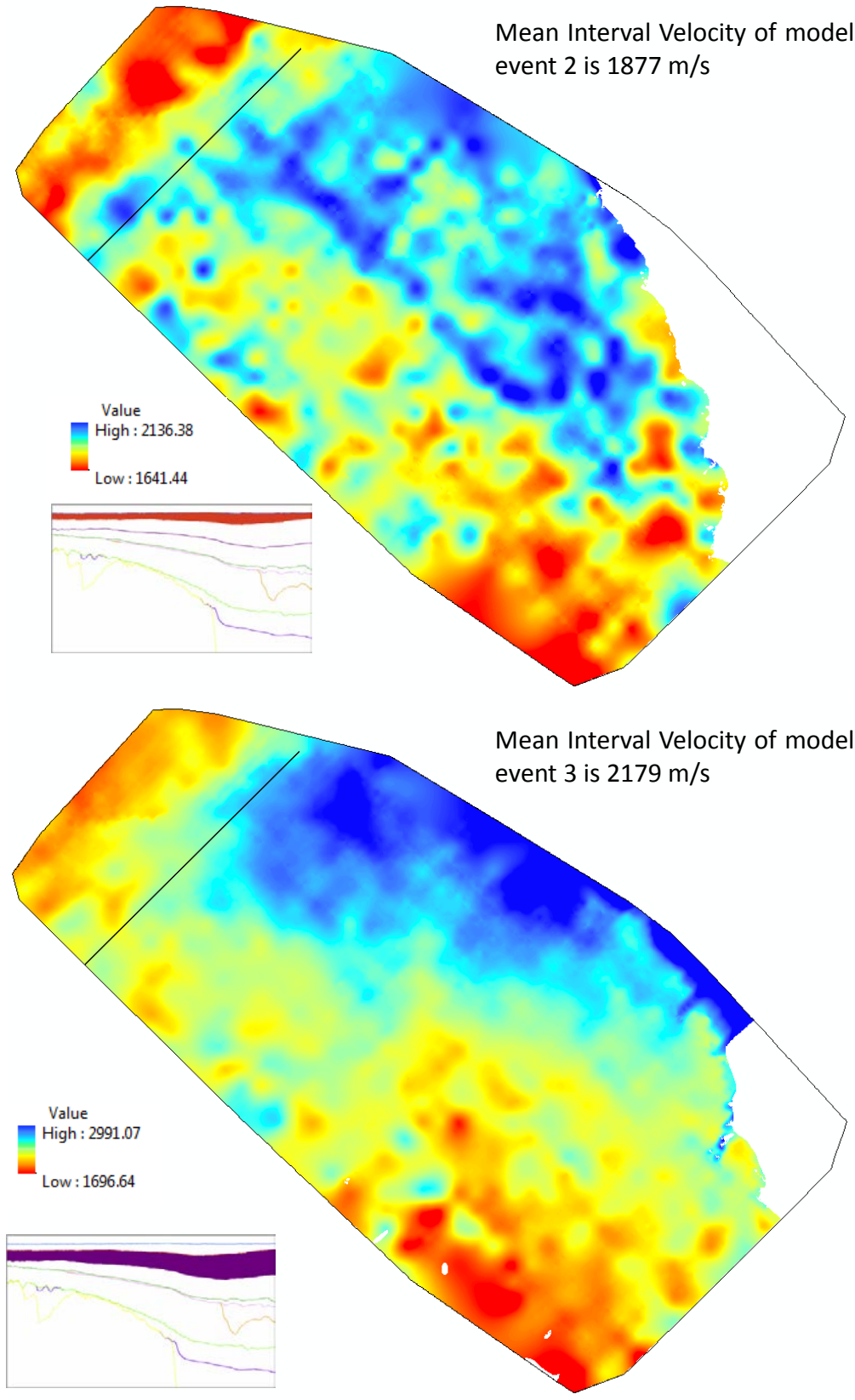

Figure 7.15 Variation of interval velocity for model events 2 (C01 Seafloor – C02 Toplap) and 3(C02 Toplap – C03 Downlap).

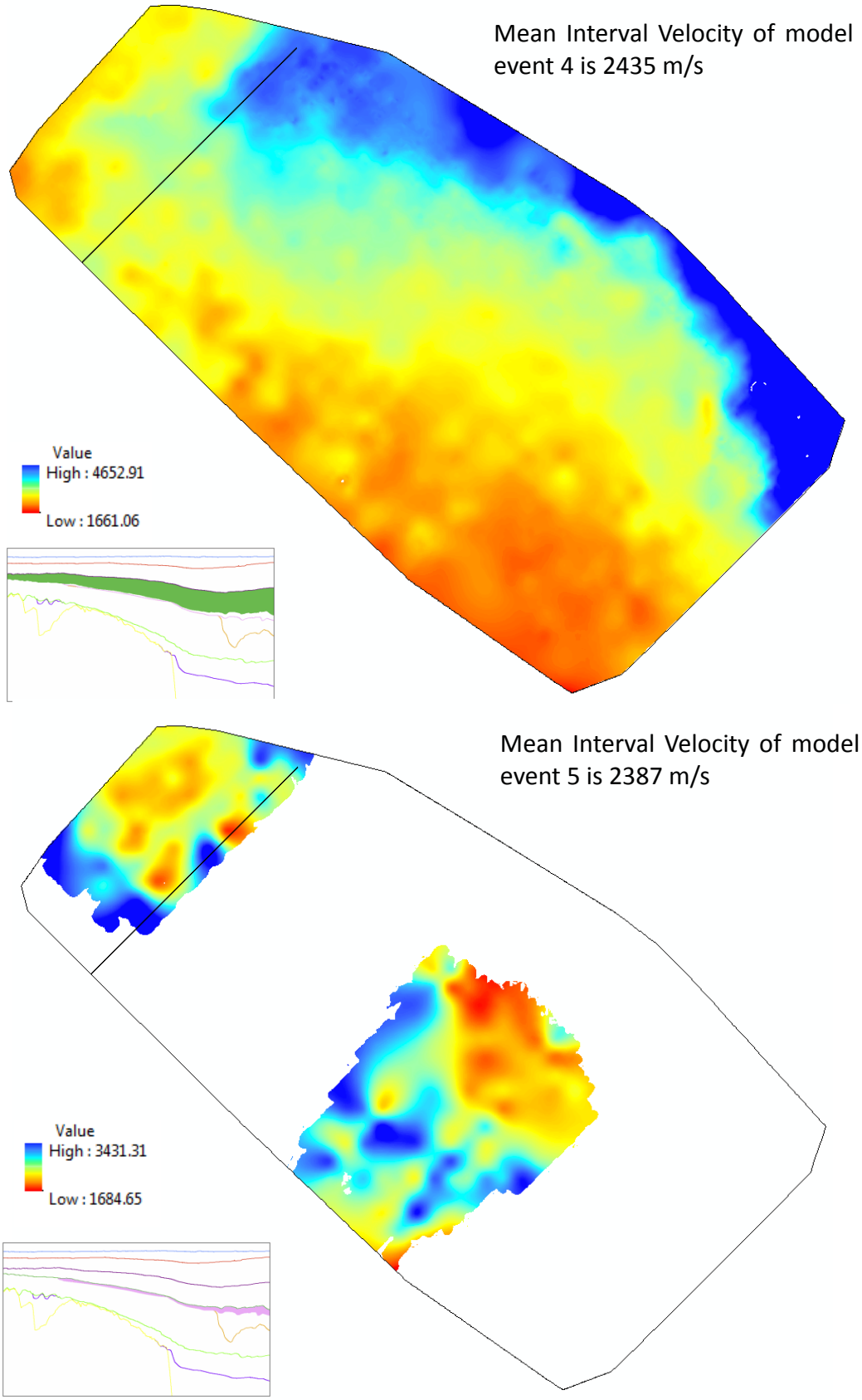

Figure 7.16 Variation of interval velocity for model events 4 (C03 Downlap – C04 Mid Miocene) and 5 (C04 Mid Miocene – C05 Slump Top).

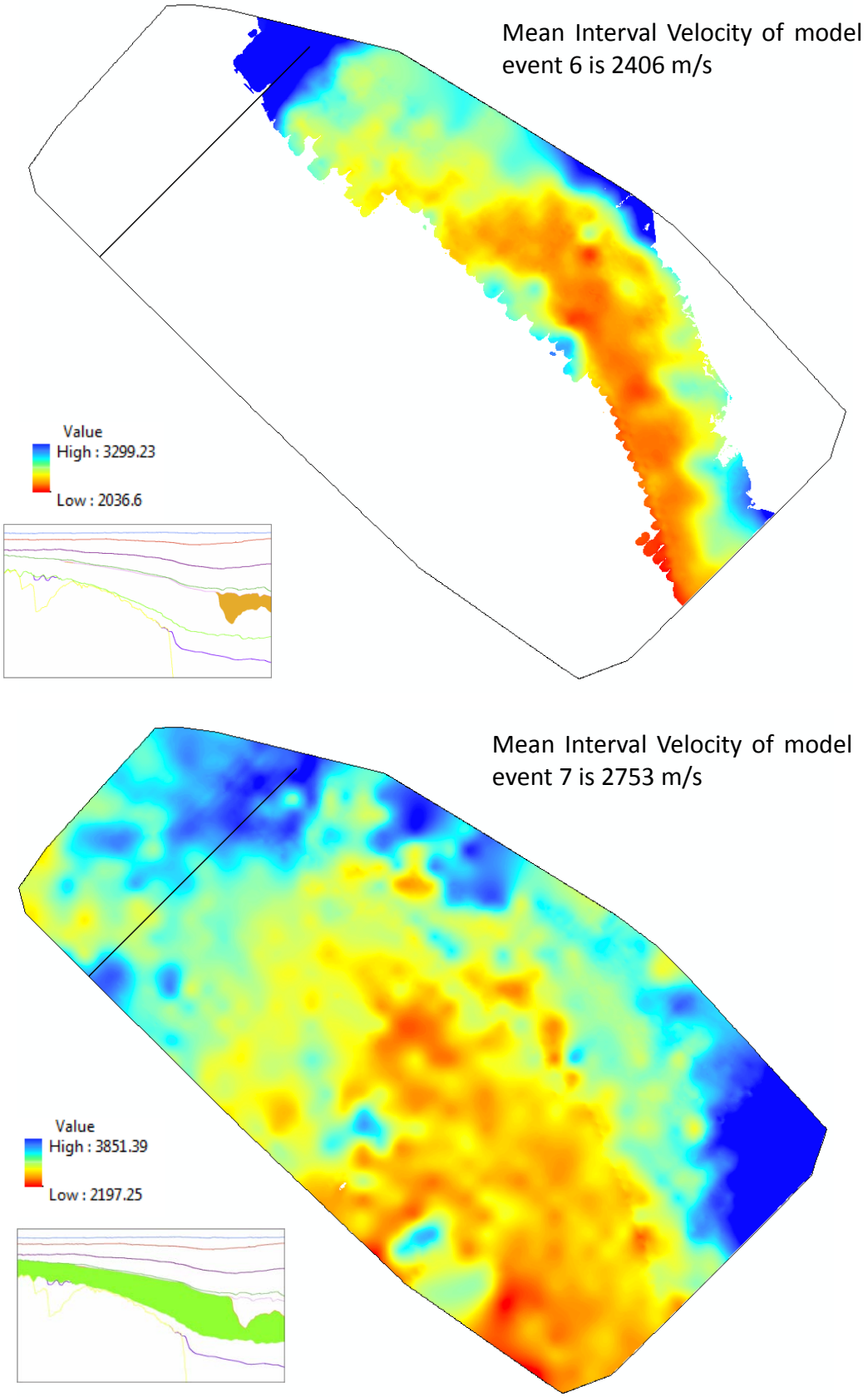

Figure 7.17 Variation of interval velocity for model events 6 (C05 Slump Top – C06 Slump Container) and 7 (C06 Slump Container – C07 Near Top Latrobe).

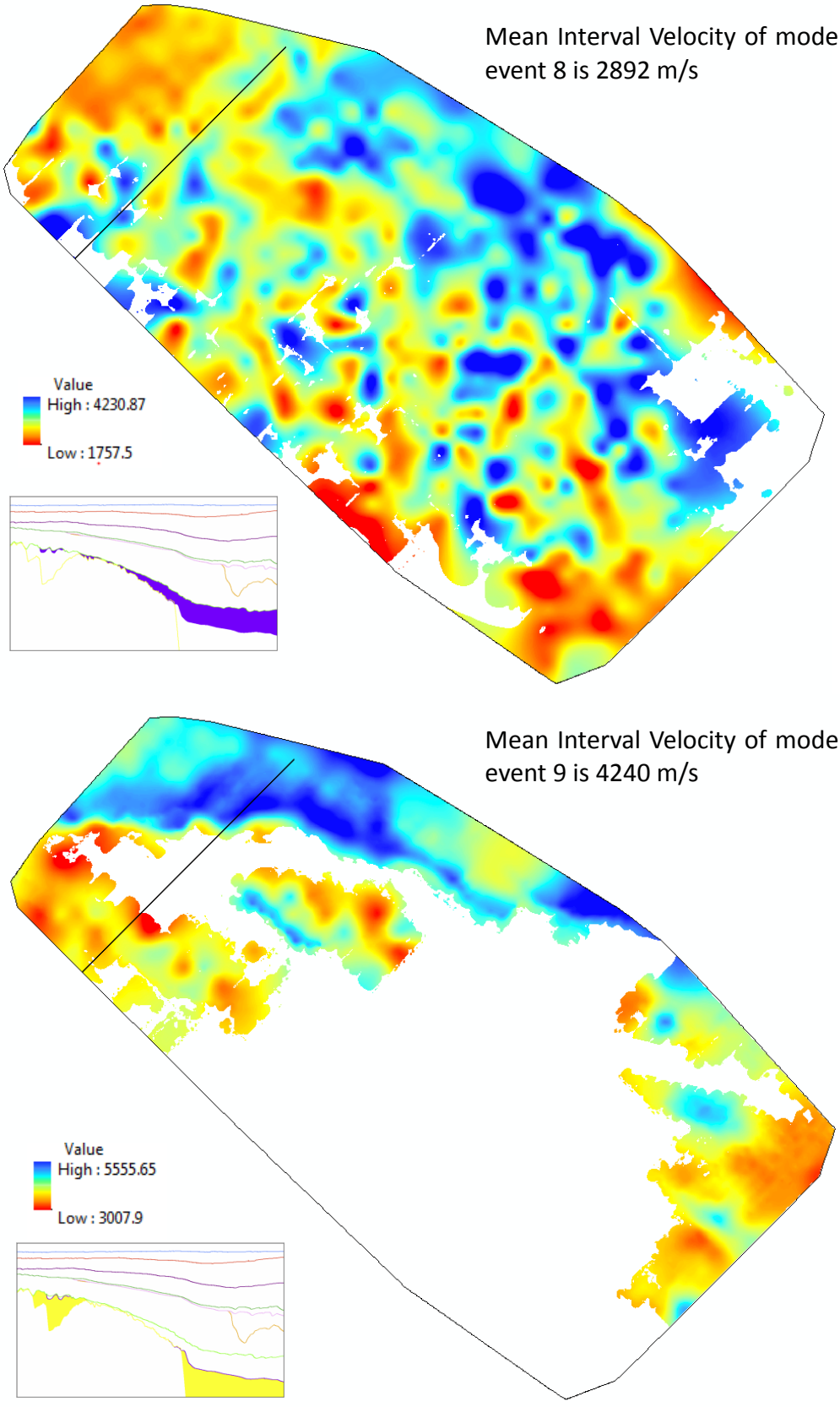

Figure 7.18 **Variation of interval velocity for model events 8 (C07 Near Top Latrobe – C08 Base Latrobe) and 9 (C08 Base Latrobe – C09 Basement).**

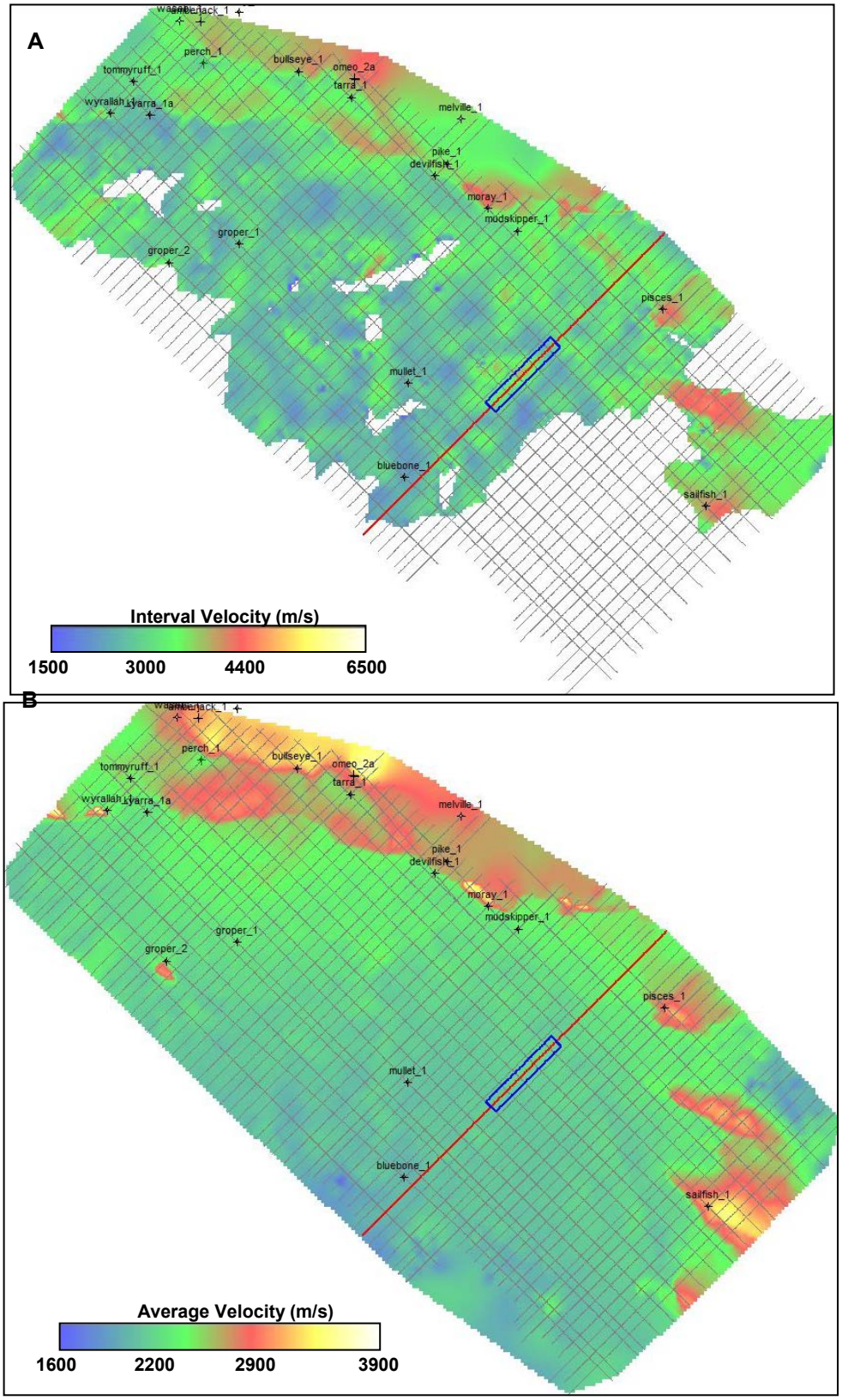

Figure 7.19 (A) Interval velocity within the Latrobe Group isopach from final interpreted horizons. (B) Average velocity at the base of the Latrobe Group.

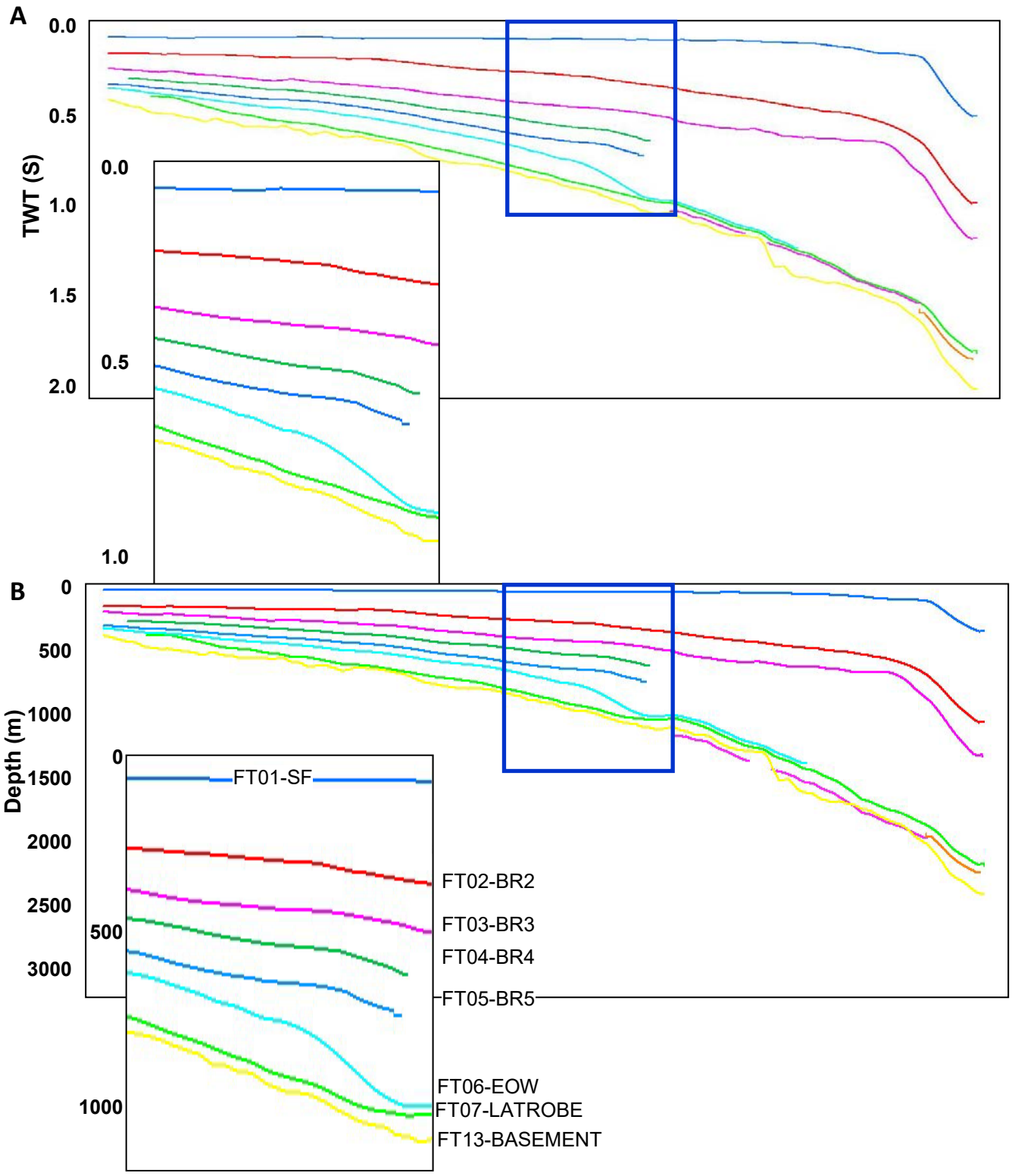

Figure 7.20 (A) Time and (B) depth sections at locations shown on previous figure. Although the interval velocity of the Latrobe isopach shows significant variability at the line location, the effect on the depth conversion is minimal. Interval velocity variability is greatest at the blue box as shown above and on the previous figure. Final interpreted horizons, not construction surfaces are shown.

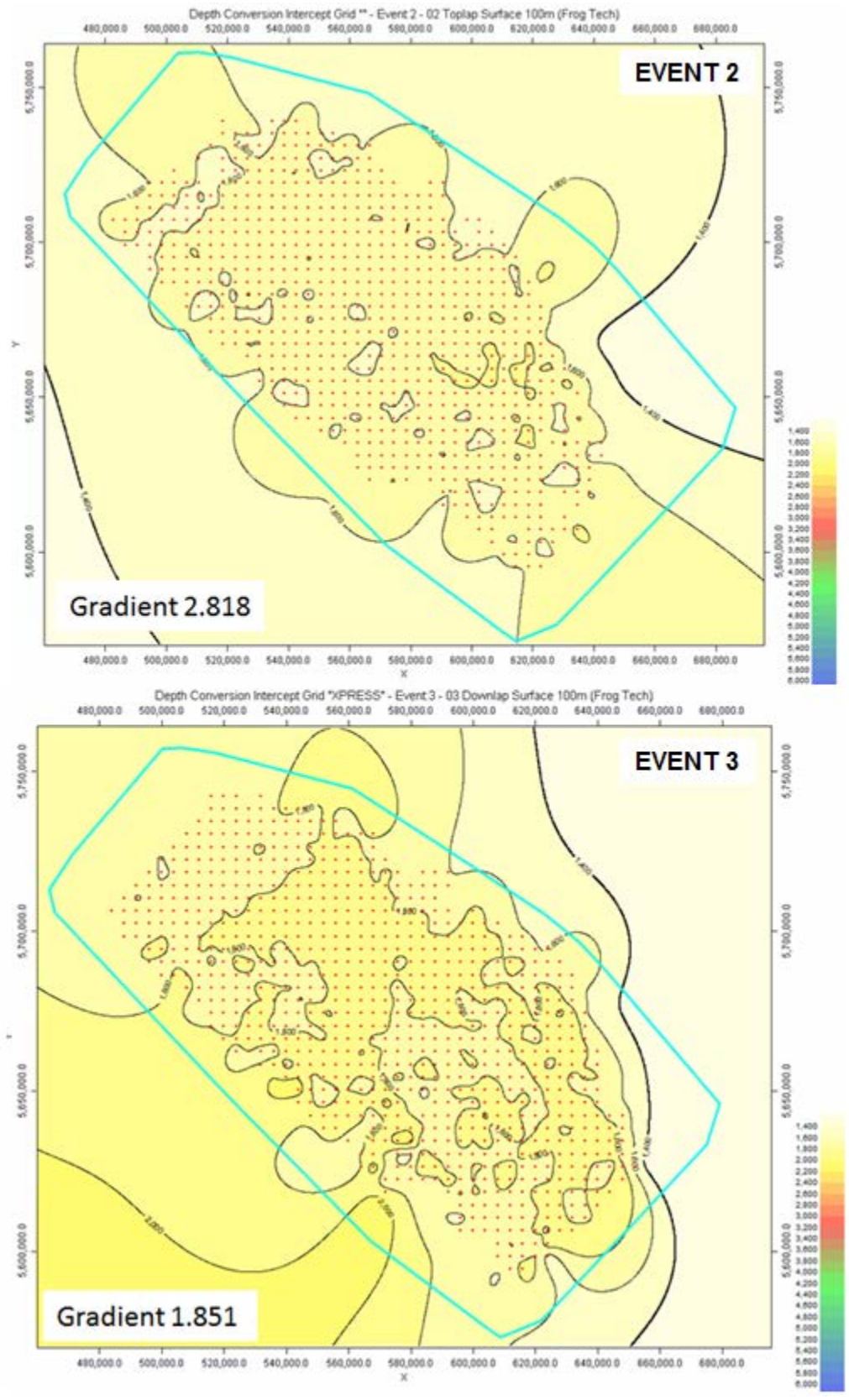

Figure 7.21 Intercept velocity (V_0) grids showing gradient (k) and pseudo-well locations for events 2 (C01 Seafloor – C02 Toplap) and 3 (C02 Toplap – C03 Downlap).

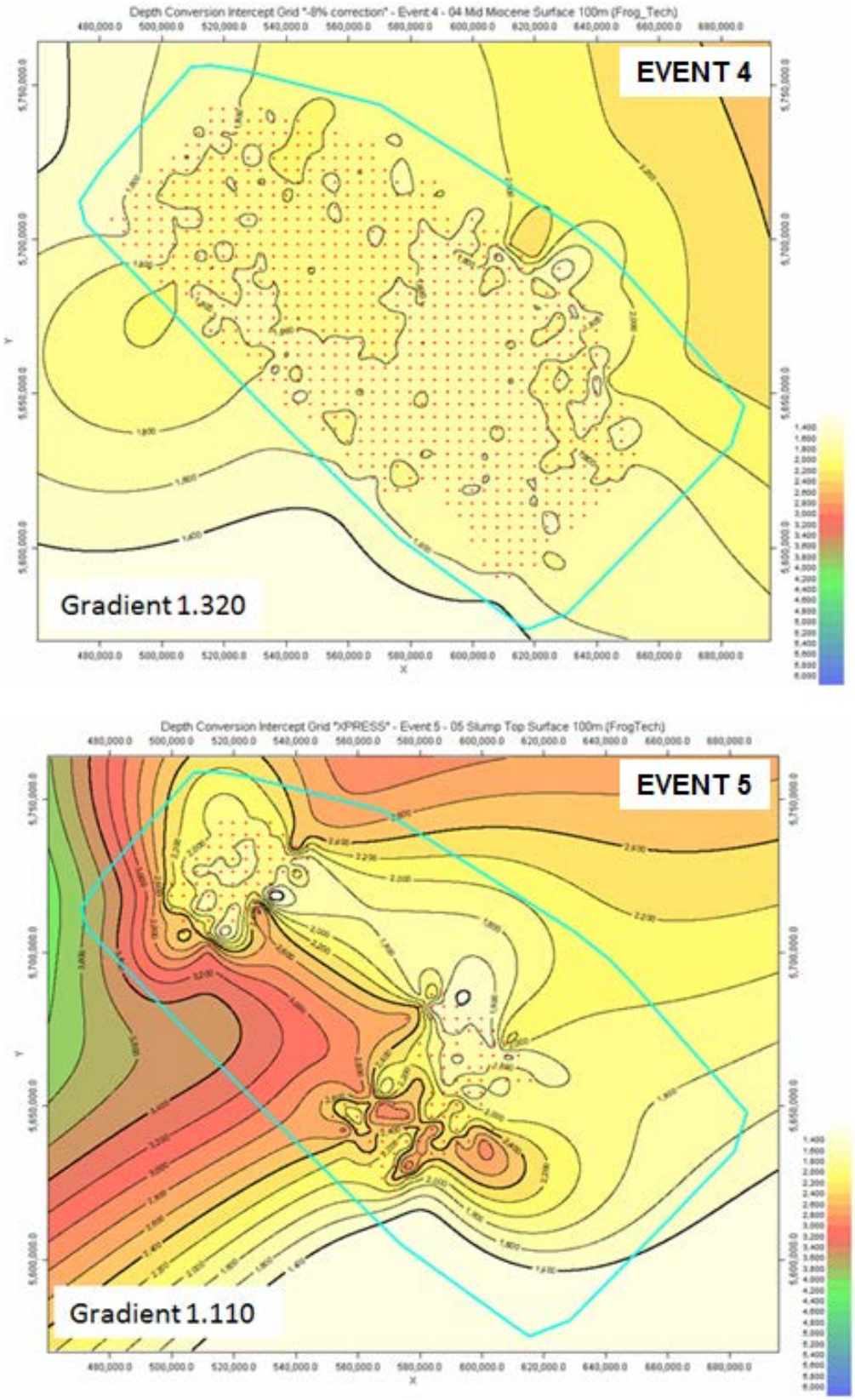

Figure 7.22 Intercept velocity (V_0) grids showing gradient (k) and pseudo-well locations for events 4 (C03 Downlap – C04 Mid Miocene) and 5 (C04 Mid Miocene – C05 Slump Top).

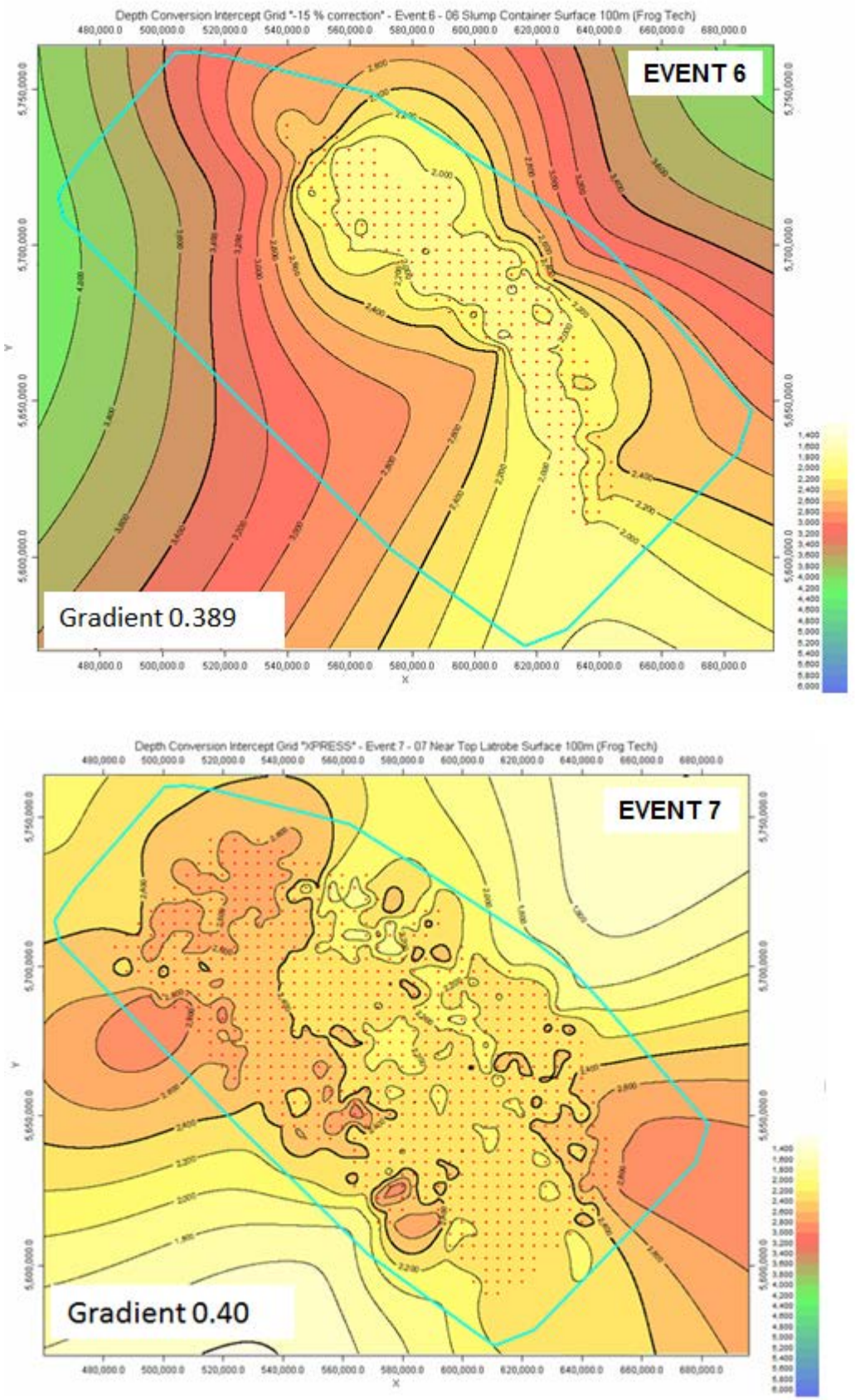

Figure 7.23 Intercept velocity (V_0) grids showing gradient (k) and pseudo-well locations for events 6 (C05 Slump Top – C06 Slump Container) and 7 (C06 Slump Container – C07 Near Top Latrobe).

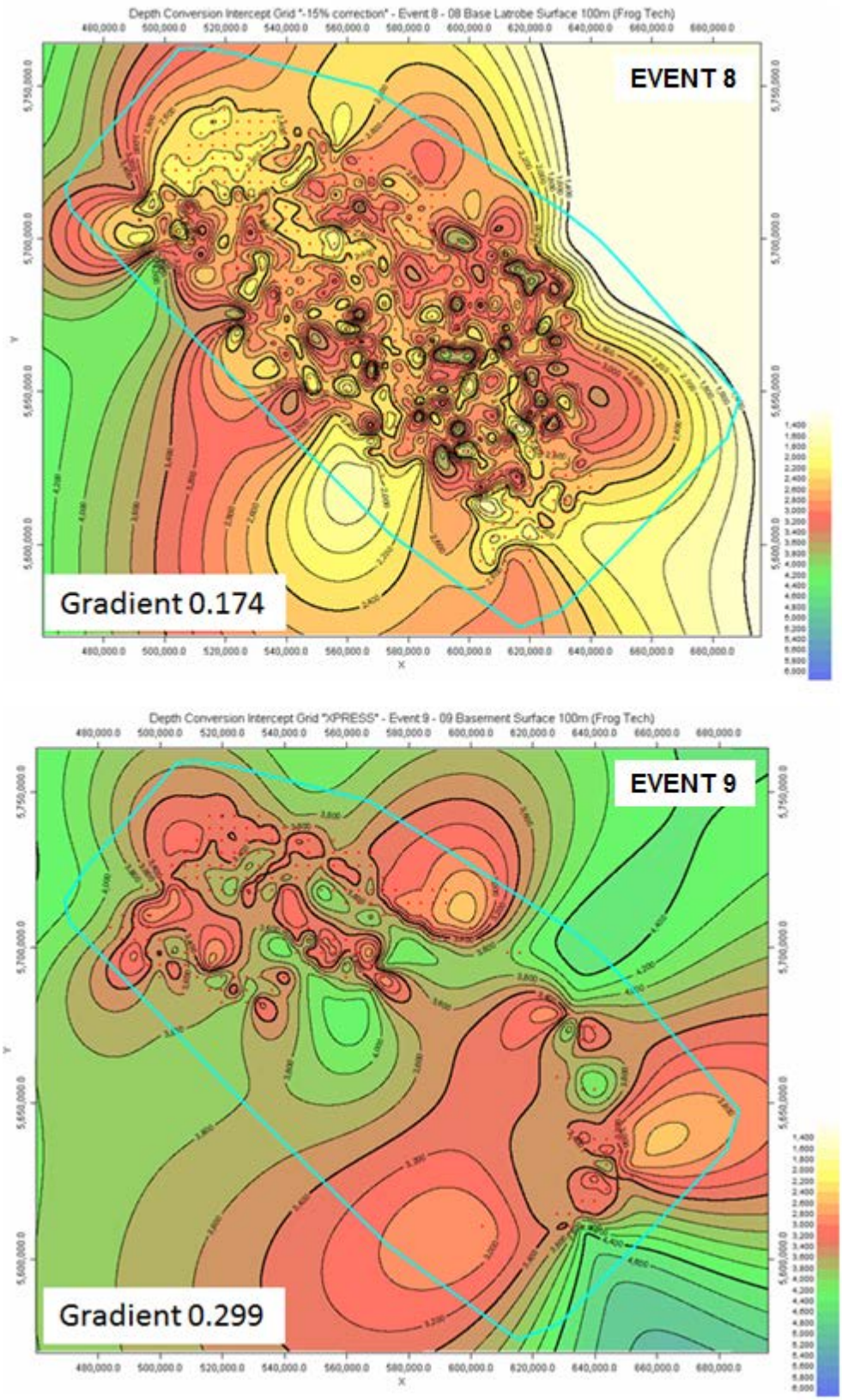

Figure 7.24 Intercept velocity (V_0) grids showing gradient (k) and pseudo-well locations for events 8 (C07 Near Top Latrobe – C08 Base Latrobe) and 9 (C08 Base Latrobe – C09 Basement).

7.3 Depth Conversion in GOCAD

The process to apply a velocity volume created in VELPAK to interpreted horizons and grids from 2D data in Kingdom 2d/3dPak does not exist within Kingdom at this stage.

GOCAD was used to bridge the gap between VELPAK and Kingdom 2d/3dPak. The average velocity model from VELPAK and gridded time surfaces from Kingdom were loaded into GOCAD and depth surfaces calculated (Figure 7.25).

7.4 Well Mis-tie Analysis and Correction using Kingdom 2d/3dPak

The final step in the depth conversion process is a correction at the well ties (Tables 7.3 and 7.4). With a few exceptions the mis-ties between the depth converted surface and the formation top pick in the wells is < +/-30 m. The FT_07_Top Latrobe Group surface is the most problematic of the suite of surfaces and required the largest corrections (Figure 7.26).

The output from this step is the final depth grid tied to well control. The final depth grids and isopachs have been presented in Section 6.

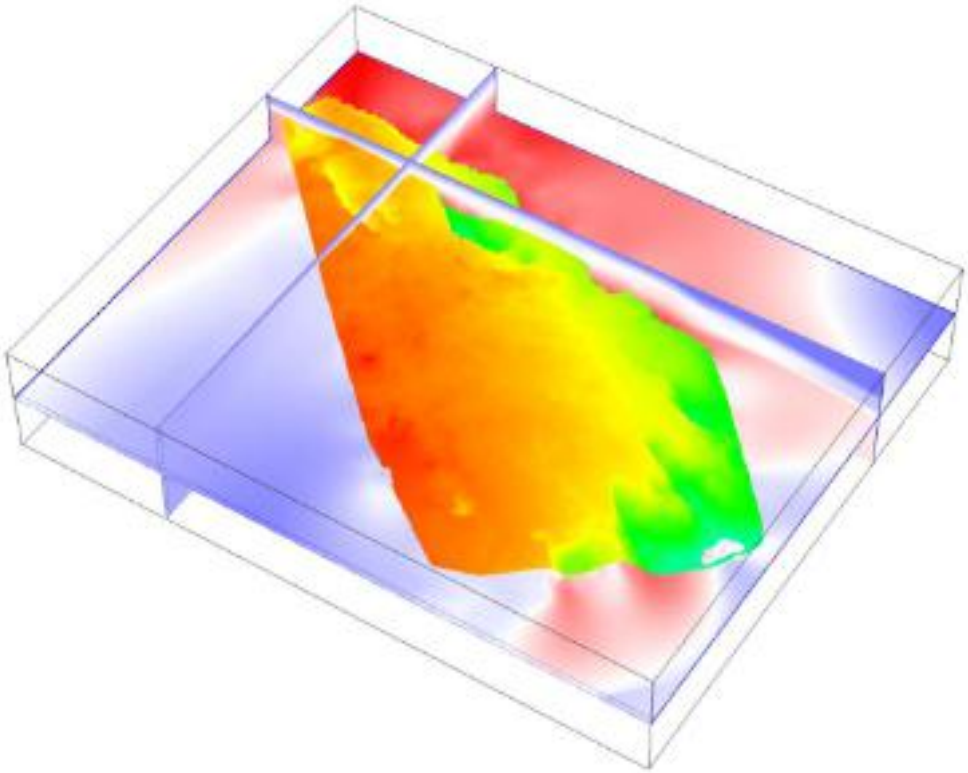

Figure 7.25 Inputs into GOCAD for the depth conversion are the gridded time surface (in this case the basement) and the average velocity volume (represented by the selected horizontal and vertical planes).

Well	X	Y	Well tie	Grid depth	Correction	Surface
amberjack_1	527608.2	5739647	37	38	-1	01 SF
bluebone_1	573123.5	5637886	38.76	54	-15.24	01 SF
bullseye_1	549449.8	5728572	58.2	61	-2.8	01 SF
devilfish_1	579967.4	5705240	74	79	-5	01 SF
groper_1	536127.6	5690092	57.6	65	-7.4	01 SF
groper_2	520632.6	5685834	59.59	63	-3.41	01 SF
kyarra_1a	516354	5718746	43.5	49	-5.5	01 SF
melville_1	585842.6	5717980	75	76	-1	01 SF
moray_1	591707	5698025	75.75	77	-1.25	01 SF
mudskipper_1	598334.4	5692905	73.99	75	-1.01	01 SF
mullet_1	574018.6	5658937	53	61	-8	01 SF
omeo_2a	561990.1	5726866	61.69	71	-9.31	01 SF
perch_1	528276.6	5730288	42.6	48	-5.4	01 SF
pike_1	582653.9	5707961	74.2	75	-0.8	01 SF
pisces_1	630915.2	5675649	122	132	-10	01 SF
sailfish_1	640502.7	5631443	85	85	0	01 SF
tarra_1	561228.7	5722701	62.5	66	-3.5	01 SF
tommyruff_1	512535.5	5726308	33	33	0	01 SF
wyrallah_1	507479.4	5719244	32	44	-12	01 SF
bluebone_1	573123.5	5637886	190.6	155	35.6	02 NT BR2
groper_1	536127.6	5690092	354.6	336	18.6	02 NT BR2
mullet_1	574018.6	5658937	250	210	40	02 NT BR2
bluebone_1	573123.5	5637886	272.6	278	-5.4	03 Top BR3
groper_1	536127.6	5690092	498.6	497	1.6	03 Top BR3
mullet_1	574018.6	5658937	373	374	-1	03 Top BR3

Table 7.3 **Comparison and defined correction between the depth-converted surfaces and formation tops in the wells for the FrOG Tech 01 Seafloor, FrOG Tech 02 Near Top Bassian Rise Unit 2 and FrOG Tech 03 Top Bassian Rise Unit 3.**

.

Well	X	Y	Well tie	Grid depth	Correction	Surface
bluebone_1	573123.5	5637886	407	400	7	05 Top BR5
mullet_1	574018.6	5658937	550	545	5	05 Top BR5
groper_1	536127.6	5690092	735	723	12	05 Top BR5
bluebone_1	573123.5	5637886	452	449	3	06 Top EOW
groper_1	536127.6	5690092	798	799	-1	06 Top EOW
kyarra_1a	516354	5718746	889	885	4	06 Top EOW
mullet_1	574018.6	5658937	609	614	-5	06 Top EOW
omeo_2a	561990.1	5726866	2160	2121	39	06 Top EOW
tommyruff_1	512535.5	5726308	819	799	20	06 Top EOW
amberjack_1	527608.2	5739647	1238	1257	-19	07 Top Lt
bullseye_1	549449.8	5728572	2062	2033	29	07 Top Lt
devilfish_1	579967.4	5705240	1617	1589	28	07 Top Lt
groper_1	536127.6	5690092	922	953	-31	07 Top Lt
kyarra_1a	516354	5718746	982	1010	-28	07 Top Lt
melville_1	585842.6	5717980	2189	2247	-58	07 Top Lt
moray_1	591707	5698025	1630	1614	16	07 Top Lt
mudskipper_1	598334.4	5692905	1448	1466	-18	07 Top Lt
mullet_1	574018.6	5658937	680	703	-23	07 Top Lt
omeo_2a	561990.1	5726866	2224	2195	29	07 Top Lt
perch_1	528276.6	5730288	1097	1140	-43	07 Top Lt
pike_1	582653.9	5707961	1808	1825	-17	07 Top Lt
pisces_1	630915.2	5675649	1774	1880	-106	07 Top Lt
tarra_1	561228.7	5722701	2109	2123	-14	07 Top Lt
tommyruff_1	512535.5	5726308	876	878	-2	07 Top Lt
wyrallah_1	507479.4	5719244	852.97	875	-22.03	07 Top Lt

Table 7.4 **Comparison and defined correction between the depth-converted surfaces and formation tops in the wells for the FrOG Tech 05 Top Bassian Rise Unit 5, FrOG Tech 06 Top Early Oligocene Wedge and FrOG Tech 07 Top Latrobe Group.**

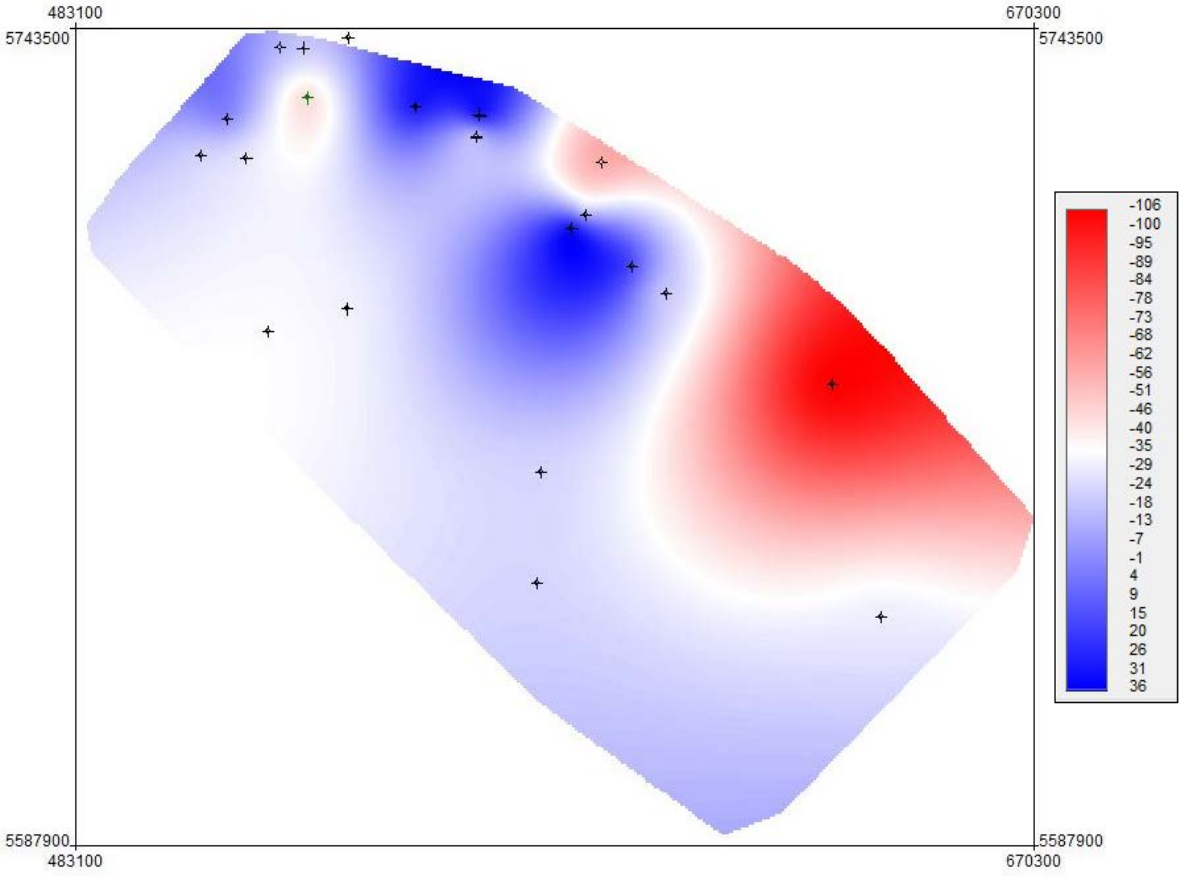

Figure 7.26 Correction grid for the FrOG Tech 07 Top Latrobe Group depth surface to tie with the formation tops in the wells.

8 Conclusions and Recommendations

FROGTECH has completed the interpretation of 13 horizons on the 8000 km seismic survey with ties to 20 key wells distributed across the Southern Flank. A velocity model was developed for the region, and calibrated to velocity information within the wells. Collectively, the resultant project is an integrated and depth-converted, seismic stratigraphic interpretation and geological model for the Southern Flank of the Gippsland Basin. The interpretation will be used by DPI and GA for continuing research on the greenhouse gas storage potential of the Gippsland Basin. Geological information will be used to construct regional geological models, and to carry-out petroleum systems modeling and prospectivity assessments. The interpretation forms part of the pre-competitive open-file data set available as a result of the acquisition of the 8000 km 2D seismic survey of the Southern Flank of the Gippsland Basin.

The 13 interpreted horizons and 10 isopach intervals (listed below) are slightly different to those requested in the DPI Tender. Changes to the deliverables were made in consultation with DPI and were driven by the geological differences between significant stratigraphic intervals on the Southern Flank (study area) relative to the Central Deep:

REQUESTED HORIZONS	INTERPRETED HORIZONS
Seafloor	FrOG Tech 01 Seafloor
	FrOG Tech 02 Near Top Bassian Rise Unit 2
Mid-Miocene Marker	FrOG Tech 03 Top Bassian Rise Unit 3
	FrOG Tech 04 Top Bassian Rise Unit 4
Top Lakes Entrance Formation	FrOG Tech 05 Top Bassian Rise Unit 5
	FrOG Tech 06 Top Early Oligocene Wedge
Top of the Latrobe Group	FrOG Tech 07 Top Latrobe Group
	FrOG Tech 08 Top Halibut Subgroup
Top Cretaceous (near K-T boundary)	
Top of Golden Beach Sub-group	FrOG Tech 09 Top Golden Beach Subgroup
	FrOG Tech 10 Top Emperor Subgroup
Top of the Strzelecki Group	FrOG Tech 11 Top Strzelecki Group
	FrOG Tech 12 Top Pre-Strzelecki Group
Basement	FrOG Tech 13 Top Basement

Listing of originally requested and final interpreted horizons from the GDPI10 2D seismic survey on the southern flank of the Gippsland Basin. Additional horizons were interpreted (bold), with only the Top Cretaceous removed from the originally requested horizons.

ISOPACH/ISOCHRON UNIT	INTERPRETED HORIZONS
Total sediment thickness	FrOG Tech 01 to FrOG Tech 13
Mid Miocene and Younger	FrOG Tech 01 to FrOG Tech 03
Mid Miocene to top EOW	FrOG Tech 03 to FrOG Tech 06
EOW	FrOG Tech 06 to FrOG Tech 07
Latrobe Group	FrOG Tech 07 to FrOG Tech 11
Cobia Subgroup	FrOG Tech 07 to FrOG Tech 08
Halibut and Golden Beach subgroups	FrOG Tech 08 to FrOG Tech 10
Emperor Subgroup	FrOG Tech 10 to FrOG Tech 11
Strzelecki Group	FrOG Tech 11 to FrOG Tech 13
?Pre-Strzelecki Group	FrOG Tech 12 to FrOG Tech 13

Listing of isopachs/isochrons generated in the project and relationship to the interpreted horizons.

8.1 Conclusions

- **Structural Framework:**

  The Top Basement depth structure map and basement fault interpretation has defined the underlying structural framework of the study area. The main controlling features are:

  1) The rigid, cratonised basement block beneath the Southern Platform. The nature of the basement has resulted in the formation of isolated half-graben during extensional events, such as the newly identified McLoughlins Sub-basin (~ 6 km deep). The effects of extension are more readily identified along the edges of the basement block with the formation of the more extensive Foster and Darriman fault systems.

2) The Foster Fault System (FFS) which separates the Southern Platform and Southern Terrace. The FFS is a fundamental structural boundary that was reactivated in the early-middle Miocene, triggering instability and collapse of the overlying carbonate shelf, resulting in a significant slump zone along the Southern Terrace. The fault system was a focus for volcanic intrusions during periods of extension. Relay zones formed important sediment pathways to the Southern Terrace and were the site for local inversion such as observed at Moray-1.

3) The rugose topography of the Southern Platform, including a central zone of basement highs, that have acted as a sediment source during deposition of the Latrobe Group and the Early Oligocene Wedge. The Southern Platform also experienced minimal subsidence and was a prominent sediment source until the Campanian.

4) The Pisces Sub-basin has been re-interpreted as a series of NE-trending en-echelon half graben that cut across the easternmost margin of the Southern Platform. The extensional faults were reactivated prior to breakup in the Tasman Sea off the Gippsland Basin. Here, sediments are locally disrupted by seismic anomalies suggesting vertical migration of fluids related to volcanism and igneous intrusions.

- **Latrobe Group Reservoirs:**

  New mapping clearly shows for the first time that the Halibut Subgroup extends from the Southern Terrace (where it has been intersected by drilling), across the Foster Fault System and well onto the Southern Platform. Within this interval, extensive sand sheets are identified between the central platform basement ridge and the FFS and funneled from the Southern Platform onto the Southern Terrace at relay points along the FFS.

  The Cobia Subgroup has also been mapped and is more extensive across the Southern Platform than previously interpreted. The Cobia Subgroup thins on the updip and eastern parts of the Southern Platform where it infills the rugose basement topography and onlaps the basement highs.

  The broader extent of both Halibut and Cobia reservoirs will have implications for greenhouse gas injection models. New maps have also been produced for the older Latrobe Group intervals (Emperor and Golden Beach subgroups) where deposition has been strongly controlled by the Foster Fault System and related structures.

- **Potential Sealing Facies and Risks– The Early Oligocene Wedge:**

  The nature and distribution of sealing facies are relatively more complex in the study area than the Central Deep. Contrary to previous interpretations, the Lakes Entrance Formation is not the regional sealing facies for Top Latrobe reservoirs across the Southern Platform. Instead, an older, thick progradational, regionally extensive succession known as the Early Oligocene Wedge (EOW) overlies Latrobe Group sediments. The EOW forms the lowermost of a series of progradational carbonate wedges that were deposited through to the late Miocene. The EOW displays mostly topset and low-angle progradational internal stratal geometries. The sealing characteristics of the basal EOW facies are here considered variable in age, thickness and lithology. The EOW is absent over the easternmost Southern Platform and thins to downlap across the Southern Terrace. In its condensed downlap location, sediments of the EOW could be confused with a thinned succession of the Gurnard Formation.

  From this interpretation two potential scenarios where the EOW could have good sealing potential are suggested:

  1) Where the wedge is thickest.

  2) Where the wedge downlaps and the distal toes could represent fine-grained condensed sedimentation.

Identified risks associated with the EOW sealing potential include:

1) Proximity to the central platform ridge.

2) Post-depositional reactivation along the Foster Fault System.

3) The slump complex which may locally consume the upper part of the EOW.

4) Local faulting of the EOW that occurs updip of the slump feature.

5) Inversion/uplift in the western basin.

An optimal area has been predicted, largely overlying the Southern Terrace, where the relative EOW seal potential is high and the risks are considered low.

- **Other Potential Seal Facies:**

  The seal assessment of the Southern Flank focused on the Cobia and Halibut subgroup reservoirs, and sealing facies of the EOW. The Gurnard Formation is here considered a more complex facies that requires further work beyond the scope of this study to determine its true age, lithology and sequence stratigraphic framework. The Gurnard Formation is predicted to be an important sealing facies in the western part of the study area. Elsewhere, the unit is too thin and underlies a condensed section of the distal EOW. The EOW does not directly overlie the Halibut Subgroup within the study area, thus seals for these reservoirs rely on intraformational shales or basal shales within the overlying Cobia Subgroup. The detailed mapping of individual intraformational seals within the Cobia and Halibut subgroups is beyond the scope of the current study but is recommended for future work.

- **Slump Complex**:

  Much of the EOW to mid-Miocene succession is consumed by a large slump zone that spans the length of the outer Southern Platform and extends across parts of the Southern Terrace. The slump is interpreted to have formed by shelf instability caused by late stage faulting along the western part of the FFS.

  The slump feature breaches and reduces the effectiveness of possible sealing units. Greenhouse gases injected into underlying reservoirs may migrate into the slump zone, where containment and migration pathways may be complex and unconstrained. The formation of release faults upslope from the slump complex have also affected the integrity of Oligocene and younger sediments that overlie the Latrobe Group.

- **Seal Failure Indicators**:

  An assessment of the GDPI10 2D seismic survey for evidence of seal failure, such as HRDZs and gas chimneys, has identified several clusters of seismic anomalies. Overall, these anomalies are interpreted to relate to the release of fluids associated with volcanic intrusions and with some component of associated fault breach. The clustering of the anomalies is more likely to relate to localised volcanic centres, rather than indications of regional seal breach points. No pervasive hydrocarbon-related anomalies were identified.

8.2 Recommendations for Future Work

- Undertake a full reinterpretation of the Gurnard Formation and the EOW to clearly distinguish the age, lithology and seal potential of these different facies. Integrate the new interpretation with wells that lie close to the Southern Platform (which are outside the current study area).

- Extend regional ties of the deeper horizons (Strzelecki, Emperor and Golden Beach) across the Darriman Fault and into the Central Deep to establish a continuous structural model for the Southern Flank. The

GDPI10 2D seismic survey only crossed the Darriman Fault in the western part of the study area, and this has compromised ties along the northern boundary of the study area.

- Seismic interpretation and the resultant gridding performed on the regional GDPI10 survey could be used to high-grade areas for further investigation. As a first step, regridding any smaller area at a higher resolution to provide additional control on the gridding algorithm and allow for a smaller grid cell size would be beneficial. Including additional interpretations from the many vintage datasets where appropriate may also enhance the current interpretation in some locations. It is considered that additional modern seismic acquisition and interpretation would be required prior to siting greenhouse gas injection wells.
- Review the geographic location of wells on the Southern Flank, as the absolute confidence of the location of older wells is relatively low.
- Reprocessing of select GDPI10 lines may enhance the imaging of structural features on the Southern Platform or the deeper stratigraphy in the Southern Terrace.
- Formation tops need to be reviewed at a number of levels, including additional biostratigraphic analysis to investigate possible alternative interpretations.
- Melville-1 is a key tie well for the survey but contains limited biostratigraphic or formation top information. Additional work on this well may provide important linkage information between the Southern Flank and the Central Deep.
- The new stratigraphic and structural interpretation provides a framework to understand existing seal capacity results (MICP) and can be used to plan future program activities to test concepts and highlight areas of interest.
- The velocity model was developed on a regional scale, using broad stratigraphic intervals to capture velocity variations and assumed increasing velocity with depth. If a more accurate depth conversion is required in localised areas then the model should be reviewed taking into account the velocity inversions noticed in the pseudo-sonic logs. This could be achieved by 'mapping' the inversion in the pseudo-logs.
- The construction surfaces used to create the velocity model could be refined by using the final interpreted surfaces of this study. This should enhance the velocity model and give an improved depth result as the boundaries where the velocity changes would be more accurately defined.
- Ensure the GDPI10 2D seismic survey is released only after the SEG-Y have been regenerated referenced to shotpoint rather than CDP.

9 References

3D-GEO, 2010. High resolution structural seismic stratigraphic analysis of the onshore & offshore Gippsland Basin, Victoria, Australia. Unpublished Report Draft 2.

BASS STRAIT OIL COMPANY, 2001. Melville-1 Well Completion Report, Volume 2: Derivative Data. Unpublished Report.

BERNECKER, T. & PARTRIDGE, A.D., 2001. Emperor and Golden Beach subgroups: The onset of Late Cretaceous sedimentation in the Gippsland Basin, SE Australia. *In* K.C. Hill & T. Bernecker (eds) *Eastern Australasian Basins Symposium: A Refocused Energy Perspective for the Future*, Petroleum Exploration Society of Australia Special Publication, pp. 391-402.

BERNECKER, T. & PARTRIDGE, A.D., 2005. Approaches to palaeogeographic reconstructions of the Latrobe Group, Gippsland Basin, southeastern Australia. *The APPEA Journal* **45(1)**, pp. 581-599.

BERNECKER, T., PARTRIDGE, A.D. & WEBB, J.A., 1997. Mid-Late Tertiary deep water temperate carbonate deposition, offshore Gippsland Basin, southeastern Australia. *In* N.P. James & J.D.A. Clarke (eds) Cool Water Carbonates, *Society of Economic Palaeontologists and Mineralogists Special Publication* **56**, pp. 221-236.

BERNECKER, T., WOOLLANDS, M.A., WONG, D., MOORE, D.H. & SMITH, M.A., 2001. Hydrocarbon prospectivity of the deep water Gippsland Basin, Victoria, Australia. *The APPEA Journal* **41(1)**, pp. 91-113.

BERNECKER, T., THOMAS, H. & DRISCOLL, J., 2003. Hydrocarbon prospectivity of areas, V03-1, V03-2, 03-1(v) and 03-2(v), offshore Gippsland Basin, Victoria, Australia. *Victorian Initiative for Minerals and Petroleum Report* **79**, Department of Primary Industries, 270 p.

BERNECKER, T., THOMAS J.H. & O'BRIEN, G.W., 2006. Hydrocarbon prospectivity of Areas V06-2, V06-3 and V06-4, southern offshore Gippsland Basin, Victoria, Australia. *Victorian Initiative for Minerals and Petroleum Report* **88**, Department of Primary Industries, 224 p.

BISHOP, M.G., 2000. Petroleum system of the Gippsland Basin, Australia. *U.S. Geological Survey Open File Report* **99-50-Q**, 40 p.

BLEVIN, J.E. & CATHRO, D.L., 2008. Australian Southern Margin Synthesis, Project GA707, Client Report to Geoscience Australia by FrOG Tech.

BLEVIN, J., BOREHAM, C.J. & TRIGG, K.R., 2003. Petroleum geology of the Bass Basin - Interpretation report/an output from the Western Tasmanian Regional Minerals Program. *Geoscience Australia Record* **2003/19**, pp. 1-255.

BROOKS, J.D. & SMITH, J.W., 1969. The diagenesis of plant lipids during the formation of coal, petroleum and natural gas. II. Coalification and the formation of oil and gas in the Gippsland Basin. *Geochimica et Cosmochimica Acta* **33**, pp. 1183-1194.

BURNS, B.J., BOSTWICK, T.R. & EMMETT, J., 1987. Gippsland terrestrial oils - Recognition of compositional variations due to maturity and biodegradation effects. *Australian Petroleum Exploration Association Journal* **27(1)**, pp. 73-84.

CANDE, S.C. & MUTTER, J.C., 1982. A revised interpretation of seafloor spreading magnetic anomalies between Australia and Antarctica. *Earth and Planetary Science Letters* **58**, pp. 151-160.

CHAN, P.K.N., 1983. Tarra No. 1 Australian Aquitaine Petroleum Well Completion Report, VIC/P17, Offshore Gippsland Basin.

CUMMINGS, A.M., HILLIS, R.R. & TINGATE, P.R., 2004. New perspectives on the structural evolution of the Bass Basin: Implications for petroleum prospectivity. *In* P.J. Boult, D.R. Johns and S.C. Lang (eds) *Eastern Australasian Basins Symposium II*, Petroleum Exploration Society of Australia Special Publication, pp. 689-694.

CURNOW, C.N., 1969. ESSO Groper-2 Well Completion Report. Unpublished Report, 36 p.

DE VERA, J., GRANADO, P. & MCCLAY, K., 2010. Structural evolution of the Orange Basin gravity-driven system, offshore Namibia. *Marine and Petroleum Geology* **27(1)**, pp. 223-237.

DEPARTMENT OF RESOURCES, ENERGY AND TOURISM, 2011. Regional geology of the Gippsland Basin. AUSTRALIA 2011 Offshore Petroleum Exploration Acreage Release, 16 p.

DUDDY, I.R. & GREEN, P.F., 1992. Tectonic development of the Gippsland Basin and environs: Identification of key episodes using Apatite Fission Track Analysis (AFTA). *In* C.M. Barton, K. Hill, C. Abele, J. Foster & N. Kempton (eds) *Energy Economics and Environment - Gippsland Basin Symposium,* Australasian Institute of Mining and Metallurgy, Melbourne Branch, pp. 111-120.

FRASER, A.R. & TILBURY, L.A., 1979. Structure and stratigraphy of the Ceduna Terrace region, Great Australian Bight. *Australian Petroleum Exploration Association Journal* **19(1)**, pp. 53-65.

FUGRO SEISMIC IMAGING PTY LTD, 2011. Seismic data processing report for Victorian DPI, Survey 2010 Southern Flank 2D.

GEOSCIENCE AUSTRALIA. Petroleum wells database (http://dbforms.ga.gov.au/www/npm.well.search)

GIBSON-POOLE, C.M., SVENDSEN, L., UNDERSCHULTZ, J., WATSON, M.N., ENNIS-KING, J., VAN RUTH, P.J., NELSON, E.J., DANIEL, R.F. & CINAR, Y., 2006. Gippsland Basin geosequestration: A potential solution for the Latrobe Valley brown coal CO_2 emissions. *The APPEA Journal* **46(1)**, pp. 413-434.

GIBSON-POOLE, C.M., SVENDSEN, L., UNDERSCHULTZ, J., WATSON, M.N., ENNIS-KING, J., VAN RUTH, P.J., NELSON, E.J., DANIEL, R.F. & CINAR, Y., 2008. Site characterisation of a basin scale CO_2 geological storage system: Gippsland Basin, southeast Australia. *Environmental Geology* **54(8)**, pp. 1583-1606.

GOETZ, J.F., DUPAL, L. & BOWLER, J., 1979. An investigation into the discrepancies between sonic log and seismic check spot velocities. *Australian Petroleum Exploration Association Journal* **19(1)**, pp. 131-141.

GOLDIE DIVKO, L.M., O'BRIEN, G.W., TINGATE, P.R. & HARRISON, M.L., 2009. Geological carbon storage in the Gippsland Basin, Australia: Containment potential. *VicGCS Report* **1**, Department of Primary Industries, 42 p. + appendices.

GOLDIE DIVKO, L.M., O'BRIEN G.W., HARRISON, M.L. & HAMILTON, P.J., 2010. Evaluation of the regional top seal in the Gippsland Basin: Implications for geological carbon storage and hydrocarbon prospectivity. *The APPEA Journal* **50,** pp. 463-486.

GRADSTEIN, F.M., OGG, J.G. & SMITH, A.G., 2004. A Geologic Time Scale 2004. University Press, Cambridge, 589 p.

GROSS, M.D., 1993. Determination of reservoir distribution over the Blackburn/Terakihi oil field, Gippsland Basin, Australia. *Australian Petroleum Exploration Association Journal* **33(1)**, pp. 1-14.

HAYES, D.E. & RINGIS, I., 1973. Seafloor spreading in the Tasman Sea. *Nature* **243**, pp. 454-458.

HILL, P.J., EXON, N.F., KEENE, J.B. & SMITH, S.M., 1998. The continental margin off east Tasmania and Gippsland: Structure and development using new multibeam sonar data. *Exploration Geophysics* **29**, pp. 410-419.

HOLDGATE, G.R., WALLACE, M.W., DANIELS, J., GALLAGHER, S.J., KEENE, J.B. & SMITH, A.J., 2000. Controls on Seaspray Group sonic velocities in the Gippsland Basin – A multidisiplinary approach to the canyon seismic velocity problem. *The APPEA Journal* **40(1)**, pp. 295-313.

KEETLEY, J., NOUROLLAH, M., TAIT, A., HOFFMAN, N., HALL, M. & ASQUITH, K., 2010. High resolution structural seismic stratigraphic analysis of the onshore and offshore Gippsland Basin, Victoria, Australia. Unpublished Report.

KOENITZ, D., WHITE, N., MCCAVE, I.N. & HOBBS, R., 2008. Internal structure of a contourite drift generated by the Antarctic Circumpolar Current. *Geochemistry Geophysics Geosystems* **9(6)**, 27 p.

MINERAL RESOURCES OF TASMANIA PUBLICATIONS.

(http://www.mrt.tas.gov.au/portal/page?_pageid=35,1&_dad=portal&_schema=PORTAL).

MOORE, P.S., BURNS, B.J., EMMETT, J.K. & GUTHRIE, D.A., 1992. Integrated source, maturation and migration analysis, Gippsland Basin, Australia. *Australian Petroleum Exploration Association Journal* **32(1)**, pp. 313-342.

NORVICK, M.S., 2005. Plate tectonic reconstructions of Australia's Southern Margin. *Geoscience Australia Record* **2005/07**, 113 p.

NORVICK, M.S. & SMITH, M.A., 2001. Mapping the plate tectonic reconstructions of southern and southeastern Australia and implications for petroleum systems. *The APPEA Journal* **41(1)**, pp. 15-35.

NORVICK, M.S., SMITH, M.A. & POWER, M.R., 2001. The plate tectonic evolution of eastern Australasia guided by the stratigraphy of the Gippsland Basin. *In* K.C. Hill & T. Bernecker (eds) *Eastern Australasian Basins Symposium: A Refocused Energy Perspective for the Future,* Petroleum Exploration Society of Australia Special Publication, pp. 15-23.

O'BRIEN, G.W. & WOODS, E.P., 1995. Hydrocarbon-related diagenetic zones (HRDZs) in the Vulcan Sub-basin, Timor Sea: Recognition and exploration implications. *Australian Petroleum Exploration Association Journa*l **35(1)**, pp. 220-252.

O'BRIEN, G.W., TINGATE, P.R., GOLDIE DIVKO, L.M., HARRISON, M.L., BOREHAM, C.J., LIU, K., ARIAN, N. & SKLADZIEN, P., 2008**.** First order sealing and hydrocarbon migration processes, Gippsland Basin, Australia: Implications for CO_2 geosequestration. *In* J.E. Blevin, Bradshaw, B.E. & C. Uruski (eds) *Eastern Australasian Basins Symposium III*, Petroleum Exploration Society of Australia Special Publication, pp. 1-28.

O'SULLIVAN, P.B., BELTON, D.X. & ORR, M., 2000. Post-orogenic thermotectonic history of the Mount Buffalo region, Lachlan Fold Belt, Australia: Evidence for Mesozoic to Cenozoic wrench-fault reactivation? *Tectonophysics* **317**, pp. 1-26.

OGG, J.G., OGG, G. & GRADSTEIN, F. M., 2008. The Concise Geologic Time Scale. University Press, Cambridge, 184 p.

PARTRIDGE, A.D., 1999. Late Cretaceous to Tertiary geological evolution of the Gippsland Basin, Victoria. PhD Thesis, Latrobe University, Bundoora, Melbourne, Australia, 439 p.

PARTRIDGE, A.D., 2001. Revised stratigraphy of the Sherbrook Group, Otway Basin. *In* K.C. Hill & T. Bernecker (eds) *Eastern Australasian Basins Symposium: A Refocused Energy Perspective for the Future*, Petroleum Exploration Society of Australia Special Publication, pp. 455-464.

PARTRIDGE, A.D., 2002. Palynological analysis of Melville-1, offshore Gippsland Basin (*Biostrata Report* **2002/01**). Appendix A of Melville-1 Well Completion Report, Volume 2, Unpublished Report.

PARTRIDGE, A.D., 2003. Early Oligocene age for top of Latrobe reservoirs in Tommyruff-1 and Wyrallah-1, southwest Gippsland Basin. Unpublished Report, 12 p.

PARTRIDGE, A.D., 2006. New observations on the Cenozoic stratigraphy of the Bassian Rise derived from a palynological study of the Groper-1, Mullet-1 and Bluebone-1 wells, offshore Gippsland Basin, southeast Australia. Unpublished Report, 41 p.

PARTRIDGE, A.D., BERNECKER, T., KELMAN, A.P., KHIDER, K., LE POIDEVIN, S. & MANTLE, D.J., 2011. Geoscience Australia: Gippsland Basin Biozonation and Stratigraphy, Chart 40.

PARTRIDGE, A.D., BERNECKER, T., KELMAN, A.P., KHIDER, K., LE POIDEVIN, S. & MANTLE, D.J., 2012. Geoscience Australia: Gippsland Basin Biozonation and Stratigraphy, Chart 40.

PHILP, R.P., 1994. Geochemical characteristics of oils derived predominantly from terrigenous source materials. *In* A.C. Scott & A.J. Fleet (eds) Coal and Coal-bearing Strata as Oil-prone Source Rocks? *Geological Society, London, Special Publication* **77**, pp. 71-91.

PLANKE, S., RASMUSSEN, T., REY, S.S. & MYKLEBUST, R., 2005. Seismic characteristics and distribution of volcanic intrusions and hydrothermal vent complexes in the Vøring and Møre basins. *In* A.G. Dore & B.A. Vinning (eds) Petroleum Geology: North-West Europe and Global Perspectives—Proceedings of the 6th Petroleum Geology Conference. *Geological Society, London, Petroleum Geology Conference Series* **6**, pp. 833–844.

POWER, M.R., HILL, K.C. & HOFFMAN, N., 2003. Structural inheritance, stress rotation, overprinting and compressional reactivation in the Gippsland Basin—Tuna 3D seismic dataset. *The APPEA Journal* **43(1)**, pp. 197-222.

POWER, M.R., HILL, K.C., HOFFMAN, N., BERNECKER, T. & NORVICK, M., 2001. The structural and tectonic evolution of the Gippsland Basin: Results from 2D section balancing and 3D structural modelling. *In* K.C. Hill & T. Bernecker (eds) *Eastern Australasian Basins Symposium: A Refocused Energy Perspective for the Future*, Petroleum Exploration Society of Australia Special Publication, pp. 373-384.

RIDER, M.H., 1996. The Geological Interpretation of Well Logs. Whittles Publishing.

ROYER, J.-Y. & ROLLET, N., 1997. Plate-tectonic setting of the Tasmanian region. *Australian Journal of Earth Sciences* **44 (5)**, pp. 543-560.

SAYERS, J., SYMONDS, P.A., DIREEN, N.G. & BERNARDEL, G., 2001. Nature of the continent-ocean transition on the non-volcanic rifted margin of the central Great Australian Bight. *In* R.C.L. Wilson, R.B. Whitmarsh, B. Taylor & N. Froitzheim (eds) Non-volcanic Rifting of Continental Margins: A Comparison of Evidence from Land and Sea. *Geological Society, London, Special Publication* **187**, pp. 51-77.

SHAW, R.D., 1979. On the evolution of the Tasman Sea and adjacent continental margins. PhD Thesis, University of Sydney, Australia, 311 p.

SMITH, G.C., 1988. Oil and Gas. *In* J.G. Douglas & J.A. Fergusson (eds) Geology of Victoria, *Geological Society of Australia Special Publication* **5**, pp. 514-531.

STAGG, H.M.V., COCKSHELL, C.D., WILLCOX, J.B., HILL, A.J., NEEDHAM, D.V.L., THOMAS, B., O'BRIEN, G.W. & HOUGH, L.P., 1990. Basins of the Great Australian Bight Region: Geology and Petroleum Potential. *BMR Continental Margins Program Folio* **5**.

STOW, D.A.V., FAUGÈRES, J.-C., VIANA, A. & GONTHIER, E., 1998. Fossil contourites: A critical review. *Sedimentary Geology* **115(1-4)**, pp. 3–31.

TAYLOR, D.J., 1966. Esso Gippsland Shelf No.1: The Mid-Tertiary Foraminiferal Sequence. Unpublished Report.

TELFORD, W., 1985. Applied Geophysics. Cambridge University Press.

TERRATEK, 2012. Independent technical advisors report, FROGTECH projectDPI702, Southern Flank GDPI10 2D seismic survey, Gippsland Basin. Unpublished Report, 181 p.

THOMAS, H., BERNECKER, T. & DRISCOLL, J., 2003. Hydrocarbon prospectivity of Areas V03-3 and V03-4 offshore Gippsland Basin, Victoria, Australia: 2003 Acreage Release. *Victorian Initiative for Minerals and Petroleum Report **80***, Department of Primary Industries, 249 p.

WEISSEL, J.K. & HAYES, D.E., 1977. Evolution of the Tasman Sea reappraised. *Earth and Planetary Science Letters* **36**, pp. 77-84.

WILLCOX, J.B. & STAGG, H.M.V., 1990. Australia's southern margin: A product of oblique extension. *Tectonophysics* **173**, pp. 269-281.

WILLCOX, J.B., COLWELL, J.B. & CONSTANTINE, A.E., 1992. New ideas on Gippsland Basin regional tectonics. *In* C.M. Barton, K. Hill, C. Abele, J. Foster & N. Kempton (eds) *Energy Economics and Environment - Gippsland Basin Symposium*, Australasian Institute of Mining and Metallurgy, Melbourne Branch, pp. 93-110.

YILMAZ, Ö., 1987. Seismic Data Processing. *Society of Exploration Geophysicists, Investigations in Geophysics Volume* **2**, 526 p.